Evaluating UK Blanket Peatland Restoration: Structure, Function, and Net Carbon Benefit

Volume 1of 1

This thesis is submitted for the degree of Doctor of Philosophy in Geography

University of Cumbria

Institute of Science and Environment

June 2025

Jack Richard Brennand

Word count: 66,500

Abstract

UK blanket peatlands are globally significant carbon stores, but widespread degradation has shifted them from net carbon sinks to sources. Restoration is increasingly implemented as a nature-based solution aligned with net-zero policy, attracting public and private investment. However, restoration outcomes are evaluated using surface proxies and assumed recovery timelines, limiting insight into sub-surface function and carbon efficiency.

This research advances scientific understanding, restoration practice, and policy by integrating surface ecological data with sub-surface bulk chemical, structural, and carbon cost indicators to evaluate restoration effectiveness in Northern England. A mixed-methods approach was developed, combining bespoke site selection with limited samples across large, heterogeneous landscapes, condition surveys, bulk and chemical analysis, innovative 3D X-ray micro-computed tomography (µCT), and the first Life Cycle Assessment (LCA) of peatland restoration interventions. New methodologies were introduced to quantify and classify peat porosity by functional behaviour, enabling assessment of structural and functional recovery alongside net carbon benefit.

Findings showed widely adopted surface indicators failed to capture sub-surface functional recovery. µCT revealed persistent drainage pathways and limited stratification, with minimal acrotelm and mesotelm development even after a decade. Turving supported atmosphere-connected pore networks indicative of a functional acrotelm, increasing surface water uptake, retention, and anoxia, suggesting its effectiveness as a revegetation strategy complimenting rewetting efforts. Carbon costs varied up to 277-fold; helicopter-installed stone dams incurred high emissions but delivered limited benefit. Greater emissions did not equate to greater function.

This research informs revisions to the IUCN UK Peatland Code and provides evidence-based recommendations for best practice. It urges policy to account for sub-surface function in restoration targets and reporting, potentially extending beyond carbon. Findings support more credible carbon crediting and encourages private investment in peatland restoration as a long-term climate mitigation strategy.

Acknowledgements

Author's Declaration

I, Jack Richard Brennand, confirm that the research included within this thesis is my own work or that where it has been carried out in collaboration with, or supported by others, that this is duly acknowledged and my contribution indicated.

I attest that I have exercised reasonable care to ensure that the work is original, and does not to the best of my knowledge break any UK law, infringe any third party's copyright or other Intellectual Property Right, or contain any confidential material. I accept that the institution has the right to use plagiarism detection software to check the electronic version of the thesis.

I confirm that this thesis has not been previously submitted for the award of a degree by this or any other university.

The copyright of this thesis rests with the author and no quotation from it or information derived from it may be published without the prior written consent of the author

Signature:

Date:

Contents

List of Tables

List of Figures

Chapter 1: Introduction

Exploitation of fossil fuels and land resources has disrupted Earth's carbon cycle, driving anthropogenic climate change. Atmospheric concentrations of carbon dioxide (CO_2) and methane (CH_4) have increased dramatically (Figure 1.1a), contributing to a rise in global temperatures of ~1.0°C since the mid-19th century (Figure 1.1b) (IPCC, 2021, 2022a, 2023b). These changes threaten the biosphere and demand action to mitigate greenhouse gas (GHG) emissions and restore carbon sinks.
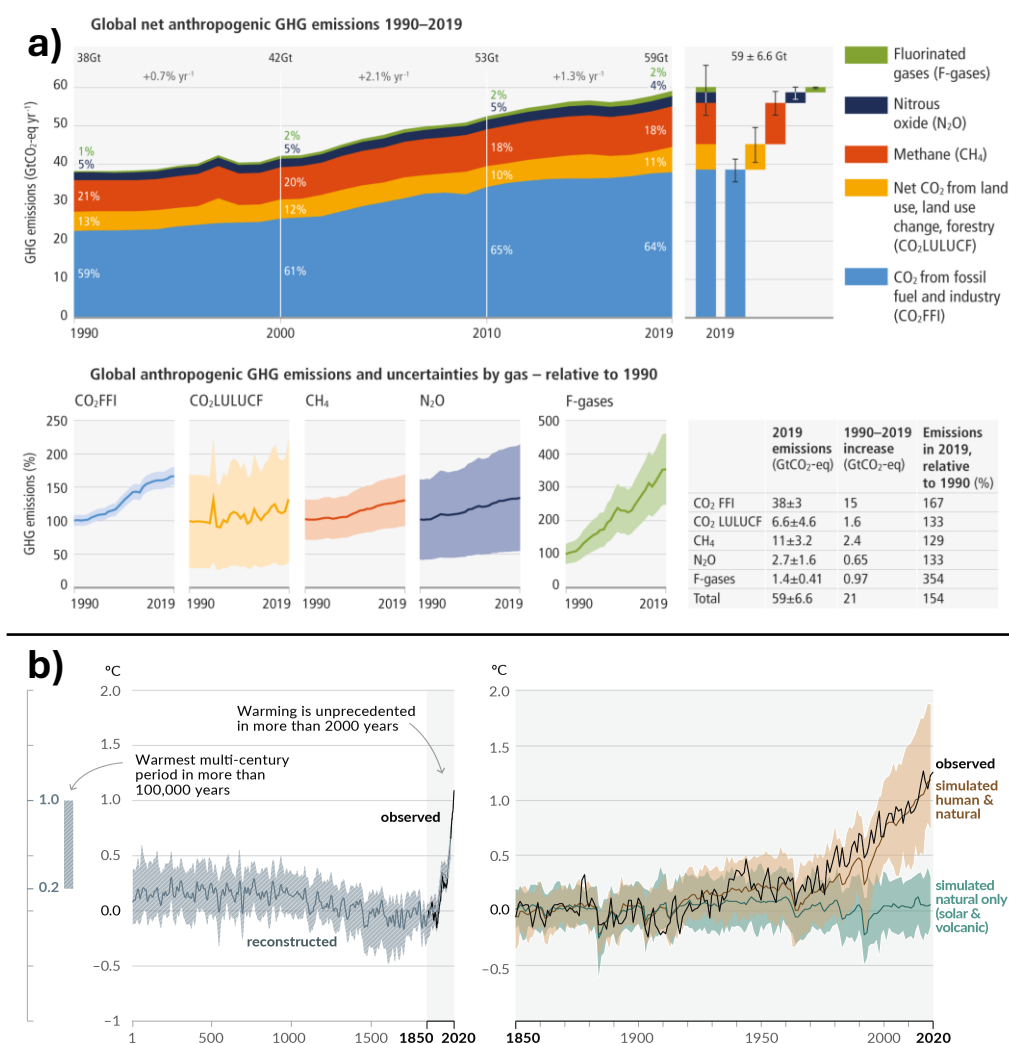
Figure 1.1: Graphs from the IPCC Sixth Assessment Report: a) Global net anthropogenic GHG emissions 1990-2019 (IPCC, 2021); b) History of global temperature change and causes of recent warming (IPCC 2022b).

The terrestrial environment, comprising vegetation, soil, and detritus, plays a fundamental role in regulating the carbon cycle (Kasischke, 2000). However, >90% of these systems have been altered by land-use change, reducing their capacity for carbon accumulation (Plumptre *et al.*, 2022). Restoring these ecosystems is now recognised as a critical nature-based solution to the climate and biodiversity crisis (IPCC, 2014, 2022b; Gibbs and Salmon, 2015).

Despite only covering ~2.84% of Earth's land surface, peatlands represent the largest terrestrial carbon store, estimated at ~550 – 612 Gt C; approximately one-third of global soil carbon (Yu *et al.*, 2010; Minasny *et al.*, 2019) and twice the amount stored in the world's rainforest biomass (Xu *et al.*, 2018). Under waterlogged, anaerobic conditions, decomposition is retarded, enabling peat accumulation at an average rate of ~1mm y^{-1} (Clymo *et al.*, 1998; Clymo and Bryant, 2008). Peatlands have historically sequestered ~500 Mt C y^{-1} (Gorham, 1991), contributing a net cooling effect on global climate (Yu, 2011). However, >50% of global peatlands have been degraded through drainage, overgrazing, burning, forestry, and extraction (Petrescu *et al.*, 2015; Joosten *et al.*, 2016b; Apori *et al.*, 2022). These disturbances have reversed their carbon sink function, with degraded peatlands emitting ~0.31 – 3.38 Gt CO_2eq y^{-1}, equivalent to ~1 – 5% of global anthropogenic emissions (Leifeld and Menichetti, 2018).

The UK contains ~3 million hectares of peatland; ~12% of its land area, including ~13% of the world's rare blanket bog (Figure 1.2) (Bain *et al.*, 2011; JNCC, 2011). These ecosystems store ~3.12 Gt C and have historically contributed as net carbon sinks (Bain *et al.*, 2011; Evans *et al.*, 2017; Gregg *et al.*, 2021). However, ~90% of UK blanket peatlands are now in a degraded condition (Artz *et al.*, 2019), contributing up to 24.5 Mt

$CO_2eq\ y^{-1}$, close to 50% of the UK's total land-use emissions (Evans *et al.*, 2017; Gregg *et al.*, 2021). In response, *peatland restoration is embedded in national climate policy* (Stoneman *et al.*, 2016; Strack *et al.*, 2022) *and supported by public and private funding* (Wentworth, 2022; Hooker and Wentworth, 2024), including through blended finance models (Moxey *et al.*, 2021). Schemes such as the IUCN UK Peatland Code aim to reverse degradation and generate measurable carbon savings for sale as credits within the unregulated voluntary carbon market (Hooker and Wentworth, 2024; IUCN, 2024a). *However, national targets remain largely unmet* (IUCN, 2024d) and many restored sites continue to act as net carbon sources for decades post-intervention (Cooper *et al.*, 2014; Vanselow-Algan *et al.*, 2015).

Figure 1.2: Restored blanket peatland at Shap Fells, Cumbria, England, representing rare UK blanket bog habitat.

Restoration is assessed using surface-based ecological indicators (JNCC, 2009; Shepherd *et al.*, 2013; Birnie *et al.*, 2023; Crowle *et al.*, 2025) and assumed emissions reductions (Couwenberg *et al.*, 2011; Birnie and Smyth, 2013; Smyth *et al.*, 2015), as seen within the IUCN UK Peatland Code (IUCN, 2024b), with limited consideration of sub-surface structural and functional recovery. *This restricts the ability to determine whether interventions actually restore long-term carbon benefits, as carbon storage dynamics are governed by belowground structural processes* (Clymo *et al.*, 1998; Rezanezhad *et al.*, 2016; McCarter *et al.*, 2020). Moreover, assessments have not empirically accounted for the carbon costs of restoration (Drever *et al.*, 2021), including emissions from material sourcing, machinery use, and helicopter transport; known to be significant in landscape-scale restoration (Chiu *et al.*, 2022). As carbon is the primary metric of success and informs blended finance, this further questions the accuracy of reported net carbon benefits and reduces investor confidence (Bonn *et al.*, 2014; Moxey *et al.*, 2021).

Despite policy and funding support, UK blanket peatland restoration has yet to deliver the functional or carbon outcomes expected of a credible nature-based solution. Rewetting and revegetation have improved ecological conditions (Strack and Zuback, 2013; Alderson *et al.*, 2019), but do not guarantee sub-surface recovery or net carbon sequestration. Reported carbon benefits are often marginal (Worrall *et al.*, 2011; Strack and Zuback, 2013), and without accounting for the emissions associated with restoration, net carbon balance remains uncertain (Drever *et al.*, 2021). This reflects over-reliance on surface proxies, limited monitoring of sub-surface impacts, and insufficient technique differentiation. *Evaluating sub-surface function and carbon efficiency is required to inform best practice and policy, increasing the credibility and investment feasibility of peatland restoration as a climate mitigation strategy.*

1.1 Aims and Purpose of the Research

The aim of this thesis is to evaluate the effectiveness of UK blanket peatland restoration based on sub-surface structural and functional recovery, as well as the net carbon benefits of interventions, accounting for their carbon costs. Rather than relying on indirect surface proxies, it examines whether restored sites recover sub-surface function, where long-term carbon accumulation occurs, and if interventions deliver a positive net carbon balance. These additions are critical to improving the credibility and climate relevance of peatland restoration as a nature-based solution, particularly where outcomes underpin carbon finance and policy commitments.

To address this, the research integrates established ecological and bulk chemical indicators of recovery with novel structural and carbon cost data associated with distinct interventions. This approach builds on and critically evaluates existing monitoring frameworks, including those based on JNCC (2009) and the IUCN UK Peatland Code, which rely on indirect surface proxies that may not capture sub-surface change. The methodology and research questions guiding this assessment are outlined in Chapter 3.

A key part of the research is the application of 3D X-ray micro-computed tomography (µCT) to visualise and quantify peat macroporosity. This enables detailed analysis of effective pore volume, shape, connectivity, and anisotropy; characteristics influencing hydrological function, solute transport, and gas exchange relevant to carbon accumulation (detailed in Chapter 2). However, µCT is resource-intensive and cannot be applied at scale. A bespoke, pragmatic sampling framework was therefore developed to support representative site selection across large, heterogeneous landscapes (outlined

in Chapter 4), while grounding μCT findings in accessible ecological and bulk chemical assessments.

To evaluate the carbon efficiency of restoration techniques, Life Cycle Assessment (LCA) was used to quantify emissions from raw materials, transport, and installation (detailed in Chapter 2). This enables direct comparison between the functional recovery delivered by interventions and their associated carbon costs; overlooked in assessments of restoration benefit. When considered alongside structural, bulk chemical, and surface indicators, these data provide the first integrated evaluation of sub-surface functional recovery and net carbon balance across different restoration techniques.

The purpose of this thesis is therefore to embed sub-surface structural and functional understanding into restoration monitoring, and to incorporate the carbon costs of interventions into project emissions reporting. This supports more robust evaluation of interventions, increases confidence in reported outcomes, and provides evidence to inform best practice and future policy in UK blanket peatland restoration.

1.2 Thesis Structure

This thesis is structured to progress from critical evaluation of current monitoring approaches to the integration of sub-surface functional and carbon cost data, providing an evidence-based assessment of peatland restoration effectiveness. **Chapter 2** reviews the scientific and policy context of UK blanket peatland degradation and restoration, identifying key limitations in existing evaluation frameworks, particularly their reliance on surface condition as an indirect proxy for carbon and function.

Chapter 3 outlines the project design and methodological approach, detailing the research questions, field measurements, laboratory techniques, and 3D X-ray micro-computed tomography (μCT) application. Justifications are provided to support the research is grounded in established protocols while facilitating the integration of innovative structural and carbon cost assessments. Considering the intensity of μCT analysis and limitations on sample numbers, **Chapter 4** presents a bespoke, spatially balanced sampling framework to support representative site selection across large, heterogeneous landscapes. This includes degraded (baseline), near-natural (target), and restored sites across a range of restoration ages and techniques.

Chapter 5 evaluates surface condition using the JNCC (2009) *Common Standards Monitoring Guidance (CSM) for Upland Habitats: Blanket Bogs*. It provides a critical assessment of surface indicators currently used in restoration monitoring and develops condition scores to evaluate success embedded in existing practice. **Chapter 6** presents results from bulk and chemical analyses of the sub-surface, examining physical and biogeochemical indicators of function with depth and assessing whether surface scores from Chapter 5 capture sub-surface processes. The potential for bulk chemical indicators to serve as accessible proxies is also evaluated, considering their alignment with standard measurement protocols.

Chapter 7 applies μCT to quantify peat pore network structure, including macroporosity, inferred microporosity, pore size, shape, complexity, connectivity, and anisotropy, offering novel insights into how restoration techniques influence fine-scale structure and function. A new porosity classification is introduced, dividing pore space into two active types and one inactive type based on spatial and functional behaviour.

Chapter 8 assesses the carbon costs of restoration using Life Cycle Assessment (LCA), quantifying emissions from raw materials, transport, and installation. This adaptive chapter presents results currently under peer review (Brennand *et al.*, 2025) and now embedded within the IUCN UK Peatland Code Carbon Savings Calculator (IUCN, 2025a). Findings enable the first direct comparison between functional outcomes and the carbon cost of restoration interventions.

Chapter 9 integrates findings across structural, bulk chemical, surface, and carbon cost datasets to evaluate restoration effectiveness and propose a definition of success grounded in sub-surface functional and carbon understanding. The research questions are addressed directly, before **Chapter 10** concludes with implications for monitoring, policy, and restoration practice.

Chapter 2: Blanket Peatland Structure, Function, Restoration, and Evaluation

Blanket peatlands are globally significant carbon sinks, historically contributing to climate regulation through long-term carbon sequestration and storage (Yu *et al.*, 2011; Joosten *et al.*, 2016b). In the UK, they cover a fraction of area yet represent the largest terrestrial carbon store (Bain *et al.*, 2011; Evans *et al.*, 2017; Gregg *et al.*, 2021). However, most UK blanket peatlands are degraded, shifting from net carbon sinks to sources (Evans *et al.*, 2017; Artz *et al.*, 2019). This has prompted widescale restoration to cap GHG emissions, supported by ambitious climate targets and substantial funding (Bain *et al.*, 2011; Bonn *et al.*, 2014, 2016a; Stoneman *et al.*, 2016; Strack *et al.*, 2022; Wentworth, 2022).

Indirect surface proxies for carbon emissions (Billett *et al.*, 2010; Couwenberg *et al.*, 2011; Petrokofsky *et al.*, 2012) and condition (JNCC, 2009; Shepherd *et al.*, 2013) have been integrated into restoration monitoring frameworks (Birnie *et al.*, 2023; Crowle *et al.*, 2025) and carbon accounting (Birnie and Smyth, 2013; Smyth *et al.*, 2015; IUCN, 2024b). However, the extent to which these indicate true functional recovery remains unknown. At the same time, a suite of restoration techniques have been implemented to rewet and revegetate degraded sites (Parry *et al.*, 2014; Thom *et al.*, 2019; NatureScot, 2021), yet their impacts on function and carbon balance are poorly understood. This includes the carbon emissions associated with restoration interventions which can be substantial (Drever *et al.*, 2021; Chiu *et al.*, 2022).

Understanding functional recovery and carbon costs is essential to the integrity of carbon credits and to shift targets toward delivering net carbon sequestration through defined restoration success (Whitfield *et al.*, 2011; Reed *et al.*, 2013, 2022; Bonn *et al.*, 2014, 2016b; Stoneman *et al.*, 2016; Moxey *et al.*, 2021).

2.1 Peatland Structure, Formation, and Significance

Peat is decaying or decayed organic matter (Holden *et al.*, 2004). It forms where photosynthetic productivity exceeds decomposition in saturated regions over long ecological timescales (Ingram, 1978; Clymo, 1984). Recognised as retarded decay, this process occurs due to the restricted diffusion rate of gases in water, limiting oxygen availability for aerobic decay. Moreover, the substantial heat capacity of water, along with high energy demand for vaporisation, contributes to lower temperatures, suppressing microbial activity and assisting peat formation (Clymo, 1984; Freeman *et al.*, 2001). Peat growth and blanket peatland succession relies on specific ombrotrophic, hydrological regimes influenced by climate, topography, and geology (Moore, 1975; Charman, 2002) (Figure 2.1).

Climate must sustain saturated conditions for at least part of the year, while topography and geology must support high water tables with minimal runoff (Charman, 2002; Holden and Burt, 2003). Chemical and biological factors regulate primary production and decay rates of organic matter (Charman, 2002). These include acidic, nutrient-poor environments created by atmospheric precipitation inputs and dominance of *Sphagnum* mosses, contributing to retarded decomposition through their high cation exchange capacity and production of phenolic and uronic acids (Gagnon and Glime, 1992; Weston *et al.*, 2015; Dunn *et al.*, 2016).

Anthropogenic activity also contributes to blanket peatland formation in the UK through the historic removal of trees (Tallis, 1998; Charman, 2002) (Figure 2.1). While debate persists over the extent of human influence (Moore, 1993; Tallis, 1995; Huang, 2002; Gallego-Sala *et al.*, 2016), palaeoecological records suggest formation occurred between ~1500 and ~9000 BP, with great expansion across ~5000-6000 BP (Tallis, 1998; Yu *et al.*, 2010; Gallego-Sala *et al.*, 2016).
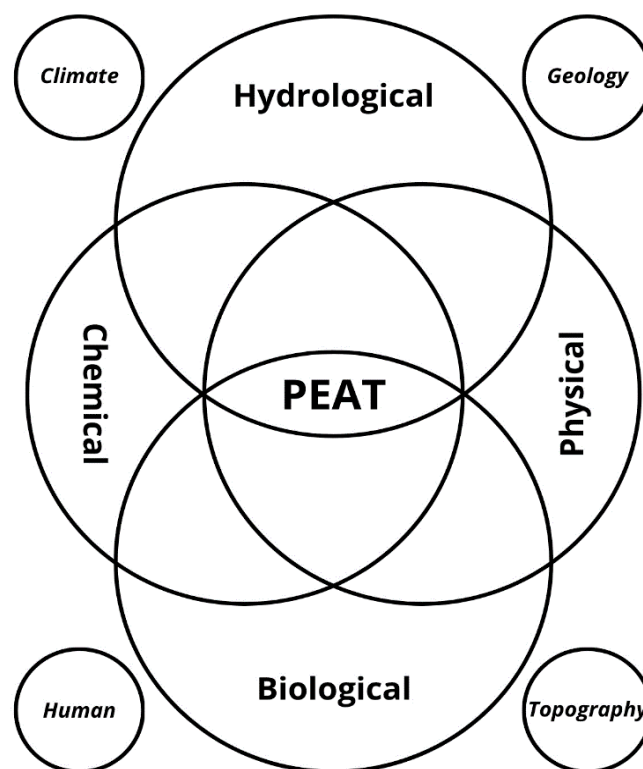
Figure 2.1: Conceptual illustration showing the core and external factors influencing blanket peat formation, adapted from Charman (2002). Factors interact in combination over long ecological timescales and across entire landscapes.

Forming under specific conditions (Figure 2.1; Charman, 2002), blanket peatlands reside in relatively warm (mean annual temperature >-1°C; warmest month ≤15°C) and wet (≥1000mm annual precipitation; ≥160 days rainfall at ≥1mm) maritime climates >40-45° latitude, where precipitation exceeds evapotranspiration (Lindsay *et al.*, 1988; Gallego-Sala *et al.*, 2016). They are primarily restricted to the uplands (>249m) of the UK in the

oceanic west and north, including the Highlands and Western Isles of Scotland, and Cumbria Fells, Central Pennines, and Yorkshire Dales in England (Figure 2.2) (House *et al.*, 2011; Natural England, 2025). However, peatland type (blanket bog, raised, bog, and fen) mapping is limited by land-use change, such as agricultural and grassland expansion over peats, which obscures ecological boundaries (Artz *et al.*, 2019; Minasny *et al.*, 2019). Volumetric extents also remain poorly defined due to inconsistent national definitions of peat depth (Section 2.4.2) and a lack of scalable, high-resolution sub-surface data for reliable depth and carbon stock estimation (Parry *et al.*, 2012; Evans *et al.*, 2017; Carless *et al.*, 2021; Natural England, 2025).
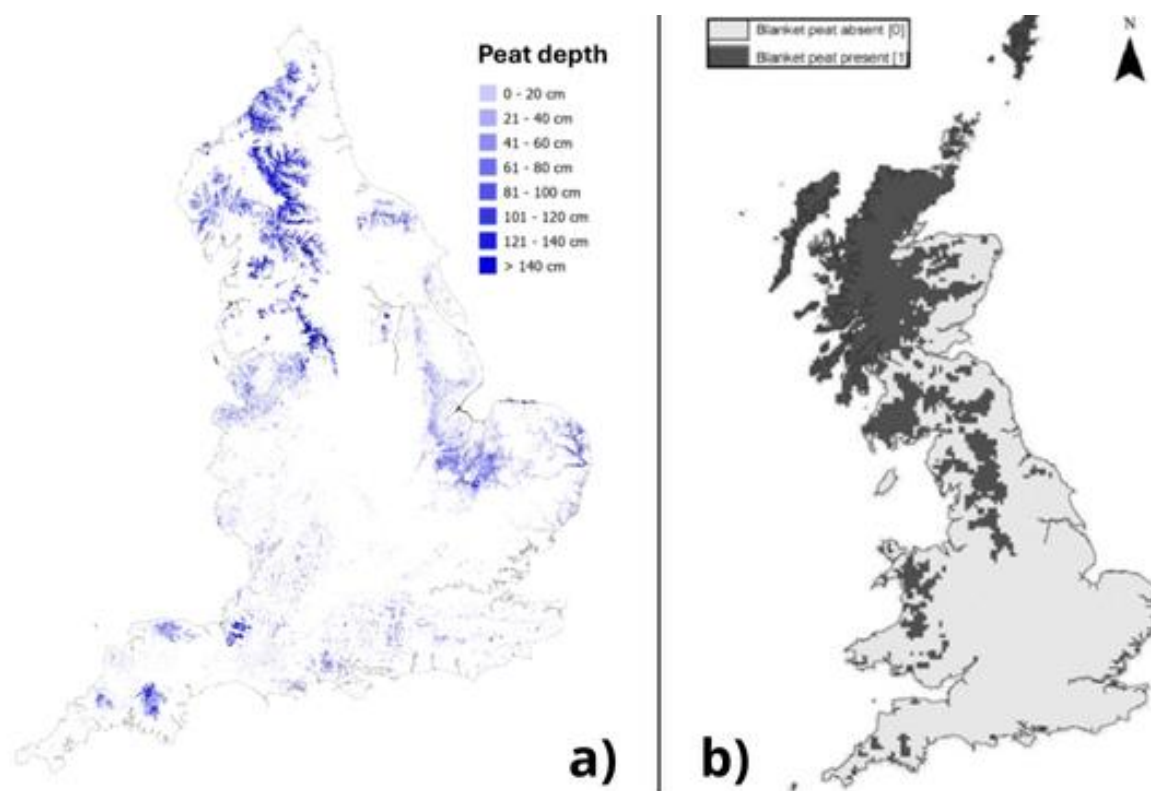
Figure 2.2: Peatland mapping in England and Great Britain: a) Highest resolution peat depth map for England, showing spatial variability in thickness but not differentiating between peatland types (Natural England, 2025); b) blanket peatland distribution across Great Britain, based on presence/absence within 5km^2 grid cells, indicating limited precision in national-scale peatland type mapping (House *et al.*, 2011).

Globally, peatlands store ~550-612 Gt C (Yu, 2012; Leifeld and Menichetti, 2018) and sequester ~0.37 Gt C y^{-1} (Gorham, 1991; Gorham *et al.*, 2012), representing the largest terrestrial carbon sink, despite comprising only ~2.84% of land area (Strack *et al.*, 2022; Minasny *et al.*, 2024). Peatlands cover ~12% of the UK's terrestrial area and store ~3.12 ± 0.3 Gt C, incorporating blanket bogs, raised bogs, and fens (Bain *et al.*, 2011; Evans *et al.*, 2017; Gregg *et al.*, 2021). Blanket peatlands contribute ~87% of UK peat cover at ~2.9 M ha (Tallis, 1998; Holden *et al.*, 2004; Ballard *et al.*, 2011), equivalent to ~13% of global blanket peatlands (Milne and Brown, 1997), and represent the largest carbon store (Gregg *et al.*, 2021).

Long-term carbon accumulation in blanket peat results from the retarded decomposition of photosynthesising species under saturated, anoxic conditions (Tolonen and Turunen, 1996; Clymo *et al.*, 1998). Consequently, carbon storage is a function of its formation (Charman, 2002; Chapin *et al.*, 2006; Lindsay, 2010a; Charman *et al.*, 2013) and is governed by its structure (Ingram, 1978; Clymo, 1984). Understanding these natural processes begins to contextualise restoration aims.

2.1.1 Peat Structure

Peat formation and carbon accumulation is governed by vertical structure, described by the diplotelmic model (Figure 2.3) (Ingram, 1978; Clymo, 1984), which forms part of the blanket peatland carbon cycle discussed in Section 2.1.2. The model divides the peat profile into the acrotelm and catotelm. The acrotelm lies above the mean annual water table and is characterised by high hydraulic conductivity and predominantly aerobic conditions. It supports living vegetation, where gross primary productivity contributes to net primary productivity, and carbon losses occur through aerobic ecosystem respiration

(CO_2 production) and gas diffusion (Section 2.1.2). The catotelm lies below the mean water table, extending to the underlaying substrate. It is fully saturated, with low hydraulic conductivity, promoting slow, anaerobic decomposition and CH_4 release. The catotelm functions as the primary layer of long-term carbon storage, where partially decomposed organic matter accumulates, supporting vertical peat growth at ~1mm y^{-1} (Clymo *et al.*, 1998). Clymo and Bryant (2008) expanded the diplotelmic model to include the pectotelm, representing the photosynthetically active surface layer, and the mesotelm, a transitional zone between the acrotelm and catotelm.
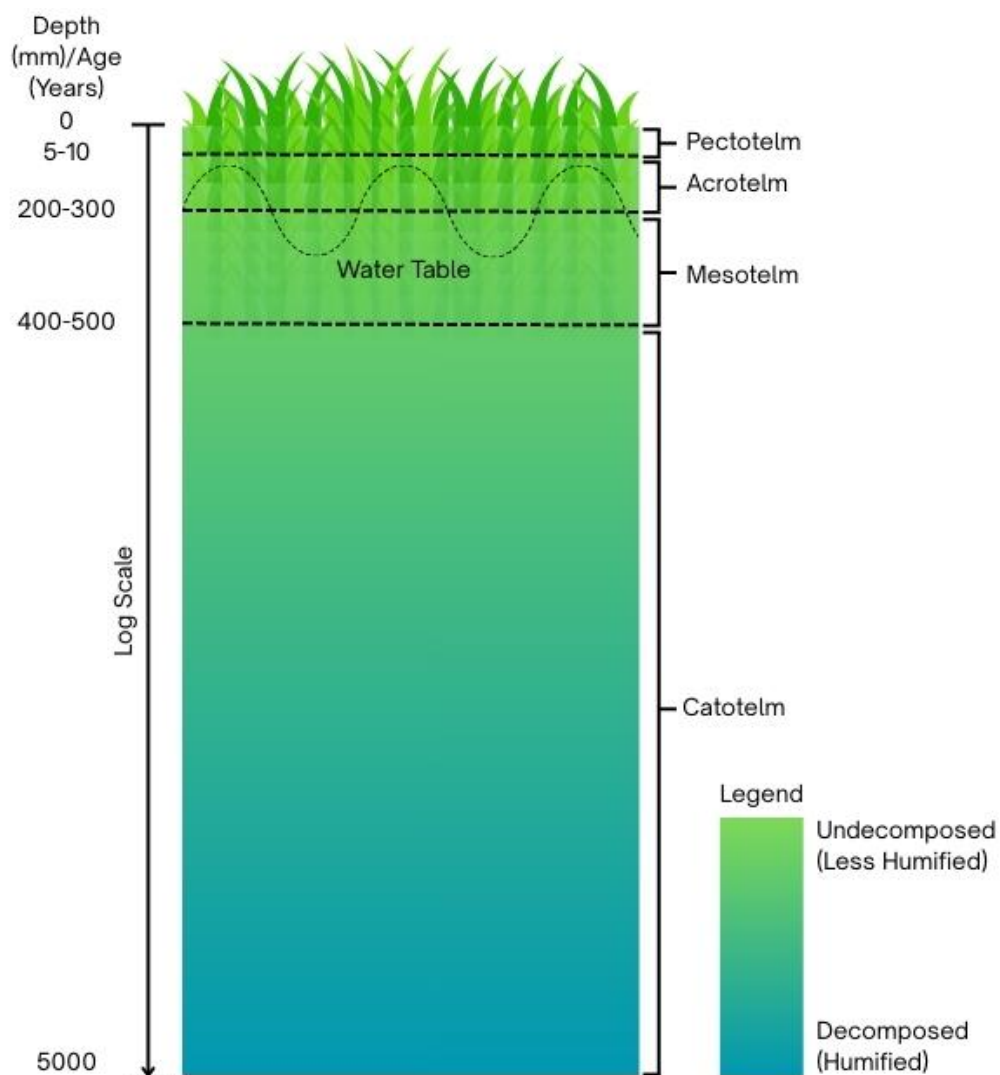
Figure 2.3: Diplotelmic model of peat formation: Ingram (1978), Clymo (1984), and Clymo and Bryant (2008). Semi-logarithmic scale represents the peatland accumulation rate assumption of ~1mm y^{-1} (Clymo *et al.*, 1998). Colour gradient and transparency of vegetation signifies the degree of decomposition with depth (mm). Depths of layers are indicative suggestions from Clymo and Bryant (2008).

However, the model has been criticised for oversimplifying peat formation and carbon storage processes. In particular, the addition of the pectotelm and mesotelm has been argued to offer limited functional insight due to insufficient characterisation (Belyea and Baird, 2006; Morris *et al.*, 2011). Its emphasis on vertical layering overlooks horizontal heterogeneity and ecohydrological complexity, which are essential for understanding carbon dynamics and functional spatial variability (Holden and Burt, 2003; Baird *et al.*, 2016). This includes microtopographic variation such as hummock to hollow complexes (Morris *et al.*, 2015), which play distinct roles in carbon accumulation (discussed further in Section 2.2.1). Morris *et al.* (2011) instead advocate for identifying functional 'hotspots' within the peat profile. Nonetheless, the diplotelmic model remains a useful conceptual tool, particularly for delineating broad functional zones in relation to decomposition and hydrological responsiveness. Its simplicity offers practical value for restoration and monitoring strategies, especially where spatial data are lacking. While it does not capture the full ecohydrological variability of peatlands, it provides a foundational framework that can be integrated with more spatially explicit or process-based models to support targeted management and assessment.

2.1.2 Carbon Accumulation in Peat

Carbon accumulation in peat is a function of its formation and structure, whereby carbon inputs exceed losses over long timescales. The Net Ecosystem Carbon Balance (NECB) model best describes this processes, integrating key fluxes regulating carbon storage (Chapin *et al.*, 2006). It can be summarised as:

$$NPP = GPP - ER$$

$$NCA = NPP - (D + O)$$

where:

- **GPP:** Gross primary productivity.

- **ER:** Ecosystem respiration.

- **NPP:** Net primary productivity.

- **D:** Decomposition.

- **O:** Other fluxes, such as dissolved organic carbon (DOC) and particulate organic carbon (POC).

- **NCA:** Net carbon accumulation.

NECB can be viewed in two parts: NPP indicates the carbon sequestration function, while NCA represents the carbon storage function. Positive NCA is achieved where carbon inputs (NPP) exceed losses from decomposition (D) and other fluxes (O).

Net primary productivity is driven by peat-forming vegetation, including bryophyte, vascular, and graminoid species (Lindsay *et al.*, 1988; Belyea and Clymo, 2001; Sottocornola *et al.*, 2009; Strack *et al.*, 2016; Bacon *et al.*, 2017). *Sphagnum* (a genus of bryophyte) frequently dominates under ombrotrophic conditions and is recognised as a pioneer species (van Breemen, 1995; Rochefort *et al.*, 2003; Strack and Price, 2009; Weston *et al.*, 2015; Bacon *et al.*, 2017). *Sphagnum* fixes atmospheric carbon through photosynthesis (gross primary productivity), while limiting autotrophic and heterotrophic respiration via releasing phenolic and uronic acids (Gagnon and Glime, 1992; van

Breemen, 1995; Verhoeven and Liefveld, 1997; Hamard *et al.*, 2019). Their hyaline cells (further discussed in Section 2.2.1) also maintain saturated, cool conditions, retarding decomposition and contributing to high net primary productivity (Kettridge and Binley, 2008; Weston *et al.*, 2015). Consequently, *Sphagnum* is considered an ecosystem engineer. While vascular plants and graminoids contribute structurally to peat formation, particularly as nurse species for bryophyte succession (Bacon *et al.*, 2017), they play a lesser role in maintaining saturation, acidity, and the cool, anaerobic conditions retarding decomposition (Zeh *et al.*, 2020).

Decomposition refers to the microbial transformation of litter and root exudates into simpler, low molecular weight compounds (Dunn *et al.*, 2016). It occurs rapidly under oxic and more slowly under anoxic conditions, releasing CO_2 and CH_4, respectively (Clymo, 1984). These gases exchange with the atmosphere through diffusion or direct pathways (Moore *et al.*, 2002; Holden, 2005b). Rates are regulated by temperature and oxygen availability, controlled by the hydrological regime (O'Kelly and Pichan, 2014; Bell *et al.*, 2018). Other carbon losses include waterborne export, such as the leaching of dissolved organic carbon and particulate organic carbon through sub-surface pathways, including peat pipes (Holden, 2005a; Evans *et al.*, 2016, 2018). These carbon fluxes are summarised in Figure 2.4.

Observed values suggest the climate regulation function of blanket peatlands depends on a fine balance between long-term carbon sequestration and GHG emissions. UK blanket peatlands have historically sequestered between -0.35 – 2.09 t C ha^{-1} y^{-1} (Billett *et al.*, 2010), though other estimates report narrower ranges of -0.56 – 0.72 t C ha^{-1} y^{-1}, including sites with negative net primary productivity (Koehler *et al.*, 2011). Expressing

net carbon balance in carbon dioxide equivalents (CO_2eq) shows additional complexity. CH_4 has a global warming potential ~28 times greater than CO_2 over a 100-year timescale (United Nations Climate Change, 2020). Consequently, CH_4 emissions can offset CO_2 sequestration. Artz *et al.* (2014) estimated average net GHG emissions from blanket peatlands at -0.76 ± 0.39 t CO_2eq ha^{-1} y^{-1}, while Worrall *et al.* (2011) modelled highs of -4.11 t CO_2eq ha^{-1} y^{-1}, though these are likely overestimates (Artz *et al.*, 2014). More recent studies suggest near-natural blanket peatlands sequester as little as -0.02 t CO_2eq ha^{-1} y^{1} (Gregg *et al.*, 2021), or -0.25 Mt CO_2eq y^{-1} (Evans *et al.*, 2017). 'Near-natural' is used in place of 'pristine' due to ongoing debate over whether they exist (Section 2.3; Evans *et al.*, 2017; Artz *et al.*, 2019). This demonstrates the sensitivity of blanket peatland carbon accumulation potential and contextualises the task of restoration.
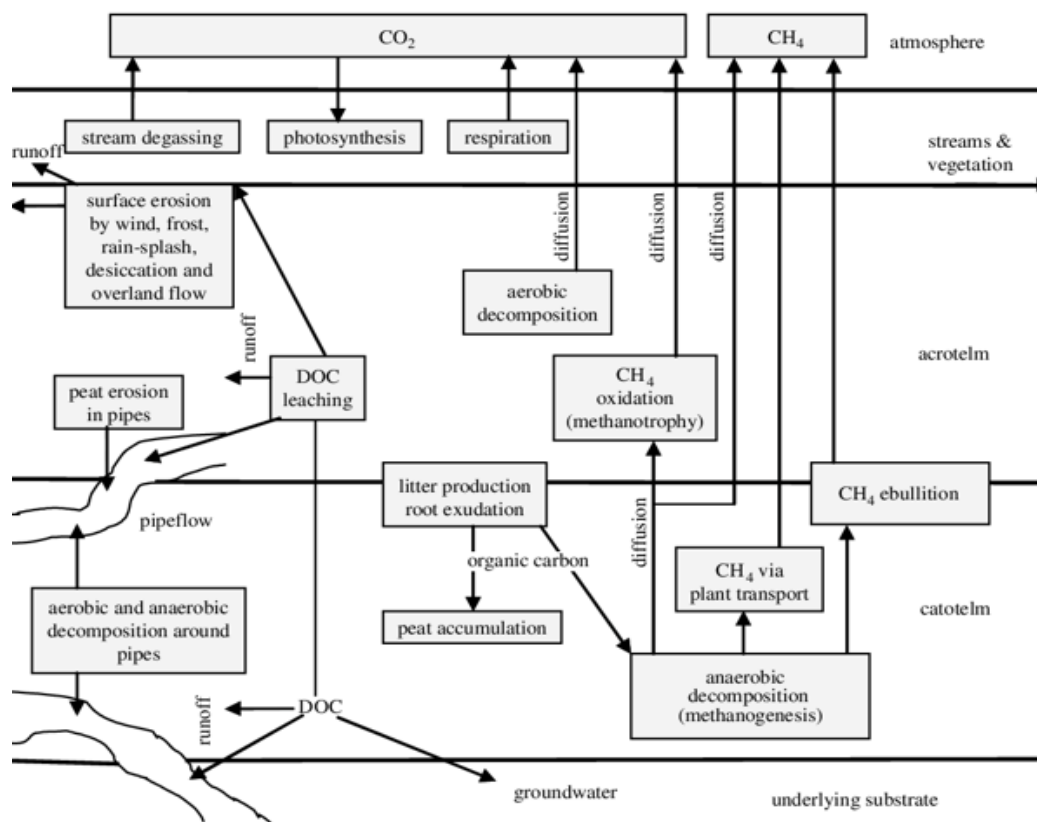
Figure 2.4: Conceptual diagram detailing the components of the carbon cycle in blanket peatlands adapted from Holden (2005b). Note POC relates to those components on the left of the diagram covering erosional processes.

2.2 Role of the Sub-Surface in Peatland Function

While carbon sequestration (positive net primary productivity) is governed by surface processes, net carbon accumulation is determined by sub-surface structure (Clymo, 1984; Clymo and Bryant, 2008; Rezanezhad *et al.*, 2016) and functions where 99% of peat carbon stored (Tallis, 1998; Belyea and Malmer, 2004; Holden, 2005b; Li *et al.*, 2024). These include water retention, solute transport, and gas exchange, which regulate decomposition (Freeman *et al.*, 2001), CO_2 and CH_4 production (Dalva and Moore, 1993; Strack and Waddington, 2007), and carbon export (Evans *et al.*, 2016). These processes are controlled by pore network structure (Rezanezhad *et al.*, 2009, 2010, 2016; Gharedaghloo *et al.*, 2018; McCarter *et al.*, 2020), critical to evaluating the long-term carbon storage function of blanket peatlands and assessing the effectiveness of restoration (Strack *et al.*, 2008; Weber *et al.*, 2017; Alderson *et al.*, 2019).

2.2.1 Water Retention and Transfer

Hydrology represents the primary control on net carbon accumulation (Holden and Burt, 2003; Belyea and Malmer, 2004; Holden, 2005b). Water table depth and saturation through water-holding pores govern the thickness of functional layers (e.g., acrotelm, mesotelm, catotelm), controlling oxygen availability and decomposition rates (Ise *et al.*, 2008; Holden *et al.*, 2011), vegetation composition (Bacon *et al.*, 2017; Li *et al.*, 2024), and carbon export (Evans *et al.*, 2016).

High water tables (~20cm below the surface) create anoxic conditions, suppressing microbial activity and promoting catotelm formation through anaerobic decay (Clymo, 1984; Dalva and Moore, 1993). Decomposition occurs ~50 times more slowly under saturated conditions (Clymo *et al.*, 1998; Clymo and Bryant, 2008), countering the

increased global warming potential of CH_4. Saturated peatlands have been shown to sequester up to 1.58 t CO_2eq ha^{-1} y^{-1} (Evans *et al.*, 2021). Waterlogging also reduces sub-surface temperatures, further retarding microbial activity (Frolking *et al.*, 2001; Hilasvuori *et al.*, 2013; Bell *et al.*, 2018). Consequently, maintaining near-surface water tables reduces carbon losses (decomposition plus other fluxes). Additionally, saturated conditions in an intact acrotelm support *Sphagnum* mosses, which help maintain high water tables. Their hyaline cells retain between 16–26 times their weight in water, trapping moisture and retarding decomposition (Figure 2.5) (Kettridge and Binley, 2008; Weston *et al.*, 2015).
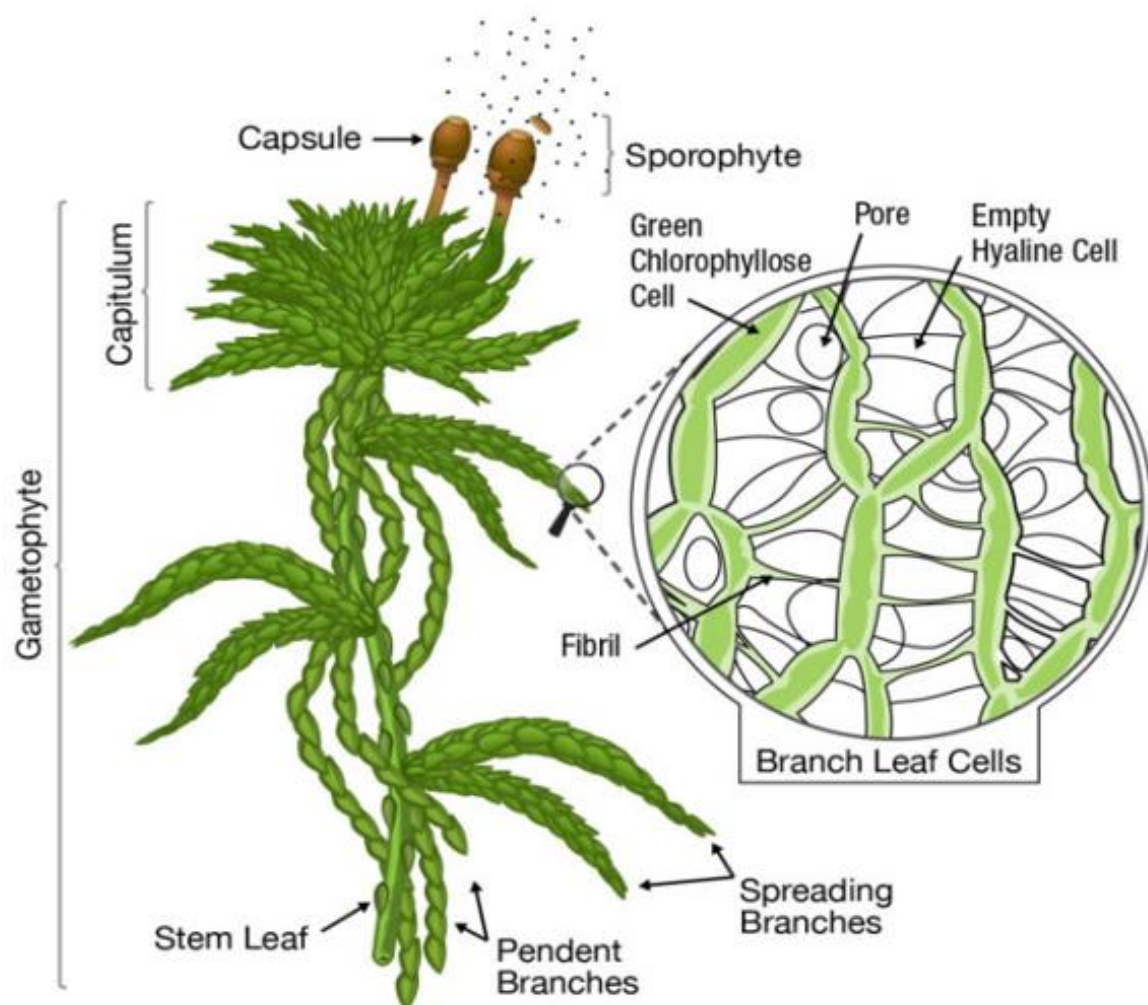
Figure 2.5: Schematic of a strand (gametophyte) of *Sphagnum* moss highlighting the hyaline cell structure responsible for water or gas retention (Weston *et al.*, 2015).

Sphagnum dominance forms hummock to hollow microtopography, which increases surface roughness and water retention from surface runoff, further supporting positive net carbon accumulation (Hogg, 1993; Van Der Molen *et al.*, 1994; Turunen *et al.*, 2004; Holden, 2005b; Holden *et al.*, 2008; Moore *et al.*, 2015; Shuttleworth *et al.*, 2019). Microtopographic variation introduces spatial heterogeneity within the acrotelm. Hummocks (>20-30cm) are more aerated and experience greater water table fluctuation, supporting dryer *Sphagnum* and vascular species, while hollows remain saturated, functionally resembling catotelm conditions and supporting bryophyte species more resilient to decomposition (Van Der Molen *et al.*, 1994; Bengtsson *et al.*, 2016). These conditions influence organic matter accumulation, bulk density, and carbon storage capacity. Hummocks exhibit higher organic carbon concentrations, while hollows may store more carbon per unit volume due to higher bulk density (Figure 2.6) (Wang *et al.*, 2021). Lawns form transitional zones, facilitating surface water accumulation and exhibiting a mix of species from both microforms (Loisel and Yu, 2013; Morris *et al.*, 2019). Consequently, diverse microtopography increases peatland resilience to climate change and contributes to long-term carbon accumulation (Hogg, 1993; Lafleur *et al.*, 2005; Morris *et al.*, 2015; Alshammari *et al.*, 2020; Wang *et al.*, 2021).

Lower water tables increase the thickness of the oxic layer, accelerating aerobic respiration and CO_2 release (Evans *et al.*, 2021; Huang *et al.*, 2021; Ma *et al.*, 2022; Li *et al.*, 2024). They also increase waterborne carbon loss through the leaching of dissolved organic carbon and particulate organic carbon (Evans *et al.*, 2016, 2018; Young *et al.*, 2017) and favour vascular and graminoid species which produce more liable litter, further increasing decomposition rates and carbon loss (Prescott, 2010; Schellekens *et al.*, 2015; Zeh *et al.*, 2020).
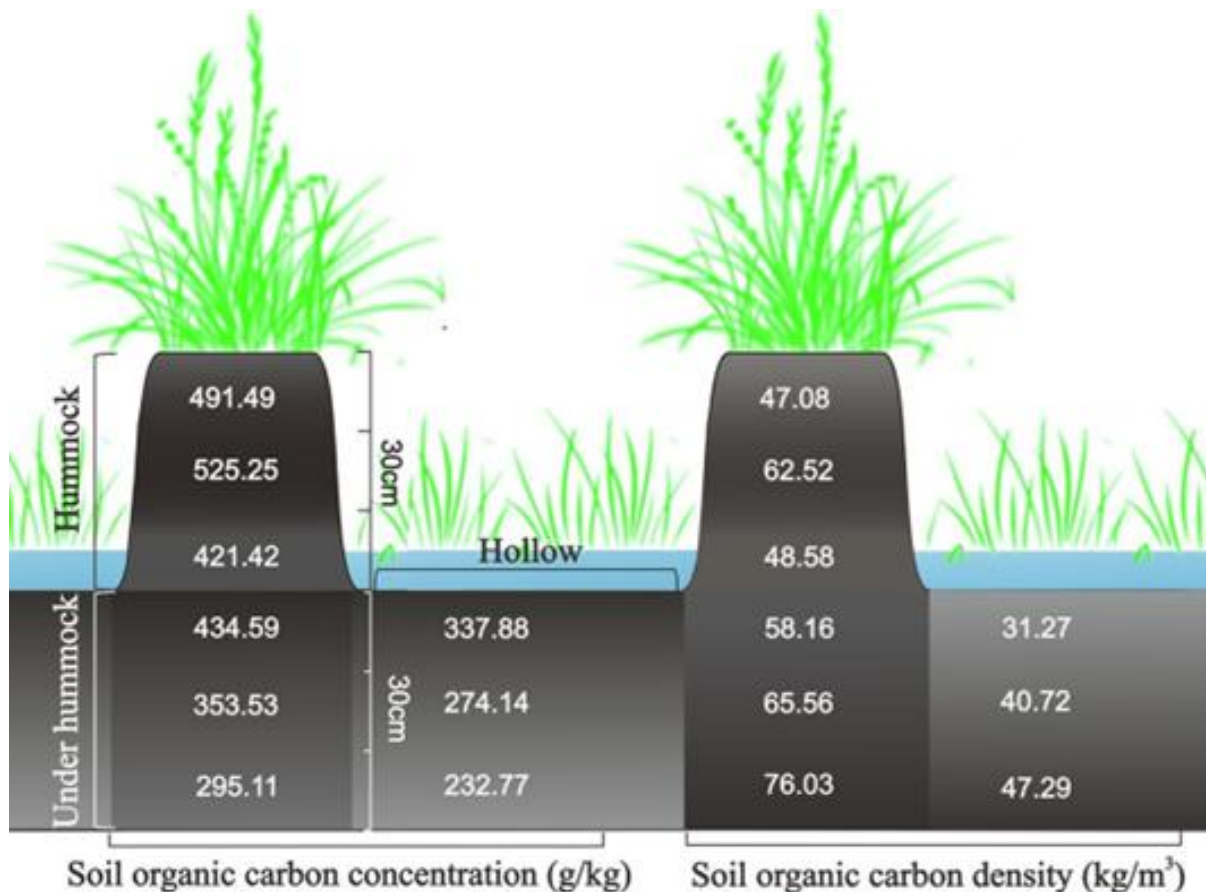
Figure 2.6: Influence of hummock to hollow microtopography on structure and carbon storage (Wang *et al.*, 2021).

While water table depth is initially regulated by precipitation and groundwater inputs (Charman, 2002), it is the ability of peat to retain water (saturation) through pores that determines sub-surface function and long-term carbon storage (Holden, 2005b; Rezanezhad *et al.*, 2016; Harenda *et al.*, 2018).

2.2.2 Gas Exchange

Gaseous exchange between the atmosphere and sub-surface contributes to net carbon accumulation, controlled by the balance of carbon inputs through gross primary productivity and outputs through ecosystem respiration and decomposition (Chapin *et al.*, 2006). While GHG production is biologically driven (CO_2 from aerobic respiration in

the acrotelm; CH_4 from anaerobic decomposition in the catotelm), the flux of these gases to the atmosphere is controlled by peat matrix properties (Clymo, 1984; Holden, 2005b; Clymo and Bryant, 2008; Kettridge and Binley, 2008; Rezanezhad *et al.*, 2016).

Gas transfer occurs through diffusion (Hoag and Price, 1997; Petrescu *et al.*, 2015), ebullition (Rosenberry *et al.*, 2003), and direct pathways (advective transport) such as vascular roots (Figure 2.7) (Moore *et al.*, 2002; Clymo and Bryant, 2008; Ise *et al.*, 2010; Kettridge and Binley, 2011). These processes are sensitive to water table position and vegetation type. For instance, saturated conditions limit diffusivity, increasing GHG retention, while vascular species can provide direct pathways for catotelm-produced CH_4 through roots and aerenchyma tissues (Moore *et al.*, 2002; Ise *et al.*, 2010). Consequently, the structure and connectivity of the sub-surface influences gas exchange capacity (Kettridge and Binley, 2008, 2011; Comas *et al.*, 2014).
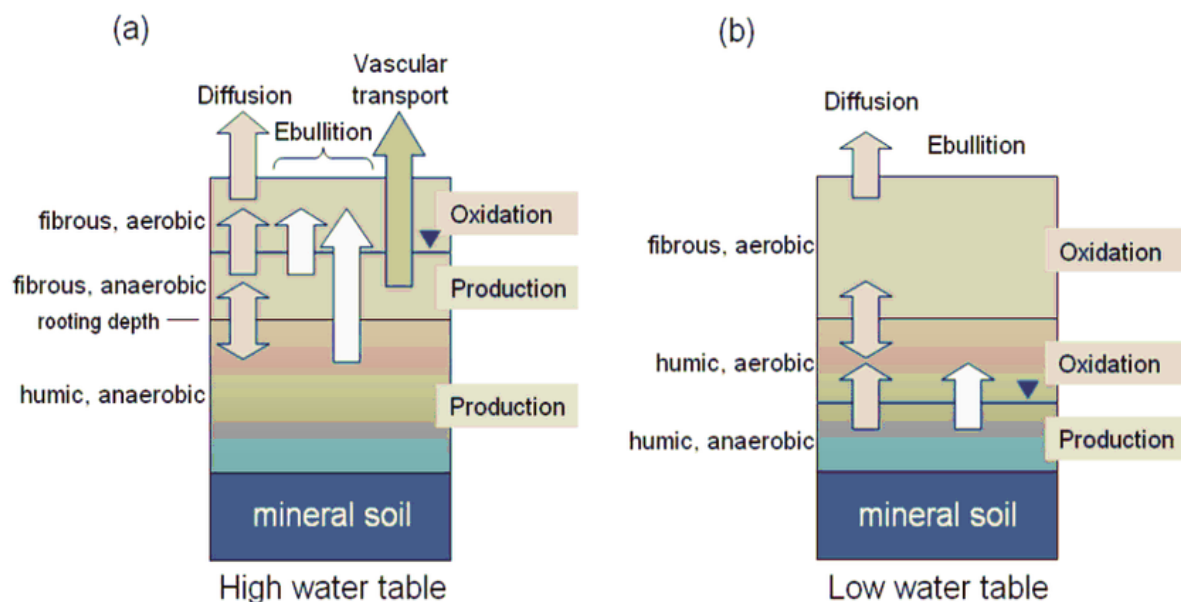
Figure 2.7: Schematic of gas flux pathways under: a) saturated; b) aerated conditions. Arrows indicate gas movement via diffusion, ebullition, and vascular transport (Ise *et al.*, 2010).

2.2.3 Pore Network Structure and Function

Water retention, solute transfer, and gas exchange in peat are regulated by pore networks, playing the most critical role in net carbon accumulation (Rezanezhad *et al.*, 2016; McCarter *et al.*, 2020). Laboratory studies suggest peat porosity ranges from 71–95%, depending on its organic composition, decomposition state (bulk density and humification), and moisture content (Boelter, 1966; Price, 1997; Rezanezhad *et al.*, 2016). However, these values are inferred from disturbed samples (Section 2.6.1), and direct in-situ quantification of pore structure remains limited, challenging the accuracy of existing estimates and their implications for functional understanding.

Pores vary in size, shape, complexity, and connectivity, forming a matrix that governs the movement of water, dissolved carbon, and gases (Hoag and Price, 1997; Quinton *et al.*, 2000, 2008, 2009; Holden, 2005b; Rezanezhad *et al.*, 2009, 2010, 2016; Gharedaghloo *et al.*, 2018; McCarter *et al.*, 2020). Studies distinguish between active (mobile) and inactive (immobile) pores (Figure 2.8) (Quinton *et al.*, 2009; Rezanezhad *et al.*, 2009, 2010, 2016). Active pores are connected and enable advective flow, typically representing macropores (>90μm) (Quinton *et al.*, 2009; Rezanezhad *et al.*, 2016). They dominate the acrotelm and may constitute up to 60% of total volume, facilitating rapid CO_2, CH_4, dissolved organic carbon, and particulate organic carbon exchange with the atmosphere and surface waters (Hoag and Price, 1997; Quinton *et al.*, 2008, 2009). Approximately 30% of mean water table depth is attributed to the uptake of surface water by these pores (Baird, 1997; Holden *et al.*, 2001; Morris *et al.*, 2019). Active pores also increase hydraulic conductivity and oxygen availability, influencing microbial activity and decomposition rates (Quinton *et al.*, 2000; Rezanezhad *et al.*, 2009, 2010, 2016; Liu *et al.*, 2020; McCarter

et al., 2020). Some may act as microbial habitats for methanotrophs, influencing CH_4 flux (Ebrahimi and Or, 2017; Tian *et al.*, 2023), and represent peat pipes (Holden, 2005a; Holden *et al.*, 2006b).

Inactive pores are isolated and typically micro (<90μm) (Quinton *et al.*, 2009; Rezanezhad *et al.*, 2016), restricting water movement and gas exchange to diffusion. They often increase with depth due to decomposition and compaction (Quinton *et al.*, 2009; Rezanezhad *et al.*, 2009; McCarter *et al.*, 2020), and occur within surface vegetation, such as the hyaline cells of *Sphagnum* (Figures 2.5; 2.8) (Kettridge and Binley, 2011; Comas *et al.*, 2014). These pores lower permeability and connectivity, promoting gas accumulation (Kettridge and Binley, 2008). For instance, Tokida *et al.* (2005) found CH_4 occupied 19.6% of peat volume. Isolated pores also support water retention dependant on geometry, retarding decomposition and supporting their role in net ecosystem carbon exchange (Quinton *et al.*, 2009; Rezanezhad *et al.*, 2009, 2010, 2016).

Pore networks are further shaped by vegetation type, particularly at fine spatial scales. *Sphagnum* mosses create complex, connected, highly porous matrices (Figure 2.8) (Clymo and Hayward, 1982; Kettridge and Binley, 2008; McCarter *et al.*, 2020), while vascular plants develop simpler networks (e.g., roots), potentially forming direct pathways for CH_4 from the catotelm to atmosphere (Moore *et al.*, 2002; Baird and Low, 2022). Decomposition, as well as freeze-thaw cycles, can also increase pore compaction and tortuosity over time, limiting hydraulic conductivity and gas diffusion (Quinton *et al.*, 2000; Rezanezhad *et al.*, 2010).
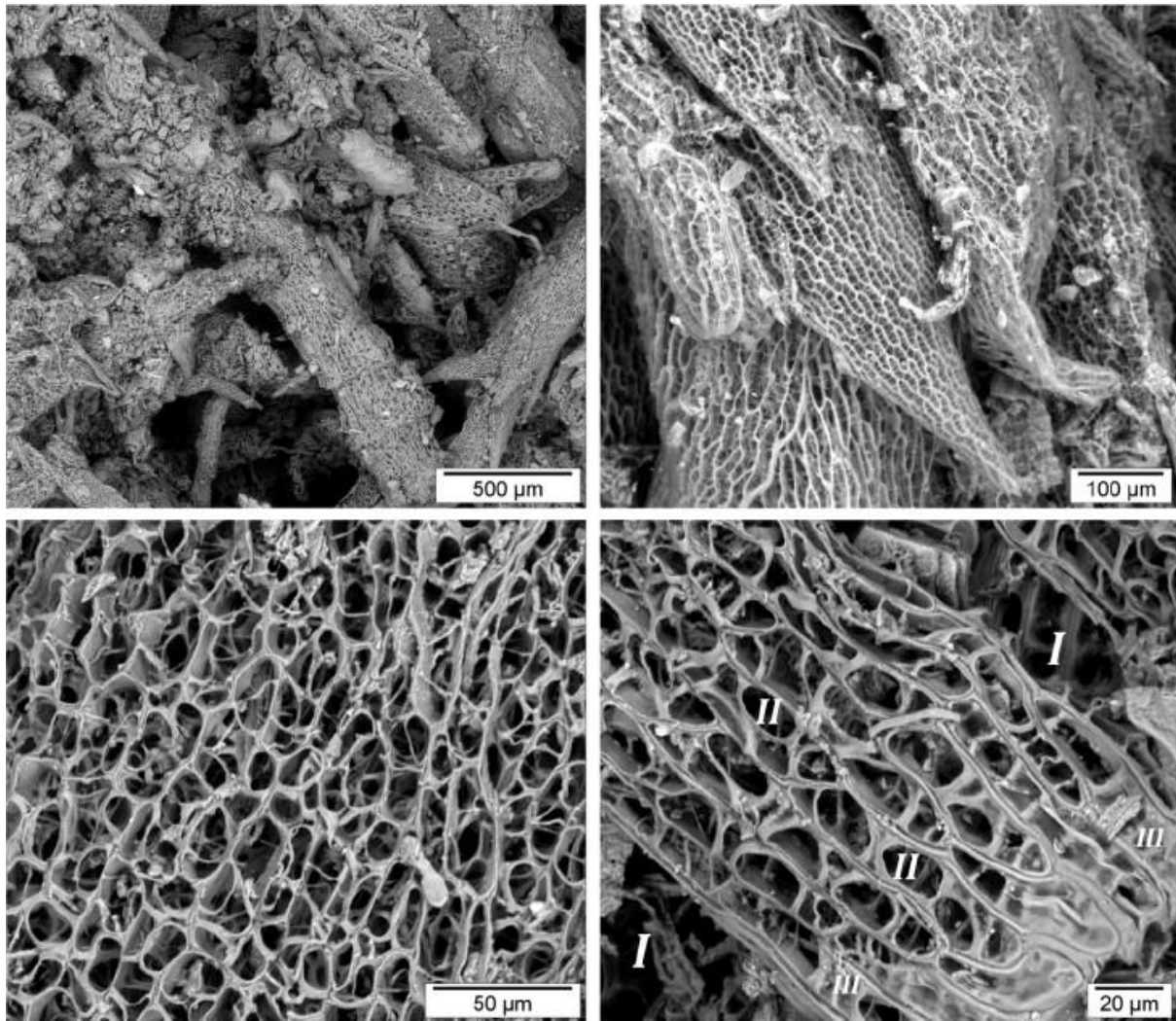
Figure 2.8: Back-scattered electron images of the pore structure of *Sphagnum* peat (Rezanezhad *et al.*, 2016). Images show differentiating pore size distributions: I) open, connected (active) macropores; II) closed or partially closed cells (inactive); III) dead-ended or isolated pores spaces (hyaline cells).

Previous research indicates a fine balance between active and inactive porosity regulates net carbon accumulation, demonstrating the delicate equilibrium between long-term carbon sequestration and GHG emissions (Section 2.1.2). However, current porosity estimates are inferred based on laboratory analysis of disturbed samples, with direct assessments restricted to the microscale. This limits understanding of in-situ pore-scale function. Additionally, the structural and functional recovery of pore networks following restoration remains unknown, restricting insight into their role in sustaining long-term carbon storage. Understanding macropore network structure is therefore critical.

2.2.4 Summary of Key Knowledge Gaps

Models of peat structure and carbon balance are widely applied to explain hydrological and gaseous functions, yet the sub-surface pore networks regulating these remain poorly characterised. This limits understanding of carbon accumulation and restoration outcomes:

- **Limited volumetric data:** National estimates of peat depth and carbon stocks are restricted by incomplete, low-resolution, or assumed sub-surface data.

- **Carbon balance uncertainty:** The high global warming potential of CH_4 introduces uncertainty into the net ecosystem carbon balance of peatlands, demonstrating the need for more accurate quantification.

- **Oversimplified models:** The diplotelmic model overlooks spatial heterogeneity and microtopographic variation, limiting its ability to represent real-world carbon dynamics.

- **Under-characterised sub-surface processes:** Controls on water retention, solute transport, and gas exchange remain poorly understood, restricting insight into structural and functional relationships.

- **Overlooked pore networks:** Despite their role in determining function, macropore networks in intact peat are rarely analysed, with research focused on microscale, discontinuous samples.

- **Uncertain restoration outcomes:** The structural and functional recovery of sub-surface pore networks post-restoration remains unknown, limiting evaluation of long-term carbon storage potential.

These gaps demonstrate the sub-surface structure determining long-term carbon storage remain poorly understood. Direct assessment of macropore networks is required to describe how sub-surface structure governs hydrological and gaseous functions, especially under degraded conditions, where disturbance compromises structural integrity.

2.3 Peatland Degradation

Anthropogenic activities, including drainage, forestry, overgrazing, burning, pollution, peat extraction, and renewable energy development, have driven widespread degradation of UK peatlands (Andersen *et al.*, 2017; Evans *et al.*, 2017; Artz *et al.*, 2019). In particular, drainage, overgrazing, and burning have had major impacts on upland blanket peatlands (Tallis, 1998; Holden *et al.*, 2004, 2007; Ramchunder *et al.*, 2009; Thom *et al.*, 2016). These pressures lower water tables (Waddington and Price, 2000; Holden *et al.*, 2004; Waddington *et al.*, 2015), alter vegetation composition (Noble *et al.*, 2018), and disrupt sub-surface structure (Lindsay *et al.*, 2014b; Moore *et al.*, 2015; Sloan *et al.*, 2018), reducing carbon sequestration and storage potential (Strack and Waddington, 2007; Smith *et al.*, 2014), as well as their resilience to climate change (Davies *et al.*, 2013; Marshall *et al.*, 2022).

Artz *et al.* (2019) estimates ~90% of UK blanket peatlands are in poor condition, with England exhibiting the highest at 98.7% (detailed in Section 2.4.1; Table 2.2) and no presence of 'pristine' due to pollution and ongoing climate change. Consequently, most have transitioned from net carbon sinks to sources. Current emissions are estimated between 23.1 – 24.5 Mt CO_2eq y^{-1} (Evans *et al.*, 2017), corresponding to 3.48 – 13.23 t

CO_2eq ha^{-1} y^{-1} (Gregg *et al.*, 2021); an increase of 4.24 – 13.99 ± 0.39 t CO_2eq ha^{-1} y^{-1} from historical records (Billett *et al.*, 2010; Artz *et al.*, 2014). These emissions contribute ~3.5% of the UK's total annual GHG emissions (an increase of 1.2% from 1990), positioning them as significant contributors to the net warming effect on global climate (BEIS, 2021; Wentworth, 2022).

2.3.1 Drainage

Drainage of UK blanket peatlands aimed to lower water tables to support livestock (Robinson and Armstrong, 1988; Holden *et al.*, 2004), game birds (Done and Muir, 2001), forestry (Cannell *et al.*, 1993; Sloan *et al.*, 2018), and peat extraction for horticulture (Alexander *et al.*, 2008). Drainage processes and subsequent land-use changes impact net ecosystem carbon balance, reducing net carbon accumulation (Waddington and Price, 2000; Holden *et al.*, 2004; Holden *et al.*, 2006a; Holden *et al.*, 2006b; Joosten, 2009; Waddington *et al.*, 2015; Young *et al.*, 2017).

Lower water tables increase oxygen availability, promoting aerobic decomposition in the acrotelm, increasing CO_2 emissions (Figure 2.9) (Waddington and Price, 2000; Lindsay, 2010a; Rowson *et al.*, 2010). Drier conditions favour graminoid and vascular vegetation, reducing net primary productivity through increased ecosystem respiration (Prescott, 2010; Schellekens *et al.*, 2015) and promoting dissolved organic carbon loss (Lindsay, 2010a; Rowson *et al.*, 2010; Evans *et al.*, 2016). Vascular plant colonisation also increases CH_4 emissions through monocot roots (Moore, 2002). Mäkilä (2011) found drainage reduced net carbon accumulation by 10.8 g C m^2 y^{-1}, while Evans *et al.* (2016) estimates carbon losses from dissolved organic carbon and particulate organic carbon contribute an additional 2.5 ± 1.5 t CO_2eq ha^{-1} y^{-1}. Although Roulet *et al.* (1993) proposed

CH₄ emission reductions from drained peatlands, more recent assessments show negligible change or offset by CH_4 release from drain bottoms and deep cracks (Figure 2.9) (Lindsay, 2010a; Evans *et al.*, 2018; Peacock *et al.*, 2019).
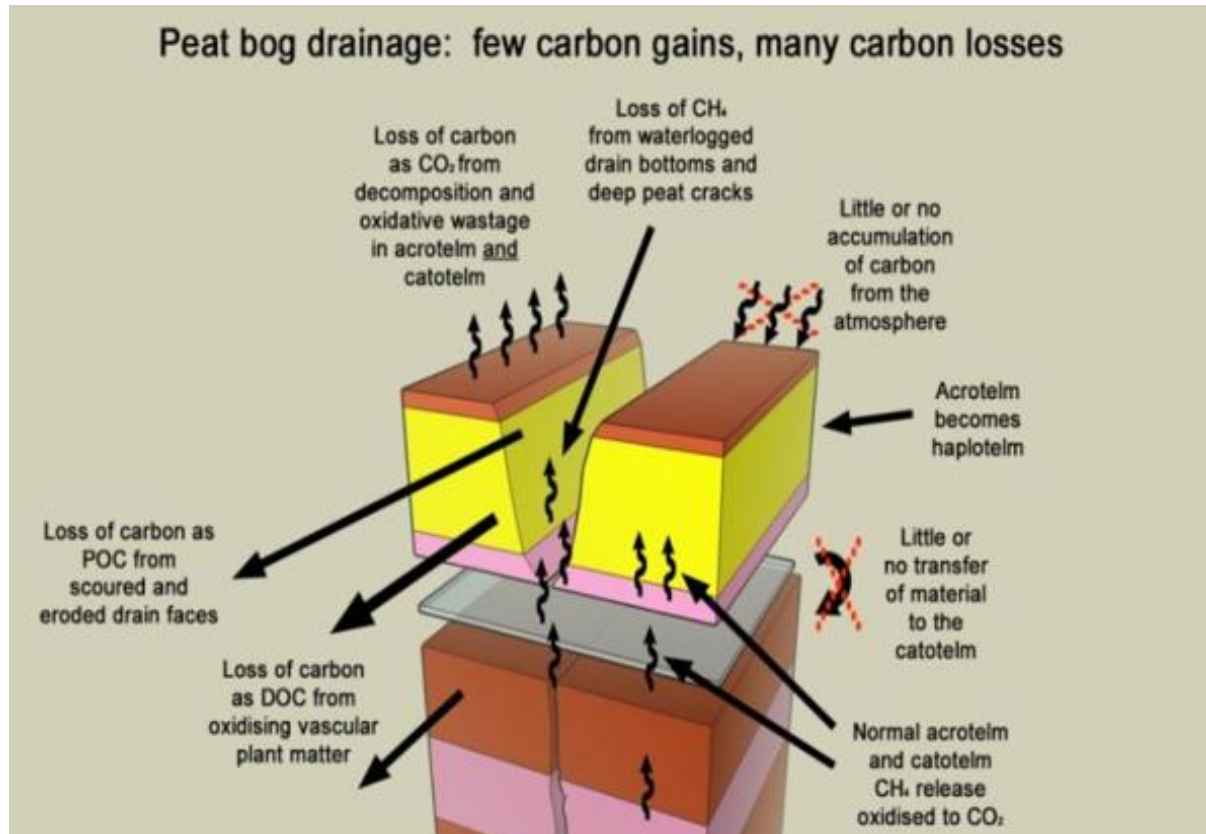
Figure 2.9: Carbon balance model of drainage for a standard cubic meter of peat (Lindsay, 2010). Note 'haplotelm' refers to a non-functioning acrotelm.

Drainage also causes peat shrinkage, subsidence, and compaction through accelerated decomposition and oxidisation (Figure 2.10) (Lindsay, 2010a; Leifeld *et al.*, 2011; Lindsay *et al.*, 2014b; Urbanová and Picek, 2019). These processes degraded the structural integrity of peat, leading to collapse and desiccation where the fibrous matrix becomes compressed and consolidated. This reduces the size and proportion of pores contributing to limited connectivity and water retention, lowering permeability and the ability to maintain surface saturation for retarded decomposition (Silins and Rothwell,

1998; Holden *et al.*, 2006b; Lindsay *et al.*, 2014b). Additional carbon is lost through increased mobilisation of particulate organic carbon (Holden, 2005b; Evans *et al.*, 2006). Silins and Rothwell (1998) recorded a decrease in saturated hydraulic conductivity from 14.46cm h^{-1} in near-natural peat to 1.69cm h^{-1} following drainage. This demonstrates the reduced capacity of drained peat to transmit water and contribute to net carbon accumulation.
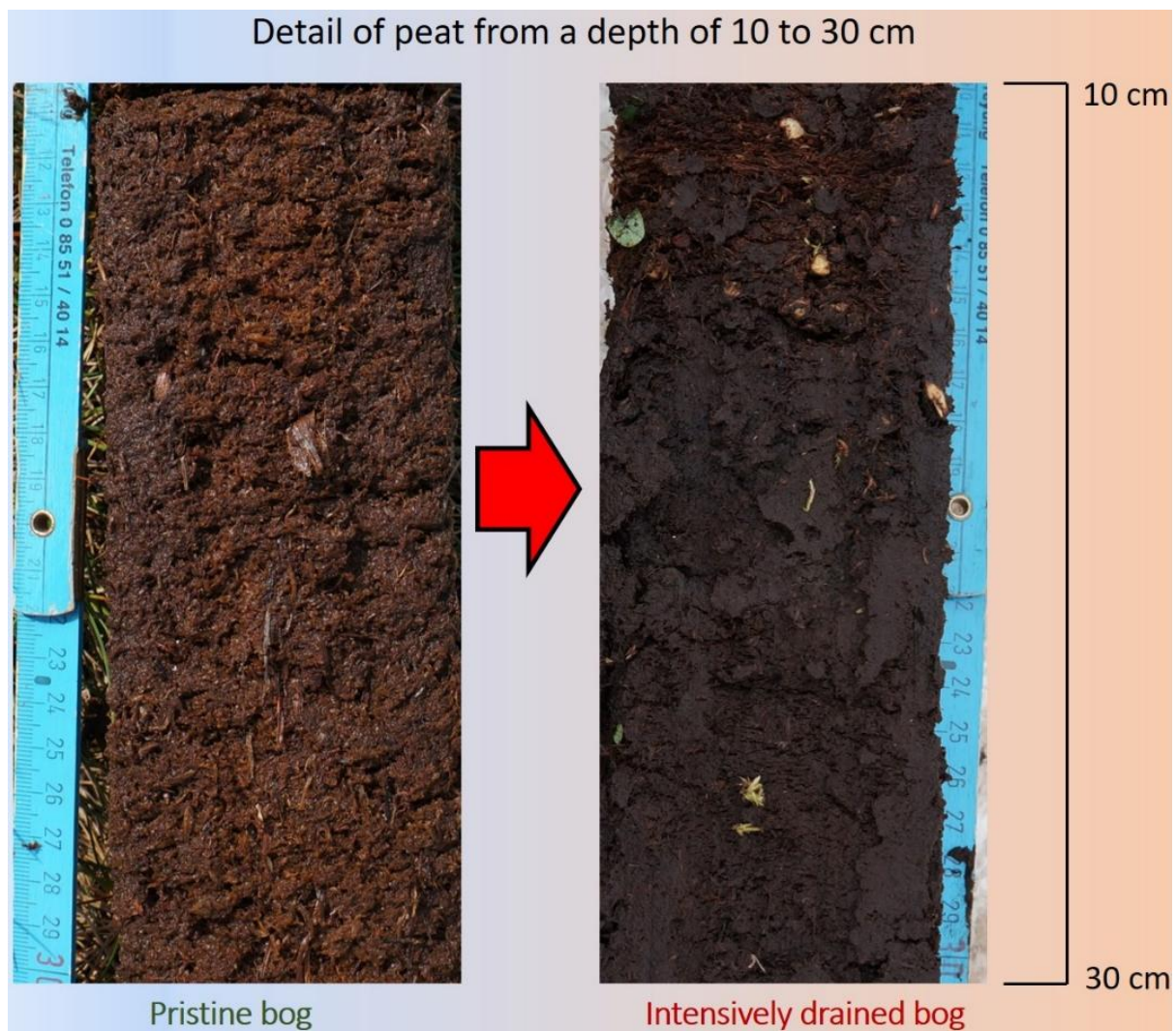
Figure 2.10: Visual comparison of peat cores from 10-30cm depth showing the effects of intensive drainage on oxidisation (colour shift) and compaction (bulk density increase) (Urbanová and Picek, 2019).

2.3.2 Overgrazing

Although absent from models of peat formation (Figure 2.1; Charman, 2002), herbivores have historically contributed through the regulation of peat-forming vegetation (Lindsay *et al.*, 2014a). At low densities (~0.4 ha^{-1}), grazing suppresses graminoid and vascular species, promoting bryophyte succession and favourable conditions for net carbon accumulation (Rowell, 1988; Clarke *et al.*, 1995; Thompson *et al.*, 1995). Trampling also supports surface microtopography, increasing local bulk density and forming shallow pools supporting *Sphagnum* (Lindsay *et al.*, 2014a).

However, overgrazing removes peat-forming vegetation and exposes bare peat; considered the most detrimental feature for net carbon accumulation (Evans, 1997; Garnett *et al.*, 2000; Ward *et al.*, 2007; Worrall *et al.*, 2011; Worrall and Clay, 2012; Parry *et al.*, 2014; Shuttleworth *et al.*, 2019). Bare peat reduces moisture retention, particularly in the surface acrotelm, accelerating aerobic decomposition and CO_2 release (Ward *et al.*, 2007; Worrall and Clay, 2012). These effects are amplified by trampling-induced compaction, which increases bulk density and reduces permeability (Lindsay *et al.*, 2014a). Erosion and the export of dissolved organic carbon and particulate organic carbon are also increased (Evans, 1997; Tallis, 1998; Ward *et al.*, 2007). Chemical changes include lowered pH, suppressing plant growth, and increased sub-surface temperatures driven by microbial activity (Malik *et al.*, 2018). Nitrate inputs from livestock further stimulate microbial decomposition through increased nutrient availability (N_2O release; Lindsay *et al.*, 2014a). Grazing effects are often coupled with drainage, amplifying carbon loss through combined impacts on vegetation, surface compaction, and water table drawdown. However, the joint hydrological and biochemical

consequences of interacting disturbances remains poorly understood, particularly in relation to long-term carbon storage and restoration outcomes (Ramchunder *et al.*, 2009; Andersen *et al.*, 2017; Artz *et al.*, 2019).

2.3.3 Burning

Burning in UK blanket peatlands includes managed burns and wildfires (Ramchunder *et al.*, 2009; Davies *et al.*, 2013, 2016; Heinemeyer *et al.*, 2018; Noble *et al.*, 2018; Gray *et al.*, 2021). Rotational strip burning is used to remove older vegetation and promote regrowth for livestock and game birds (Pearce-Higgins and Yalden, 2004; Robertson *et al.*, 2017; Heinemeyer *et al.*, 2018; Whitehead and Baines, 2018). It affects ~15-18% of UK blanket peatlands (Anderson *et al.*, 2009; Worrall *et al.*, 2010), while wildfires account for an additional ~2,500 ha y^{-1} (Baker *et al.*, 2025), linked to drought and climate change (Davies *et al.*, 2013; Kettridge *et al.*, 2015; Andersen *et al.*, 2024).

Best practice rotational strip burning (~5cm deep, every 4 years) can increase gross primary productivity by stimulating new growth and introduce stored carbon through charcoal deposition (Heinemeyer *et al.*, 2018). However, burns lower water tables, expose bare peat, and cause direct carbon losses through CO_2, CH_4, dissolved organic carbon, and particulate organic carbon export, countering increased gross primary productivity (Ward *et al.*, 2007; Douglas *et al.*, 2015; Noble *et al.*, 2018). Additionally, burning reduces resilience, increasing vulnerability to wildfires, responsible for the greatest fire-related carbon losses in the UK (Baker *et al.*, 2025). A wildfire in a blanket peatland in Scotland released ~290 Kt C across six days, equivalent to >2% of Scotland's total anthropogenic GHG emissions (Wiltshire *et al.*, 2019). Across the UK, peatland

wildfires emitted ~0.8 Tg C between 2001 and 2021, accounting for >90% of the UK's total annual fire-related carbon emissions (Baker *et al.*, 2025).

2.3.4 Implications of Other Forms of Degradation

Other anthropogenic pressures, including forestry (Tallis, 1998; Sloan *et al.*, 2018), industrial pollution (Ferguson and Lee, 1983; Proctor and Maltby, 1998), peat extraction for horticulture (Tallis, 1998; Alexander *et al.*, 2008), and renewable energy development (Grieve and Gilvear, 2008; Smith *et al.*, 2014; Mello *et al.*, 2020), also reduce the net carbon accumulation potential of blanket peatlands through bulk and chemical changes. While carbon emissions from degradation are relatively well quantified, the sub-surface structural and functional changes informing these emissions remain poorly understood, leading to unknown tipping points of restoration feasibility. This presents a challenge for effective restoration and assessments of long-term recovery.

2.3.5 Summary of Key Knowledge Gaps

Although carbon losses from degraded blanket peatlands are increasingly well-recognised, the sub-surface structural changes regulating these fluxes remain poorly understood. This limits the ability to assess degradation impacts or design effective restoration strategies based on structural baselines:

- **Poorly characterised structural impacts:** Compaction and collapse reduce water retention and carbon storage potential but remain difficult to quantify in situ.
- **Unclear degradation thresholds:** Tipping points beyond which structural damage becomes irreversible are unknown, limiting prediction of restoration potential.

- **Limited understanding of compound pressures:** Degradation often occurs through multiple pressures, but their combined effects on hydrology, structure, and carbon balance remain underexplored.

- **Unresolved impacts of burning:** While rotational burning may increase short-term productivity, its long-term impact on structure and resilience remains contested.

> These gaps demonstrate the importance of accounting for sub-surface structural integrity in policy, restoration, and practice. Establishing robust structural baselines is essential to align restoration design with long-term carbon outcomes and to support an evolving policy landscape.

2.4 UK Policy Drivers and Aims of Restoration

Peatland restoration is increasingly recognised as a nature-based solution to the climate and biodiversity crises (Bonn *et al.*, 2014, 2016a; Stoneman *et al.*, 2016; Reed *et al.*, 2022; Strack *et al.*, 2022). While early international policies focussed on wildlife and freshwater regulation (Ramsar Convention, 1971, 2003; European Union, 1992), recent understanding of anthropogenic climate change and the role of degraded peatlands (IPCC, 2023a) has shifted focus toward carbon mitigation (United Nations, 2011, 2015; IPCC, 2013; UNEP, 2017). In the UK, this is acknowledged in the integration of peatland restoration into net-zero targets (IUCN, 2018; CCC, 2020; DEFRA, 2021a; Government, 2021; Wentworth, 2022) and substantial funding (DEFRA, 2021b; Government, 2021; Natural England and DEFRA, 2021; Hooker and Wentworth, 2024). However, progress monitoring remains incomplete, and current evidence suggests restoration targets are not on track to be met (Andersen *et al.*, 2017; Artz *et al.*, 2019; IUCN, 2024d). This

demonstrates a disconnect between science, practice, and policy in UK peatland restoration. For example, even the most recent Natural England peat map has been criticised for inaccuracies, yet underpins policy and funding decisions, highlighting a critical limitation in evidence-led restoration planning (Natural England, 2025). Moreover, England's goal to restore 35,000 ha over ~5 years (DEFRA, 2021a) appears unrealistic considering leading peatland restoration contractors have delivered only ~30,000 ha over the past ~25-years due to small-scale project tenders. Despite clear aims to rewet and revegetate degraded systems, practical constraints and project scales are often overlooked, with monetary cost justifying technique selection in tenders. Interventions seek to support net carbon balance by increasing net primary productivity and reducing carbon losses (e.g., dissolved and particulate organic carbon through erosion), improve water storage and quality, and support biodiversity (Andersen *et al.*, 2017; Evans *et al.*, 2017; IUCN, 2018; Alderson *et al.*, 2019; Artz *et al.*, 2019). However, carbon remains the dominant metric of success which often fails to capture these broader ecosystem benefits.

2.4.1 UK Policy, Funding, and Governance

International recognition of peatlands as carbon sinks (UNFCC, 1998; United Nations, 2011, 2015; IPCC, 2013; UNEP, 2017) and their degradation as contributors to global warming (IPCC, 2023a) has shaped their inclusion in UK climate policy (Bonn *et al.*, 2016a; Joosten *et al.*, 2016). Peatlands are included in the UK's legally binding 2050 net-zero target through protection and restoration (Government, 2021). However, no UK-wide peatland policy exists (Artz *et al.*, 2019). Instead, devolved nations have developed separate strategies with individual targets, funding, and support (Table 2.1). The UK

Peatland Strategy sets a shared 2040 vision, but implementation remains fragmented and carbon-focused (IUCN, 2018). Critically, sub-surface functions informing long-term carbon sequestration and broader ecosystem services are rarely integrated, limiting the development of a holistic metric of restoration success.

Public funding has traditionally driven peatland restoration in the UK. In England, the Nature for Climate Fund allocated £50 million through the Peatland Grant Scheme (NCPGS) to restore 35,000 ha by 2025 (DEFRA, 2021a; Natural England and DEFRA, 2021). However, the NCPGS required ≥25% of project costs sourced from non-exchequer contributions, such as private finance or charitable donations (Natural England and DEFRA, 2021). With the Environmental Land Management (ELM) scheme to replace NCPGS beyond 2025 (DEFRA, 2021b), this requirement is expected to persist, making access to funding increasingly competitive, particularly with Countryside Stewardship schemes (DEFRA and Rural Payments Agency, 2024). Consequently, private finance has become critical to future delivery (Bonn *et al.*, 2014; Reed *et al.*, 2022). One mechanism is the sale of carbon credits within the unregulated carbon market (Dunn and Freeman, 2011; Bonn *et al.*, 2014; Moxey *et al.*, 2021; Chen *et al.*, 2023; Hooker and Wentworth, 2024). The IUCN UK Peatland Code provides a toolkit to estimate, verify, and convert CO_2eq savings from peatland restoration into saleable Pending Issuance Units (PIUs) (IUCN, 2024a). Alongside the UK Woodland Carbon Code, it is recognised as a high-integrity framework supporting blended finance (Reed *et al.*, 2013; IUCN, 2024a). As of February 2025, 337 projects are registered, but uptake remains slow with no current trading. Investor confidence is restricted by uncertain carbon outcomes and limited evidence of long-term returns (Smyth *et al.*, 2015; Moxey *et al.*, 2021; Mackenzie, 2024).

Table 2.1: Overview of UK peatland strategies and key national restoration targets.

Devolved Nation	Peatland Strategy	Governing Body	Key Targets	References
England	England Peat Action Plan (2021)	Department for Environment, Food & Rural Affairs (DEFRA)	Restore 35,000 ha by 2025 through the Nature for Climate Peatland Grant Scheme (NCPGS), Develop an updated peat map by 2024. Ban the sale of peat in the amateur horticulture sector by 2024.	DEFRA (2021a)
Wales	National Peatland Action Programme (2020-2025)	Natural Resources Wales (NRW)	Restore 600-800 ha y^{-1}. Achieve a total of 3000 ha by 2025.	NRW (2020)
Scotland	Scotland's National Peatland Plan: Working for Our Future (2015)	NatureScot (formerly Scottish Natural Heritage)	Restore 250,000 ha by 2030.	SNH (2015)
Northern Ireland	Northern Ireland Peatland Strategy 2022-2040	Department of Agriculture, Environment & Rural Affairs (DAERA)	Restore degraded peatlands to favourable conservation status by 2030. Manage all semi-natural peatlands for biodiversity and ecosystem function by 2040.	DAERA (2022)

While carbon has become the dominant metric for valuing peatland restoration, it represents only part of the story. Restored peatlands provide a range of ecosystem benefits, including biodiversity increase and water regulation (Grand-Clement *et al.*, 2013; Bonn *et al.*, 2014, 2016a; Thom *et al.*, 2016; Alderson *et al.*, 2019), which are not captured by current carbon evaluation. Emerging efforts to develop biodiversity credits demonstrates a shift toward more holistic financing mechanisms, aiming to account for ecological integrity and species recovery (IUCN, 2025b). However, these tools remain in early development and lack the methodologies and validations associated with carbon markets (Moxey *et al.*, 2021; IUCN, 2025b). For example, alternative schemes to the IUCN UK Peatland Code, such as Wilder Carbon, offer a blended biodiversity and carbon credit model (Wilder Carbon, 2024), which could significantly increase credit values (Section 2.7). However, the methodologies for such schemes remain unclear. Consequently, carbon currently remains the most viable and scalable mechanism for attracting private finance and continues to inform current policy frameworks (Dunn and Freeman, 2011; Reed *et al.*, 2013; Smyth *et al.*, 2015).

Further disconnection between science and policy is evidenced in Table 2.2. By comparing restoration targets outlined in devolved nation policies (Table 2.1) with national carbon inventory data (Bain *et al.*, 2011; Evans *et al.*, 2017; Artz *et al.*, 2019; Gregg *et al.*, 2021), Table 2.2 estimates if national restoration goals were achieved, ~3.2-8.0 Mt CO_2eq y^{-1} could be mitigated. Note this assumes immediate emissions reductions, discussed in the following section. However, this potential accounts for only 13-35% of total UK peatland emissions (excluding Northern Ireland due to data gaps) (Evans *et al.*, 2017). Assuming a linear relationship, the lower estimate suggests current national targets would fail in meeting UK-wide net-zero targets by 2050. This demonstrates a

significant misalignment between emissions reduction ambitions and the scale of action in policy. Moreover, targets aim to cap emissions rather than promote net sequestration. This risks underestimating the role of peatlands as nature-based climate solutions and may direct restoration towards sub-optimal outcomes. Table 2.2 therefore demonstrates a critical disconnect between the scale of restoration, carbon mitigation potential, and the extent to which scientific understanding of functional recovery is considered.

Table 2.2: Summary of peatland extent, condition, emissions, restoration targets, and estimated carbon savings potential across UK nations. Data represents a synthesis of devolved nation policy documents (Table 2.1) and published carbon data from Bain *et al*. (2011), Evans *et al*. (2017), Artz *et al*. (2019), and Gregg *et al*. (2021).

Metric	Wales	Northern Ireland	Scotland	England	UK (Total)
Shallow Peat (ha)	359,200	141,700	3,461,200	527,193	**4,489,293**
Deep Peat (ha)	90,050	242,622	1,947,750	495,828	**2,776,250**
Peaty Soils (ha)	42,980	348,200	Included in Shallow	186,372 (Wasted) 211,424 (Peaty Pockets)	**/**
Estimated Carbon Store (Mt C)	193	165	2,322	440	**3,120**
% of Peat Degradation	70% (314,475 ha)	86% (330,517 ha)	80% (1,558,200 ha)	98.7% (1,193,671 ha)	**83.7% Average**
GHG Emissions (Mt C)	510,000	2,232,000	9,637,000	10,863,000	**23,242,000**
GHG Emissions for Deep Peat (Mt C)	-1,000	175,000	-30,000	1,426,000	**1,573,000**
Estimated Restoration (ha)	5,557	2,862	90,000	42,805	**141,224**
Potential Carbon Savings - Table 2.1 (Mt C)	300,000	N/A	500,000 - 4,800,000	2,400,000	**3.2–8.0**

2.4.2 Progress of Peatland Restoration in the UK

As a function of policy, there is a clear imperative to restore degraded blanket peatlands across the UK, with a range of approaches outlined in Section 2.5. Despite these commitments and investment, restoration progress is lagging. IUCN (2024c) estimates ~250,000 ha of UK peatlands have been restored; half the area required to meet 2040 targets. This delivery pace has not changed since earlier assessments (Table 2.2; Artz *et al.*, 2019). Scotland's target of 250,000 ha by 2030 requires ~16,500 ha y^{-1}, yet the average rate since 2015 remains at ~5,675 ha y^{-1} (Dipper, 2022). In England, only 50% of the 35,000 ha target for 2025 has been funded and delivered. Wales has achieved just one third of its planned restoration, while Northern Ireland remains in the draft phase of reporting (IUCN, 2024d). These failings demonstrate shortfalls in the implementation of the UK's peatland strategies.

Barriers include inconsistent definitions of peat depth across devolved nations. Scotland defines peat as >50cm deep (SNH, 2015); Wales and Northern Ireland use >40cm (NRW, 2020; DAERA, 2022); and England distinguishes <30cm (shallow) from >50cm (deep) (Table 2.2; Evans *et al.*, 2017; Artz *et al.*, 2019; DEFRA, 2021a). Mapping also remains incomplete, with ~50% of UK peatlands adequately surveyed, and restoration is prioritised on designated sites (e.g., SSSIs), excluding many degraded areas from eligibility (Stoneman *et al.*, 2016; Andersen *et al.*, 2017; Artz *et al.*, 2019). These discrepancies restrict accurate carbon stock estimation (Section 2.1.2; Bain *et al.*, 2011; Evans *et al.*, 2017) and complicate evaluation of peatland restoration as a nature-based solution.

Monitoring progress if further restricted by a lack of standardised protocols, limiting consistent assessment of restoration outcomes (Andersen *et al.*, 2017; Artz *et al.*, 2019; IUCN, 2024d). Funding remains one of the most persistent barriers, particularly in meeting the scale of restoration required under devolved policy targets (Tables 2.1; 2.2). Requirements to secure match funding from non-exchequer sources, such as the NCPGS and the forthcoming ELM scheme, limit access for many projects. Given the policy imperative to deliver large-scale restoration, this reliance on co-financing mechanisms places greater emphasis on attracting private investment and delivery through blended finance models (Dunn and Freeman, 2011; Moxey *et al.*, 2021; Reed *et al.*, 2022). Consequently, a clearer understanding of restoration processes and outcomes is required to reduce investor uncertainty and build market confidence. This would also support the awarding of tenders based on more than just the lowest price.

Despite barriers and shortfalls in delivery, peatland restoration delivers positive outcomes (Figure 2.11). Pilkington *et al.* (2016) reported complete revegetation of bare peat within five growing seasons, while Alderson *et al.* (2019) observed significant increases of JNCC (2009) favourable condition species after two years (Figure 2.11). Hydrological recovery has also been documented. Holden *et al.* (2017) recorded a five-fold reduction in catchment discharge within six months of ditch blocking, and Alderson *et al.* (2019) reported a mean rise of 8mm y^{-1} in water table depth across 12 years (Figure 2.11).
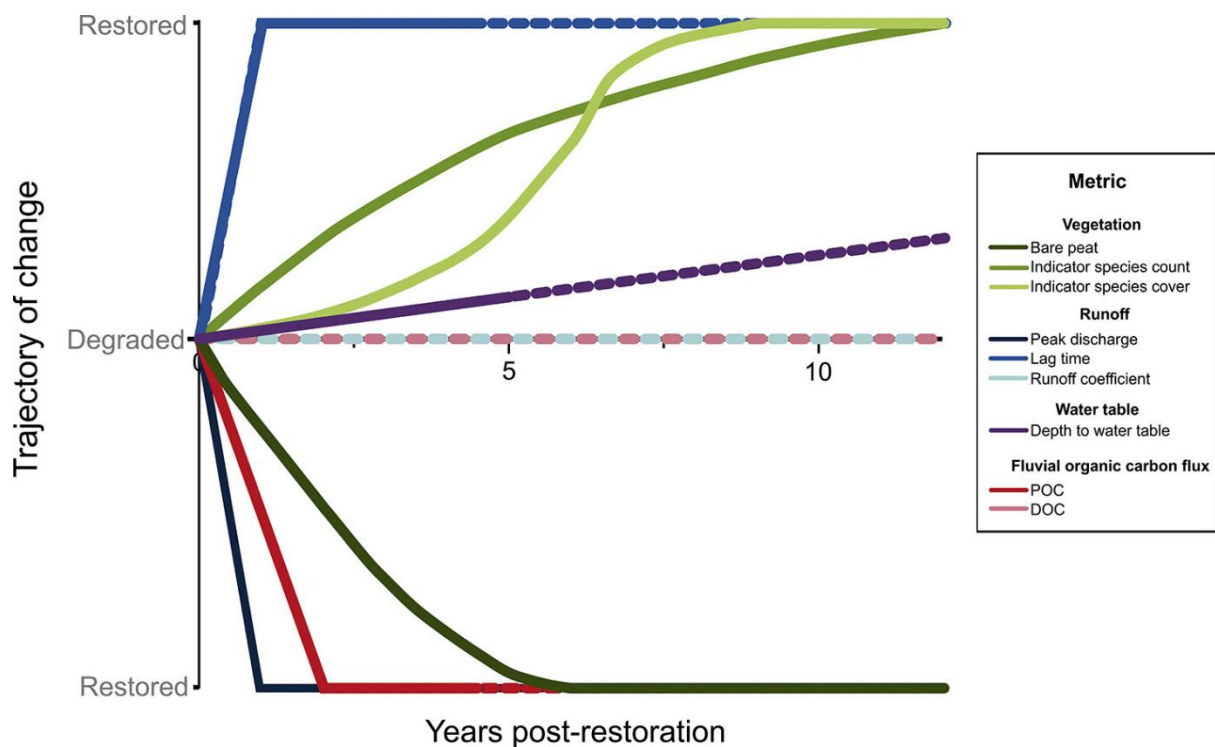
Figure 2.11: Trajectories of ecosystem change in blanket peatlands (Alderson *et al.*, 2019). Figure shows positive ecological, hydrological, and carbon impacts over time.

Improved net carbon accumulation following restoration is well evidenced. Strack and Zuback (2013) showed restored sites exhibited lower ecosystem respiration, reduced CO_2 exchange, and decreased net ecosystem exchange after ~10 years (Figure 2.12). Worrall *et al.* (2011) reported emissions reductions of ~170 – 613 t C km^2 y^{-1} across sites, with a blanket bog transitioning from a source to sink after ~4 years, accumulating ~91 ± 13 t C km^2 y^{-1}. Wilson *et al.* (2011), Turner *et al.* (2013), and Evans *et al.* (2018) also documented reductions in dissolved organic carbon and particulate organic carbon export, including a 7% decline in dissolved organic carbon loss within the first year post-restoration (Turner *et al.*, 2013). These support the potential for restoration to reduce carbon emissions. However, outcomes vary with site condition and intervention technique (Chapman *et al.*, 2012; Alderson *et al.*, 2019; Artz *et al.*, 2019). For example,

Figure 2.12c shows a restored drained site still exhibited positive net ecosystem exchange after ~10 years, whereas the source to sink transition reported by Worrall *et al.* (2011) after ~4 years occurred at a relatively intact site. This poses challenges for scaling predictions of net ecosystem carbon balance and using carbon as a metric for success.
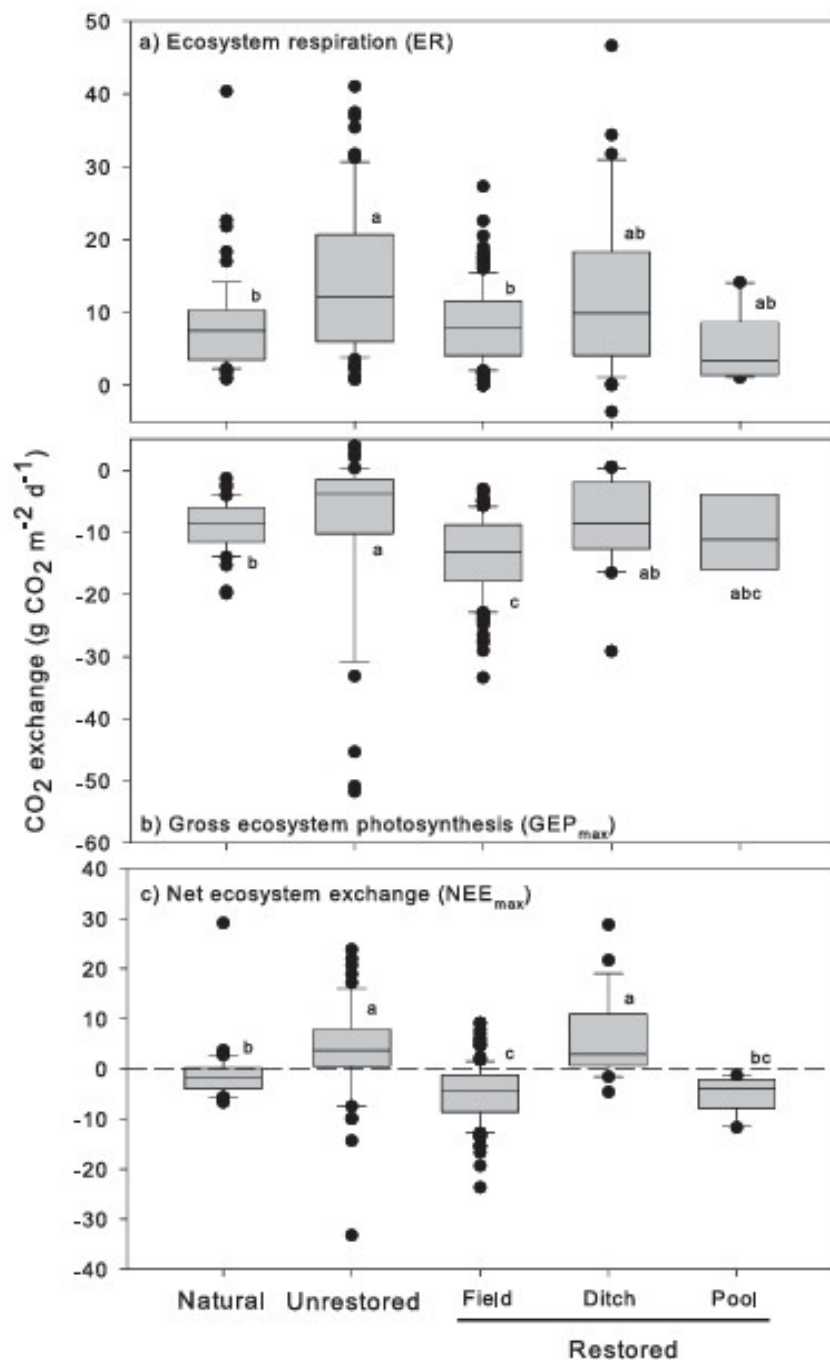
Figure 2.12: Comparison of CO_2 fluxes across natural, degraded (unrestored), and restored peatland sites (Strack and Zuback, 2013): a) ecosystem respiration (ER); b) gross ecosystem photosynthesis (GEP_{max}); c) net ecosystem exchange (NEE_{max}). Restored sites are differentiated by treatment type (field, ditch, pool). Negative NEE indicate net carbon uptake.

Although rewetting reduces CO_2 emissions (Joosten, 2009; Strack *et al.*, 2016), CH_4 emissions frequently increase, particularly in graminoid-dominated sites. Cooper *et al.* (2014) reported an increase of 76kg CH_4 ha^{-1} y^{-1} following rewetting and Vanselow-Algan *et al.* (2015) found increased CH_4 emissions persisting >30 years post-restoration. These fluxes reduce net carbon accumulation in CO_2eq due to global warming potentials (Section 2.1.2) (Baird *et al.*, 2009; Wilson *et al.*, 2009; IUCN, 2024c). Alternatively, restoration may have little effect on net carbon accumulation (Green *et al.*, 2018). Although, resent studies suggest restoration reduces climate warming despite CH_4 emissions (Günther *et al.*, 2020; Kalhori *et al.*, 2024). Nonetheless, restoration responses are variable and transitions to net carbon sinks often extend beyond typical ~5-year monitoring cycles (Baird *et al.*, 2009; Bacon *et al.*, 2017; Young *et al.*, 2019, 2021). As shown in Figures 2.11 and 2.12, some sites remain in recovery ~10 years post-intervention. However, limited monitoring durations constrained by funding obstruct detection of long-term carbon trends, potentially resulting in under or overestimation of restoration impacts (Green *et al.*, 2018; Artz *et al.*, 2019; Young *et al.*, 2019).

Outcomes demonstrate a fundamental flaw in UK peatland restoration policy, which assumes rapid carbon savings post-intervention. Targets prioritise emissions reduction (IUCN, 2018; CCC, 2020; Government, 2021), yet restored peatlands often continue to emit carbon (particularly CH_4) for decades post-restoration (Cooper *et al.*, 2014; Vanselow-Algan *et al.*, 2015). This assumption is embedded in the IUCN UK Peatland Code, which projects net carbon savings within 5 years (Section 2.7; IUCN, 2024a). Additionally, net ecosystem carbon balance post-restoration remains poorly quantified. This uncertainty undermines confidence in restoration as a nature-based climate solution and limits the adoption of private finance mechanisms which depend on robust,

verifiable carbon estimates (Reed *et al.*, 2013, 2022; Bonn *et al.*, 2014; Moxey *et al.*, 2021; Strack *et al.*, 2022). Understanding where, when, and how functional recovery occurs in restored peatlands is therefore critical to aligning policy with net carbon accumulation.

2.4.3 Summary of Key Knowledge Gaps

Devolved nation policy is driven by overambitious targets exceeding delivery capacity, yet fails to meet UK-wide net-zero commitments. This disconnect between policy ambition, limited scientific acknowledgement, and practical implementation, both financially and operationally restricts the development of effective peatland restoration strategies:

- **Targets misaligned with mitigation need:** National restoration targets are insufficient to meet net-zero commitments and aim to cap emissions rather than promote net carbon sequestration.

- **Carbon as a poor metric of success:** Current policy and finance prioritise carbon reduction, overlooking wider ecosystem benefits such as biodiversity and water regulation.

- **Uncertain restoration outcomes:** Carbon impacts of restoration vary with site condition and intervention type, challenging assumptions of linear and immediate recovery.

- **Inconsistent definitions and data gaps:** Alternate peat classifications and incomplete mapping undermine national inventories and limit restoration eligibility, particularly beyond designated sites.

- **Funding and finance shortfalls:** Progress is restricted by competitive co-financing. While biodiversity credits are emerging, the carbon market remains the dominant lever despite slow uptake and low investor confidence.

- **Limited long-term monitoring:** Projects often only extend ~5-years, missing delayed or variable recovery, especially net carbon balance.

> Addressing these gaps is essential to align restoration policy with delivery capability, capacity, and functional outcomes. A more closely integrated, evidence-based approach is fundamental to support public confidence in investment and blended finance. Understanding how specific techniques influence long-term recovery is critical to achieving restoration targets and meeting climate objectives.

2.5 Restoration Techniques

Restoration of blanket peatlands aims to reverse the impacts of degradation (Section 2.3) through a combination of rewetting and revegetation, often supplemented by site management and chemical interventions (Parry *et al.*, 2014; Thom *et al.*, 2016). It targets physical features driving emissions and instability, including drainage ditches, grips, erosion gullies, hags, and bare peat (Figure 2.13). The *Conserving Bogs: The Management Handbook* (Thom *et al.*, 2019) and *Peatland ACTION – Technical Compendium* (NatureScot, 2021) provide guidance on intervention delivery in the UK. However, there has been little research into the effectiveness of individual techniques, where multiple options are available for the same goal. This includes their relative environmental impact, contributing to unknown carbon costs, which may impact the carbon balance from restoration (Drever *et al.*, 2021).
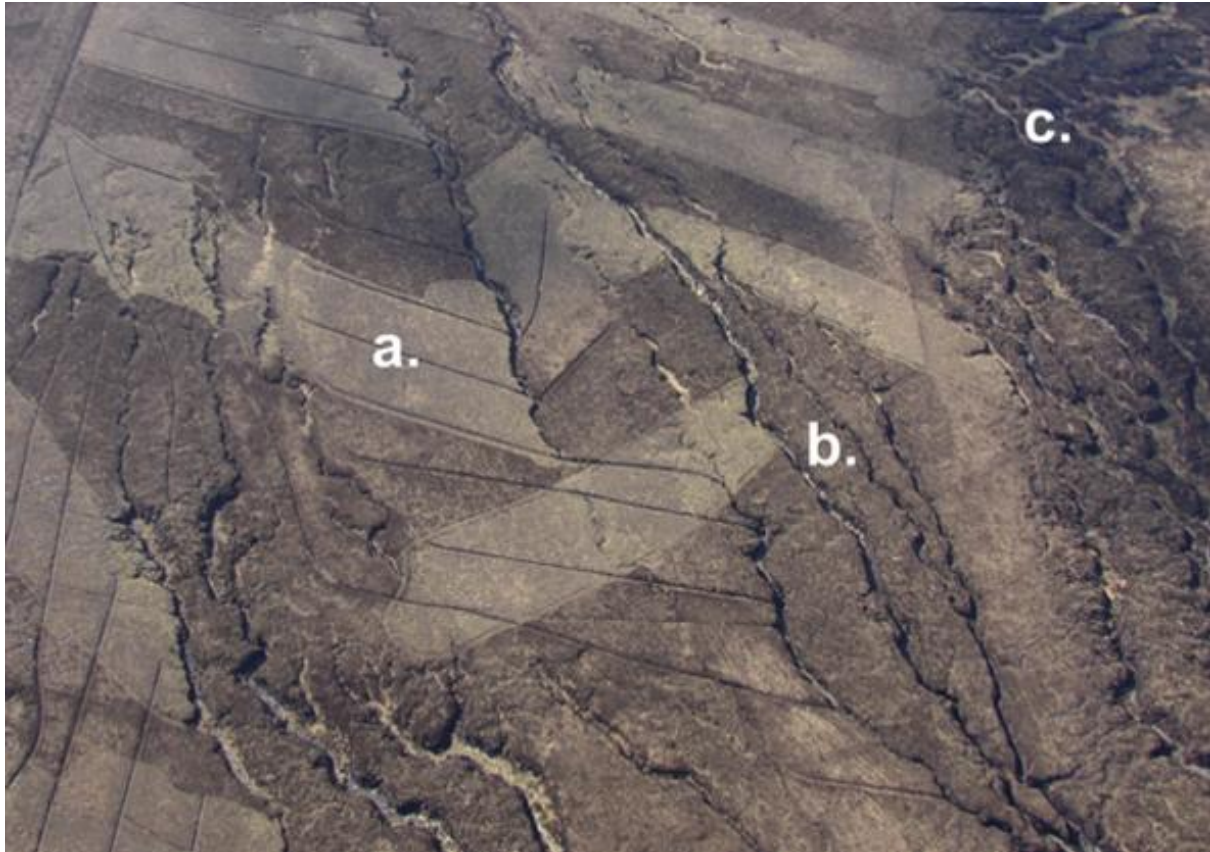
Figure 2.13: Aerial image of blanket peatland degradation features as depicted in Parry *et al.* (2014): a. represents artificial drainage channels; b. illustrates erosional gully networks; c. shows hag formations and the presence of bare peat pans (darker areas), possibly formed through burning.

2.5.1 Rewetting

Rewetting aims to restore high water tables to limit oxidation and increase carbon storage through retarded decomposition (Strack and Zuback, 2013; Thom *et al.*, 2016; Joosten, 2021). Interventions also reduce erosion, encouraging sediment deposition, and restrict dissolved and particulate organic carbon export (Armstrong *et al.*, 2010; Shuttleworth *et al.*, 2015; Evans *et al.*, 2018). By increasing surface moisture, rewetting supports the establishment of peat-forming species, such as *Sphagnum* (Allott *et al.*, 2009; Holden *et al.*, 2017). Techniques target drainage ditches, erosion gullies, and hags, as well as involve bunding to create surface pools (Armstrong *et al.*, 2009; Parry *et al.*, 2014; Thom *et al.*, 2019; Howson *et al.*, 2023).

Ditch and gully blocking involves damming channels (Figure 2.14). Interventions are typically selected based on channel dimensions. For large channels (>3m wide; >1.5m deep), stone dams or plastic piling are common, while smaller ones (<2m wide; <1m deep) often use timber, heather bales, or peat (Figure 2.15). Where channels extend to the mineral layer, impermeable materials are prioritised (Thom *et al.*, 2019; NatureScot, 2021).
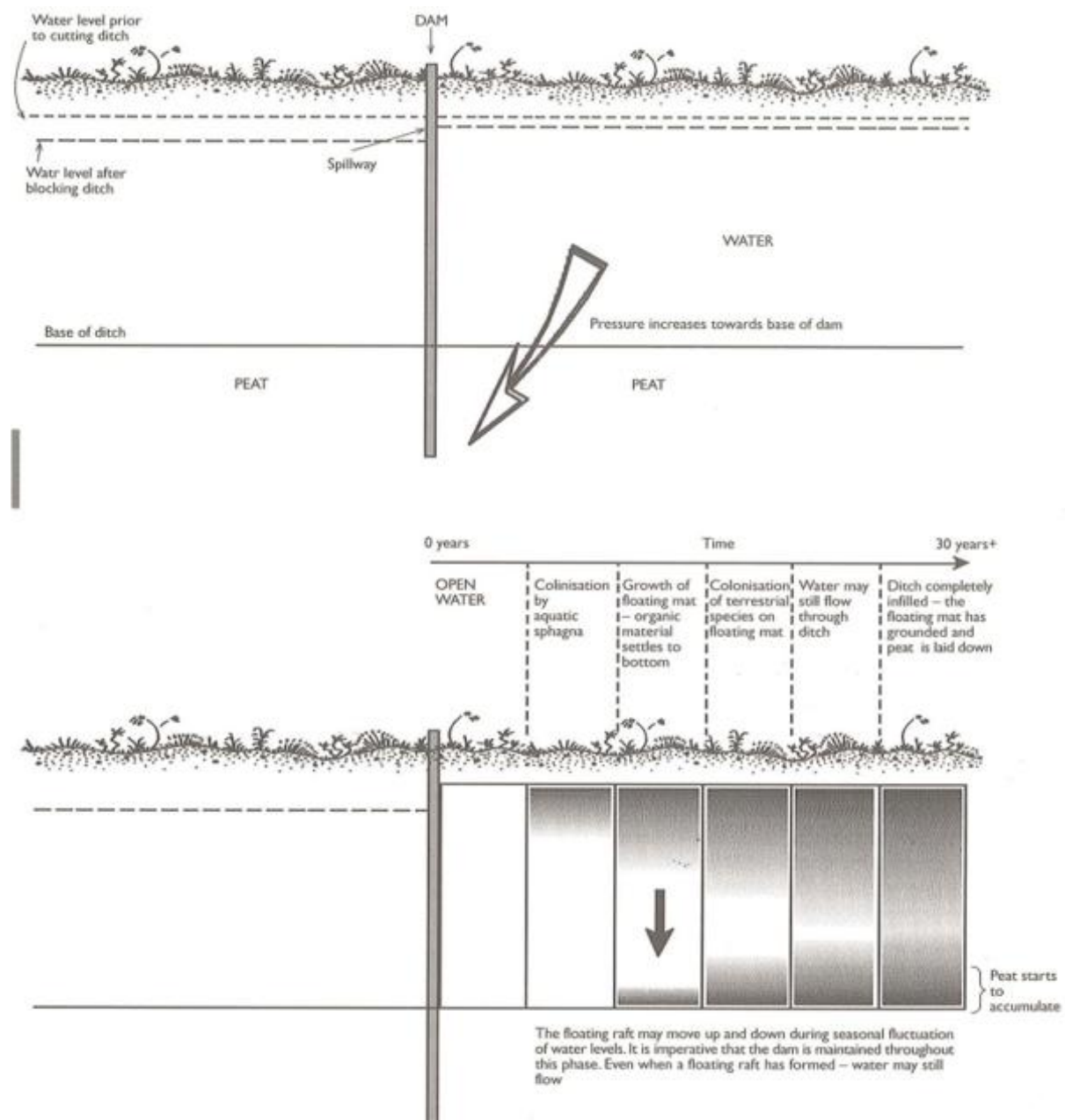
Figure 2.14: Principles of dam installation as a blanket peatland rewetting technique, as depicted in Thom *et al.* (2019).

Material choice also influences delivery. Stone dams typically require helicopter assistance due to their weight (~775kg), whereas peat dams can be installed using low-pressure ground machinery, and timber dams are suitable for manual (by hand) installation (Figure 2.15).

Figure 2.15: Examples of ditch and gully blocking interventions (Thom *et al.*, 2019; NatureScot, 2021): a. helicopter installation of a stone dam, used to block large erosion gullies; b. timber dam installed by hand, working as a water and sediment trap; c. plastic pilling installed to block drainage ditches, inserted by hand; d. peat dam created using low-pressure ground machinery (excavator), supporting water retention and *Sphagnum* growth.

Reprofiling is often conducted alongside ditch and gully blocking and involves reshaping steep gully and hag sides to gradients of 33° – 45° using excavators. This angle creates optimum slope stability, reduces erosion risk (including dissolved and particulate organic carbon loss), and facilitates vegetation re-establishment (Figure 2.16). Reprofiling also promotes sediment accumulation in channel bases and supports shallower water tables, supporting hydrological recovery (Parry *et al.*, 2014; Thom *et al.*, 2016, 2019).
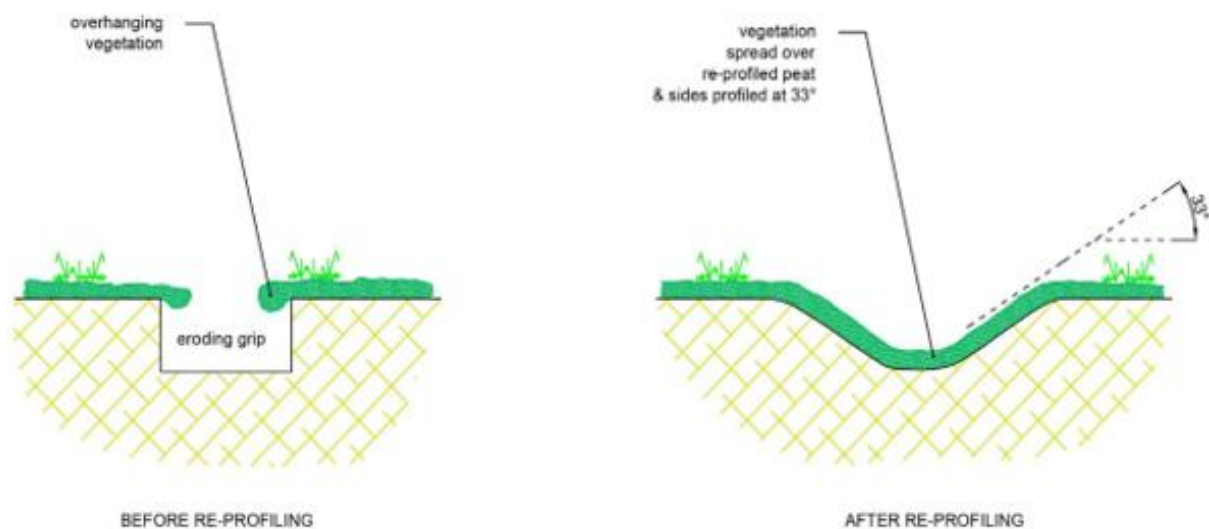
Figure 2.16: Illustration of reprofiling, including its combined role in revegetation (Thom *et al.*, 2019).

Bunding involves creating raised embankments to retain surface water, reduce flow velocity, and promote saturation (Holden *et al.*, 2006; Ramchunder *et al.*, 2009; Shuttleworth *et al.*, 2019). Surface bunds, typically made from permeable materials such as coir or fibrous peat, are designed to slow overland flow, trap sediment, and create microhabitats for bryophyte colonisation (Figure 2.17). Peripheral bunds, constructed along restoration margins, use impermeable materials like well-humified peat or mineral substrate to minimise water loss (Thom *et al.*, 2019; NatureScot, 2021).

Bunds also promote surface pool formation in shallow depressions, enhancing moisture retention and supporting *Sphagnum* establishment (Parry *et al.*, 2014; Howson *et al.*, 2023). Their size, placement, and materials vary with site topography, rewetting goals, and access (Thom *et al.*, 2019; NatureScot, 2021).
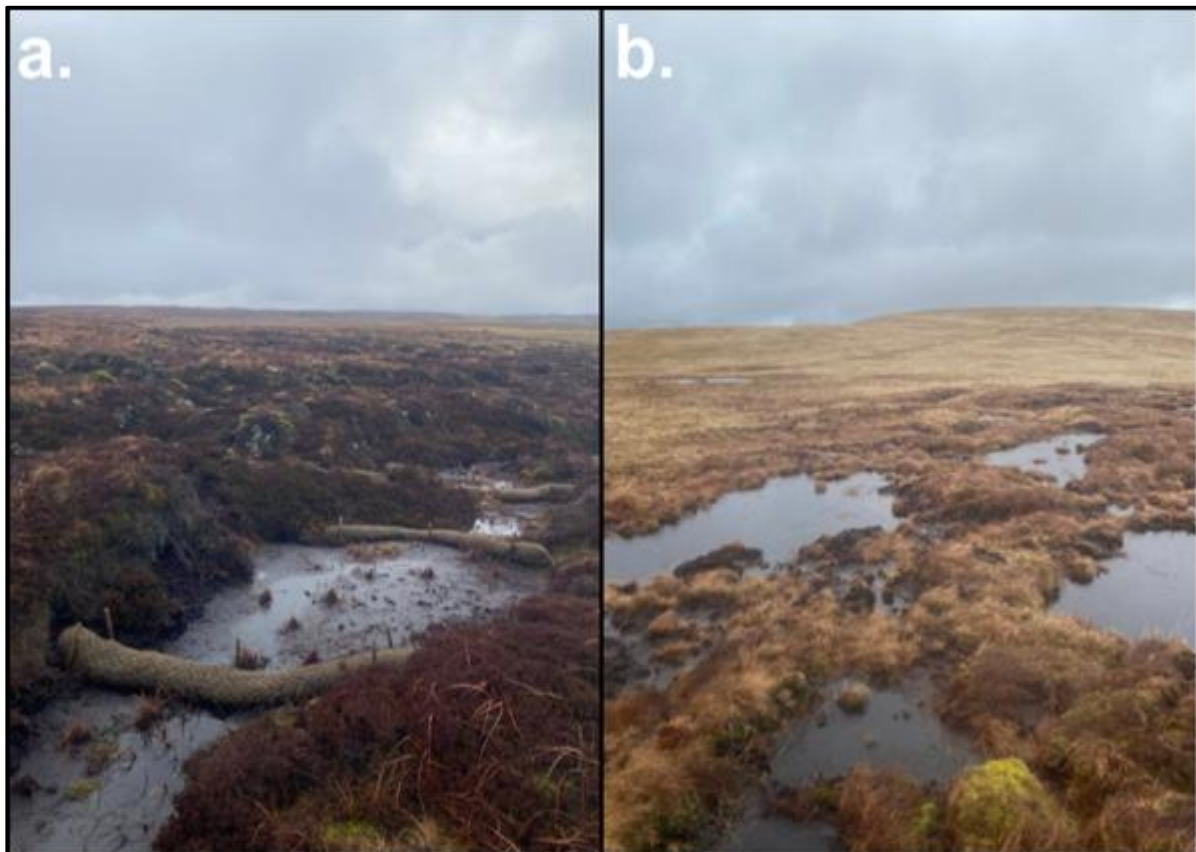
Figure 2.17: Examples of bund construction in blanket peatland restoration (Thom *et al.*, 2019; NatureScot, 2021): a. surface bunds made from coir logs installed across an eroding gully to reduce flow and retain water; b. formation of surface pools in a restored area using fibrous peat, promoting conditions suitable for *Sphagnum*.

2.5.2 Revegetation

Revegetation aims to re-establish peat-forming vegetation and stabilise bare peat to promote carbon sequestration and storage (Worrall *et al.*, 2011; Parry *et al.*, 2014; Thom *et al.*, 2016). Vegetation cover also reduces surface runoff by increasing friction and introducing microtopographic variation, which increases water retention and infiltration

(Section 2.2.1) (Holden *et al.*, 2001, 2004; Evans and Warburton, 2005; Wilson *et al.*, 2010). Interventions target bare peat features such as pans, reprofiled gully sides, and exposed hags (Parry *et al.*, 2014; Thom *et al.*, 2016).

Direct approaches reintroduce peat-forming vegetation to bare peat surfaces. **Turving** involves transplanting ~1m^2, 10-30cm deep sections of healthy surface (acrotelm) peat from adjacent borrow pits or donor sites onto exposed areas such as reprofiled gullies or peat bunds (Armstrong *et al.*, 2009; Parry *et al.*, 2014; Thom *et al.*, 2019). These are pressed into place using the underside of an excavator bucket, providing immediate surface coverage and structure (Figure 2.18a). Where donor material is limited or bare peat pans persist, **plug planting** is adopted. This involves hand planting *Sphagnum* plugs, typically sourced through micropropagation, at densities of 1 per 1-4m^2 to promote bryophyte colonisation and microtopographic variation (Figure 2.18b) (Parry *et al.*, 2014; Andersen *et al.*, 2017; Thom *et al.*, 2019). Plugs can vary from *Sphagnum* capitulums and gel capsules to multi-species plugs ~15cm^3 (Thom *et al.*, 2019). For extensive or inaccessible areas, **brash spreading** distributes cut vegetation (typically heather or grass mix) across bare peat surfaces by hand, low-pressure ground vehicle, or helicopter (Figure 2.18c). Full surface coverage is essential to maximise establishment, although excessive layering can cause compaction and light limitation (Thom *et al.*, 2019). Consequently, a broad application of ~220-250kg ha^{-1} is recommended (Thom *et al.*, 2019; NatureScot, 2021). These interventions demonstrate multiple installation options to achieve the same goal. However, uncertainty remains over which technique offers the most effective or resilient long-term outcomes, with trade-offs between material availability, scalability, and functional suitability.
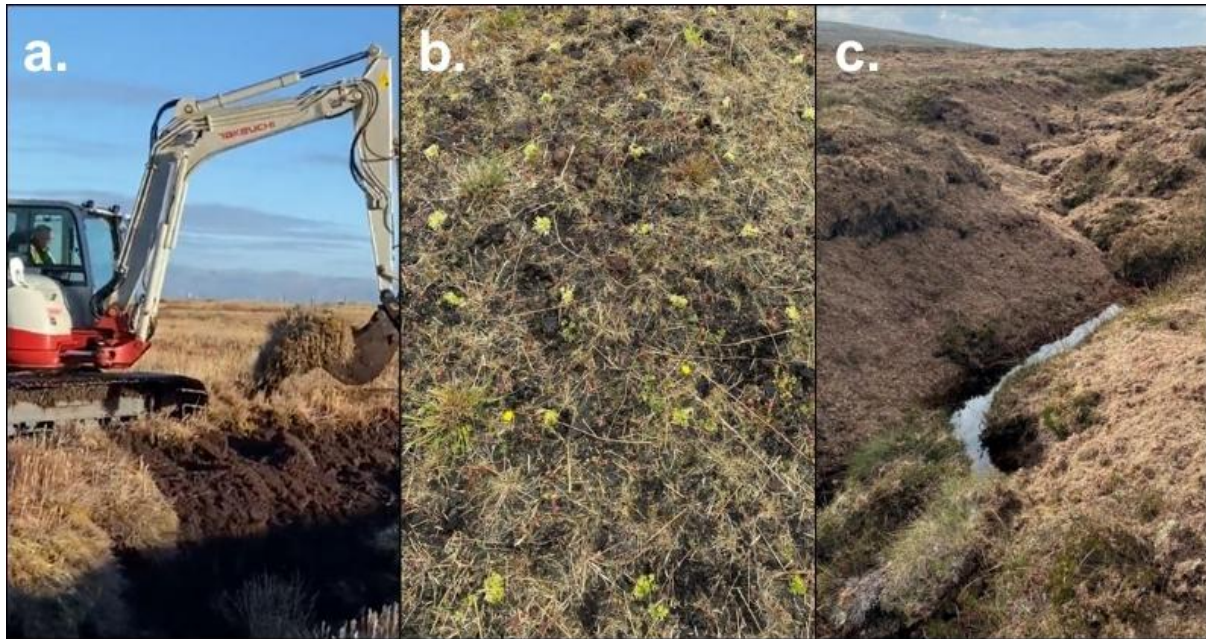
Figure 2.18: Examples of direct revegetation techniques as applied to bare peat surfaces on blanket peatlands (Thom *et al.*, 2019; NatureScot, 2021): a. turving using an excavator to transplant turves onto reprofiled gully slopes; b. plug planting of micropropagated *Sphagnum* to promote bryophyte colonisation; c. heather brash spreading across reprofiled gully slopes to act as a nurse layer.

Indirect revegetation techniques modify surface conditions to support vegetation establishment, particularly where acidity, nutrient limitation, or erosion restrict recovery (Parry *et al.*, 2014). **Lime and fertiliser application** raises pH and introduce nutrients, favouring the growth of graminoid and vascular species on severely degraded sites. Lime is typically applied at ~1 t ha^{-1}, with N:P:K fertiliser at ~40kg ha^{-1}, using helicopters and often requiring reapplication (Figure 2.19a). This is frequently combined with grass seed to introduce hardy nurse species that bind to the surface, reducing erosion and facilitating peat-forming species growth (Thom *et al.*, 2019; NatureScot, 2021). **Geotextiles**, such as coir-based Geojute, are used to stabilise exposed peat or reprofiled slopes, minimising aeolian erosion and protecting applied vegetation (Figure 2.18b) (Andersen *et al.*, 2017; Thom *et al.*, 2019; NatureScot, 2021). Geojute is typically hand-pinned into the peat surface using wooden, plastic, or steel pegs (Thom *et al.*, 2019).

These techniques provide structural support where physical degradation restricts direct planting and demonstrate intensive approaches to restore severely degraded areas. In less degraded systems, indirect site management, including **livestock exclusion** or **reduced grazing** pressure, is implemented to mitigate overgrazing impacts (Section 2.3.2) (Parry *et al.*, 2014).
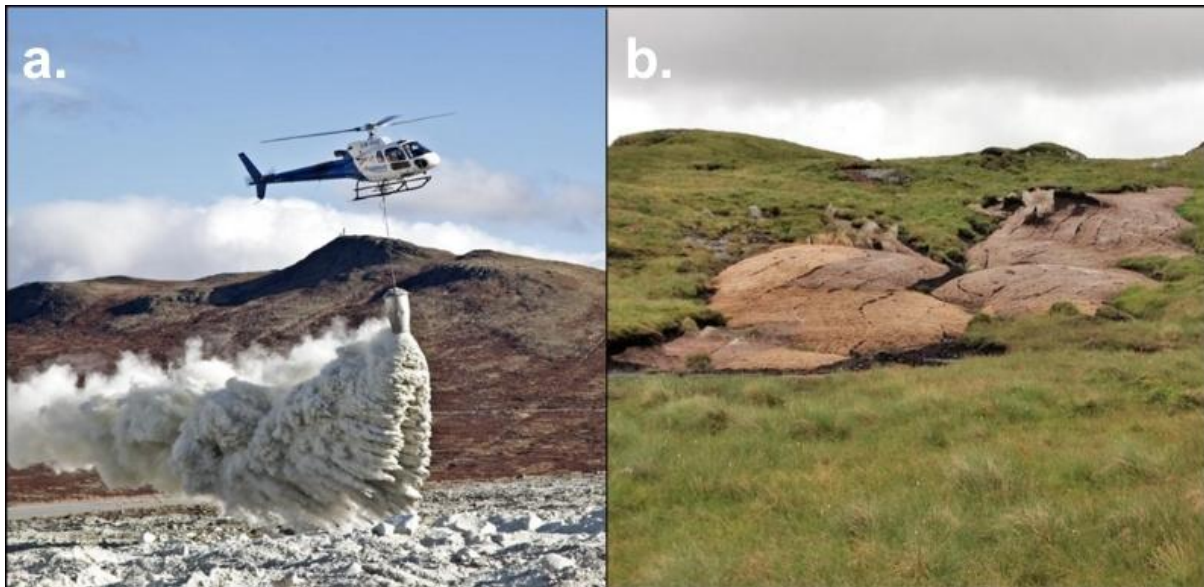
Figure 2.19: Examples of indirect revegetation techniques, typically applied to severely degraded blanket peatlands (Thom *et al.*, 2019; NatureScot, 2021): a. aerial application of lime to raise pH and support graminoid and vascular succession; b. Geojute mesh application on reprofiled, grass-seed-treated gully sides to stabilise surfaces.

2.5.3 Technique Effectiveness

The above sections demonstrate a range of techniques to rewet and revegetate degraded blanket peatlands, offering multiple options to achieve similar outcomes (Thom *et al.*, 2019; NatureScot, 2021). For instance, 2 ≤ 3m wide and 1 ≤ 1.5m deep gullies not eroded to mineral base can be blocked using peat, plastic, timber, or stone (Table 2.3), while brash can be spread by hand, low-pressure ground vehicles, or helicopter (Thom *et al.*,

2019). Despite their widespread adoption, the effectiveness of individual techniques and

materials in restoring functionality remains unknown.

Table 2.3: Damming guidelines extracted from Thom *et al.* (2019) directing towards material use to block erosion gullies based on size, depth, and proximity of mineral base.

Width	Depth	Eroded to Mineral Base?	Material
≤ 1m	≤ 1m	Yes	Peat
			Heather Bale
			Stone
		No	Peat
			Heather Bale
			Plastic
			Timber
1 ≤ 2m	1 ≤ 1.5m	Yes	Stone
		No	Timber
			Plastic
			Stone
2 ≤ 3m	1 ≤ 1.5m	Yes	Stone
		No	**Peat**
			Plastic
			Timber
			Stone
> 3m	> 1.5m	Yes	Stone
		No	Stone
			Plastic

Previous studies have assessed combinations of interventions (e.g., 'grip blocking')

without isolating impacts of individual materials or delivery methods (Worrall *et al.*, 2011;

Evans *et al.*, 2018; Alderson *et al.*, 2019; Howson *et al.*, 2023). Consequently, technique

evolution has progressed without research evidence. An exception is the application of

lime and fertiliser; likely studied due to its adoption on severely degraded sites,

particularly in the Pennines of England (Alderson *et al.*, 2019; Howson *et al.*, 2023).

Findings suggest mixed outcomes. Stimson *et al.* (2017) reported modest reductions in GHG emissions compared to bare peat, while Biasi *et al.* (2008) found increased CO_2 release. This demonstrates individual techniques can produce variable effects on function and may reduce net carbon accumulation.

Options also differ in their relative carbon intensity. Interventions requiring exotic materials imported through global supply chains or transported by helicopter (e.g., stone dams, coir logs) are likely to generate higher carbon emissions than those using local materials and low-pressure ground machinery (e.g., peat dams, turves). However, these emissions remain unquantified, representing a significant gap in understanding and introducing ambiguity into restoration carbon accounting (Drever *et al.*, 2021).

From a policy perspective, restoration success is increasingly defined by its ability to reduce net carbon emissions, aligning with national and international climate targets (Section 2.4.1). Yet without reliable data on carbon costs, assessments of net benefit remain unreliable. This is particularly important for the voluntary carbon market, where overestimated savings risk undermining investor confidence and the credibility of carbon credit audits (Bonn *et al.*, 2014; Moxey *et al.*, 2021). These uncertainties demonstrate the requirement for robust frameworks evaluating the functional recovery and carbon efficiency of specific restoration techniques.

2.5.4 Summary of Key Knowledge Gaps

Although numerous techniques exist to rewet and revegetate degraded blanket peatlands, their effectiveness and carbon impacts remain poorly understood.

- **Lack of technique-specific evidence:** Most studies assess combinations of techniques, meaning the functional effectiveness of isolated interventions is poorly understood.

- **Unclear best practices:** Multiple rewetting and revegetation options exist, but their effectiveness, resilience, and site suitability remain underexplored.

- **Limited data on carbon impacts:** The ability of specific techniques to reduce emissions or increase carbon sequestration is under-quantified, limiting confidence in their mitigation potential.

- **Unaccounted carbon costs:** Emissions from materials, transport, and installation are rarely included, limiting the accuracy and transparency of net carbon benefit.

- **Misalignment with policy:** Restoration success is determined by net carbon reductions, yet the absence of technique specific carbon data weakens the accuracy of policy reporting and crediting frameworks.

- **Risks to carbon market integrity:** Without robust evidence of carbon savings and delivery costs, projects risk overestimating benefits; undermining investor confidence and the credibility of carbon finance schemes (already weakened due to assumptions of immediate impact; Section 2.4.2).

The lack of robust evidence limits the ability to evaluate restoration success, particularly in the context of carbon markets and policy frameworks requiring measurable outcomes. This undermines confidence in reported carbon savings and may partly explain the slow uptake and absence of credit trading under schemes such as the IUCN UK Peatland Code. Addressing these gaps requires a transparent, evidence-based approach to evaluating restoration techniques, integrating both functional recovery (beyond carbon) and carbon efficiency (balancing benefits and costs). Such an approach would support the development of robust monitoring, reporting, and verification frameworks, while enabling the inclusion of wider ecosystem benefits.

2.6 Monitoring and Evaluation of Peatland Restoration Success

The effectiveness of blanket peatland restoration is assessed through monitoring and reporting frameworks aligned with current policy, focussing on net carbon reduction (Section 2.4). Carbon outcomes remain the metric of success, informing restoration design (Section 2.5) and financial mechanisms such as carbon crediting (Section 2.7). High-resolution methods, including direct GHG flux monitoring (Billett *et al.*, 2010; Rowson *et al.*, 2010), bulk and chemical analysis (Petrokofsky *et al.*, 2012; Strack and Zuback, 2013), and solute export measurements (Evans *et al.*, 2016; Swenson *et al.*, 2019) offer insight into functional recovery (net ecosystem carbon balance). However, they are costly, labour-intensive, and often destructive, limiting their scalability (Rowell, 1994; Couwenberg *et al.*, 2011; Petrokofsky *et al.*, 2012). Consequently, restoration impacts are inferred using low-cost surface proxies such as vegetation cover, bare peat

extent, and hydrological features (JNCC, 2009; Couwenberg *et al.*, 2011; Shepherd *et al.*, 2013; Birnie *et al.*, 2023; Crowle *et al.*, 2025). Yet these indicators have weak empirical associations to sub-surface processes (Section 2.2), limiting their capacity to evaluate functional recovery. Moreover, they fail to capture wider ecosystem benefits, including water regulation. Despite these limitations, proxy-based assessments remain central to national reporting and carbon accreditation schemes (Birnie and Smyth, 2013; Smyth *et al.*, 2015; IUCN, 2024b), and rarely incorporate the carbon costs associated with restoration delivery (Section 2.5.3). This reliance on incomplete metrics of success presents a critical challenge for policy, finance, and the credibility of peatland restoration as a nature-based solution.

2.6.1 Direct Approaches to Measure Net Carbon Accumulation

Direct monitoring approaches quantify key carbon fluxes and sequestration functions in blanket peatlands, including water table dynamics and gaseous and aquatic pathways (Billett *et al.*, 2010; Petrokofsky *et al.*, 2012; Evans *et al.*, 2018; Green *et al.*, 2018). These include GHG exchange measurements, dipwells, bulk and chemical analysis of peat cores, and monitoring of waterborne carbon exports.

GHG exchange is typically assessed using eddy covariance towers or gas chambers (Figure 2.20). Eddy covariance provides continuous, large-scale (~1km^2 in blanket peatlands) estimates of net primary productivity, integrating gross primary productivity and ecosystem respiration (Frolking *et al.*, 2002; Baldocchi, 2003; Billett *et al.*, 2010; Levy and Gray, 2015; Strack *et al.*, 2016). While valuable for understanding carbon dynamics and assessing functional response of restoration (Strack *et al.*, 2016; Peacock *et al.*, 2019), its adoption in UK uplands is restricted by topographic variance, meteorological

instability, and high costs (Baldocchi, 2003; Petrokofsky *et al.*, 2012; Rebmann *et al.*, 2018; Scholz *et al.*, 2021). Alternatively, closed and open gas chambers allow finer-scale measurements of CO_2 and CH_4, as well as N_2O fluxes under controlled light and temperature conditions (Hutchinson and Mosier, 1981; Strack and Zuback, 2013; Levy and Gray, 2015; Vanselow-Algan *et al.*, 2015; Strack *et al.*, 2016; Evans *et al.*, 2021). Chambers can be installed on terrestrial or aquatic surfaces (Figure 2.20), but require frequent calibration and maintenance limiting scalability (Billett *et al.*, 2010; Petrokofsky *et al.*, 2012). Both have contributed to carbon flux modelling, but remain impractical for routine monitoring across restoration projects.
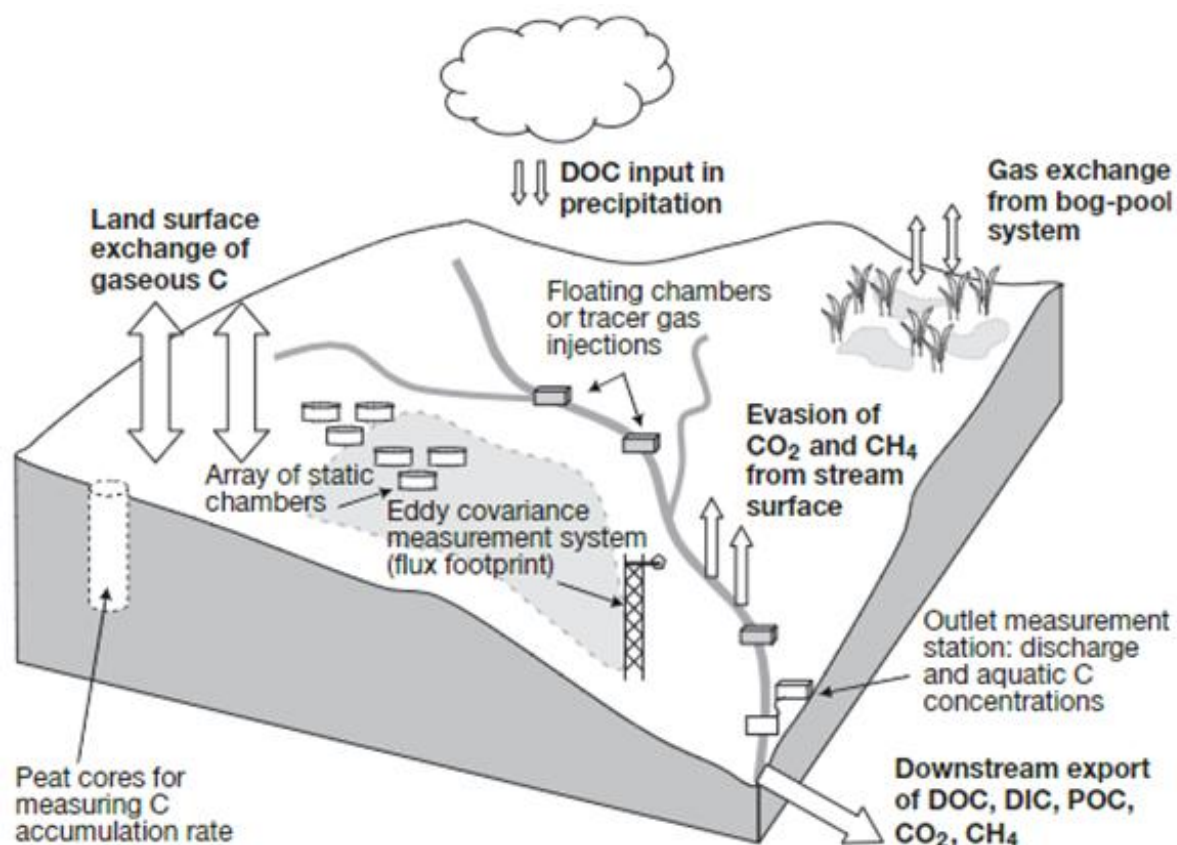
Figure 2.20: Illustration of the direct approaches to measure net carbon accumulation in blanket peatlands (Billiet *et al.*, 2010). Size of the arrows suggests the magnitude of fluxes in peat-forming systems.

Bulk chemical analysis of peat cores offers insight into decomposition processes, hydrology, and carbon storage (Figure 2.20). Key indicators include total organic carbon (TOC), carbon-to-nitrogen (C:N) ratios, bulk density, moisture content, and degree of humification, alongside pH, redox potential (Eh), and temperature (Boelter, 1966; Rowell, 1994; Chapman *et al.*, 2009; Chambers *et al.*, 2011; Morris *et al.*, 2015; Susilawati *et al.*, 2016; Alderson *et al.*, 2019; Peacock *et al.*, 2019). TOC and C:N are quantified through loss-on-ignition (LOI) or elemental analysis, indicating rates of organic matter accumulation (Rowell, 1994; Chambers *et al.*, 2011; Schulte and Hopkins, 2015; Green *et al.*, 2018; Peacock *et al.*, 2019). Bulk density and humification increase with peat degradation (Boelter, 1966; Clymo, 1984), while high moisture content can indicate lower decomposition and greater hydraulic conductivity (Kechavarzi *et al.*, 2010; Petrokofsky *et al.*, 2012; McCarter and Price, 2013; Morris *et al.*, 2019). Moisture content, derived gravimetrically, can also be used to estimate porosity, providing insight into peat's water retention capacity (Rowell, 1994; Strack and Price, 2009; Prat-Guitart *et al.*, 2016; Chapman *et al.*, 2017). pH and Eh, representing acidity and anoxia, are typically assessed in the field using probes (Kahlert *et al.*, 2004; Joshi *et al.*, 2021). Low pH (~4.0) and negative Eh are characteristic of functioning, ombrotrophic systems, while very low (<3.5) or raised pH (>5.0) and positive Eh suggest drainage and disturbance (Urquhart and Gore, 1973; Proctor and Maltby, 1998; Niedermeier and Robinson, 2007; Rowson *et al.*, 2010; Susilawati *et al.*, 2016).

Although bulk and chemical assessments are generally cost-effective, they require destructive sampling and laboratory access (except for probes), and can be restricted by peat type or legacy degradation (Givele *et al.*, 2004; Petrokofsky *et al.*, 2012; Chimner *et al.*, 2014; Kettridge *et al.*, 2015). These indicators primarily demonstrate cumulative

condition over time rather than short-term change, making direct attribution to restoration challenging (Strack *et al.*, 2008; Page and Baird, 2016; Wilson *et al.*, 2016; Evans *et al.*, 2017). However, few studies have assessed these bulk and chemical indicators in combination post-restoration, and parameters such as pH and Eh remain overlooked despite their biochemical relevance to carbon function (Urquhart and Gore, 1973; Susilawati *et al.*, 2016). Nonetheless, bulk and chemical properties provide insight into sub-surface condition and can offer valuable context on restoration impact, particularly if correlations with scalable surface indicators can be established.

Waterborne carbon losses such as dissolved organic carbon, particulate organic carbon, and dissolved CO_2 and CH_4 represent key components of net ecosystem carbon balance, particularly in degraded and restored blanket peatlands (Rowson *et al.*, 2010; Worrall *et al.*, 2011; Evans *et al.*, 2016, 2018; Young *et al.*, 2017). These fluxes are typically measured at outlet stations (Figure 2.20), with concentrations quantified through laboratory analysis (Worrall *et al.*, 2003; Wallage *et al.*, 2006; Turner *et al.*, 2013; Evans *et al.*, 2018). While important for understanding downstream carbon loss, outlet monitoring poses logistical challenges for installation and maintenance across remote upland sites (Worrall *et al.*, 2003; Billett *et al.*, 2006). Links to sub-surface recovery remain poorly understood, though pore structure likely governs export potential (Holden *et al.*, 2006b; Wickland *et al.*, 2006; Armstrong *et al.*, 2012; Peacock *et al.*, 2018).

While these direct approaches offer insights into carbon functions, particularly in combination, their cost, complexity, and limited scalability have led to the widespread adoption of surface proxies as indicators of restoration success (Couwenberg *et al.*, 2011; Petrokofsky *et al.*, 2012).

2.6.2 Surface Proxies as a Measure of Restoration Success

Surface proxies include ecological indicators, such as vegetation composition, cover, and species richness, as well as physical degradation features (JNCC, 2009; Billett *et al.*, 2010; Couwenberg *et al.*, 2011; Liu *et al.*, 2020). The *Common Standards Monitoring Guidance (CSM) for Upland Habitats: Blanket Bogs* (JNCC, 2009) informs statutory condition assessments across the UK (Shepherd *et al.*, 2013; Alderson *et al.*, 2019; Gregg *et al.*, 2021; Birnie *et al.*, 2023; Crowle *et al.*, 2025), while remote sensing is increasingly used to scale these assessments (Luscombe *et al.*, 2015; Lees *et al.*, 2019, 2021; Alshammari *et al.*, 2020; Minasny *et al.*, 2024). However, their connection to sub-surface structure, which governs many of the functions they are used to infer (Section 2.2), remains poorly understood.

The *common standards monitoring guidance: blanket bogs* provides a method to assess blanket peatland condition using surface vegetation and structural indicators (JNCC, 2009). It outlines a series of mandatory attributes and targets required for a site to qualify as near-natural H7130 blanket bog (Table 2.4). Indicator species are drawn from National Vegetation Classification (NVC) types associated with high water tables, serving as proxies for surface wetness (Haapalehto *et al.*, 2011; JNCC, 2011; Rydin and Jeglum, 2013; Lees *et al.*, 2019). These species also act as proxies for GHG flux and net carbon accumulation (Couwenberg *et al.*, 2011; Liu *et al.*, 2020). Consequently, JNCC (2009) indicators are embedded within restoration monitoring across the UK. Natural England applies them to define favourable condition in restored sites (Shepherd *et al.*, 2013; Crowle *et al.*, 2025), while NatureScot incorporates them into restoration assessment protocols (Birnie *et al.*, 2023). However, the common standards monitoring guidance was

not developed to assess restoration; rather the feasibility of sites to be restored (JNCC, 2009). Therefore, it does not capture gradients of recovery or directly assess restoration success, including the effectiveness of interventions in returning functionality.

Remote sensing technologies are increasingly used to upscale surface condition monitoring across restored sites (Andersen *et al.*, 2017; Minasny *et al.*, 2024). Spectral, UAV, and LiDAR imagery enable the detection of bare peat, vegetation type, and surface structure, which are then used to infer GHG flux and surface wetness (Luscombe *et al.*, 2015; Lees *et al.*, 2019, 2021; Alshammari *et al.*, 2020). Novel approaches such as bog breathing, measuring surface deformation as a proxy for water table fluctuation, offer further insight into functional processes, including moisture retention potential and microtopography (Howie and Hebda, 2018; Andersen *et al.*, 2021; Lees *et al.*, 2021).

Table 2.4: Simplified summary of key attributes and example targets from the common standards monitoring guidance for blanket bogs (JNCC, 2009).

Mandatory Attributes	Targets
Vegetation composition – frequency of indicator species	At least 6 indicator species should be present.
Vegetation composition – cover of indicator species	At least 50% of vegetation cover should consist of at least 3 indicator species - *Sphagnum* cover should not consist only of *Sphagnum fallax*. Any one of *Eriophorum vaginatum*, Ericaceous species collectively, or *Trichophorum* should not individually exceed 75% of vegetation cover.
Vegetation composition – cover of other species	Less than 1% of vegetation should consist of invasive species (10% for trees and shrub).
Vegetation structure – indicators of browsing	Less than 33% of the last complete growing season's shoots should not show signs of browsing.
Vegetation structure – disturbance	There should be no observable signs of burning.
Physical structure – peat erosion	The extent of eroding peat should not exceed new peat growth.
Physical structure – indicators of active drainage and/or ground disturbance due to herbivore or human activity	Less than 10% of the total feature area should be disturbed bare ground and/or show signs of active drainage. Less than 10% of *Sphagnum* should be damaged.

However, associations between surface indicators and sub-surface structure remain unexplored. For instance, incorporating pore network complexity (e.g., volume of isolated pores and tortuosity) could explain the 'how' of bog breathing, adding a sub-surface functional dimension to proxy-based assessment. While surface proxies offer scalability to monitoring restoration, their weak association to sub-surface processes limits their ability to assess functional recovery. Despite this, they form the foundation of reporting carbon benefits from projects, as seen within the IUCN UK Peatland Code.

2.6.3 Summary of Key Knowledge Gaps

Current monitoring and assessment approaches in blanket peatland restoration rarely include evidence of sub-surface processes, limiting their ability to evaluate functional outcomes critical to long-term success and wider ecosystem benefits beyond carbon:

- **Carbon as the dominant metric:** While biodiversity is often recorded, assessments use surface ecology as an indirect proxy for carbon, despite broader restoration goals.

- **Limited scalability of direct methods:** High-resolution techniques are costly, destructive, and impractical for routine or landscape-scale monitoring.

- **Weak associations between surface proxies and sub-surface function:** Surface indicators lack empirical correlation with sub-surface processes such as water retention or gas exchange which determine net carbon accumulation.

- **Absence of integrated frameworks:** No standardised approach combines scalable surface metrics with validated indicators of sub-surface function or carbon costs of intervention.

- **Misalignment with restoration objectives:** Existing frameworks were not designed to assess functional recovery and fail to capture long-term structural impacts.

Current monitoring strategies focus on carbon, yet rely on indirect proxies which fail to capture functional recovery or broader ecosystem benefits. This limits the accuracy of reported outcomes and weakens investor confidence, as carbon alone is not sufficient to fund the scale of restoration required (Section 2.4.1). A more integrated, functionally evidenced monitoring strategy is therefore required to improve reporting accuracy and establish a robust definition of restoration. Embedding indicators of functional recovery and wider ecosystem services within carbon accounting would enhance their credibility and investability.

3D X-ray micro-computed tomography (µCT) offers a potential solution to the limitations outlined in this section, particularly the inability of current proxies to explain why a peatland stores carbon. As outlined in Section 2.2.3, pore networks govern the hydrological and biochemical processes controlling carbon accumulation (Hoag and Price, 1997; Holden, 2005b; Quinton *et al.*, 2009; Rezanezhad *et al.*, 2016; Gharedaghloo *et al.*, 2018). However, conventional laboratory techniques, such as gravimetric porosity and loss-on-ignition, are destructive and provide limited structural insight (Section 2.6.1), restricting their ability to characterise sub-surface functional behaviour.

µCT provides a non-destructive, high-resolution method for visualising and quantifying pore networks in 3D (Cnudde and Boone, 2013; Rezanezhad *et al.*, 2016; Hanna and Ketcham, 2017). Advances in resolution and sample preparation, including advanced trimming, have extended its applicability to saturated organic soils (Carr *et al.*, 2020). Applications in restored saltmarshes have demonstrated post-restoration increases in microporosity and connectivity, with implications for water retention and carbon storage

(Spencer *et al.*, 2017; Dale *et al.*, 2019; Chirol *et al.*, 2021). Adapting these methods to peatlands could demonstrate how restoration alters pore structure and influences key sub-surface functions, such as maintaining high water tables, retarding decomposition, and supporting carbon sequestration (Section 2.1.2).

µCT therefore offers a valuable tool for assessing sub-surface structural responses to restoration and embedding functional understanding within evaluation frameworks, strengthening proxy-based monitoring and the evidence base for peatland restoration outcomes. Further details of its applicability are provided in Chapter 3; Section 3.5.

2.7 Quantifying Carbon Savings of Restoration Under the IUCN UK Peatland Code

The IUCN UK Peatland Code is the primary mechanism for quantifying and reporting carbon benefits from peatland restoration projects (Reed *et al.*, 2013; Moxey *et al.*, 2021; Hooker and Wentworth, 2024; IUCN, 2024a). It estimates carbon emissions (CO_2eq) reductions over time using indirect surface proxies of condition (Birnie and Smyth, 2013; Smyth *et al.*, 2015; IUCN, 2024b). The scheme aims to enable private investment by converting ecosystem change into verifiable carbon outcomes (Reed *et al.*, 2013; IUCN, 2024a). Until 2025, a fixed 10% buffer was applied to carbon savings estimates to account for emissions associated with restoration delivery; a static value applied irrespective of site or technique with no empirical basis (IUCN, 2024a). *As a direct consequence of this research, the IUCN UK Peatland Code has begun incorporating technique-specific carbon cost data (Chapter 8)*, though this has yet to be widely applied in practice (IUCN, 2025a).

The IUCN UK Peatland Code Field Protocol is built on a modified version of the European Greenhouse gas Emission Site Type (GEST) framework (Couwenberg *et al.*, 2011), tailored to UK blanket and raised bogs. It defines six pre-restoration ecosystem states based on surface condition indicators, including vegetation structure and degradation features (e.g., bare peat, gullies), each assigned a standard emissions factor derived from average GHG flux data (Table 2.5) (Birnie and Smyth, 2013; Smyth *et al.*, 2015; IUCN, 2024b).

Table 2.5: Simplified summary of the six pre-restoration (baseline) condition categories for raised and blanket bogs (IUCN, 2024b).

Pre-Restoration Condition Category	Emission Factor (t CO_2eq ha^{-1} y^{-1})
Actively Eroding: Hagg/Gully	17.72
Actively Eroding: Flat Bare	17.72
Drained: Artificial	3.32
Drained: Hagg/Gully	2.51
Modified	2.51
Near-Natural	0.32

Emission factors are used to calculate a site's pre-restoration baseline. Projected reductions, expressed as Pending Issuance Units (PIUs), are then modelled at 5-year intervals over a typical 100-year lifespan, based on changes in ecosystem state following restoration (IUCN, 2024b). Restoration impacts are verified through intermittent audits to confirm interventions were implemented to specification (IUCN, 2024a). PIUs can then be converted into Peatland Carbon Units (PCUs).

As discussed in Section 2.4.2, restored sites may continue to emit increased carbon for decades post-intervention (Cooper *et al.*, 2014; Vanselow-Algan *et al.*, 2015; Bacon *et al.*, 2017). Assuming net reductions begin after only five years therefore risks overestimating carbon savings (Moxey *et al.*, 2021) and demonstrate the limited incorporation of sub-surface functional processes into monitoring frameworks. Additionally, there is little evaluation of functional intervention success, such as the effectiveness of ditch blocking or turve placement, limiting ability to assess restoration resilience. This is particularly important across long project timescales (typically 100 years) and with increasing climate change pressures.

The IUCN UK Peatland Code applies a risk buffer to account for errors, leakages, and restoration-related emissions (IUCN, 2024a). In Version 2.1, this buffer was uniformly increased from 15% to 20%, with 10% attributed to the carbon costs of restoration. However, there was no empirical evidence for this figure. Considering the variation in intervention type, materials, and delivery methods (Section 2.5), applying a fixed deduction introduces uncertainty into reported carbon savings and limits transparency for investors. *This research addressed that gap by providing the first quantification of carbon costs associated with specific restoration techniques (Chapter 8). As a result, the IUCN has begun integrating this data into the Peatland Code, offering more robust, site-specific carbon accounting (IUCN, 2025a).* Incorporating these costs increases the credibility of reported carbon savings and could increase investor confidence, critical given the IUCN UK Peatland Code's growing role in enabling private finance (Section 2.4.1).

Nonetheless, carbon valuation remains inconsistent and frequently low when in isolation, limiting private investment (Worrall *et al.*, 2009; Dunn and Freeman, 2011; Reed *et al.*, 2013; Bonn *et al.*, 2014; Smyth *et al.*, 2015; Moxey *et al.*, 2021; Mackenzie, 2024). Peatland Code projects in the UK currently generate PIUs valued at ~£25 per tonne, while the price of verified PCUs remains uncertain but is expected to be between £15 and £25 per tonne (IUCN, 2025c). Alternatively, combined carbon and biodiversity credits, such as those issued by Wilder Carbon, can exceed £75 – £100 per tonne (Wilder Carbon, 2024), though the methodology supporting these claims is unknown (Section 2.4.1).

This variability and uncertainty, driven by the absence of standardised, evidence-based valuation, undermines market stability and investor confidence. Although carbon remains the main driver for restoration finance, current metrics fail to indicate functional recovery. Projects report projected carbon savings without consideration of sub-surface recovery which supports long-term carbon accumulation (Section 2.2). Developing scalable indicators of sub-surface function is therefore essential to support credited carbon outcomes. Without them, peatland restoration risks becoming financially driven rather than functionally effective.

2.7.1 Summary of Key Knowledge Gaps

Although the IUCN UK Peatland Code now includes intervention carbon costs informed by this research, limitations remain. These continue to undermine the accuracy, credibility, and investment potential of restoration carbon accounting:

- **Functional processes are poorly represented:** Projected carbon savings (PIUs) rely on static ecosystem state changes and surface proxies, which have limited empirical correlation to sub-surface processes responsible for net carbon accumulation.

- **Assumed recovery timelines:** Emissions reductions are presumed to occur after 5-years, despite evidence of restored sites remaining net carbon sources for decades (Section 2.4.2).

- **Variability in carbon price:** The lack of standardised, evidence-based valuation (un-regulation) results in significant variability in credit pricing, reducing investor confidence and market reliability.

- **Carbon cost integration – RESOLVED:** Prior to this research, no empirical data informed deductions for emissions associated with restoration delivery.

> Integrating carbon costs improves transparency, but embedding functional indicators is required to support credited savings reflect true outcomes and long-term success.

Life Cycle Assessment (LCA) offers a scalable, standardised method for quantifying the environmental impacts of a product, process, or service across its entire lifespan (ISO, 2006; Curran, 2013; Hauschild *et al.*, 2017). It accounts for emissions, energy use, resource depletion, and pollution, typically expressed in CO_2eq (Bjørn *et al.*, 2017). While traditionally applied to products and services, LCA is increasingly used to evaluate landscape-scale 'events', such as river habitat restoration, by quantifying the carbon costs of materials, transport, and implementation (Chiu *et al.*, 2022). These insights support more transparent, evidence-based planning (Rebitzer *et al.*, 2004), aligning with wider sustainability goals.

In peatland restoration, LCA addresses a key limitation of current monitoring frameworks relying on indirect surface proxies of carbon savings and assumed recovery timelines. By enabling more accurate net carbon accounting, LCA demonstrates the overlooked

carbon costs of intensive techniques, such as those requiring exotic materials and helicopter transport, highlighting differences in intervention efficiency (Drever *et al.*, 2021). This supports the development of transparent, comparable, and credible restoration claims, increasing investor confidence and strengthening carbon finance mechanisms such as the IUCN UK Peatland Code. As illustrated in Figure 2.21, LCA accounts for all stages of the intervention life cycle, supporting µCT-based structural assessments by adding a carbon cost dimension to restoration evaluation (see Chapters 3; Section 3.6 and Chapter 8 for further details).
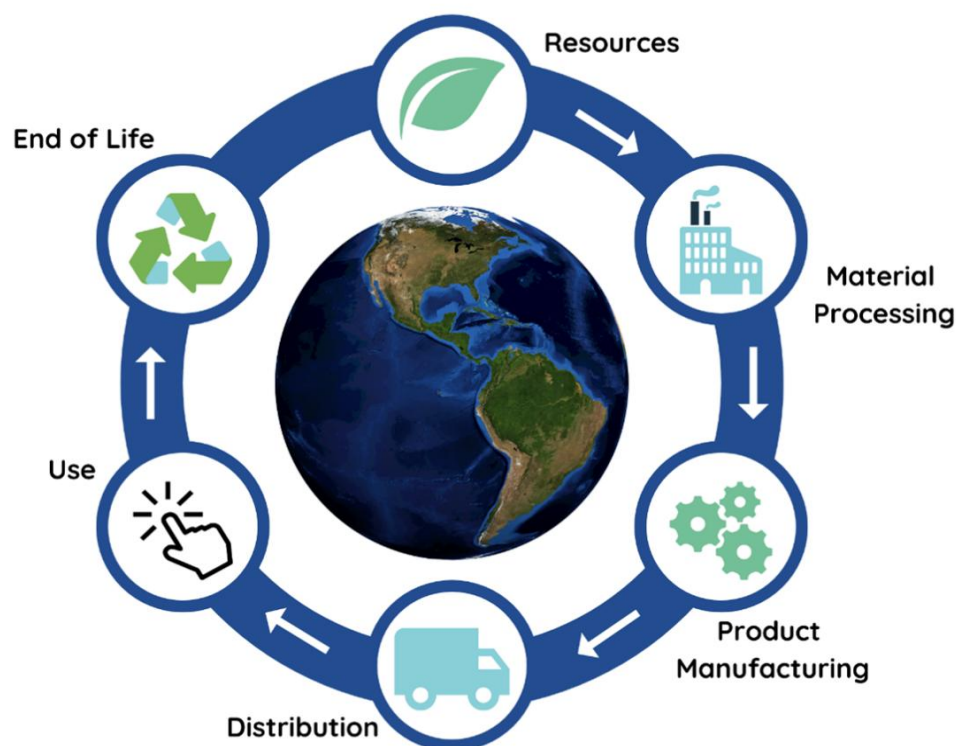
Figure 2.21: Conceptual illustration of the components of LCA as described in Hauschild *et al.* (2017).

2.8 Chapter Synthesis and Discussion

UK blanket peatlands represent a globally significant carbon store. However, historical land-use change and anthropogenic pressures, including drainage, overgrazing, and burning, have shifted sites from net carbon sinks to sources. Recognising their mitigation potential, the restoration and protection of peatlands is now embedded in national and international climate policy as a nature-based solution for reducing GHG emissions and achieving net-zero commitments.

Multiple rewetting and revegetation techniques exist to restore degraded peat, yet their carbon effectiveness, including the relative carbon costs, remains poorly understood due to limited assessment of interventions in isolation. Moreover, restored sites may remain net emitters for decades due to sustained CH_4 emissions. These unknowns and variability challenge assumptions of immediate carbon benefits and undermine the reliability of restoration success reporting. Although carbon remains the dominant metric underpinning policy and finance morels for restoration, it responds inconsistently to restoration and also misses the wider benefits such as biodiversity and water regulation, restricting its capacity as an indicator of restoration success.

These issues are amplified by current evaluation and carbon accounting frameworks, which rely on surface proxies and assumed 5-year recovery timelines. However, long-term carbon storage is controlled by sub-surface structure, particularly pore networks regulating water retention, gas exchange, and decomposition. Despite their importance, these below-ground processes remain unmeasured at fine spatial scales, reducing confidence in reported outcomes and the credibility of restoration reporting.

Devolved nation policy is driven by overambitious targets exceeding delivery capacity, yet fails to meet UK-wide net-zero commitments. These targets also focus on reducing emissions, rather than supporting net carbon sequestration, further demonstrating the limited consideration of natural sub-surface processes regulating long-term carbon accumulation. This disconnect between policy ambition, practical constraints, and the scientific evidence underpinning processes and dynamics highlights the requirement for more functionally grounded evidence to inform target-setting and restoration evaluation.

Meeting such targets exceeds the capacity of public funding, prompting a shift toward blended finance models. The IUCN UK Peatland Code has emerged as the principal mechanism for enabling this, but uptake remains slow, restricted by low carbon prices, outcome uncertainty, and a lack of transparency. More robust, evidence-based assessments of sub-surface functional recovery and intervention-related carbon costs could increase credibility and support improved carbon pricing in voluntary markets.

Few studies have directly assessed sub-surface structural and functional recovery following restoration, and none alongside the carbon costs of interventions. Most evaluations focus on short-term surface changes and do not distinguish the efficiency or net benefit of individual techniques. This limits the ability to identify best practice and determine which interventions deliver the most effective benefits. As carbon markets evolve, transparent reporting of savings and costs will be essential to support more robust and verifiable carbon claims.

Chapter 3: Methodology and Project Design

A multi-method research design is adopted to address the research gaps identified in Chapter 2, combining surface condition assessment, sub-surface bulk and chemical analyses, 3D X-ray micro-computed tomography (μCT), and Life Cycle Assessment (LCA) across degraded, restored, and near-natural sites. These methods evaluate the structural and functional recovery of restored blanket peatlands, assess associations between surface and sub-surface indicators, and quantify the carbon costs of restoration interventions relative to baseline and target conditions.

The aim of the analyses is to evaluate the effectiveness of blanket peatland restoration. This is achieved by assessing whether surface and sub-surface indicators demonstrate functional recovery, and whether such outcomes justify the carbon costs of intervention. These three research questions establish a better understanding of restoration success grounded in structural, functional, and carbon cost evidence:

Research Question 1: Can surface indicators be used as a proxy to infer changes in sub-surface structure and function post-restoration?

Surface condition assessments are widely adopted in peatland restoration monitoring, offering insights into vegetation cover, degradation state, hydrology, and proxy GHG emissions (Chapter 2; Section 2.6.2). However, the extent to which these indicators demonstrate sub-surface structure and function remains unclear (Chapter 2; Sections 2.2; 2.6.1), limiting their value as tools to assess restoration effectiveness. This question evaluates whether surface condition corresponds with sub-surface recovery, and

whether accessible indicators can serve as reliable proxies for structural and functional change post-restoration.

Objectives:

1. **Surface condition assessments** are conducted using JNCC (2009) *Common Standards Monitoring Guidance (CSM) for Upland Habitats: Blanket Bogs*, evaluating vegetation composition and structure, as well as physical degradation features to determine restoration condition aligning with current monitoring practices (Chapter 2; Section 2.6.2; methodology detailed in Chapter 4).

2. **Sub-surface bulk and chemical properties** are selected as indicators of sub-surface function, using accessible and inexpensive methods suitable for routine monitoring (Chapter 2; Section 2.6.1).

3. **Proxy assessment:**

    a. **Surface condition versus sub-surface bulk properties:** Surface conditions are quantified and statistically compared with sub-surface bulk and chemical properties to assess whether current surface indicators demonstrate broad sub-surface processes.

    b. **Sub-surface bulk properties versus structure:** Bulk and chemical properties are compared with µCT-derived structural parameters to evaluate their potential to act as proxies for sub-surface structure. This comparison also grounds µCT within established indicators of peatland function, increasing interpretability and relevance.

c. **Integrated assessment:** Where bulk properties correspond with µCT structure and surface condition, the potential for surface indicators to infer sub-surface function is evaluated for integration into restoration monitoring frameworks. Assessments are framed relative to structural baselines (degraded) and target conditions (near-natural) to contextualise recovery trajectories and improve relevance to monitoring.

> These comparisons support the refinement of monitoring frameworks through the inclusion of scalable indicators of sub-surface recovery.

Research Question 2: To what extent does the restoration of degraded blanket peatlands support the recovery of sub-surface structure and function?

Sub-surface structure controls the long-term carbon storage function of blanket peatlands, yet their response to restoration remains poorly understood (Chapter 2; Section 2.2). This question evaluates whether restoration interventions support the recovery of key structural and bulk and chemical properties over time, and whether restored sites transition away from degraded toward near-natural baselines.

Objectives:

1. **3D X-ray micro-computed tomography (µCT)** is used to characterise total macroporosity and pore network structure, providing insight into storage capacity, retention, and water, solute, and gas exchange efficiency, which control carbon

accumulation (Chapter 2; Section 2.2). Structural change is evaluated relative to degraded and near-natural baselines to assess recovery.

2. **Bulk and chemical analysis** is used to quantify properties associated with microbial activity, decomposition, structure, moisture retention, acidity, and anoxia, which influence long-term carbon storage (Chapter 2; Sections 2.2, 2.6.1).

> These metrics provide a comprehensive assessment of sub-surface structure and function, enabling evaluation of restoration effectiveness across different techniques and timescales, with reference to baseline and target conditions.

Research Question 3: How do the carbon costs of interventions impact the carbon benefit potential of restoration?

While peatland restoration aims to reduce GHG emissions and support long-term carbon storage (Chapter 2; Sections 2.4), the use of exotic materials and machinery can introduce considerable carbon costs (Chapter 2; Section 2.5). These include emissions from raw materials, transportation, and installation, which may offset or delay net climate benefits. This question evaluates the carbon balance between intervention costs and the extent of sub-surface functional recovery to determine whether restoration techniques deliver varying net benefits over time.

Objective:

1. **Life Cycle Assessment (LCA)** is used to quantify the carbon costs of restoration interventions using LCA data and emissions factors.

2. **Functional outcomes of restoration** are characterised through μCT structural parameters, bulk and chemical indicators, and surface features (Research Questions 1 and 2), providing a basis for evaluating restoration effectiveness.

3. **Integrated assessment** is conducted by combining carbon cost data with functional recovery indicators to assess the carbon efficiency of different interventions. Results are also contextualised within a real-world case study and evaluated against IUCN UK Peatland Code carbon savings assumptions to determine whether current carbon crediting approaches adequately indicate carbon costs and benefits.

Findings support the refinement of carbon accounting methodologies and inform decision-making for restoration tendering, carbon credit issuance, and policy development.

3.1 Sampling Framework

A bespoke, systematic sampling strategy is required to select representative conditions, including degraded samples as baselines and near-natural as functional targets for comparison. This is particularly challenging within large, heterogeneous landscapes, where traditional random or transect-based sampling may fail to capture spatial variability (Kermorvant *et al.*, 2019; Mastrantonis *et al.*, 2024). This is compounded where highly specialised and intensive techniques such as X-ray CT limit the number of samples that can be collected or analysed within a research project. The strategy adopted is outlined in the following chapter, indicating the requirement for detailed justification of site selection and sampling design given the complexity of the study area and methods.

3.2 Field Measurements

pH, redox potential (Eh), and temperature were selected as sub-surface indicators of function due to their role in regulating microbial activity, nutrient cycling, and decomposition (Chapter 2; Sections 2.2; 2.6.1). They were prioritised for their sensitivity to restoration outcomes, cost-effectiveness, and scalability within standard field protocols (Urquhart and Gore, 1973; Petrokofsky *et al.*, 2012; Tokarz and Urban, 2015; Howson *et al.*, 2023). Although additional chemical assessments such as electrical conductivity (EC) were available, EC indicates salinity and ion concentration, providing less functional insight into anaerobic conditions or GHG production (Grootjans *et al.*, 2016; Howson *et al.*, 2023). pH, Eh, and temperature are associated with vegetation, hydrology, and decomposition indicating carbon accumulation (Chapter 2; Section 2.1.2). Eh was used as a proxy for snapshot water table depth, with transitions between oxic and anoxic conditions (~0–400 mV) indicating saturation levels (Urquhart and Gore, 1973; Callebaut *et al.*, 1982; Seybold *et al.*, 2002). This provided a rapid, non-destructive estimate of saturation, facilitating interpretation of real-time water retention capacity.

In-situ measurements were prioritised to capture undisturbed conditions. Although laboratory settings offer greater control, observed differences during a 72-hour delay between recovery and analysis indicated storage affected results (Figure 3.1). pH increased across all depths in the laboratory, likely due to reduced microbial respiration at 4°C and the accumulation of alkaline byproducts (Preston *et al.*, 2012). Eh became less responsive to depth, likely indicating the absence of water table flux during storage. Effects justify real-time field measurements for representative biochemical data. Temperature was recorded in the field to support interpretation.
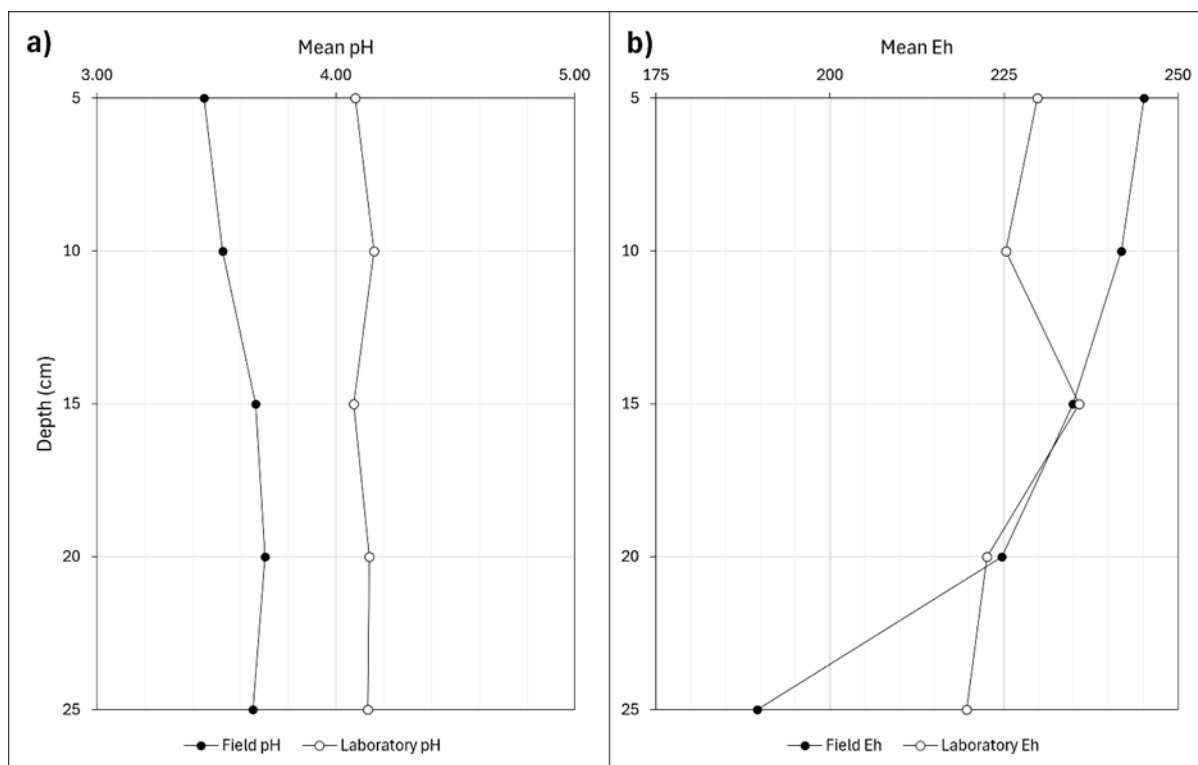
Figure 3.1: Comparison of mean field and laboratory measurements: a) pH; b) redox potential (Eh).

Although pH and Eh are recognised as indicators of biochemical function, they are rarely assessed continuously throughout the peat profile, particularly Eh (Urquhart and Gore, 1973; Haraguchi, 1991). Most studies rely on discrete or surface-only measurements, limiting understanding of vertical biochemical processes. By measuring pH, Eh, and temperature at 5cm intervals from 0–30cm, this study captures depth-dependent gradients across the acrotelm, mesotelm, and upper catotelm. Due to the remoteness of study areas and budget constraints, local meteorological data such as air temperature and precipitation were unavailable to support interpretation of sub-surface temperature. Consequently, normalised changes with depth are used to support functional interpretation.

These data enable comparison with sub-surface structural and bulk properties, supporting an integrated assessment of restoration impact on functionality.

3.2.1 Field Measurement of pH, Redox Potential, and Temperature

pH and temperature was measured in the field using a calibrated Hanna Instruments HI-99121 meter. The probe was pre-calibrated with buffer solutions before deployment. Measurements were taken within the hollow left by core extraction to minimise disturbance and spatial variation (Figure 3.2). Readings were recorded at 5cm depth intervals from 0–30cm, using the west-facing wall to support consistent aspect and alignment with laboratory sub-sample depths (explained in the following section). The probe was inserted directly into the peat matrix, and values were recorded once stabilised (~2 minutes). Between measurements, the electrode was rinsed with deionised water to prevent cross-contamination.

Figure 3.2: Field measurements: a) Surface (0cm) pH, Eh, and temperature assessments; b) Sub-surface pH, Eh, and temperature readings at 5cm intervals from the west-facing wall.

Eh was measured simultaneously using a Pen Type ORP redox meter, pre-calibrated with an ORP 220 mV standard solution. Readings were taken at the same intervals, with the platinum electrode inserted into the peat and values recorded upon stabilisation. The electrode was rinsed with deionised water between measurements and re-calibrated daily to support accuracy. Drift effects were not observed.

3.3 Sample Recovery and Preparation for Laboratory Analyses

3D X-ray micro-computed tomography (µCT) requirements dictated sample dimensions, extraction depth, and recovery method to support undisturbed, continuous cores while balancing resolution restrictions with sample size.

Cores were extracted to 300mm depth using 110mm internal diameter tubes, providing high-resolution data while maintaining sample continuity and alignment with England's definition of deep peat (Chapter 2; Section 2.4.2). Resolution restrictions are discussed further in Section 3.5.2. Custom 3mm thick unplasticised polyvinyl chloride (uPVC) tubes with sharpened edges were used to minimise disturbance during insertion (Figure 3.3). Plastic was selected to avoid interfering with X-ray attenuation during scanning (Section 3.5.2), while providing rigidity for field use.

Cores were recovered using the advanced trimming method described by Carr *et al*. (2020), previously adopted for undisturbed sediment sampling by Spencer *et al*. (2017) and Chirol *et al*. (2021). This technique relies on gravity, minimising disturbance compared to rotary drilling, percussion/vibrocorers, or gouge augers, which introduce friction, compressive and tensile stresses, and sample shortening or smearing (Carr *et al.*, 2020). While friction could not be entirely eliminated, gravitational extraction minimised mechanical stress, preserving structural integrity for µCT assessment.

Figure 3.3: uPVC sample tube (110mm diameter x 300mm depth) used for undisturbed peat coring. The bottom edge (top of tube) is sharpened to aid insertion and minimise disturbance.

Core extraction was conducted centrally on south-facing gully sides (Figure 3.4). Sampling targeted the upper 0–30cm, representing the primary functional zone for carbon sequestration, storage, and surface water uptake where the acrotelm transitions into the mesotelm and catotelm layers (Ingram, 1978; Clymo, 1984; Holden, 2005b; Clymo and Bryant, 2008). Sampling beyond this depth while maintaining the resolution required for μCT imaging was not feasible (Section 3.5.3).
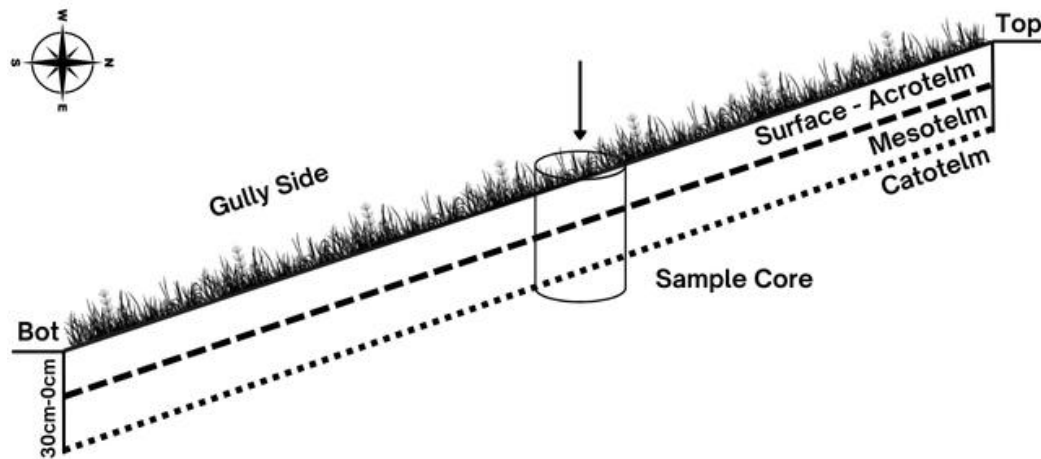
Figure 3.4: Cross-section showing core extraction from south-facing gully sides. Diagram illustrates the spatial position of samples in relation to the peat profile, including the surface, acrotelm, mesotelm, and catotelm layers.

Vegetation was cleared within a 50cm^2 buffer using serrated and non-serrated knives and trowels to aid core extraction and site restoration (Figure 3.5a). Samples were carefully removed by cutting around the tube circumference and allowing gravity to lower the core until flush with the surface (Figure 3.5b). Scissors were used where roots were dense. A clean cut was made at the base and the sample lifted using a flat trowel.
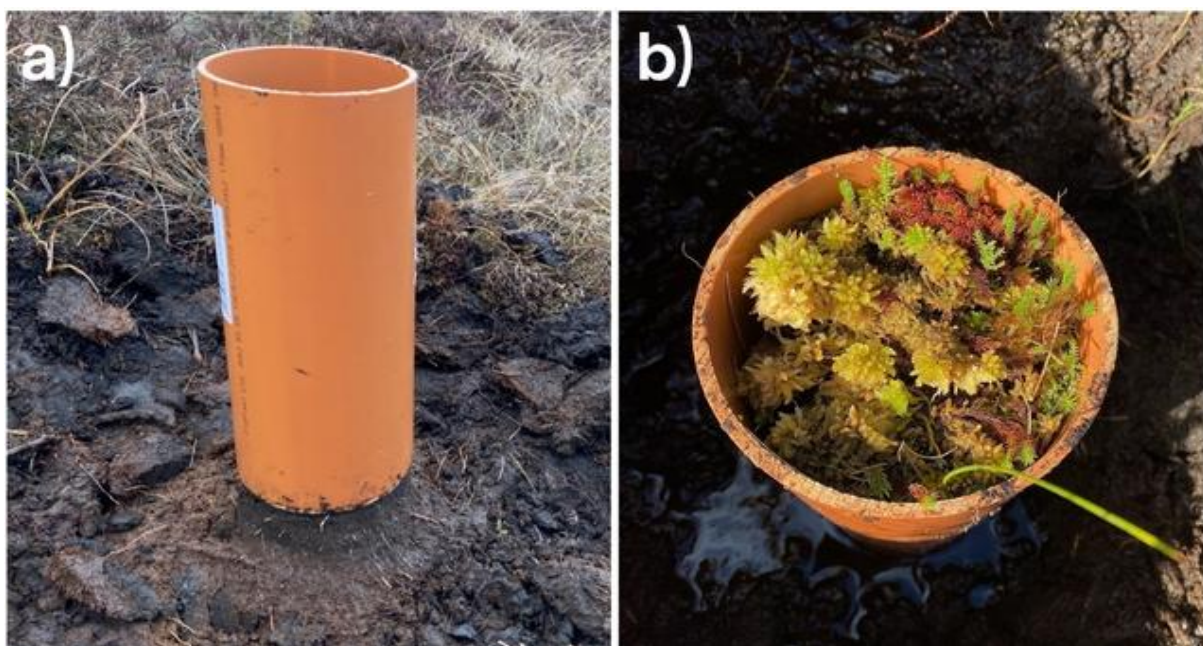
Figure 3.5: Core extraction processes: a) Advanced trimming method (Carr *et al.*, 2020) showing careful vegetation removal to minimise disturbance and enable site restoration; b) Undisturbed core with minimal deformation and preserved internal structure.

This supported minimal disturbance, preserving intact pore and root networks representative of in-situ conditions. Samples were sealed using custom Low-Density Polyethylene (LDPE) end caps (110mm diameter by 39mm depth, 1mm thick), heavy-duty pallet wrap, and cloth tape, creating an air and watertight seal to maintain air-filled and water-filled pore networks. Cores were stored upright in protected cool boxes to preserve structure during transit and maintained at 4°C to limit decomposition (Figure 3.6) (Cook *et al.*, 2016; Collier *et al.*, 2020; Howson *et al.*, 2023). While freezing at -18°C is recommended to completely stop decomposition (Givele *et al.*, 2004; Preston *et al.*, 2012) freeze-thaw processes would destroy structural integrity. A plastic button was taped on the north-facing wall to preserve orientation (Section 3.5.4b).

Figure 3.6: Vertical storage of extracted and sealed peat cores at 4°C prior to scanning and laboratory assessment.

Laboratory-based bulk and chemical analyses required sub-sampling (Section 3.4). Scanned cores were used to support alignment and representivity with μCT datasets. Cores were recovered, scanned, and received in the laboratory within 72 hours, maintaining consistent transit conditions to minimise disturbance and decomposition. Core tubes were opened longitudinally using a rotary cutting tool to preserve depth profiles and avoid compaction.

Sub-samples were extracted from the central vertical face of each core by halving the sample and sub-sampling at midpoints of evenly spaced 5cm intervals from 2.5-27.5cm (Figure 3.7a). This supported consistent sampling across depth and alignment with μCT datasets, enabling direct comparison across structural, chemical, and field assessments. A modified 10ml syringe with a serrated edge was used to control volume, supporting accurate and repeatable subsampling (Figure 3.7b).
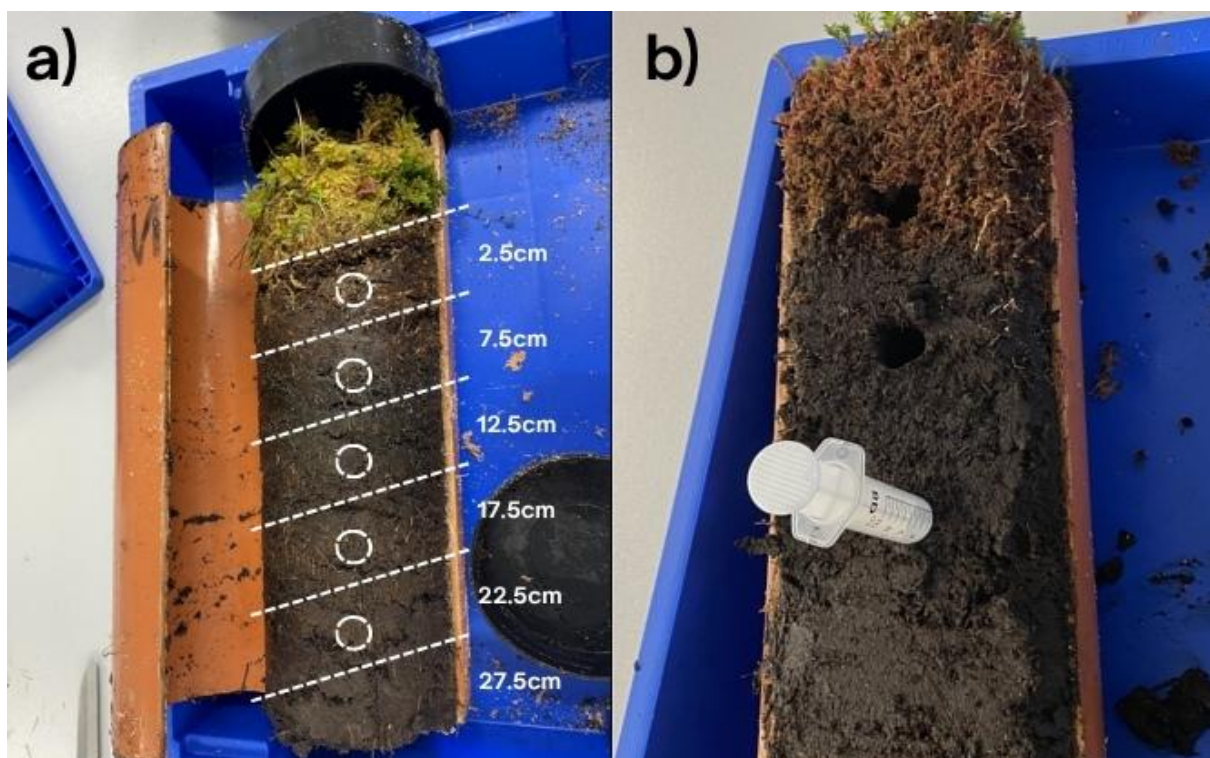
Figure 3.7: Preparation and sub-sampling of a peat core for bulk chemical analysis: a) halved core face with 5cm intervals and sampling depths; b) sub-sampling using a modified 10ml syringe with a serrated edge to extract known volume samples.

A minimum threshold of 5ml per sub-sample was set according to laboratory protocols (Section 3.4). Sub-samples were assessed immediately to limit oxidation. Where extensive root networks were present, scissors were used to cut above and below the sub-sample interval, ensuring roots remained intact.

3.4 Laboratory Bulk and Chemical Assessment

As noted above, bulk and chemical analyses were conducted on sub-samples from scanned cores following imaging due to the destructive nature of the methods (Section 2.6.1). Moisture content, bulk density, organic carbon content, and Von-Post humification were selected as key indicators of sub-surface function, providing insight into physical structure, decomposition rates, hydrological properties, and carbon storage capacity (Chapter 2; Sections 2.1.1; 2.2). Metrics align with µCT-derived parameters (Section 3.5.8), enabling direct comparison between bulk properties and sub-surface structure and function. Standard, cost-effective, and established techniques were prioritised to increase relevance for restoration evaluation, proxy development, and to ground µCT interpretation within existing assessment.

3.4.1 Bulk Density and Moisture Content (Oven-Drying)

Moisture content (MC) and bulk density (BD) were selected as indicators of sub-surface function due to their relevance to structure, hydrology, and decomposition, as well as the rewetting aim of restoration (Chapter 2; Sections 2.1.1; 2.2; 2.5). MC was defined as the mass ratio of pore water to solid particles, expressed as a percentage (Equation 3.1), while BD represented the dry mass per total sample volume (Equation 3.2). Both support interpretation of µCT-derived porosity and water-holding capacity (Section 3.5.8).

MC and BD can be measured using direct (gravimetric) or indirect (sensor-based) methods. Direct methods such as oven-drying are cost-effective and standardised (BSI, 1990b; Rowell, 1994; ASTM, 2000; Chambers *et al.*, 2011), though destructive and susceptible to volatilisation loss (O'Kelly and Sivakumar, 2014). Indirect approaches, including regression and radiometric techniques, are non-destructive but expensive and require specialist equipment (Chambers *et al.*, 2011).

Oven-drying (thermogravimetric) was selected for its simplicity and capacity to simultaneously determine MC, BD, and organic carbon content (Section 3.4.2). Samples were dried at 105 ± 5°C for >16 hours, following standard protocols (Figure 3.8a) (BSI, 1990b; ASTM, 2000). Although lower drying temperatures (60–90°C) are recommended for organic soils to minimise volatilisation, complete drying was necessary to support complete pore water removal. O'Kelly and Sivakumar (2014) confirm organic matter losses at 105°C are negligible in decomposed peat, making this approach suitable for structural and functional analysis. Known-volume sub-samples were placed in coded ashing crucibles (Figure 3.8b), wet-weighed, and oven-dried.

MC was calculated as:

$$MC(\%) = \frac{wet\ weight - dry\ weight}{dry\ weight}\ X\ 100$$

Equation 3.1

BD was calculated as:

$$BD(g/cm^3) = \frac{dry\ weight}{total\ volume\ (ml)}$$

Equation 3.2

Figure 3.8: Laboratory assessments: a) Oven used to dry samples; b) wet sub-sample preparation example for oven-drying.

3.4.2 Organic Carbon Content (Loss-on-Ignition)

Organic carbon content (OC) was used as an indicator of carbon storage capacity, inferring long-term decomposition and historic degradation. It supported structural interpretation alongside µCT-derived porosity (Section 3.5.8). OC is associated with moisture content, bulk density, and humification, providing a functional carbon context for evaluating sub-surface function (Chapter 2; Sections 2.1; 2.2; 2.6.1). OC was defined as the percentage of organic carbon in the organic matter (OM), following Klingenfuß *et al*. (2014) (Equations 3.3; 3.4).

OC was calculated from OM determined via Loss-on-Ignition (LOI), a widely adopted and cost-effective method aligned with standard protocols (BSI, 1990a; 1990b ASTM, 2007). Although LOI may underestimate OC due to mineral or volatile losses, this risk is limited in deep peats with low mineral content (Rowell, 1994; Petrokofsky *et al.*, 2012; Farmer *et al.*, 2014). LOI was therefore selected over elemental analysis for its affordability,

accessibility, and compatibility with standardised bulk sampling (Turetsky *et al.*, 2002; Petrokofsky *et al.*, 2012).

Oven-dried sub-samples were combusted at 550°C for 4 hours in a muffle furnace (Figure 3.9a). Following ignition, crucibles were reweighed (Figure 3.9b), and OM was calculated as:

$$OM(\%) = \frac{dry\ weight - ash\ weight}{dry\ weight} \ X\ 100$$

Equation 3.3

OM values were converted to OC using a standard factor of 0.578, appropriate for ombrotrophic peat in the Northern Hemisphere (Klingenfuß *et al.*, 2014):

$$OC\ (\%) = \ OM(\%)\ X\ 0.578$$

Equation 3.4
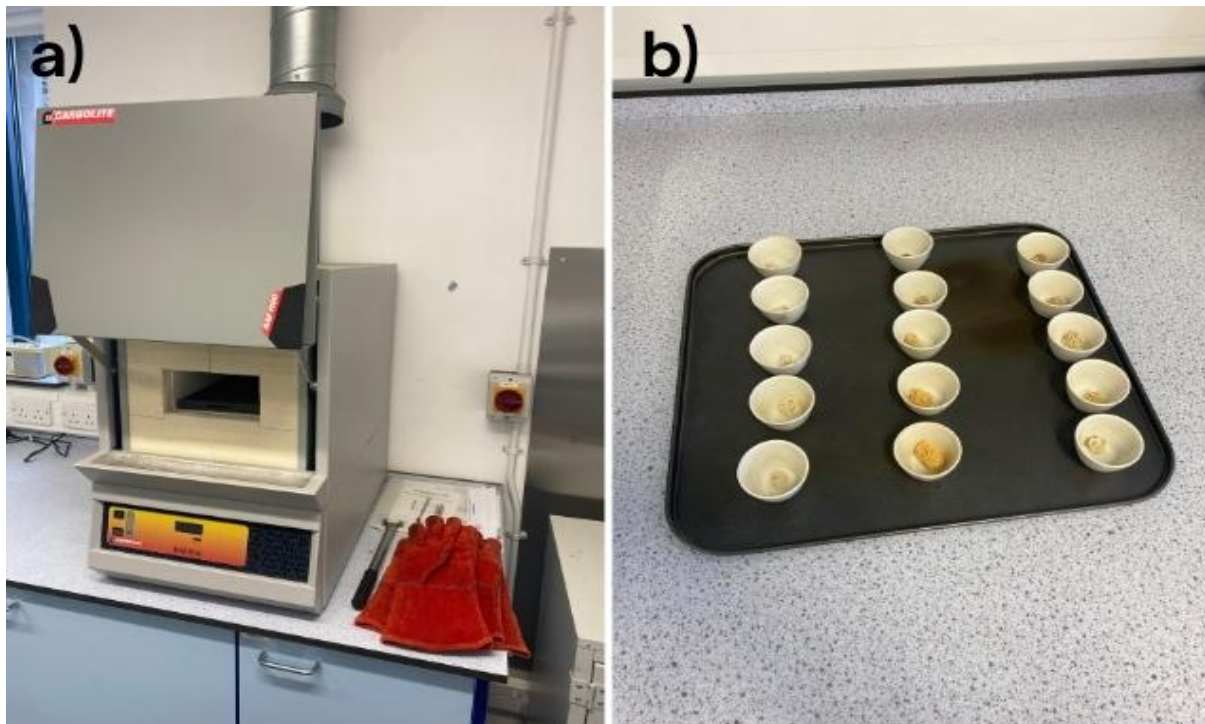
Figure 3.9: Laboratory assessments: a) Carbolite muffle furnace used to combust oven-dried peat samples at 550°C; b) ashed sub-samples following LOI, retained in coded crucibles for reweighing.

3.4.3 Von-Post Humification

Humification was used to assess decomposition and degradation history, as well as support the interpretation of sub-surface structure, microporosity, and stratification (Chapter 2; Sections 2.1; 2.2.3). Alongside μCT data, it can provide insight into restoration layering, indicating whether added material (e.g., turves) are structurally integrated with underlaying peat (micro- and macroporosity), or whether discontinuity exists, affecting hydrological and carbon function (Section 3.5.8). Microporosity was inferred through combined assessment of μCT grayscale density with Von-Post humification following (Spencer *et al.*, 2017), providing an accessible proxy.

The Von-Post Humification Scale (H1–H10) was adopted as a rapid and low-cost semi-qualitative method (von Post, 1922; Wijeyesekera *et al.*, 2016). While more advanced methods such as FTIR or NMR offer molecular-level detail (Artz *et al.*, 2008), they are resource-intensive and unsuitable for standardised monitoring (Chambers *et al.*, 2011). The Von-Post method supports functional interpretation by relating fibre content, amorphous material, and exudate characteristics to decomposition state (Table 3.1).

Sub-samples were collected by hand from the vertical face of each core, adjacent to the sub-samples extracted for MC, BC, and OC at 5cm intervals (Figure 3.10). The Von-Post test was applied consistently by the same operator using the standard squeeze method. Laboratory assessment was preferred over field application to support consistent environmental conditions and improved visibility of decomposition characteristics.

Table 3.1: Von-Post humification scale as outlined in Wijeyesekera *et al*. (2016).

Degree of Humification (Von-Post)	Decomposition	Plant Structure	Amorphous Material	Colour of Released Water	Escape of Material on Squeezing	Nature of Residue
H1	None	Easily identified	None	Clear	None	None
H2	Insignificant	Easily identified	None	Clear or yellowish	None	None
H3	Very slight	Still identifiable	None		None	Not pasty
H4	Slight	Not easily identifiable	Very slight amount	Muddy brown	None	Somewhat pasty
H5	Moderate	Recognised but vague	Very slight amount	Muddy brown	Very small amount	Somewhat pasty
H6	Moderately strong	Indistinct	Very slight amount	Muddy brown	About one third escapes	Somewhat pasty
H7	Strong	Very faintly recognisable	Lots		About one half escapes	Fibres and roots more resistant to decomposition remain in hand
H8	Very strong	Very indistinct	Large quantity	Very dark and almost pasty	About two thirds escape	Fibres and roots more resistant to decomposition remain in hand
H9	Nearly complete	Almost undiscernible	Large quantity	Very dark and almost pasty	About two thirds escape	Fibres and roots more resistant to decomposition remain in hand
H10	Complete	Not discernible	Large quantity	Very dark and almost pasty	All peat escapes	Fibres and roots more resistant to decomposition remain in hand

Figure 3.10: Example of Von-Post humification assessment at 5cm intervals.

3.4.4 Summary of Bulk and Chemical Parameters

Table 3.2 defines and summarises the functional relevance of each bulk and chemical

parameter selected.

Table 3.2: Summary of bulk chemical properties investigated, method of assessment, and their functional relevance to sub-surface processes.

Bulk Property	Method	Relative Function	References
Organic carbon content	**Laboratory:** Loss-on-ignition (LOI)	**Carbon storage:** Indicates cumulative peat accumulation and degradation history.	(Rowell, 1994; Chambers *et al.*, 2011; Alderson *et al.*, 2019)
Temperature	**Field:** Probe	**Microbial activity:** Regulates enzymatic processes and respiration rates, influencing decomposition and gas flux.	(Freeman *et al.*, 2001; Prescott, 2010; Strack *et al.*, 2016)
Humification	**Laboratory:** Von-Post	**Decomposition:** Indicates degree of decomposition; rapid suggests oxic, slow indicates anoxic.	(von Post, 1922; Stanek and Silc, 1977; Wijeyesekera *et al.*, 2016)
Bulk density	**Laboratory:** Oven-drying	**Physical structure:** Indicates compaction, linked to porosity, water retention, and gas exchange capacity; may indicate rapid decomposition.	(Boelter, 1966; Rowell, 1994; Givele *et al.*, 2004; Chambers *et al.*, 2011; Rezanezhad *et al.*, 2016)
Moisture content	**Laboratory:** Oven-drying	**Water retention:** Indicates water holding capacity and aeration; relates to temperature, decomposition, and microbial activity.	(Rowell, 1994; O'Kelly, 2004; Rezanezhad *et al.*, 2016; Perdana *et al.*, 2018)
pH	**Field:** Probe	**Acidity:** Regulates microbial processes, vegetation composition, and nutrient cycling; linked to oxygen in the profile (organic acid production).	(Urquhart and Gore, 1973; Proctor and Maltby, 1998; Freeman *et al.*, 2001)
Redox potential	**Field:** Probe	**Anoxia:** Proxy for oxygen availability, regulating CO_2 and CH_4 production, as well as microbial activity.	(Urquhart and Gore, 1973; Freeman *et al.*, 2001; Niedermeier and Robinson, 2007)

3.5 3D X-ray Micro-Computed Tomography

3D X-ray Micro-Computed Tomography (µCT) offers a non-destructive, high-resolution method for visualising and quantifying pore networks, enabling functional interpretation of hydrology, gas exchange, and carbon storage (Chapter 2; Section 2.6.3). While µCT is increasingly applied in soil science and sedimentology, its use in peatlands remains limited and has not yet been extended to restored sites. Furthermore, no standardised methodology exists for analysing continuous peat cores. Figure 3.11 outlines the µCT workflow developed in this study, adapted from Spencer *et al*. (2017) and Chirol *et al*. (2021) for large, intact peat cores. The approach balances resolution with core volume while minimising artefacts and preserving sample integrity. Total pore space is classified into atmosphere-connected (ACP), boundary-connected (BCP), and isolated porosity (IP) to support structural interpretation of restoration impacts on functionality. Full scanning and processing parameters are provided in the Appendices (A – E).
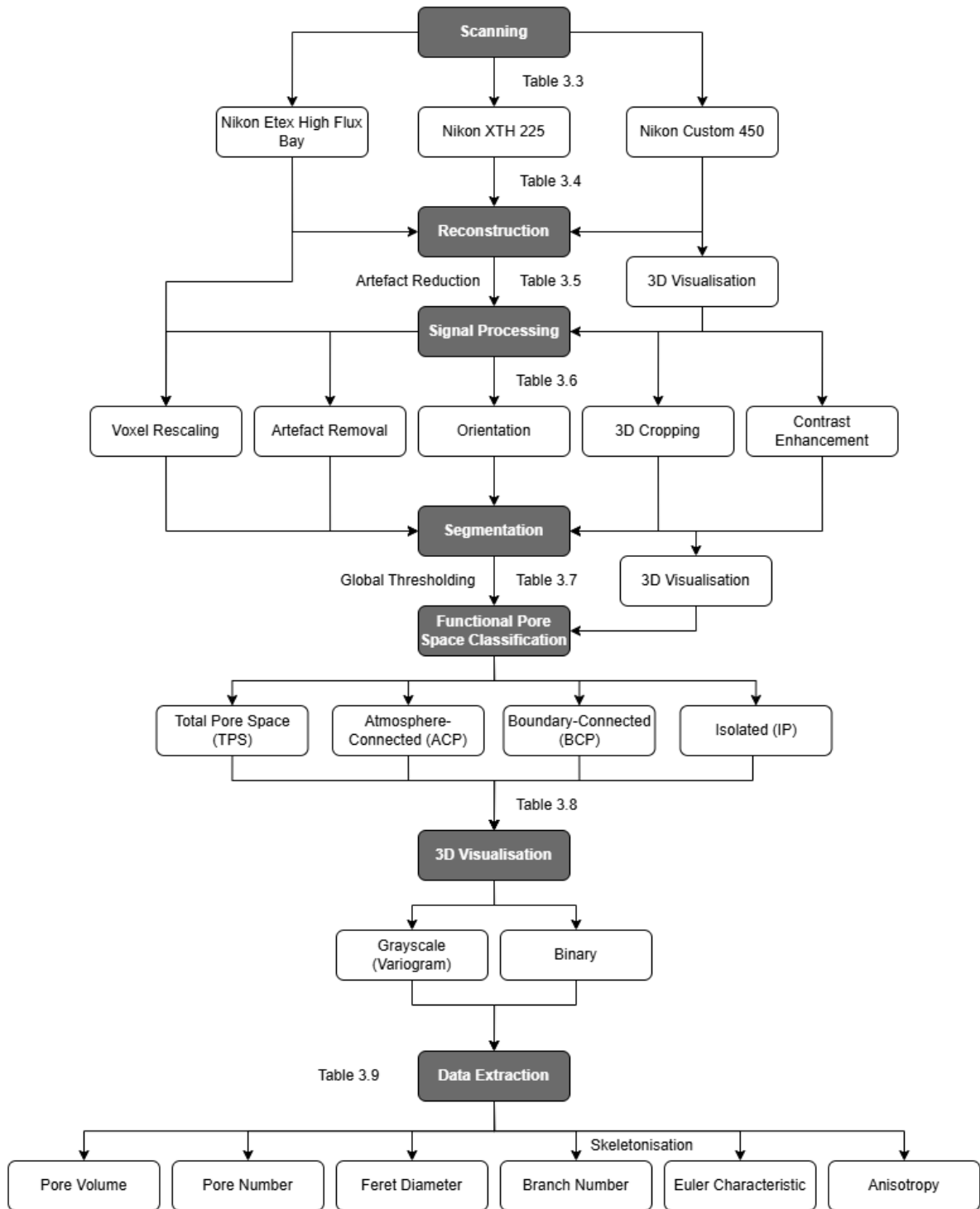
Figure 3.11: Workflow of μCT data acquisition, processing, and analysis used. Dark grey = process; white = measured/classified parameters.

3.5.1 μCT in Sedimentology: A Brief Review

Traditional methods for assessing sub-surface structure in soils and sediments, such as sieving, root washing, gravitational drainage, and manual dissection, are destructive, introduce sampling errors, and fail to preserve intact pore structure (Chapter 2; Section 2.6.1; Davey *et al.*, 2011; Al-Shammary *et al.*, 2018). They also lack the resolution to quantify fine-scale attributes such as pore complexity and connectivity, limiting interpretation of hydrological function and carbon storage (Chapter 2; Section 2.2.3). In response, imaging-based approaches have emerged. Gribbe *et al.* (2020) used photographic slicing of frozen peat monoliths to reconstruct pore and root networks in 3D, improving structural characterisation. However, freezing and slicing remains destructive and risks compromising the integrity of fine-scale pore networks.

μCT represents a non-destructive, high-resolution alternative for quantifying internal structure based on X-ray attenuation (Cnudde and Boone, 2013; Hanna and Ketcham, 2017). Compared to medical CAT scanning, μCT in geoscience employs higher energy sources, smaller X-ray focal spots, and longer acquisition times, enabling micron-scale resolutions (Cnudde and Boone, 2013). Its application in soil science has supported quantification and analysis of pore space in agricultural soils (Helliwell *et al.*, 2013; Keller *et al.*, 2013) and wetland sediments (Davey *et al.*, 2011; Dale *et al.*, 2019; Chirol *et al.*, 2021), including restored saltmarshes (Spencer *et al.*, 2017). These studies demonstrate the method's potential to associate pore structure to functional behaviour in restored systems. For instance, Spencer *et al.* (2017) reported increased microporosity and macropore connectivity post-restoration, with implications for water retention and carbon sequestration (Figure 3.12).
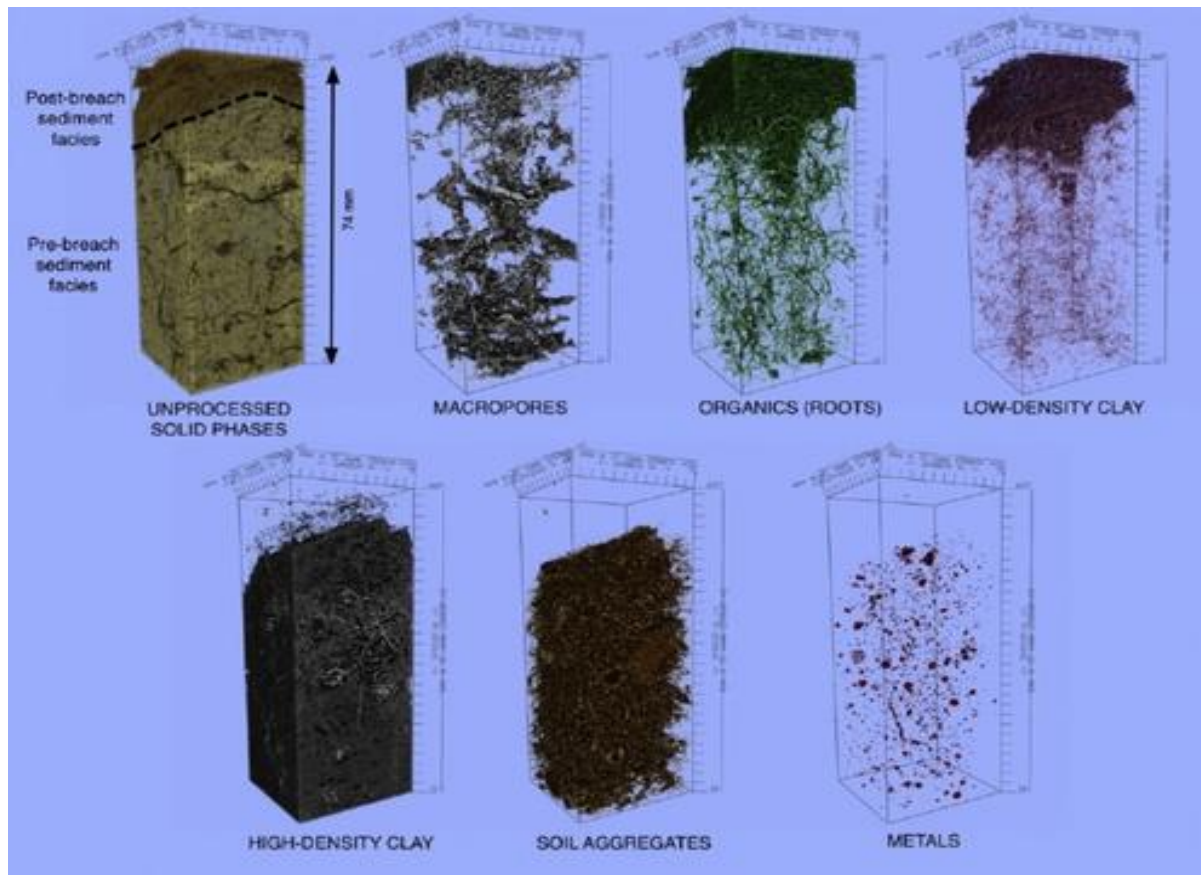
Figure 3.12: Example of μCT applied to restored (de-embanked) saltmarsh cores in Spencer *et al.* (2017). Figure demonstrates the ability of μCT to segment, quantify, and visualise in 3D structural elements of restored wetland soils, including intact macropore networks.

However, application to peat remains limited to a small number of studies using discontinuous sub-samples (Kettridge and Binley, 2008; Quinton *et al.*, 2009; Rezanezhad *et al.*, 2009, 2010; 2016; Kettridge and Binley, 2011; Comas *et al.*, 2014; Gharedaghloo *et al.*, 2018; McCarter *et al.*, 2020), with no established methodology for continuous, intact cores from restored sites. Most focus on discrete depths, limiting capacity to capture the full vertical gradient across the acrotelm, mesotelm, and catotelm. For example, Rezanezhad *et al.* (2016) identified large, connected (active) pores at 0–6 cm, contrasting with small, disconnected (inactive) pores at 61–67 cm (Figure 3.13), but did not assess how this transition influences water and gas transfer throughout the profile.
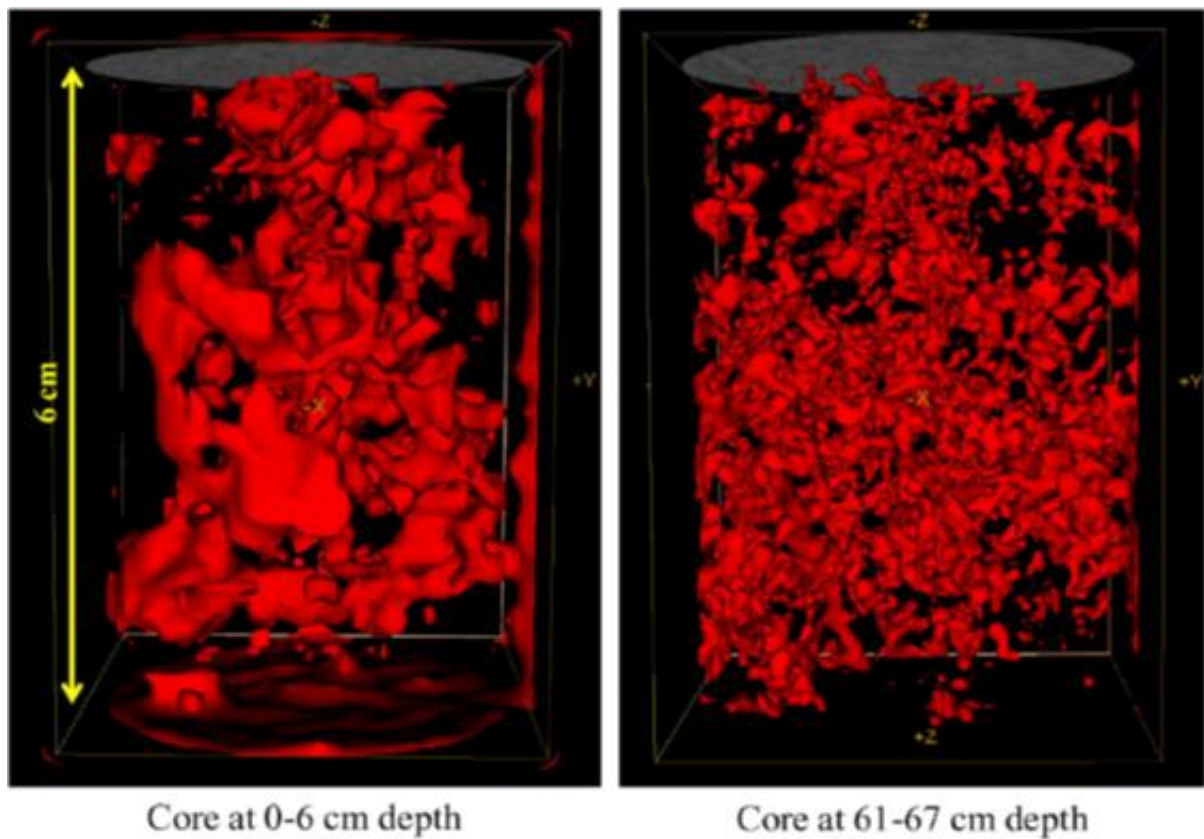
Figure 3.13: 3D reconstructions of peat porosity at contrasting depths from Rezanezhad *et al*. (2016).

This research advances the application of µCT into peatland restoration assessment by developing a tailored methodology for large, undisturbed, continuous cores, enabling more robust evaluation of structural and functional recovery.

3.5.2 Key Principles of µCT

µCT projects X-rays through a rotating sample to generate a series of 2D radiographs, which are reconstructed into a 3D voxel-based image stack. X-rays are produced by accelerating electrons from a heated tungsten cathode toward a target and metal anode (typically copper) inside a vacuum tube (Figure 3.14). Deceleration at the anode upon collision produces a broad spectrum of X-ray photons, which are typically emitted in a cone-beam configuration toward the sample (Figure 3.15).
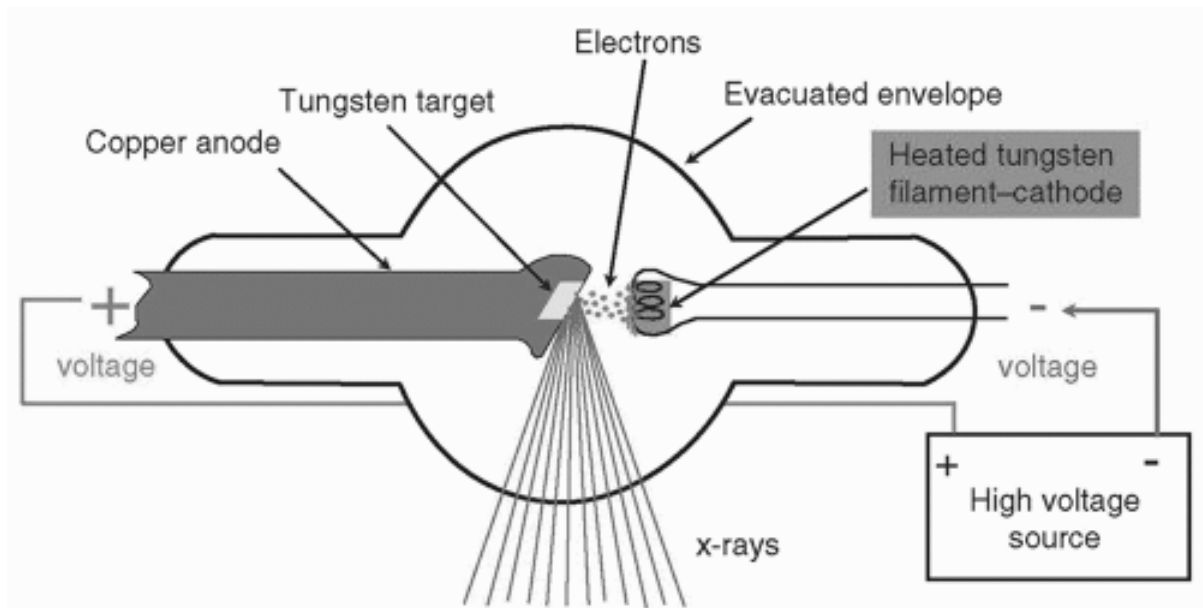
Figure 3.14: Minimum requirements for X-ray production, illustrating the source, target, vacuum, and connection of electrodes to high-voltage sources which form the X-ray tube (inferred from Bushberg, 2013).

X-rays interact with internal structures as they penetrate and are attenuated and absorbed or scattered depending on material properties. A flat-panel silicon detector records attenuation (Figure 3.15), converting transmitted X-ray intensity into electrical signals, forming greyscale images. Denser materials attenuate more X-rays and appear brighter; less dense materials attenuate less and appear darker (Section 3.5.3). Image contrast is therefore regulated by differences in X-ray attenuation.
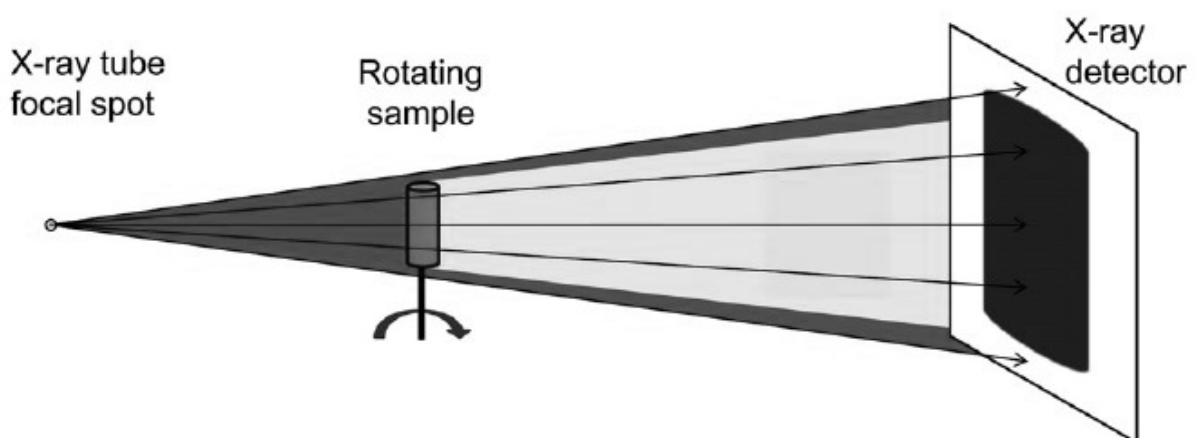
Figure 3.15: Schematic diagram of a typical lab-based μCT setup with a conical X-ray beam. Figure source: Cnudde & Boone (2013).

X-ray attenuation is influenced by:

1. **Photoelectric absorption (Figure 3.16a):** Low-energy photons are absorbed, especially in low atomic number materials.

2. **Compton scattering (Figure 3.16b):** Photons are deflected with partial energy loss.

3. **Rayleigh scattering (Figure 3.16c):** Photons are elastically deflected without energy loss.

These effects contribute to image artefacts, varying depending on material composition and energy spectrum of the X-ray source (Section 3.5.3). Attenuation is explained using Beer's Law, describing the exponential decay of X-ray intensity through a material:

$$I = I_o e - \int \mu(s)ds$$

Equation 3.5

where *I* is the transmitted intensity, $I_o e$ is the incident beam intensity, $\mu(s)$ is the local attenuation coefficient, and *ds* is the path length through the material. This relationship enables μCT to reconstruct internal structures based on variations in grayscale density and composition.

Bushberg (2013) provides the detail for μCT imaging principles, while Cnudde and Boone (2013) and Hanna and Ketcham (2017) describe its application in geoscience.
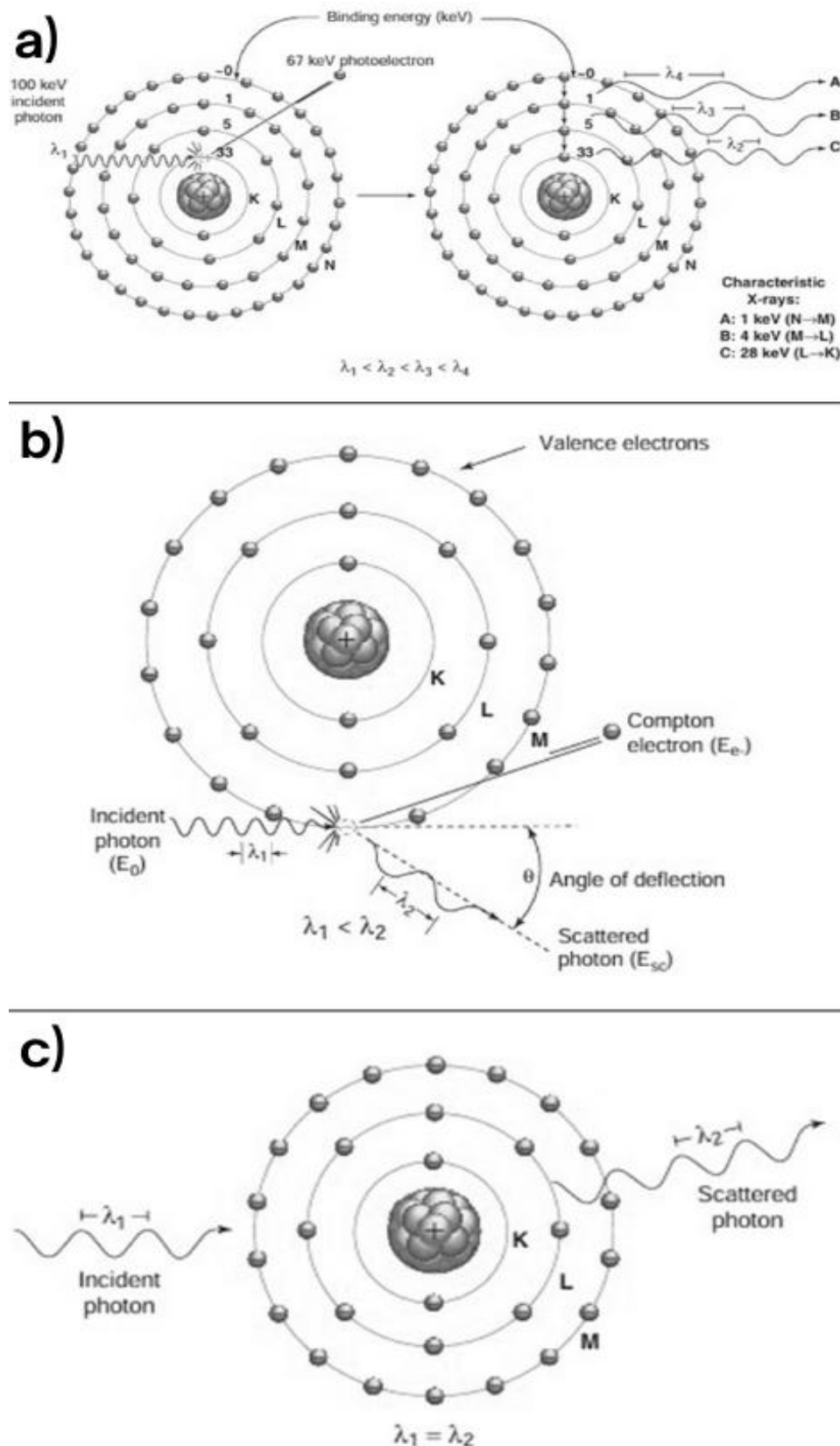
Figure 3.16: Primary X-ray attenuation mechanisms adapted from Bushberg (2013): a) Photoelectric absorption – a high-energy photon ejects a K-shell electron (absorbed), with subsequent electron transitions emitting characteristic X-rays; b) Compton scattering – the incident photon loses energy upon ejecting a loosely bound valence electron, producing a scattered photon at a deflection angle (θ); c) Rayleigh scattering – the photon is elastically scattered without energy loss, maintaining wavelength and directionality.

3.5.3 Scanning, Reconstruction, and Initial Artefact Reduction

Previous studies on peat achieved high resolutions (<20μm) by scanning small sub-samples (1–6cm^3) (Kettridge and Binley, 2008; Quinton *et al.*, 2009; Rezanezhad *et al.*, 2009, 2010; Kettridge and Binley, 2011; Comas *et al.*, 2014; Rezanezhad *et al.*, 2016). However, such resolutions are not feasible for continuous cores due to field-of-view (FOV) and geometric magnification constraints (Figure 3.17). Scanning parameters were therefore optimised to achieve the smallest voxel size with complete sample inclusion.
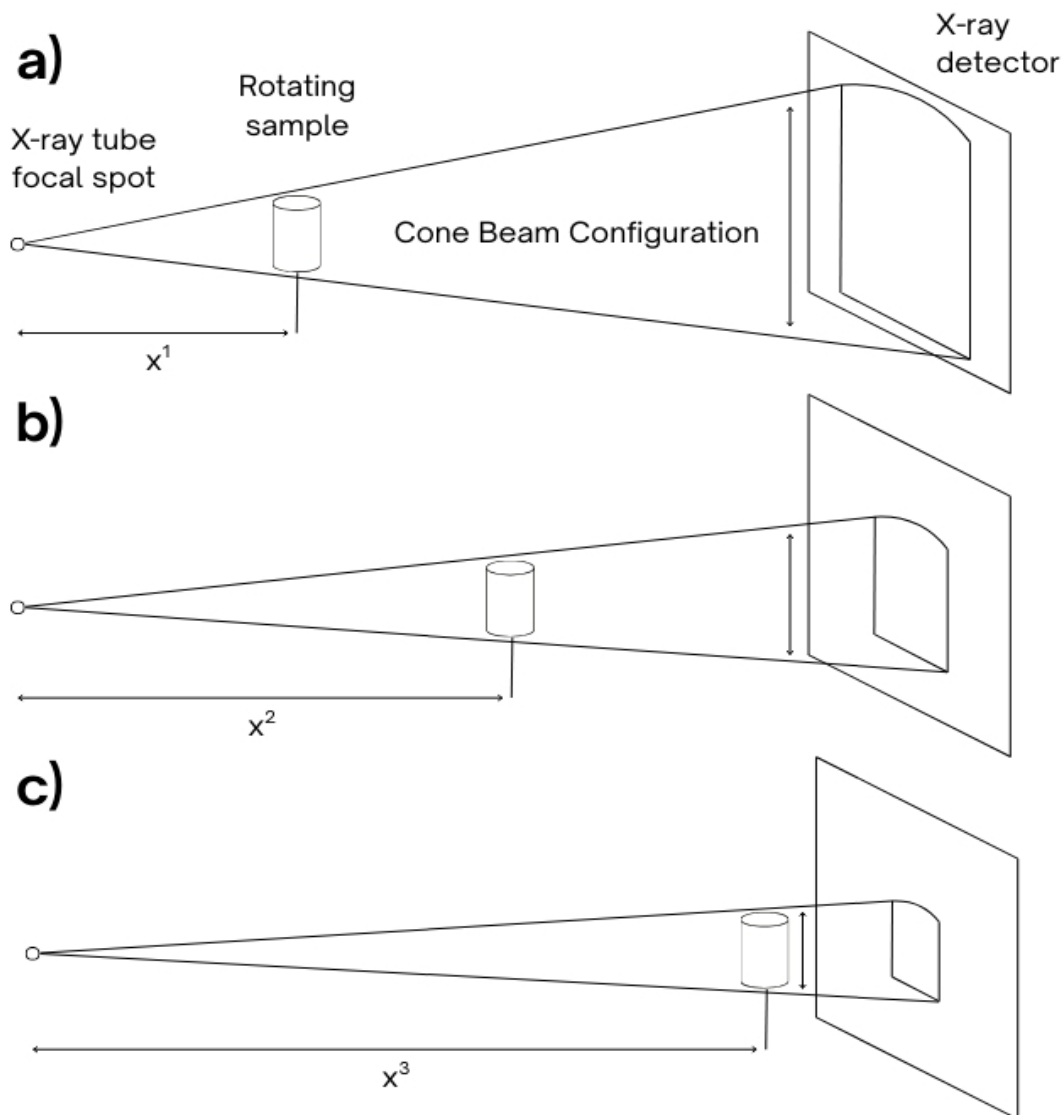
Figure 3.17: Effect of sample position (stage) on FOV and magnification in cone-beam μCT scanning: a) Sample positioned close to the X-ray source increases magnification and resolution, but reduces the FOV; b) Central position provides a balance between resolution and FOV; and c) Sample positioned closer to the detector increases FOV but reduces resolution.

Samples were scanned at the University of Manchester's Henry Moseley National X-ray Computed Tomography facility (NXCT) using the Nikon Xtek 225kV High Flux Bay system (Figure 3.18). The system was equipped with a 225kV static tungsten target (minimum focal spot of 3µm) and a 16-bit, 4096 x 4096 (4k) pixel amorphous silicon flat-panel detector, capable of imaging large volumes in a cone-beam configuration.
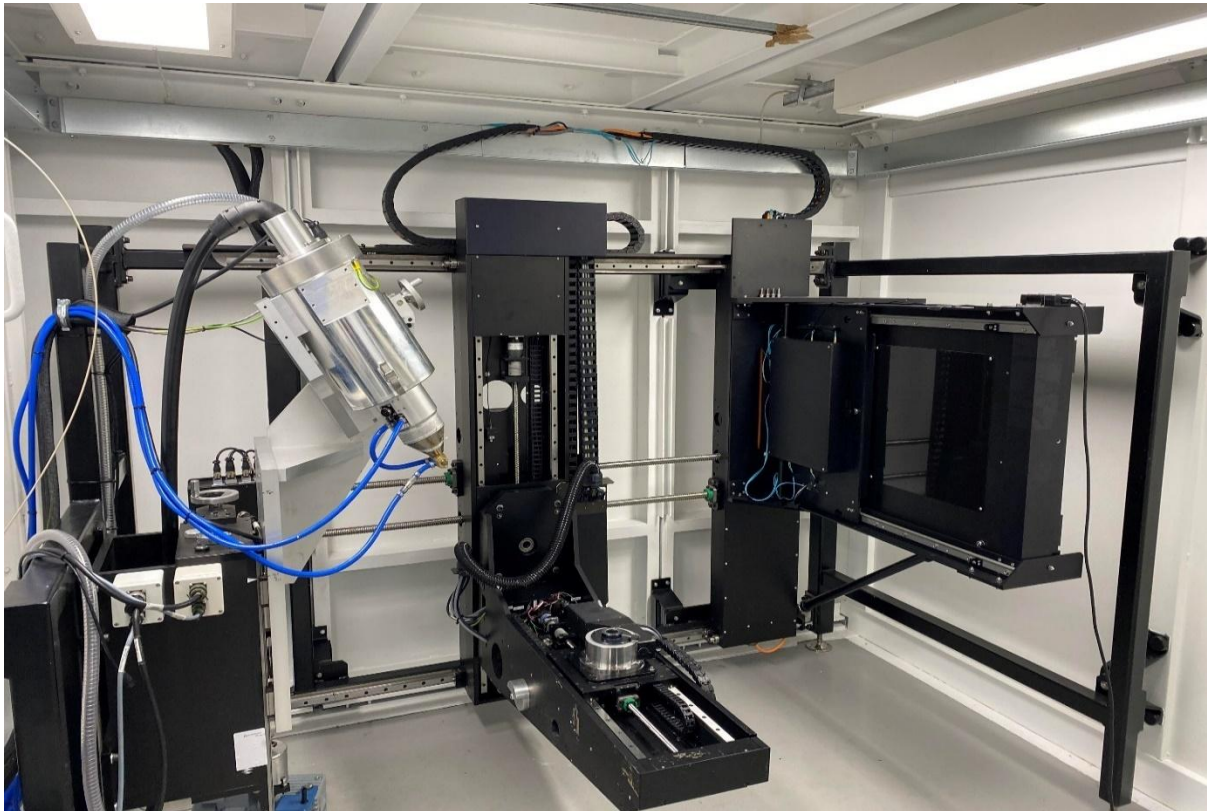
Figure 3.18: University of Manchester's Henry Mosely NXCT Nikon Xtek 225kV High Flux system. Image shows the X-ray source on the left (cone beam), sample stage in the centre, and 4k detector on the right in a walk-in bay.

Consistent scanning parameters were applied to support comparability of attenuated data across cores (Table 3.3). Samples were mounted vertically using a base-lock mechanism (Figure 3.19), with stage settings (rotation, Y-position, zoom, and tilt) adjusted to maintain core inclusion and minimum voxel size. A voxel resolution of 51.11µm was achieved (Table 3.3).

Table 3.3: Nikon Xtek 225kV High Flux Bay scanning and acquisition parameters. Table summarises stage positioning, beam settings, geometric magnification, pixel resolution, and projection acquisition used for core scans.

Scanner: Nikon Xtek 225kV High Flux Bay				
Stage Position		**Optimise Image**		
X	Locked	Binning		x1
Y	420	Digital Correction		x2
Magnification	708	Beam Energy		190
Rotation	360°	Beam Current		100
Tilt	Locked	Resulting Power		19
Imaging	0			
Stage Position Results		**Optimise Image Results**		
Geometric Magnification	1.956	Exposure		1.00fps
		Exposure Time		1.00s
Effective Pixel Size	51.11µm	Gain		30dB
Projection Setup		**Acquisition**		
Num. Projections	3201	~4 hours		
Frames	2			
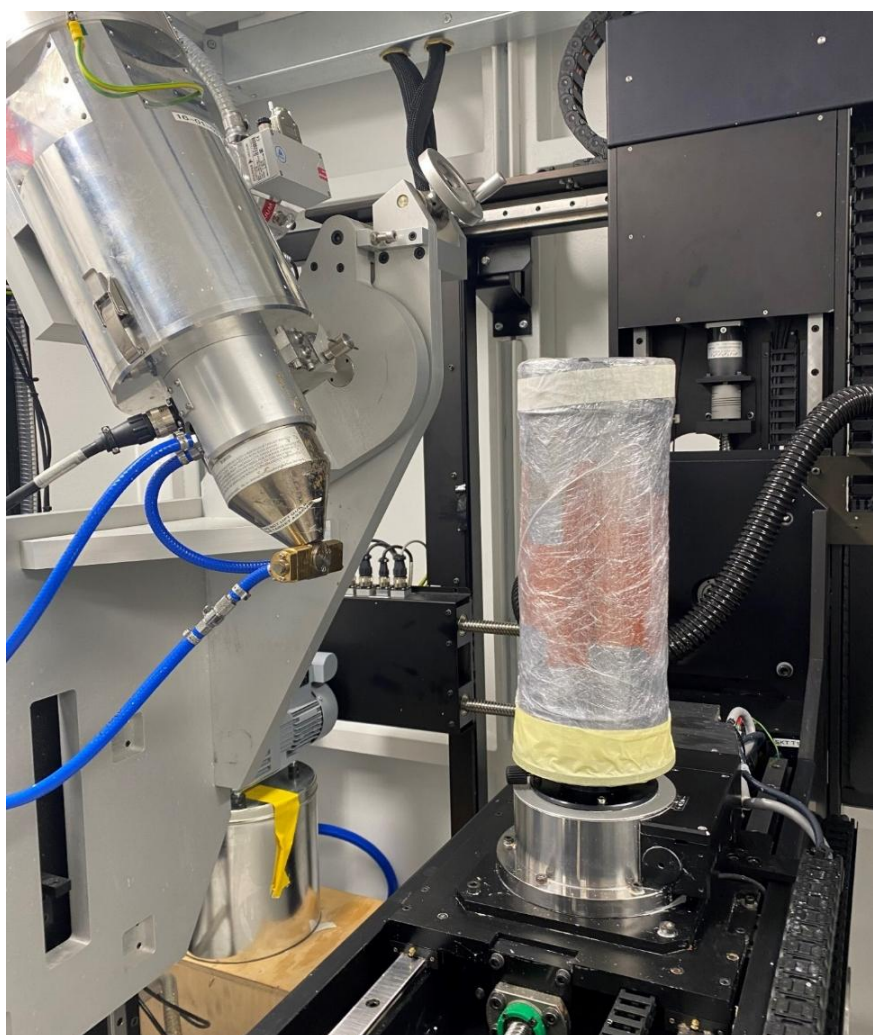
Figure 3.19: Example of a sample vertically mounted and secured on the rotation stage and manipulator within the Nikon Xtek 225 kV High Flux Bay system.

When the High Flux Bay was unavailable, four samples were scanned using the Nikon

XTH 225 and Nikon Custom 450 systems. Both were capable of a grayscale range

between 0–65,535, consistent with the High Flux Bay. However, due to reduced detector

size (2024 x 2024 pixels) and housing (Figure 3.20), FOV and magnification limitations

restricted achievable voxel size to 81.55µm. Scans were rescaled to this resolution during

signal processing to support consistency across cores (Section 3.5.4). Alternative

scanning parameters are provided in Appendix A, and impacts of voxel rescaling are

discussed in Section 3.5.9.

Figure 3.20: Nikon XTH 225 system used for alternative scans. Its smaller housing and reduced detector size limited FOV and geometric magnification.

Raw projections were captured as 16-bit TIFF radiographs showing cumulative X-ray attenuation (Figure 3.21a). These have low internal contrast, with materials appearing dark and void space bright due to detector response. Reconstruction in CTPro3D (Nikon Metrology) used filtered back-projection to generate high-resolution Z-slices (Figure 3.21b), compiled into 3D image stacks (Cnudde and Boone, 2013). This inverts contrast, so bright (high-density) voxels typically indicate organic matter, while dark (low-density) voxels represent air or water-filled porosity (Kettridge and Binley, 2011; Rezanezhad *et al.*, 2016).
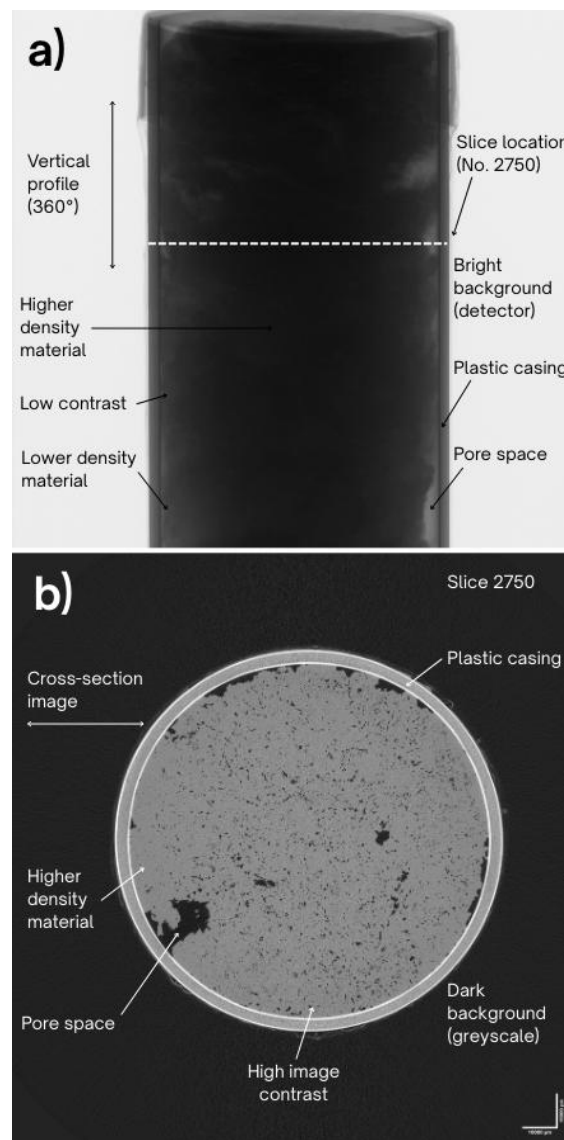
Figure 3.21: Raw TIFF images: a) Raw projection image (vertical profile, 360°) before reconstruction; b) Reconstructed grayscale cross-sectional Z-slice.

Reconstruction parameters are summarised in Table 3.4. Output stacks were saved in TIFF format, preserving greyscale values and metadata required for quantitative analysis (Cnudde and Boone, 2013). Alternative reconstruction parameters are provided in Appendix B for scans using the Nikon XTH 225 and Nikon Custom 450 systems.

Table 3.4: Reconstruction settings used for Nikon Xtek 225kV High Flux Bay scans.

Software: CTPro3D (Filtered Back-Projection Algorithm)			
Centre of Rotation		**Initial Processing**	
Automatic?	Yes	Beam Hardening	Preset 2
Accuracy	High Quality	Scatter Reduction	0
Slice Detection	Dual	Noise Reduction	Preset 1
Outputs:			
Interpolation?		Yes (Linear)	
Attenuation Scaling		0.20 (low) – 99.80 (high)	
Format		TIFF Stack Single	
Processing Time		~4.5 hours	

Raw projections were susceptible to artefacts due to attenuation (absorption and scatter; Section 3.5.2) and trade-offs made to capture the entire sample at minimal voxel size in heterogeneous peat. These artefacts degraded image quality and reduced segmentation accuracy (Cnudde and Boone, 2013). Table 3.5 summarises artefact types, their causes, and the correction strategies applied, while Figure 3.22 provides visual examples.

Table 3.5: μCT imaging artefacts observed, with causes, effects, and applied correction methods.

Artefact	Cause	Effect	Correction Applied (Tables 3.3; 3.4)
Beam hardening	Low-energy photon absorption exaggerates internal contrast gradients.	Central darkening and concave greyscale profiles; reduced contrast and segmentation accuracy (Figure 3.22a).	1) 0.25mm Al filter to pre-harden the beam; 2) CTPro3D Beam Hardening Correction Preset 2
Detector saturation	Excess photon counts from dense features or heavy metals.	Loss of detail in bright regions; risk of exceeding dynamic range (Figure 3.22b).	1) Grayscale range capped below 60,000 counts for stability; 2) Digital gain set to 30dB
Partial-volume effect	Voxel contains more than one material (e.g., peat and air), causing greyscale averaging.	Blurring and smearing at material boundaries (Figure 3.22c).	1) Voxel resolution maximised; 2) Minimum 10-voxel volume filter applied during segmentation (Section 3.5.5)
Image noise	Photon starvation, detector instability, or stochastic variation.	Speckling and poor edge definition; reduced segmentation accuracy (Figure 3.22d).	1) Frame averaging (×2); 2) Noise Reduction Preset 1; 3) Attenuation scaling (0.2–99.8%); 4) Shading correction; 5) Despeckling during signal processing (Section 3.5.4)

Corrections enhanced image clarity, improved contrast between pore space and organic matter, and enabled more reliable thresholding during segmentation (Section 3.5.5). Visual inspection and histogram checks confirmed uniform greyscale profiles across samples. Cnudde and Boone (2013) provide further details on artefacts and correction processes. Artefact correction parameters specific to scans using the Nikon XTH 225 and Nikon Custom 450 systems are provided in Appendix A and B.
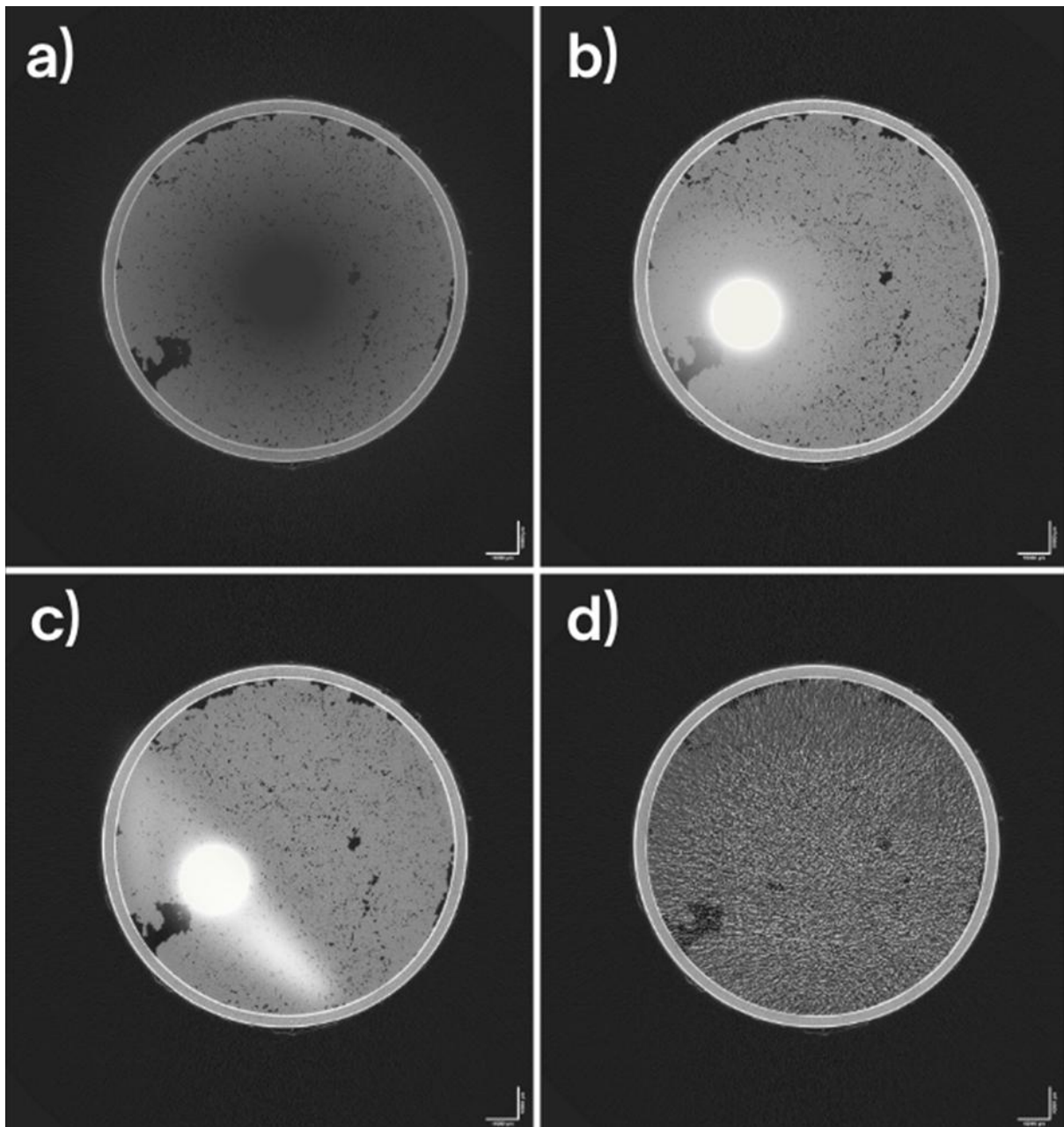
Figure 3.22: Conceptual illustration of common image artefacts during micro-CT scanning and reconstruction: a) Beam hardening – central darkening due to photoelectric absorption; b) Partial volume effect – greyscale distortion at material boundaries from voxel averaging, especially near high-density materials (shown in white); c) Scatter – bright streaking caused by photon deflection (scatter), often around high-density features; d) Image noise – high-frequency speckling unrelated to material structure, caused by electronic interference or photon starvation.

3.5.4 Signal Processing

Figure 3.23 and Table 3.6 summarise the image processing steps applied to prepare stacks for segmentation. Processing was conducted using Fiji's ImageJ software (Schindelin *et al.*, 2012) to reduce artefacts, optimise grayscale contrast, and reduce file size for efficient analysis. These steps were necessary for enabling more accurate segmentation and reliable pore network characterisation across varying scan resolutions.
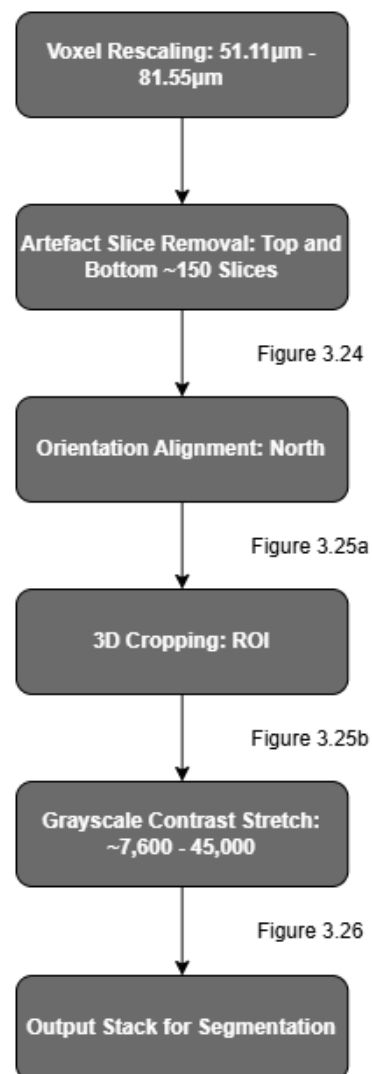
Figure 3.23: Signal processing workflow.

Table 3.6: Signal processing steps applied to image stacks prior to segmentation. Steps were designed to standardise resolution, remove artefacts, align orientation, define ROI, and optimise grayscale contrast, supporting consistent and reliable pore segmentation.

Step	Purpose	Method	Outcome
1) Voxel Rescaling	Standardise voxel resolution across cores due to scanning system differences.	Rescaled 51.11µm scans to 81.55µm using a scale factor of 62.6732%.	Enabled direct comparison and reduced file size by ~30GB, though increased risk of partial volume effects (Section 3.5.3; Table 3.5).
2) Artefact Slice Removal	Eliminate artefacts caused by plastic end caps and stage base.	Removed ~150 slices from the top and bottom due to scatter and beam hardening artefacts (Figure 3.24).	Retained functional core volume (1.22–28.78cm) while avoiding artefact inclusion; reduced file size by ~6GB.
3) Orientation Alignment	Standardise orientation (axial reference) across stacks.	Rotated image stacks to align north using field sampling markers (Figure 3.25a).	Increased consistency for directionally sensitive metrics (e.g., anisotropy).
4) 3D Cropping	Define region of interest (ROI) and support voxel uniformity.	Cropped to square ROI within cylindrical boundary (Figure 3.25b).	Reduced file size by ~5GB; supported compatibility with segmentation and rendering tools requiring cubic voxel areas.
5) Grayscale Contrast Stretch	Enhance grayscale separation of pore and organic phases.	Applied linear contrast stretch to grayscale histogram (~7,600–45,000) (Figure 3.26).	Improved thresholding precision and binarisation consistency across samples.

a) Artefact Slice Removal

Figure 3.24 illustrates the scatter and beam hardening effects found in the top and bottom ~150 slices due to plastic end caps and proximity to the stage base.
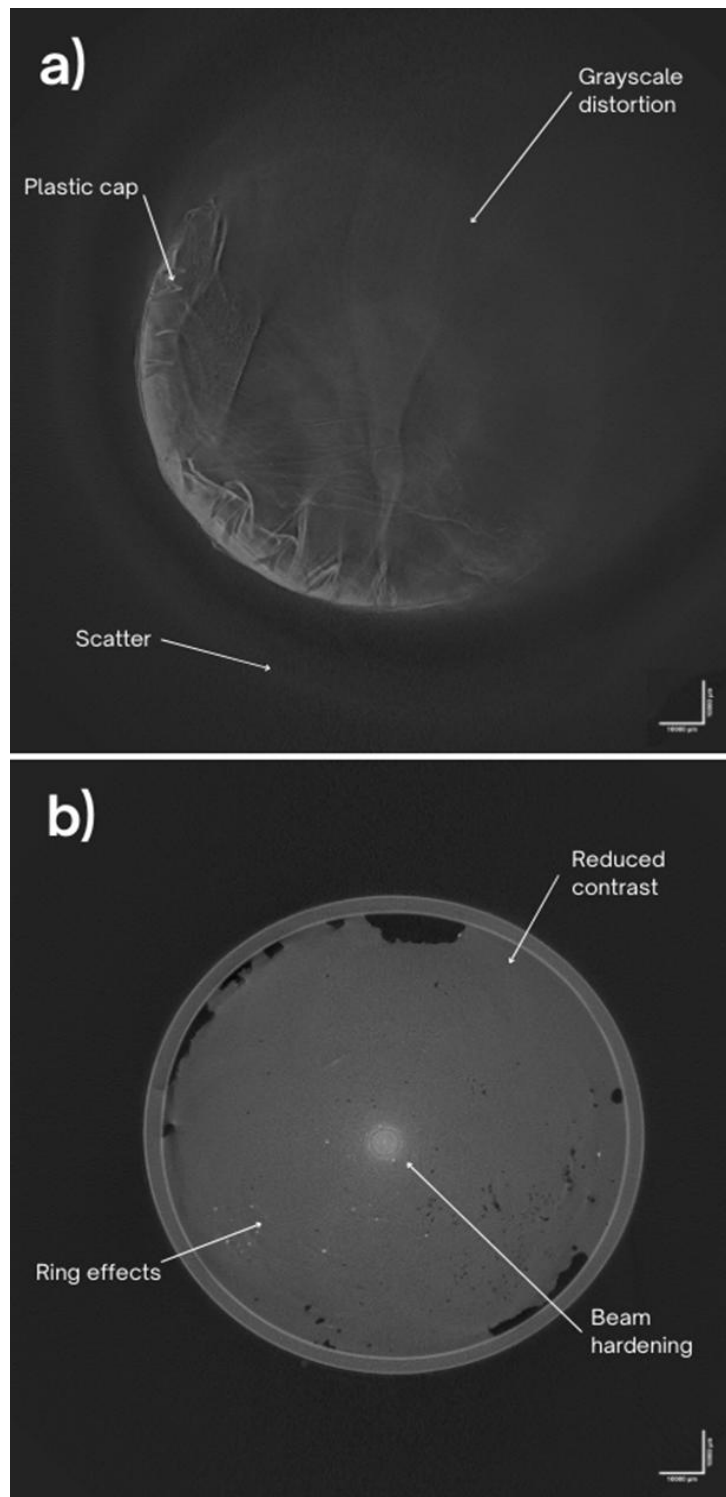
Figure 3.24: End-of-core artefacts: a) Top slices exhibiting structural distortion due to plastic cap and X-ray scatter; b) Bottom slice example affected by beam hardening and stage base proximity.

b) Orientation and Cropping

Figure 3.25a shows stack rotation toward the north using the field marker (plastic button), while Figure 3.25b demonstrates 3D cropping (X, Y, Z plane) to the maximum square ROI.
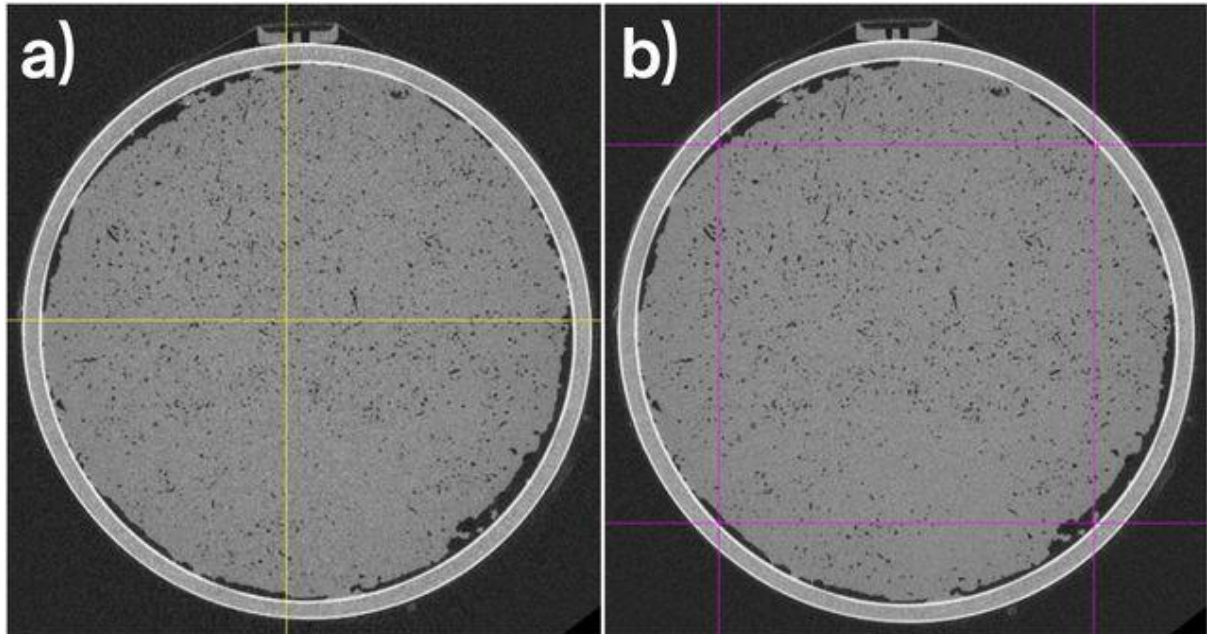
Figure 3.25: Signal processing in ImageJ (Z-slices): a) Sample orientation aligned northward using the field marker (plastic button) to standardise axial reference across image stacks; b) 3D cropping of image stacks to the largest square ROI within the cylindrical core boundary, ensuring compatibility with cubic voxel-based processing.

c) Grayscale Contrast Stretch

Figure 3.26 shows the impact of grayscale contrast stretching, highlighting improved visual and computational separation between dark pore spaces and lighter organics.

A full breakdown of processing steps and adjustments for alternative scan systems is provided in Appendix C.
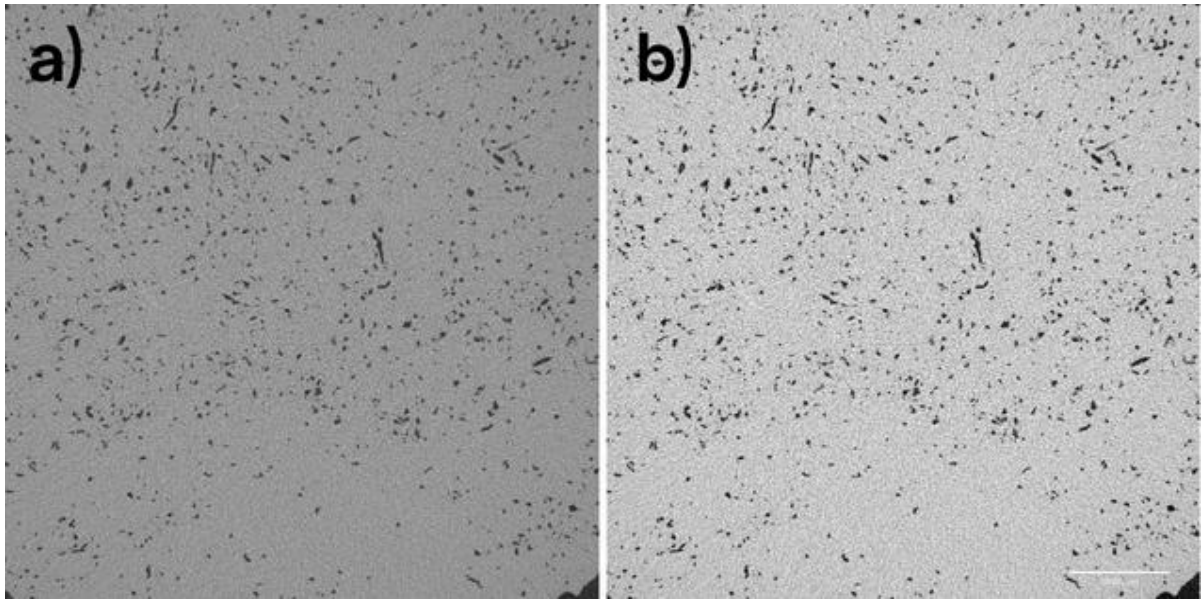
Figure 3.26: Grayscale linear contrast stretch: a) Pre-stretch image showing poor differentiation between pore space and organic matter; b) Post-stretch image (applied ~7600–45000 grayscale range), improving separation of low-density pore (dark) and high-density organic (light) phases.

3.5.5 Segmentation

Segmentation converts grayscale image stacks into binary volumes, distinguishing voids (pore space) from solids (organic matter). As voxel intensity indicates material density, segmentation accuracy determines the reliability of structural metrics such as pore volume, geometry, and connectivity (Cnudde and Boone, 2013). While some inaccuracies are unavoidable, especially partial volume effects in heterogeneous materials (Section 3.5.3), Figure 3.27 and Table 3.7 outline the workflow developed to minimise artefact interference and optimise segmentation accuracy.
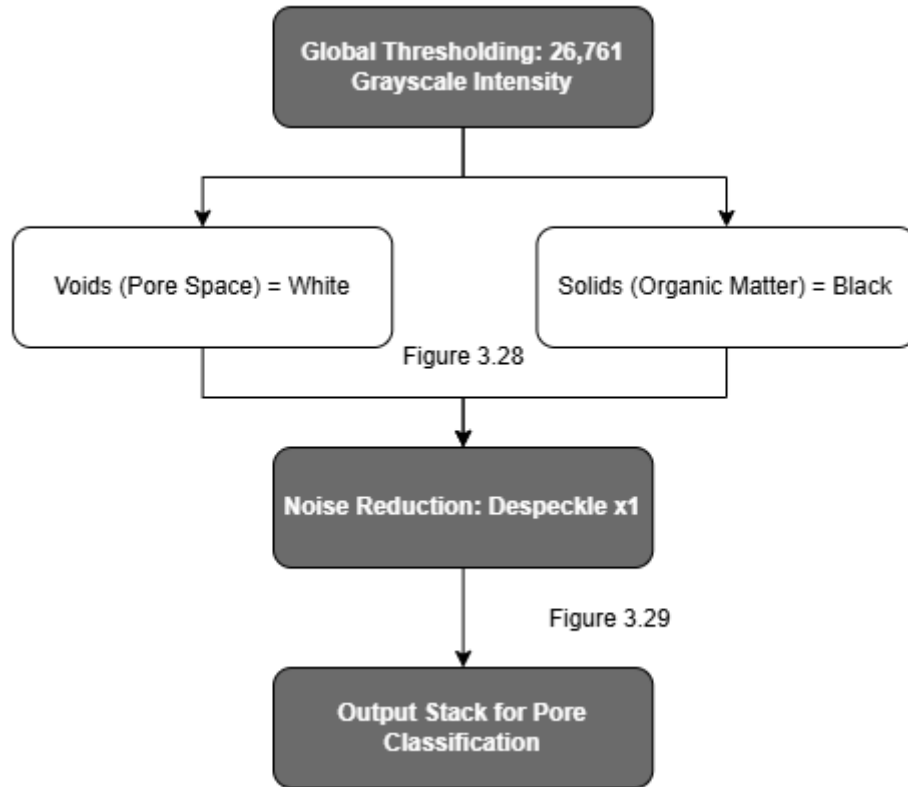
Figure 3.27: Segmentation workflow. Dark grey = process; white = measured/classified parameters.

Table 3.7: Segmentation steps applied to image stacks prior to pore space classification. Steps were designed to enable accurate phase separation and minimise noise interference.

Step	Purpose	Method	Outcome
1) Thresholding	Classify grayscale voxels as pore space (voids) or organic matter (solids).	Global thresholding at intensity 26,741 (out of 45,000) classified <26,741 as voids and >26,741 as soils; manually optimised and visually verified (Figure 3.28).	Consistent binary separation of phases across all samples.
2) Noise Reduction	Remove misclassified single-voxel noise.	Despeckling operation (x1) removed isolated single voxels (Figure 3.29).	Reduced segmentation noise without affecting bulk porosity; improved accuracy.

a) Thresholding

Figure 3.28 shows the binarisation of a contrast-stretched grayscale stack, separating void/pore space (white) from solid/organic matter (black). While machine learning approaches such as Trainable WEKA Segmentation can improve classification accuracy when phases overlap (Arganda-Carreras *et al.*, 2017), they are less suited to large datasets and unnecessary when preprocessing provides clear grayscale separation (Bendle *et al.*, 2015).
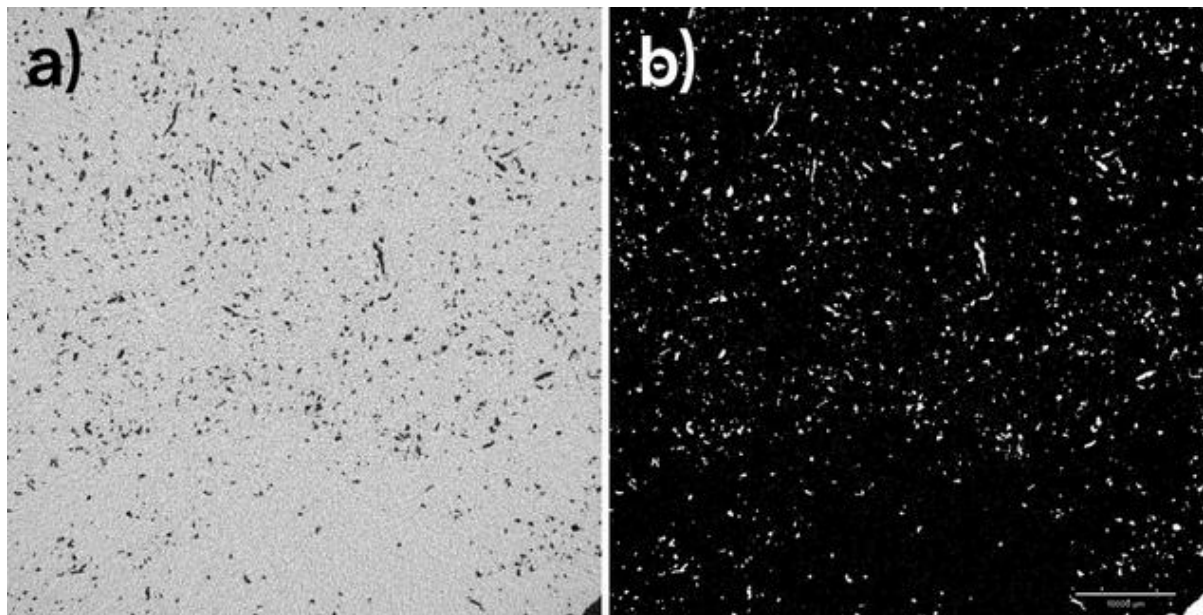
Figure 3.28: Global thresholding: a) Contrast-stretched grayscale image (Figure 3.26b) prior to binarisation; b) Binary volume post-thresholding, with pore/void space = white and organic/solid matter = black.

b) Noise Reduction

Figure 3.29 demonstrates the impact of a single despeckling operation to remove isolated noise voxels. Although some of these may represent actual pores, their limited volume and structural irrelevance warranted exclusion. Volume tests before and after despeckling confirmed negligible impact on bulk porosity.
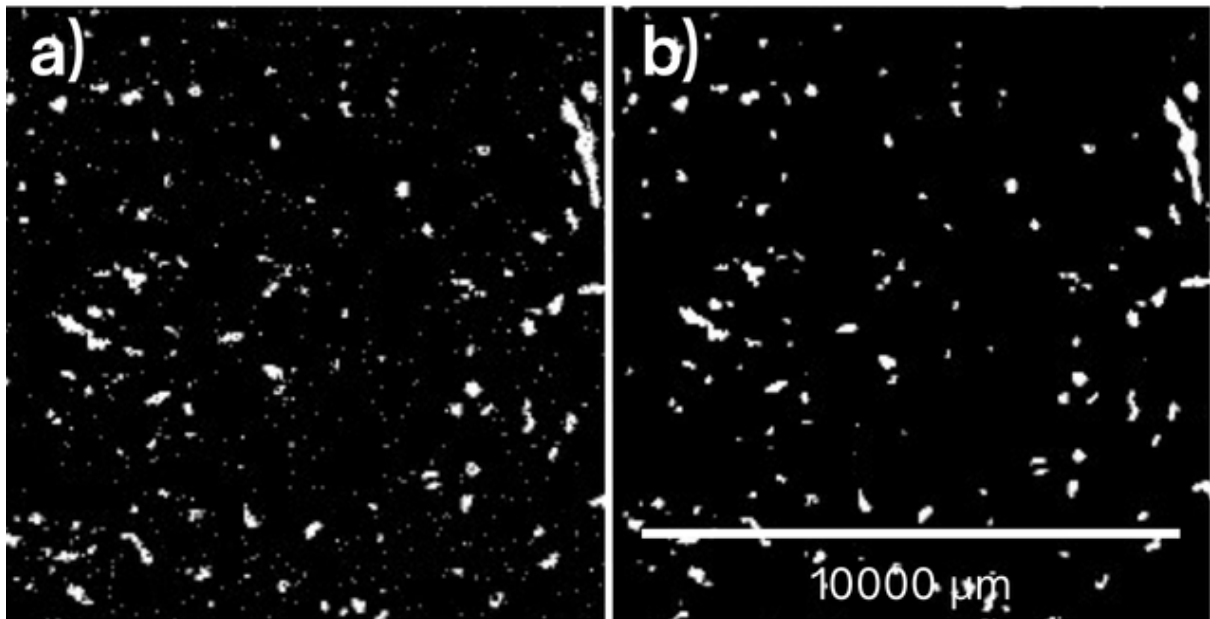
Figure 3.29: Noise reduction using despeckle operation: a) Binary volume before despeckling with isolated noise voxels; b) Post-despeckle output showing cleaner segmentation.

A detailed segmentation workflow, including threshold validation procedures and scan-specific adjustments is provided in Appendix D.

3.5.6 Functional Pore Space Classification and Isolation

Total Pore Space (TPS) was divided into three spatially and functionally distinct types to evaluate sub-surface structure and function: Isolated Porosity (IP); Atmosphere-Connected Porosity (ACP); and Boundary-Connected Porosity (BCP). This builds on early classifications of mobile and immobile porosity (Chapter 2; Section 2.2.3: Quinton *et al.*, 2009; Rezanezhad *et al.*, 2009, 2010, 2016) by introducing spatial connectivity as a basis for functional classification. These classes associate pore structure to surface and sub-surface exchange, water retention, drainage pathways, and carbon accumulation (Chapter 2; Section 2.2.3). Table 3.8 and Figure 3.30 summarise and visualise functional pore space types.

Table 3.8: Functional pore space types, associated function, and method of isolation to enable meaningful sub-surface structure quantification for functional behaviour interpretation.

Pore Space Type	Description	Functional Relevance	Method of Isolation
Isolated Porosity (IP)	Enclosed voids not connected to any image stack boundary or surface.	Structurally inert, limiting water and solute transport – comparable to inactive pore descriptions (Quinton *et al.*, 2009). May indicate trapped gases, particularly within vegetation (e.g., *Sphagnum* hyaline cells) or fibrous, decomposed peat (Kettridge and Binley, 2008).	BoneJ's Exclude Edges function; visually verified.
Atmosphere-Connected Porosity (ACP)	Pores continuously connected to the sample surface (top slice at 1.22cm). Minimum width set to ≥2mm following Rowell (1994).	Surface to sub-surface exchange: Supports surface water infiltration (Holden, 2005b) and direct GHG exchange with the atmosphere. Associated with surface vegetation and saturation, providing a proxy for acrotelm functions.	ImageJ morphological tools: erode–dilate, smoothing, Gaussian filtering; subtraction of surface air layer. Minimum surface connected width of ≥2mm excluded finer pores involved in gaseous exchange; morphological tools smoothed pore geometry (Appendix E). Limitations are considered in data interpretation.
Boundary-Connected Porosity (BCP)	Pores connected to the image stack sides or base (28.78cm), but not the surface (≥2.5cm).	Lateral and vertical sub-surface connectivity beyond sample limits: Supports internal transfers, drainage, and horizon integration (acrotelm-mesotelm-catotelm stratification) and broader site interpretations of restoration effectiveness.	BoneJ Particle Analyser; remaining pores after excluding ACP and IP.
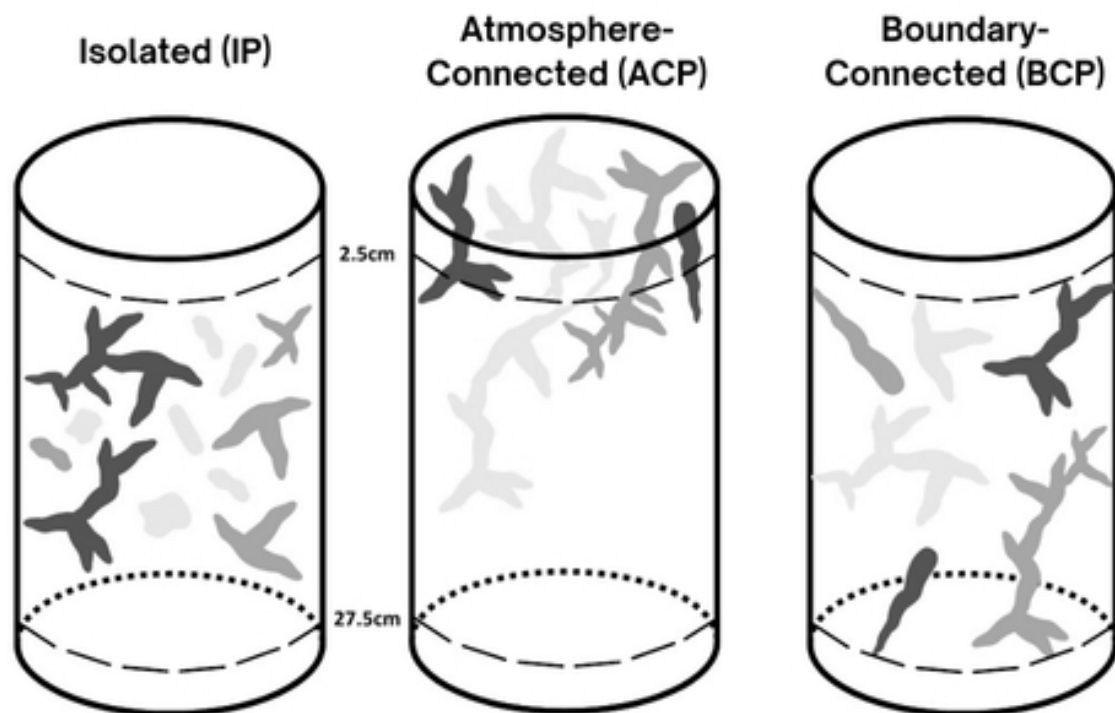
Figure 3.30: Conceptual illustrations of functional pore space types: a) isolated porosity (IP), fully enclosed voids with no boundary contact; b) atmosphere-connected porosity (ACP), pores with a continuous path to the surface; and c) boundary-connected porosity (BCP), pores connected to the base or sides of the sample but not the surface.

Detailed isolation workflows and adjustments for alternative scan systems are provided in Appendix E.

3.5.7 Volume Rendering and Visualisation

3D volume rendering was used to visually verify reconstruction, signal processing, segmentation, and explore pore network structure beyond Z-slices, as seen in the data acquisition workflow (Figure 3.11). Drishti v3.2 (Limaye, 2012) was used due to its compatibility with 16-bit TIFF stacks, support for greyscale and binary datasets, and ability to render high-resolution volumes without compression (Hu *et al.*, 2020).

a) Model Generation and Rendering

TIFF stacks were imported into Drishti Import and converted into cubic voxel volumes (.pvl.nc format). These were rendered in Drishti Render using custom transfer functions to control voxel colour, opacity, and intensity:

- **Greyscale volumes:** Variogram-based segmentation was used to initially isolate bulk phases or artefacts by grayscale intensity (Figure 3.31). Figure 3.32a demonstrates how these can be used to interpret materials and explore datasets.

- **Binary volumes:** Segmented pore networks were rendered as solid structures. Surface shaders enhanced pore boundaries and internal geometry, aiding data interpretation (Figure 3.32b).
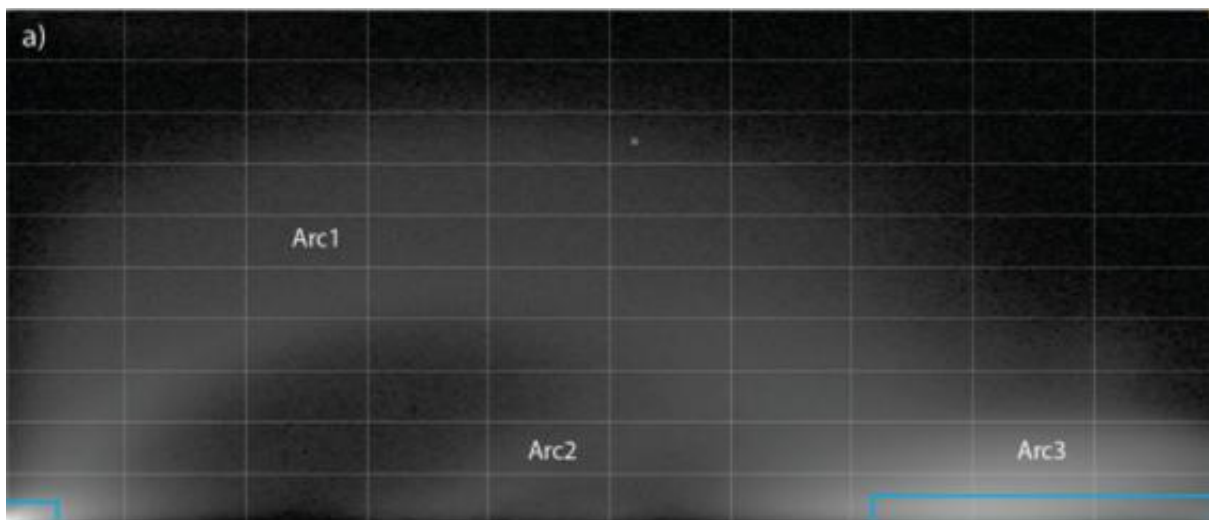
Figure 3.31: Variogram plot of voxel intensity values used in Drishti to guide phase segmentation. Arc 1 = low to medium density (e.g., pore space; air – water filled); Arc 2 = medium to high density (e.g., intact vegetation – decomposed); Arc 3 = high density (e.g., humified peat/heavy metals). Transitional arcs may represent alternative materials or boundary artefacts/partial volume effects. Figure source: Groves (2017).

Rendered binary volumes are used in the results to visualise pore structures across degraded, near-natural, and restored samples. They support structural interpretation and improved transparency by associating quantitative analysis with visual representations.
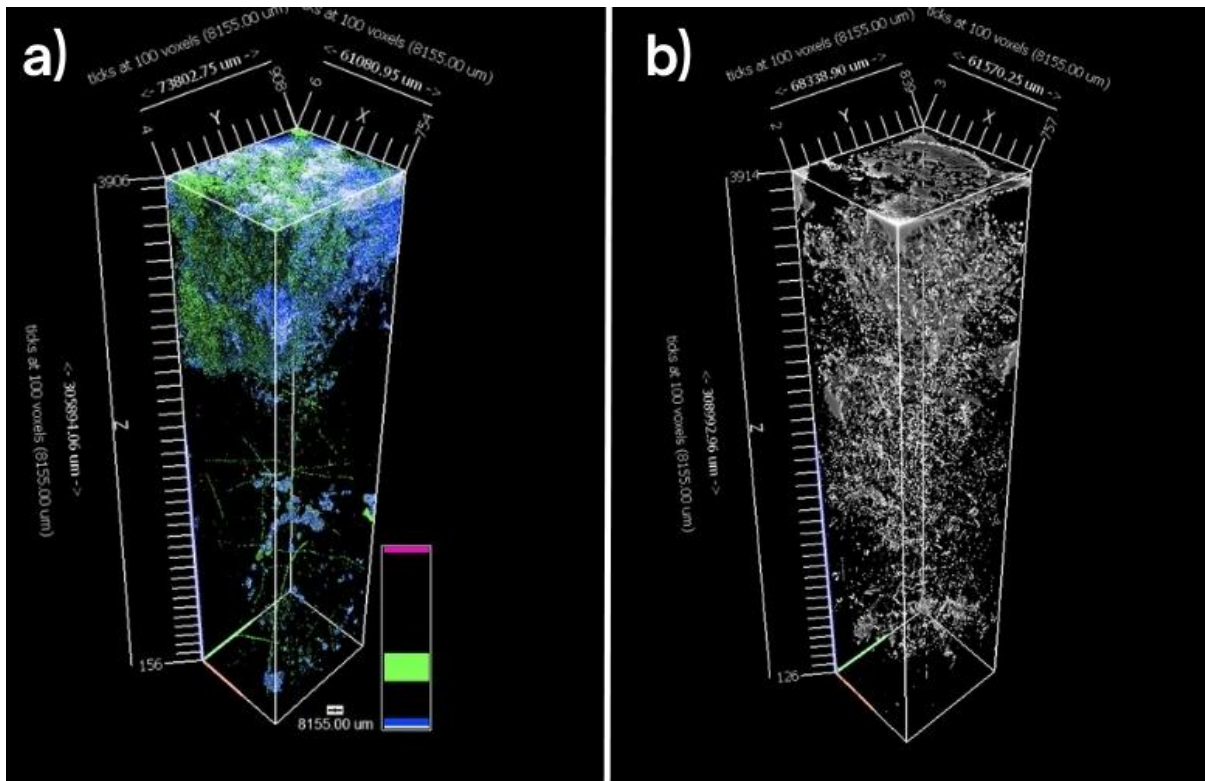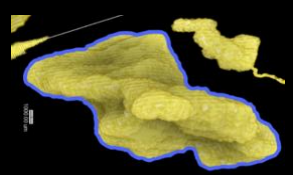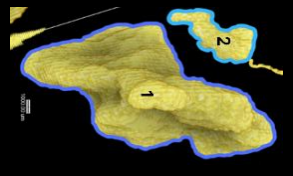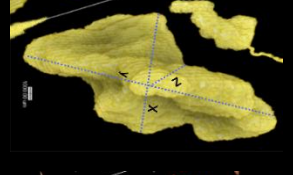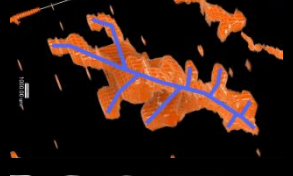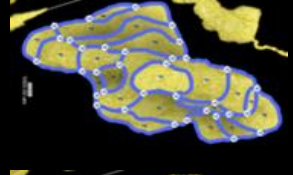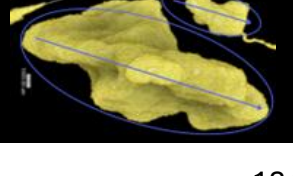
Figure 3.32: 3D volume rendering examples from Drishti: a) Initial greyscale segmentation via variogram-defined intensity thresholds. Interpreted phases: white = air; blue = water; green = vegetation; pink = dense inclusions; black/transparent = peat matrix - Note these are visual approximations used for data exploration, not absolute classifications; b) Segmented binary pore network with surface shading applied to enhance geometry and pore boundary clarity.

3.5.8 Pore Space Data Extraction

Quantitative metrics were extracted from each pore space type (Section 3.5.6; Table 3.8) using BoneJ plugins in ImageJ (Doube *et al.*, 2010). These parameters characterise sub-surface structure in relation to water retention, gas exchange, and carbon storage (Chapter 2; Section 2.2), enabling direct evaluation of functional recovery across restored samples. Data were extracted at 5cm depth intervals (2.5-27.5cm) to support consistency in volume across cores and comparison with field and laboratory datasets (Sections 3.2; 3.4). Table 3.9 details selected metrics.

Table 3.9: Summary of 3D pore network parameters extracted from segmented data for each pore class (TPS, ACP, BCP, IP).

Parameter	Definition/Calculation	Application/Functional Relevance	References	Illustration
Pore Volume (%/µm³)	1) Total bulk porosity as a volume fraction: $$\left(\frac{Total\ Pore\ Volume}{Total\ Sample\ Volume}\right) X\ 100$$ 2) Individual pore volumes.	1) Indicates total storage/transport capacity. 2) Used to derive pore size classes and distribution, distinguishing small retentive versus large conductive pores and identifying dominant volumes.	Cnudde & Boone (2013); Rezanezhad et al. (2016)	
Pore Number (*n*)	Count of discrete pores in each volume.	Indicates network density. Used alongside pore volume in size distribution. High counts of small pores suggest fragmentation; lower counts of larger pores suggest efficient, dominant pathways.	Quinton et al. (2009); Rezanezhad et al. (2009)	
Feret Diameter (µm)	Maximum bounding length in X, Y, Z axes.	Used to classify pore shape via Sneed & Folk ternary diagrams. Shape is a proxy for function: compact = retention/gas bubbles; elongate = flow channels (e.g., root pathways).	Sneed and Folk, (1958); Benn and Ballantyne (1993)	
Branch Number	Count of discrete branches extending from the main body of pores – Uses the Skeletonization feature within BoneJ (Doube et al., 2011).	Used as a metric of complexity (contributing to tortuosity alongside the Euler number). Higher branch numbers indicate more complex structures, potentially increasing retention and promoting diffusive transport, while lower values suggest simpler, more direct flow paths.	Cnudde & Boone (2013); Spencer et al., (2017)	
Euler Characteristic	Topological connectivity (tortuosity) measure of individual pores: $$Objects - (Tunnels + Holes)$$	Lower values imply greater connectivity and continuity of flow paths. Used alongside branch number, Euler number distinguishes between connected and dead-ended paths, informing tortuosity. Useful for inferring permeability and sub-surface drainage.	Doube et al. (2011)	
Anisotropy	Directionality index (0 = isotropic; 1 = highly anisotropic), derived from voxel orientation.	Indicates orientation of pore networks. Higher values suggest directional flow structures (e.g., gully sides); lower values indicate isotropic retention. Important for assessing structural re-profiling and turve placement.	Ketcham (2005); Gharedaghloo et al. (2018)	

These metrics provide a quantitative basis for evaluating pore network structure and function, with interpretation dependent on pore type and depth. For example, high pore volume or connectivity in atmosphere-connected pores near the surface (acrotelm) may suggest efficient water infiltration (Chapter 2; Section 2.2.1; Holden, 2005b), while pores at depth (catotelm) may indicate CH_4 transport through monocot roots (Chapter 2; Section 2.2.2; Moore, 2002). Functional interpretations by pore type and depth are outlined at the start of Chapter 7.

Graphical statistics based on Hoey (2004) were used to interpret pore size distributions, including graphical mean (ϕ), standard deviation, and skewness. The Sneed and Folk (1958) particle shape classification, recommended by Benn and Ballantyne (1993), was used to evaluate pore geometry, providing additional insight into structural function.

3.5.9 Rescaling Effects

Cores scanned at 51.11μm resolution using the Nikon Xtex 225kV High Flux Bay and Nikon Custom 450 systems were rescaled to match the 81.55μm resolutions of scans conducted on the Nikon XTH 225 to support comparability. This processes inevitably resulted in a degree of data loss, particularly in the representation of microporosity. This was tested by comparing the total bulk porosity across three select samples scanned on the Nikon Xtex 225kV High Flux Bay (Table 3.10).

Table 3.10: Total bulk porosity (% of total volume) of Total Pore Space (TPS) across select samples at 51.11μm and 81.11μm scanning resolutions (pre- and post-rescaling).

Resolution	SF_Nat (near-natural target)	BC_LT_2 (Bampton Common – local turving (2))	BC_Deg (degraded baseline)
51.11μm	3.42	3.81	3.04
81.55μm	2.88	3.03	2.73

Signal loss from rescaling averaged ~18% and is visualised in Figure 3.33. However, this study focuses on macroporosity >90µm due to its role in facilitating water and solute transfer (Beven and Germann, 2013), and comparability across samples was essential for evaluating restoration technique effectiveness. Moreover, microporosity can still be inferred from greyscale density values, as all scan acquisition parameters remained consistent (Section 3.4.3).
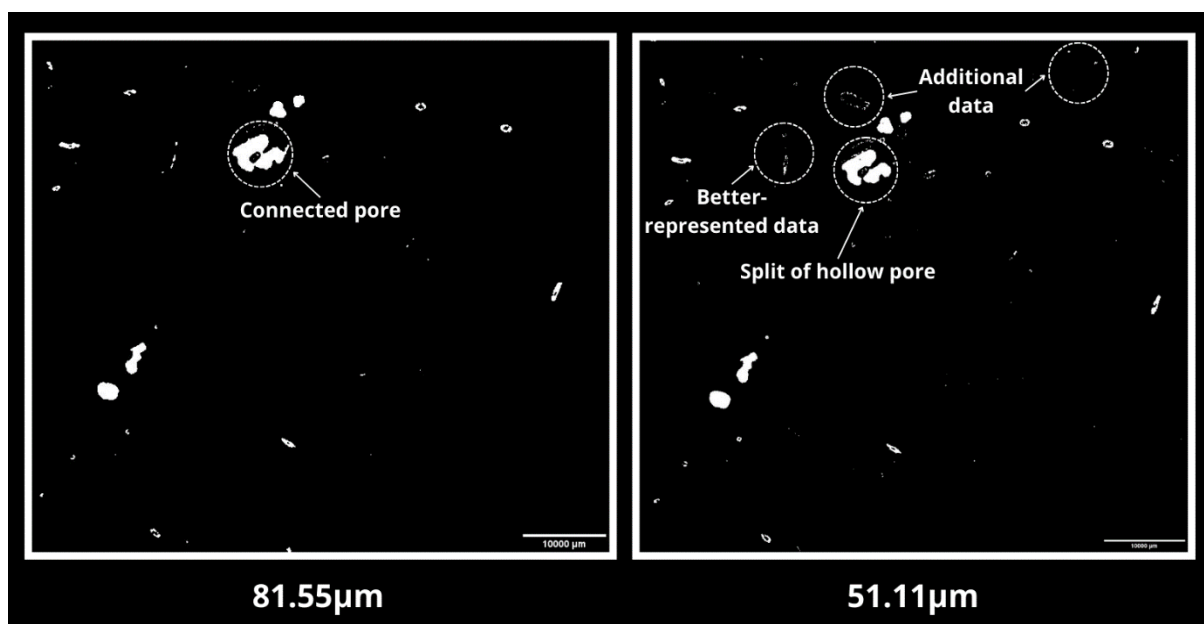
Figure 3.33: Comparison of the same Z-slice from SF_Nat Total Pore Space (TPS). Left shows the re-scaled 81.55µm; right demonstrates the original 51.11µm volume.

3.6 Life Cycle Assessment

Life Cycle Assessment (LCA) was used to quantify the carbon costs of common blanket peatland restoration interventions (Chapter 2; Section 2.5; Thom *et al.*, 2019; NatureScot, 2021), encompassing emissions from raw material production, processing, transport (of materials, machinery, and personnel, including on-site), and installation. The assessment followed ISO 14040/14044 guidelines (ISO, 2006) and adopted a conservative 'cradle-to-site' approach, reflecting the point of delivery and installation of

restoration materials. Carbon costs were calculated in CO_2eq using emissions factors from UK Government conversion datasets, peer-reviewed literature, and LCA databases such as GaBi (BEIS, 2022; IPCC, 2023). Analysis accounted for Scope 1, Scope 2, and Scope 3 emissions, providing a comprehensive estimate of intervention carbon costs (Figure 3.34).

This is the first application of LCA to peatland restoration. The approach enables transparent, replicable evaluation of intervention carbon efficiency, addressing a key limitation in frameworks such as the IUCN UK Peatland Code (Chapter 2; Section 2.7). Considering the complexity and policy relevance of this analysis, full methodological details, assumptions, and a real-world case study are presented in Chapter 8, with outputs now incorporated into the updated IUCN UK Peatland Code Carbon Savings Calculator (Brennand *et al*., 2025; IUCN, 2025a).
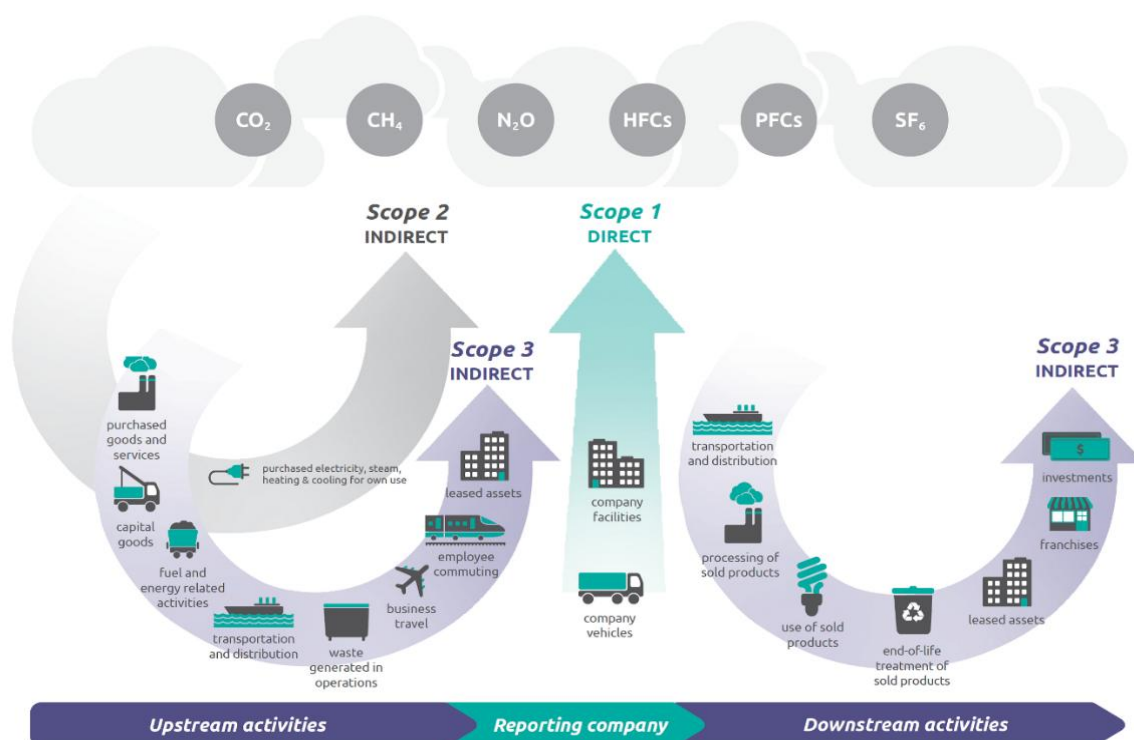
Figure 3.34: Overview of GHG emissions scopes under the Greenhouse Gas Protocol (WRS & WBCSD, 2011). Scope 1 refers to direct emissions from owned or controlled sources; Scope 2 includes indirect emissions from the generation of purchased energy; Scope 3 covers all other indirect emissions across the value chain, including upstream and downstream activities (e.g., transport, procurement, and waste).

3.7 Chapter Synthesis and Discussion

A multi-method framework was adopted to evaluate blanket peatland restoration against functional baselines. Surface condition assessment (covered in the next chapter), sub-surface bulk and chemical analyses, µCT, and LCA were used to *assess structural recovery, functional behaviour, and carbon efficiency*, directly addressing the research questions and knowledge gaps outlined in Chapter 2.

Sub-surface function was quantified using indicators including pH (acidity), Eh (anoxia), temperature (microbial activity), bulk density (compaction), moisture content (saturation), organic carbon (carbon store), and Von-Post humification (decomposition). *These metrics were selected for their interpretability, cost-effectiveness, and suitability as proxies for structure*. They also help contextualise µCT outputs within existing monitoring frameworks.

µCT enables characterisation of total macroporosity, inferred microporosity (alongside Von-Post humification), and pore network properties including volume, size, shape, complexity, connectivity, and anisotropy *associated with functional behaviour*. Pores were classified as atmosphere-connected (ACP), boundary-connected (BCP), or isolated (IP), *indicating their roles in retention, drainage, and gas exchange*. Degraded cores served as baselines, while near-natural cores provided functional targets.

LCA quantified the carbon costs of interventions, including emissions from materials, machinery, and installation (Chapter 8). *These data support assessment of net carbon benefit and inform the IUCN UK Peatland Code's carbon accounting framework*.

Considering the complexity of methods adopted, identifying representative degraded (baseline), near-natural (target), and restored sites was critical. This required a bespoke approach, incorporating geospatial analysis, ground-truthing, and condition assessment, particularly challenging across large, heterogeneous landscapes.

Chapter 4: Site Selection and Representative Sampling

A multi-method approach combining established techniques with intensive µCT imaging (Chapter 3; Section 3.1) of sub-surface structure requires a strategic sampling framework to support representative samples. In particular, data from degraded and near-natural baselines (Chapter 2; Section 2.2.4) are required to contextualise recovery trajectories, while restored sites need to cover varying techniques and timescales to address the research questions and evaluate restoration effectiveness.

However, identifying representative sampling points in blanket peatlands is challenging due to their size, heterogeneity, and fine-scale variation (Chapter 1; Section 1.1; Chapter 3; Section 3.1). Microtopographic differences at the sub-meter scale (e.g., hummocks and hollows) can influence carbon dynamics (Chapter 2; Section 2.2.1), and spatial variability is often greater in restored environments (Cunliffe *et al.*, 2013; Parry *et al.*, 2014; Young *et al.*, 2017). Previous studies have overlooked this, applying random (Parry *et al.*, 2014; Alshehri *et al.*, 2020; Howson *et al.*, 2023) or transect-based sampling (Green *et al.*, 2017; Holden *et al.*, 2017; Young *et al.*, 2017). Instead, 'spatially balanced' approaches are recommended to better capture landscape heterogeneity and meet research objectives (Kermorvant *et al.*, 2019; Mastrantonis *et al.*, 2024).

Additional logistical constraints, such as site remoteness, uneven terrain, and access, further complicated undisturbed sampling (Chapter 3; Section 3.3; Carr *et al.*, 2020). Fieldwork was restricted to springtime to avoid nesting birds (Thom *et al.*, 2019; NatureScot, 2021) and align with optimal ecological survey conditions (JNCC, 2009).

Game management also imposed seasonal access restrictions on occasion. A bespoke, pragmatic framework was therefore developed, drawing on principles of 'spatially balanced' sampling. This approach aimed to support comparability and representativeness across degraded, near-natural, and restored sites. The specific objectives were to:

1. **Develop a reproducible sampling strategy for large, heterogenous landscapes:** Considering the limited number of samples for μCT due to its intensity (n = 15), the approach prioritised representativeness over statistical meaningfulness.

2. **Support sample representativeness despite low sample population:** Control cores represented well-characterised degraded or near-natural conditions, while restored sites were selected to capture key techniques and timescales. Site choice was informed by spatial data, ground-truthing, and field reconnaissance.

3. **Optimise comparability across site types:** Within each survey area, restored cores were taken from locations considered examples of 'successful' intervention, avoiding known failures. Control sites were selected to maximise contrast with restored cores while remaining comparable.

Site selection followed the *Common Standards Monitoring Guidance (CSM) for Upland Habitats: Blanket Bogs* (JNCC, 2009), supporting the extraction of cores from representative areas of their respective states (degraded, restored, or near-natural).

4.1 Region Selection

Approximately 70-90% of England's blanket peat is in the North (Figure 4.1), primarily in the Pennines (~30%, 100,000 ha), Yorkshire (~27%, 93,000 ha), and Cumbria (~13%, 31,000 ha) (IUCN, 2018; Natural England, 2025). They persist due to relatively warm (8.5–

10.6°C) and wet (≥1000mm annual rainfall) maritime conditions, with ≥160 days of rainfall (≥1mm) annually (Cfb and Cfc zones; Beck *et al.*, 2018). Approximately 90% of these blanket peatlands have undergone anthropogenic degradation (Chapter 2; Section 2.4.1; Table 2.2; Artz *et al.*, 2019), prompting large-scale restoration initiatives, including the Great North Bog project (North Pennines National Landscape, 2024).

Figure 4.1: Distribution of blanket bogs in England based on Natural England's 2016 Priority Habitat data. Dataset includes Sites of Special Scientific Interest (SSSI) designations, condition assessment areas, Environmental Stewardship (ES) and Countryside Stewardship (CS) management options, and Living England classifications for blanket bogs (excluding deciduous woodland).

4.1.1 Regional Breakdown

To support comparable and representative site selection while meeting the study's objectives: 1) assessing undisturbed samples; 2) adhering to standard definitions; and 3) maintaining logistical feasibility, the following criteria were applied to refine the sample area:

1. **H7130 Blanket bog designation:** Sites had to be classified under the EU Habitats Directive (Annex I), with National Vegetation Classifications (NVC) types including one or more of the following:

    a. **M17** *Scirpus cespitosus – Eriophorum vaginatum* blanket mire.

    b. **M18** *Erica tetralix – Sphagnum papillosum* raised and blanket mire.

    c. **M19** *Calluna vulgaris – Eriophorum vaginatum* blanket mire.

    d. **M20** *Eriophorum vaginatum* blanket and raised mire.

    e. **M25** *Molinia caerulea – Potentilla erecta* mire.

This supported vegetation consistency across selected sites (JNCC, 2009).

2. **Peat depth >30cm:** Aligning with England's minimum threshold for deep peat (Chapter 2; Section 2.4.2; Lindsay, 2010).

3. **Proximity to research facilities:** Sites had to be within a two-hour travel time (by train or car) from the National X-ray Computed Tomography facility (NXCT) in Manchester and research base in Ambleside, Cumbria, minimising disturbance during transport and reducing decomposition risk.

4. **Altitude >249m:** Meeting the upland classification for England (Natural England, 2001).

Natural England's Priority Habitats Inventory – Blanket Bogs (2022) dataset was used in QGIS to identify designated H7130 blanket bogs (Criterion 1) (Natural England, 2022). Peat depth data from the Peaty Soils Locations database was applied to isolate areas >30cm depth (Criterion 2) (Natural England, 2016). A two-hour travel zone from NXCT Manchester and Ambleside was overlaid (Criterion 3), reducing the potential sampling area to ~93,000 ha (Figure 4.2a). Sites meeting altitude Criterion 4 (>249m) were identified using the Ordnance Survey Terrain 50m DTM (2019) from OS Digimap within the regional-scale scoping area, refining the sampling area to ~87,000 ha (Figure 4.2b).
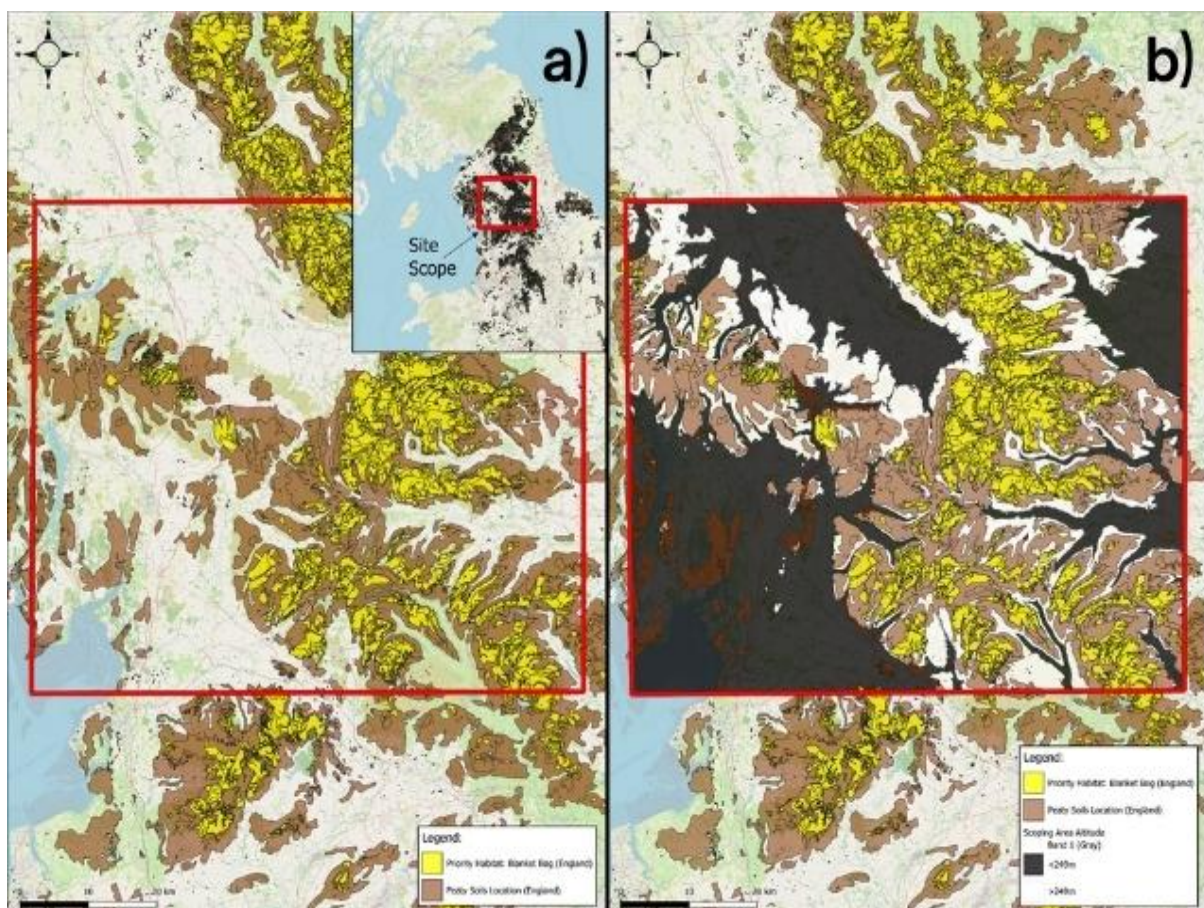
Figure 4.2: Site scope and altitude: a) Peaty Soil Locations (Natural England, 2016) and Priority Habitats Inventory – Blanket Bogs (Natural England, 2022) in northern England. Red box delineates the two-hour travel zone from NXCT Manchester and Ambleside, Cumbria, used to refine site selection (scoping area). Priority habitats include SSSI designations, condition assessment areas, ES and CS management options, and Living England classifications for blanket bogs (excluding deciduous woodland); b) Upland (>300m) peaty soils (Natural England, 2016) and Priority Habitats Inventory – Blanket Bogs (Natural England, 2022) in Northwest England. Red box outlines the site scoping area. Dark gray areas represent land below the 300m upland threshold, while white areas meet the upland criteria. Elevation data is sourced from Ordnance Survey Terrain 50m DTM (2019).

4.2 Project Site Selection

Although ~87,000 ha of blanket peatland met the regional filtering criteria, further refinement was required to identify restoration project sites suitable for sub-sampling of restored, degraded, and near-natural peat. A stratified systematic sampling approach was adopted to support representative distribution of restoration ages and techniques.

An initial pool of sites was compiled based on restoration project tenders issued between 2010 and 2022. Sites were filtered through a multi-stage processes, considering restoration age, technique, data availability, accessibility, and logical feasibility. Considering the objective to extract undisturbed cores, proximity to access routes and terrain suitability were critical. In addition, permissions for access and sample extraction were essential due to designation status and land use. Permission restrictions formed the final filtering criterion (Table 4.1).

Table 4.1: Site selection process and filtering criteria used to refine the initial pool of restoration projects.

Selection Stage	Filtering Criteria	Sites
Initial Pool	Invitations to tender (2010 – 2022)	Flow Moss, Grimwith Moor, **Borrowdale Head**, East Arkengarthdale, Stags Fell, Birkdale, Mungrisdale, Mossdale, Whatshaw Common, Fleet Moss, Gouthwaite, Heathfield, Ramsgill, Raydale, West Arkengarthdale, Kidbeck Moss, Croglin Fell, Matterdale Common, Tebay Common, **Bampton Common**, Allerdale, Vance Lodge, Bowes Moor, Eycott Hill, Melbecks Moor, **Shap Fells**, Martindale Common, **Stake Moss**
Temporal Classification	Old (~7-10 years)	Flow Moss, Grimwith Moor, **Borrowdale Head**, East Arkengarthdale, Stags Fell
	Intermediate (~4-7 years)	Birkdale, Mungrisdale, Mossdale, Whatshaw Common, Fleet Moss, Gouthwaite, Heathfield, Ramsgill, Raydale, West Arkengarthdale, Kidbeck Moss, Croglin Fell, Matterdale Common, Tebay Common, **Bampton Common**, Allerdale, Vance Lodge
	Young (~1-4 years)	Bowes Moor, Eycott Hill, Melbecks Moor, **Shap Fells**, Martindale Common, **Stake Moss**
Restoration Approach	Local materials used (e.g., peat)	Grimwith Moor, **Borrowdale Head**, East Arkengarthdale, Birkdale, Mungrisdale, Mossdale, Whatshaw Common, Ramsgill, West Arkengarthdale, Kidbeck Moss, Tebay Common, **Bampton Common**, Allderdale, **Shap Fells**, Martindale Common
	Exotic materials used (e.g., coir, stone)	Flow Moss, Stags Fell, Fleet Moss, Gouthwaite, Heathfield, Raydale, Croglin Fell, Matterdale Common, Vance Lodge, Bowes Moor, Eycott Hill, Melbecks Moor, **Stake Moss**
Data Quality	Geospatially referenced shapefiles	**Borrowdale Head**, Stags Fell, Birkdale, Mossdale, Fleet Moss, Gouthwaite, Heathfield, Ramsgill, Raydale, West Arkengarthdale, Matterdale Common, Tebay Common, **Bampton Common**, Vance Lodge, Bowes Moor, **Shap Fells**, Martindale Common, **Stake Moss**
Accessibility	Geospatially referenced access or viable access from remote sensing analysis	**Borrowdale Head**, Fleet Moss, Gouthwaite, Heathfield, **Bampton Common, Shap Fells, Stake Moss**
Logistical Feasibility	≤5km from an access road	**Borrowdale Head**, Fleet Moss, Gouthwaite, Heathfield, **Bampton Common, Shap Fells, Stake Moss**
Permissions Granted	Landowner permissions possible	**Borrowdale Head, Bampton Common, Shap Fells, Stake Moss**

Four sites met the criteria and were selected for further evaluation: Borrowdale Head or 'Borrowdale' (BW), Bampton Common (BC), Shap Fells (SF), and Stake Moss (SM) (Table 4.2). Figure 4.3 provides a geospatial representation of selected sites.

Table 4.2: Summary of final restoration project sites meeting selection criteria.

Site Name/ Code	Age	Restoration Techniques	Peat Depth (cm)	Altitude (m)	Access Route	Road Dist. (km)
Borrowdale (BW)	Old (~10 years)	Local: Reduced grazing, gully & hag reprofiling, local turving	>50cm – Deep Peat	~525	OS Footpath	~3.1
Bampton Common (BC)	Intermediate (~5 years)	Local: Reduced grazing, gully & hag reprofiling, local and imported turving, peat/mineral dams, peat bunds	>50cm – Deep Peat	~575	OS Footpath	~4
Shap Fells (SF)	Young (~2 years)	Local: Grazing exclusion, gully & hag reprofiling, local and imported turving, peat dams, peat bunds	>50cm – Deep Peat	~475	Machinery Access Route	~4.4-4.8
Stake Moss (SM)	Young (~2 years)	Exotic: Gully & hag reprofiling, heather brash spread, coir logs, stone/timber dams, peat bunds, plug planting, lime application	>50cm – Deep Peat	~450	Local Road	~1
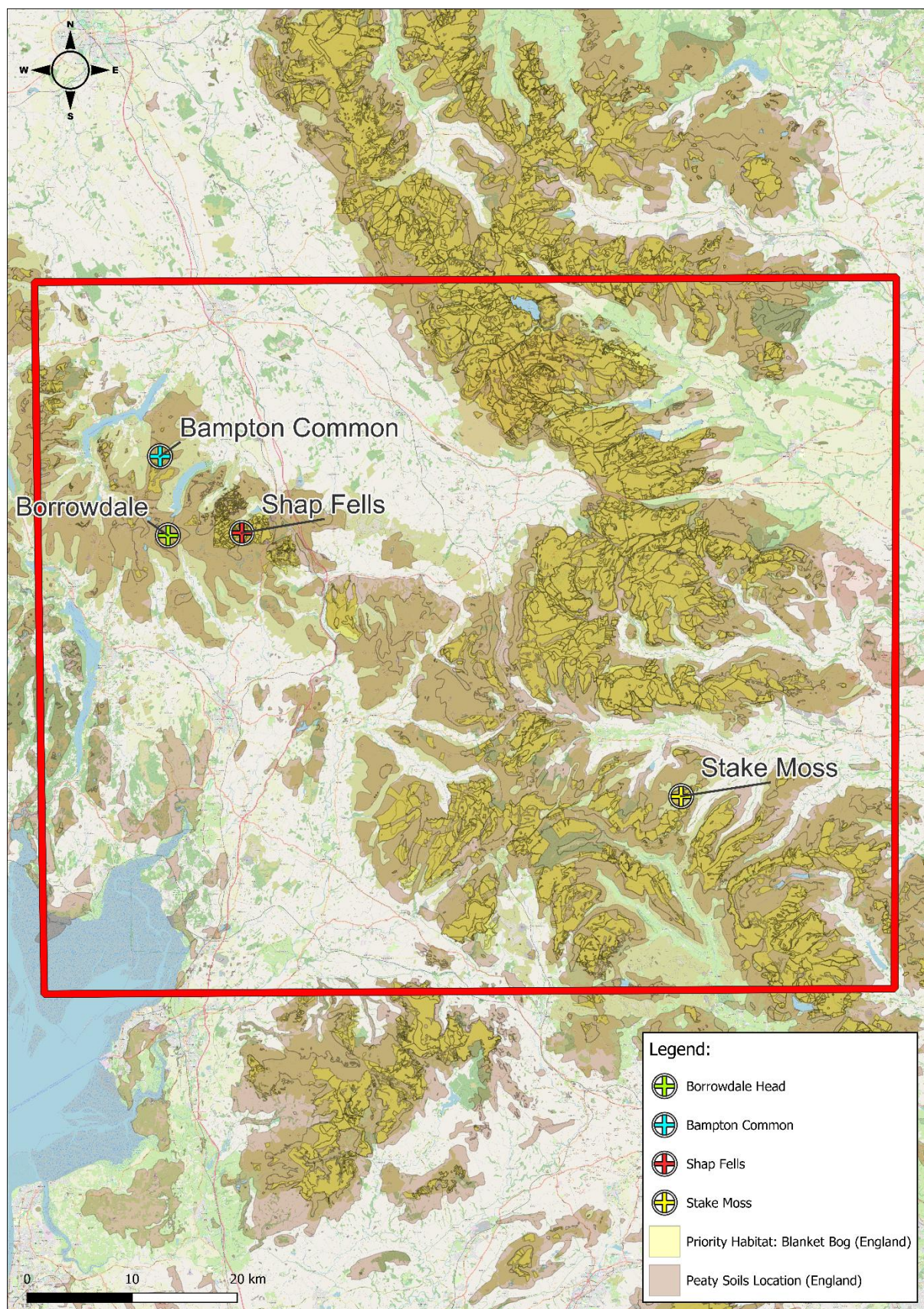
Figure 4.3: Geospatial distribution of selected restoration sites (Table 4.2) based on relevant selection criteria.

4.2.1 Selected Site Descriptions

Selected sites represent a sufficient range of restoration approaches, conditions, and timescales since intervention. Table 4.3 summarises key geological, ecological, and conservation attributes of each site, demonstrating comparability based on selection criteria (Table 4.1). Figure 4.4 provide a geospatial map of each site.

Table 4.3: Summary of site attributes for the four selected restoration projects.

Attribute	Borrowdale (BW)	Bampton Common (BC)	Shap Fells (SF)	Stake Moss (SM)
Location	Borrowdale, East Lake District (NY 52117 05154)	High Street, East Lake District (NY 46152 16511)	High Street, East Lake District (NY 51951 08767)	Yorkshire Dales National Park (SD 93567 82373)
Total Area (ha)	≥800	≥2,580	≥7,700	≥313
Altitude Range (m)	400–650	200–800	300–650	350–500
Deep Peat Coverage (ha)	~173 (325–475m)	~550 (450–675m)	~1,300 (400–650m)	~256 (375–500m)
Peatland Type	Blanket bog (H7130)	Degraded/modified blanket bog (H7130)	Blanket bog (H7130), wet/dry heath (H4030)	Modified blanket bog (H7130), calcareous grassland
Designation	County Wildlife Site	RSPB Reserve; Drinking Water Protected Area	SSSI; SAC; Drinking Water Protected Area	Yorkshire Dales National Park
Catchment	River Kent (SSSI, SAC)	Environment Agency (EA) – Drinking Water	EA – Drinking Water	Groundwater protection zone
Geology	Andesite, dacite	Andesite, dacite	Andesite; granite outcrop (excluded)	Millstone grit; sandstone
Primary Degradation	Overgrazing; drainage	Overgrazing; drainage; local peat cutting	Gripping; local peat cutting; overgrazing	Gripping; overgrazing
Restoration Area (ha)	~1.27	~220	~340	~166
Restoration Years	2011 (~10 years)	2017–2018 (~5 years)	2013 initial; 2020–2022 (~2 years)	2018–2021 (~2 years)
Restoration Technique	Local: reprofiling, turving, grazing reduction	Local: reprofiling, turving, bunds, bare peat stabilisation	Local: reprofiling, turving, bunds, stabilisation, herbivore exclusion	Exotic: reprofiling, heather brash, coir, dams, lime, planting
Objectives	Stabilise peat; reduce runoff; flood mitigation	Reduce carbon loss; stabilise peat; improve retention	Reduce carbon loss; improve water quality; stabilise peat	Reduce carbon loss; limit erosion; support biodiversity
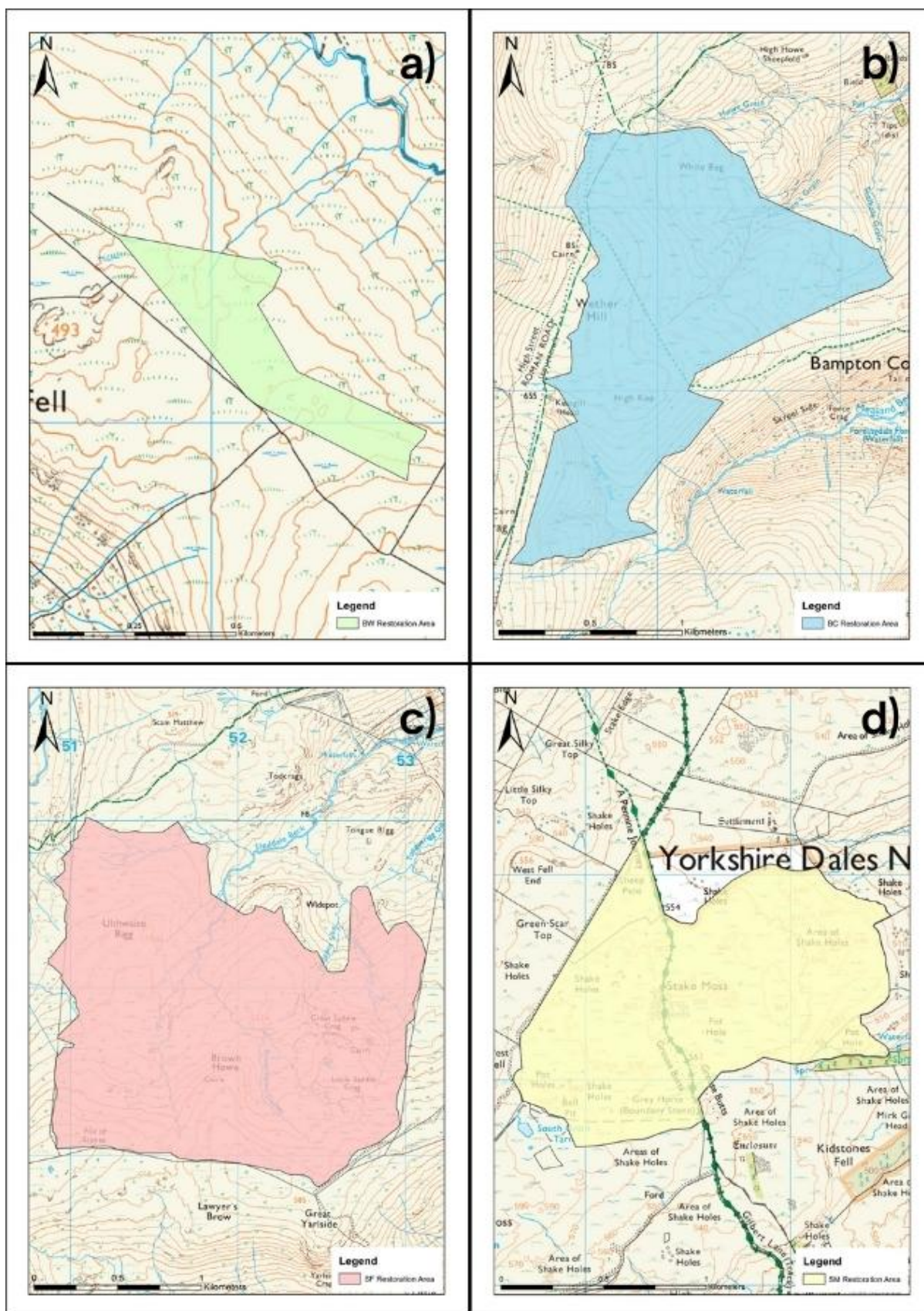
Figure 4.4: Selected site extents: a) Borrowdale (BW) restoration area. Central grid reference: NY 52117 05154; b) Bampton Common (BC) restoration area. Central grid reference: NY 46152 16511; c) Shap Fells (SF) restoration area. Central grid reference: NY 51951 08767; d) Stake Moss (SM) restoration area. Central grid reference: SD 93567 82373.

4.3 Survey Area Selection

Project sites covered ~730 ha, providing a sufficiently large area for investigation. However, further refinement was necessary to isolate specific restoration techniques (e.g., turving and brash spreading areas) and to assess relative condition, enabling selection of representative degraded, near-natural, and restored plots for sampling.

4.3.1 Restoration Technique Selection

Although selected sites exhibited a range of rewetting and revegetation interventions, gully restoration was the primary focus across sites, enabling a targeted assessment of technique effectiveness. Based on the site selection criteria (Table 4.1) and the applied interventions (Table 4.3), Table 4.4 outlines the restoration techniques selected for analysis and their justification.

Table 4.4: Selected restoration techniques, descriptions, and justifications for inclusion based on site-specific applications.

Restoration Technique	Description	Justification
Local Turving (Local)	Application of locally sourced turves (within excavator reach) to revegetate reprofiled gully sides	Applied at BW, BC, and SF, enabling assessment of long-term restoration effectiveness (~2–10 years)
Imported Turving (Local)	Application of imported turves (sourced from a borrow pit within/from a near-by bog) to revegetate reprofiled gully sides	Applied at BC and SF, allowing evaluation of restoration effectiveness (~2–5 years) and comparison of local turving approaches
Heather Brash Spread (Exotic)	Application of heather brash to revegetate reprofiled gully sides	Applied at SM, allowing assessment of technique efficiency, particularly exotic versus local techniques (SF)
Coir Logs (Exotic)	Placement of coir logs in gullies to promote rewetting	Applied at SM, enabling evaluation of exotic versus local techniques (SF)
Stone/Timber Dams (Exotic)	Installation of stone or timber dams in gullies to promote rewetting	Applied at SM, facilitating comparisons with SF and enabling assessment of different exotic rewetting approaches (stone/timber dams versus coir logs)

While selected techniques are comparable, rewetting and revegetation serve distinct functions and are therefore interpreted separately, particularly at the plot scale (Chapter 2; Section 2.5). Supplementary interventions, such as peat dams, plug planting, and lime application, were recorded during field assessment and accounted for in the sampling design, but not evaluated independently.

Technique selection was used to refine each project site to focused sampling areas based on applied interventions. At Borrowdale (BW), sampling focused on ~1,000m of reprofiled gullies revegetated with **local turves** (Figure 4.5a). At Bampton Common (BC), the focus extended to ~40,000m of reprofiled and revegetated gullies using **local and imported turves** (Figure 4.5b). Shap Fells (SF) included ~100,000m of reprofiled gullies, again using **local and imported turves** (Figure 4.5c). Stake Moss (SM) featured ~22,000m of reprofiled gullies treated with **heather brash**, along with ~1,000 **coir logs** and 423 **stone/timber dams** (Figure 4.5d).
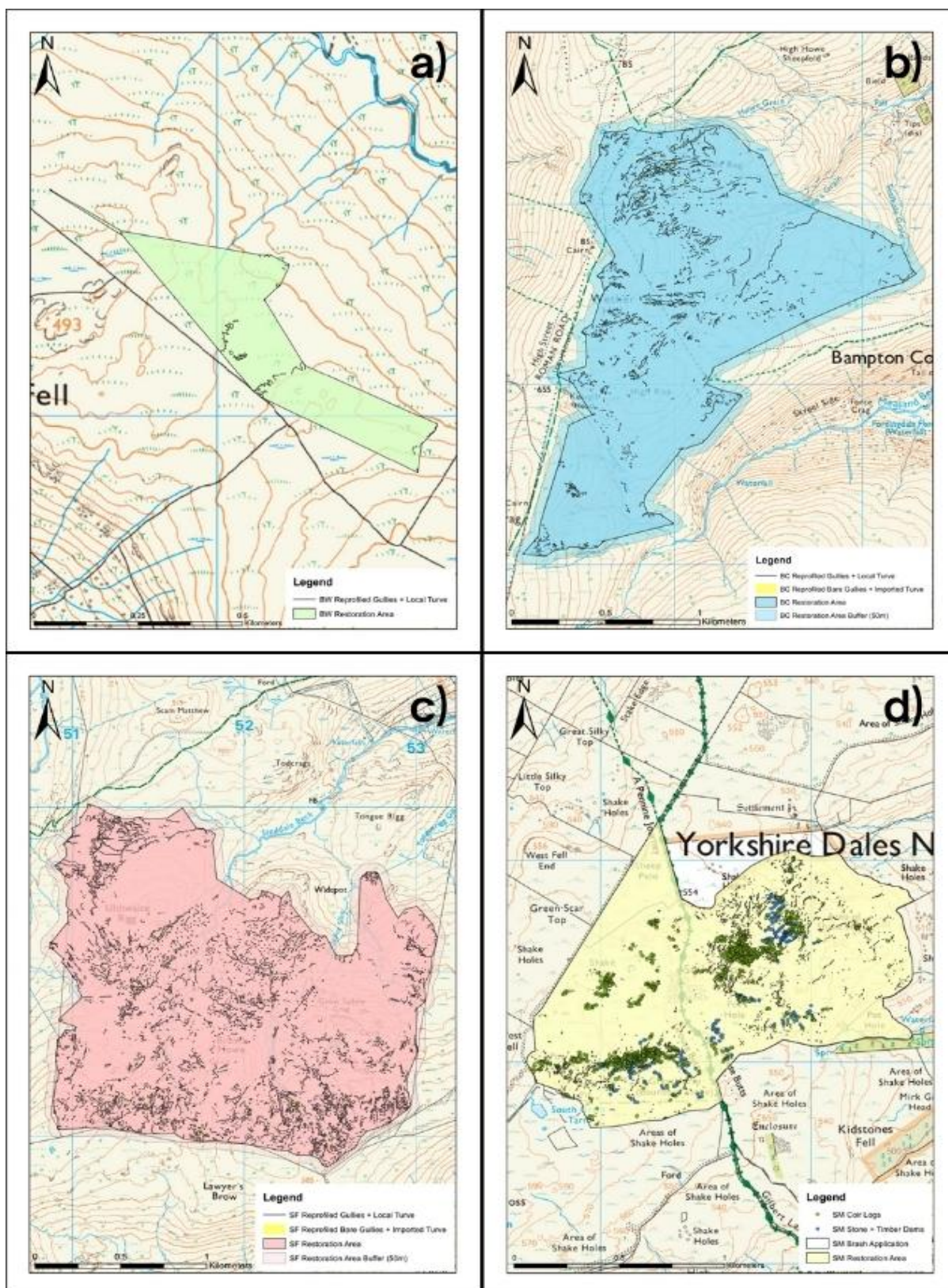
Figure 4.5: Selected site restoration extents: a) Borrowdale (BW) restoration area, showing the spatial extent of assessed peatland restoration interventions (local turving); b) Bampton Common (BC) restoration area, showing the spatial extent of assessed peatland restoration interventions (local and imported turving); c) Shap Fells (SF) restoration area, showing the spatial extent of assessed peatland restoration interventions (local and imported turving); d) Stake Moss (SM) restoration area, showing the spatial extent of assessed peatland restoration interventions (heather brash spreading, coir log installation, and stone/timber dam application).

4.3.2 Stratified Grid Selection

Although restoration technique selection refined the project area, further stratification was required to systematically identify representative sampling locations. A 50x50m fishnet grid was applied to each restoration area in ArcGIS (Figure 4.6), following Parry *et al*. (2012) and NRW (2022). This provides standardised sampling units, balancing spatial heterogeneity with logical feasibility for ground-truthing.
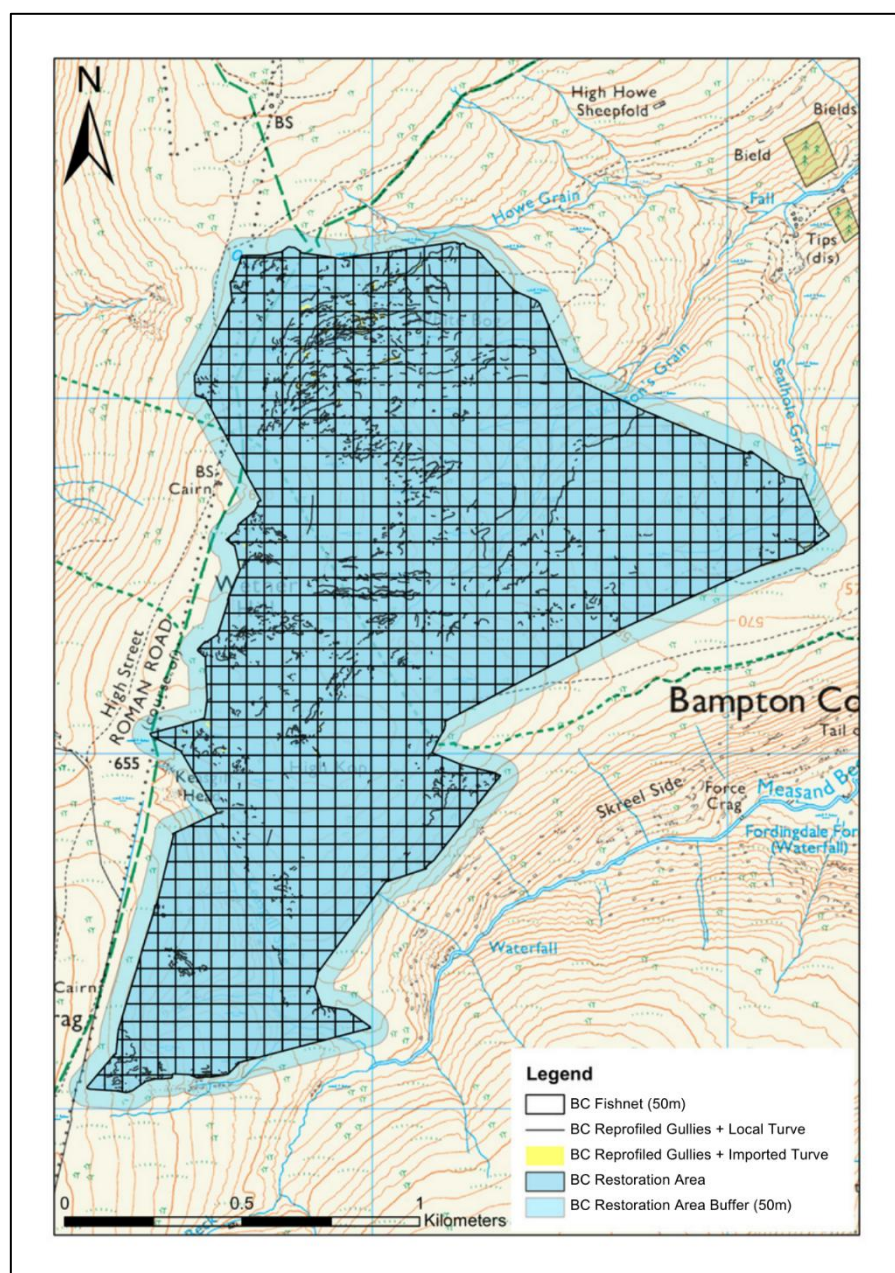
Figure 4.6: Example adoption of a 50x50m fishnet grid at Bampton Common (BC) to create standardised sampling units for further investigation.

Areas of maximum restoration intensity were prioritised to evaluate restoration effectiveness, assuming greater intervention indicated more severe degradation and reduced the risk of selecting minimally degraded areas. This also enabled selection of representative plots showing the best examples of restoration (Section 4.4), supporting standardised, repeatable site selection. For each site, total lengths, areas, and counts of selected techniques (Table 4.4) were calculated per 50x50m grid unit in ArcGIS. The three most intensive units were then ground-truthed, exemplified in Figure 4.7 (Appendix F provides the selected grid squares for other sites).
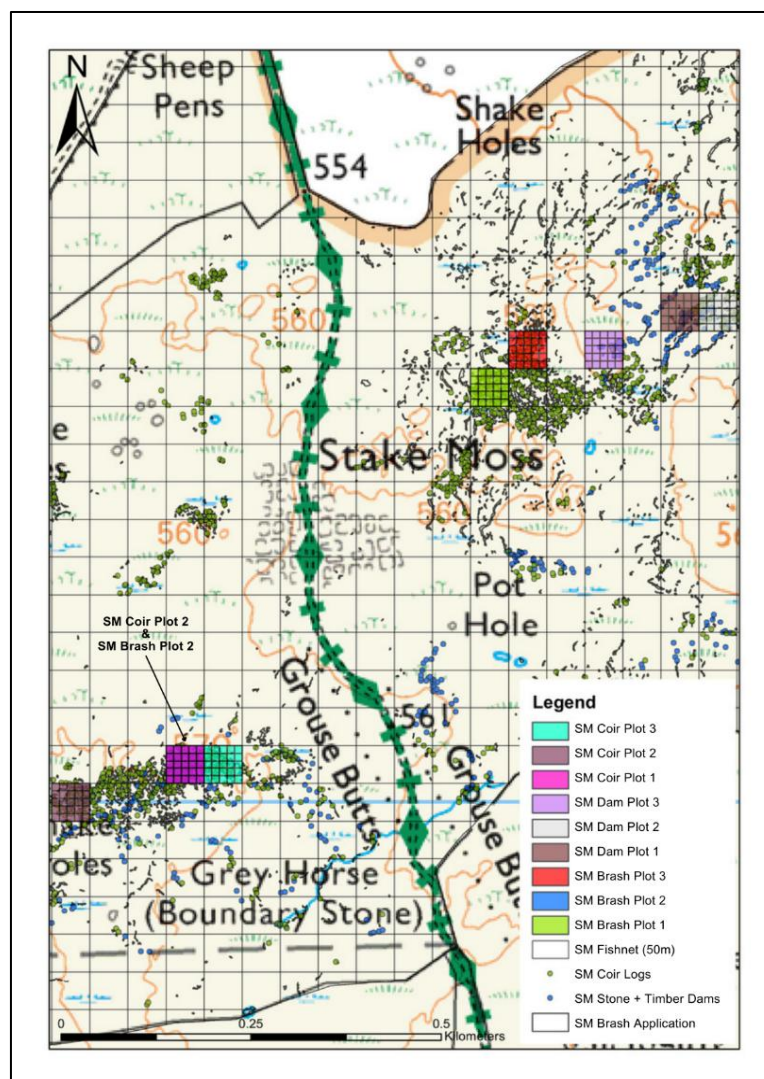
Figure 4.7: Selected top three most intensive 50x50m grid units at Stake Moss (SM) for total area of heather brash spread (Brash), quantity of stone/timber dams (Dam), and quantity of coir logs (Coir) within gullies. Internal grids relate to ground-truthing assessments.

4.3.3 Control Area Selection

Representative degraded and near-natural areas were selected to establish baseline conditions and assess restoration targets. Control sites were located within the Bampton Common (BC) and Shap Fells (SF) peatlands, avoiding selection from different systems to the restored, supporting comparability. Bampton Common and Shap Fells were chosen based on existing designations (Table 4.3). Bampton Common is characterised as degraded, while Shap Fells is more likely to indicate near-natural condition. Additionally, both form part of the wider High Street blanket peatland complex, providing a consistent geographical context. Restoration areas were excluded ensuring control plots remained within the same peatland but were spatially distinct, maintaining control integrity. A 50m buffer was applied around sites to minimise restoration influence while maintaining environmental comparability (seen in Figures 4.5; 4.6). This also supported logistical feasibility for access.

Considering the increasing role of Earth observation imagery in monitoring large, heterogeneous landscapes (Trippier *et al.*, 2020), initial site scoping was conducted using 2019 high-resolution (25cm) aerial imagery from Edina Digimap. Within the Bampton Common buffer zone, degraded areas were identified by the presence of gullies, hags, and bare peat (Figure 4.8a). In contrast, green *Sphagnum* lawns were observed within the Shap Fells buffer zone, indicative of near-natural conditions (Figure 4.8b).
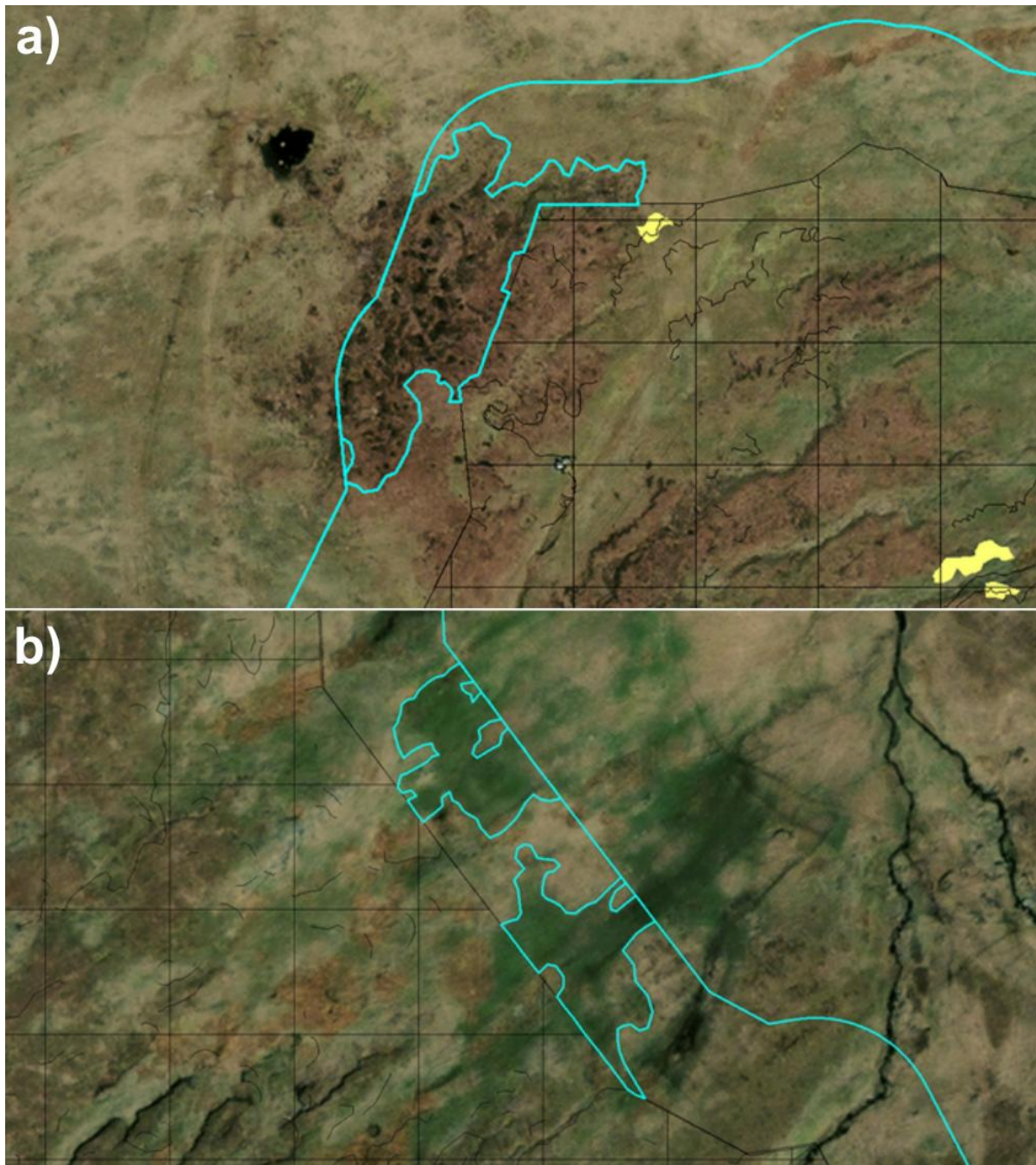
Figure 4.8: Initial control site selection through aerial imagery (Edina Digimaps 2019 (25cm resolution)): a) Example of degraded site selection within the buffer zone of Bampton Common (BC); b) Example of near-natural site selection within the buffer zone of Shap Fells (SF).

Applying the same 'maximum intensity' approach used for restoration sites, the three largest degraded and near-natural areas were selected for further investigation at Bampton Common (Figure 4.9a) and Shap Fells (Figure 4.9b).
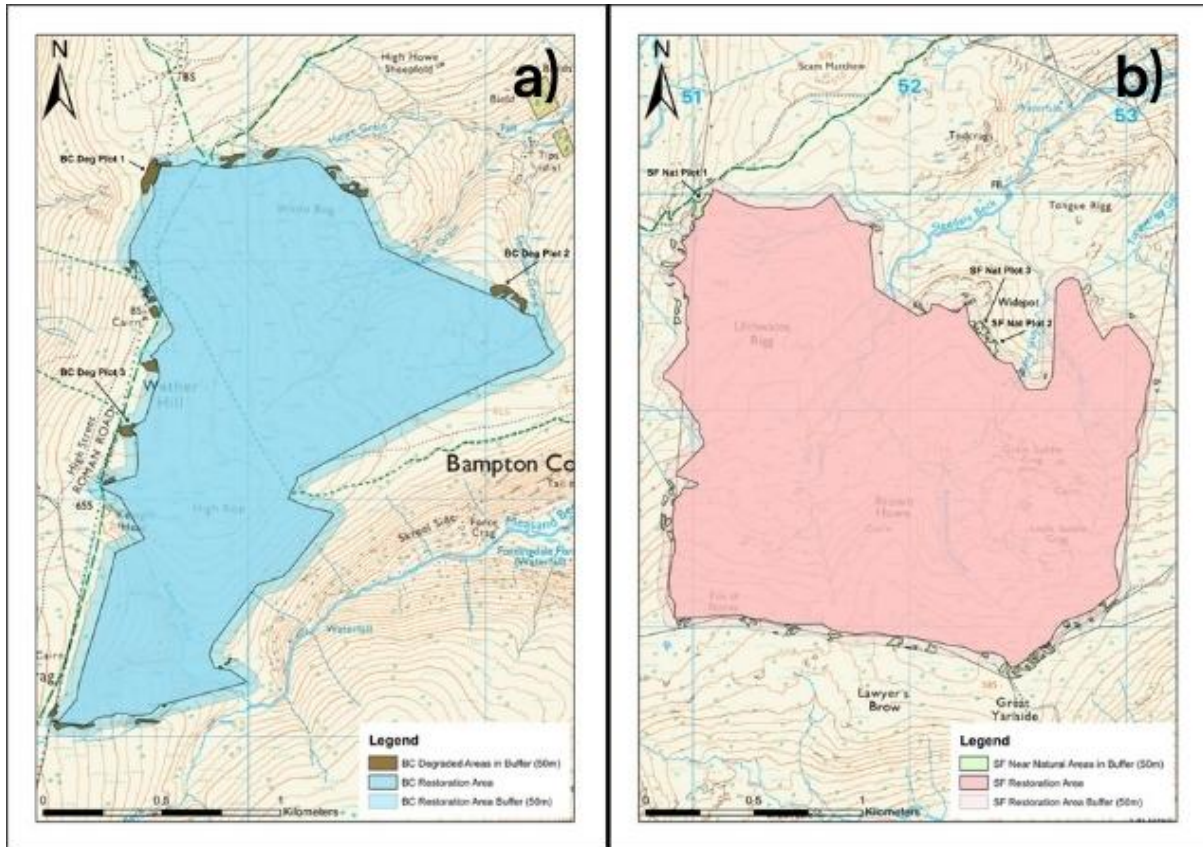
Figure 4.9: Potential control area extents: a) Degraded areas identified using aerial imagery within the 50m buffer zone of Bampton Common (BC). Figure shows the three largest degraded areas selected for further investigation as potential control plots; b) Near-natural areas identified using aerial imagery within the 50m buffer zone of Shap Fells (SF). Figure shows the three largest near-natural areas selected for further investigation as potential control plots.

4.3.4 Ground-Truthing

Ground-truthing was conducted to verify the accuracy of geospatial datasets, including Natural England's Peaty Soils Locations (2016), Edina Digimap aerial imagery (2019), and restoration shapefiles (2011 onwards). At restoration sites, this involved:

1. **Peat depth ≥30cm:** Measured every 10m within each 50x50m grid unit using a peat probe and Garmin eTrex 10 GPS (Figure 4.7 shows the 10x10m sub-grids used).

2. **Restoration techniques:** Visually confirmed the presence of expected interventions.

3. **Restoration extent:** Validated intervention length, area, and quantity using direct measurement or a Microsoft BAP Precision S-Series.

4. **Site topography:** Visually assessed slope variability and compared against the OS 2019 Terrain 50m DTM (Figure 4.2).

5. **Anomalies:** Identified unmapped interventions or disturbances affecting site suitability.

At control sites, peat depth, topography, and anomalies were similarly assessed to validate their suitability and consistency with expected condition.

a) Restored Areas

Ground-truthing was carried out between February and April 2022 under clear ground conditions. Peat depth exceeded 30cm at all locations, with Bampton Common – Reprofiled Gullies + Imported Turves Plot 1 (BC RG + IT Plot 1) recording the lowest average depth (~50cm). Restoration techniques and extents closely matched spatial data, with a maximum offset of ~8m. As expected for designated blanket bogs, slopes ranged from 5–10°, although BC RG + LT Plot 1 and Plot 3 were closer to 10°. No anomalies were identified. Findings validated the geospatial selection process, confirming spatial data provided accurate and representative sampling locations.

b) Control Areas

Ground-truthing was conducted between February and April 2022 in clear conditions. At Bampton Common – Degraded Plot 1 (BC Deg Plot 1), peat depth averaged ~20cm and did not consistently meet the ≥30cm threshold. The adjacent Roman Road, used by walkers and quad bikes (Figure 4.9a), further compromised site suitability (e.g., footpath disturbance). Plot 2 met peat depth requirements but exhibited a steeper slope (~20°) than other sites and was excluded. Plot 3 was again influenced by the Roman Road, raising concerns from Historic England about core extraction.

At Shap Fells – Near-Natural Plot 1 (SF Nat Plot 1), the public footpath (Figure 4.9b) and an unmarked fence compromised site integrity. SF Nat Plot 2 and Plot 3 met the scoping criteria, but an unmapped tributary caused fen species dominance (e.g., *Phragmites australis*), challenging its classification as H7130 blanket bog.

Findings demonstrated limitations of aerial imagery in identifying degraded and near-natural areas. Higher-resolution imagery, machine learning, or random regression modelling may improve future site selection (Trippier *et al.*, 2020). Inaccuracies may also indicate changes in peatland condition since 2019, the most recent imagery available at the time. As shown in Figure 4.10, site condition/feature extent can shift over three years, influencing selection outcomes.
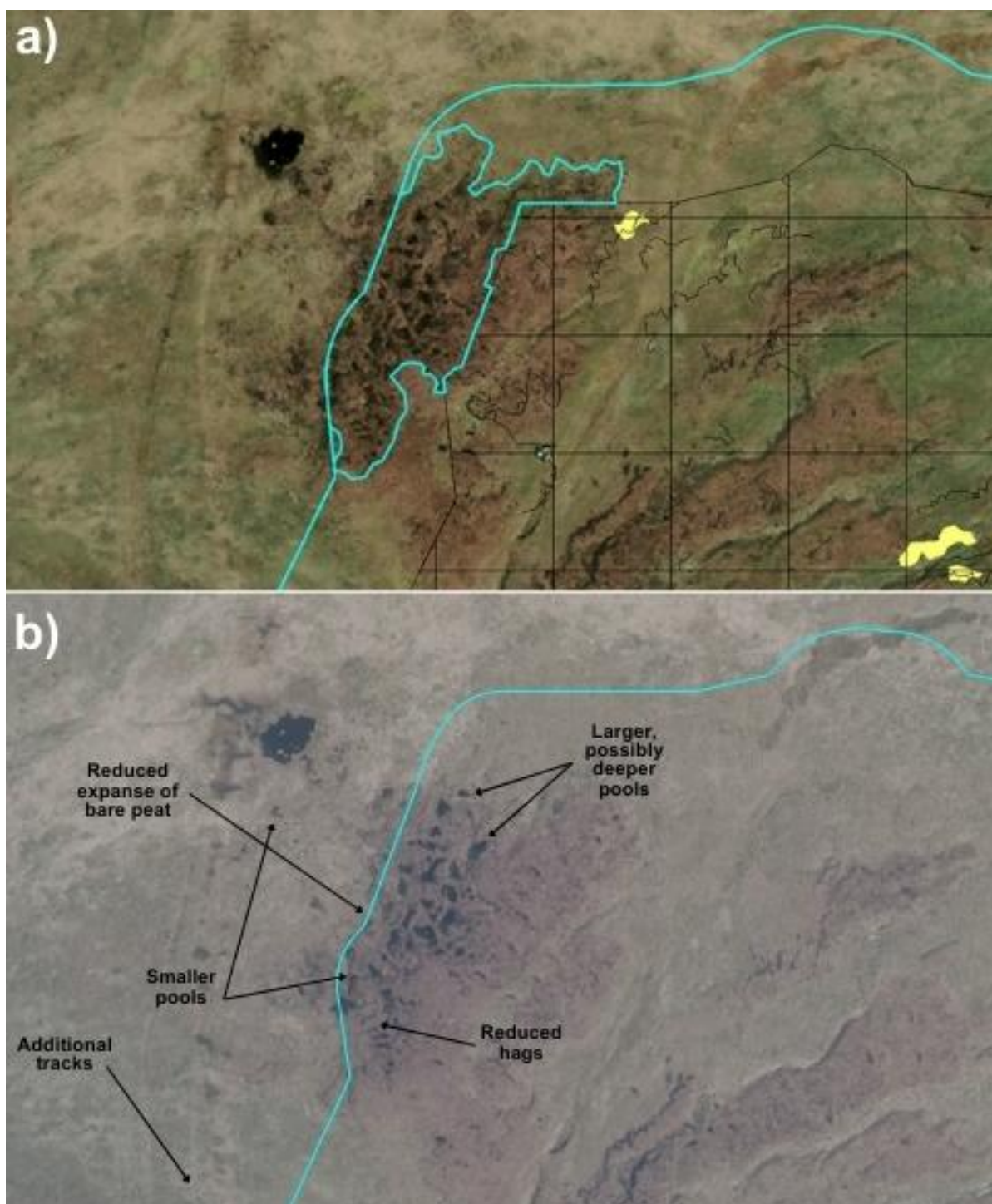
Figure 4.10: Temporal changes across Bampton Common – Degraded Plot 1 (BC Deg Plot 1): a) 2019 aerial imagery from Edina Digimap; b) 2022 aerial imagery from Edina Digimap. Figure reveals changes in surface conditions over a 3-year period.

An opportunistic sampling approach was adopted to address these limitations. During ground-truthing, alternative mapped degraded and near-natural areas were assessed within the buffer zones of Bampton Common and Shap Fells (Figure 4.9). Scoping proceeded southward from BC Deg Plot 1 and SF Nat Plot 1, both located in the northwest of their respective complexes, supporting consistency. The first areas meeting the ground-truthing criteria were selected as control sites for further evaluation. Figure 4.11 shows the spatial distribution of the selected control sites at Bampton Common and Shap Fells, respectively.
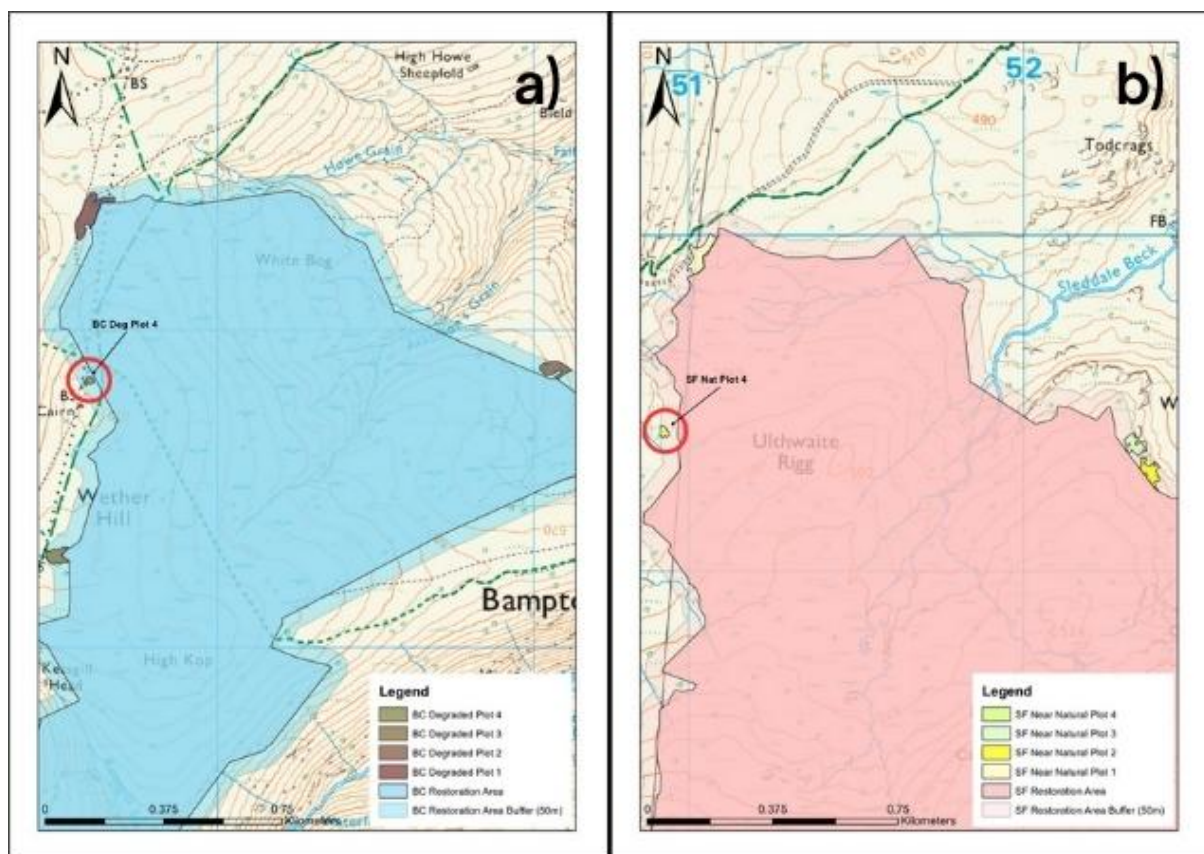
Figure 4.11: Selected control plots: a) Assessed degraded sites within the buffer zone of Bampton Common (BC). Figure shows the opportunistically assessed Bampton Common – Degraded Plot 4 (BC Deg Plot 4), as other sites failed ground-truthing criteria; b) Assessed near-natural sites within the buffer zone of Shap Fells (SF). Figure shows the opportunistically assessed Shap Fells – Near-Natural Plot 4 (SF Nat Plot 4), as other sites failed ground-truthing criteria.

4.3.5 Condition Assessment Approach

The JNCC (2009) *Common Standards Monitoring Guidance for Upland Habitats: Blanket Bogs* was used to assess surface condition across restored, degraded, and near-natural sites. JNCC (2009) assesses key surface indicators, including vegetation, bare peat, and erosion, evaluating the surface response to restoration. It was selected for its adoption in designations and post-restoration monitoring (Chapter 2; Sections 2.4.2; 2.6.2). The assessment also provides a baseline for evaluating surface recovery across sites which is explored in the following chapter.

a) JNCC (2009) Common Standards Monitoring Guidance

JNCC (2009) employs a $4m^2$ quadrat approach to assess condition across blanket peatlands. It evaluates eight mandatory attributes capturing vegetation composition, structure, and physical indicators of degradation. Table 4.5 builds on the summary of JNCC (2009) attributes presented in Chapter 2; Section 2.6.2; Table 2.4 to describe the mandatory targets alongside their assessment method.

Table 4.5: Summary of JNCC (2009) mandatory attributes, condition targets, and quadrat assessment methods.

Attribute	Target	Assessment
1. Feature Extent	No measurable decline in blanket bog area	Field comparison with baseline maps, systematic grid sampling, or patch-based recording
2. Vegetation Composition – Frequency of Indicator Species	≥6 indicator species present (Appendix G)	Visual assessment at 4m² scale, scoring each *Sphagnum* separately
3. Vegetation Composition – Cover of Indicator Species	≥50% of vegetation cover consists of ≥3 indicator species; *Sphagnum* cover must not be *Sphagnum fallax* dominant	Visual assessment at 4m² scale
4. Vegetation Composition – Cover of Other Species	<1% cover of non-native species; <10% scattered native trees/shrubs	Visual estimate of entire feature from sample location and at 4m² scale
5. Vegetation Structure – Browsing Impact	<33% browsing of previous growing season's dwarf-shrub shoots	Visual estimate at 4m² scale
6. Vegetation Structure – Disturbance	No visible signs of burning into moss layer; no disturbance in sensitive areas (Appendix G)	Visual estimate for entire feature from sample location
7. Physical Structure – Peat Erosion	Eroding peat extent < stable redeposited peat with vegetation regrowth	Aggregate visual estimate at sample locations
8. Ground Disturbance – Drainage & Trampling	<10% of total feature area disturbed by ditches, heavy trampling, or vehicle tracks	Visual assessment of diffuse disturbance at 4m² scale, with targeted assessments of defined paths/tracks

4.3.6 Final Survey Area Selection

Considering the JNCC (2009) quadrat approach, refinement of the 50x50m units was necessary to support feasibility. The maximum intensity approach (Section 4.3.1) was re-applied to select 10x10m sub-plots within each grid (previously mapped for ground-truthing, Figure 4.7) to balance methodological rigour with logistical constraints. An example of survey area selection is shown in Figure 4.12 (refer to Appendix H for other sites).
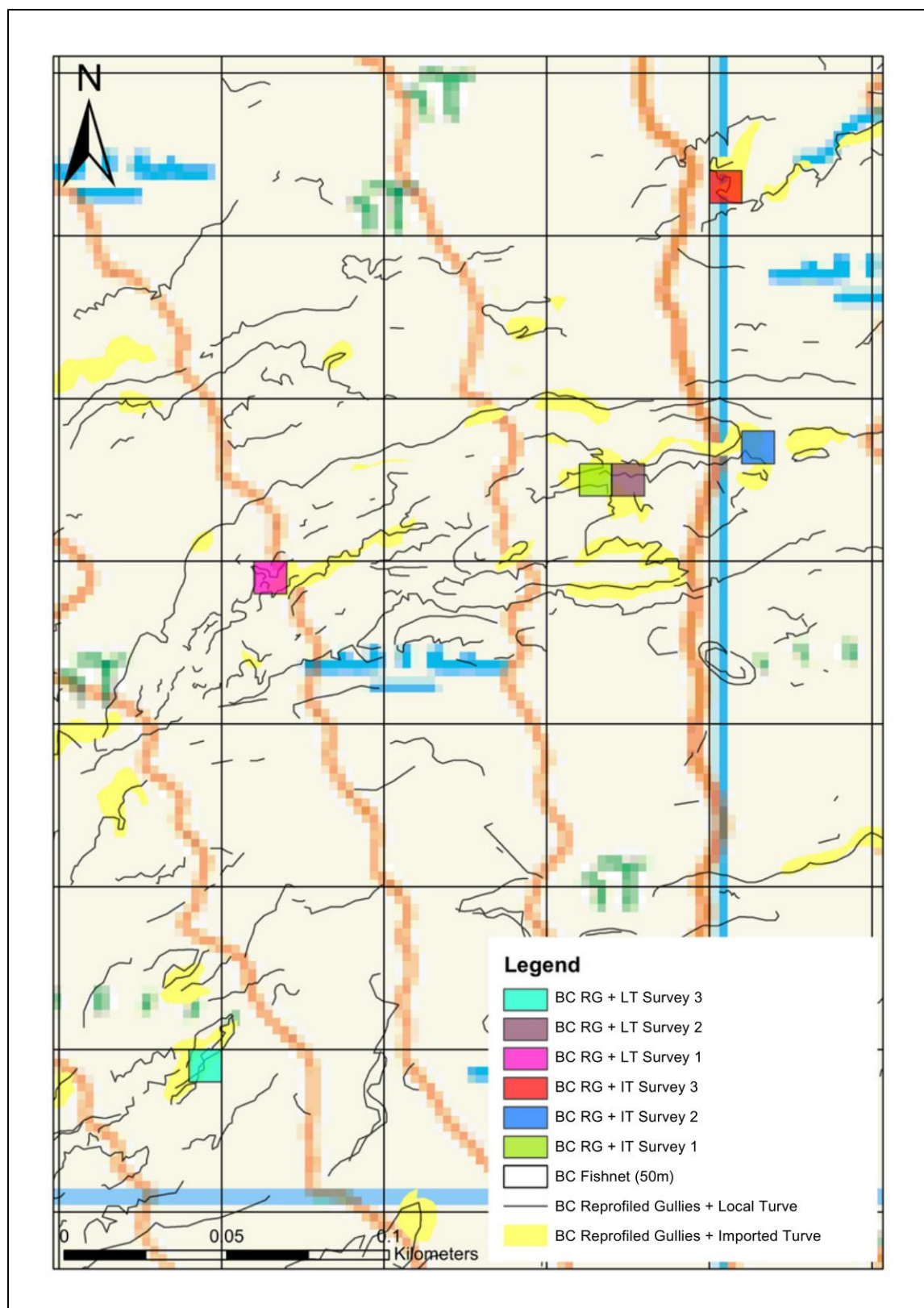
Figure 4.12: Selected 10x10m survey sub-plots at Bampton Common (BC) for total lengths of reprofiled and locally turved (RG + LT) and reprofiled and imported turved (RG + IT) gullies.

A 10x10m survey area was established around the central coordinate of each control site to account for their smaller extent (Section 4.3.4b). This supported consistent and unbiased sampling, minimised edge effects, and provided a representative snapshot of site conditions while maintaining comparability with restored areas. Figure 4.13 shows the selected survey areas for the control sites.
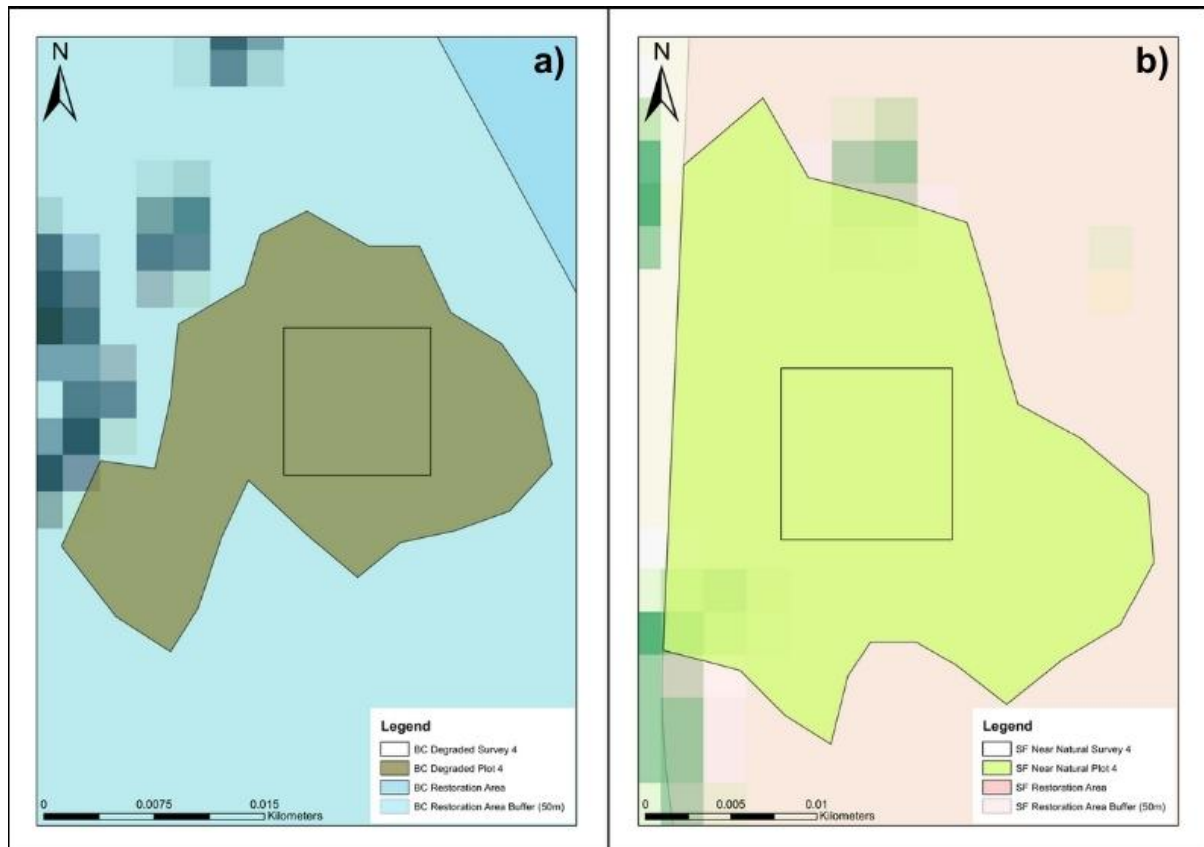
Figure 4.13: 10x10m survey plots for the control sites: a) degraded at Bampton Common; b) near-natural at Shap Fells.

4.3.7 Survey Approach

Surveying aimed to identify the most representative sites for sub-sampling, supporting selected areas indicated successful restoration outcomes associated with specific techniques and post-restoration timescales. JNCC (2009) assessments also provided

surface condition data to contextualise sub-surface analyses (discussed in the following chapter).

a) Methodology

A standardised quadrat approach was implemented following JNCC (2009) to evaluate peatland condition and restoration effectiveness. Data collection aligned with Table 4.5 and focused on:

1. **Peat regrowth:** Percentage cover (Attribute 1).

2. **Vegetation composition and structure:** Richness and cover of key indicator species (Attributes 2 and 3; Appendix G).

3. **Degradation features:** Extent of bare peat, drainage, erosion, browsing, burning, ground disturbance, *Sphagnum* damage, and invasive species cover (Attributes 4–8).

JNCC (2009) sensitive areas (Appendix G) were also recorded, including:

1. **Survey location type:** Dominant feature within the quadrat (e.g., gully tops, sides, bog pools).

2. **Microtopography:** Number of hummock–hollow complexes (≥20cm elevation difference).

3. **Bog pool proximity:** Distance to the nearest bog pool.

4. **Restoration technique isolation:** Distance to the nearest additional restoration feature (e.g., bunds, dams).

This supported sensitive areas (e.g., bog pools) were avoided where sampling was impractical. It also enabled consistent plot selection and isolation of individual restoration techniques. Data collection followed JNCC (2009) visual assessment, with

percentage cover recorded categorically to the nearest 0 or 5 (Appendix I). While this may equate to totals exceeding 100%, it reduces observer bias, improves efficiency, and supports a robust, repeatable framework for large-scale assessment. Quadrats were surveyed using a systematic grid with a north-oriented serpentine transect pattern (Figure 4.14), supporting repeatable spatial coverage and consistent aspect mapping. Surveys were conducted by the same individual to minimise observer bias.
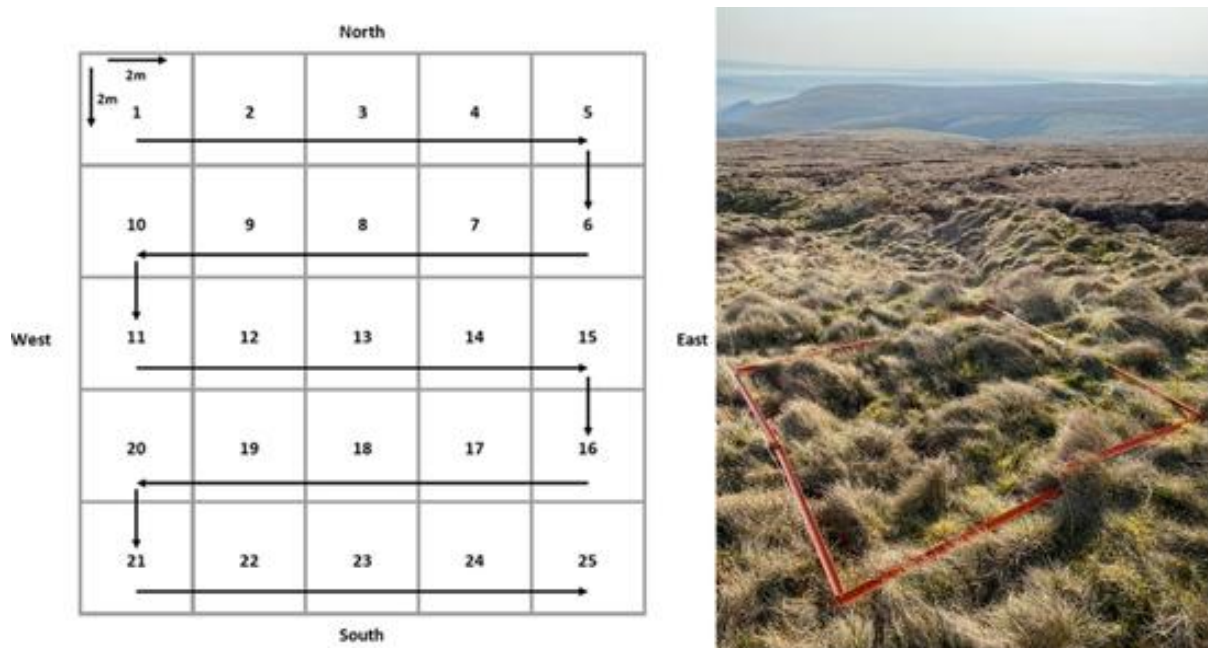
Figure 4.14: Systematic grid-based serpentine quadrat approach used to collect JNCC (2009) data.

b) Restoration Success Selection

Surveys were conducted across the 26 restored and control plots between March and May 2022. As only 15 peat cores could be selected for µCT analysis (Chapter 2; Section 3.1), further refinement was required to identify the most representative plots for sub-sampling. Surface condition scores from JNCC (2009) assessments were categorised into favourable and unfavourable attributes based on criteria (Table 4.6).

Table 4.6: JNCC (2009) mandatory attributes (Table 4.5) categorised into favourable (near-natural) and unfavourable (degraded) based on their descriptions (JNCC, 2009).

Favourability Category	Attribute (Extent)
Favourable	1. Peat regrowth
	2 & 3. Indicator species
Unfavourable	4. Invasive species
	5. Browsing
	6. Burning
	7. Erosion
	8. Bare peat, active drainage, damaged ground, and *Sphagnum* damage

At the survey scale, a favourability score was calculated by subtracting the total number of unfavourable attributes from favourable. These were normalised to a 0–100 scale, where 0% represented the degraded and 100% the near-natural control. Within each restoration intervention, the highest-scoring plot among the top three was selected for sampling (Table 4.7), allowing consistent and objective site selection. Detailed mandatory attribute (Table 4.5) findings are presented in the following chapter.

Selecting the most favourable condition outcome within the most severely degraded areas (inferred from restoration intensity) captured the maximum potential for restoration success. This approach minimised inclusion of failed or poorly implemented interventions, avoiding the effects of operational error and facilitating a fair evaluation of the intended functional outcome of each technique. While selecting midpoints could provide a broader understanding of average recovery, it risks underrepresenting the purpose of each intervention. By focussing on more favourable examples within severely degraded contexts, this approach balances severe baseline conditions with observed surface recovery, enabling robust assessment of intervention effectiveness under the most challenging scenarios.

Table 4.7: JNCC (2009) favourability score findings used to select the most representative sites for sub-sampling. BW = Borrowdale (~10 years old); BC = Bampton Common (~5 years old); SF = Shap Fells (~2 years old); SM = Stake Moss (~2 years old). Bold demonstrates selected areas; controls are highlighted in italics.

Survey Site	Total Favourable Attributes	Total Unfavourable Attributes	'Favourability Score'	Normalised Score
BC Degraded 4	*1065*	*3610*	*-2545*	*0.00*
BW RG + LT 1	**1540**	**645**	**895**	**78.99**
BW RG + LT 2	1315	855	460	69.00
BW RG + LT 3	925	480	445	68.66
BC RG + IT 1	**1845**	**945**	**900**	**79.10**
BC RG + IT 2	1255	1350	-95	56.26
BC RG + IT 3	1285	700	585	71.87
BC RG + LT 1	**1795**	**900**	**895**	**78.99**
BC RG + LT 2	1520	810	710	74.74
BC RG + LT 3	1320	755	565	71.41
SF RG + IT 1	1545	1895	-350	50.40
SF RG + IT 2	**1745**	**1070**	**675**	**73.94**
SF RG + IT 3	1625	1690	-65	56.95
SF RG + LT 1	1880	1465	415	67.97
SF RG + LT 2	1600	1300	300	65.33
SF RG + LT 3	**2250**	**1155**	**1095**	**83.58**
SM Brash 1	990	1910	-920	37.31
SM Brash 2	**1650**	**1390**	**260**	**64.41**
SM Brash 3	1305	1715	-410	49.02
SM Coir 1	1750	1430	320	65.79
SM Coir 2	1495	970	525	70.49
SM Coir 3	**1830**	**1115**	**715**	**74.86**
SM Dam 1	**1875**	**1315**	**560**	**71.30**
SM Dam 2	1370	1340	30	59.13
SM Dam 3	1450	995	455	68.89
SF Near Natural 4	*2370*	*560*	*1810*	*100.00*

4.4 Plot Selection

A structured approach was required to support systematic and representative selection of samples for sub-surface assessment. Plot selection was based on:

1. **Spatial distribution of core samples.**

2. **Dominant surface feature recorded within each quadrat.**

3. **Criteria used to define 4m^2 sampling plots.**

4. **Resulting dataset used in subsequent analysis.**

This supported consistency across sites and enabled robust comparison of local restoration impacts on sub-surface structure.

4.4.1 Peat Core Sample Distribution

The 15 peat cores were distributed to capture variation in restoration technique and timescale. Temporal assessment was prioritised, as time since intervention is critical for evaluating restoration effectiveness as a carbon reduction strategy. Technique comparisons were also included, though direct comparisons are limited by differing functional aims. **One plot** was selected within **each control site** (degraded and near-natural) to represent baseline conditions. **Two plots** were sampled for **each turving method**, enabling temporal assessment and comparison between local and imported turves. **One plot** was selected from **each Stake Moss intervention** (**brash spread, coir log application, and stone/timber dam installation**) to support comparability between alternate approaches and turving and heather brash spreading as a revegetation technique. This distribution allowed restoration effects to be assessed across intervention types while maintaining consistency across sites.

4.4.2 Dominant Feature Selection

Gully sides were selected for sampling based on JNCC (2009) survey data. Although their slopes are comparable to sensitive conditions (Appendix G), they were directly targeted by restoration interventions, including turve placement and heather brash application. Focusing on gully systems supported this feature was present at all sites, providing a consistent restoration context. This consistency enabled more robust assessment of how restoration affects sub-surface structure across sites.

4.4.3 Selection Approach

Individual survey plots (4m^2 sub-plots) were selected using the approach in Section 4.4.1, prioritising highest-scoring areas to maintain consistency and maximise assessment of restoration effectiveness. South-facing aspect was also considered, as these plots receiving more sunlight were expected to show more advanced seasonal growth early in the survey period, supporting consistent vegetation assessment across sites. For each sub-plot, the top two scoring alternatives were also identified in case of site constraints related to JNCC (2009) sensitive areas (Appendix G) or proximity to other interventions. Given the standard 8–10m spacing of peat dams (Thom *et al.*, 2019; NatureScot, 2021) a minimum buffer of 5m was applied to isolate the effects of selected restoration techniques. At Shap Fells – Restored Gully + Local Turving (SF RG + LT), the third highest-scoring plot was selected, as the highest-scoring plots were located on a steep northwest-facing section (>20°) with visible turve slippage, making it unsuitable under JNCC (2009) sensitive area criteria (Appendix G) and in line with the aims of the investigation. Figure 4.15 shows non-normalised favourability scores and spatial distribution of selected sub-plots for sampling.
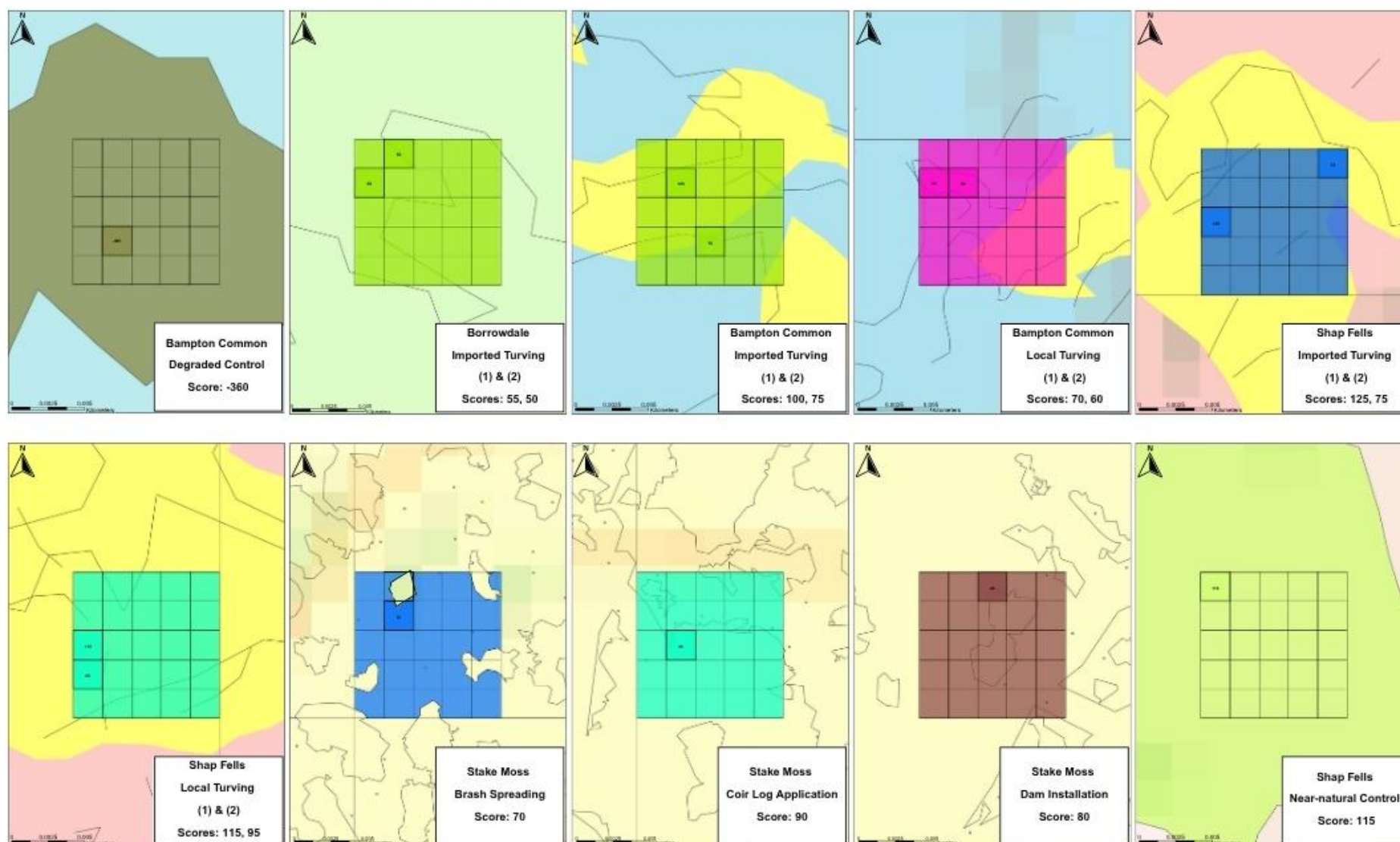
Figure 4.15: Spatial distribution of selected 10x10m survey plots across restored, degraded, and near-natural sites, showing final 4m^2 plot locations and JNCC (2009) relative non-normalised favourability scores.

4.5 Chapter Synthesis and Discussion

A bespoke, structured, pragmatic sampling framework was developed to support more robust evaluation of peatland restoration effectiveness using a multi-method approach. Recognising the challenges of working in large, heterogeneous uplands, the framework combined geospatial filtering, stratified selection, ground-truthing, and systematic field survey to *enable representative sampling across degraded, near-natural, and restored sites.*

Opportunistic sampling, common across geosciences due to logistical constraints, introduces bias, particularly where sample numbers are limited and spatial variability is high (Cunliffe *et al.*, 2013; Parry *et al.*, 2014; Young *et al.*, 2017). Yet this issue remains largely unacknowledged in ecological and environmental studies, where random (Parry *et al.*, 2014; Alshehri *et al.*, 2020; Howson *et al.*, 2023) and transect-based approaches (Green *et al.*, 2017; Holden *et al.*, 2017; Young *et al.*, 2017) are still widely adopted. By explicitly addressing this limitation, *the adopted approach supports comparability and repeatability, drawing on principles of 'spatially balanced' sampling designed to account for spatial heterogeneity and align sampling with research objectives* (Kermorvant *et al.*, 2019; Mastrantonis *et al.*, 2024). Although this bespoke approach was developed for peatlands, its underlying principles are transferable to other large, heterogeneous landscapes. *It offers a novel framework for sampling complex systems with limited samples and demonstrates how intensive methods can yield wider-scale insights.*

Although only 15 cores were available for µCT analysis, the *integration of spatial analysis, condition assessment, and restoration intensity mapping enabled the selection of samples indicative of wider restoration contexts. This supports more meaningful*

discussion of restoration outcomes. Restored plots were selected based on favourability scores within the most degraded areas (inferred through restoration intensity), capturing the maximum potential for recovery and indicating the goals of restoration. While this approach enables functional interpretation of restoration success, it is acknowledged alternative studies may prioritise average or unfavourable conditions depending on their objectives (e.g., incorporating restoration 'failure').

Control plots were selected from within the same peatland complexes to support ecological comparability while avoiding impacts from restoration. Remote sensing, while increasingly adopted in ecological monitoring, was found to have limited utility in distinguishing degraded from near-natural conditions at the resolution required, demonstrating the challenges in accurate mapping discussed in Chapter 2; Section 2.1 and highlighting the value of integrated, ground-based assessments.

By combining geospatial datasets, field survey, and ground-truthing, *this framework addressed key limitations of previous assessment methods and enables identification of more representative sampling points. It offers a repeatable foundation for evaluating large, heterogenous systems using intensive techniques, balancing methodological rigour with practical feasibility.* Site selection and survey design followed the *Common Standards Monitoring Guidance (CSM) for Upland Habitats: Blanket Bogs* (JNCC, 2009), *supporting alignment with national monitoring protocols and comparability with policy reporting* (Chapter 2; Section 2.4.2; 2.6.2).

The sampling framework supports subsequent analysis of surface condition, sub-surface bulk and chemical composition, and structural function, providing confidence that selected plots capture representative examples of their respective condition.

Chapter 5: Evaluating the Effectiveness of Restoration Using Surface Proxies

In the UK, peatland condition is primarily assessed through surface features, which capture ecology, degradation, and habitat quality (Chapter 1; Section 1.1). These indicators also function as proxies for restoration success in monitoring and carbon accounting frameworks (Chapter 2; Sections 2.6.2; 2.7). The JNCC (2009) *Common Standards Monitoring Guidance (CSM) for Upland Habitats: Blanket Bogs* provides the basis for such assessments and informs national protocols, including Natural England's *Favourable Condition Tables* (Shepherd *et al.*, 2013; Crowle *et al.*, 2025) and NatureScot's (Peatland ACTION) *Peatland Condition Assessment* (Birnie *et al.*, 2023). While multiple condition assessment methods exist (Chapter 2; Section 2.6.2), JNCC (2009) informs most practical and policy-aligned evaluations of blanket bogs (Chapter 2; Sections 2.4.2; 2.6.2), classifying sites as favourable or unfavourable based on vegetation composition, physical structure, and disturbance (Chapter 4; Section 4.3.5a; Table 4.5). These indicators are also used to estimate GHG emissions reduction through restoration (Couwenberg *et al.*, 2011; Evans *et al.*, 2017; Alderson *et al.*, 2019).

Surface proxies similarly inform carbon credit calculations under the IUCN UK Peatland Code *Field Protocol* (IUCN, 2024b), where vegetation and surface features inform estimates of carbon savings through static ecosystem state changes (Birnie and Smyth, 2013; Smyth *et al.*, 2015). Despite availability of detailed biodiversity and ecosystem service metrics, surface proxies continue to dominate carbon benefit estimations (Chapter 2; Sections 2.4; 2.6.2).

In addition to informing representative site selection through comparison of unfavourable and favourable indicators (Chapter 4; Section 4.3.7), detailed JNCC (2009) condition assessments were conducted to address three objectives:

1. **Evaluate restoration effectiveness:** Assess how surface condition varies across intervention techniques and timescales, using surface indicators to infer recovery trajectories.

2. **Critically examine JNCC (2009):** Evaluate whether the framework captures recovery, including broader ecosystem benefits relevant to monitoring and carbon reporting.

3. **Establish surface baselines for sub-surface comparison:** Generate localised surface condition data to contextualise bulk and chemical properties as well as μCT-derived structural analyses, enabling assessment of surface to sub-surface alignment.

For each JNCC (2009) mandatory attribute (Chapter 4; Section 4.3.5a; Table 4.5), data were collected at the $100m^2$ (10x10m) (25, $4m^2$ plots; Chapter 4; Section 4.3.2; Figure 4.7) and $4m^2$ (Chapter 4; Section 4.3.6; Figure 4.12) scale. Average surface condition data are presented and evaluated at the $100m^2$ site scale to support wider interpretation of restoration effectiveness, facilitating more robust extrapolation of findings. This approach also avoids the disproportionate influence of localised anomalies or sensitive areas observed at the $4m^2$ scale (Chapter 4; Section 4.4.3; Appendix G). Detailed plot-level results remain available in Appendix J.

5.1 Vegetation Composition – Indicator Species Richness

JNCC (2009) classifies an area as favourable if at least six indicator species (Chapter 4; Section 4.3.5a; Table 4.5) are present within a $4m^2$ plot. This corresponds to an average of six indicator species at the $100m^2$ site scale for a site to be classified as favourable.
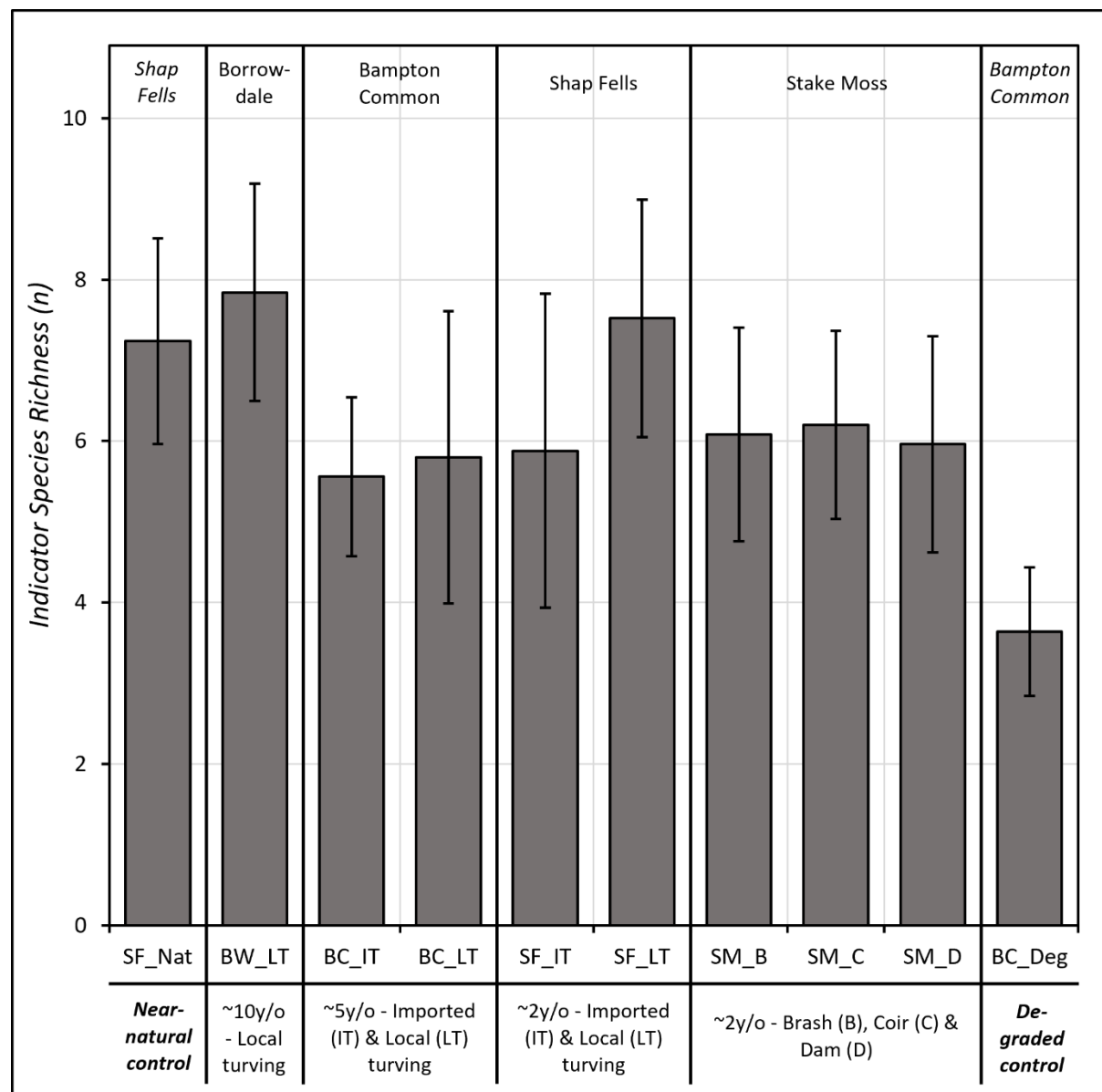
Figure 5.1: Average indicator species richness (JNCC, 2009) across restoration and control sites ($100m^2$). Bars show standard deviation. Black vertical lines separate sites based on restoration age and technique (described in bottom text). The blanket bog complex for each site is labelled at the top.

5.1.1 Control Sites

SF_Nat (near-natural control) exhibits high species richness (~7.2 ± 1.2), consistently maintaining favourable conditions. BC_Deg (degraded control) has the lowest species richness (~3.6 ± 0.8), with low variability, indicating stable unfavourable conditions. *Findings confirm JNCC (2009) effectively differentiates between degraded and near-natural conditions, capturing the impact of long-term degradation on indicator species diversity.*

5.1.2 Restoration Age

The oldest site (~10 years, Borrowdale) exhibits the highest species richness (~7.9 ± 1.4), surpassing near-natural conditions. Intermediate-aged sites (~5 years, Bampton Common) show lower species richness (~5.7–5.8) with variable standard deviation, suggesting average unfavourable conditions. The youngest sites (~2 years, Shap Fells and Stake Moss) also generally exhibit lower species richness (~6.3 on average) with high variability (± 1.5 on average), indicating restoration has initiated recovery but remains inconsistent across sites. *Findings suggest a non-linear recovery trajectory, with species richness increasing rapidly in the first ~2 years, stabilising between 2–5 years, and improving again after ~10 years.*

5.1.3 Restoration Technique

Local turving consistently supports higher species richness than imported turving. At Shap Fells, local turving (SF_LT) exhibits species richness (~7.5 ± 1.5), comparable to near-natural conditions. At Bampton Common, local turving (BC_LT) supports slightly higher species richness (~0.2 ± 0.8) than imported turving (BC_IT). *Findings suggest local*

turves support species recovery, likely due to the retention of site-adapted propagules and reduced disturbance during transport. Minimal difference is observed between heather brash spread at Stake Moss (SM_B) and imported turving at Shap Fells (SF_IT), suggesting both are capable of species recovery, although local turving demonstrates increased species richness (SF_LT).

5.2 Vegetation Composition – Indicator Species Cover

JNCC (2009) defines a plot favourable if ≥50% of total vegetation cover consists of at least three indicator species (Appendix G). Additionally, *Sphagnum* cover must not be exclusively *Sphagnum fallax*, and no single species or species group, including *Eriophorum vaginatum*, *Ericaceous* species (*Calluna vulgaris*, *Erica spp*., *Vaccinium spp*.), or *Trichophorum cespitosum*, should exceed 75% of total vegetation cover. Non-native species must also be absent.

Figure 5.2 presents average indicator species cover proportions across restored, near-natural, and degraded sites, assessed against these thresholds. No non-native species were recorded, so this criterion is not assessed further. Analysis evaluates whether each site meets the cover requirements and examines how species composition varies with restoration age and technique.
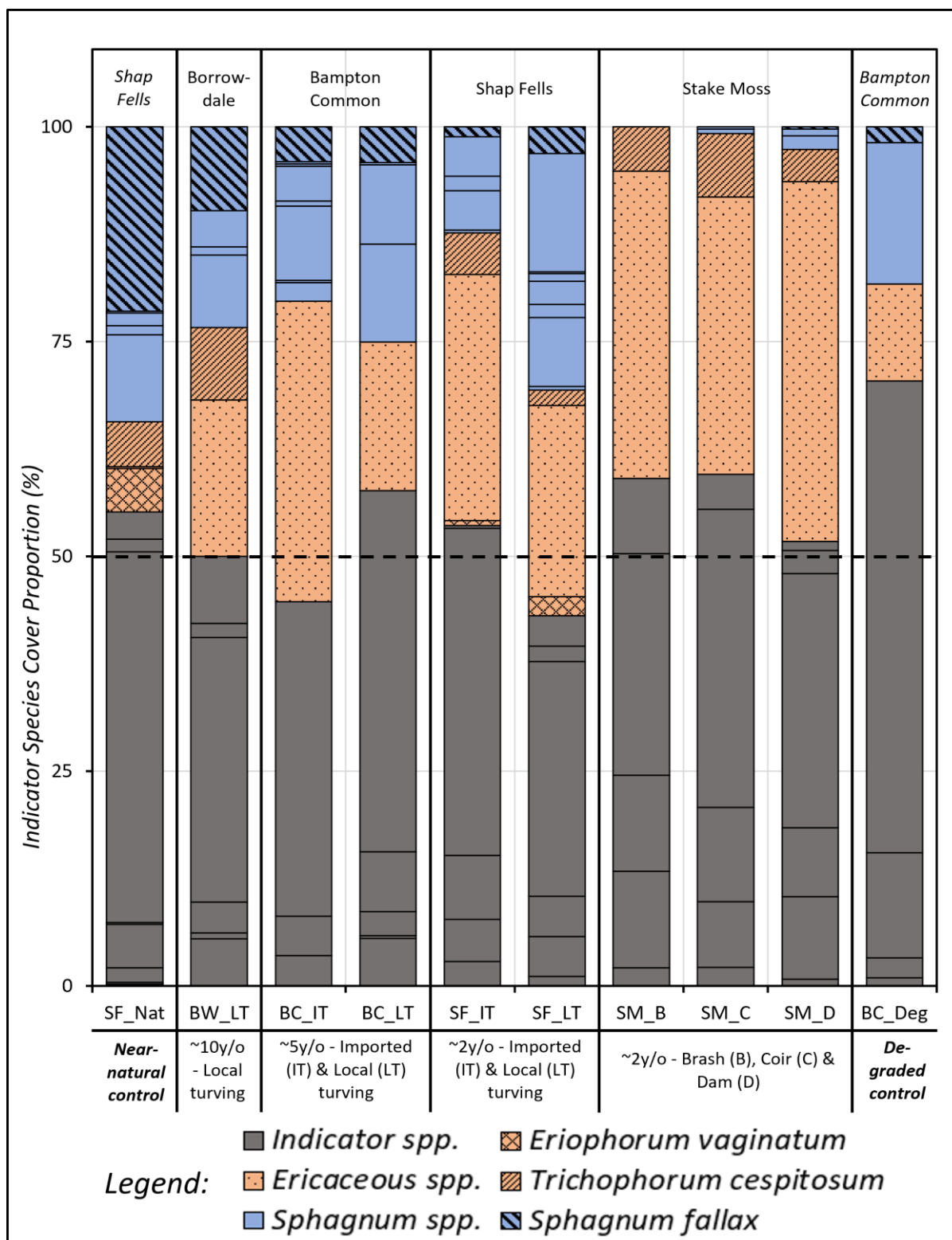
Figure 5.2: Average indicator species contribution to average vegetation cover (JNCC, 2009) across restored and control sites (100m²). Stacked bars show the proportional contribution of indicator species. *Eriophorum vaginatum*, *Ericaceous* species, and *Trichophorum cespitosum* are highlighted in orange and assessed against the dominance threshold (>75% total cover). *Sphagnum* species are displayed in blue, with *Sphagnum fallax* distinguished by bold diagonal lines to assess whether it constitutes 100% of *Sphagnum* cover. Other indicator species are outlined in grey. The dashed horizontal line at 50% marks the cover threshold, indicating whether at least three indicator species contribute to this proportion (black lines separating species contributions above or below). Black vertical lines separate sites by restoration age and technique, with blanket bog complexes labelled at the top.

Figure 5.2 demonstrates all sites meet JNCC (2009) favourable conditions. At least three indicator species contribute to ≥50% of average vegetation cover across all sites. *Eriophorum vaginatum*, *Trichophorum cespitosum*, and *Ericaceous* species do not individually or collectively exceed the 75% dominance threshold, and *Sphagnum* cover is never composed exclusively of *Sphagnum fallax*.

Findings suggest JNCC (2009) indicator species cover thresholds fail to differentiate between near-natural and degraded conditions or capture the effectiveness of restoration. The lack of a total vegetation cover requirement limits its ability to assess cover variance. Additionally, sites with differing species compositions can still be classified as favourable, preventing assessment of recovery trajectories. For instance, Stake Moss – heather brash (SM_B) meets favourable criteria, despite having no *Sphagnum* cover. Moving beyond threshold-based classification allows for relative comparisons, identifying 'more favourable' sites and improving assessment of restoration.

Figure 5.3 presents total average indicator species cover, allowing for actual data comparisons. While all sites remain favourable under JNCC (2009), this breakdown facilitates an evaluation of whether restoration age or technique influences conditions.
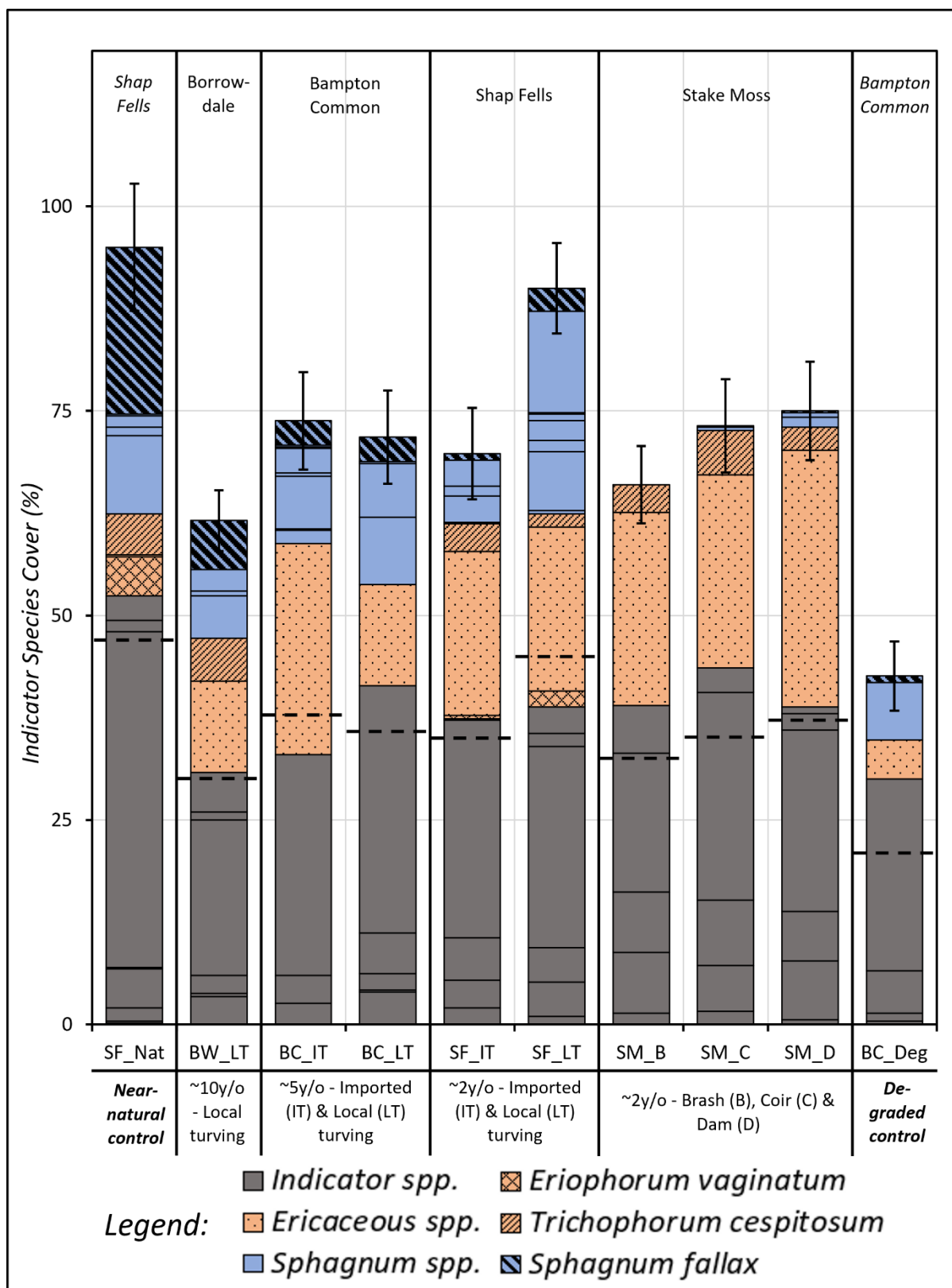
Figure 5.3: Total average indicator species cover (JNCC, 2009) across restoration and control sites (100m^2). Stacked bars represent the actual contribution of indicator species. *Eriophorum vaginatum*, *Ericaceous* species, and *Trichophorum cespitosum* are highlighted in orange. *Sphagnum* species are shown in blue, with *Sphagnum fallax* distinguished by bold diagonal lines. Other indicator species are outlined in grey. Dashed horizontal lines mark the 50% cover threshold. Error bars represent total standard deviation. Black vertical lines separate sites by restoration age and technique, with blanket bog complexes labelled at the top.

5.2.1 Control Sites

SF_Nat (near-natural control) has the highest average indicator species cover (~95 ± 8%) and the greatest *Sphagnum* contribution (~33%), with *Sphagnum fallax* comprising ~20%, ensuring a diverse *Sphagnum* community. BC_Deg (degraded control) has the lowest indicator species cover (~43 ± 4%) and minimal *Sphagnum* (~8%). SF_Nat also contains lower proportions of *Eriophorum vaginatum*, *Trichophorum cespitosum*, and *Ericaceous* species relative to its total vegetation cover. While BC_Deg also has low coverage of these species, this likely indicates overall low indicator species cover rather than a balanced composition. *Findings suggest, beyond binary classification, JNCC (2009) data can distinguish near-natural from degraded conditions. Assessing relative species contributions provides a more detailed evaluation of peatland condition.*

5.2.2 Restoration Age

The oldest site (~10 years, Borrowdale) has lower cover (~62 ± 4%) than some younger sites (~2 years, Shap Fells and Stake Moss). Intermediate-aged (~5 years, Bampton Common) show mixed results (~72–74 ± 6%), comparable to younger sites (~2 years, SF_LT, SF_IT, SM_B, SM_C, SM_D), which range from ~66–90% with high variability. *Findings demonstrate no linear increase in average indicator species cover with restoration age. However, all restored sites exceed degraded conditions (BC_Deg), confirming restoration rapidly establishes 'more favourable' indicator species cover.*

Older (~10 years, Borrowdale) and intermediate (~5 years, Bampton Common) sites exhibit the highest and most consistent *Sphagnum* cover. Younger sites (~2 years, Shap Fells and Stake Moss) have lower *Sphagnum* proportions, except for Shap Fells – imported turves (SF_IT), which records the highest *Sphagnum* proportion (~31%). This

may indicate operational factors, such as careful extraction and placement of turves, preserving their quality (or higher source quality). Nonetheless, *Sphagnum* contribution increases with restoration age. Additionally, *Sphagnum fallax* cover increases from ~0.2% at Stake Moss to ~6% at Borrowdale, aligning more closely with near-natural conditions. *Findings challenge JNCC (2009) assumptions that Sphagnum fallax dominance indicates unfavourable conditions, suggesting instead its presence indicates natural successional processes in restored settings.*

5.2.3 Restoration Technique

Turving techniques support higher *Sphagnum* cover and lower proportions of *Eriophorum vaginatum*, *Trichophorum cespitosum*, and *Ericaceous* species compared to other methods (Stake Moss sites), particularly heather brash spread (SM_B). *This supports turving directly establishes Sphagnum, while other revegetation techniques depend on longer-term natural colonisation.*

Local turving supports greater *Sphagnum* cover and lower *Eriophorum vaginatum*, *Trichophorum cespitosum*, and *Ericaceous* species than imported turving. *Findings suggest Sphagnum is sensitive to transport, with relocation disrupting established communities and allowing vascular and graminoid species to dominate.*

5.2.4 Species Composition Trends

Utilising actual indicator species cover values, Figure 5.4 demonstrates how JNCC (2009) data can support broader analysis of species composition trends beyond threshold-based classification.
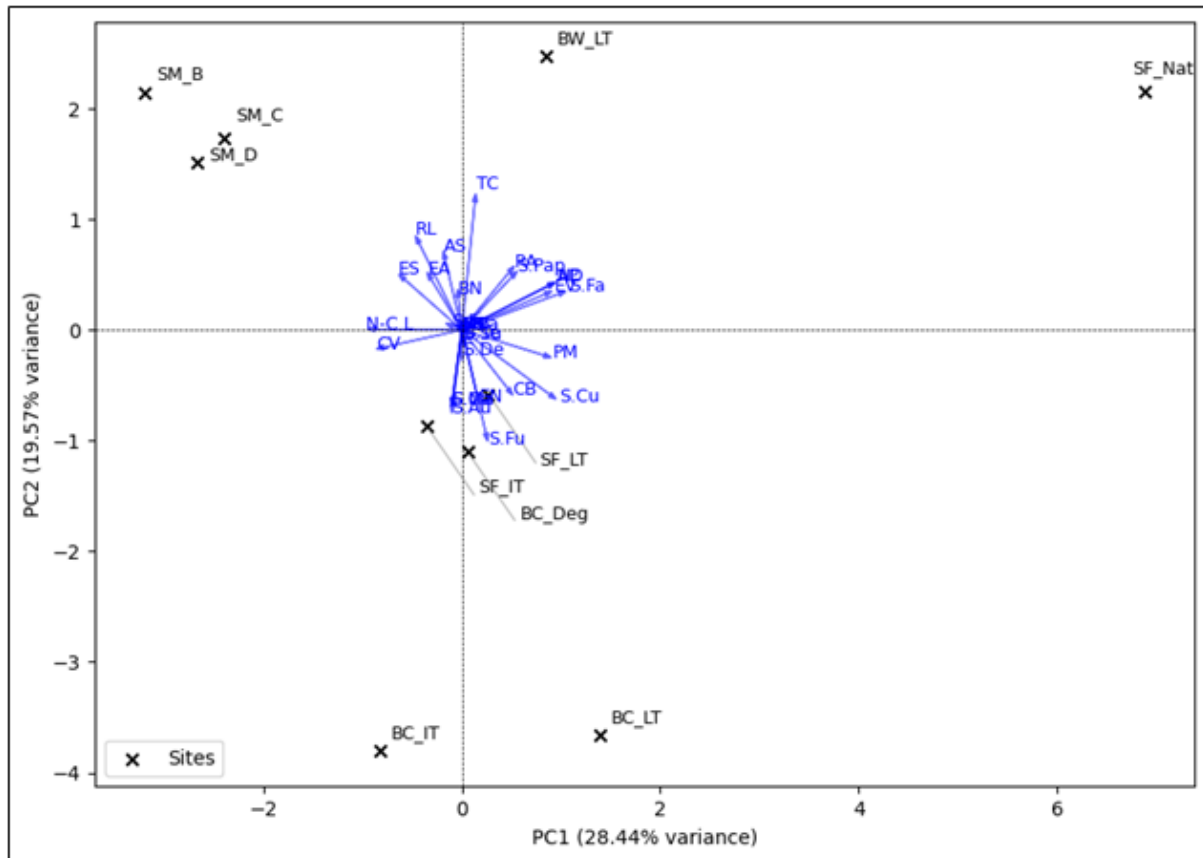
Figure 5.4: Principal Component Analysis (PCA) biplot of average indicator species cover across restored, near-natural, and degraded sites. Black crosses represent sites, and blue vectors represent species contributions. PC1 (28.44% variance) differentiates sites based on species composition. PC2 (19.57% variance) captures additional variation.

While not accounting for total variance, SF_Nat (near-natural conditions) and BC_Deg (degraded conditions) are in opposing quadrants, suggesting different species composition supporting earlier observations (Figure 5.4). SF_Nat and BW_LT are in the same quadrant, indicating more similar species composition. However, BW_LT remains distinct from SF_Nat, suggesting alignment with near-natural conditions has not occurred after ~10 years. BC_Deg clusters with the youngest turved sites (~2 years; SF_LT and SF_IT), indicating early-stage turving retains more degraded species composition.

Stake Moss sites (~2 years, SM_B, SM_C, SM_D) form a distinct cluster in the upper-left quadrant, differing from degraded and restored turved sites. This suggests brash

spreading, coir logs, and stone/timber dams establish unique species compositions that do not align with either degraded or near-natural conditions. Site-specific factors, such as differing peatland mesotopes, may contribute to this variation, consistent with the relatively low total variance explained by the PCA (~48%).

Intermediate-aged sites (~5 years, BC_IT and BC_LT) also occupy a distinct position, supporting restoration creates transitional communities that evolve over time. Alternatively, variation between mesotopes may account for compositional differences, despite consistent NVC classifications as H7130 blanket bog (Chapter 4; Section 4.1.1).

Species vectors indicate no single species drives observed variance. However, *Sphagnum fallax* aligns with SF_Nat and BW_LT, suggesting a potential association with recovering systems, challenging JNCC (2009) guidance, which considers its dominance indicative of unfavourable condition. *Trichophorum cespitosum* shows greater directionality toward BW_LT, indicating it may also suggest longer-term recovery.

Despite low PCA variance, Figure 5.4 suggests restoration improves species composition but does not replicate near-natural conditions within a ~10-year timeframe. Findings highlight the demand to clarify restoration goals, distinguishing between ecosystem replication and functional improvement beyond degraded states.

5.3 Vegetation Structure – Indicators of Browsing

JNCC (2009) defines favourable conditions if less than 33% of indicator dwarf shrub species (*Arctostaphylos* spp.*, Calluna vulgaris*, *Erica* spp.*, Empetrum nigrum*, and *Vaccinium* spp.) show signs of browsing, while *Betula nana* and *Myrica gale* should not exceed 66%.

Figure 5.5 presents average indicator dwarf shrub species proportions alongside browsing evidence (Chapter 4; Section 4.3.5a; Table 4.5) across restored, near-natural, and degraded sites. JNCC (2009) thresholds have been converted into averages for comparison, with a 33% browsing limit for dwarf shrubs and a 66% limit for *Betula nana* and *Myrica gale*. This data evaluates browsing impacts on surface conditions and the effectiveness of JNCC (2009) criteria. *Myrica gale* was not recorded in any plots and is therefore excluded from assessment.
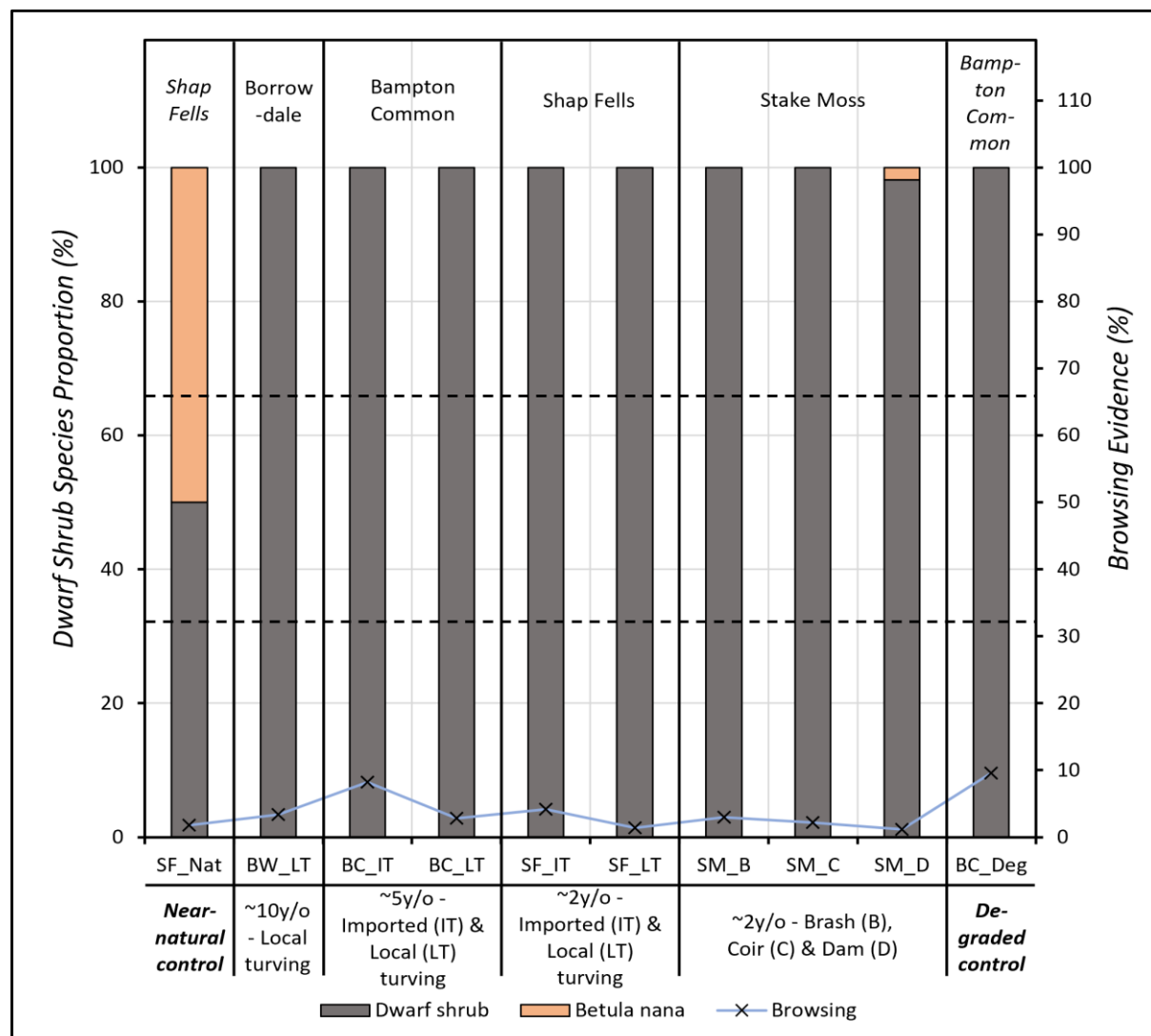
Figure 5.5: Average dwarf shrub species proportions and browsing evidence across restored, near-natural, and degraded sites (100m^2). *Betula nana* is highlighted in orange to assess whether browsing exceeds the 66% threshold (indicated by a horizontal dashed line), while all other dwarf shrub species are shown in grey, with the 33% threshold also marked by a horizontal dashed line. The blue line represents average browsing evidence. Black vertical lines separate sites by restoration age and technique, with blanket bog complexes labelled at the top.

Browsing evidence remains below JNCC (2009) thresholds at all sites, classifying them favourable. Similar to indicator species contributions (Figure 5.2), assessment fails to differentiate between near-natural (SF_Nat) and degraded (BC_Deg) conditions. Although, BC_Deg has low total vegetation cover (Figure 5.3), limiting browsing opportunities. Despite this, data variations reveal sites that are moderately 'more favourable' than others.

5.3.1 Control Sites

BC_Deg (degraded control) exhibits the highest average browsing evidence (9.6%), while SF_Nat (near-natural control) records one of the lowest (1.8%). This is important, as SF_Nat also has the highest average indicator species cover (95%, Figure 5.3), whereas BC_Deg has the lowest (42.6%, Figure 5.3). Although both remain within JNCC (2009) favourable limits, findings suggest near-natural conditions experience lower grazing pressure. *This indicates grazing exclusion was effective at Shap Fells, where fencing and intensive herbivore management were implemented*, unlike at Bampton Common (Chapter 3; Section 4.2.1; Table 4.3). Alternatively, more waterlogged terrain at Shap Fells may have naturally limited herbivore access.

5.3.2 Restored Sites

Browsing evidence across restored plots ranged from 1.2–8.2%, with no clear trend based on restoration age or technique. *This suggests grazing pressure is influenced more by land management than by restoration design*, as most interventions focused on direct rewetting and revegetation rather than herbivore control. Notably, Bampton Common was the only restored site exposed to ongoing sheep grazing. BC_IT (~5 years, imported turves) recorded the highest browsing pressure (8.2%), comparable to the degraded

control. This indicates grazing may affect restoration outcomes, including turve establishment and species composition. Nonetheless, all restored sites remained within JNCC (2009) browsing thresholds, even accounting for dwarf-shrub dominance (*Ericaceous spp.*; Figure 5.3).

5.4 Physical Structure – Degradation Extent

JNCC (2009) defines favourable conditions based on the extent of degradation features, with the following criteria (extracted from Chapter 4; Section 4.3.5a; Table 4.5):

1. **No evidence of burning.**

2. **Eroding peat must cover less area than stable re-deposited peat and new growth.**

3. **Disturbed ground, bare peat, and/or signs of active drainage must cover less than 10% of area.**

4. **Less than 10% of *Sphagnum* cover should be damaged.**

Figure 5.6 presents total average degradation cover and the proportional contribution of each degradation feature across restored, near-natural, and degraded sites. This assessment quantifies physical degradation extent, establishing a baseline for evaluating restoration effectiveness in relation to JNCC (2009) thresholds. Burning was not observed in any plot and is therefore excluded from further analysis.
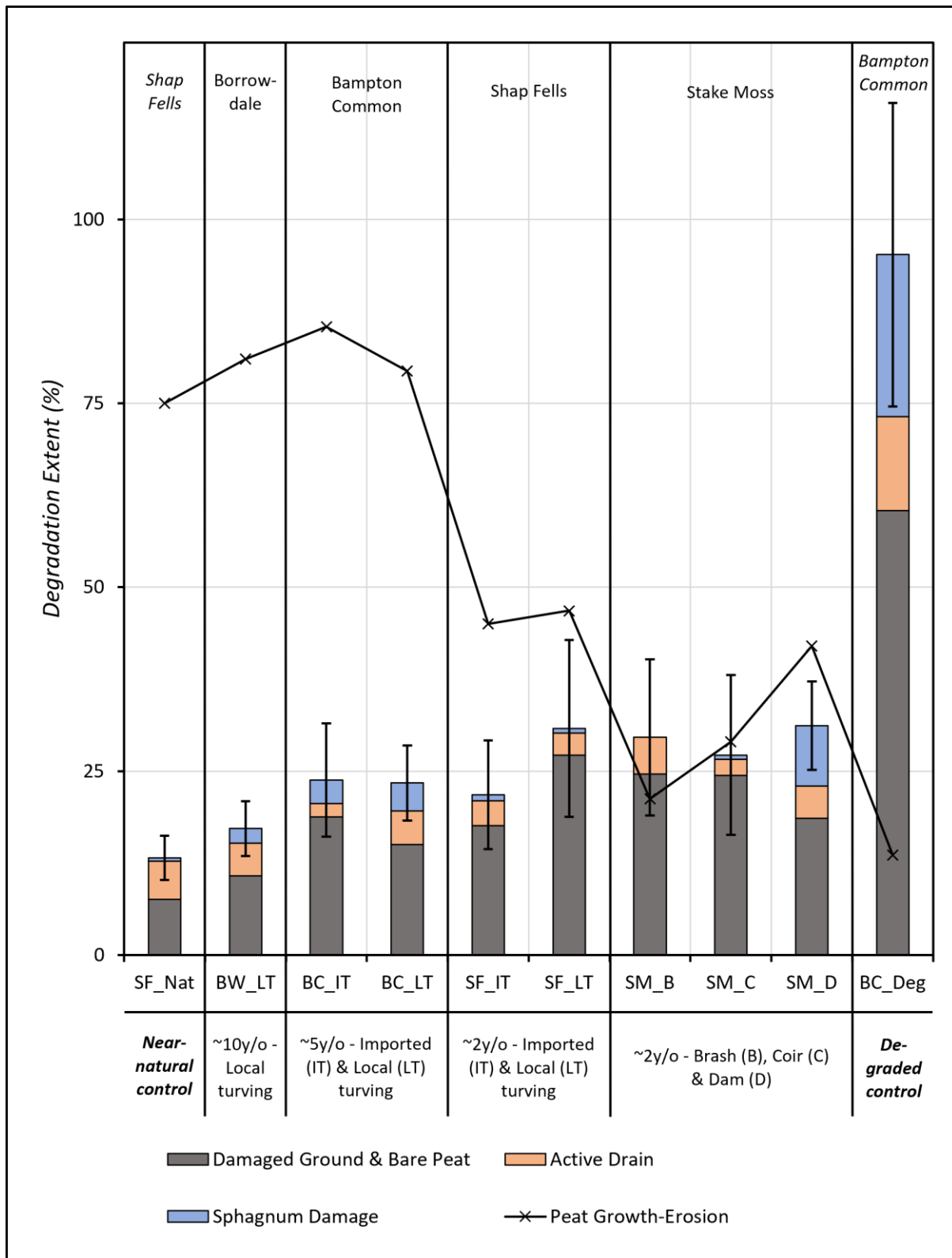
Figure 5.6: Average degradation cover (JNCC, 2009) and relative contributions of damaged ground and bare peat (grey), active drains (orange), and *Sphagnum* damage (blue) across restored, near-natural, and degraded sites (100m^2). Peat growth minus erosion is represented by the black line. Black vertical lines separate sites by restoration age and technique, with blanket bog complexes labelled at the top.

5.4.1 Control Sites

Near-natural (SF_Nat) and degraded (BC_Deg) controls meet JNCC (2009) favourable criteria for erosion, with peat regrowth exceeding erosion extent (positive values: 75% and 13.6%, respectively). However, SF_Nat exhibits 61.4% greater peat regrowth, supporting its 'more favourable' condition and greater carbon sequestration potential. BC_Deg meets the criterion, but its low value (13.6%) highlights the ambiguity of JNCC (2009), which lacks a clear threshold.

SF_Nat remains within JNCC (2009) limits for disturbed ground and bare peat (7.6%), while BC_Deg exceeds the 10% threshold (60.4%). Similarly, SF_Nat meets the drainage threshold (5.2%), whereas BC_Deg surpasses (12.8%), demonstrating JNCC (2009) differentiates near-natural and degraded conditions based on drainage extent. *Sphagnum* damage is minimal at SF_Nat (0.4%), indicating healthy moss cover, while BC_Deg records 22%, classifying as unfavourable. *Findings support the utility of JNCC (2009) in distinguishing near-natural from degraded conditions across key degradation indicators, with the exception of erosion.* This limitation may indicate the framework's vague guidance on erosion, which states regrowth should exceed eroding peat but provides no quantitative threshold.

5.4.2 Restoration Age

Restored sites meet JNCC (2009) favourable criteria for peat regrowth, with positive growth versus erosion values. However, extent varies by restoration age. Older (~10 years, Borrowdale) and intermediate (~5 years, Bampton Common) sites exhibit high values (79.4–85.4%), while younger (~2 years, Shap Fells and Stake Moss) show lower values (21.2–46.8%), suggesting peat regrowth remains limited early on but improves after ~5

years. No restored site meets JNCC (2009) favourable criteria for disturbed ground and bare peat, though both decline over time. The youngest sites (~2 years) exhibit 22.5% coverage, intermediate (~5 years) show 16.9%, and the oldest (~10 years) records 10.8%, approaching SF_Nat conditions. This suggests restoration disturbance (e.g., tracking, turve placement) and vegetation succession contribute to surface stabilisation. Some unfavourable features persist even after ~10 years. Restored sites meet JNCC (2009) thresholds for drainage extent and *Sphagnum* damage (<10%), indicating restoration reduces active drainage and improves *Sphagnum* quality via wetter conditions (effective rewetting). However, Stake Moss sites contain little to no *Sphagnum* cover (Figure 5.3), questioning whether JNCC (2009) should include a minimum *Sphagnum* threshold.

Findings highlight the limitations of JNCC (2009) thresholds in assessing restoration impacts on degradation, as sites are classified as either favourable or unfavourable without capturing trajectories. While degradation features decline over time, no restored site fully meets SF_Nat (near-natural) conditions, suggesting restoration may not achieve favourable status within a decade.

5.4.3 Restoration Technique

Stake Moss sites restored using heather brash (SM_B), coir logs (SM_C), and stone/timber dams (SM_D) exhibit higher degradation totals and lower peat regrowth versus erosion values than the comparable 2-year-old Shap Fells site. This difference is especially clear when comparing heather brash spreading to turving as a revegetation approach, suggesting turving may accelerate recovery by directly introducing peat-forming vegetation. Beyond this, restoration technique has minimal influence on degradation extent under JNCC (2009).

5.4.4 Site Degradation Trends

Adopting the actual degradation cover values, Figure 5.7 builds on the previous threshold-based assessment by revealing broader site-level trends in degradation extent, as captured by JNCC (2009) indicators.
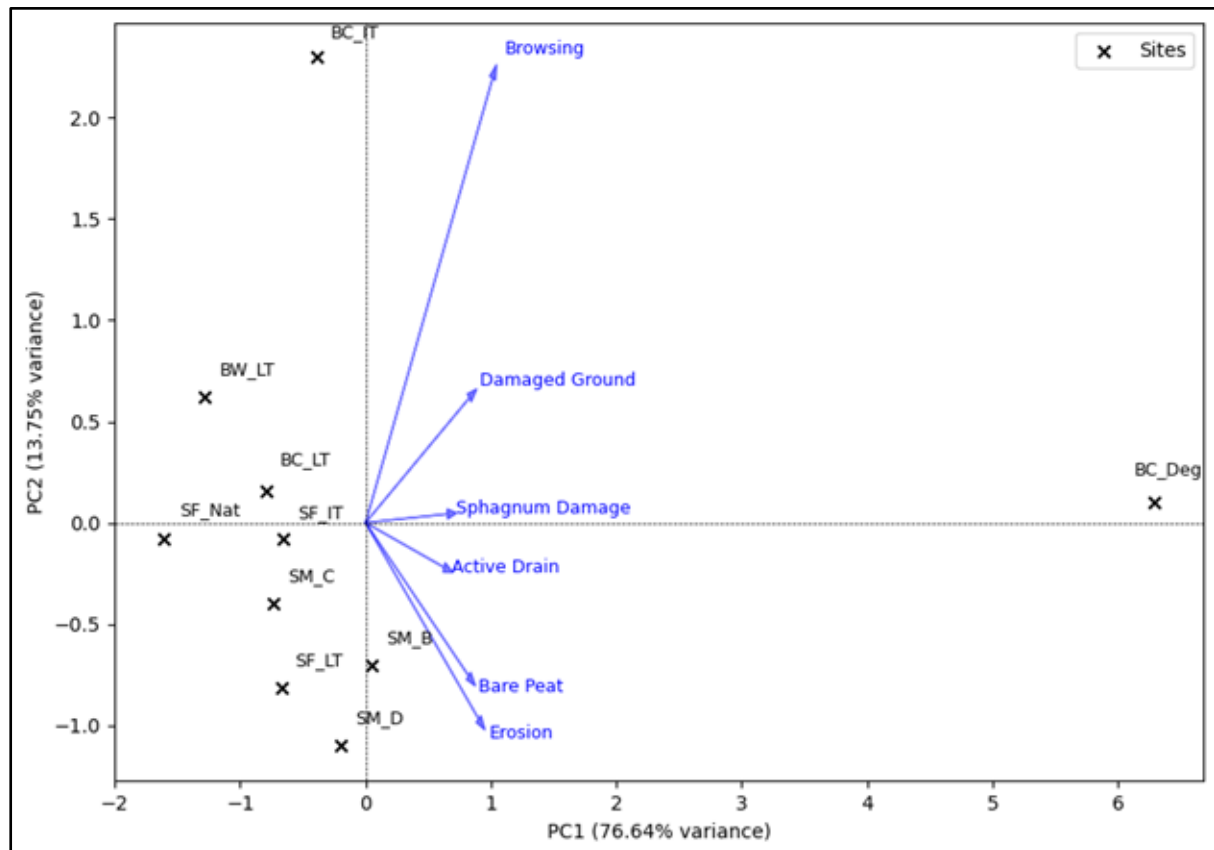
Figure 5.7: Principal Component Analysis (PCA) biplot of average degradation extent across restored, near-natural, and degraded sites. Black crosses represent sites, and blue vectors represent degradation type contributions. PC1 (76.64% variance) differentiates sites based on degradation type and extent. PC2 (19.57% variance) captures additional variation.

BC_Deg (degraded control) is positioned in the far-right quadrant, influenced by damaged ground, *Sphagnum* damage, and active drainage, while SF_Nat (near-natural control) is in the far-left. This confirms degradation composition and extent differ between near-natural and degraded conditions and that JNCC (2009) data effectively captures this (>76% variance captured in PCA).

Restored sites cluster closer to SF_Nat than BC_Deg, supporting restoration initiates rapid surface recovery within ~2 years. BW_LT (~10 years, Borrowdale – local turving) is closest to SF_Nat, followed by BC_LT (~5 years, Bampton Common – local turving). Younger restored sites (~2 years, Stake Moss and Shap Fells) are positioned further towards BC_Deg, indicating early restoration stages retaining some degradation features. This supports degradation declining with time since restoration.

Vectors show bare peat, erosion, and active drainage cluster near the youngest restored sites, indicating these features persist in early-stage restoration (~2 years). Their closer association suggests they interact, potentially compounding degradation effects. Browsing, damaged ground, and *Sphagnum* damage align with intermediate to older restored sites. The connection between browsing and vegetation damage suggests beyond ~5 years, site-level management interventions (e.g., herbivore exclusion) may play a larger role in reducing degradation. This is supported by BC_IT (~5 years, Bampton Common – imported turving) aligning with the browsing vector, suggesting sheep grazing influences degradation composition. *Findings demonstrate the importance of assessing degradation impacts in combination, rather than in isolation (e.g., drainage; Chapter 2; Section 2.3.5).*

5.5 JNCC Outcomes Summary

JNCC (2009) mandates all criteria relating to vegetation composition, vegetation structure, and physical structure must be met for a site to be classified as favourable (Chapter 4; Section 4.3.5a; Table 4.5). A simplified version of these criteria was used in Chapter 4 to inform representative site selection, whereas the full JNCC framework is applied here to evaluate outcomes. Under these criteria, only SF_Nat (near-natural

control) meets the standard (Table 5.2). While this confirms the representativity of site selection (Chapter 4), it highlights the framework's inability to differentiate between restored and degraded sites along a gradient of recovery; restored sites remain classified as unfavourable even after a decade despite clear improvements. *Findings support the original purpose of JNCC (2009) was to assess ecological condition rather than evaluate restoration effectiveness (Chapter 2; Section 2.6.2).*

However, beyond mandatory classification, JNCC (2009) criteria begin to allow for a more nuanced evaluation, categorising sites as 'more favourable' or 'less unfavourable' based on specific restoration outcomes. These criteria are re-summarised in Table 5.1.

Table 5.1: Summary of JNCC (2009) attributes, criteria, and thresholds for favourable condition.

Attribute	Criterion	Threshold/Condition
Vegetation Composition	1. Indicator species richness	≥6 species (Appendix G)
	2.1 Indicator species cover: ≥3 species	≥50% total vegetation cover
	2.2 Indicator species cover: *Sphagnum fallax*	Must not be dominant
	2.3 Indicator species cover: *Calluna vulgaris*, *Erica spp.*, *Vaccinium spp.*	≤75% total vegetation cover
Vegetation Structure	3. Browsing pressure on indicator dwarf shrubs	<33% of vegetation cover
	4. Browsing pressure on *Betula nana* and *Myrica gale*	<66% of vegetation cover
Physical Structure	5. Eroding peat versus stable regrowth	Erosion < regrowth across area
	6. Disturbed ground and bare peat	<10% of area
	7. Active drainage	<10% of area
	8. *Sphagnum* damage	<10% of *Sphagnum* cover

Table 5.2 presents the number of criteria met per site, along with specific criteria that were not met.

Table 5.2: JNCC (2009) favourable condition criteria achieved by restored, near-natural, and degraded sites.

Site	Criteria Achieved (*n*)	Criteria Failed
SF_Nat	*10*	*N/A*
BW_LT	9	6: <10% of area should be disturbed ground or bare peat.
BC_IT	8	1: ≥6 indicator species. 6: <10% of area should be disturbed ground or bare peat.
BC_LT	8	1: ≥6 indicator species. 6: <10% of area should be disturbed ground or bare peat.
SF_IT	8	1: ≥6 indicator species. 6: <10% of area should be disturbed ground or bare peat.
SF_LT	9	6: <10% of area should be disturbed ground or bare peat.
SM_B	9	6: <10% of area should be disturbed ground or bare peat.
SM_C	9	6: <10% of area should be disturbed ground or bare peat.
SM_D	8	1: ≥6 indicator species. 6: <10% of area should be disturbed ground or bare peat.
BC_Deg	*6*	*1: >6 indicator species.* *6: <10% of area should be disturbed ground or bare peat.* *7: <10% of area should show signs of active drainage.* *8: <10% of total Sphagnum cover should be damaged.*

Table 5.2 confirms SF_Nat is the only site meeting all criteria, classifying as favourable under JNCC (2009). BC_Deg fails four criteria, including vegetation composition and three of the four physical structure indicators, supporting its classification as degraded. Restored sites consistently failed the disturbed ground and bare peat criterion (<10%), suggesting degraded surface features can persist for over a decade post-restoration, or certain techniques may not fully mitigate damage. An alternative explanation is restoration-induced disturbance, such as machinery tracking, or site-level failings like turve slippage, may persist despite efforts to avoid these during site selection (Chapter 4; Section 4.3).

Some restored sites also failed the indicator species richness criterion of >6 species (BC_IT, BC_LT, SF_IT, SM_D), often in combination with high levels of disturbed ground or bare peat. This suggests a possible relationship between limited vegetation succession and persistent surface degradation, supporting the value of assessing combined degradation impacts rather than isolated indicators (Chapter 2; Section 2.3.5). *While these findings offer insight into restoration effectiveness, the categorical framework of JNCC (2009) still fails to account for restoration age or technique, limiting its ability to capture trajectories of recovery.*

5.5.1 Revised Surface Condition Scoring

JNCC (2009) condition data were converted into a continuous, quantitative format to overcome binary and threshold-based limitations and enable more effective evaluation of restoration success. Findings showed restored sites improved relative to the degraded control, with increases in indicator species richness (Section 5.1; Figure 5.1), cover (Section 5.2; Figure 5.3), and reductions in degradation extent (Sections 5.3; Figure 5.5; 5.4; Figure 5.6). Variation among sites was attributed to restoration age and technique, with generally 'more favourable' scores in older sites and those restored using local turving. However, to enable more meaningful statistical comparison and summarise trends, values were normalised onto a 0–1 scale across the JNCC (2009) surface indicators assessed (Chapter 4; Section 4.3.5a; Table 4.5). This also enables direct comparison with sub-surface metrics assessed in subsequent chapters. Table 5.3 outlines the normalisation process, while Table 5.4 presents the resulting site-level scores. Plot-level (4m^2) data are provided in Appendix J.

Table 5.3: Summary of refined surface condition scoring criteria.

Criterion	Description	Raw Metric	Scoring (0-1)	Notes
1	Indicator species richness	Total number of indicator species	Richness/Max richness observed	No cap; higher = better
2	Indicator species cover	% cover of all indicator species	Cover %/Max cover % observed	Indicates dominance of indicator flora
3	*Sphagnum* cover	% cover of all *Sphagnum* species	*Sphagnum* %/Max observed	Replaces S. *fallax* dominance; higher = better
4	Vascular dominance	Max % of dominant vascular spp. (*Eriophorum*, *Calluna*, etc.)	1 – (Dominant %/75), capped at 1 and floored at 0	Inverse scaled; JNCC threshold = 75%
5	Browsing pressure	% of all relevant species browsed	1 – (Browsing %/Max observed), capped at 1	Combines dwarf shrubs, *Betula*, *Myrica*
6	Surface regrowth	Regrowth % – erosion %	(Value – Min)/(Max – Min)	Min-max normalised; can be negative
7	Bare peat extent	% of surface covered by bare peat	1 – (Bare peat %/Max observed), capped at 1	Worst degradation feature
8	Disturbed ground extent	% of surface disturbance	1 – (Disturbed %/Max observed), capped at 1	Captures herbivore prints, machinery etc.
9	Active drainage	% of plot affected by active drainage	1 – (Drainage %/Max observed), capped at 1	Indicates hydrological degradation
10	*Sphagnum* damage	% of *Sphagnum* visibly damaged	If present: 1 – (Damage %/Max observed) If absent: Score = 0	Absence of *Sphagnum* = unfavourable

Table 5.4: Revised average condition scores for each site across surface indicators (JNCC, 2009), calculated using a gradient-based scoring system (0–1).

Criterion	*BC_Deg*	BW_LT	BC_IT	BC_LT	SF_IT	SF_LT	SM_B	SM_C	SM_D	*SF_Nat*
C1	0.46	1.00	0.71	0.74	0.75	0.96	0.78	0.79	0.76	0.92
C2	0.45	0.65	0.78	0.76	0.73	0.95	0.69	0.77	0.79	1.00
C3	0.24	0.44	0.46	0.55	0.26	0.85	0.00	0.02	0.06	1.00
C4	0.94	0.78	0.66	0.83	0.68	0.69	0.64	0.61	0.54	0.87
C5	0.00	0.65	0.15	0.71	0.56	0.85	0.69	0.77	0.88	0.81
C6	0.00	0.94	1.00	0.92	0.44	0.46	0.11	0.21	0.40	0.86
C7	0.00	0.89	0.84	0.79	0.65	0.46	0.56	0.57	0.63	0.91
C8	0.00	0.72	0.47	0.69	0.79	0.67	0.64	0.63	0.79	0.83
C9	0.00	0.66	0.86	0.64	0.73	0.77	0.61	0.83	0.66	0.59
C10	0.00	0.91	0.85	0.83	0.96	0.97	0.00	0.97	0.63	0.98
Score	0.21	0.76	0.68	0.75	0.66	0.76	0.47	0.62	0.61	0.88

Using normalised scores derived from continuous JNCC (2009) values, Table 5.4 demonstrates clearer contrasts between control and restored conditions. SF_Nat (near-natural control) exhibited the highest score (0.88), indicating diverse vegetation, minimal disturbance, and extensive *Sphagnum* cover. BC_Deg (degraded control) recorded the lowest (0.54), characterised by low species richness, vascular dominance, and erosion. *Findings validate the effectiveness of the sampling strategy (Chapter 4) and support confidence in subsequent condition-based inferences*.

Restored sites scored between these baselines. Borrowdale (~10 years post-restoration) achieved the highest score (0.76), indicating substantial improvements in species composition and surface stability. Bampton Common (~5 years post-restoration) also scored highly, with BC_LT (local turves) and BC_IT (imported turves) recording 0.68 and 0.75, respectively. Younger sites (~2 years post-restoration), such as Shap Fells and Stake Moss, showed slightly lower and more variable scores (0.60–0.72). Locally turved plots (LT) generally outperformed imported turves (IT) at the same sites, likely due to improved structural integrity and retention of site-specific propagules.

Stake Moss sites consistently scored closer to BC_Deg, particularly SM_B (heather brash spreading), suggesting turving may offer a more effective revegetation approach. This may be related to the direct transfer of acrotelm in turving, in contrast to the natural development associated with spreading techniques. Nonetheless, all restored sites outperformed BC_Deg, indicating measurable recovery. *Most, particularly older restorations, showed closer alignment with SF_Nat, though none achieved equivalent favourable status, suggesting restoration outcomes remain functionally distinct from near-natural conditions after a decade*.

5.5.2 Role of *Sphagnum* and Microtopographic Variation

As discussed in Section 5.2, JNCC (2009) does not set a minimum threshold for bryophyte or *Sphagnum* presence, despite its importance in peat-formation and carbon accumulation (Chapter 2; Section 2.1). Instead, it only provides a maximum threshold for *Sphagnum fallax* dominance, which findings suggest could limit the ability of JNCC (2009) to assess restoration effectiveness (Section 5.2). Moreover, microtopographic variation is excluded from assessment criteria, only recorded as a 'sensitive area' (Appendix G) despite its functional importance for water retention and surface structure (Chapter 2; Section 2.2.1).

As part of the surveying approach (Chapter 4; Section 4.5.5; Appendix I), bryophyte and *Sphagnum* species composition and microtopographic variation were recorded. This included the cover of specific species and counts of hummock and hollows (>20cm elevation difference, following Givele *et al.*, 2004), enabling further analysis of their role in surface condition and restoration effectiveness.

a) *Sphagnum Composition*

Figure 5.8 presents the average cover of bryophyte and *Sphagnum* species, classified as mosses under JNCC (2009), alongside the dominant species recorded at each site.
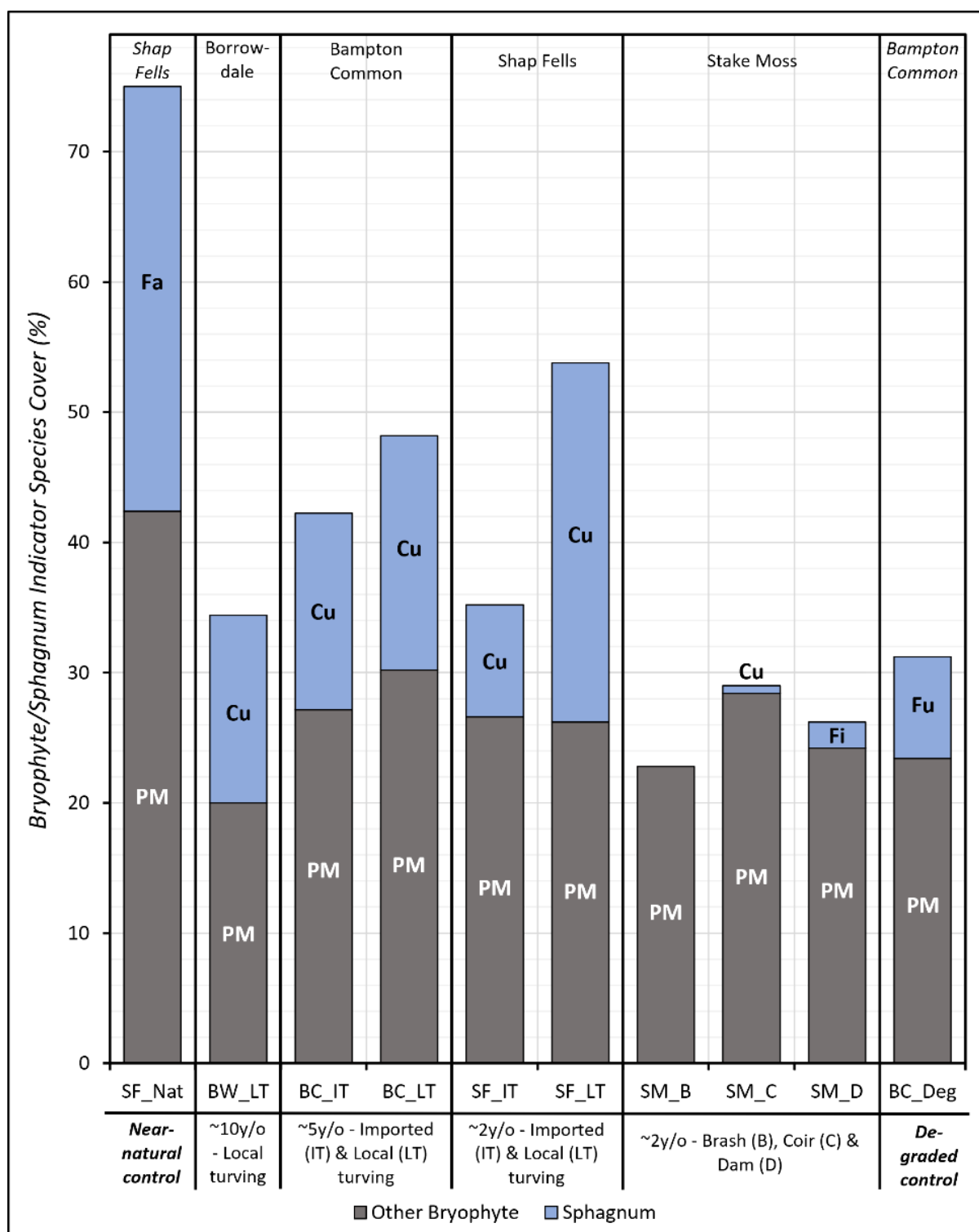
Figure 5.8: Breakdown of JNCC (2009) moss indicator species cover across restored and control sites. Average bryophyte cover proportions (Figure 5.3) are categorised into *Sphagnum* (blue) and other mosses (dark grey). Dashed horizontal lines mark the 50% cover threshold. Error bars represent total standard deviation. Black vertical lines separate sites by restoration age and technique, with blanket bog complexes labelled at the top.

i) Control Sites:

SF_Nat (near-natural control) exhibited the highest *Sphagnum* cover (32.6%) within the greatest total bryophyte indicator species cover (Figure 5.3). *Sphagnum fallax* was the dominant species, unique to SF_Nat. BC_Deg (degraded control) recorded lower *Sphagnum* cover (7.8%) within a limited bryophyte extent and was the only site where *Sphagnum fuscum* dominated. Pleurocarpous mosses were the dominant non-*Sphagnum* bryophytes across controls and restored sites. *Findings suggest quantifying Sphagnum cover and identifying dominant species enables clearer distinction between degraded and near-natural conditions.* This aligns with condition scores in Table 5.4 and supports the inclusion of specific *Sphagnum* data within future iterations of the JNCC (2009) framework or evaluation protocols.

ii) Restoration Technique:

While no clear trends were observed with restoration age, restoration technique appeared influential. Turved sites consistently supported higher bryophyte and *Sphagnum* cover than sites restored using alternative methods (Stake Moss), especially heather brash spreading (SM_B), which exhibited no *Sphagnum*. *This indicates turving more effectively reintroduces Sphagnum through direct acrotelm placement than techniques relying on natural succession.*

Species differences were also evident. Turves sites were dominated by *Sphagnum cuspidatum*, associated with waterlogged conditions and resilience (Van Der Molen *et al.*, 1994; Breeuwer *et al.*, 2009; Bengtsson *et al.*, 2016), while Stake Moss sites exhibited more variable species, including *Sphagnum fimbriatum*. *This suggests turving supports more effective rewetting through water-retentive Sphagnum hyaline cells (Chapter 2;*

Section 2.2.1). Locally sourced turves further outperformed imported in *Sphagnum* cover, likely due to retained structural integrity and native propagules.

Findings further support the inclusion of *Sphagnum* metrics in restoration assessment, offering a sensitive indicator of early-stage functional recovery.

b) Microtopographic Variation

Figure 5.9 presents the average number of hummock to hollow complexes recorded per site, features designated as 'sensitive areas' under JNCC (2009) (Appendix G).
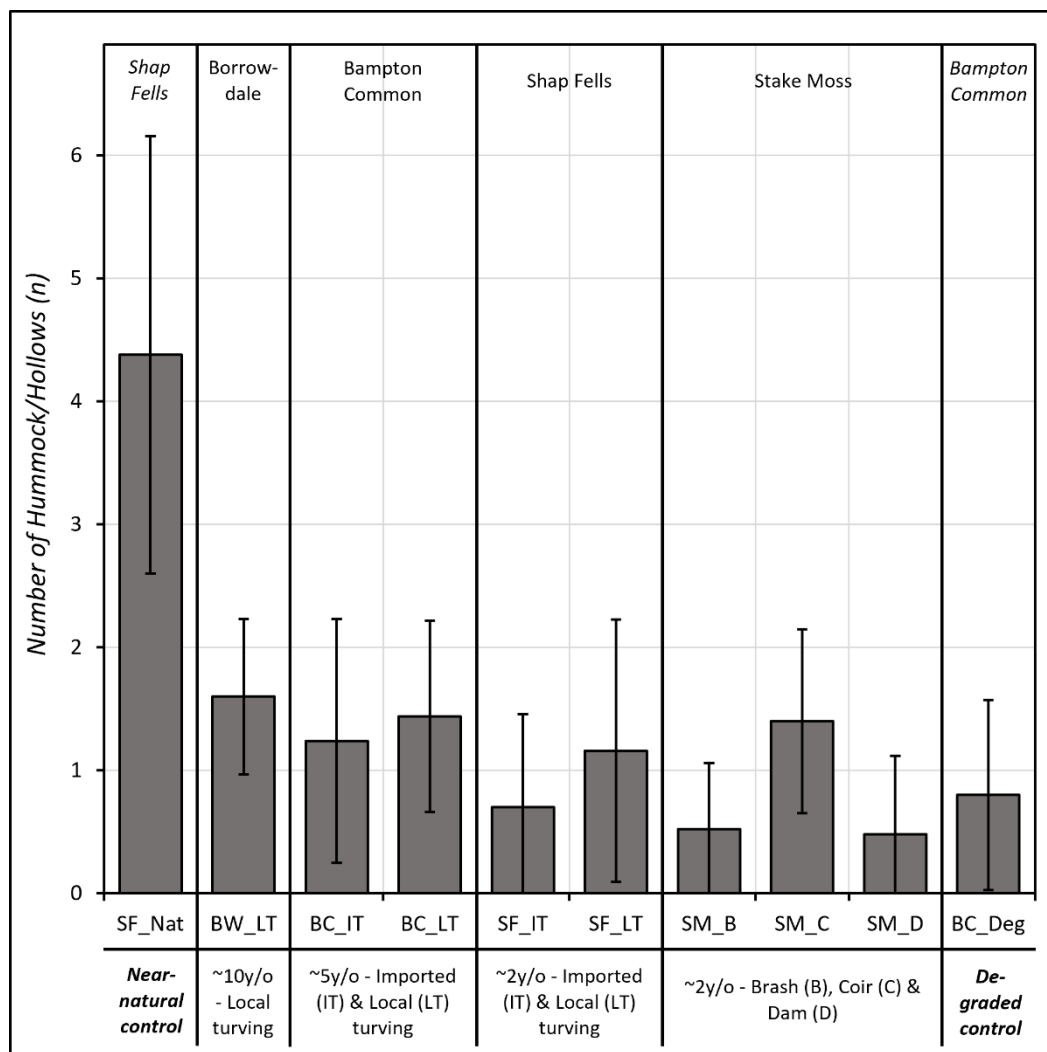
Figure 5.9: Average number of hummock to hollow complexes ('sensitive areas'; JNCC, 2009) across restoration and control sites (100m^2). Bars show standard deviation. Black vertical lines separate sites based on restoration age and technique (described in bottom text). The blanket bog complex for each site is labelled at the top.

i) Control Sites:

SF_Nat (near-natural control) exhibited a high average number of hummock–hollow complexes (~4.5 per plot), indicating natural microtopographic variation consistent with favourable condition. BC_Deg averaged fewer than one complex per plot, suggesting a more homogenous surface prone to rapid runoff (Chapter 2; Section 2.2.1). This indicates reduced surface water uptake capacity and highlights a clear microtopographic distinction between near-natural and degraded sites, supporting its inclusion in condition assessments.

ii) Restored Sites:

No strong relationship was observed between microtopography and restoration age or technique. However, most restored sites showed greater microtopographic variation than BC_Deg, and older turved sites (e.g., Borrowdale, ~10 years; Bampton Common, ~5 years) were closest to SF_Nat. This suggests restoration can increase surface complexity, improving water retention and resilience (Chapter 2; Section 2.2.1). Nonetheless, SF_Nat exhibited higher values, indicating restoration does not fully replicate near-natural microtopography even after a decade. *Although less strongly associated with surface condition scores than Sphagnum, microtopographic patterns suggest related trends*. SF_Nat showed the greatest variation alongside the highest *Sphagnum* cover and dominance of *Sphagnum fallax*, challenging its exclusion from favourable classification under JNCC (2009). Restored sites showed greater variation than BC_Deg, supporting its potential as an additional indicator of favourable condition.

> Microtopography is a clear indicator of near-natural functional condition, though within a decade, there is little indication restoration supports its development.

5.6 Chapter Synthesis and Discussion

The JNCC (2009) *Common Standards Monitoring Guidance (CSM) for Upland Habitats: Blanket Bogs* effectively differentiates degraded from near-natural conditions, fulfilling its role as a monitoring tool (Chapter 2, Section 2.6.2) and justifying its use for representative site selection (Chapter 4, Section 4.3.5). *However, its binary, threshold-based classification limits its ability to distinguish restored from degraded sites, despite ecological improvements* (Shepherd *et al.*, 2013; Birnie *et al.*, 2023; Crowle *et al.*, 2025).

5.6.1 Refinements through Continuous Data and Normalisation

Normalising condition scores onto a continuous scale addressed this limitation, enabling a more sensitive and quantitative assessment. Once thresholds were removed, restored sites consistently outperformed the degraded, showing higher indicator species richness and cover and reduced bare peat extent. These improvements became clear when restoration age and technique were evaluated along a continuum from 'less' to 'more favourable' condition. *Findings support re-evaluating or removing fixed thresholds when assessing restoration outcomes*.

5.6.2 Impact of Technique and Time

Surface recovery was greatest at turved sites, particularly where local turves were used, likely due to retained propagules and intact acrotelm structure (Chapter 2; Sections 2.1; 2.5.2). In contrast, heather brash plots at Stake Moss (~2 years post-restoration) exhibited lower species richness, increased bare peat, and reduced *Sphagnum* cover, demonstrating the influence of revegetation technique on specific indicators. Older turved sites (e.g., Borrowdale, ~10 years) showed further gains and fewer disturbance

features, suggesting benefits over time as systems stabilise. Grazing exclusions also supported *Sphagnum* and dwarf shrub recovery by reducing browsing pressure. *These findings support turving, particularly with local material, as a more effective revegetation technique than alternatives such as heather brash spreading and challenge assumptions that recovery is achieved within five years* (Chapter 2; Section 2.7).

5.6.3 Interacting Pressures

PCA results reinforced degradation pressures occur in combination. *Sphagnum* damage clustered with drainage, likely reflecting desiccation, while erosion and bare peat formed a second cluster, indicating compounding impacts from trampling and surface instability (Chapter 2; Section 2.5.4). *These interdependencies show multi-indicator frameworks are better suited to capture the interacting pressures relevant to restoration* (Chapter 2; Section 2.3).

5.6.4 Expanded Assessment

Expanding assessment attributes beyond JNCC (2009) criteria improved interpretation. Assessing *Sphagnum* composition showed the presence of any species, rather than simply the absence of *Sphagnum fallax* dominance, better indicated surface recovery. Similarly, microtopographic variation, though not included in JNCC (2009) criteria, consistently distinguished near-natural from degraded and early-stage restored sites, supporting its relevance to hydrological function and ecosystem resilience (Chapter 2; Section 2.2.1). *Findings support Sphagnum as an independent indicator species, particularly given its role in water retention and carbon accumulation* (Chapter 2; Section 2.2.1).

5.6.5 Towards Integration with Sub-Surface Function

Refining and normalising surface indicators also enables integration with sub-surface metrics. Chapters 6 and 7 evaluate bulk, chemical, and structural properties, and aligning these with surface scores supports a more holistic assessment of functional recovery. *Surface indicators could help evaluate restoration trajectories beyond ecological condition, associating hydrological and carbon function* (Chapter 2; Section 2.6.2). *This directly addresses limitations in current carbon accounting frameworks such as the IUCN UK Peatland Code, which assume static recovery timelines* (Chapter 2; Section 2.7). While surface metrics provide valuable insights into ecological change, they do not fully explain how recovery occurs (Spencer *et al.*, 2017; Chirol *et al.*, 2021). Understanding the processes regulating water movement, retention, decomposition, and carbon accumulation requires assessment of sub-surface structure and function.

Table 5.5: Summary of research questions addressed in Chapter 5.

Research Question	Contribution/Implications
Research Question 1: Can surface indicators be used as a proxy to infer changes in sub-surface structure and function post-restoration?	Standard JNCC (2009) protocols fail to differentiate restored from degraded conditions. However, refined indicators (e.g., species composition, bare peat extent) show potential for proxy development (explored in Chapter 6 and 7)
Research Question 2: To what extent does the restoration of degraded blanket peatlands support the recovery of sub-surface structure and function?	Surface metrics provide early signs of ecological recovery across techniques and ages, offering a framework to contextualise sub-surface responses evaluated in Chapters 6 and 7.
Research Question 3: How do the carbon costs of interventions impact the carbon benefit potential of restoration?	Surface outcomes vary with technique (e.g., turving versus heather brash), which may relate to sub-surface function (Chapters 6 and 7) and carbon cost-efficiency (Chapter 8).

Chapter 6: Restoration Effectiveness as Indicated by Bulk and Chemical Properties

While surface indictors from the JNCC (2009) *Common Standards Monitoring Guidance (CSM) for Upland Habitats: Blanket Bogs* differentiated degraded from near-natural conditions, and when refined, provided indication of recovery trajectories in restored sites (Chapter 5), their capacity to indicate sub-surface recovery remains unclear (Chapter 2; Section 2.6). In particular, surface scores did not consistently capture variation associated with restoration technique or age, suggesting key aspects of functional response may operate independently of surface condition.

Sub-surface processes control hydrological regulation, decomposition dynamics, and carbon accumulation (Chapter 2; Sections 2.2; 2.6.1). However, few studies directly associate surface indicators to the sub-surface properties regulating these functions, particularly using intact, continuous samples (Anderson and Peace, 2017). Urquhart and Gore (1973) provide one of the few investigations of biochemical properties with depth in continuous peat extending from the surface. Such analyses have not been conducted in restored peatlands, demonstrating a key gap in understanding sub-surface restoration responses, as well as baseline conditions (Chapter 2; Sections 2.2.4; 2.6.1; 2.6.3).

Bulk and chemical properties identified as functionally relevant (Chapter 2; Section 2.6.1; Chapter 3; Section 3.4) are assessed across degraded, restored, and near-natural conditions to evaluate sub-surface restoration effectiveness relative to baseline and target states. Analyses include temperature, pH, Eh, moisture content, bulk density, organic carbon content, and humification (Chapter 3; Section 3.4.4; Table 3.2). Widely

adopted, cost-effective techniques are applied to the same cores assessed using μCT imaging in Chapter 7, enabling direct comparison between structural and functional recovery in intact samples. Results assess whether surface condition indicates sub-surface response and whether bulk and chemical properties can serve as reliable proxies for sub-surface function in restored blanket peatlands.

6.1 Sub-Surface Bulk and Chemical Properties

Sub-surface bulk and chemical properties offer insights into hydrological and biogeochemical functions not captured by surface indicators. These metrics govern water retention, microbial activity, decomposition, and carbon storage, and often respond more slowly to restoration than surface vegetation (Chapter 2; Sections 2.2; 2.6.2). Parameters assessed are defined and justified in Chapter 3; Section 3.4.4; Table 3.2, with each selected for its relevance to functional recovery and compatibility with cost-effective assessment.

6.1.1 Organic Carbon Content

Organic carbon content provides a long-term record of carbon accumulation and degradation. It is widely used to infer carbon storage capacity and degradation history (Chapter 3; Section 3.4.4; Table 3.2). Organic carbon content was measured via loss-on-ignition (LOI) and is presented as a scatter plot to illustrate the range of values across depth for each core.
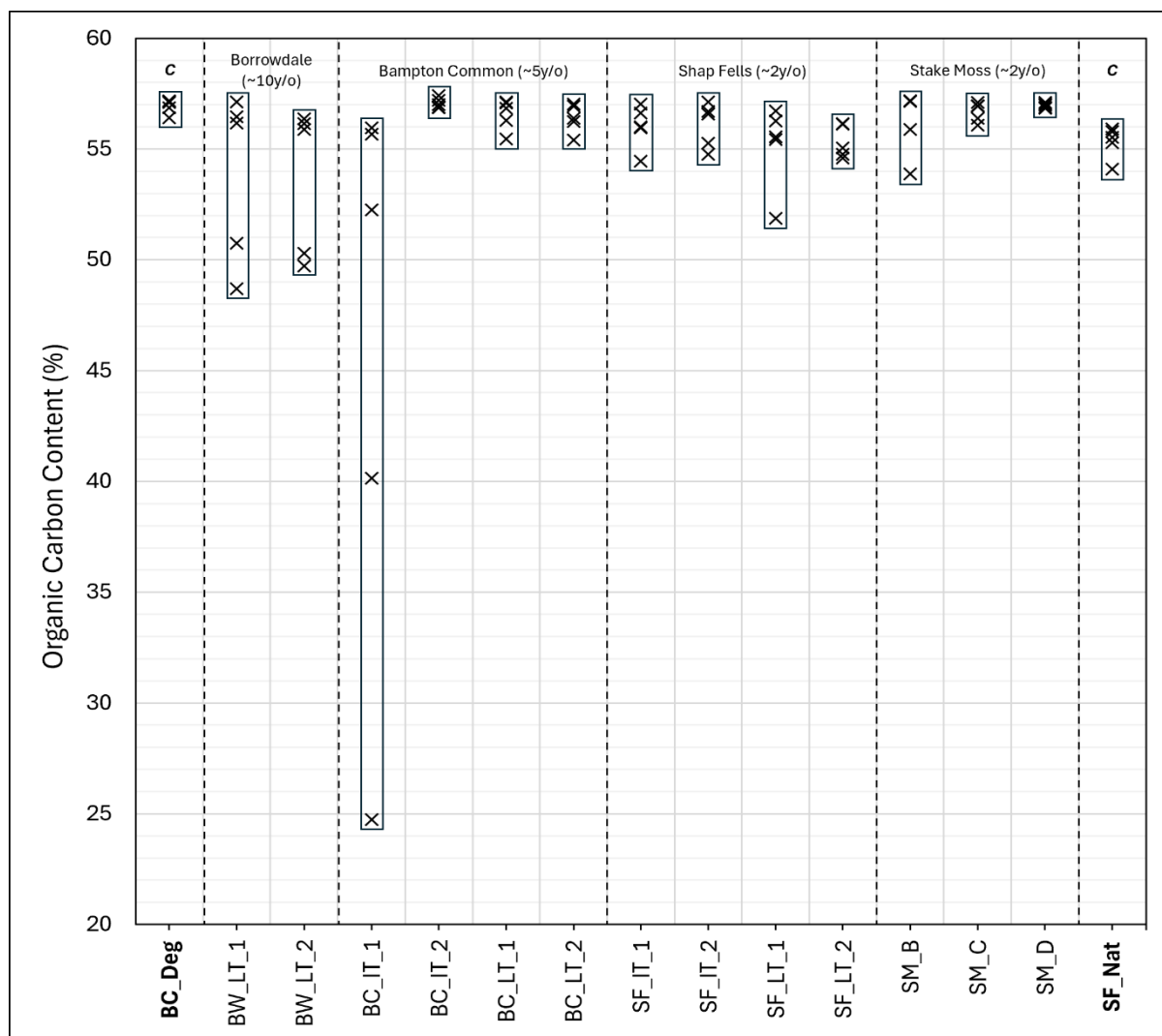
Figure 6.1: Organic carbon content (%) across cores, grouped by site and restoration age. Values represent 5cm depth intervals from 5–25cm.

Figure 6.1 demonstrates organic carbon content was consistently high across samples (>50%), confirming the organic nature of peat. This indicates long-term carbon storage across sites, suggesting recent degradation (<100 years). Bampton Common – Imported Turves (1) shows lower values. This indicates a mineral horizon identified in the field, possibly linked to past human disturbance, such as construction of a nearby Roman road (Chapter 4; Section 4.3.4). This is supported by its origin between 15-25cm, equivalent to ~1500 – 2500 years of formation. Alternatively, it may indicate poor turve quality, sourced from a shallow or mineral-rich site.

6.1.2 Temperature

Temperature regulates microbial activity, decomposition, and GHG production (Chapter 3; Section 3.4.4; Table 3.2). Although absolute values could not be determined due to limited local meteorological data (Chapter 3; Section 3.2), relative (normalised) profiles provide insight into sub-surface thermal dynamics. Depth profiles are first presented for the control sites to establish baseline contrasts between degraded and near-natural conditions. Restored cores are then presented alongside controls to evaluate changes in thermal structure, with emphasis on deviations from degraded conditions as indicators of functional recovery.

a) Controls
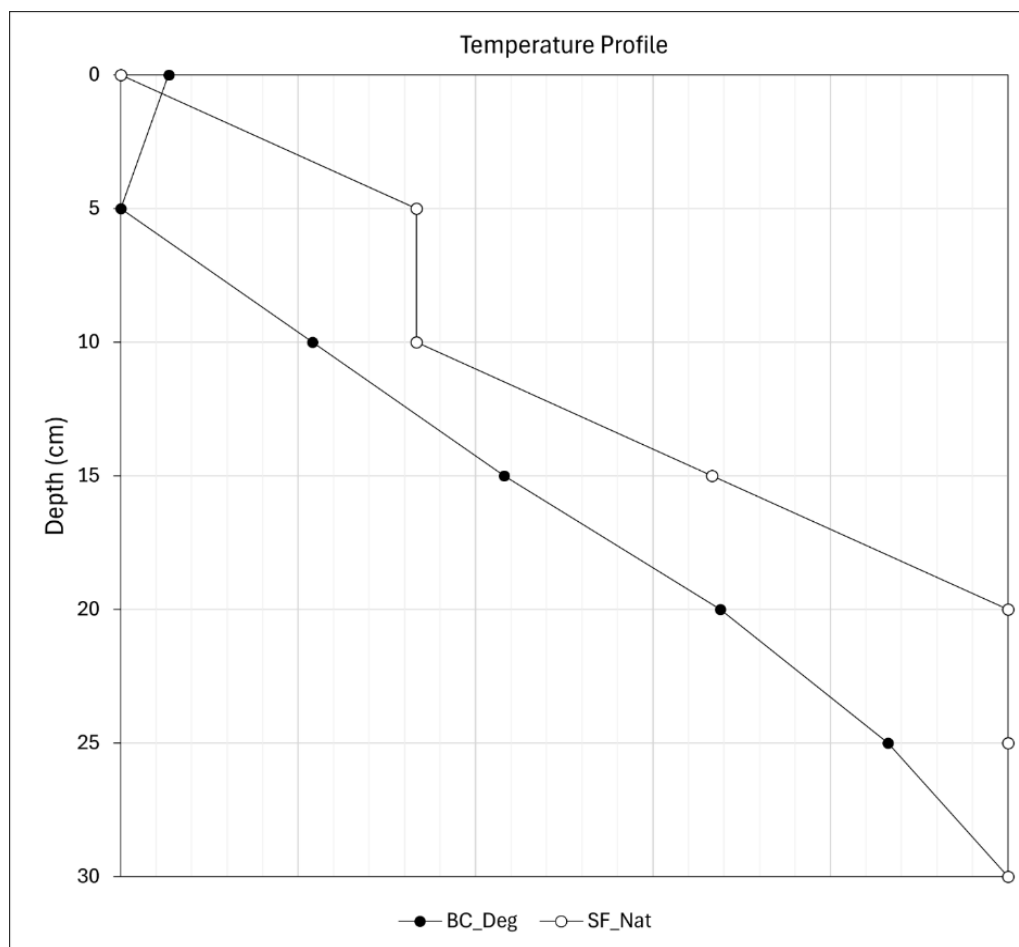
Figure 6.2: Temperature profiles with depth for the degraded (BC_Deg) and near-natural (SF_Nat) control cores. Values are normalised due to a lack of local meteorological data.

Figure 6.2 shows control sites exhibit increasing temperature with depth, consistent with increased microbial activity. The near-natural control (SF_Nat) displays a more gradual profile, with stable values at 5–10cm likely indicating high moisture content near the water table limit, which buffers thermal change. BC_Deg shows a steeper gradient, indicating drier, aerated conditions favouring aerobic decomposition and CO_2 production. However, similar profiles below 10cm suggest continued microbial activity in SF_Nat, supporting its classification as near-natural rather than pristine (Chapter 2; Sections 2.1.2; 2.5).
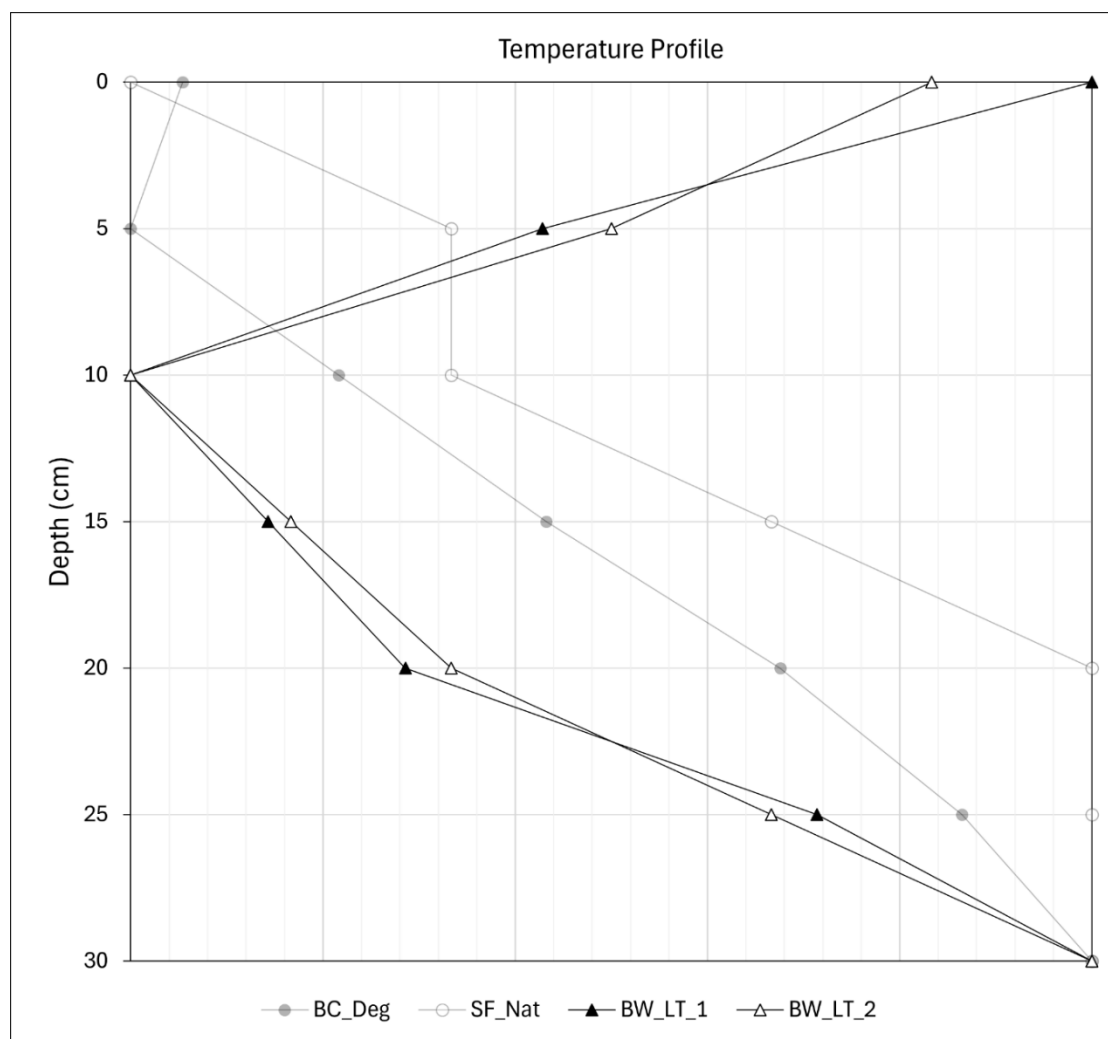
b) Borrowdale

Figure 6.3: Temperature profiles with depth for the Borrowdale (~10 years old; local turving) cores. Values are normalised due to a lack of local meteorological data.

Figure 6.3 demonstrates Borrowdale cores exhibit higher surface temperatures, declining to 10cm, then increasing with depth, indicating control profiles. This likely indicates surface air temperature influence due to limited thermal buffering, suggesting low moisture and aerobic conditions in the acrotelm. Below 10cm, increasing temperatures suggest increased microbial activity in the catotelm, supporting CH_4 production. Similar profiles across replicates indicate low spatial variability.

c) Bampton Common
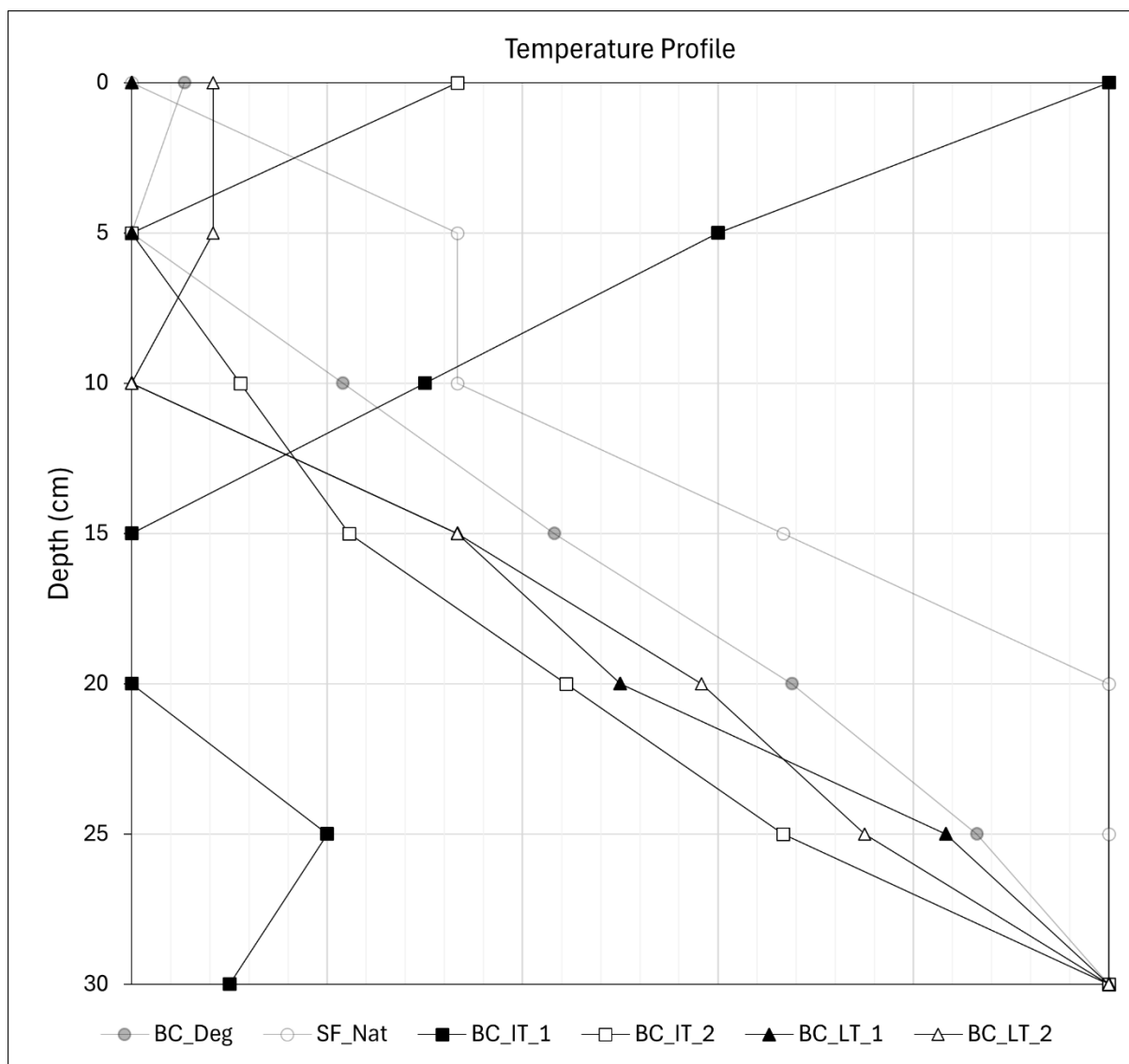
Figure 6.4: Temperature profiles with depth for the Bampton Common (~5 years old; imported and local turving) cores. Values are normalised due to a lack of local meteorological data.

Figure 6.4 shows most Bampton Common cores display profiles consistent with the controls, with temperature increasing with depth. Imported Turve (2) and both Local Turve cores exhibit near-surface thermal buffering (0–5cm), suggesting increased surface moisture similar to near-natural conditions. Imported Turve (1) shows a reversed profile with declining temperature with depth, likely indicating reduced microbial activity associated with lower organic content (Section 6.1.1). This shows turve quality or disturbance influences sub-surface recovery and deviation from degraded conditions.

d) Shap Fells
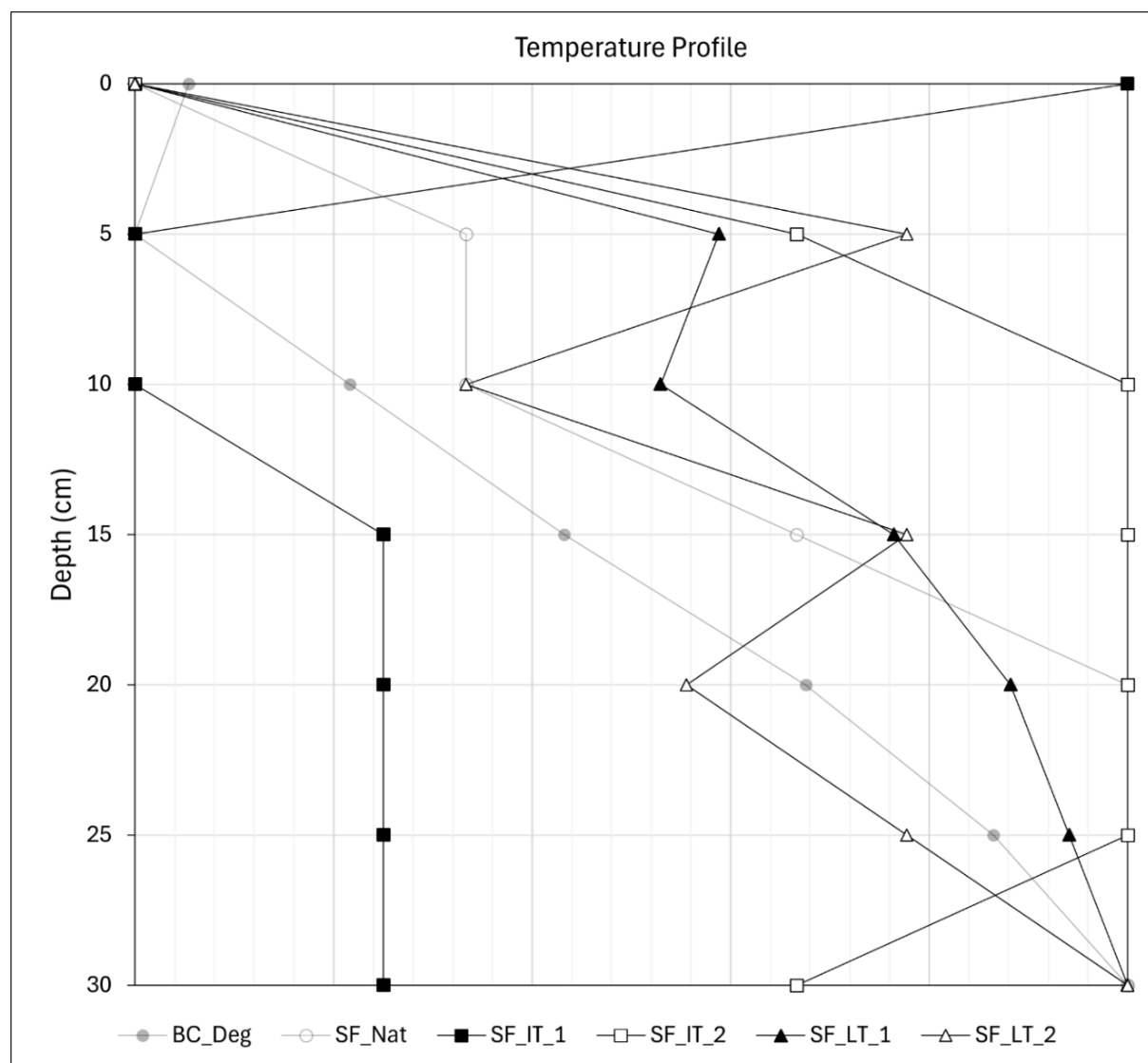
Figure 6.5: Temperature profiles with depth for the Shap Fells (~2 years old; imported and local turving) cores. Values are normalised due to a lack of local meteorological data.

Figure 6.5 demonstrates Shap Fells cores generally display increasing temperature with depth, indicating microbial activity in deeper layers. However, greater variability between profiles suggests inconsistent water retention and limited acrotelm – mesotelm – catotelm stratification. Shap Fells – Imported Turve (1) shows decreasing temperature with depth, similar to Bampton Common – Imported Turve (1), supporting the influence of turve quality. This highlights local turving as a more effective approach for restoring near-natural thermal conditions. Results suggest ongoing sub-surface recovery ~2 years post-restoration.
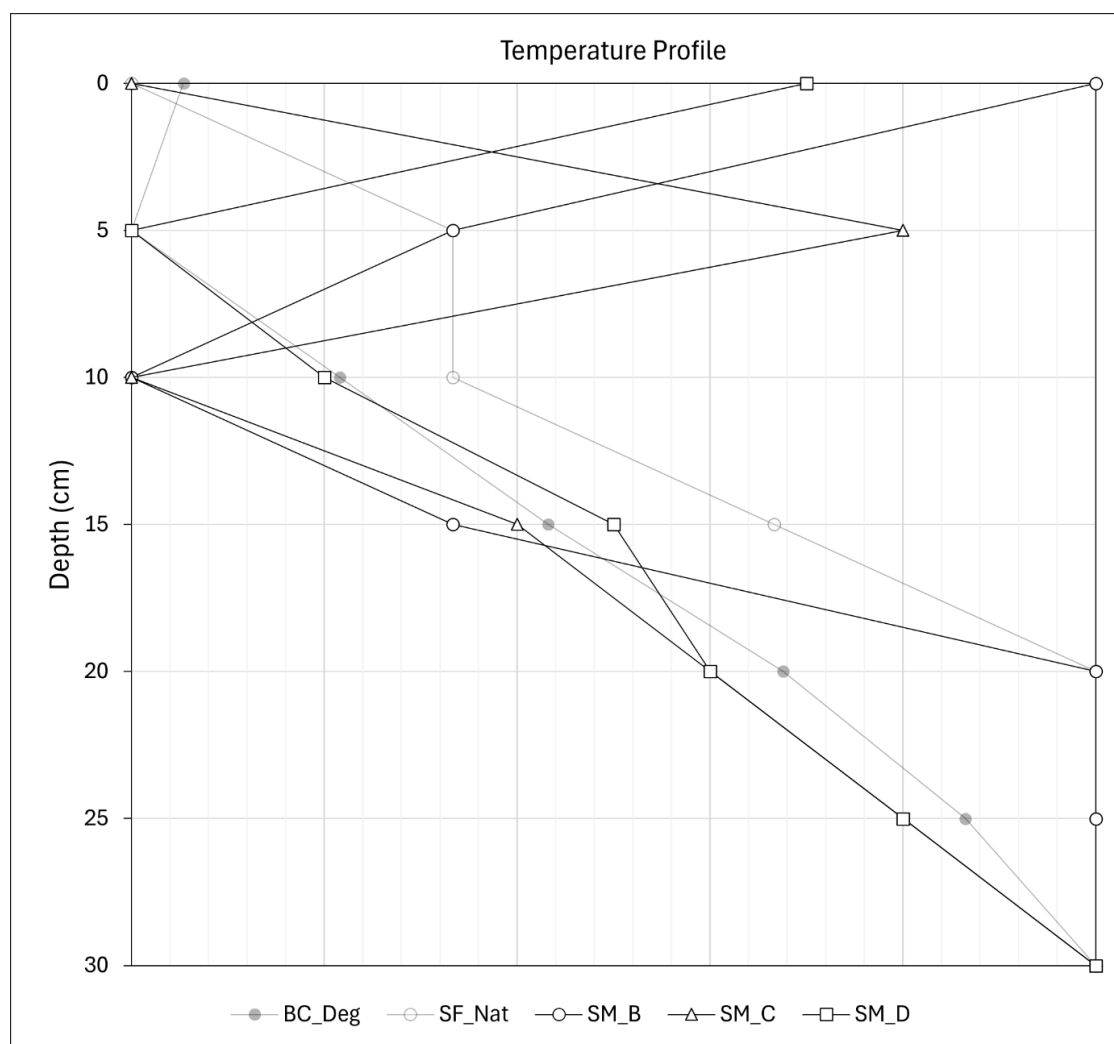
e) Stake Moss

Figure 6.6: Temperature profiles with depth for the Stake Moss (~2 years old; heather brash, coir, and stone/timber dam) cores. Values are normalised due to a lack of local meteorological data.

Figure 6.6 shows Stake Moss cores generally exhibit increasing temperature with depth, indicating microbial activity in deeper layers, but with variability in the surface 0–10cm. Stake Moss – Brash and Dam show declining temperature between 0–5cm, suggesting surface thermal buffering linked to increased moisture ~2 years post restoration. Stake Moss – Coir displays a divergent profile with greater variability. Deeper layers remain consistent with degraded conditions, indicating non-turving interventions influence surface thermal dynamics but have limited effect on deeper sub-surface hydrology.

f) Summary and Interpretation

Most cores exhibit increasing temperature with depth, consistent with high microbial activity and GHG production in deeper (catotelm) layers (Chapter 2; Section 2.2; Clymo, 1984; Freeman *et al.*, 2001; Prescott, 2010; Strack *et al.*, 2016). Near-surface variability (0–10cm) indicates differences in moisture content, with thermal buffering in some restored cores as a result of increased surface wetness (Section 6.1.5). Local turving more closely aligned with near-natural thermal profiles in Bampton Common and Shap Fells. However, sub-surface change remained limited below ~10cm. Variability in surface results may also indicate meteorological influences since cores were not extracted simultaneously across locations (Chapter 3; Section 3.3).

6.1.3 Humification

Humification provides a proxy for long-term decomposition, with rates influenced by oxygen availability and historic water table position. Higher humification indicates prolonged aerobic conditions, while lower values indicate accumulation under anoxic conditions (Chapter 3; Section 3.4.4; Table 3.2). Combined with μCT-inferred density, humification can also suggest microporosity (Chapter 7; Section 7.2.3). Humification

was assessed using the Von-Post scale, a widely applied, standard method. Humification trends across sites are first presented, followed by depth profiles for control and restored cores to evaluate whether restoration influences sub-surface decomposition.
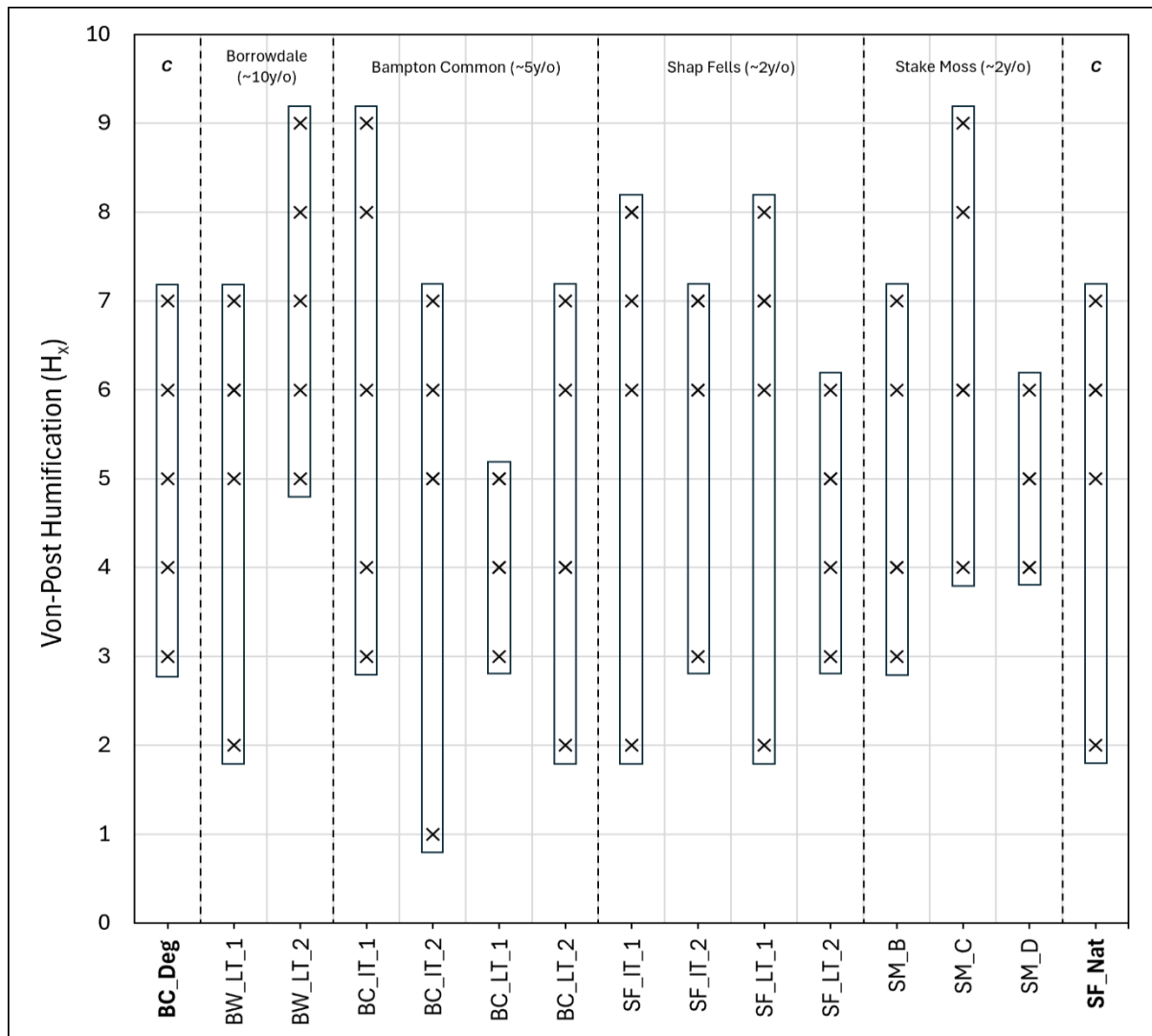
Figure 6.7: Von-Post humification scores (H$_x$) across cores, grouped by site and restoration age. Values represent 5cm depth intervals from 5–25cm.

Figure 6.7 shows a range of Von-Post humification scores (H1-H9), indicating variable levels of decomposition and potential microporosity within the upper 30cm. The degraded (BC_Deg) and near-natural (SF_Nat) controls range from low (H2-H3) to moderately high (H7), indicating some degree of surface aeration and decomposition in the acrotelm and upper catotelm. This supports classification of SF_Nat as near-natural

rather than pristine (Chapter 2; Sections 2.1.2; 2.5), where anoxic conditions up to 5cm depth would be expected (low H_x). Restored sites tend to exhibit higher and more uniform humification values (typically H3-H8), suggesting decomposition is more consistent throughout. This indicates while restoration may stabilise the surface (Chapter 5), it does not fully replicate the anoxic conditions necessary for retarded decomposition in deeper layers. This may reduce long-term carbon sequestration potential.

a) Controls
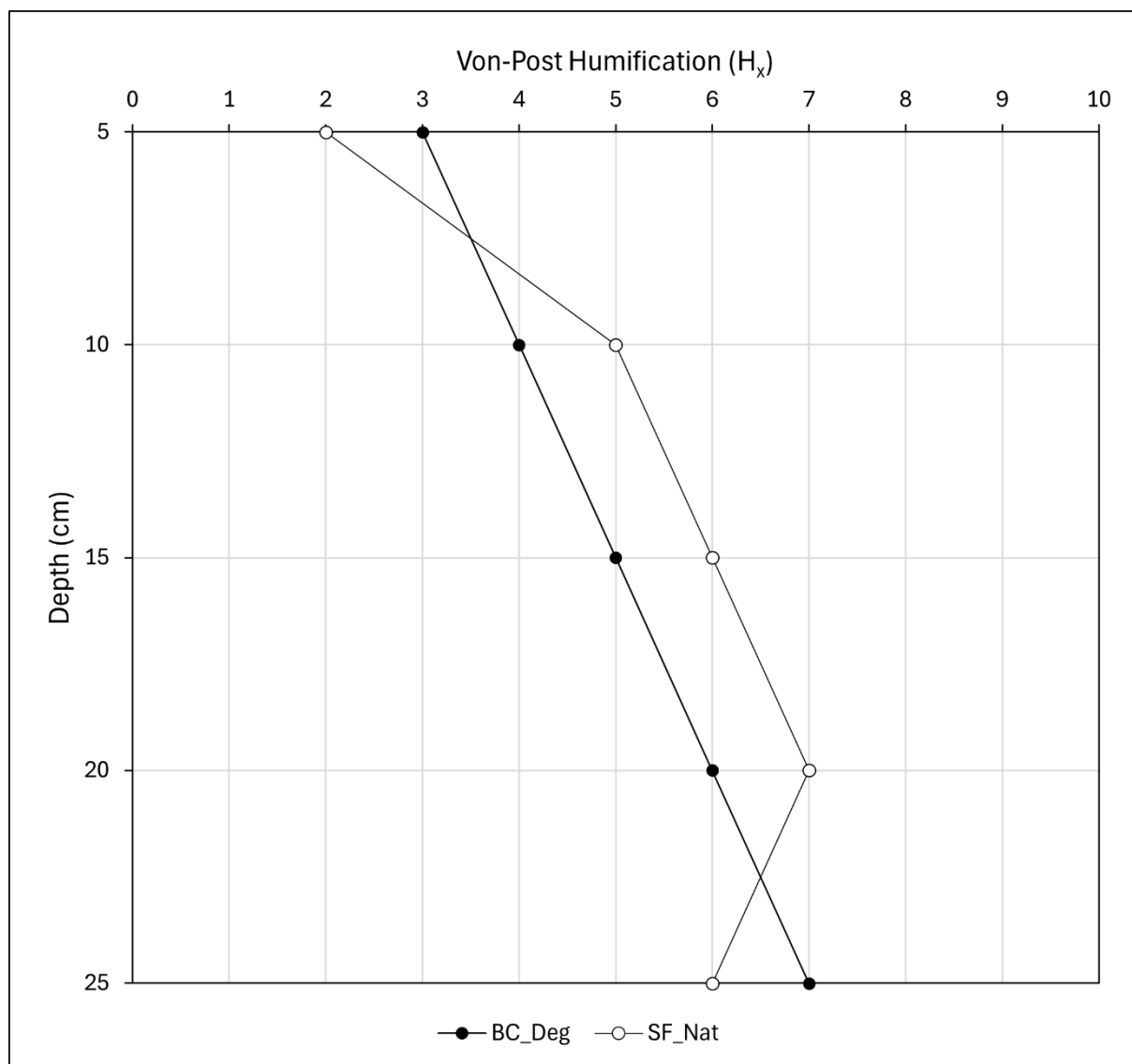
Figure 6.8: Von-Post humification profiles with depth for the degraded (BC_Deg) and near-natural (SF_Nat) control cores.

Figure 6.8 demonstrates the degraded (BC_Deg) and near-natural (SF_Nat) controls exhibit increasing decomposition with depth. SF_Nat shows a sharper increase between 5-10cm, indicating a long-term saturated surface (Section 6.1.5) but aerated sub-surface (section 6.1.7), as supported by temperature findings (Section 6.1.2), while BC_Deg follows a uniform gradient. However, limited variation supports the classification of SF_Nat as near-natural rather than pristine (Chapter 2; Sections 2.1.2; 2.5).
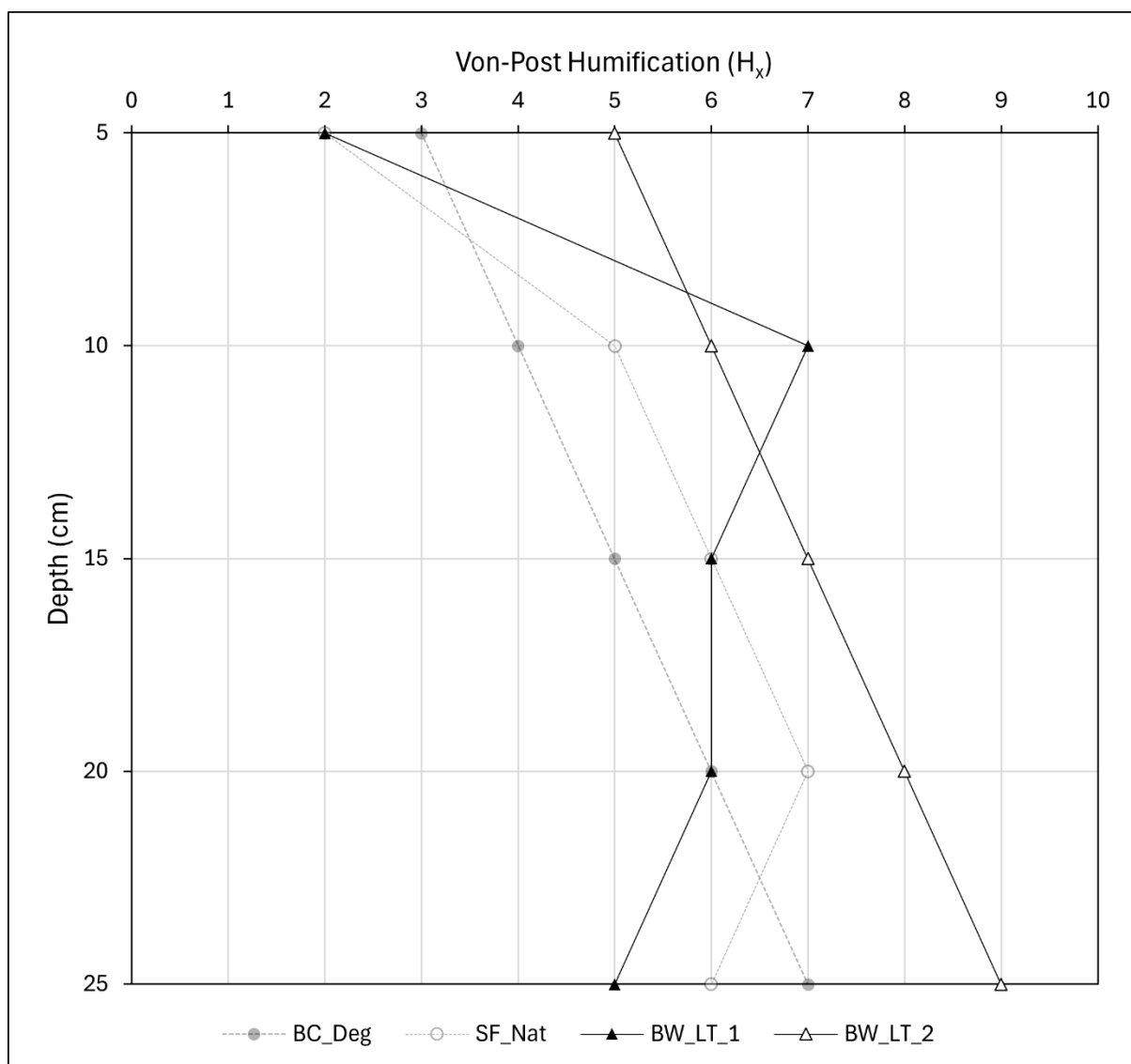
b) Borrowdale

Figure 6.9: Von-Post profiles with depth for the Borrowdale (~10 years old; local turving) cores.

Figure 6.9 shows Borrowdale – Local Turve (1) displays a profile more similar to near-natural, with a sharper increase between 5–10cm, suggesting surface saturation but greater sub-surface aeration, promoting CO_2 production. Borrowdale – Local Turve (2) shows consistently higher humification, resembling the degraded profile and indicating increased decomposition. Variability between cores indicates the spatial heterogeneity of restored peatlands, contrasting with temperature findings (Section 6.1.2), while higher humification suggests continued or increased decomposition even after a decade.

c) Bampton Common
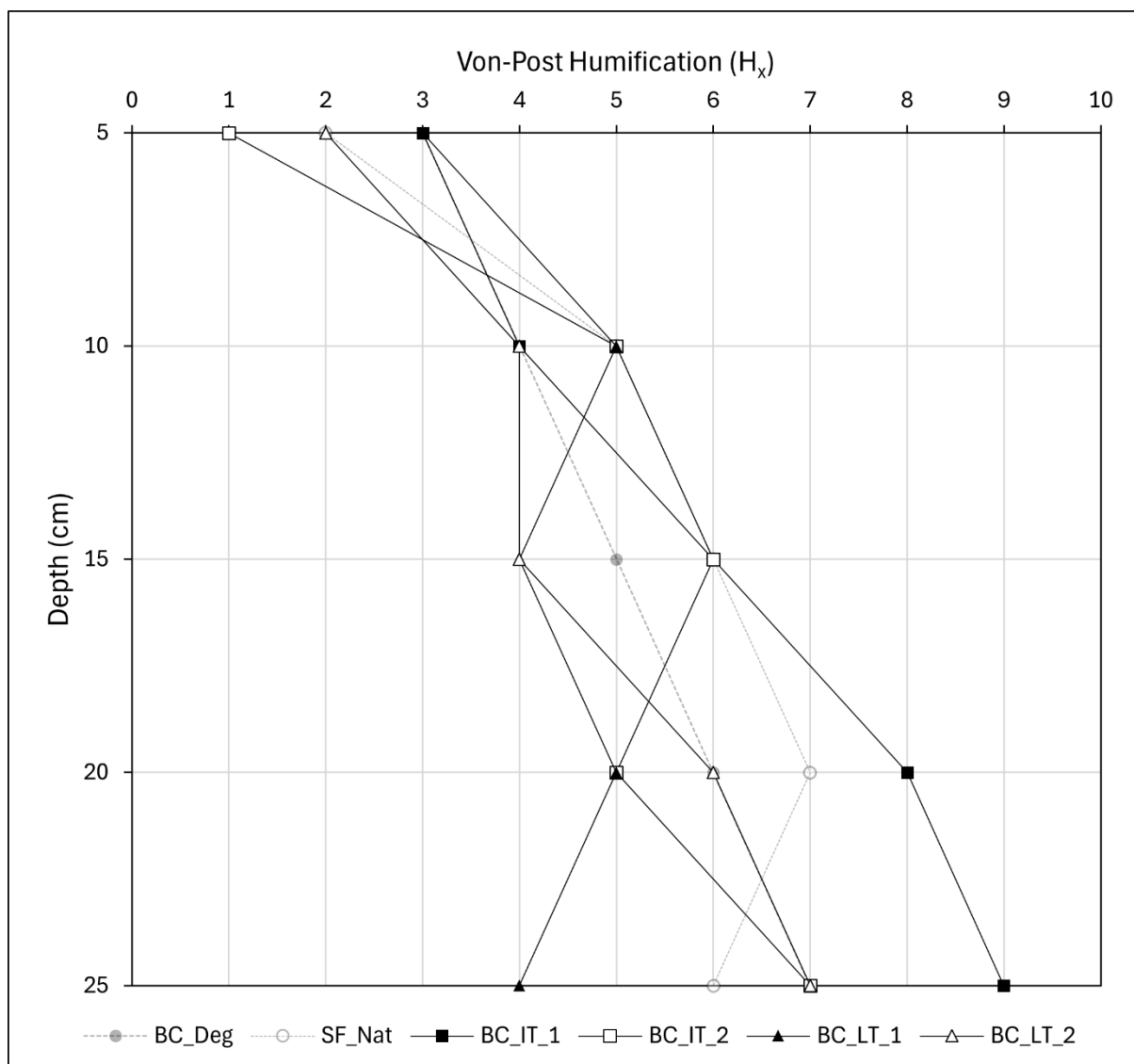
Figure 6.10: Von-Post profiles with depth for the Bampton Common (~5 years old; imported and local turving) cores.

Figure 6.10 demonstrates Bampton Common cores exhibit increasing decomposition with depth, with low surface values and increases between 5-10cm, resembling the near-natural profile, indicating surface wetness. Imported Turve (2) and Local Turve (2) show gradual increases similar to controls, while Imported Turve (1) and Local Turve (1) diverge beyond 15cm. Local Turve (1) decreases below 15cm, indicating a higher local water table suppressing decomposition, whereas Imported Turve (1) increases to H9, suggesting increased sub-surface decomposition and carbon loss.

d) Shap Fells
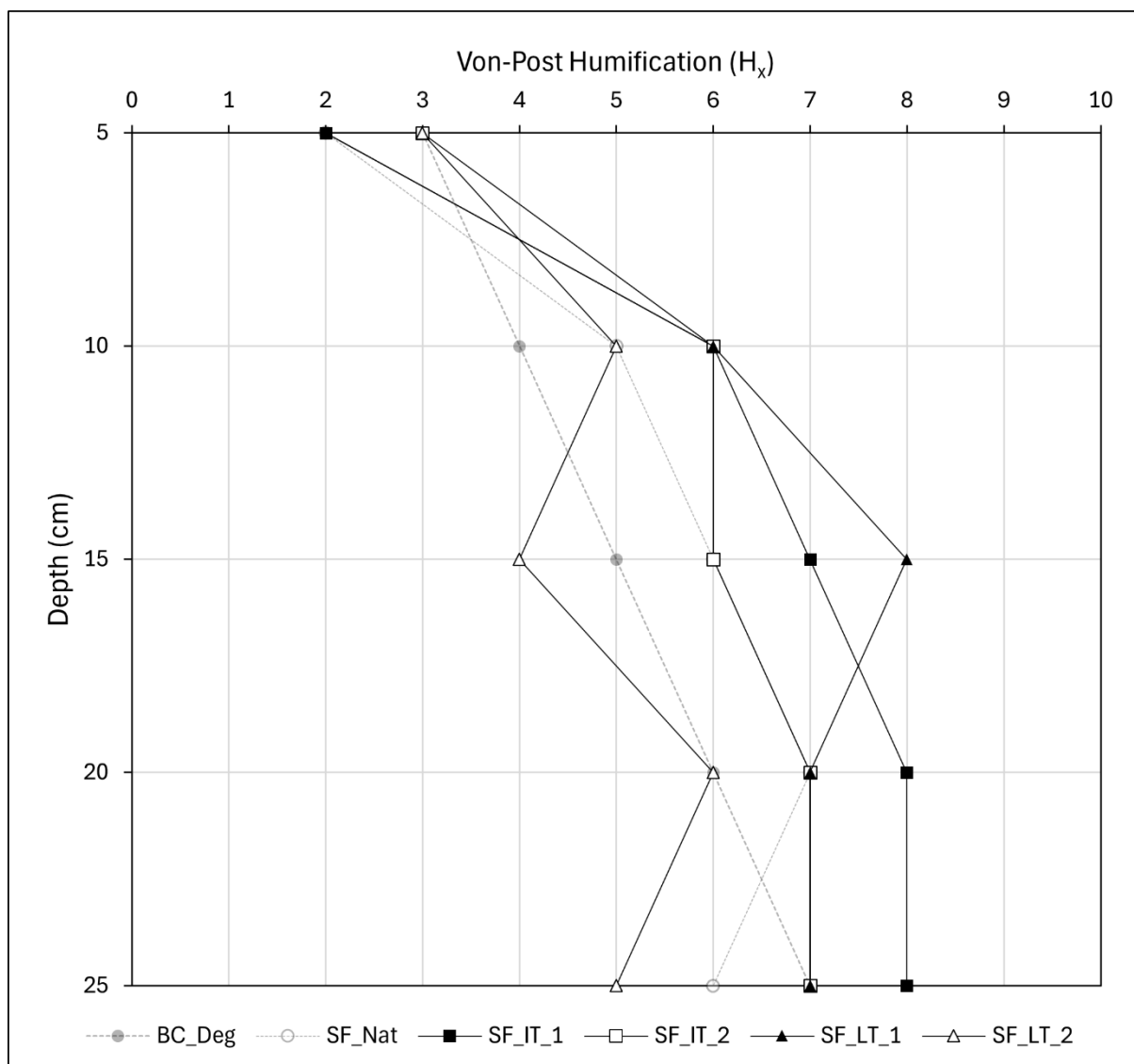
Figure 6.11: Von-Post profiles with depth for the Shap Fells (~2 years old; imported and local turving) cores.

Figure 6.11 shows Shap Fell cores exhibit low surface humification (H2–H3) with an increase between 5–10cm, resembling the near-natural profile. However, deeper layers trend toward higher humification, suggesting ongoing or relict sub-surface decomposition. This may indicate limited effectiveness of rewetting after ~2 years. Shap Fell – Local Turve (2) shows slightly lower sub-surface values, indicating localised water table recovery or retention capacity may be sufficient to slow decomposition in some areas.

e) Stake Moss
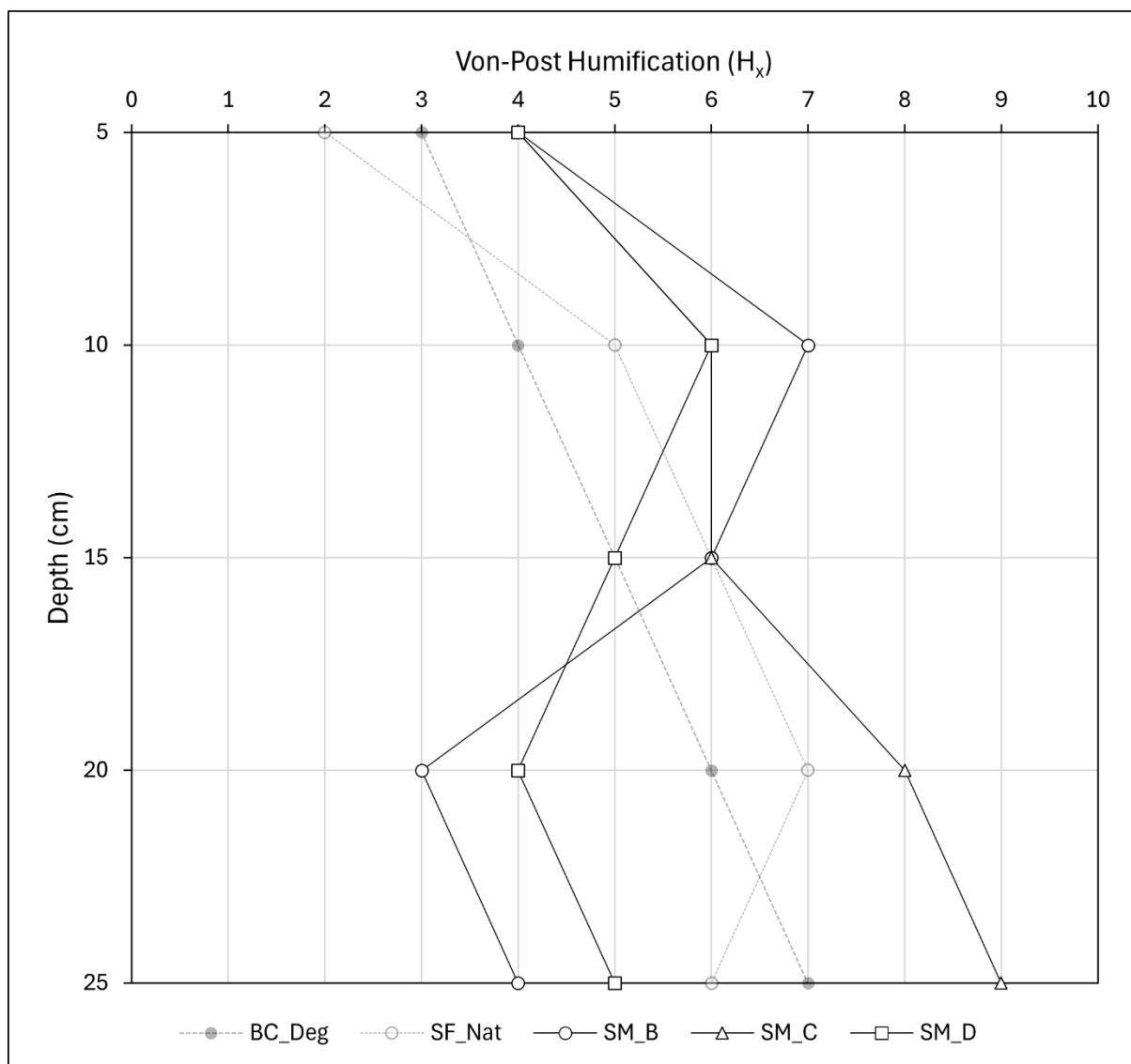
Figure 6.12: Von-Post profiles with depth for the Stake Moss (~2 years old; heather brash, coir, and stone/timber dam) cores.

Figure 6.12 demonstrates Stake Moss cores exhibit higher surface humification (H4) and diverge with depth, indicating different decomposition gradients compared to the controls and turved sites. Stake Moss – Brash and Dam show oscillating values below 15cm, possibly indicating variable water retention and microporosity between layers (Chapter 7; Section 7.2.3), while Coir increases to H9, suggesting sustained sub-surface aeration and decomposition. Variation may indicate limited effectiveness of alternative techniques compared to turving.

f) Summary and Interpretation

Increases in humification between 5-10cm in the near-natural and most restored cores supports re-establishment of a saturated surface layer (>5cm) (Section 6.1.5), consistent with acrotelm development (Chapter 2; Sections 2.1.1; 2.2.1). However, decomposition remains high throughout profiles, indicating thin or incomplete acrotelms and sustained sub-surface aeration (Section 6.1.7), supported by temperature findings (Section 6.1.2). This promotes CO_2 release, limiting the extent to which restoration has re-established anoxic conditions necessary for long-term carbon accumulation (Clymo *et al.*, 1998; Scanlon and Moore, 2000; Clymo and Bryant, 2008; Rowson *et al.*, 2010; Fenner and Freeman, 2011). Findings demonstrate a potential disconnect between surface condition (Chapter 5) and sub-surface decomposition rates. Furthermore, Von-Post was not sensitive to the mineral layer in Bampton Common – Imported Turve (1) identified in Section 6.1.1, challenging its ability to assess humification post restoration.

6.1.4 Bulk Density

Bulk density indicates the mass of peat per unit volume and serves as a proxy for compaction associated with decomposition and disturbance. In the upper 30cm, higher

values typically indicate degradation, associated with reduced peat-forming species, porosity, limited water retention and infiltration, and increased potential for GHG diffusion (Chapter 3; Section 3.4.4; Table 3.2). Restoration is expected to reduce bulk density relative to degraded states by re-establishing vegetation structure and increasing water retention potential (McCarter and Price, 2013; Morris *et al.*, 2019; Howson *et al.*, 2023). Patterns are assessed across sites and with depth to evaluate whether interventions support structural recovery relative to control conditions. Along with humification, findings are expected to correlate with μCT-derived porosity values (Kettridge and Binley, 2008; Spencer *et al.*, 2017).
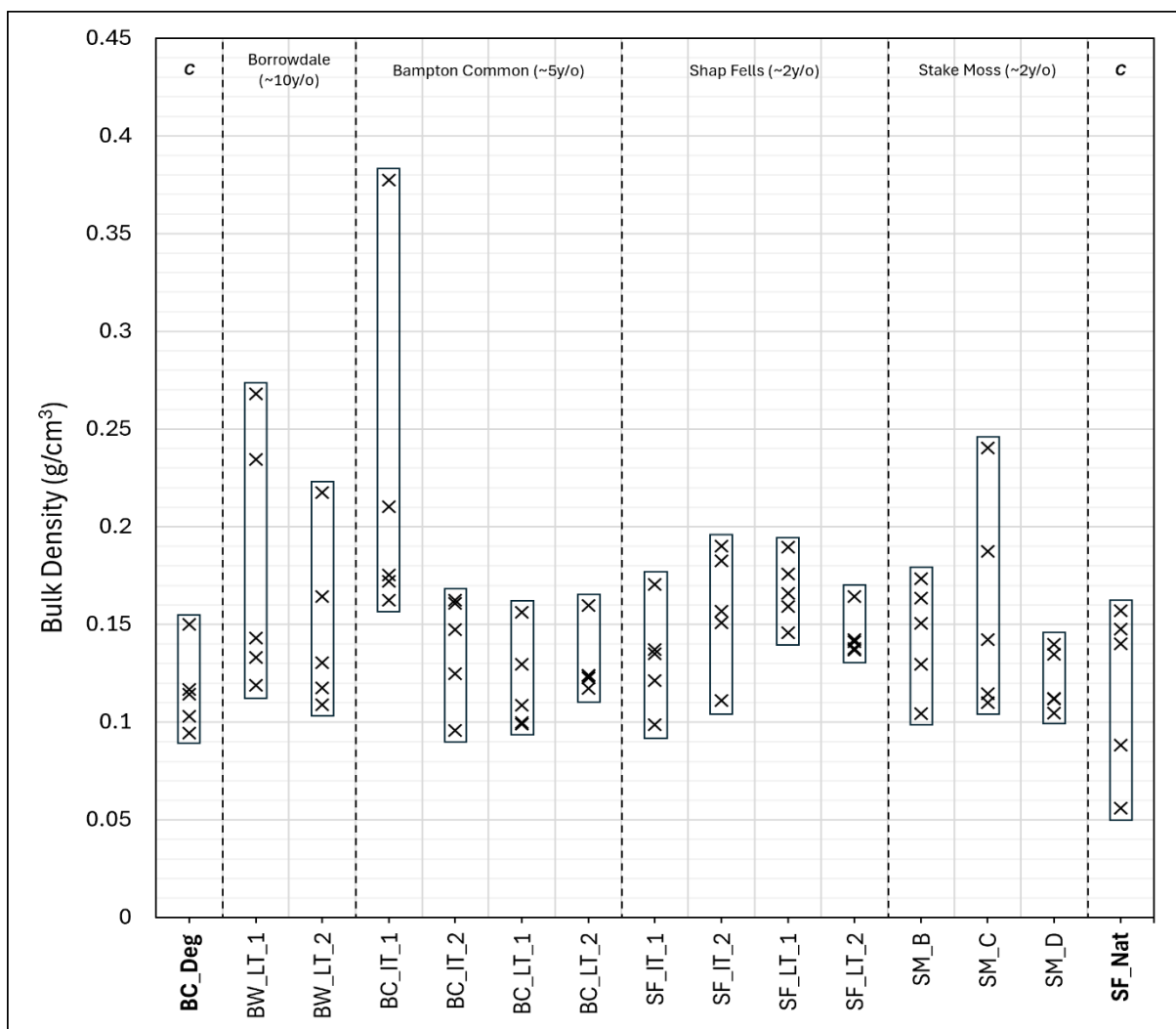
Figure 6.13: Bulk density (g/cm³) across cores, grouped by site and restoration age. Values represent 5cm depth intervals from 5–25cm.

Figure 6.13 shows bulk density is generally low across samples, consistent with the porous nature of peat (Chapter 2; Section 2.2.3). However, restored cores tend to exhibit higher values than the degraded (BC_Deg) and near-natural (SF_Nat). SF_Nat includes two of the lowest recorded values (e.g., 0.06 g/cm^3), indicating limited compaction and intact porosity. Restored sites, particularly Borrowdale (~10 years old), show higher surface and sub-surface values, suggesting increased compaction persisting a decade post-restoration. This could be linked to increased decomposition (Section 6.1.3), limiting water-holding capacity (Section 6.1.5) and functional recovery. Alternatively, restoration practice, such as turve pressing or machinery tracking, may impose irreversible compaction (within ~10 years). A distinct increase in Bampton Common – Imported Turve (1) supports the presence of a mineral layer identified in Section 6.1.1.

a) Controls
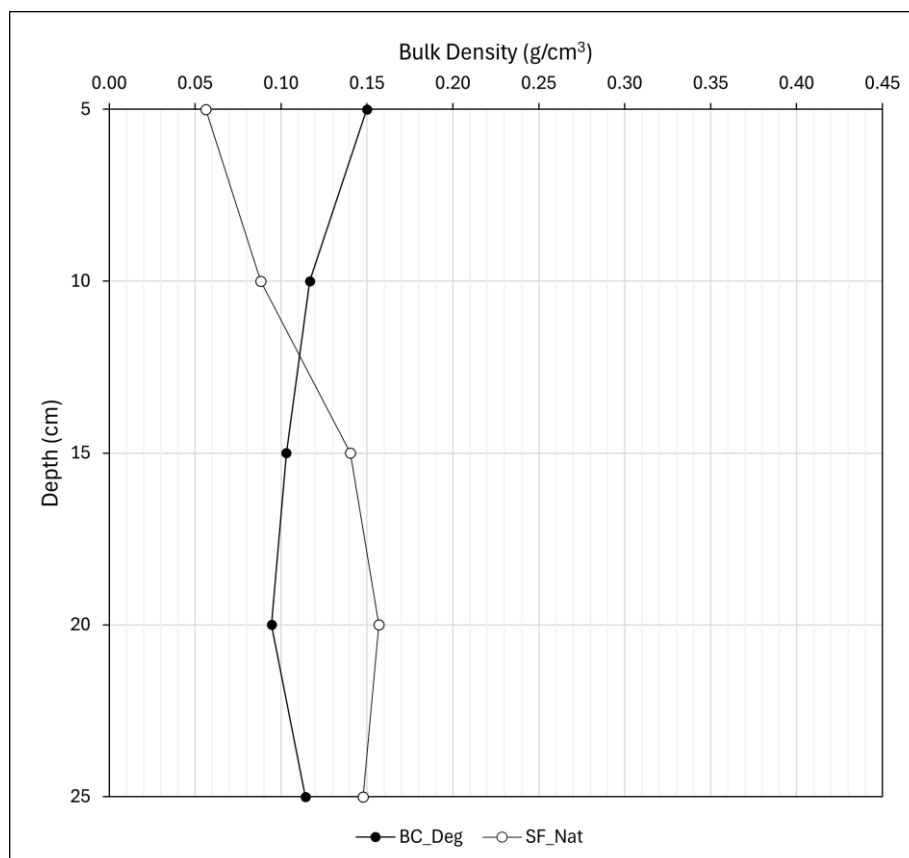
Figure 6.14: Bulk density profiles with depth for the degraded (BC_Deg) and near-natural (SF_Nat) control cores.

Figure 6.14 demonstrates the degraded control (BC_Deg) exhibits higher surface bulk density (0.15 g/cm^3) that decreases with depth (~0.11 g/cm^3), indicating surface compaction likely linked to aerobic decomposition (Section 6.1.7) and possibly gas expansion in deeper layers. The near-natural control (SF_Nat) shows low surface density (0.06 g/cm^3), suggesting a porous acrotelm, with increasing density at depth indicating decomposition (Section 6.1.3). Contrasting profiles support SF_Nat as more functional, with porous structure conducive to water retention and carbon storage, while BC_Deg remains degraded, particularly at the surface.

b) Borrowdale
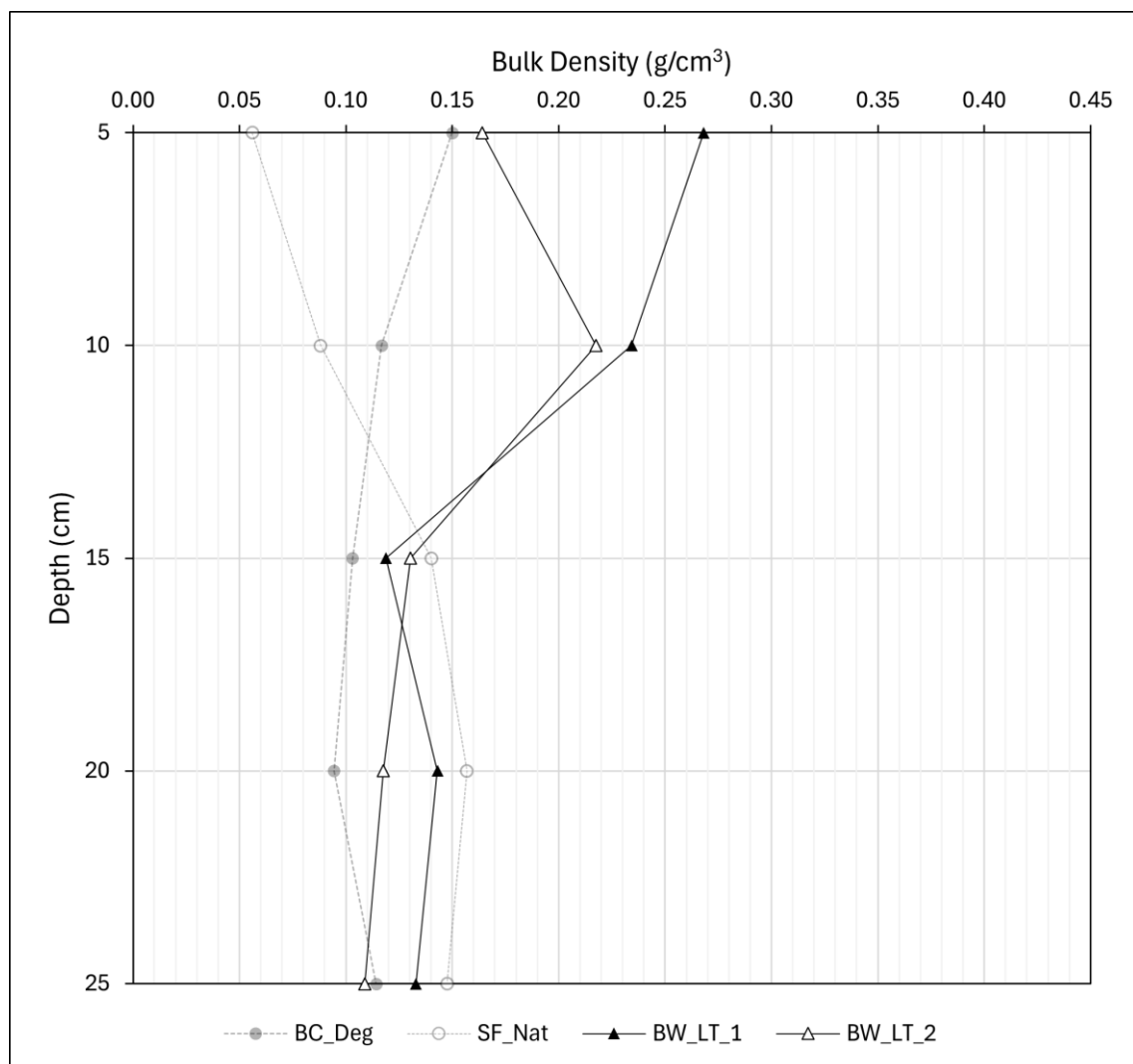
Figure 6.15: Bulk density profiles with depth for the Borrowdale (~10 years old; local turving) cores.

Figure 6.15 shows Borrowdale cores exhibit higher surface bulk density than controls, particularly Local Turve (1) with 0.27 g/cm^3 at 5cm. This suggests persistent surface compaction a decade post-restoration, possibly attributed to aerobic decomposition (Sections 6.1.3; 6.1.7) or restoration practice (disturbance; Chapter 5; Section 5.4). Local Turve (2) shows a more stratified profile but increases at 10cm (0.22 g/cm^3), possibly representing the original peat surface where a turve was placed. This highlights the compaction legacy of restoration, with variability indicating spatial heterogeneity in restored peatlands.

c) Bampton Common
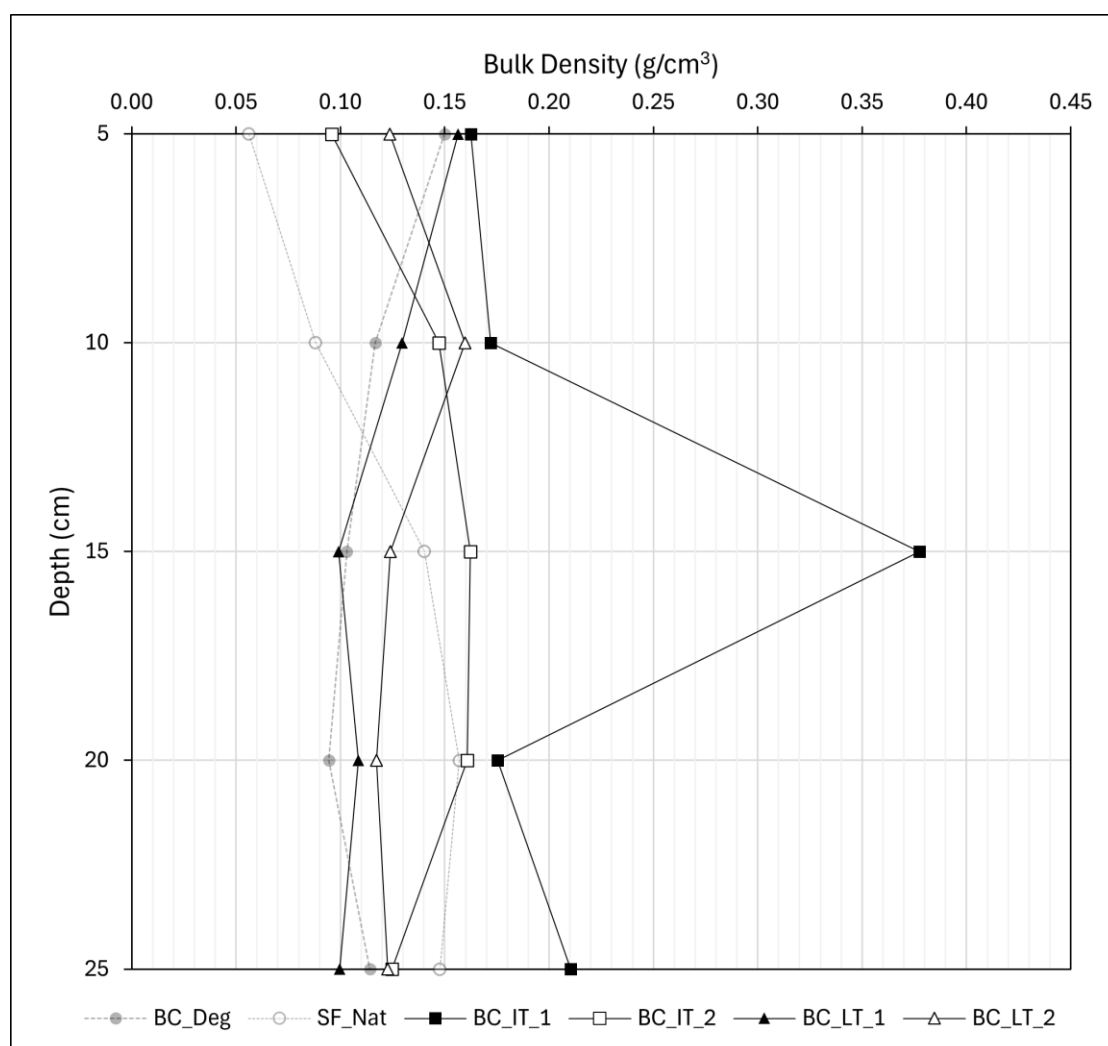
Figure 6.16: Bulk density profiles with depth for the Bampton Common (~5 years old; imported and local turving) cores.

Figure 6.16 demonstrates higher surface bulk densities than the controls, with diverging profiles below 10cm. Bampton Common - Local Turve (1) and (2) align with the degraded profile, with decreasing density with depth, likely indicating surface decomposition and sub-surface gas expansion (Chapter 2; Section 2.2.2). Imported Turve (2) trends more like the near-natural profile but with higher values, suggesting compaction from restoration and partial structural recovery. An increase at 15cm in Imported Turve (1) (0.38 g/cm^3) indicates the mineral layer identified in Section 6.1.1.

d) Shap Fells
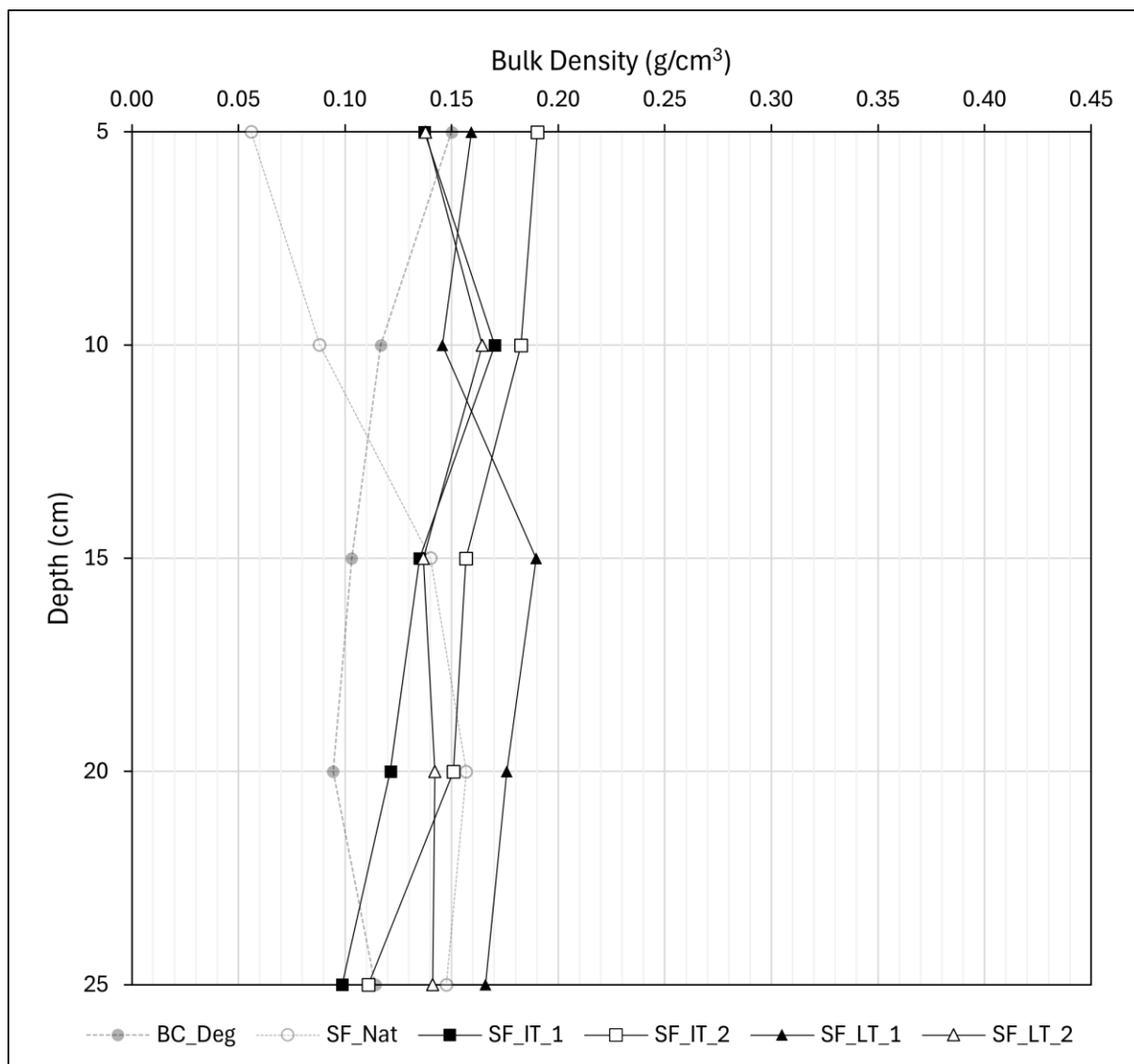
Figure 6.17: Bulk density profiles with depth for the Shap Fells (~2 years old; imported and local turving) cores.

Figure 6.17 shows Shap Fell cores consistently exhibit higher surface bulk density than the controls (0.14 – 0.19 g/cm³), with decreasing values with depth, resembling the degraded profile. This suggests surface compaction, attributed to continued decomposition (Section 6.1.3), sub-surface gas expansion, or physical disturbance from restoration (e.g., turve pressing or tracking) persisting ~2 years post-intervention (Chapter 5; Section 5.4).

e) Stake Moss
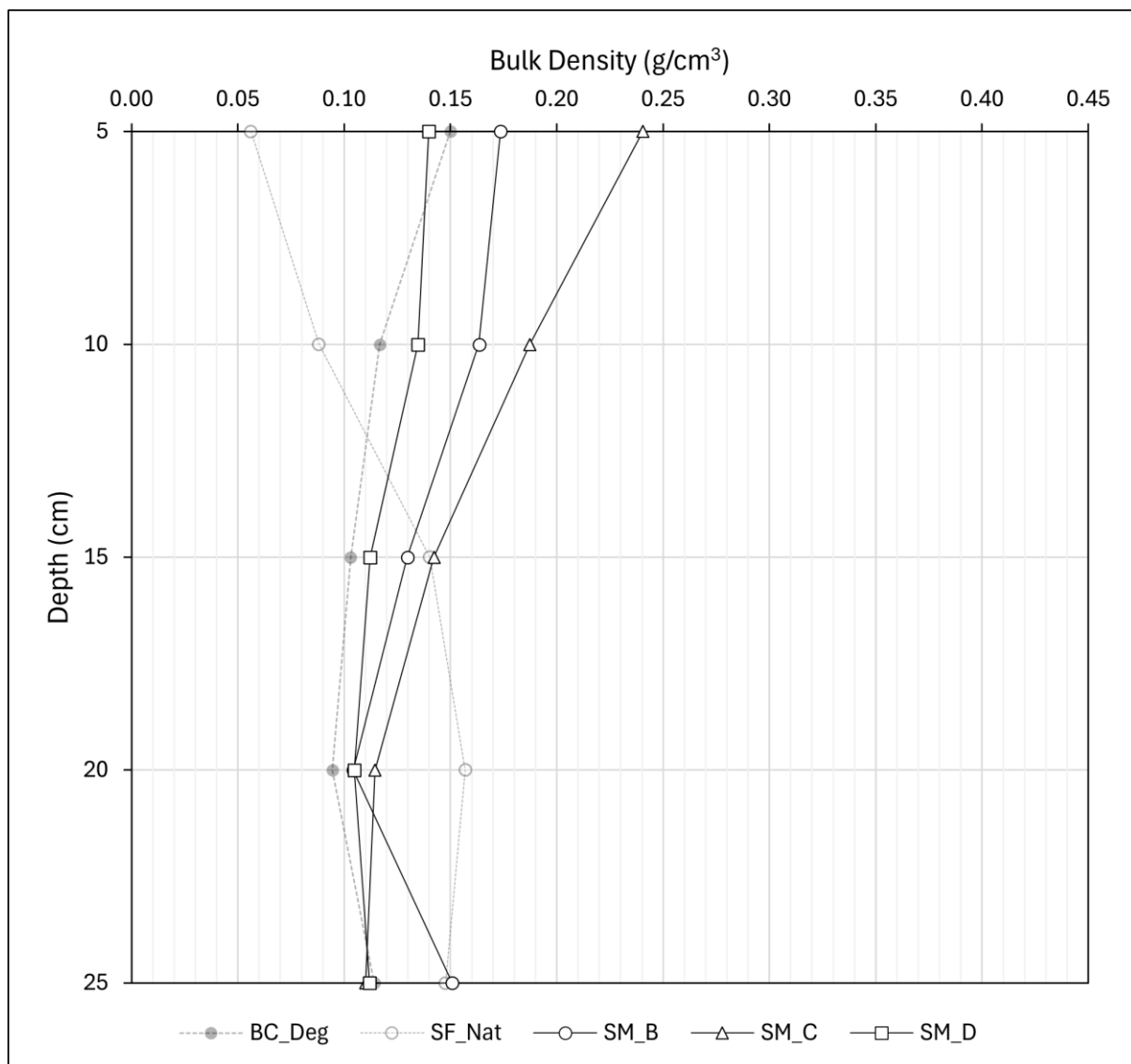
Figure 6.18: Bulk density profiles with depth for the Stake Moss (~2 years old; heather brash, coir, and stone/timber dam) cores.

Figure 6.18 demonstrates Stake Moss cores exhibit similar trends to the ~2 years old turved sites at Shap Fells, though with increased surface bulk density (~0.17–0.24 g/cm^3) and greater reduction with depth. This supports increased surface compaction and sub-surface gas expansion through more rapid decomposition (Section 6.1.3) or from alternative restoration techniques, such as brash spreading and dam installation, which typically require intensive machinery use (discussed in Chapter 8).

f) Summary and Interpretation

Restored sites consistently exhibited higher surface bulk density, indicating persistent compaction after a decade. This may result from prolonged decomposition (Chapter 2; Section 2.3.1) or structural disturbance from restoration activities such as turve pressing or machinery tracking (Chapter 5; Section 5.4). Most restored cores showed decreasing density with depth, resembling the degraded profile and contrasting with stratification observed in near-natural conditions. This may indicate sub-surface gas expansion or porosity increases driven by decomposition, limiting water retention (shown in the following section) and long-term carbon storage (Chapter 2; Section 2.2.3). While turved sites may be more effective at reducing surface compaction, they do not fully transition toward the structural conditions of near-natural.

6.1.5 Moisture Content

Moisture content indicates water-holding capacity and is a key indicator of hydrological function (Chapter 2; Section 2.2.1). High values support anoxic conditions, retarded decomposition, and promote carbon accumulation (Chapter 3; Section 3.4.4; Table 3.2). In degraded sites, drainage and compaction reduce moisture content, increasing oxygen availability and CO_2 production (Chapter 2; Section 2.3.1; Waddington and Price, 2000;

220

Strack and Waddington, 2007; Lindsay *et al.*, 2014b). Restoration aims to increase moisture retention by raising water tables and re-establishing vegetation (Chapter 2; Section 3.5). Moisture content is presented first across sites, then with depth, to assess hydrological recovery and divergence from degraded conditions.
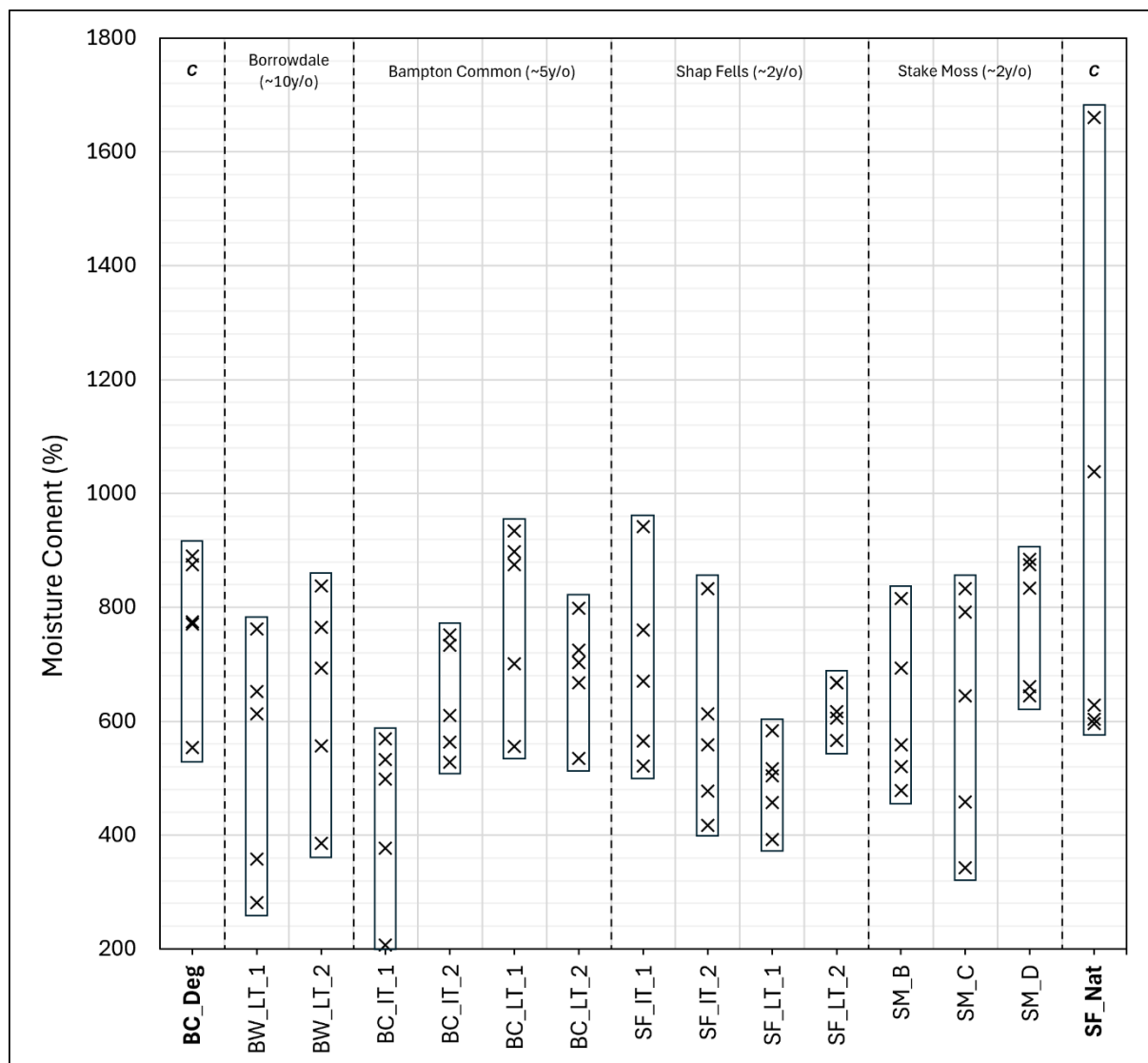
Figure 6.19: Moisture content (% dry weight) across cores, grouped by site and restoration age. Values represent 5cm depth intervals from 5–25cm.

Figure 6.19 shows samples exhibit high moisture content, exceeding dry weight in all cases, indicating the water-retention function of peat. However, there is variation across cores. The near-natural control (SF_Nat) records the highest values (e.g., 1661%),

indicating high water retention and anoxic conditions favouring carbon storage. The degraded control (BC_Deg) shows lower values (550–890%), suggesting limited water-holding capacity and increased potential for oxic decomposition. Restored sites fall within or below this degraded range, indicating restoration has not transitioned moisture content towards near-natural levels, even after a decade. The lowest value in Bampton Common – Imported Turve (1) aligns with the mineral layer identified in Section 6.1.1, supporting links between water retention, compaction, and carbon storage.

a) Controls
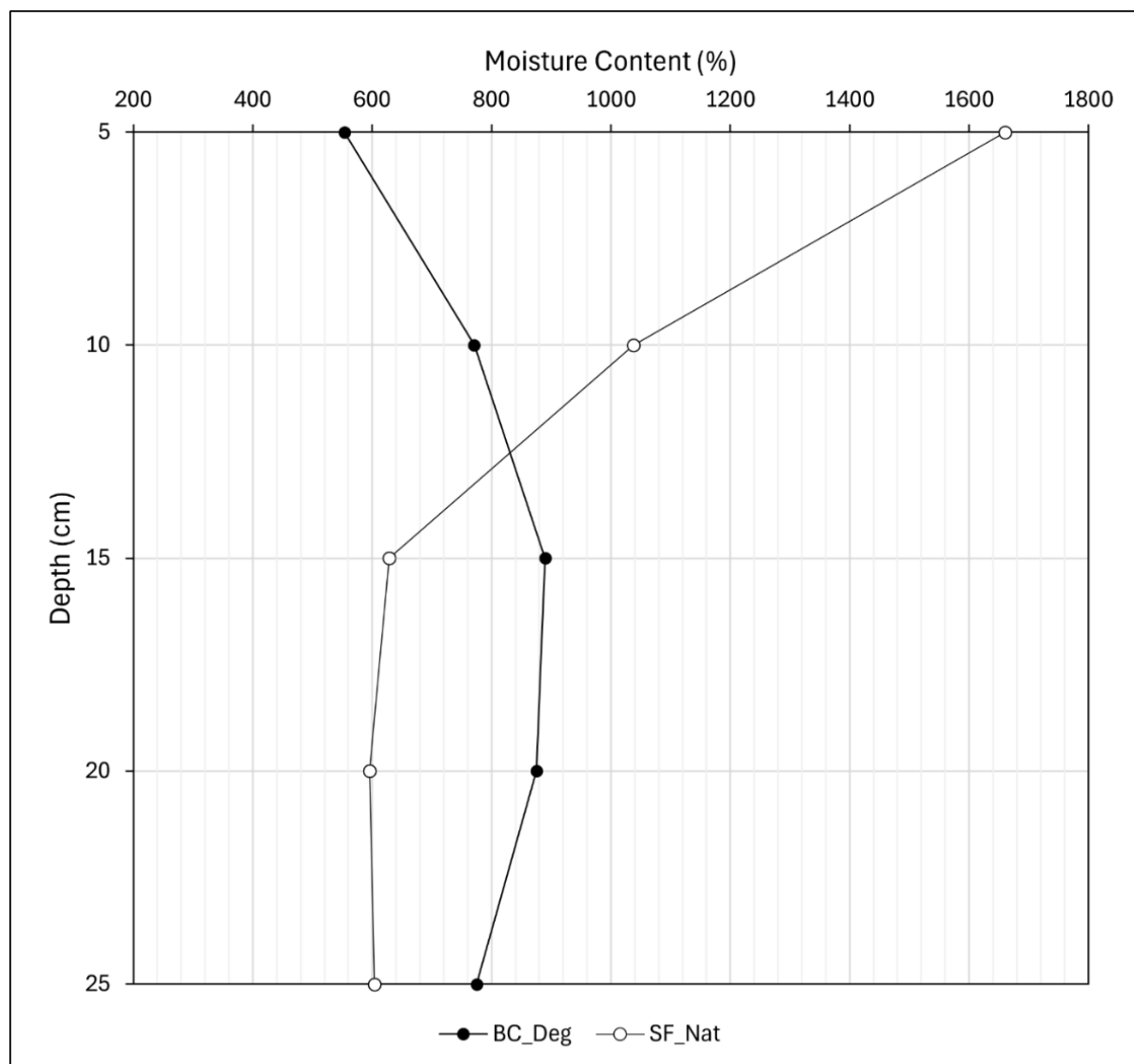
Figure 6.20: Moisture content profiles with depth for the degraded (BC_Deg) and near-natural (SF_Nat) control cores.

Figure 6.20 demonstrates contrasting moisture profiles between the degraded (BC_Deg) and near-natural (SF_Nat) controls. BC_Deg shows increasing moisture with depth, indicating a drier surface layer associated with aerobic decomposition (Sections 6.1.3; 6.1.7) and compaction (Section 6.1.4). SF_Nat records considerably high surface moisture (>1600% at 5cm), declining with depth, indicating a saturated acrotelm and progressive anoxic decomposition (Section 6.1.7), supported by surface temperature (Section 6.1.2). Contrasts suggest surface pore structure, influenced by vegetation (Chapter 5), plays a role in water retention; SF_Nat supports more anoxic conditions and retarded decomposition near the surface, while BC_Deg indicates surface hydrophobicity and aeration, favouring CO_2 release.

b) Borrowdale
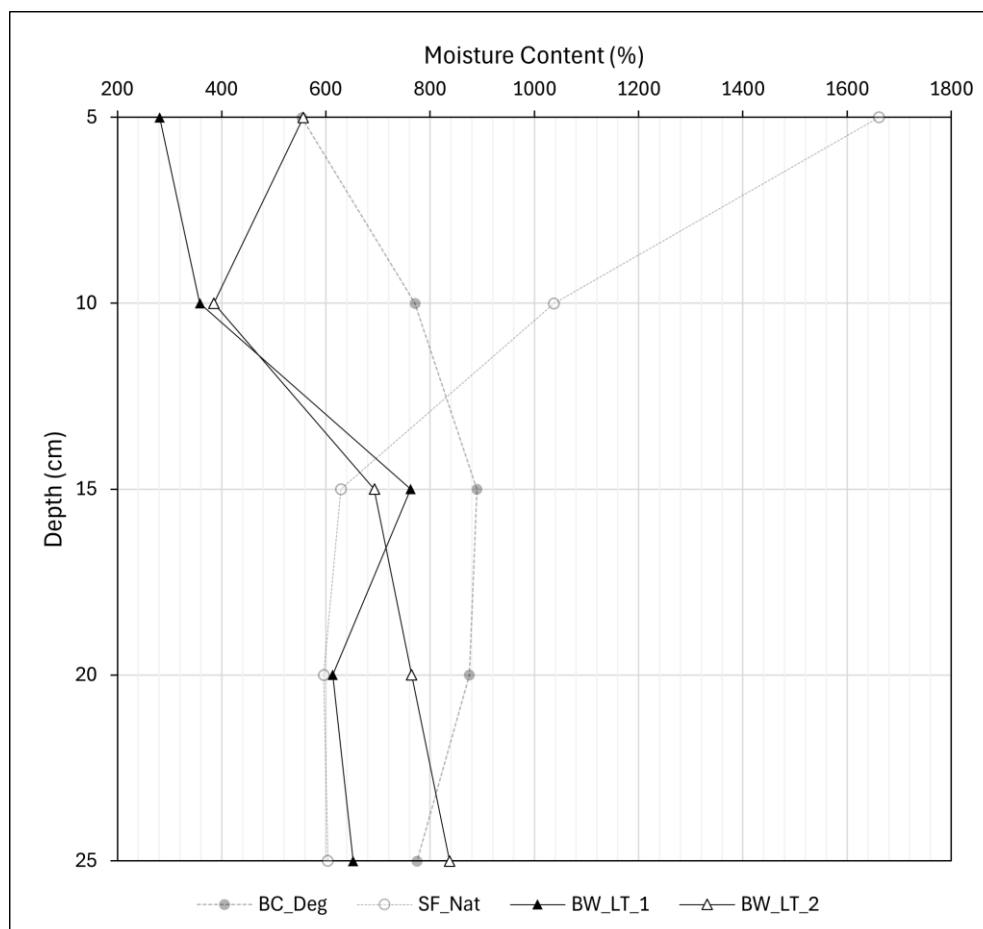
Figure 6.21: Moisture content profiles with depth for the Borrowdale (~10 years old; local turving) cores.

Figure 6.21 shows Borrowdale – Local Turve cores exhibit reduced surface moisture, particularly in Local Turve (1) (281%), consistent with low surface temperature (Section 6.1.2), high humification (Section 6.1.3), and bulk density (Section 6.1.4), indicating persistent compaction and rapid decomposition. Moisture increases with depth, suggesting partial rewetting below 10cm and a transition to more anoxic conditions (Section 6.1.7). Differences from the controls indicate restoration may support deeper hydrological recovery (increased water tables), though surface compaction continues to limit water retention a decade post-intervention. This may be associated with surface vegetation transitions (Chapter 5; Section 5.2).

c) Bampton Common
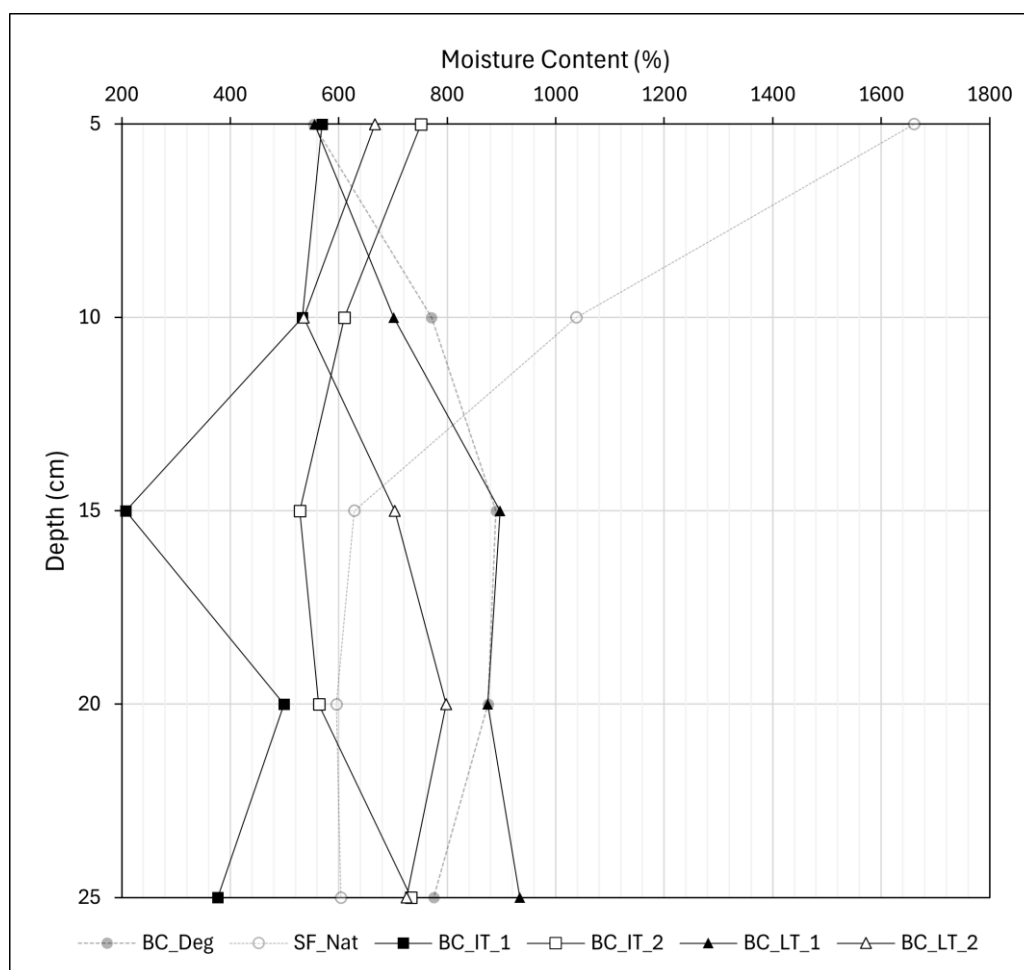
Figure 6.22: Moisture content profiles with depth for the Bampton Common (~5 years old; imported and local turving) cores.

Figure 6.22 demonstrates Bampton Common cores exhibit variable moisture profiles. Imported Turve (2) shows high surface moisture (751%) and a gradual decline with depth, suggesting partial recovery but still aligned with degraded values. Local Turve (1) and (2) indicate the degraded profile, showing continued surface hydrophobicity and sub-surface decomposition. Imported Turve (1) records the lowest moisture (207% at 15cm), consistent with the mineral layer (Section 6.1.1) and high bulk density (Section 6.1.4). Restoration may support some rewetting and water retention, but persistent compaction and aeration (Section 6.1.7) appear to limit functional recovery after ~5 years.

d) Shap Fells
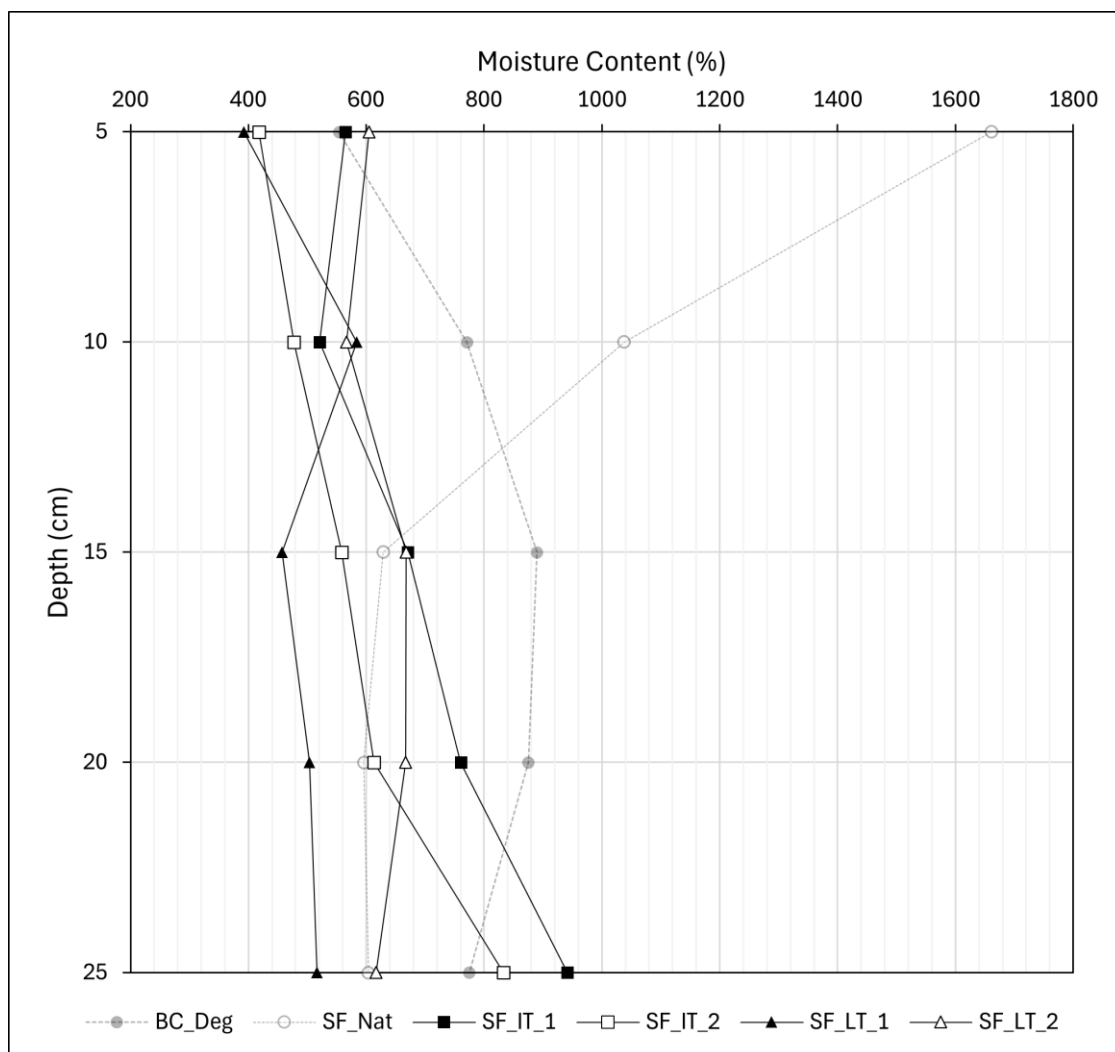
Figure 6.23: Moisture content profiles with depth for the Shap Fells (~2 years old; imported and local turving) cores.

Figure 6.23 shows Shap Fell cores consistently exhibit lower surface moisture content than controls, with minimal variation across depth. Values typically remain lower than those recorded at BC_Deg, indicating limited surface saturation and sub-surface water retention. This suggests continued surface decomposition (Section 6.1.3) and compaction (Section 6.1.4), with restricted hydrological recovery ~2 years post-restoration.
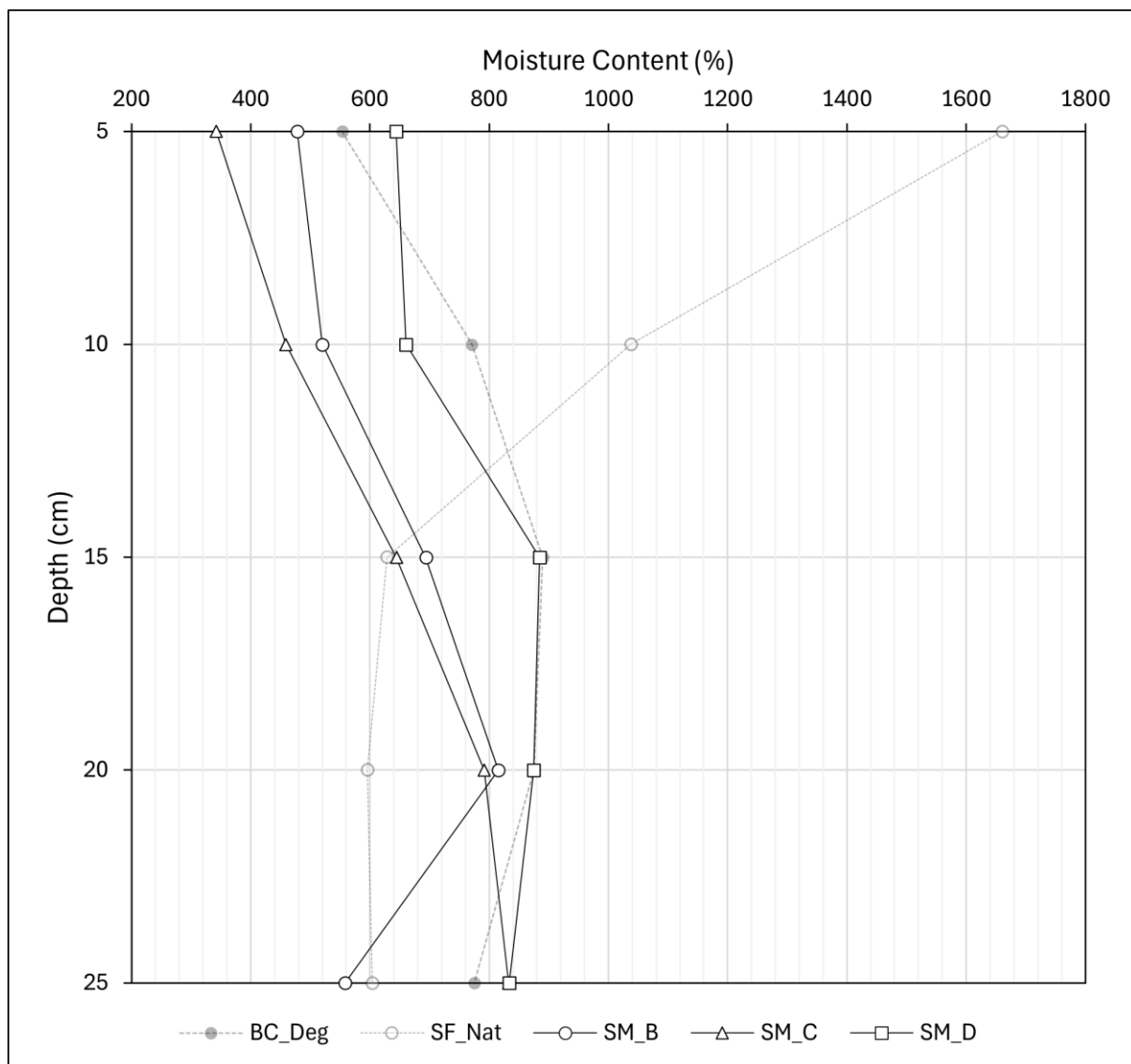
e) Stake Moss

Figure 6.24: Moisture content profiles with depth for the Stake Moss (~2 years old; heather brash, coir, and stone/timber dam) cores.

Figure 6.24 demonstrates Stake Moss cores exhibit low surface moisture content; lower than controls and turved sites at Shap Fells. Profiles increase with depth, but remain within the degraded range. This suggests limited surface water retention, likely due to compaction (Section 6.1.4). Despite some increase below 15cm, findings indicate minimal hydrological recovery ~2 years post-restoration using non-turving interventions.

f) Summary and Interpretation

Restored sites exhibited considerably lower surface moisture content than the near-natural control, indicating limited acrotelm recovery and the persistence of a hydrophobic surface layer caused by decomposition and compaction (Holden *et al.*, 2001, 2011; Morris *et al.*, 2019). Increases with depth suggest some hydrological recovery, though this may indicate water table position rather than water retention (porosity change). Shap Fells and Stake Moss (~2 years post-restoration) show consistently low profiles with minimal variability, suggesting limited early recovery. Greater heterogeneity at Bampton Common (~5 years) may indicate improved rewetting over time, supporting deeper water tables and increased carbon storage (Chapter 2; Section 2.2.1). However, even after a decade, surface recovery remains incomplete, with decomposition and compaction continuing to limit moisture retention.

6.1.6 pH

pH regulates microbial processes, nutrient cycling, and vegetation composition, making it a key indicator of biochemical function. In ombrotrophic systems, degradation lowers pH due to increased oxygen availability and organic acid production. Higher pH values, though still acidic (<5 pH), are typically associated with saturated, near-natural conditions that support diverse peat-forming vegetation (Chapter 3; Section 3.4.4; Table

3.2). Restoration is expected to increase pH through rewetting and reduction of aerobic decomposition (Urquhart and Gore, 1973; Proctor and Maltby, 1998; Freeman *et al.*, 2001). pH is presented across sites and with depth to assess biochemical recovery relative to degraded and near-natural states.
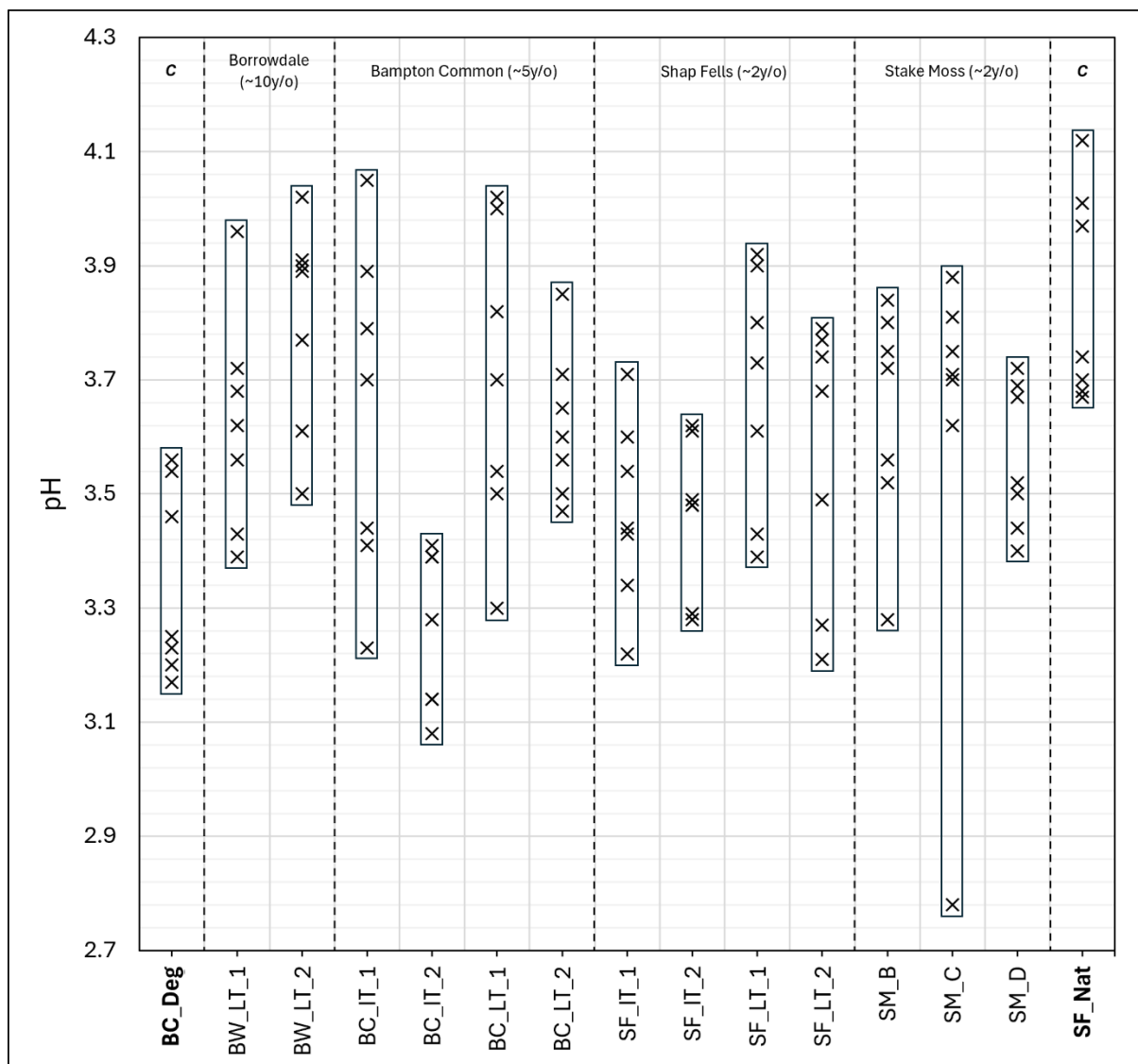
Figure 6.25: pH across cores, grouped by site and restoration age. Values represent 5cm depth intervals from 0–30cm.

Figure 6.25 indicates restoration may influence pH. The degraded control (BC_Deg) records the lowest values (~3.1–3.6), consistent with oxygen exposure (Section 6.1.7) and acid production in an ombrotrophic environment, potentially limiting vegetation

establishment (Chapter 5; Sections 5.1; 5.2). SF_Nat (near-natural control) maintains higher pH (~3.7–4.1), optimal for peat-forming vegetation and anoxia. Most restored sites show higher pH compared to BC_Deg, supporting partial hydrological recovery. Increases are generally greater at older sites (e.g., Borrowdale, ~10 years), suggesting rewetting and oxygen reduction over time. Lower values at Stake Moss – Coir and Bampton Common – Imported Turve (2) indicate incomplete rewetting or localised oxidation (Section 6.1.7).

a) Controls
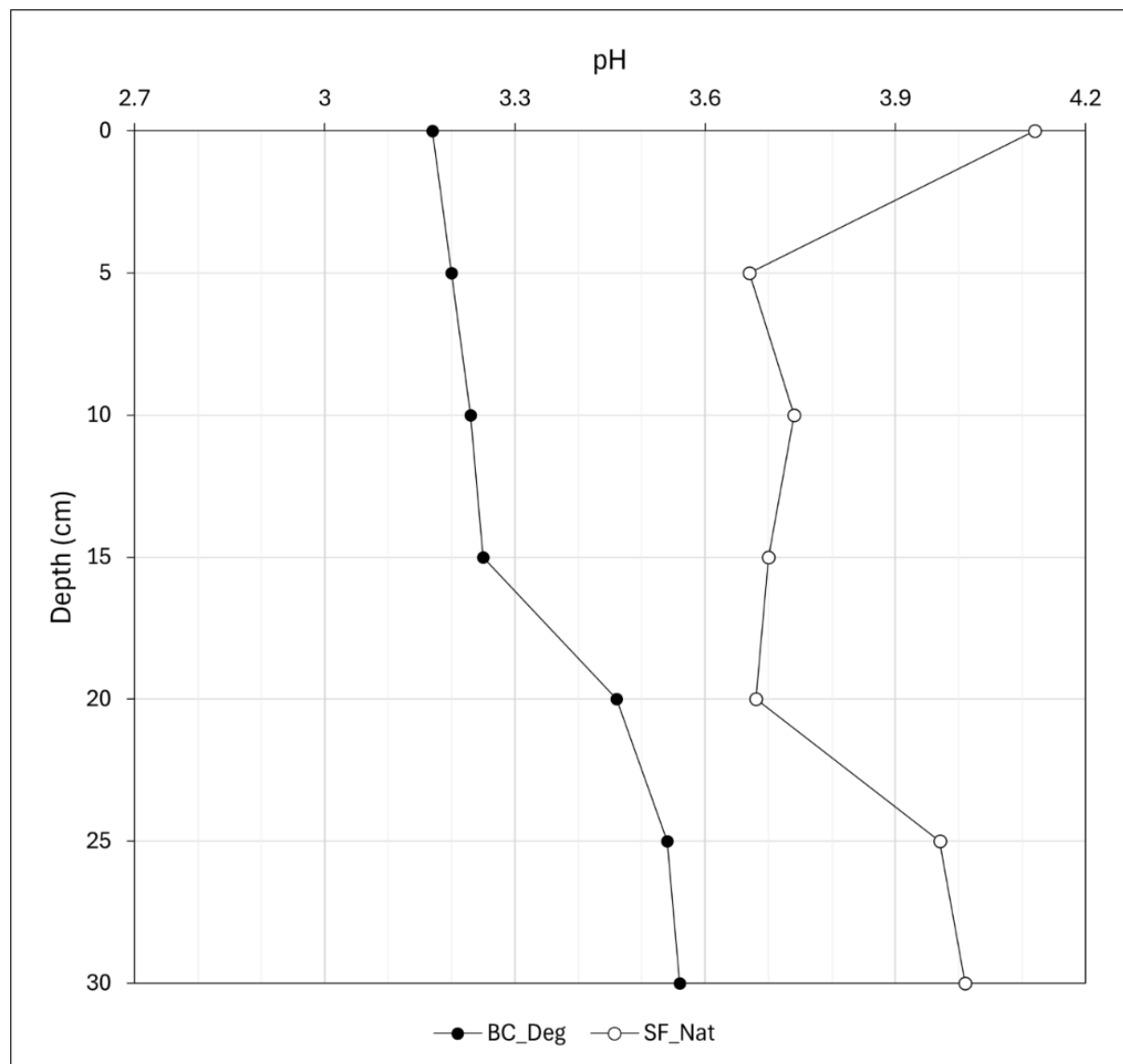
Figure 6.26: pH profiles with depth for the degraded (BC_Deg) and near-natural (SF_Nat) control cores.

Figure 6.26 shows generally increasing pH depth profiles in controls though values remain lower in the degraded core (BC_Deg). This suggests sustained oxygen availability (Section 6.1.7) and organic acid production, consistent with an un-vegetated (Chapter 5; Sections 5.1; 5.2), aerated surface (Section 6.1.5). SF_Nat (near-natural control) shows higher pH, particularly at the surface, supporting saturated (Section 6.1.5), anoxic conditions (Section 6.1.7) maintained by peat-forming vegetation (Chapter 5; Sections 5.1; 5.2). Differences in acidity highlight the role of surface structure in regulating pH and decomposition.

b) Borrowdale
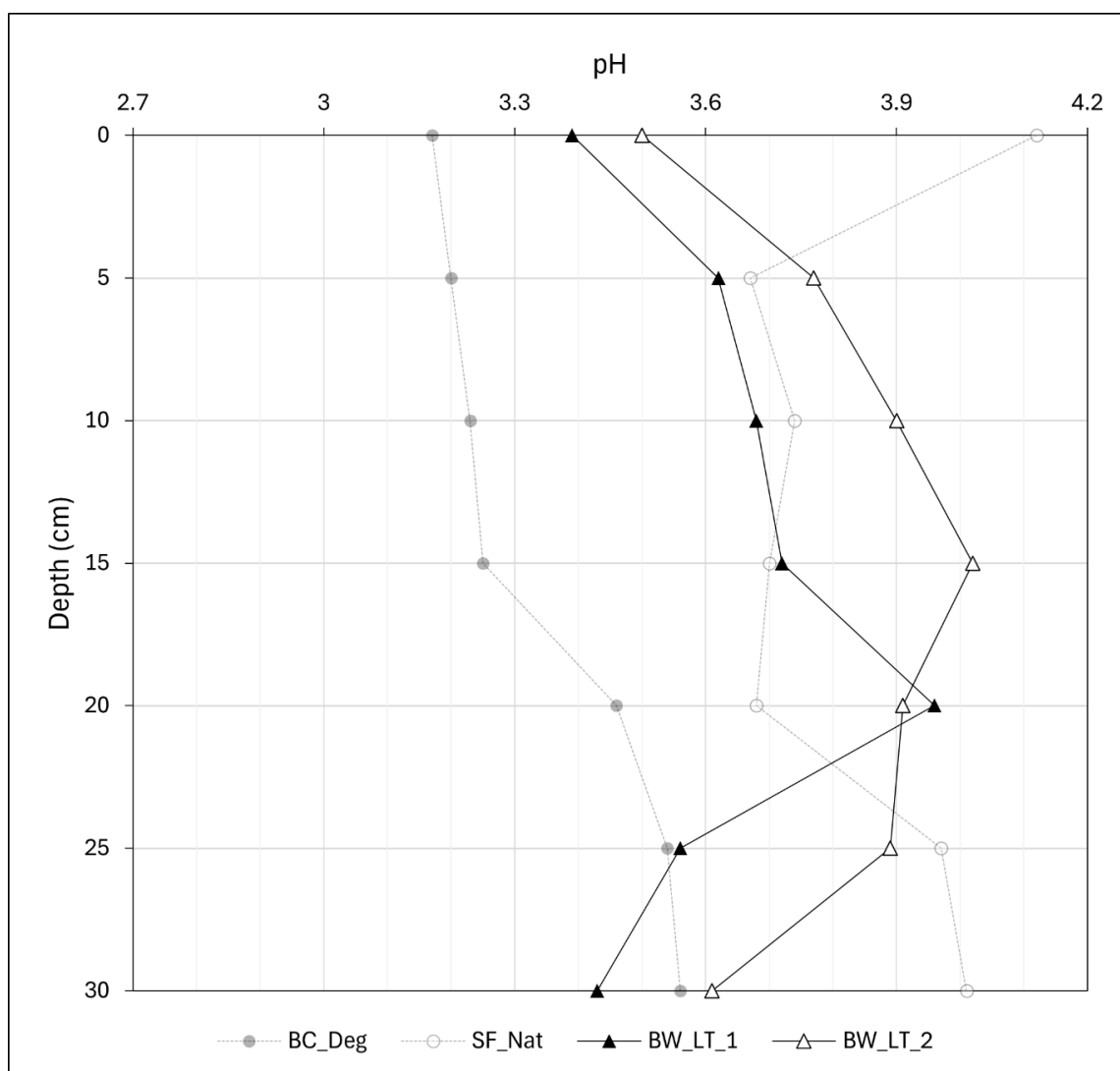
Figure 6.27: pH profiles with depth for the Borrowdale (~10 years old; local turving) cores.

Figure 6.27 demonstrates Borrowdale – Local Turve cores exhibit higher pH than BC_Deg, particularly in the upper 25cm, suggesting partial recovery of a saturated (Section 6.1.5), less oxygenated acrotelm (Section 6.1.7). Surface pH remains lower than the near-natural, potentially indicating a vegetation transition toward *Sphagnum*, *Eriophorum vaginatum*, and *Ericaceous* species a decade post-restoration (Chapter 5; Section 5.2). A decline in pH at 30cm suggests lower restoration impact at depth, potentially indicating the original degraded surface, with higher pH above representing the placed turve. This may indicate a disconnect between turves and underlaying peat.

c) Bampton Common
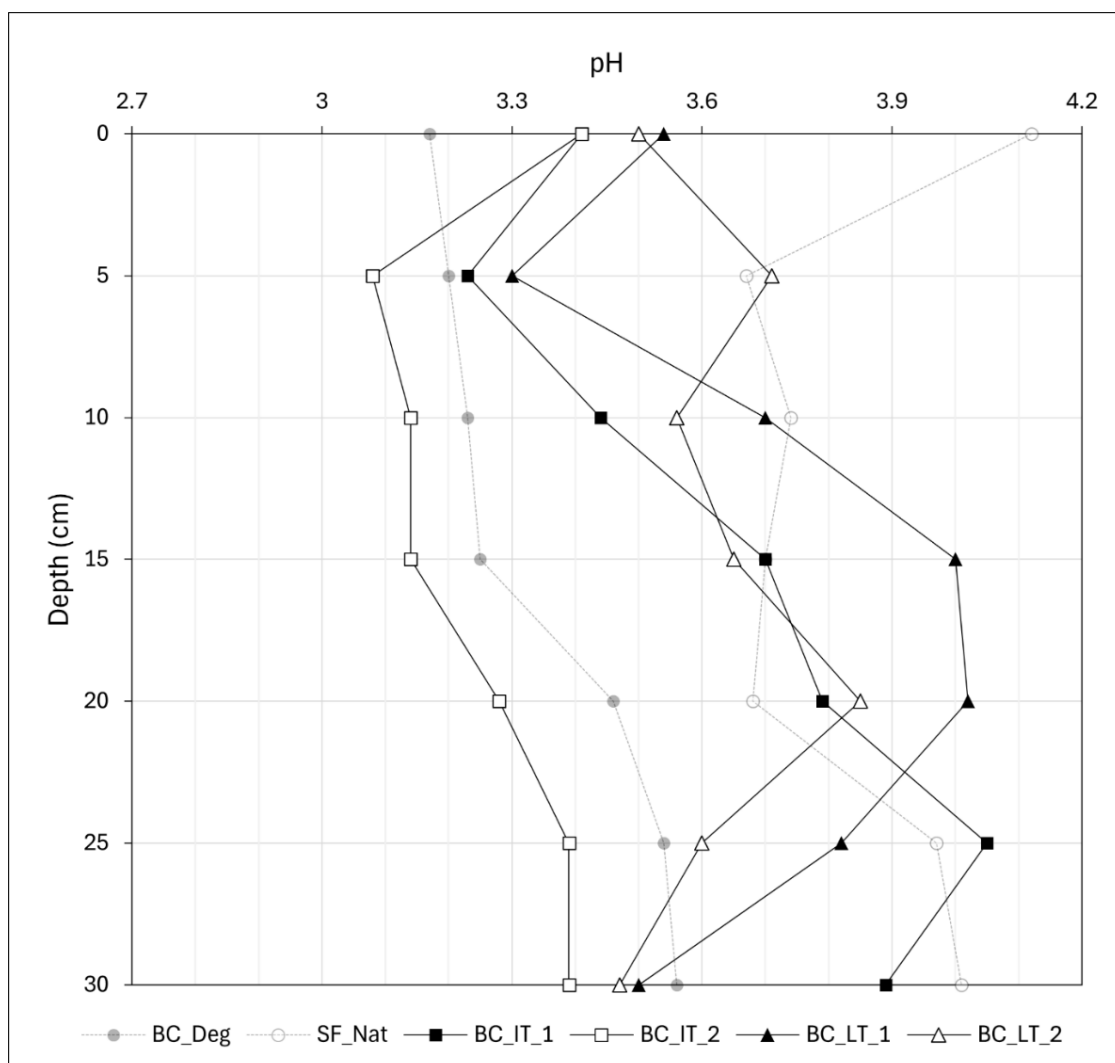
Figure 6.28: pH profiles with depth for the Bampton Common (~5 years old; imported and local turving) cores.

Figure 6.28 shows most Bampton Common cores exhibit increasing pH with depth, approaching near-natural values. This suggests partial recovery of saturated (Section 6.1.5), low-oxygen (Section 6.1.7) conditions regulating acidity and retarded decomposition. However, Imported Turve (2) remains more acidic than the degraded control, indicating limited recovery and suggesting variability in turve quality or placement. Other profiles show increased pH down to ~20–25cm before declining, consistent with turving restoration only affecting the placed acrotelm (as seen in Borrowdale). This indicates limited functional improvement at depth after ~5 years, with restrictions for long-term carbon storage and hydrological resilience.

d) Shap Fells
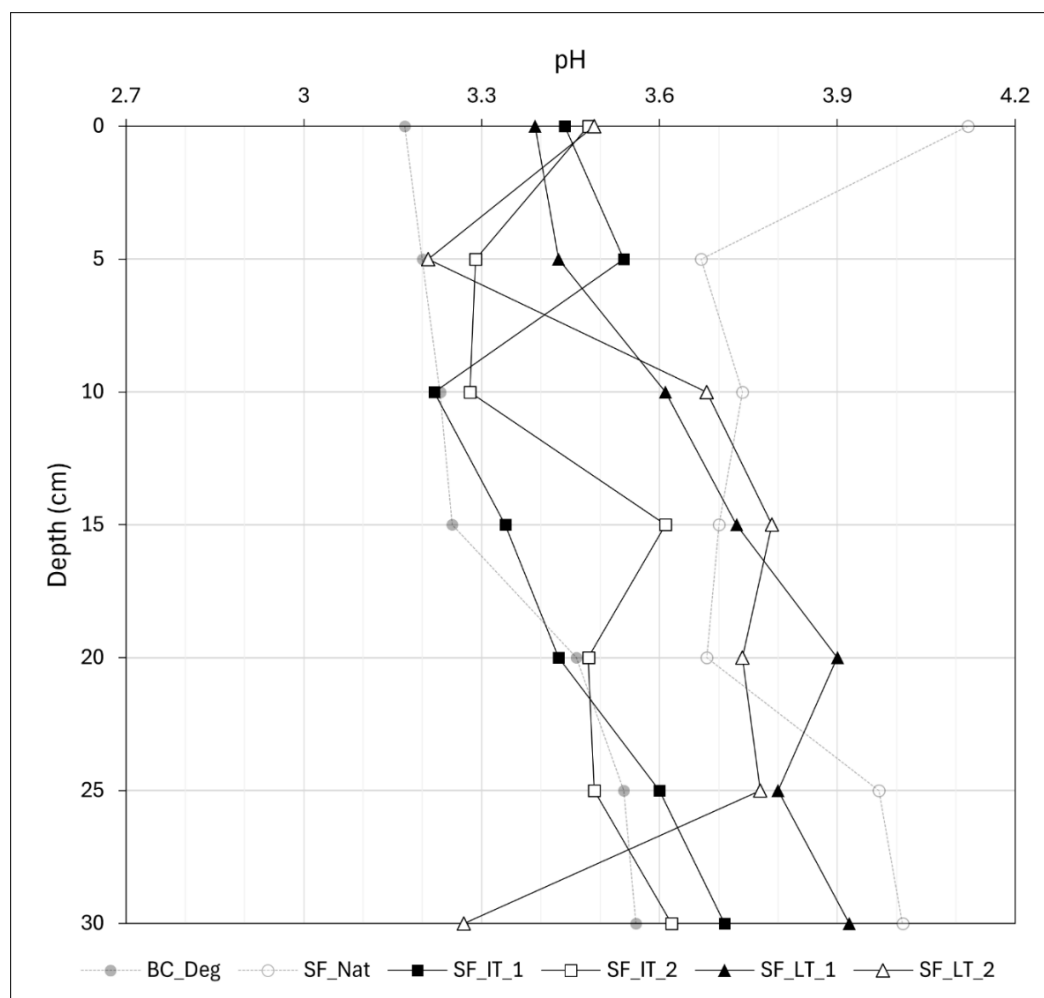
Figure 6.29: pH profiles with depth for the Shap Fells (~2 years old; imported and local turving) cores.

Figure 6.29 demonstrates pH generally increases with depth across Shap Fell cores but remains below near-natural values. This suggests partial recovery from acidic, oxygenated conditions (Section 6.1.7), with limited restoration of saturated, anoxic conditions for long-term carbon storage. Increases in surface pH indicate improved moisture conditions (Section 6.1.5), but profiles remain structurally and chemically aligned with degradation or show high variability (e.g., Shap Fell - Local Turve (2)). Findings indicate inconsistent biochemical recovery required for peat-forming species and carbon accumulation after ~2 years.

e) Stake Moss
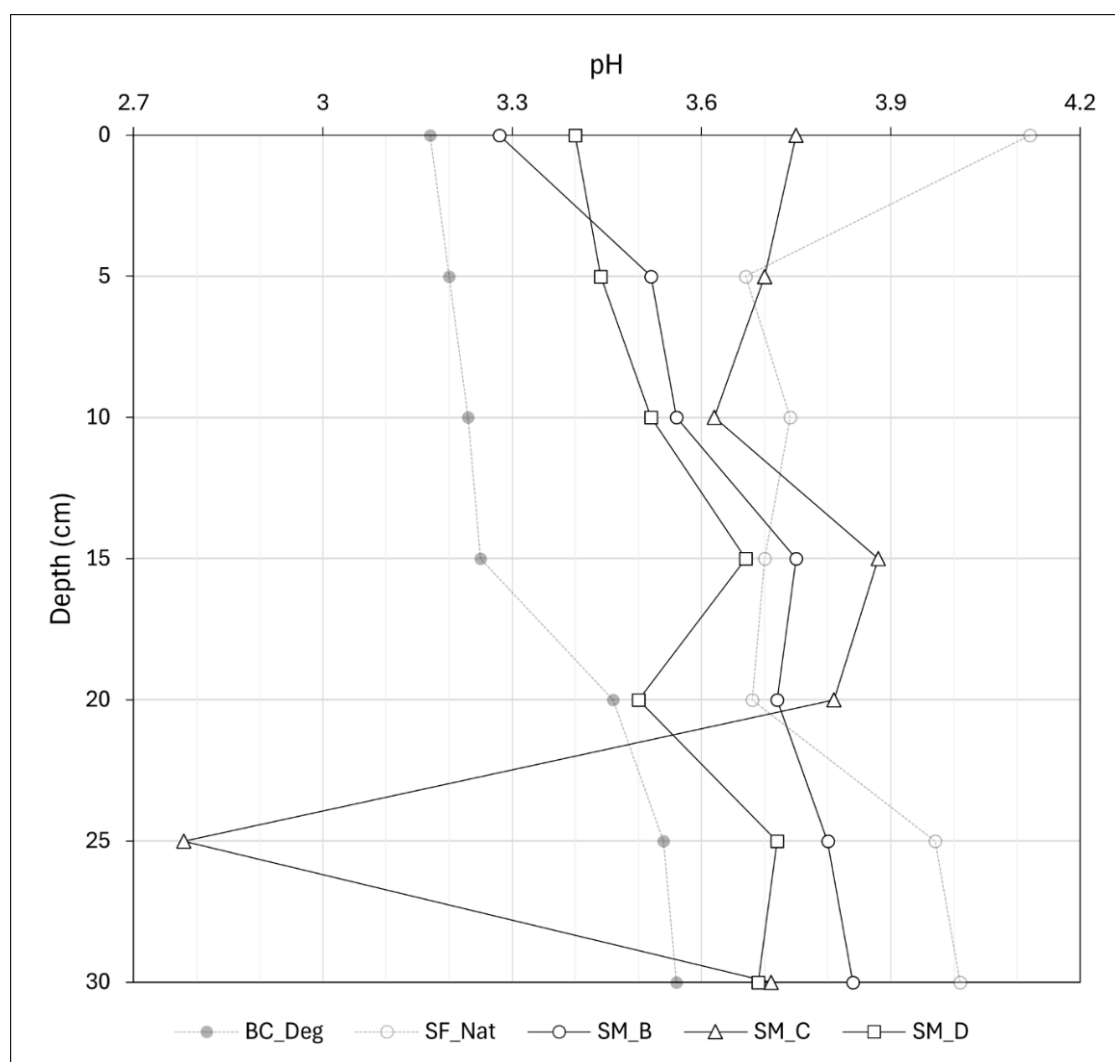
Figure 6.30: pH profiles with depth for the Stake Moss (~2 years old; heather brash, coir, and stone/timber dam) cores.

Figure 6.30 shows pH generally increases with depth across Stake Moss cores, suggesting early signs (~2 years) of biochemical recovery. Stake Moss – Brash and Dam exhibit increases and indicate the control profiles, indicating reduced acidity and potential surface saturation (Section 6.1.5). Stake Moss - Coir shows higher surface pH comparable to SF_Nat, but a decline to 2.78 at 25cm suggests localised acidification. This may indicate site-specific conditions or relic acidic inputs. Results suggest non-turving interventions may reduce acidity within ~2 years, but findings remain inconsistent and could be regulated by vascular and graminoid species (Chapter 5; Section 5.2).

f) Summary and Interpretation

Restoration increases pH across most cores, indicating partial reduction in acidity and oxygen exposure (Section 6.1.7). Older sites (e.g., Borrowdale, ~10 years post-restoration) show the greatest increase, supporting a trajectory of biochemical recovery over time. Surface pH remains lower than near-natural in all restored samples, suggesting incomplete re-establishment of saturated, anoxic conditions (Section 6.1.7) required for peat-forming vegetation and long-term carbon storage (Urquhart and Gore, 1973; Proctor and Maltby, 1998; Freeman *et al.*, 2001). pH increases are often confined to the first 20-25cm, with deeper layers remaining acidic, indicating limited structural integration of placed turves and restricted functional improvement at depth. Variability across sites highlight potential influences from local conditions or vegetation. While restoration can support biochemical function, evidence suggests this improvement is spatially and temporally inconsistent within the first decade. However, weak relationships between pH and surface condition were observed (Section 6.2.4), offering a potential proxy of restoration assessment.

6.1.7 Redox Potential

Redox potential (Eh) provides a proxy for oxygen availability and is a key indicator of sub-surface biochemical function (Chapter 3; Section 3.4.4; Table 3.2). Lower Eh values indicate anoxic conditions retarding decomposition and promoting long-term carbon storage through slow CH_4 production. Higher Eh values indicate aerobic conditions favouring rapid CO_2 release. Restoration aims to reduce Eh by re-establishing saturation and limiting oxygen diffusion (Urquhart and Gore, 1973; Freeman *et al.*, 2001; Niedermeier and Robinson, 2007). Eh is presented across sites and with depth to assess sub-surface anoxia change following restoration.
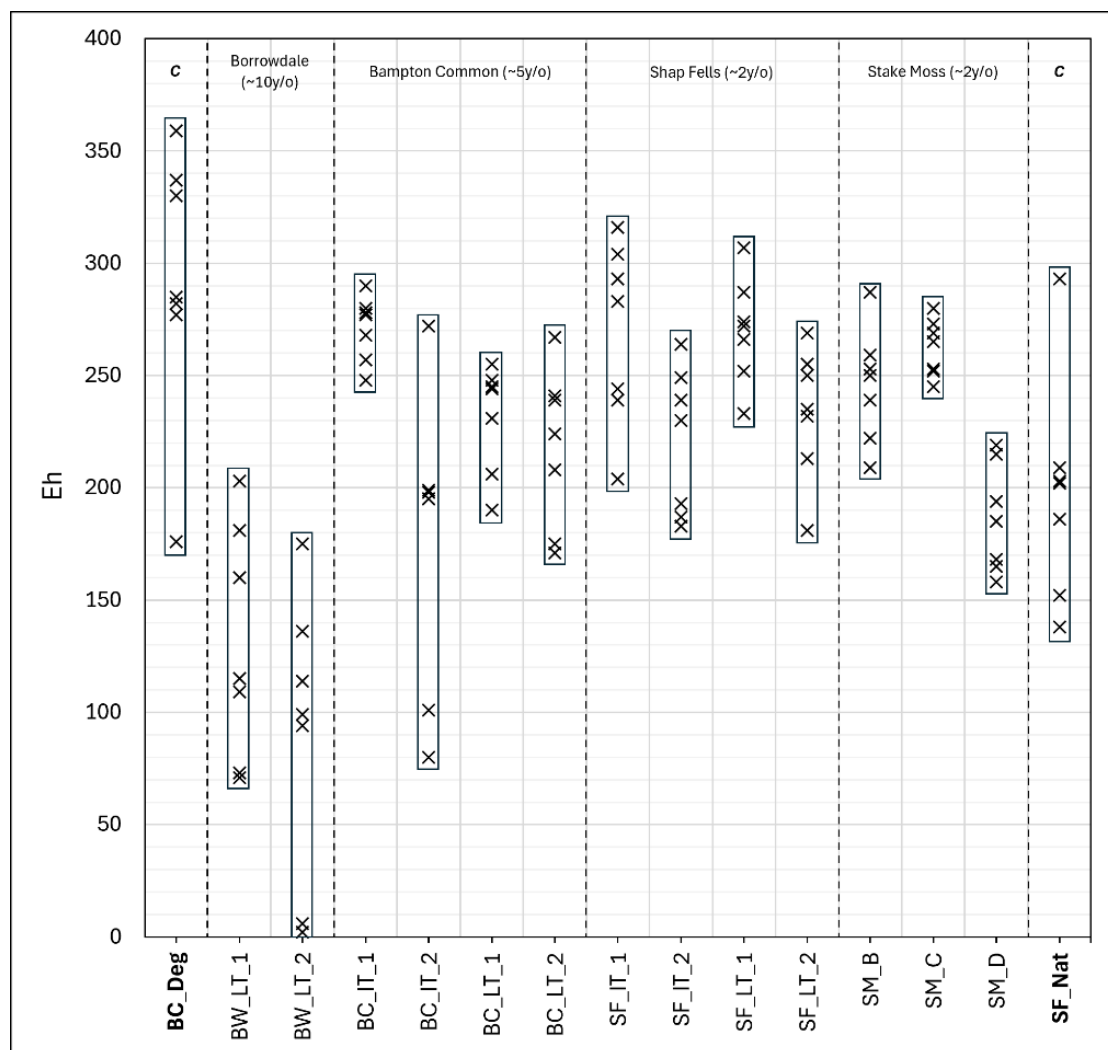
Figure 6.31: Redox potential (Eh) across cores, grouped by site and restoration age. Values represent 5cm depth intervals from 0–30cm.

Figure 6.31 demonstrates Eh indicates patterns observed for pH. The degraded control (BC_Deg) records three of the highest values, indicative of aerobic conditions and oxic decomposition, producing CO_2. SF_Nat (near-natural control) shows lower Eh, consistent with high moisture content (Section 6.1.5) and anoxic conditions supporting carbon accumulation. Restored sites generally exhibit reduced Eh relative to BC_Deg, suggesting partial rewetting. Older sites, particularly Borrowdale (~10 years) and Bampton Common (~5 years), exhibit lower Eh than recent interventions (~2 years), indicating recovery over time. At Borrowdale, Eh falls below SF_Nat, potentially due to increased bulk density (Section 6.1.4), which may restrict gas diffusion (Chapter 2; Section 2.2.3). Findings suggest restoration can lower Eh over time, with implications for long-term carbon retention and microbial activity.

a) Controls
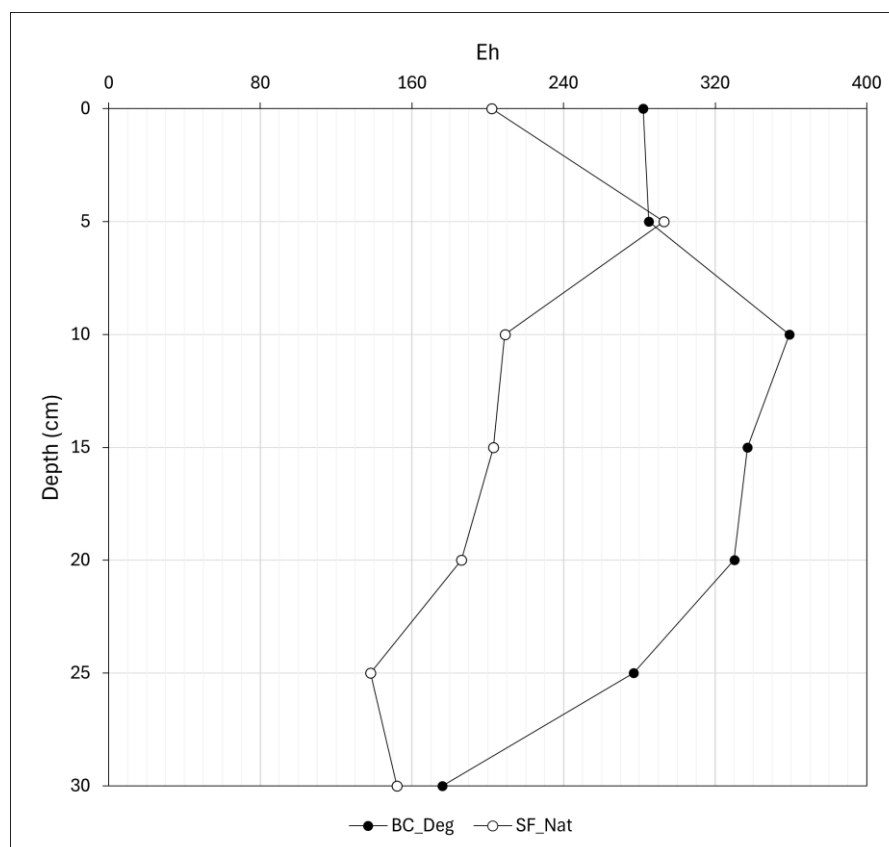
Figure 6.32: Eh profiles with depth for the degraded (BC_Deg) and near-natural (SF_Nat) control cores.

Figure 6.32 shows contrasting Eh profiles between the degraded (BC_Deg) and near-natural (SF_Nat) controls. SF_Nat exhibits lower Eh indicative of more anoxic conditions, promoting retarded decomposition and carbon storage. However, profiles converge at 5cm. This aligns with trends in higher humification (decomposition; Section 6.1.3), moisture content (Section 6.1.5), and lower pH (Section 6.1.6), suggesting a thin aerobic layer within SF_Nat. This supports some surface disturbance (Chapter 5; Sections 5.3; 5.4), consistent with its near-natural classification, rather than pristine (Chapter 2; Sections 2.1.2; 2.5).
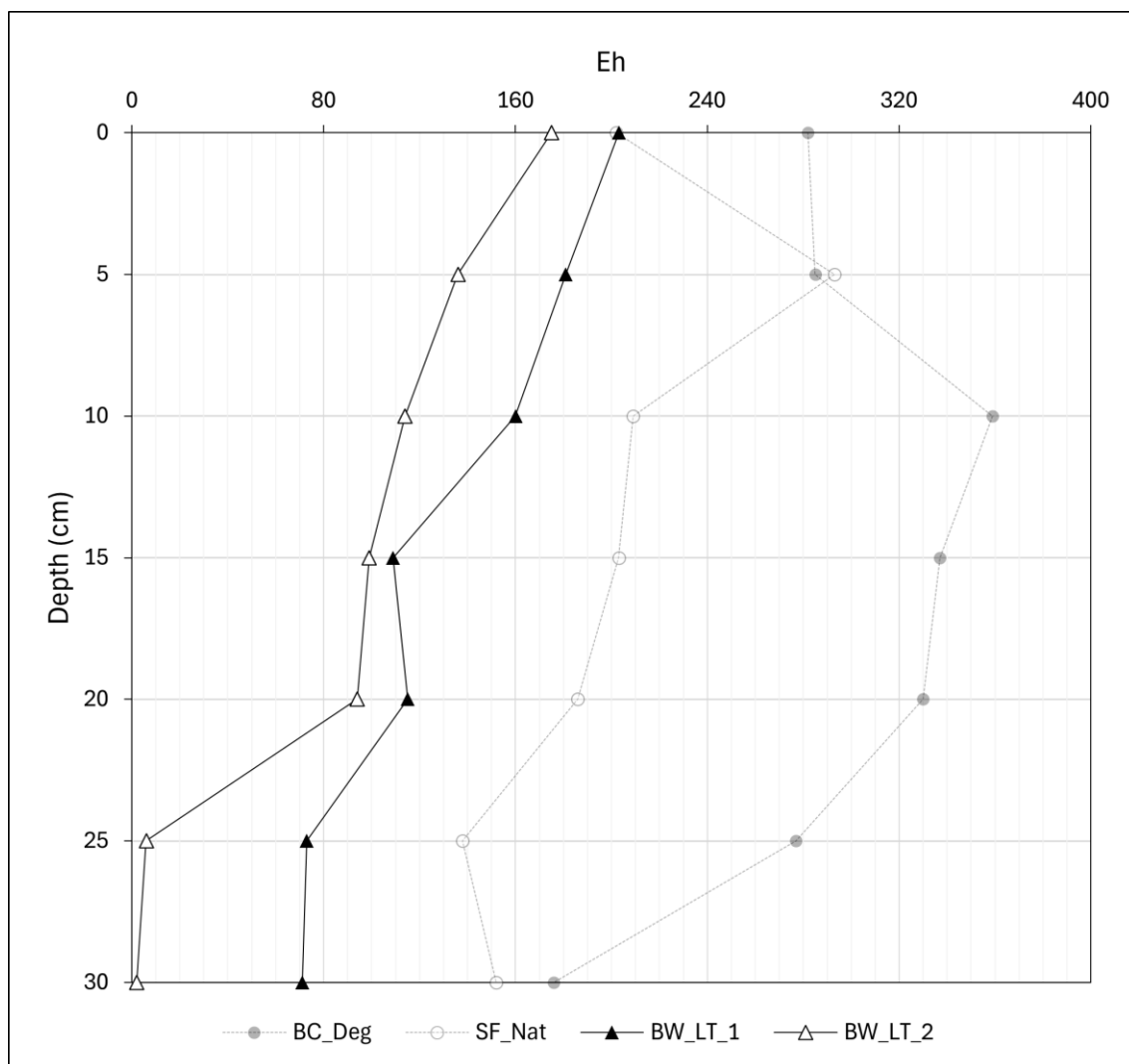
b) Borrowdale

Figure 6.33: Eh profiles with depth for the Borrowdale (~10 years old; local turving) cores.

Figure 6.33 demonstrates Borrowdale – Local Turve cores exhibit consistently lower Eh than the degraded control, indicating increased anoxia and retarded decomposition. Values are lower than SF_Nat, suggesting stronger reducing conditions despite lower moisture content to near-natural conditions (Section 6.1.5). This may indicate differences in element availability through vegetation composition (Chapter 5; Section 5.2), or unobserved chemical disturbance not captured in surface assessments. Higher Eh at near-surface depths may indicate increased temperature (Section 6.1.2), persistent compaction (Section 6.1.4), and incomplete surface saturation (Section 6.1.5). Profiles suggest partial anoxic recovery ~10 years post-restoration, potentially under altered structural or biochemical conditions.

c) Bampton Common
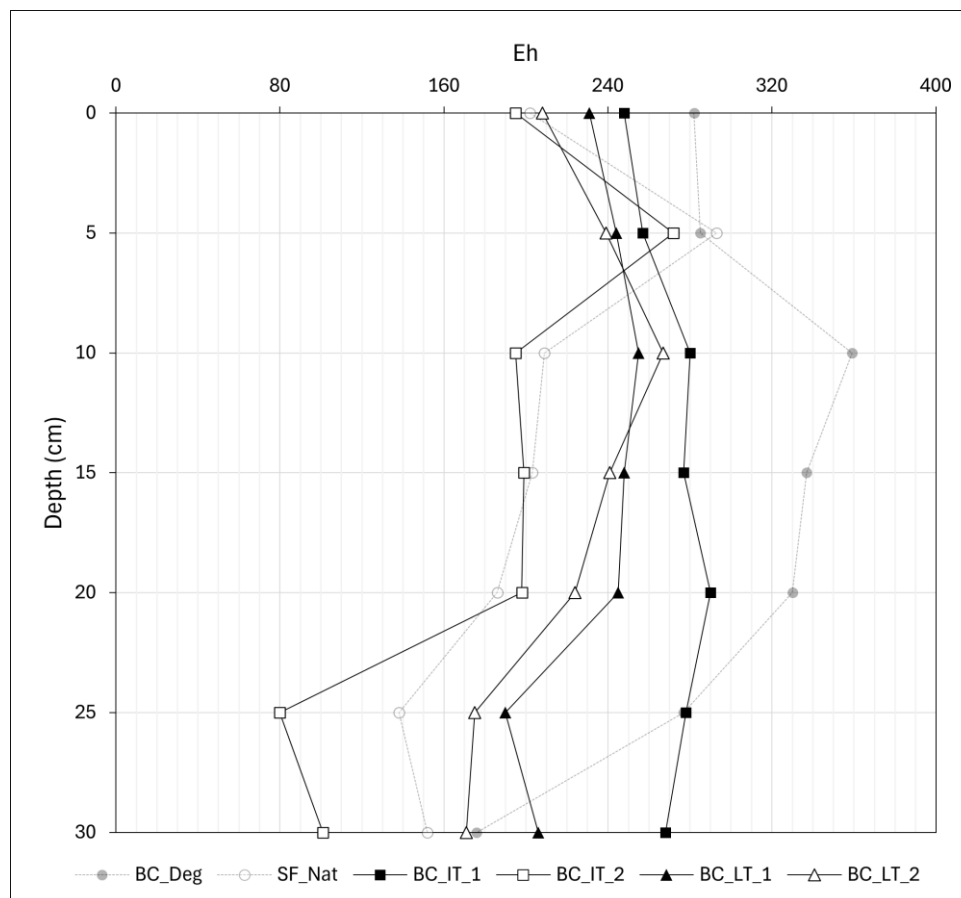
Figure 6.34: Eh profiles with depth for the Bampton Common (~5 years old; imported and local turving) cores.

Figure 6.34 shows Bampton Common cores exhibit lower Eh than the degraded control and align with near-natural profiles, indicating increased anoxia and potential for retarded decomposition ~5 years post-restoration. Bampton Common – Imported Turve (1) shows increased Eh, particularly below 25cm, exceeding degraded values. This likely indicates biochemical disturbance associated with the mineral layer (Sections 6.1.1, 6.1.4, 6.1.5), demonstrating interactions between organic carbon (Section 6.1.1), compaction (Section 6.1.4), and water retention (Section 6.1.5) on redox dynamics, indicative of pore structural influence (Rezanezhad *et al.*, 2016; Spencer *et al.*, 2017).

d) Shap Fells
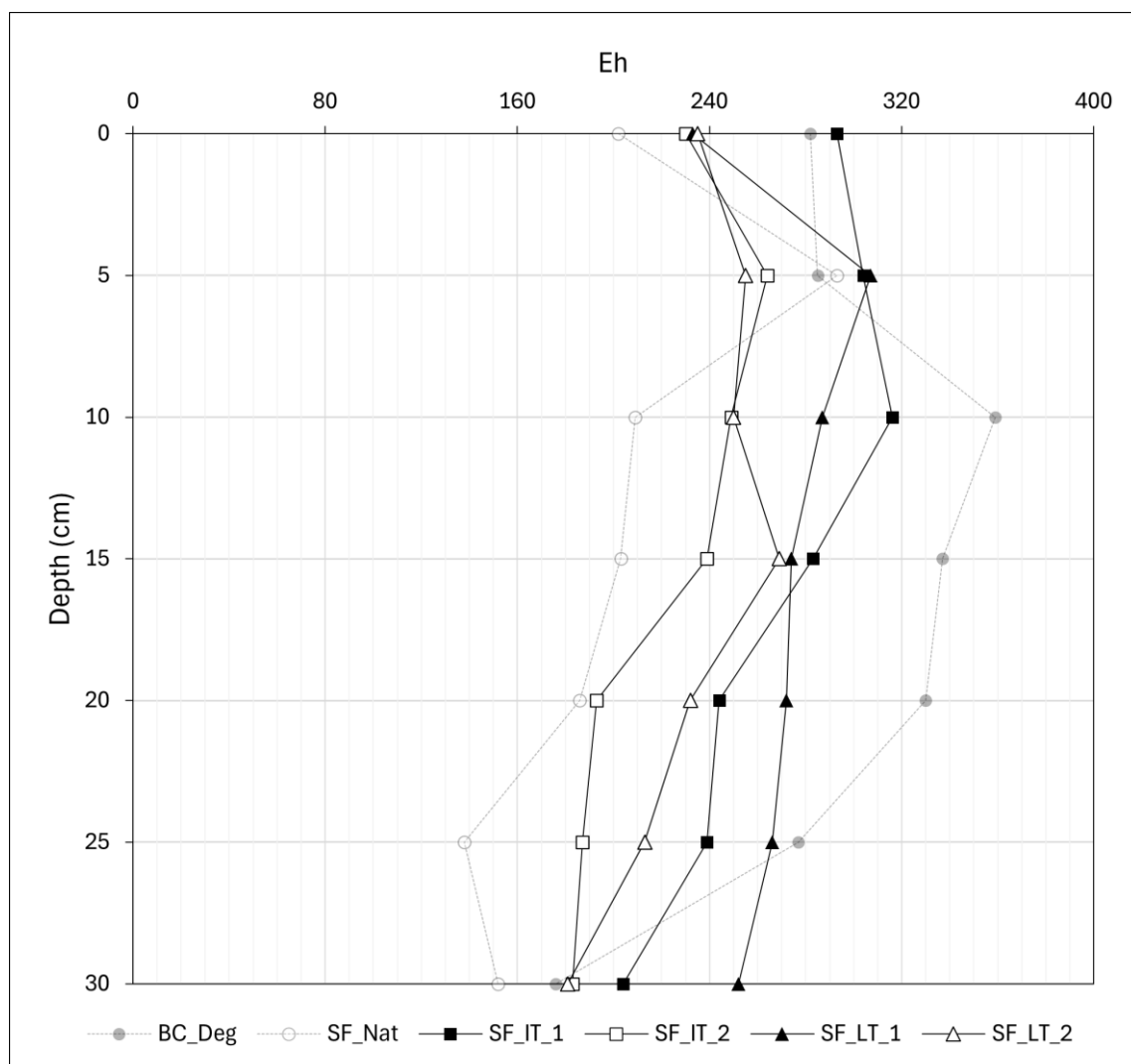
Figure 6.35: Eh profiles with depth for the Shap Fells (~2 years old; imported and local turving) cores.

Figure 6.35 demonstrates Shap Fell cores exhibit Eh values lower than the degraded control but higher than near-natural conditions. This indicates partial rewetting (water retention) ~2 years post-restoration, supported by temperature (Section 6.1.2) and moisture content (Section 6.1.5), suggesting increasing anoxia and potential for carbon storage. Limitations on further Eh reduction may relate to persistent compaction restricting water retention (Section 6.1.4).

e) Stake Moss
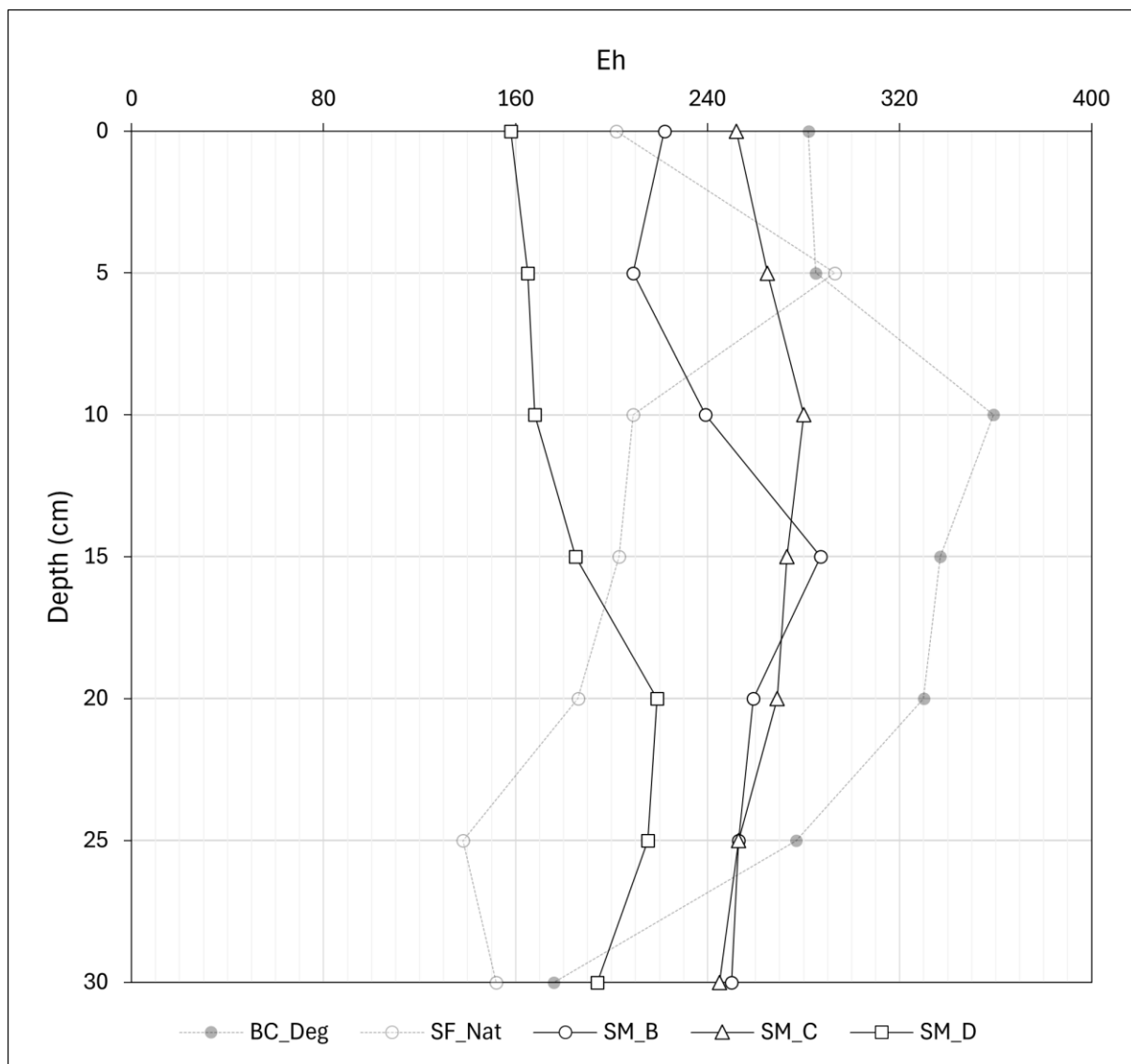
Figure 6.36: Eh profiles with depth for the Stake Moss (~2 years old; heather brash, coir, and stone/timber dam) cores.

Figure 6.36 shows Eh in Stake Moss cores is lower than the degraded control, indicating early signs of re-wetting (Section 6.1.5) and increased anoxia after ~2 years. However, values generally remain above near-natural conditions, suggesting incomplete functional recovery. Stake Moss – Dam records the lowest Eh, more closely aligning with SF_Nat, demonstrating the potential success of localised re-wetting associated with stone/timber dams.

f) Summary and Interpretation

Restored sites generally exhibited reduced Eh, indicating partial rewetting and increased anoxia relative to degraded conditions. Recovery appears time-dependent, with older sites (~5–10 years) showing lower Eh than more recent interventions (~2 years). Technique also plays a role, with effective rewetting (e.g., Stake Moss – Dam) promoting reduced Eh within ~2 years. Findings suggest Eh decreases with restoration age and intervention type, supporting sub-surface recovery and more long-term carbon storage (Urquhart and Gore, 1973; Freeman *et al.*, 2001; Niedermeier and Robinson, 2007).

6.2 Surface Condition Versus Sub-Surface Properties

Comparing mean sub-surface bulk and chemical properties with average surface condition scores (Chapter 5; Section 5.5.1; Table 5.4) evaluates whether bulk indicators indicate restoration success. This adds functional insight to existing surface assessments and identifies accessible metrics for monitoring sub-surface recovery (Chapter 2; Section 2.6.3 and Research Question 1). Polynomial regression is used to explore non-linear relationships. Organic carbon content is excluded due to limited short-term sensitivity, and temperature is removed as absolute values were unavailable (Chapter 3; Section 3.2.1). Remaining parameters, including humification, bulk density,

moisture content, pH, and redox potential (Eh), are assessed for their potential as proxies of sub-surface function and their alignment with surface monitoring. Comparisons form the basis of incorporating sub-surface structural understanding into monitoring functional response in the following chapter (Research Question 2).

6.2.1 Humification

Mean Von-Post humification values were compared with average JNCC (2009) site condition scores from Chapter 5; Section 5.5.1; Table 5.4 to assess whether surface condition indicates sub-surface decomposition (Figure 6.37).
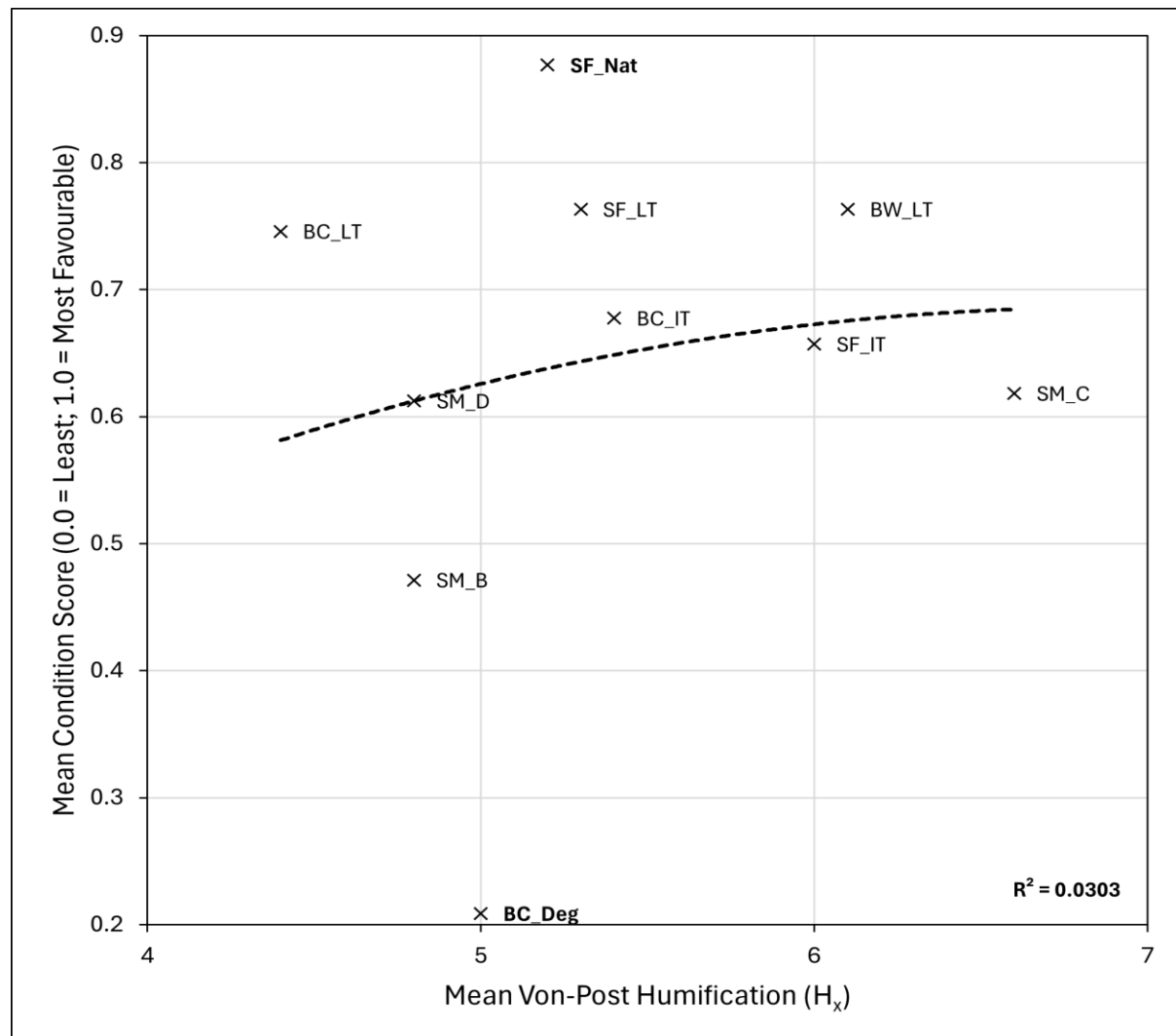
Figure 6.37: Relationship between mean sub-surface Von-Post humification (H_x) and mean site condition score. Each point represents the mean across 5cm depth intervals. For turved sites with duplicate cores, values are averaged across both.

Figure 6.37 demonstrates no meaningful relationship between mean sub-surface Von-Post humification and surface condition score (R^2 = 0.0303). This suggests limited association between surface recovery and sub-surface decomposition, indicating the insensitivity of Von-Post to short-term restoration impacts (Chapter 3; Section 3.4.4; Table 3.2).

6.2.2 Bulk Density

Mean bulk density values were compared with average JNCC (2009) site condition scores from Chapter 5; Section 5.5.1; Table 5.4 to assess whether surface condition indicates sub-surface compaction (Figure 6.38).
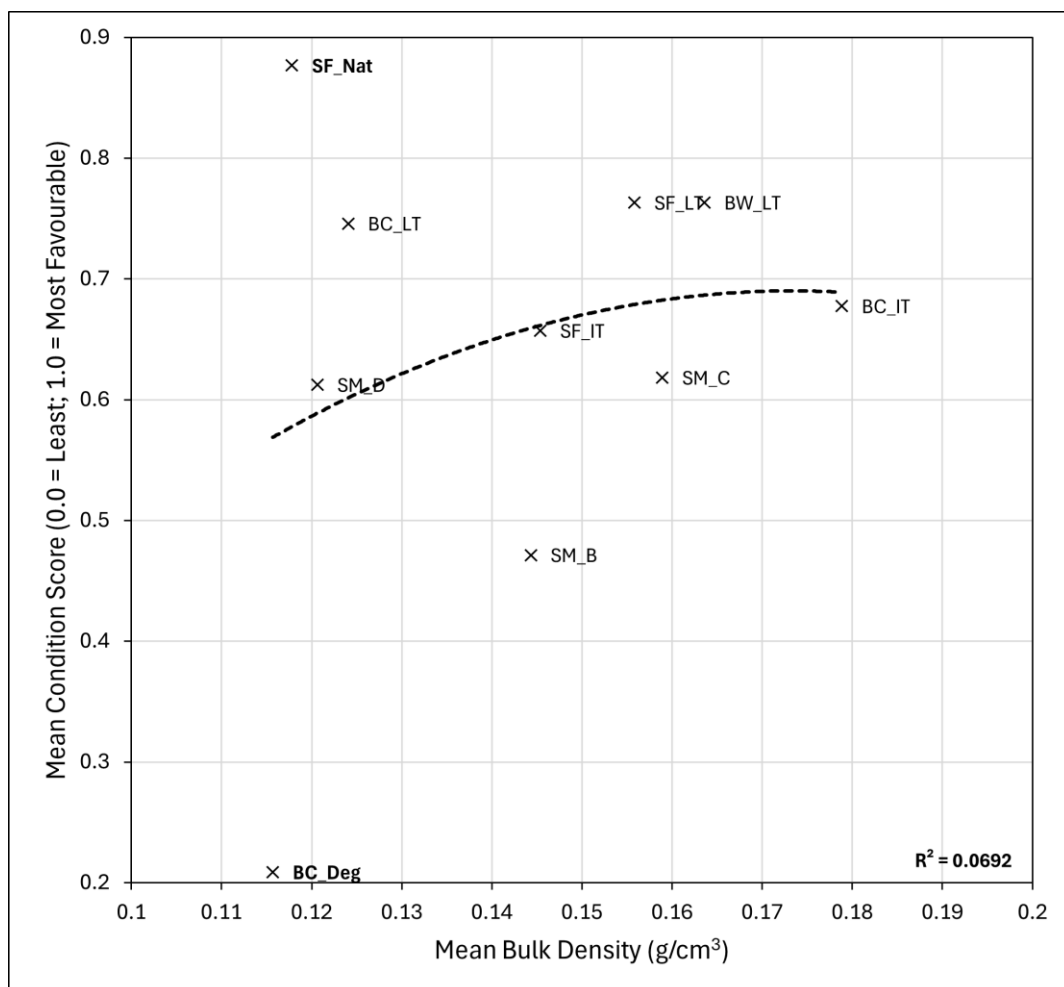
Figure 6.38: Relationship between mean sub-surface bulk density (g/cm^3) and mean site condition score. Each point represents the mean across 5cm depth intervals. For turved sites with duplicate cores, values are averaged across both.

Figure 6.38 shows no meaningful relationship between mean sub-surface bulk density and surface condition score (R^2 = 0.0692). While the degraded control (BC_Deg) exhibits low condition (unfavourable) and high compaction, restored and near-natural sites display a range of bulk densities despite similar surface scores. This suggests minimal association between surface condition and sub-surface compaction, indicating an insensitivity of bulk density to porosity change. Consistent with the literature, this may indicate limitations of the oven-drying method, which is destructive, obscuring fine-scale variation (Rowell, 1994; Couwenberg *et al.*, 2011; Petrokofsky *et al.*, 2012). µCT-derived porosity provides a more effective measure of compaction impacts and is explored in the following chapter.

6.2.3 Moisture Content

Mean moisture content values were compared with average JNCC (2009) site condition scores from Chapter 5; Section 5.5.1; Table 5.4 to assess whether surface condition indicates sub-surface water retention (Figure 6.39).
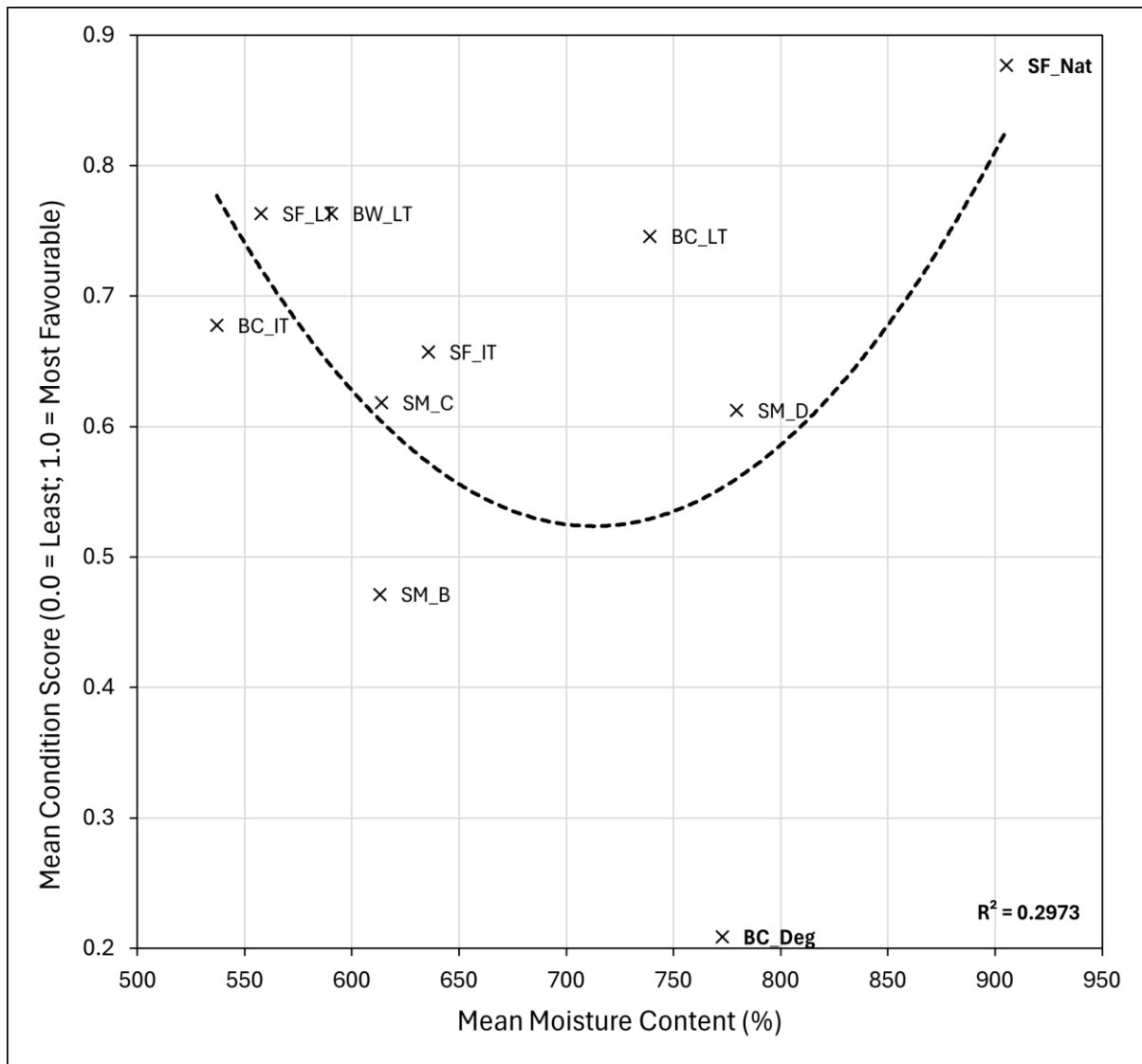
Figure 6.39: Relationship between mean sub-surface bulk density (% dry weight) and mean site condition score. Each point represents the mean across 5cm depth intervals. For turved sites with duplicate cores, values are averaged across both.

Figure 6.39 shows a weak positive relationship between mean sub-surface moisture content and surface condition score (R^2 = 0.2973), though there is no consistent pattern. Higher condition (more favourable) generally associates with high sub-surface moisture, suggesting some correspondence between surface recovery and water retention. However, overlap at mid-range values and low scores at high moisture (e.g., BC_Deg) indicate moisture alone is not a reliable proxy for condition. Additionally, surface saturation (e.g., >1600% at 5cm in SF_Nat; Section 6.1.5) is not captured in depth-

averaged means, potentially masking stronger surface to sub-surface hydrological relationships (Holden *et al.*, 2001, 2011; Morris *et al.*, 2019).

6.2.4 pH

Mean pH values were compared with average JNCC (2009) site condition scores from Chapter 5; Section 5.5.1; Table 5.4 to assess whether surface condition indicates sub-surface acidity (Figure 6.40).
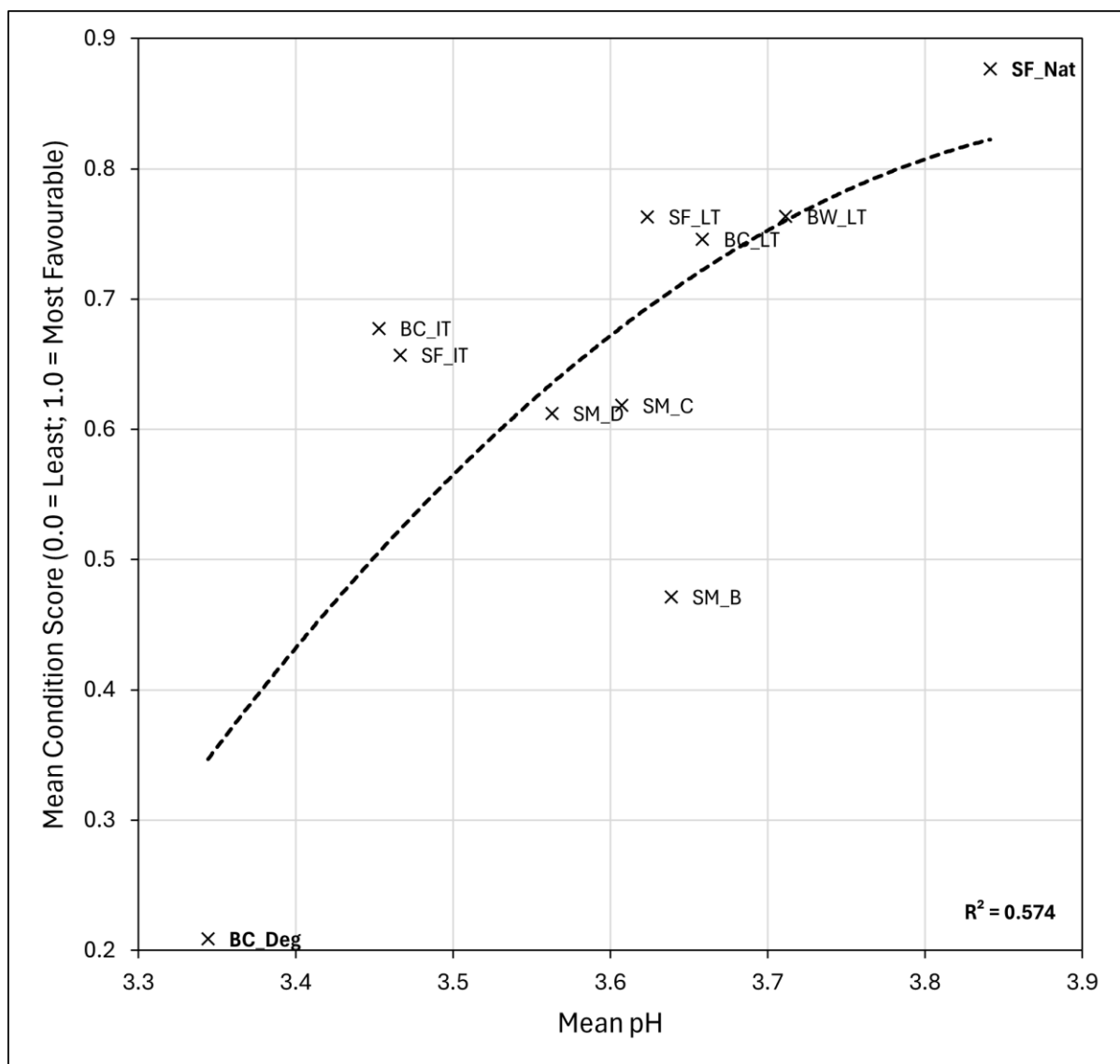
Figure 6.40: Relationship between mean sub-surface pH and mean site condition score. Each point represents the mean across 5cm depth intervals. For turved sites with duplicate cores, values are averaged across both.

Figure 6.40 demonstrates a moderate positive relationship between mean sub-surface pH and surface condition score (R^2 = 0.574), suggesting higher pH aligns with more favourable surface condition. This may indicate reduced acidity and increased surface saturation, which support peat-forming vegetation (Urquhart and Gore, 1973; Proctor and Maltby, 1998; Freeman *et al.*, 2001). The degraded control (BC_Deg) shows the lowest pH and condition score, while near-natural (SF_Nat) and more favourable restored sites (e.g., Borrowdale – Local Turve; Shap Fells – Local Turve) exhibit higher values. Outliers such as Stake Moss – Brash illustrate pH alone does not determine surface condition, but results support its potential as a proxy for functional recovery. Additionally, caution is warranted in that findings may represent the conditions within the placed turve, rather than the complete profile, where there is a structural disconnect (explored in the following chapter).

6.2.5 Redox Potential

Mean Eh values were compared with average JNCC (2009) site condition scores from Chapter 5; Section 5.5.1; Table 5.4 to assess whether surface condition indicates sub-surface anoxia (Figure 6.41).
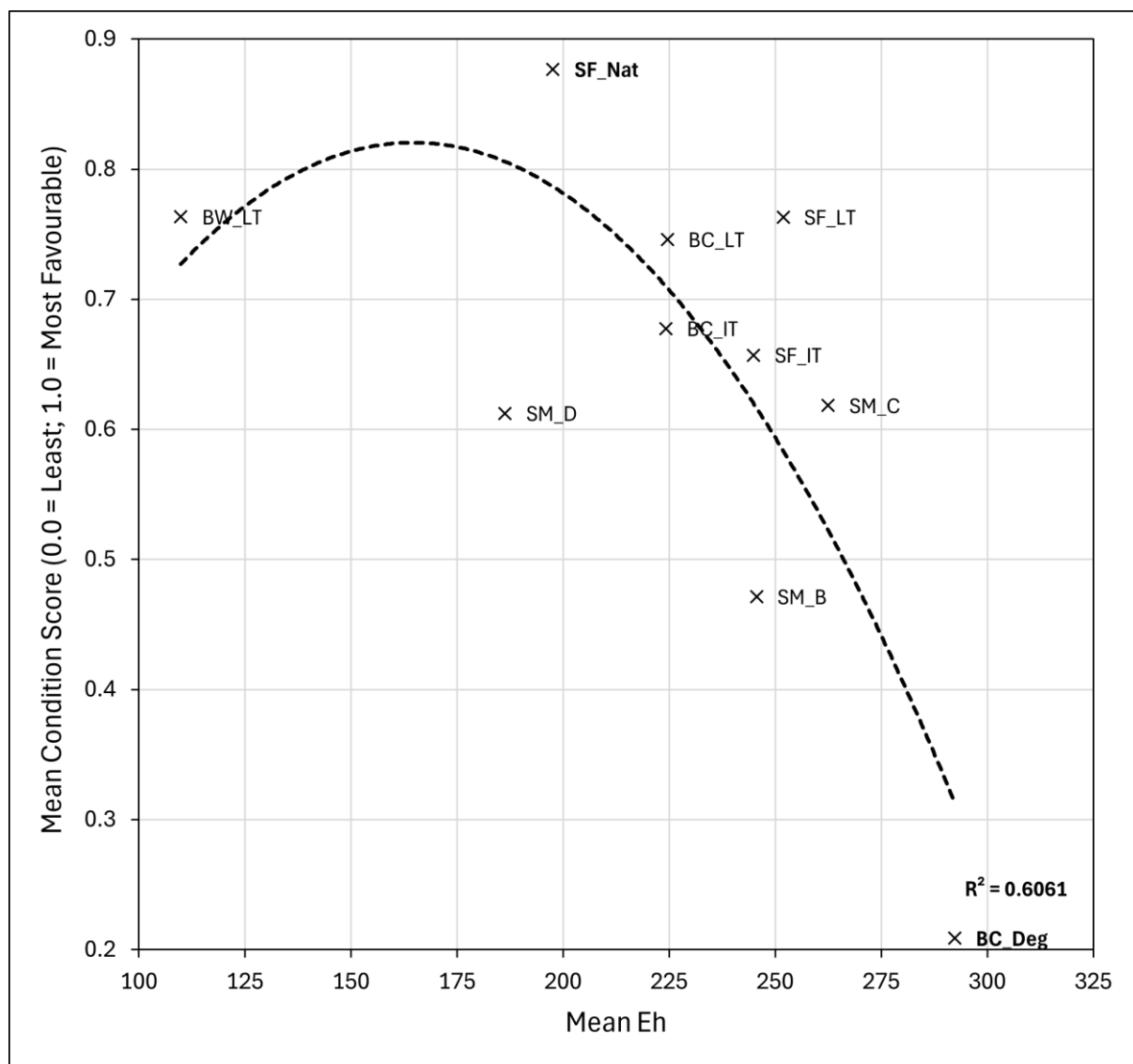
Figure 6.41: Relationship between mean sub-surface Eh and mean site condition score. Each point represents the mean across 5cm depth intervals. For turved sites with duplicate cores, values are averaged across both.

Figure 6.41 shows a moderate negative relationship between mean sub-surface Eh and surface condition score (R^2 = 0.6061), with lower Eh generally aligning with more favourable surface conditions. This supports the role of anoxia in promoting peatland function, where saturated conditions retard decomposition and increase long-term carbon storage through peat accumulation (Urquhart and Gore, 1973; Clymo, 1984; Clymo *et al.*, 1998; Freeman *et al.*, 2001; Niedermeier and Robinson, 2007). The degraded control (BC_Deg) exhibits the highest Eh and lowest condition score, while near-natural

(SF_Nat) and more favourable restored sites (e.g., Borrowdale – Local Turves) show lower Eh and increased surface condition scores. Results suggest Eh may serve as a more viable proxy for assessing sub-surface rewetting; more sensitive than destructive oven-drying methods of moisture content (Section 6.2.3).

6.3 Chapter Synthesis and Discussion

Bulk and chemical properties derived from continuous peat cores were evaluated to determine whether they effectively characterise sub-surface recovery in restored blanket peatlands (Chapter 1; Section 1.1). Functionally relevant indicators were assessed across degraded, near-natural, and restored sites to examine whether restoration age and technique influence belowground function, and to evaluate the extent to which these metrics support surface-based condition assessments, as discussed in Chapter 2; Section 2.6.3, where the limitations of surface monitoring frameworks were identified.

6.3.1 Characterising Conditions

Bulk and chemical indicators effectively distinguished degraded from near-natural conditions. The near-natural control consistently exhibited lower bulk density, higher moisture content, lower Eh, and higher pH, indicative of less compact, saturated peat capable of water retention (particularly in the acrotelm) and supporting peat-forming *Sphagnum* species (Chapter 2; Sections 2.1; 2.2; Price *et al.*, 2003; McCarter and Price, 2013; Alderson *et al.*, 2019), contributing to net carbon accumulation (Clymo *et al.*, 1998; Strack and Waddington, 2007; Strack and Price, 2009). The degraded control showed higher bulk density, reduced moisture content, and increased Eh, consistent with oxic decomposition and accelerated carbon loss through CO_2 production (Chapter 2; Section 2.3; Waddington and Price, 2000; Worrall *et al.*, 2011).

Restored cores displayed varying degrees of sub-surface recovery along a spectrum influenced by restoration age and technique, enabling differentiation from degraded conditions. Older sites such as Borrowdale (~10 years) and Bampton Common (~5 years) generally showed parameters more closely aligned with near-natural conditions, while younger restorations (Shap Fells and Stake Moss, ~2 years) exhibited greater variability but some improvement relative to the degraded baseline. *Turved sites, particularly those using local turves, more closely aligned with near-natural profiles than non-turved interventions, supporting its application over heather brash spreading*. However, bulk density and moisture content in restored cores remained more similar to degraded than near-natural conditions, demonstrating the critical influence of sub-surface structure not captured by these methods. *No restored core fully replicated the stratification (acrotelm – mesotelm – catotelm), or functional characteristics of the near-natural target, suggesting sub-surface recovery remains incomplete*.

6.3.2 Indicator Sensitivity and Functional Relevance

Not all indicators were equally sensitive or functionally meaningful. Organic carbon content, while confirming the organic nature of peat, was insensitive to recent restoration impacts. Von-Post humification and bulk density failed to clearly distinguish restored from degraded samples. Although increased decomposition and compaction were acknowledged in restored sites, *the limited precision of these parameters restricted their ability to detect fine-scale variation linked to pore structure (Chapter 2; Section 2.2.3; Kettridge and Binley, 2008; Rezanezhad et al., 2016)*.

Eh and pH more effectively captured functional differences, showing degradation-related shifts and recovery gradients with restoration age. Moisture content showed some

250

alignment with water retention and hydrological function, particularly within the acrotelm, supporting the role of the surface layer in regulating sub-surface hydrology (Holden *et al.*, 2001; Holden, 2005b; Morris *et al.*, 2019), However, interpretation was restricted by the destructive nature of sampling and by depth averaging. *Results suggest while some bulk and chemical indicators provide useful context, more sensitive techniques are required to characterise restoration outcomes* (Chapter 3; Sections 3.4.1; 3.4.2).

6.3.3 Value of Continuous Sampling

Assessing profiles facilitated direct observation of vertical stratification, offering insight into acrotelm – mesotelm – catotelm development. For example, humification, temperature, and redox profiles often indicated surface saturation (acrotelm) underlain by more decomposed peat (Ingram, 1978; Clymo, 1984; Clymo and Bryant, 2008). This stratification would not have been evident from surface observations or depth-averaged values alone (Quinton *et al.*, 2009; Rezanezhad *et al.*, 2016). However, many restored cores exhibited shallow stratification or homogenised profiles, especially where compaction or poor turve integration was indicated. *This demonstrates the value of continuous sampling in identifying structural recovery and vertical disconnects within the peat profile, including potential sub-surface 'hot spots' of decomposition or aeration* (Chapter 2; Section 2.1.1; Morris *et al.*, 2011).

6.3.4 Surface Condition Versus Sub-Surface Response

Comparison with surface condition scores (Chapter 5; Section 5.5.1; Table 5.4) showed weak correspondence between surface recovery and sub-surface functional parameters. Indicators such as humification, bulk density, and moisture content showed

no meaningful relationship with surface scores. pH and Eh displayed moderate associations (R^2 = 0.574 and 0.606, respectively), suggesting limited potential as proxies for belowground biochemical function. *Findings confirm a disconnect between surface and sub-surface condition, demonstrating the risk of miss-classifying restoration success when using surface indicators alone* (Chapter 2; Sections 2.2.4; 2.6.3). Although some metrics show potential for proxy development (Eh and pH), none consistently captured sub-surface structural or functional recovery.

Bulk and chemical indicators begin to explain how certain surface features occur, such as high surface moisture content, higher pH, and low Eh indicate *Sphagnum* presence and potential for carbon accumulation, but they do not explain why they persist or form. In particular, they do not account for the fine-scale structural aspects which govern water retention, solute transport, and gas exchange contributing to functionality and carbon storage (Chapter 2; Section 2.2.3). This understanding is critical to effectively assessing restoration's capability to recover sub-surface structure and function.

Table 6.1: Summary of research questions addressed in Chapter 6.

Research Question	Contribution/Implications
Research Question 1: Can surface indicators be used as a proxy to infer changes in sub-surface structure and function post-restoration?	Weak relationships were observed between surface scores and sub-surface bulk and chemical properties. While Eh and pH showed moderate associations, key structural indicators (e.g., bulk density, humification, moisture content) did not align with surface condition. This confirms standard surface indicators are limited in their ability to infer sub-surface functional behaviour.
Research Question 2: To what extent does the restoration of degraded blanket peatlands support the recovery of sub-surface structure and function?	Bulk and chemical profiles indicated partial recovery, with restored sites showing some improvement over degraded controls. Older and turved sites more closely resembled near-natural conditions, but no site fully replicated vertical stratification or functional properties. This suggests ongoing recovery dependent on time and technique, which could be explained by sub-surface structure (Chapter 7)
Research Question 3: How do the carbon costs of interventions impact the carbon benefit potential of restoration?	Limited functional recovery in early-stage restorations, despite ecological improvements, suggests carbon benefits may lag behind initial surface improvements. This emphasises the relevance of sub-surface structure and function when assessing restoration carbon efficiency (Chapter 8).

Chapter 7: Impacts of Restoration on Sub-Surface Structure and Function

Although surface indicators are widely used to assess functional recovery in restored blanket peatlands (Chapter 2; Sections 2.6, 2.7), Chapter 6 demonstrated a weak relationship between surface condition and sub-surface bulk and chemical properties indicative of key ecosystem functions (Chapter 3; Section 3.4.4; Table 3.2). While surface indicators (Chapter 5) and bulk chemical metrics (Chapter 6) could distinguish near-natural from degraded conditions, both individually and collectively, they failed to assess recovery in restored sites. This limitation was evident even when relying on surface indicators of ecological recovery (Chapter 5; Section 5.6), confirming a disconnect between surface and belowground processes, and demonstrating current evaluation protocols do not adequately capture functional recovery (Chapter 1; Section 1.1).

Moreover, bulk and chemical properties alone did not account for all observed variation (Chapter 6; Section 6.3). In particular, their limited sensitivity to decomposition in restored sites indicates the importance of finer-scale structural features, with porosity representing the principal driver of sub-surface functional recovery (Chapter 2; Section 2.2.3). Pore network characteristics govern water and gas dynamics, which influence surface and bulk chemical indicators. Specifically, sub-surface porosity governs hydraulic conductivity (Quinton *et al.*, 2008; Rezanezhad *et al.*, 2009, 2010), gas exchange and retention (Kettridge and Binley, 2008; Comas *et al.*, 2014), and solute transport (Rezanezhad *et al.*, 2016; McCarter *et al.*, 2020); key processes determining

carbon accumulation and long-term ecosystem function (Chapter 2; Section 2.2.3). However, these remain unaccounted for in surface-level monitoring approaches.

3D X-ray micro-computed tomography (μCT) offers a method to quantify how restoration influences sub-surface pore structure and what it means for ecosystem function (Chapter 3; Section 3.5), potentially explaining observed surface, bulk, and chemical properties. Integrating μCT into restoration assessment would improve current evaluation protocols by providing a greater understanding of sub-surface recovery. This could support more robust carbon accounting methodologies and increase confidence in carbon credits from peatland restoration (Chapter 2; Section 2.7); generating greater investment potential and advancing peatlands as a nature-based solution in policy (Chapter 2; Section 2.4).

Additionally, μCT can help evaluate the effectiveness of individual restoration techniques. As discussed in Chapter 6, bulk and chemical indicators suggest continued integration between restoration interventions and the original peat surface, such as the bonding of turves. By assessing pore network structure, μCT enables these effects to be analysed, supporting evidence-based recommendations for improving restoration practice (Chapter 2; Section 2.5.3; Thom *et al.*, 2019; NatureScot, 2022). This would strengthen peatlands' role as a nature-based solution in policy by promoting more effective interventions and increasing confidence in reported restoration outcomes.

A first-order analysis of μCT data (Figure 7.1) was conducted across a spectrum of restoration sites to evaluate whether sub-surface structure and function recover toward near-natural conditions relative to a degraded baseline. Structural trends were examined with respect to depth, restoration age, and intervention technique. Analyses focused on

macroporosity, close to the 90μm threshold proposed by Beven and Germann (2013), aligning with the scan resolution limit of 81.55μm (Chapter 3; Section 3.5.3).
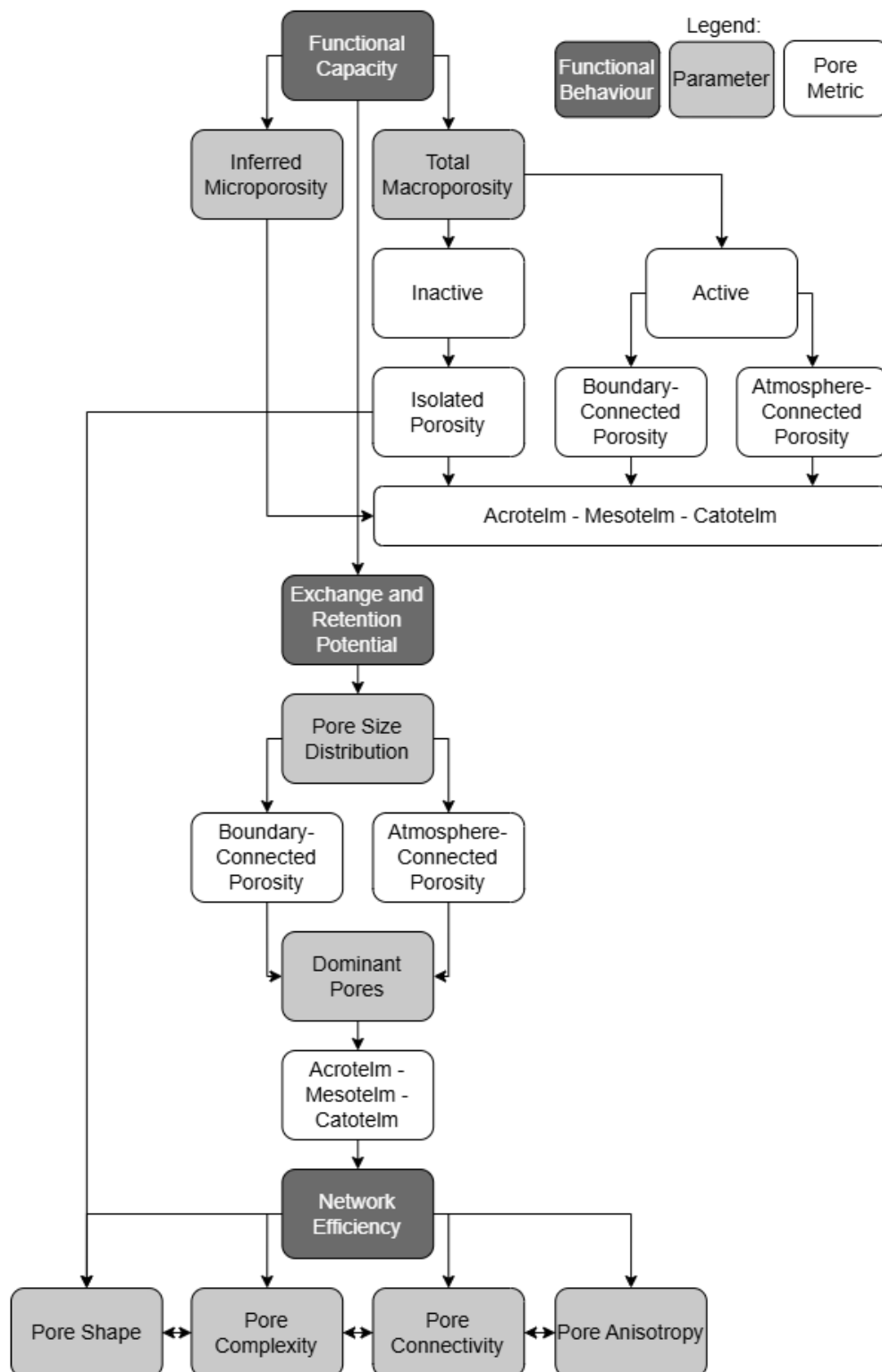
Figure 7.1: Conceptual framework used to infer functional behaviour from sub-surface pore structure.

Pore space was classified into Total Pore Space (TPS), Atmosphere-Connected Porosity (ACP), Boundary-Connected Porosity (BCP), and Isolated Porosity (IP) (Chapter 3; Section 3.5.8). This classification supports functional interpretation by distinguishing between active pores (ACP and BCP), which facilitate infiltration, lateral and vertical flow, and gas exchange, and inactive pores (IP), which primarily contribute to water retention and restricted exchange (Quinton *et al.*, 2009; Rezanezhad *et al.*, 2009, 2010, 2016).

Structural and functional interpretations are based on µCT-derived parameters outlined in Chapter 3; Section 3.5.8; Table 3.9, including pore volume (bulk and size distribution), pore number, Feret diameter (shape), branch number (complexity), Euler characteristic (connectivity), and anisotropy (directionality). These metrics allow evaluation of functional capacity, exchange and retention potential, and network efficiency; key determinants of hydrological and gaseous function (Chapter 2; Section 2.2.3).

Core IDs are used throughout to refer to site, technique, and replicate number where applicable (Table 7.1).

Table 7.1: Core ID glossary.

Core ID	Site	Age	Technique
SF_Nat	*Shap Fells*	*N/A*	*Near-natural control*
BW_LT_1	Borrowdale	~10 years old	Local turving (core 1)
BW_LT_2			Local turving (core 2)
BC_IT_1	Bampton Common	~5 years old	Imported turving (core 1)
BC_IT_2			Imported turving (core 2)
BC_LT_1			Local turving (core 1)
BC_LT_2			Local turving (core 2)
SF_IT_1	Shap Fells	~2 years old	Imported turving (core 1)
SF_IT_2			Imported turving (core 2)
SF_LT_1			Local turving (core 1)
SF_LT_2			Local turving (core 2)
SM_B	Stake Moss	~2 years old	Heather brash spread
SM_C			Coir logs
SM_D			Stone/timber dams
BC_Deg	*Bampton Common*	*N/A*	*Degraded control*

7.1 Control Samples

Comparison between near-natural and degraded cores establishes structural and functional baselines for evaluating restoration effectiveness. SF_Nat (near-natural) represents the target condition, while BC_Deg (degraded) serves as an unfavourable baseline. 3D visualisations provide a qualitative overview of pore network structure to support subsequent quantitative comparison. Figure 7.2 presents renderings of SF_Nat and BC_Deg cores, illustrating contrasts in pore stratification, spatial distribution, complexity, and connectivity.
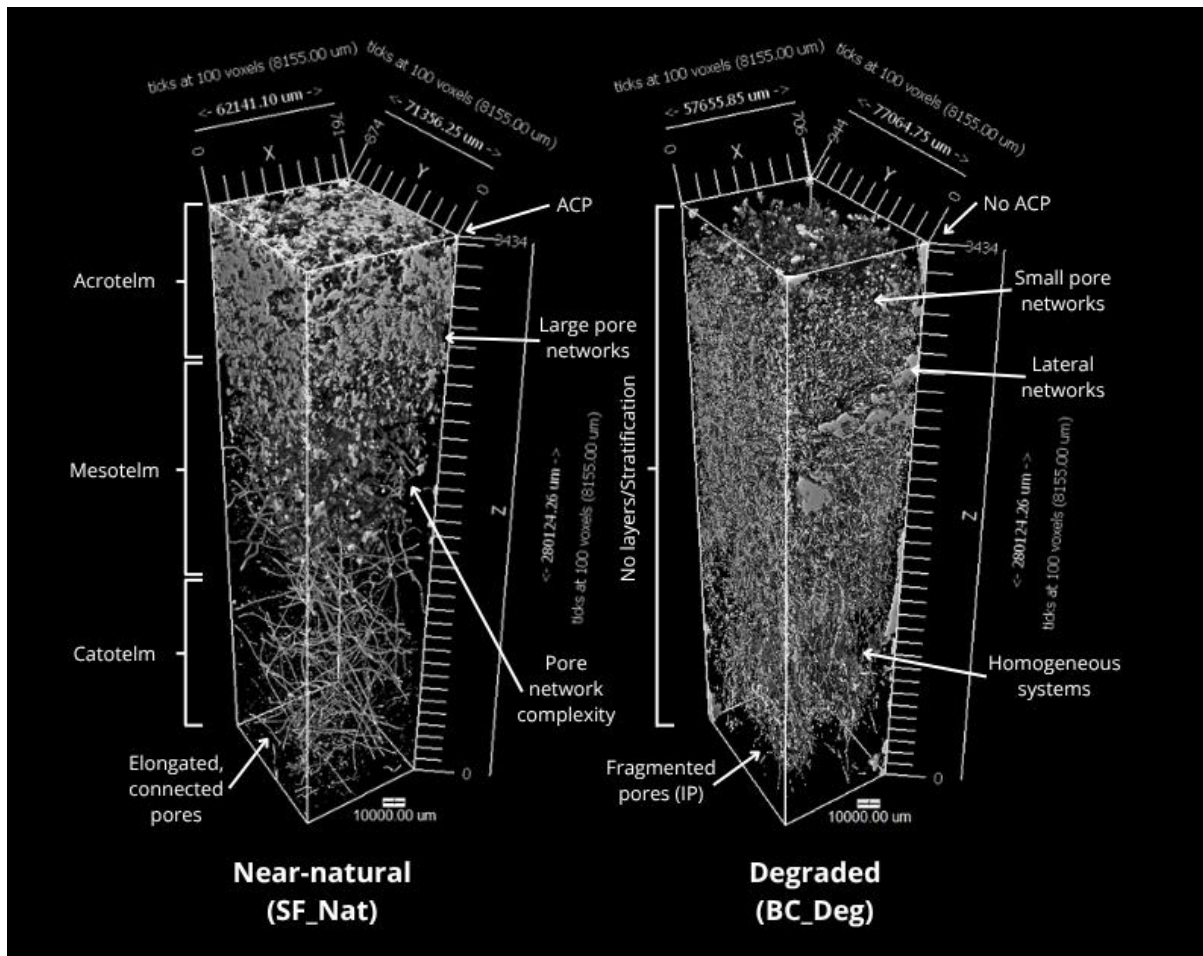
Figure 7.2: Annotated 3D visualisations of Total Pore Space (TPS) representative of near-natural (SF_Nat) and degraded (BC_Deg) control cores at ≥81.55µm resolution.

7.1.1 Structural Description

SF_Nat exhibits vertical stratification. Upper layers (~2.5-12.5cm) contain large, complex, and well-connected pore networks, while lower layers (~12.5-27.5cm) are dominated by elongated, vertically orientated pores. This indicates an intact acrotelm – mesotelm – catotelm profile. Pore networks appear dense and spatially consistent, extending from surface to depth. Atmosphere-connected pores are identifiable in the acrotelm.

BC_Deg displays a compact and homogenous structure. Pores are smaller, more rounded, and largely disconnected, with no stratification. Lateral voids and larger irregular spaces occur sporadically in lower layers. Absence of vertically continuous structures suggest limited connectivity. Surface porosity appears low, with no evidence of atmosphere-connected porosity.

7.1.2 Functional Interpretation

Connected pore networks extending from the surface in **SF_Nat** are indicative of atmosphere-connected porosity, consistent with surface water infiltration and the maintenance of a high water table (Chapter 2; Section 2.2; Holden *et al.*, 2001; Holden and Burt, 2003; Holden, 2005b). Elongated, vertically aligned pores in the lower profile indicate boundary-connected porosity, associated with vascular and graminoid roots facilitating vertical and lateral water and solute transport (Moore *et al.*, 2002; Rowson *et al.*, 2010; Chirol *et al.*, 2021; Baird and Low, 2022). Isolated porosity appears minimal, suggesting limited gas accumulation and reduced aerobic decomposition (CO_2 production and loss). Features support a stratified and functionally intact sub-surface, facilitating saturation and long-term carbon storage.

The fragmented and disconnected structure of **BC_Deg** indicates high isolated porosity, associated with reduced permeability and gas production under oxic conditions (Section 7.4.1a). Absence of atmosphere-connected porosity suggests limited infiltration and poor surface saturation (Holden *et al.*, 2001; Holden, 2005b; Morris *et al.*, 2019). Lateral voids and irregular boundary-connected pores in the lower profile are interpreted as indicators of structural collapse or peat slippage, consistent with drainage, erosional instability, and carbon loss through dissolved and particulate organic carbon export

(Chapter 2; Section 2.2.3). No acrotelm – mesotelm – catotelm profile indicates functional degradation, with reduced water retention, limited solute regulation, and increased GHG exchange through diffusion (Clymo, 1984; Clymo *et al.*, 1998; McCarter *et al.*, 2020).

> BC_Deg exhibits a compact, fragmented profile with disconnected pores and reduced hydrological function, while SF_Nat displays vertically stratified, well-connected pore networks indicative of an intact acrotelm–catotelm structure.

7.1.3 Functional Capacity of Control Samples

Building on visual observations, quantitative analysis of bulk macroporosity provides a comparative assessment of functional capacity under near-natural and degraded conditions. Total pore space (TPS) suggests the maximum volume available for water, solute, or gas storage and transfer. TPS is further subdivided into:

- **Atmosphere-connected porosity (ACP):** Indicates surface-connected pathways, supporting water infiltration and direct gas exchange with the atmosphere.

- **Boundary-connected porosity (BCP):** Signifies sub-surface lateral and vertical connectivity for water and solute transport.

- **Isolated porosity (IP):** Represents disconnected voids with potential for gas accumulation or water and solute retention.

Depth specific analysis supports interpretation by associating porosity type to acrotelm, mesotelm, or catotelm layers. 3D visualisations of ACP, BCP, and IP are also provided to support interpretation of spatial patterns.

Although μCT resolution limits analysis to pores ≥81.55μm, microporosity (<81.55μm) was inferred by subtracting detected macroporosity from the total grayscale volume. Remaining matrix grayscale values were interpreted as proxies for material density, with lower grayscale densities suggesting higher microporosity (Spencer *et al.*, 2017). This inference was supported by comparison with Von-Post humification, where less decomposed peat (lower H_x) was typically associated with lower matrix density and presumed higher microporosity (Chapter 3; Section 3.4.3).

Microporosity is functionally important, regulating capillary water retention and gas exchange via diffusion (Spencer *et al.*, 2017; McCarter *et al.*, 2020), particularly within the acrotelm and mesotelm (Kettridge and Binley, 2008; Quinton *et al.*, 2009; Rezanezhad *et al.*, 2010, 2016). Its inclusion supports interpretation by capturing functions overlooked in macroporosity assessments, especially in evaluating how restoration influences fine-scale pore structure (Section 7.2.3b).

a) Total Macroporosity

Quantifying total macroporosity provides a baseline for assessing differences in functional capacity and stratification between control cores.

Table 7.2: Bulk macroporosity for near-natural (SF_Nat) and degraded (BC_Deg) cores across 5cm depth intervals.

Depth (cm)	SF_Nat (%)	BC_Deg (%)
2.5-7.5 (5)	2.00	0.91
7.5-12.5 (10)	0.52	0.97
12.5-17.5 (15)	0.23	0.48
17.5-22.5 (20)	0.05	0.14
22.5-27.5 (25)	0.07	0.21
Total:	**2.88**	**2.73**

i) Structural Description:

Table 7.2 shows similar total bulk macroporosity between **near-natural (SF_Nat:** 2.88%) and **degraded** (**BC_Deg:** 2.73%) controls, suggesting equal functional capacity. However, opposing vertical distributions indicate contrasting structure and functions. SF_Nat exhibits high surface porosity (2.00% at 5cm), with a continuous decline to 0.07% by 25cm. BC_Deg displays a more homogeneous profile, with no clear vertical trend and a peak at 10cm (0.97%).

ii) Functional Interpretation:

Surface dominance of macroporosity in **SF_Nat** indicates an intact acrotelm with high atmospheric connectivity, supporting water infiltration and surface saturation. Declining porosity with depth corresponds to reduced oxygen availability and retarded decomposition across the mesotelm and catotelm, indicative of vertical functional layering and long-term carbon storage potential.

The more uniform macroporosity profile in **BC_Deg** suggests a disrupted acrotelm– catotelm structure. Absence of stratification with higher porosity at depth relative to SF_Nat, supports structural fragmentation identified in Figure 7.2 and is consistent with ongoing decomposition and gas accumulation (later confirmed in Section 7.4.1a). The 10cm peak may indicate lateral sub-surface drainage features or voids formed through structural collapse beyond the scanned volume (Figure 7.2).

BC_Deg exhibits reduced surface connectivity and limited functional differentiation with depth, while SF_Nat supports stratified hydrological regulation and surface to sub-surface interaction.

b) Inferred Microporosity

While the near-natural (SF_Nat) and degraded (BC_Deg) controls exhibit comparable total macroporosity, low values (2.88% and 2.73%, respectively) suggest a substantial proportion of pore space occurs below the detection threshold (<81.55µm). This is supported by laboratory studies reporting bulk porosity ranging from 71-95% (Chapter 2; Section 2.2.3; Rezanezhad *et al.*, 2016). Alternatively, laboratory methods may overestimate bulk porosity, particularly where high water content or structural disturbance exaggerates measured void space. Nonetheless, microporosity is functionally significant, supporting capillary water retention and diffusion-driven gas exchange. Opposing macroporosity profiles with depth further suggest differences in microporosity between SF_Nat and BC_Deg. Figure 9.3 presents grayscale density as a proxy for microporosity, based on material density, and compares this with Von-Post humification values to support interpretations, following the approach of Spencer *et al*. (2017) (Chapter 3; Section 3.4.3).
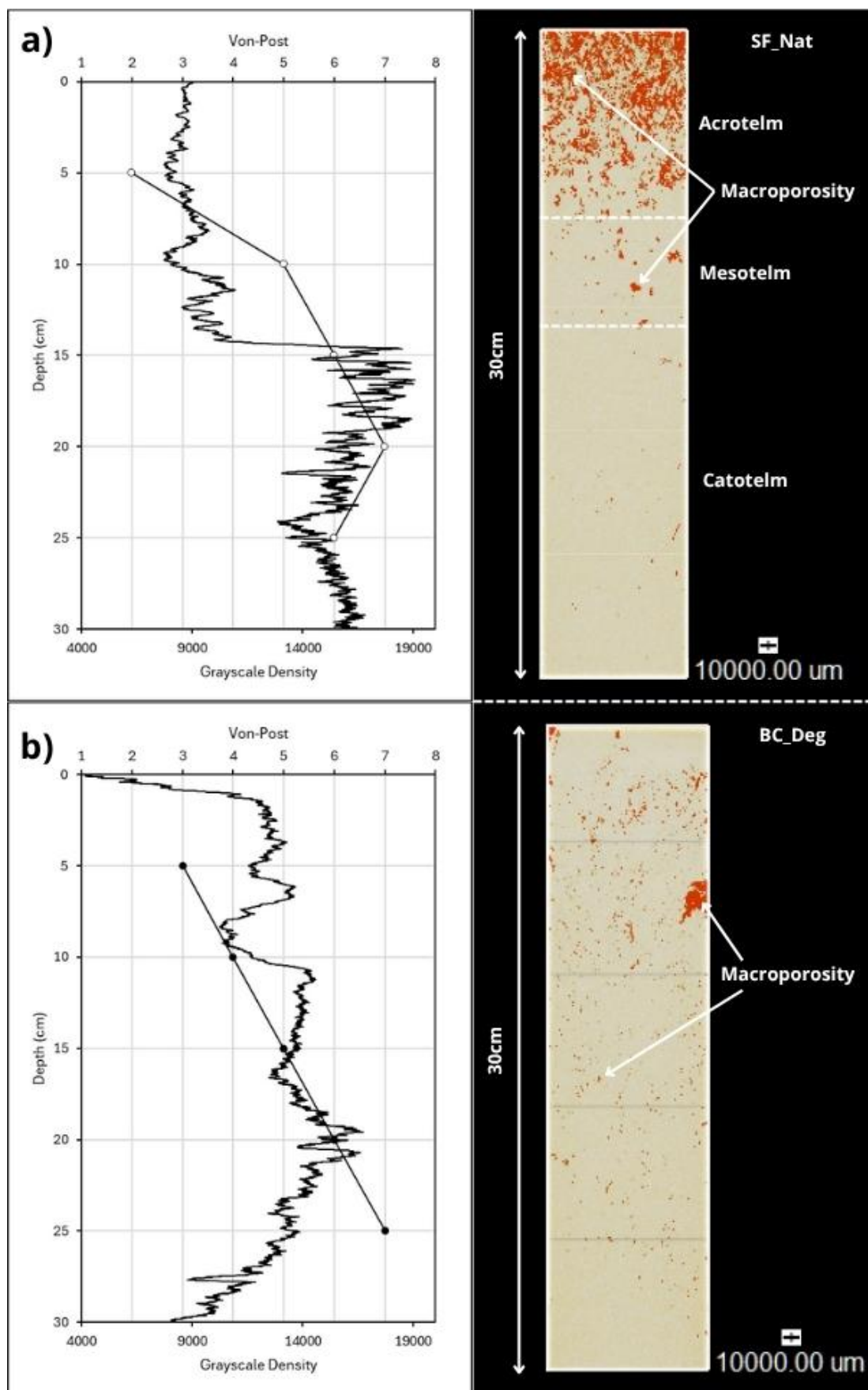
Figure 7.3: Microporosity inference using grayscale density profiles and Von-Post humification plotted alongside μCT visualisations of excluded macroporosity (red): a) near-natural control (SF_Nat); b) degraded control (BC_Deg).

i) Porosity Comparison:

Microporosity is probable across control cores with grayscale values ranging from ~4000–19,000. Following macroporosity exclusion, this range covers ~50% of the attenuation spectrum. While not all low-density regions represent pore space, demonstrating the limitation of grayscale-based inference, findings suggest laboratory methods may overestimate porosity, possibly due to their destructive approach (Chapter 2; Section 2.6.1). Values within the lower half of the grayscale range are more likely to represent true microporosity, and are consistent with other µCT observations (Quinton *et al.*, 2009; Rezanezhad *et al.*, 2016).

ii) Structural Description:

Contrasting grayscale density is evident between control cores, particularly within the acrotelm. **SF_Nat** exhibits lower grayscale density in the upper 15cm (~9000), with increasing values through the mesotelm and catotelm. This aligns with Von-Post humification, which transitions from H2 near the surface to H6–H7 at depth. **BC_Deg** displays a more homogeneous grayscale profile, with higher surface values (~11,000) and limited variation with depth. Uniform Von-Post humification supports the more consistent density profile.

iii) Functional Interpretation:

Low grayscale density and humification in the acrotelm of **SF_Nat** indicates high microporosity, likely associated with *Sphagnum* presence (hyaline cells), supporting capillary water retention and slow diffusion-driven gas exchange (Kettridge and Binley, 2008, 2011; Comas *et al.*, 2014). Combined with high surface macroporosity (Section 7.1.3a), this suggests SF_Nat retains a deep (~15cm), functional acrotelm capable of

surface water uptake and saturation, promoting carbon accumulation. Increase in grayscale density at ~15cm represents a transition into the mesotelm and catotelm, where lower microporosity indicates retarded decomposition and compaction, limiting gaseous diffusion and enhancing long-term carbon storage.

BC_Deg exhibits reduced microporosity in the acrotelm. Although the grayscale profile begins at ~4000, this likely indicates retained surface air due to core slope (Chapter 3; Section 3.3). Below ~1cm, higher grayscale density indicates a compacted, low-porosity surface layer, supporting earlier interpretations of a structurally disrupted acrotelm with limited capacity for surface water uptake or saturation. Increasing microporosity at depth may result from gas expansion linked to decomposition, suggesting increased gas production and associated carbon loss through diffusion.

BC_Deg shows limited micropore stratification, reduced surface water retention capacity, and increased gas production at depth, while SF_Nat displays stratified microporosity supporting acrotelm to catotelm function.

c) Macroporosity Types

While microporosity supports capillary water retention and slow diffusion, water, solute, and gas exchange occurs primarily within macropores. Subdividing total macroporosity into atmosphere-connected (ACP), boundary-connected (BCP), and isolated (IP) refines functional interpretation by distinguishing active (ACP, BCP) from inactive (IP) voids. Assessing these in control cores establishes a baseline for evaluating restoration recovery of functionally relevant pore space. 3D visualisations of ACP, BCP, and IP offer a qualitative overview, supporting subsequent quantitative comparison. Figure 7.4

presents ACP, BCP, and IP renderings for SF_Nat and BC_Deg, demonstrating differences

in connectivity and potential for exchange or retention.
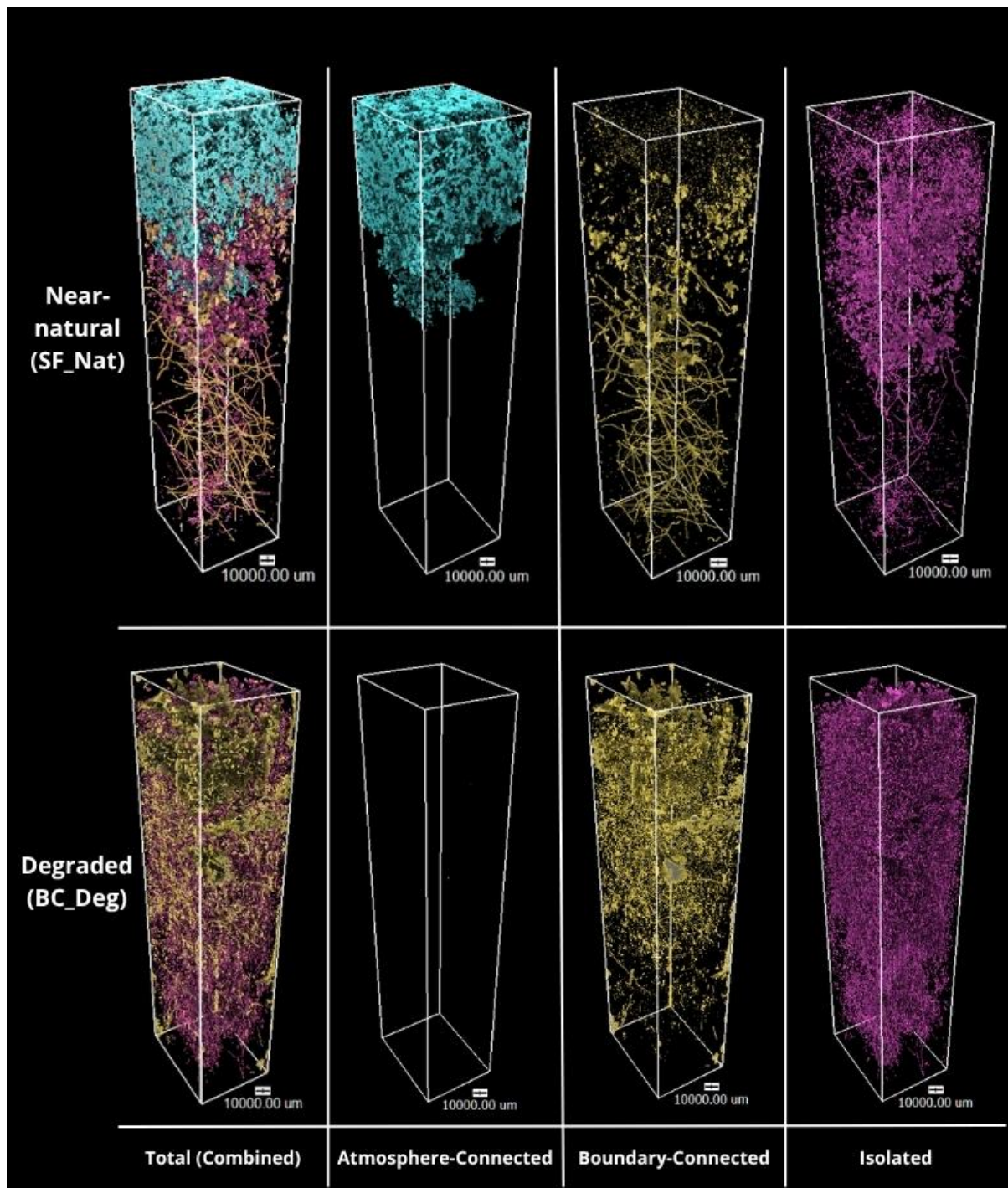
Figure 7.4: 3D visualisations of atmosphere-connected (blue), boundary-connected (orange), and isolated porosity (pink) in near-natural (SF_Nat) and degraded (BC_Deg) cores (≥81.55µm).

i) Structural Description:

SF_Nat exhibits atmosphere-connected porosity concentrated in the acrotelm, extending to ~15cm depth (mesotelm). Boundary-connected porosity appears elongated and laterally connected, particularly in the catotelm between ~20-25cm. Isolated porosity is largely distributed throughout the acrotelm (<15cm), with a fragmented and irregular geometry decreasing with depth.

BC_Deg shows no observable atmosphere-connected porosity. Boundary-connected porosity is predominantly in the acrotelm (~15cm), forming platy structures near the surface. Isolated porosity is densely and homogenously distributed throughout, dominated by small, spherical voids.

ii) Functional Interpretation:

Atmosphere-connected porosity is confined to the acrotelm and upper mesotelm in **SF_Nat**, indicating effective surface water infiltration and maintenance of high water tables. Connectivity in these upper layers supports oxygen availability and aerobic respiration (confirmed in Section 7.4.3), favouring CO_2 release rather than CH_4 from penetrating paths extending to the catotelm (>15cm), such as monocot roots (Chapter 2; Section 2.2.2; Moore *et al.*, 2002). Boundary-connected porosity in the catotelm suggests lateral and vertical sub-surface connectivity, potentially facilitating water, nutrient, and solute redistribution, and enhancing system resilience to pressures such as drought. Fragmented, irregular isolated porosity in the acrotelm suggests water-holding voids in undecomposed or partially decomposed material, such as the hyaline cells of *Sphagnum* (Chapter 2; Section 2.2.1), which reduces with depth as structure becomes more compact (Chapter 6; Section 6.1.4).

Absence of atmosphere-connected porosity in **BC_Deg** supports surface hydrophobicity (Chapter 6; Section 6.1.4) and restricted water infiltration, resulting from compaction associated with prolonged aerobic decomposition (Chapter 6; Section 6.1.7) or disturbance (Chapter 5; Section 5.4). Near-surface, platy boundary-connected porosity may indicate structural collapse or desiccation features, contributing to lateral flow, hydrophobicity, and increased potential for gas diffusion, limiting the formation of a functional acrotelm. Dense, homogeneous isolated porosity throughout the profile is indicative of structural fragmentation and gas accumulation, consistent with oxic decomposition and functional degradation. Findings begin to demonstrate relationships with bulk and chemical properties (Chapter 6), presented in Chapter 9.

BC_Deg shows disrupted stratification, surface hydrophobicity, and pore features consistent with decomposition and GHG release, while SF_Nat exhibits a stratified, intact structure supporting surface-water infiltration, restricted CH_4 release, sub-surface connectivity, and conditions favourable for long-term carbon storage and resilience.

---

d) Atmosphere, Boundary, and Isolated Porosity Contributions

Quantifying atmosphere-connected (ACP), boundary-connected (BCP), and isolated porosity (IP) provides a baseline for assessing differences in functionally relevant pore space between control cores.

Table 7.3: Bulk macroporosity by type in near-natural (SF_Nat) and degraded (BC_Deg) cores across 5cm depth intervals.

Depth (cm)	BC_Deg			SF_Nat		
	ACP	BCP	IP	ACP	BCP	IP
2.5-7.5 (5)	0.00	0.44	0.47	1.88	0.03	0.10
7.5-12.5 (10)	0.00	0.45	0.53	0.14	0.09	0.29
12.5-17.5 (15)	0.00	0.05	0.43	0.00	0.07	0.16
17.5-22.5 (20)	0.00	0.02	0.12	0.00	0.05	0.01
22.5-27.5 (25)	0.00	0.04	0.17	0.00	0.05	0.02
Total:	**0.00**	**1.00**	**1.73**	**2.02**	**0.28**	**0.58**

i) Structural Description:

Table 7.3 shows atmosphere-connected porosity in **SF_Nat** is concentrated in the acrotelm (2.5–7.5cm), contributing 1.88% (~65% of total macroporosity). It declines with depth and is absent beyond 12.5cm. Boundary-connected porosity is present throughout but remains low (<0.09%). Isolated porosity is concentrated in the acrotelm and upper catotelm, decreasing with depth, consistent with visual observations (Figure 7.4).

BC_Deg shows no atmosphere-connected porosity. Boundary-connected porosity is higher in the acrotelm and upper mesotelm, peaking at 0.45% between 7.5–12.5cm, with lower values at depth. Isolated porosity dominates across all layers, exceeding 0.43% from 2.5–17.5cm, with a more uniform distribution than in SF_Nat.

ii) Functional Interpretation:

Dominant atmosphere-connected porosity in the **SF_Nat** acrotelm supports surface water infiltration and saturated conditions, maintaining high water tables for retarded decomposition and carbon storage (Chapter 2; Section 2.2). Its absence beyond 12.5cm supports earlier interpretations that direct atmospheric pathways do not penetrate into

the anoxic catotelm, restricting CH_4 release to slowed diffusion. Low but consistent boundary-connected porosity suggests regulated sub-surface redistribution without promoting drainage. Isolated porosity in the acrotelm likely indicates water-holding voids in undecomposed or partially decomposed vegetation, decreasing with depth as peat becomes more compact and anaerobic.

Absence of atmosphere-connected porosity in **BC_Deg** supports earlier interpretations of surface hydrophobicity and compaction, restricting infiltration and contributing to drier sub-surface conditions which promote carbon loss. Increased boundary-connected porosity near the surface (0.44–0.45% at 2.5–12.5cm) indicates desiccation cracking, enhancing sub-surface drainage and increasing the potential for dissolved and particulate organic carbon losses (Chapter 2; Section 2.3.1), as well as promoting surface hydrophobicity. High and evenly distributed isolated porosity aligns with the visual presence of dense, spherical voids, interpreted as CO_2 gas bubbles produced under oxic decomposition (Section 7.4.1a).

BC_Deg exhibits a homogeneous, fragmented structure limiting hydrological function (particularly surface-water uptake) and increasing vulnerability to carbon loss, while SF_Nat demonstrates vertical separation of aerobic and anaerobic zones through stratified, functionally active pore networks, regulating water, solute, and gas transfer.

7.1.4 Summary of Structural Characteristics in Control Samples

Clear structural contrasts in bulk porosity between degraded (BC_Deg) and near-natural (SF_Nat) control cores indicate differences in surface water infiltration, retention, and solute and gas exchange potential, establishing a functional baseline for evaluating restoration.

BC_Deg (degraded):

- Exhibits a compact, fragmented structure with disconnected pores and no vertical stratification.

- Macroporosity is evenly distributed but likely inefficient; inferred microporosity lacks depth organisation and shows surface compaction indicative of disturbance (Chapter 5; Section 5.4).

- Atmosphere-connected porosity is absent, suggesting a hydrophobic surface restricting water infiltration and promoting drier sub-surface conditions (Holden *et al.*, 2001; Holden, 2005b; Morris *et al.*, 2019).

- Boundary-connected pores are shallow, appear platy, and laterally aligned, likely formed by desiccation or collapse, contributing to drainage, reduced water and solute retention, and carbon loss.

- Isolated porosity dominates across depth, limiting connectivity and supporting oxic decomposition and gas accumulation (Section 7.4.1a).

SF_Nat (near-natural):

- Displays vertical stratification, consistent with an intact acrotelm–mesotelm–catotelm profile.

- Surface-dominated macroporosity and layered inferred microporosity promote water infiltration, retention, and gas regulation under saturated conditions, demonstrating an association with high surface moisture content (Chapter 6; Section 6.1.5).

- Atmosphere-connected porosity dominates in the acrotelm, supporting surface water uptake (Holden, 2005b), high water tables (Holden *et al.*, 2001; Holden and Burt, 2003), and restricted CH_4 exchange (Moore *et al.*, 2002).

- Boundary-connected porosity occurs at depth with moderate volumes, facilitating vertical redistribution and regulated flow.

- Isolated pores are infrequent and decline with depth, reducing gas accumulation and supporting vertical connectivity (with conditions favouring CO_2 over CH_4 production).

> Findings indicate degradation leads to structural fragmentation, impaired infiltration and retention, and increased gas accumulation, creating vulnerability to carbon loss. Near-natural structure supports stratified layering, effective hydrological regulation, and conditions conducive to long-term carbon storage. This baseline enables robust assessment of structural and functional recovery in restored cores.

7.2 Restored Samples

Restored cores are evaluated against controls to examine structural and functional recovery. Variation is assessed by restoration age and technique (Table 7.1). Analyses follow the same structure as control samples (Figure 7.1), enabling comparison of porosity across depth. Comparisons support evaluation of restoration effectiveness in re-establishing functionally relevant pore space. Figure 7.5 presents 3D visualisations of total macroporosity in restored cores and controls for qualitative comparison.
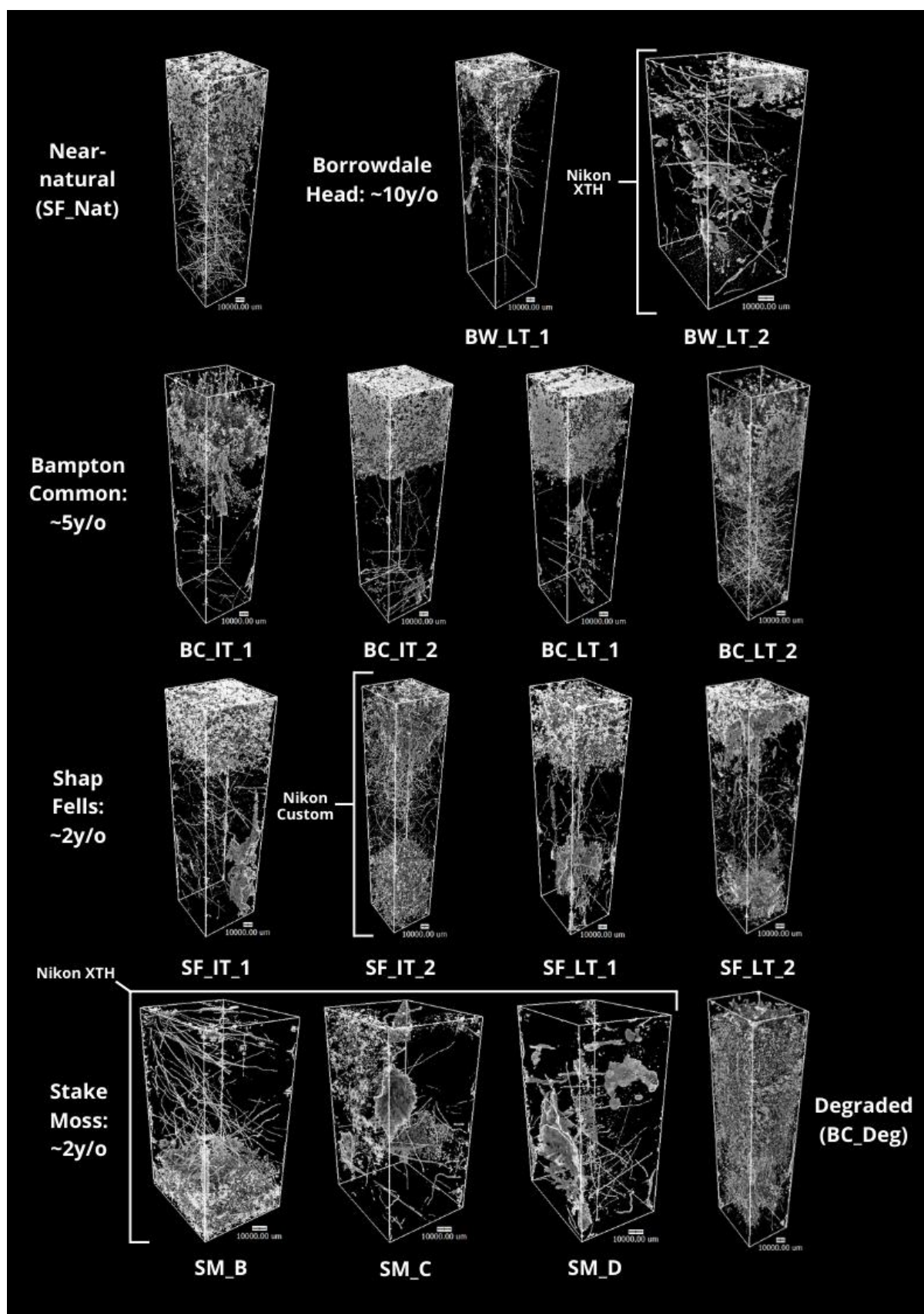
Figure 7.5: 3D visualisations of total macroporosity in restored and control cores (≥81.55μm resolution). Cores are grouped by restoration age (site) and technique. Visualisations are scaled equally; scanner type is noted where alternatives to the Nikon High Flux Bay were used (explaining bounding box variance).

7.2.1 Structural Description

Turved samples including **Borrowdale** and **Bampton Common** exhibit transitional stratification and elongate pores at depth, though surface porosity and mesotelm continuity vary between cores (Figure 7.6a). **Shap Fells** cores show surface layering and vertical pore alignment, but large voids persist in the lower profile (~20–30cm), contrasting with the more compact catotelm of SF_Nat (Figure 7.6b). **Stake Moss** cores (heather brash, coir logs, stone/timber dams) differ, with limited surface porosity, resembling BC_Deg, and fragmented, elongated pores dominating at depth (Figure 7.6c). Variability across sites appears linked to restoration age and technique, with younger (Shape Fells) and non-turved (Stake Moss) cores more frequently exhibiting deep macroporosity dominance and incomplete acrotelm–mesotelm–catotelm stratification.

7.2.2 Functional Interpretation

Visualisations indicate early sub-surface recovery (~2 years), particularly in turved cores (Shap Fells) where acrotelm development and vertical layering appear. No restored core replicates the stratification of SF_Nat (especially the mesotelm transition), or the compact, disconnected structure of BC_Deg (also seen in Chapter 6). Acrotelm re-establishment is common, but mesotelm – catotelm development remains limited, with deep macroporosity persisting, particularly in non-turved cores (Stake Moss), suggesting continued drainage and reduced hydrological function.

> Restored cores show improved surface structure supporting surface to sub-surface interactions relative to degraded conditions, but limited structural response at depth, potentially restricting long-term carbon storage.
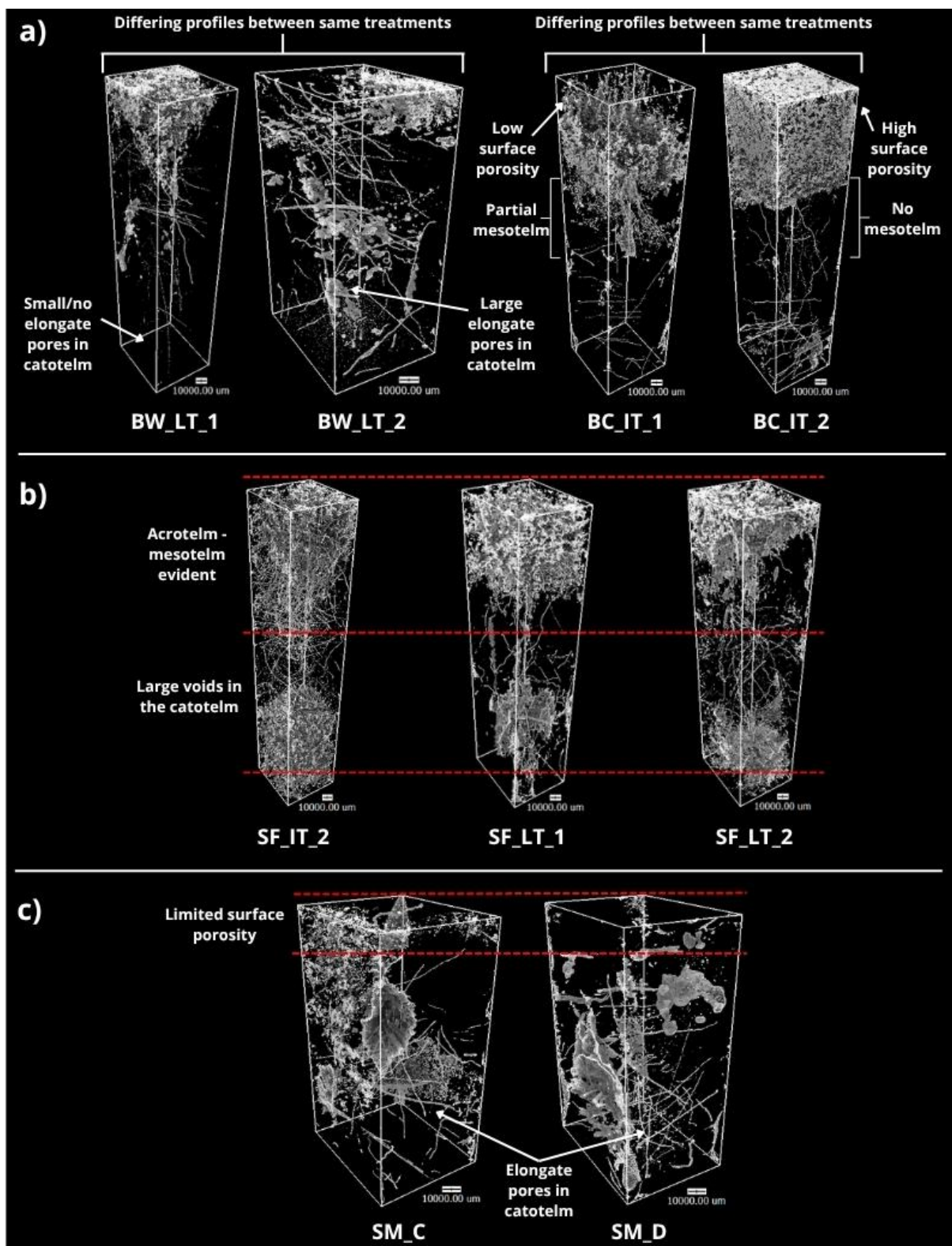
Figure 7.6: 3D visualisations of total macroporosity in selected restored cores: a) Borrowdale (Local Turve) and Bampton Common (Imported Turve) - contrasting profiles under similar treatments after ~10 and ~5 years, respectively; b) Shap Fells (Imported and Local Turve) - show early (~2 years) acrotelm–mesotelm development, with large catotelm macropores persisting; c) Stake Moss (coir log and dam installation) shows limited surface porosity and persistent deep macroporosity.

7.2.3 Functional Capacity of Restored Samples

Following qualitative observations, the functional capacity of restored samples is assessed through quantitative analysis. Total macroporosity and functionally classified pore types (atmosphere-connected; ACP, boundary-connected; BCP, and isolated; IP) are examined across depth, with inferred microporosity included to evaluate water retention and diffusion potential below the 81.55μm resolution threshold. Comparisons with control baselines are used to identify trajectories of structural and functional recovery.

a) Total Macroporosity

Quantifying total macroporosity enables direct comparison of functional capacity and vertical stratification between restored and control cores (Table 7.4).

Table 7.4: Bulk macroporosity by 5cm depth intervals across restored and control cores organised by site.

Depth	BC_Deg	BW_LT_1	BW_LT_2	BC_IT_1	BC_IT_2	BC_LT_1	BC_LT_2	SF_IT_1	SF_IT_2	SF_LT_1	SF_LT_2	SM_B	SM_C	SM_D	SF_Nat
5cm	0.91	0.41	0.74	0.66	3.13	3.18	1.45	1.35	0.47	0.89	0.84	0.09	0.28	0.07	2.00
10cm	0.97	0.08	0.13	0.30	0.85	0.69	1.31	0.08	0.12	0.15	0.15	0.04	0.77	0.91	0.52
15cm	0.48	0.11	0.13	0.17	0.03	0.08	0.11	0.15	0.04	0.10	0.03	0.07	0.10	0.60	0.23
20cm	0.14	0.01	0.07	0.06	0.01	0.12	0.05	0.65	0.72	0.45	0.13	0.43	0.31	0.47	0.05
25cm	0.21	0.00	0.04	0.07	0.22	0.07	0.10	1.02	0.56	0.19	0.43	1.01	0.12	0.28	0.07
Total:	2.73	0.61	1.10	1.27	4.23	4.15	3.03	3.25	1.92	1.77	1.57	1.63	1.58	2.32	2.88

i) Structural Description:

Borrowdale cores exhibit consistently low porosity across (0.61% and 1.10%). **Bampton Common** cores show high surface porosity, particularly in BC_IT_2 and BC_LT_1 (>3%), followed by declines with depth, resembling SF_Nat. **Shap Fells** cores have lower surface porosity similar to BC_Deg, but values increase at depth (e.g., >0.5% at 25cm in SF_IT_2 and SF_LT_1). **Stake Moss** cores record the lowest surface porosity (≤0.28%), though SM_B and SM_D show increased porosity at depth, corresponding to trends in Shap Fells (also ~2 years post restoration).

ii) Functional Interpretation:

Surface macroporosity in restored cores, particularly turved sites (e.g., **BC_IT_2**, **BC_LT_1**), suggests re-establishment of an acrotelm structure supporting surface to sub-surface interactions (surface water uptake and gaseous exchange). However, more rapid declines in porosity with depth than SF_Nat indicate incomplete mesotelm development and limited vertical continuity (Figure 7.6a). In **Borrowdale**, low porosity suggests a 10-year shift toward microporosity associated with *Sphagnum* recovery (explored in the next section). **Shap Fells** and **Stake Moss** cores show increased porosity at depth despite low surface porosity, suggesting relict drainage features and limited acrotelm formation after ~2 years. This is most apparent in Stake Moss, suggesting turving could accelerate acrotelm re-establishment.

> Early structural recovery is evident in surface layers relative to degraded conditions, particularly in turved samples, but impact at depth remains limited and no core replicates the profile of SF_Nat, particularly the mesotelm, even after a decade.

b) Inferred Microporosity

Restored cores exhibit similarly low total macroporosity to controls, considerably below laboratory-reported values (Chapter 2; Section 2.2.3), implying a high proportion of undetected microporosity. Variation in inferred microporosity is examined to evaluate how restoration age and technique influence capillary water retention (Waddington and Price, 2000; Weber *et al.*, 2017) and diffusion-driven gas exchange (Strack *et al.*, 2005; Clymo and Bryant, 2008; Kettridge and Binley, 2008; Comas *et al.*, 2014; Petrescu *et al.*, 2015) at fine spatial scales relative to control baselines.

i) Controls:
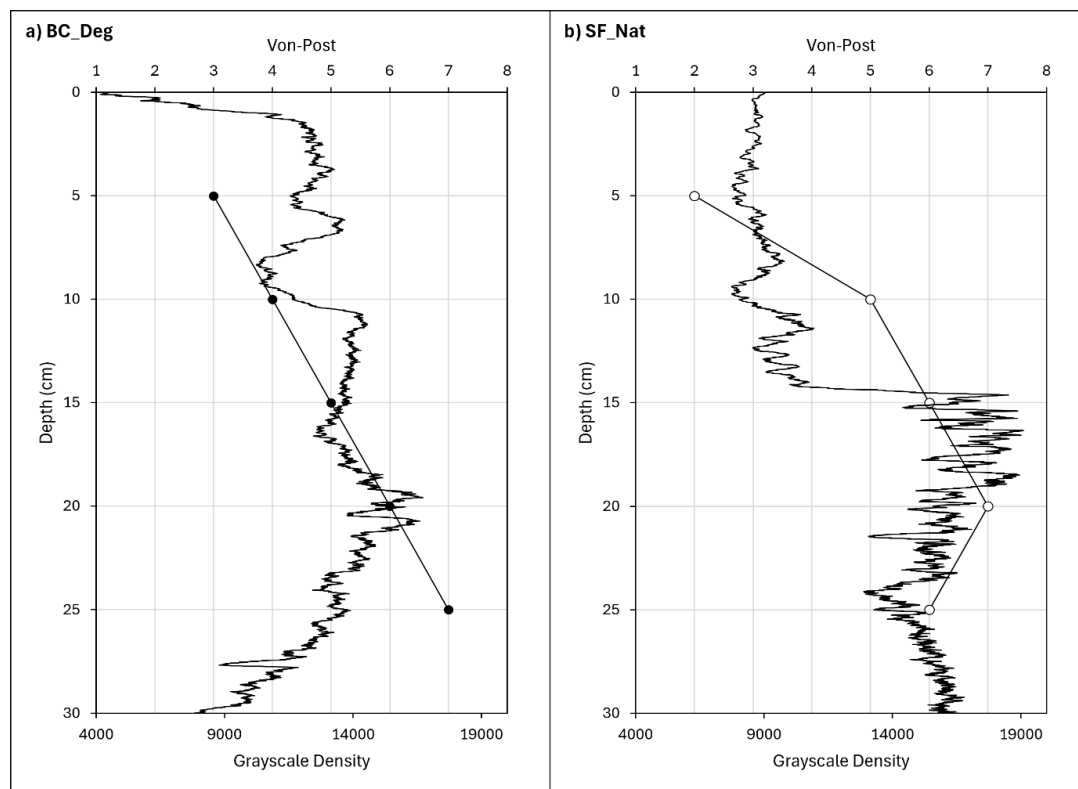
Figure 7.7: Grayscale density profiles (with macropores excluded) and Von-Post humification across control cores. Profiles are used to infer microporosity distribution with depth: a) Degraded - BC_Deg (High Flux Bay); b) Near-natural – SF_Nat (High Flux Bay).

Figure 7.7 presents control grayscale density and Von-Post humification profiles to support interpretation of inferred microporosity within restored cores.

ii) Borrowdale:
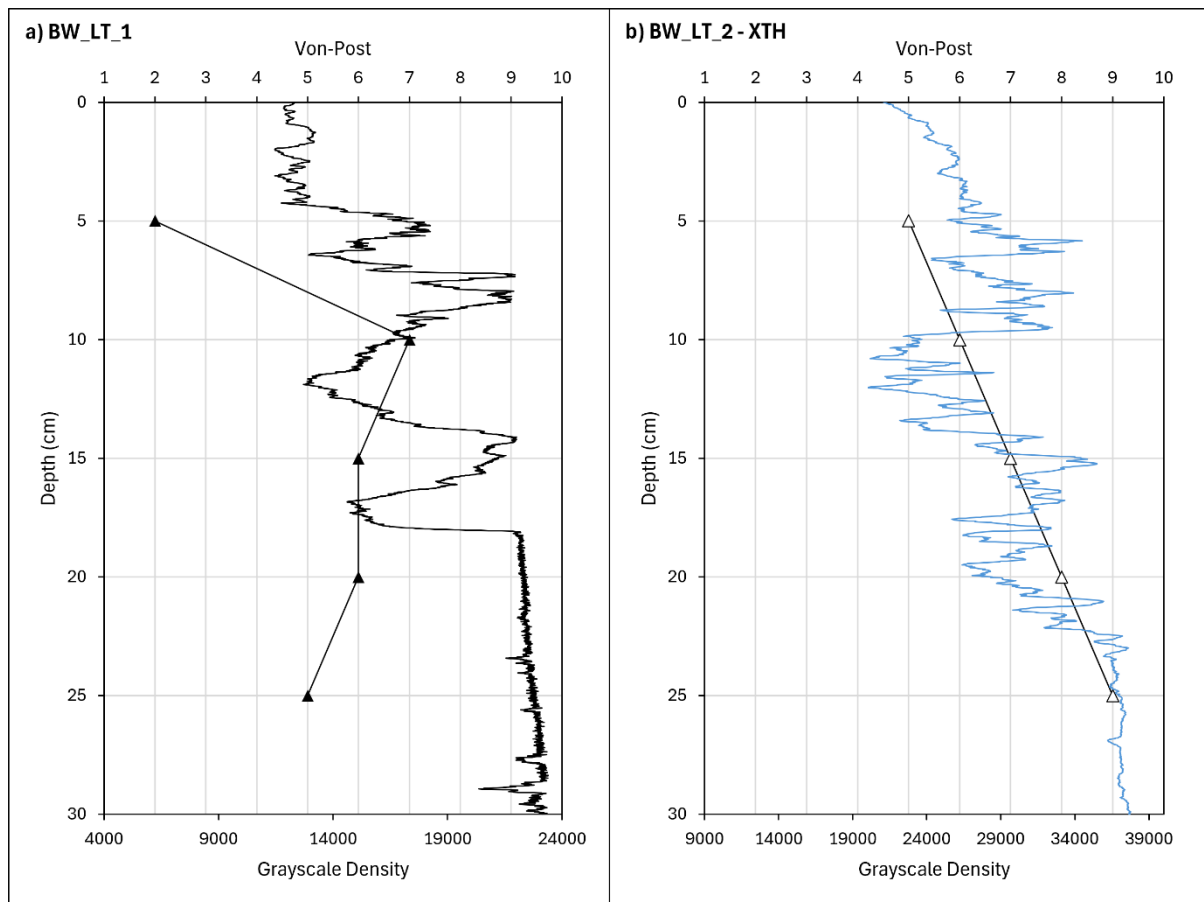
Figure 7.8: Grayscale density profiles (with macropores excluded) and Von-Post humification across Borrowdale cores (~10 years post-restoration, local turving). Profiles are used to infer microporosity distribution with depth: a) BW_LT_1 (High Flux Bay scan); b) BW_LT_2 (XTH scan) – Grayscale values not comparable.

Structural Description:

Borrowdale cores exhibit low grayscale density in the upper acrotelm (~0-5cm), within increasing density at depth, indicating bulk density (Chapter 6; Section 6.1.4). Grayscale values remain higher in BW_LT_1 than SF_Nat but follow a similar profile. Both cores show oscillating grayscale values between ~5–20cm, with a more stable and gradual increase observed in the catotelm (Chapter 6; Section 6.1.4). Von-Post humification generally corresponds to grayscale trends, although deviations are apparent in BW_LT_1 between ~10–20cm.

Functional Interpretation:

Lower grayscale density in the upper ~5cm suggests higher microporosity, supporting earlier suggestions of acrotelm recovery and *Sphagnum* influence at the micro-scale. However, higher grayscale density than SF_Nat suggest persistent surface compaction after a decade, restricting capillary water retention potential. Oscillations between ~5–20cm indicate some mesotelm development, with the transition less clear than in SF_Nat. Increasing density beyond ~20cm indicates deeper compaction and limited gas accumulation, with BW_LT_1 exceeding SF_Nat by ~5000 grayscale units. Divergence in Von-Post humification confirms its limited sensitivity to sub-surface structural characteristics in restored samples (Chapter 6; Section 6.1.3) and supports the need for caution when inferring microporosity from grayscale density. Findings also suggest relationships with bulk density (Chapter 6; Section 6.1.4) and potentially represent a more sensitive metric, explored in Chapter 9.
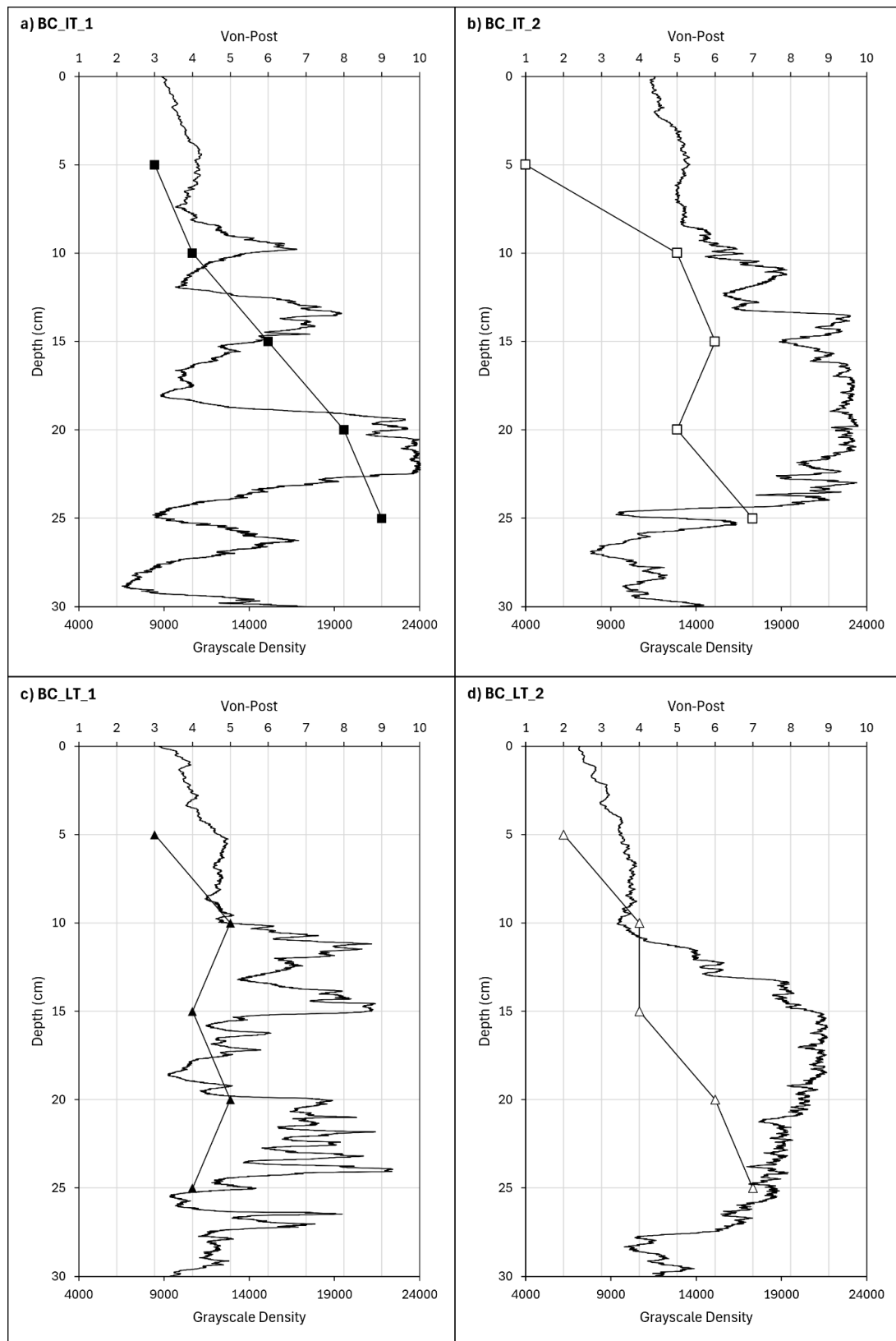
Figure 7.9: Grayscale density profiles (with macropores excluded) and Von-Post humification across Bampton Common cores (~5 years post-restoration, imported and local turving). Profiles are used to infer microporosity distribution with depth. All samples were scanned using the High Flux Bay system, directly comparable to controls: a) BC_IT_1; b) BC_IT_2; c) BC_LT_1; d) BC_LT_2.

Structural Description:

Bampton Common cores show low grayscale density at the surface, with values similar to SF_Nat extending to ~10cm. BC_IT_2 and BC_LT_2 exhibit increased density at ~15cm, followed by a decline in the catotelm (~25cm). BC_IT_1 and BC_LT_1 display oscillating grayscale profiles beyond ~10cm, generally aligning with Von-Post humification.

Functional Interpretation:

Low grayscale density between ~0–10cm suggests high surface microporosity, supporting capillary water retention through *Sphagnum*. However, shallower penetration compared to SF_Nat (~15cm) indicates incomplete acrotelm recovery ~5 years post-turving. Nonetheless, values penetrate deeper and are lower than in Borrowdale, suggesting turve quality or thickness may influence acrotelm development and water retention capacity. Oscillations in BC_IT_1 and BC_LT_1 imply limited mesotelm–catotelm stratification and minimal restoration impact on deeper microporosity. Increases at ~15cm in BC_IT_2 and BC_LT_2 support mesotelm development, though deeper profiles resembling BC_Deg indicate gas accumulation and ongoing oxic decomposition, leading to CO_2 release through diffusion.

vi) Shap Fells:
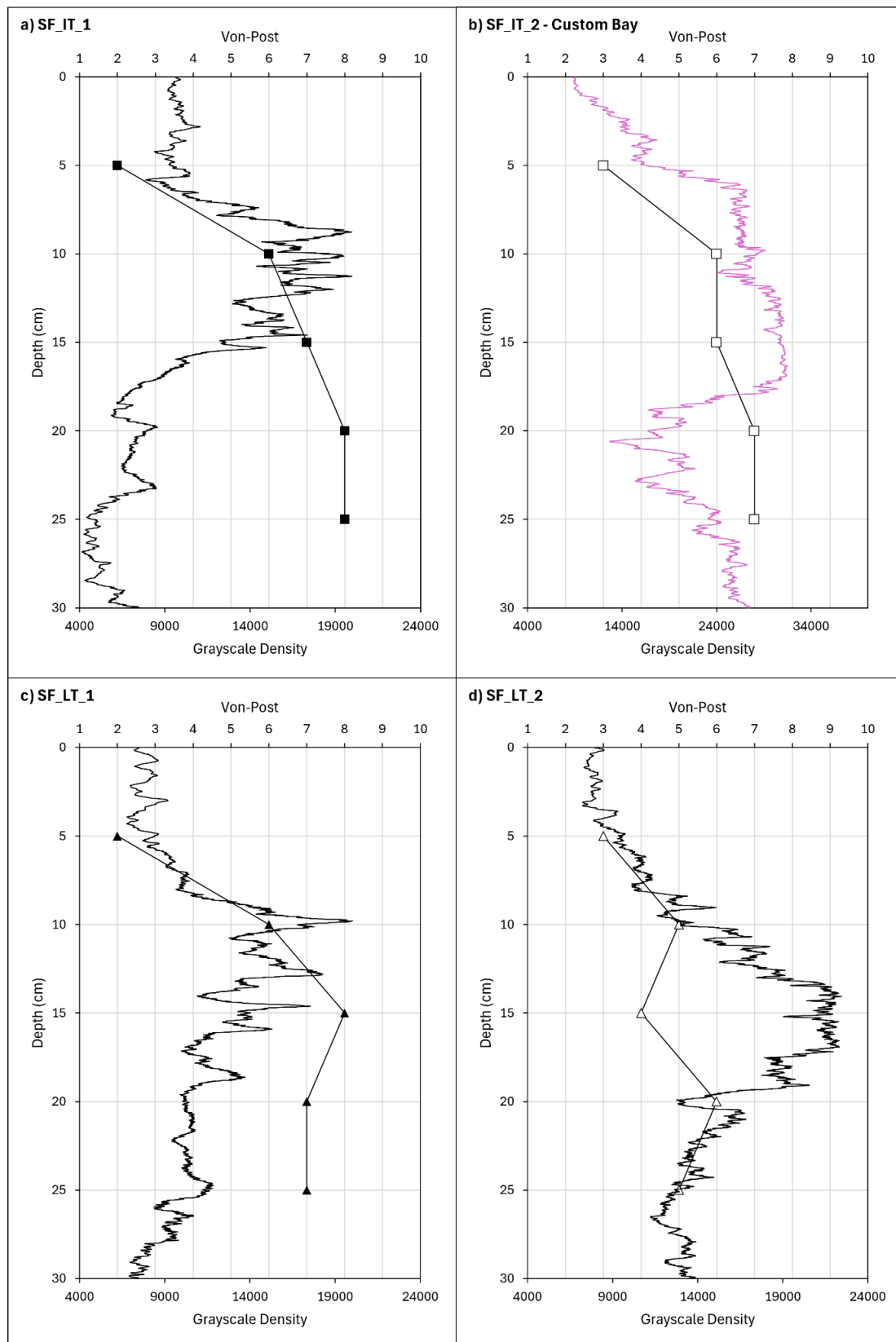
Figure 7.10: Grayscale density profiles (with macropores excluded) and Von-Post humification across Shap Fells cores (~2 years post-restoration, imported and local turving). Profiles are used to infer microporosity distribution with depth: a) SF_IT_1 (High Flux Bay); b) SF_IT_2 (Custom Bay); c) SF_LT_1 (High Flux Bay); d) SF_LT_2 (High Flux Bay).

Structural Description:

Shap Fells cores show low grayscale density in the upper ~5cm, followed by an increase between ~10–20cm and decline to values ~4000 in the catotelm. While Von-Post humification corresponds with mid-profile density increases, it fails to indicate the deeper decreases observed in grayscale values except for SF_LT_2.

Functional Interpretation:

Low grayscale density in the upper ~5cm suggests increased microporosity and early-stage acrotelm development through *Sphagnum* presence, though the shallower extent compared to Bampton Common and SF_Nat demonstrates the role of time in restoring surface water retention. Increased density between ~10–20cm indicates partial mesotelm development ~2 years post-turving. Below ~20cm, low grayscale values suggest gas accumulation from decomposition, often falling below those in BC_Deg, potentially indicating early-stage CH_4 production during rewetting (Chapter 2; Section 2.3.1). Persistently high Von-Post scores at depth in three cores supports its insensitivity to sub-surface structural recovery (Chapter 6; Section 6.1.3).
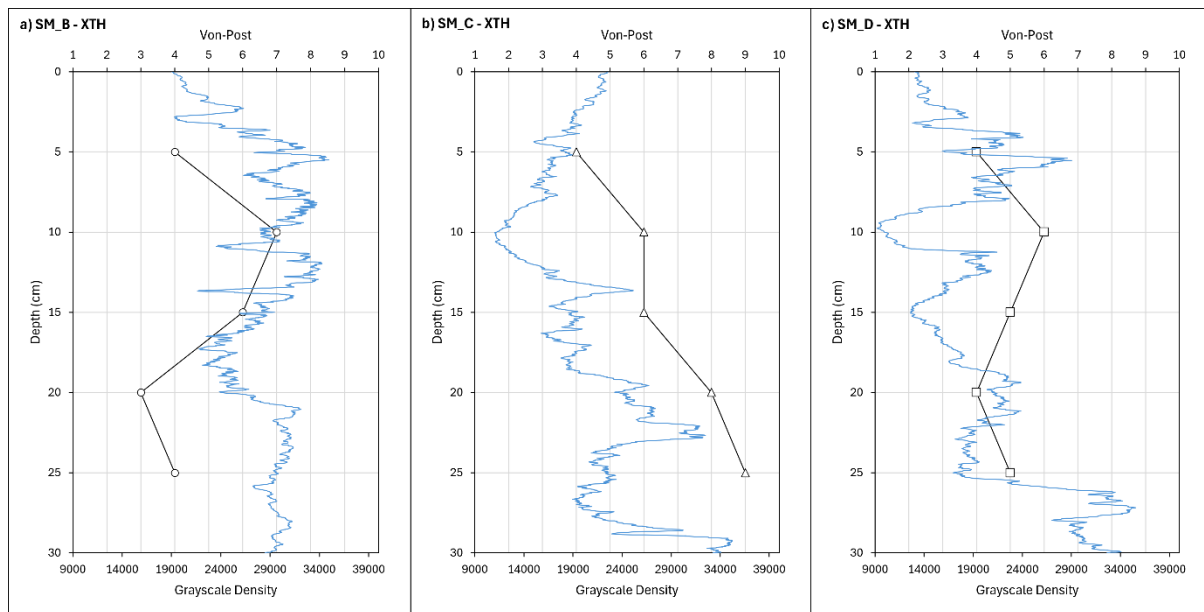
Figure 7.11: Grayscale density profiles (with macropores excluded) and Von-Post humification across Stake Moss cores (~2 years post-restoration, heather brash, coir logs, stone/timber dams). Profiles are used to infer microporosity distribution with depth. All samples were scanned using the XTH system, meaning values are not comparable to controls: a) SM_B; b) SM_C; c) SM_D.

Structural Description:

Stake Moss cores display variable grayscale density and Von-Post humification profiles, with no consistent low-density zone in the upper 0–15cm, unlike SF_Nat and other turved cores. Grayscale values oscillate with depth, with SM_C and SM_D showing fluctuations but an overall increasing density trend, supported by Von-Post humification (and bulk density; Chapter 6; Section 6.1.4). SM_B presents a more uniform profile, similar to BC_Deg.

Functional Interpretation:

Absence of low grayscale density in the acrotelm suggests limited microporosity and no evidence of capillary water retention through *Sphagnum*, supporting Chapter 5 observations (Section 5.2). This contrasts with turved sites and

288

indicates slower development of capillary water retention under alternative revegetation methods like heather brash spreading. Lack of consistent structure across depth implies no microscale stratification into acrotelm – mesotelm – catotelm layers. Declines in microporosity at depth suggest potential CO_2 diffusion hotspots in the upper 15cm, while deeper microporosity may favour CH_4 release. Findings support further relationships with surface indicators (Chapter 5), as well as bulk and chemical properties (Chapter 6), which are discussed in Chapter 9.

Restored cores show variable inferred microporosity, influenced by restoration age and technique; turved sites display early signs of capillary water retention in the acrotelm and partial mesotelm development, while non-turved sites lack stratification and retain microporosity patterns similar to degraded conditions. Von-Post distinguishes intact acrotelms, but does not capture fine-scale transitions.

c) Atmosphere, Boundary, and Isolated Porosity Contributions

Refocussing on macroporosity, where most transport and exchange processes occur (Chapter 2; Section 2.2.3), quantification of atmosphere-connected (ACP), boundary-connected (BCP), and isolated porosity (IP) distinguishes functionally relevant pore space types and enables direct comparison with control baselines.

Table 7.5: Total bulk macroporosity for each connectivity-based porosity type (atmosphere-connected; ACP, boundary-connected; BCP, isolated porosity; IP) across restored and control cores.

Core ID	ACP	BCP	IP
BC_Deg	*0.00*	*1.00*	*1.73*
BW_LT_1	0.29	0.20	0.12
BW_LT_2	0.48	0.35	0.27
BC_IT_1	0.82	0.36	0.09
BC_IT_2	3.40	0.36	0.47
BC_LT_1	2.95	0.22	0.98
BC_LT_2	1.90	0.59	0.54
SF_IT_1	1.22	1.88	0.15
SF_IT_2	0.38	0.47	1.07
SF_LT_1	0.88	0.73	0.17
SF_LT_2	0.78	0.32	0.47
SM_B	0.01	1.06	0.57
SM_C	0.13	1.30	0.14
SM_D	0.01	2.19	0.12
SF_Nat	*2.02*	*0.28*	*0.58*

i) Structural Description:

Borrowdale cores exhibit low atmosphere-connected porosity (0.29–0.48%), though it is the dominant porosity type (~48% and ~44%, respectively). **Bampton Common** shows the highest atmosphere-connected porosity among restored sites, particularly in BC_IT_2 (3.40%) and BC_LT_1 (2.95%), with boundary-connected and isolated porosity consistently lower than BC_Deg. **Shap Fells** cores demonstrate moderate atmosphere-connected porosity (0.38–1.22%) and higher boundary-connected (0.32–1.88%), with variable isolated porosity. **Stake Moss** cores record limited atmosphere-connected

porosity (<0.15%) and the highest boundary-connected across sites (1.06–2.19%), exceeding BC_Deg (1.00%), while isolated porosity remains low (0.12–0.57%).

ii) Functional Interpretation:

Borrowdale cores show limited but dominant atmosphere-connected porosity, suggesting restricted yet potential water infiltration, with low boundary and isolated porosity indicating regulated sub-surface transfer rates and retention after ~10 years.

Bampton Common samples exhibit high atmosphere-connected porosity, implying effective surface water infiltration. However, exceedance of near-natural conditions (e.g., BC_IT_2 and BC_LT_1) could suggest higher rates of CO_2 exchange with the atmosphere. Nevertheless, lower boundary and isolated porosity than BC_Deg supports functional recovery after ~5 years. **Shap Fells** and **Stake Moss** cores show moderate to low atmosphere-connected porosity alongside higher boundary-connected and variable isolated porosity, consistent with early-stage recovery and ongoing drainage at ~2 years post-restoration.

> No restored core replicates near-natural conditions, but turving accelerates atmosphere to sub-surface connectivity, supporting early acrotelm development.

d) Depth Profiles of Atmosphere, Boundary, and Isolated Porosity

Beyond bulk porosity, depth profiles of atmosphere-connected (ACP), boundary-connected (BCP), and isolated macroporosity (IP) are assessed for each restored core to support functional interpretation relative to degraded and near-natural controls.
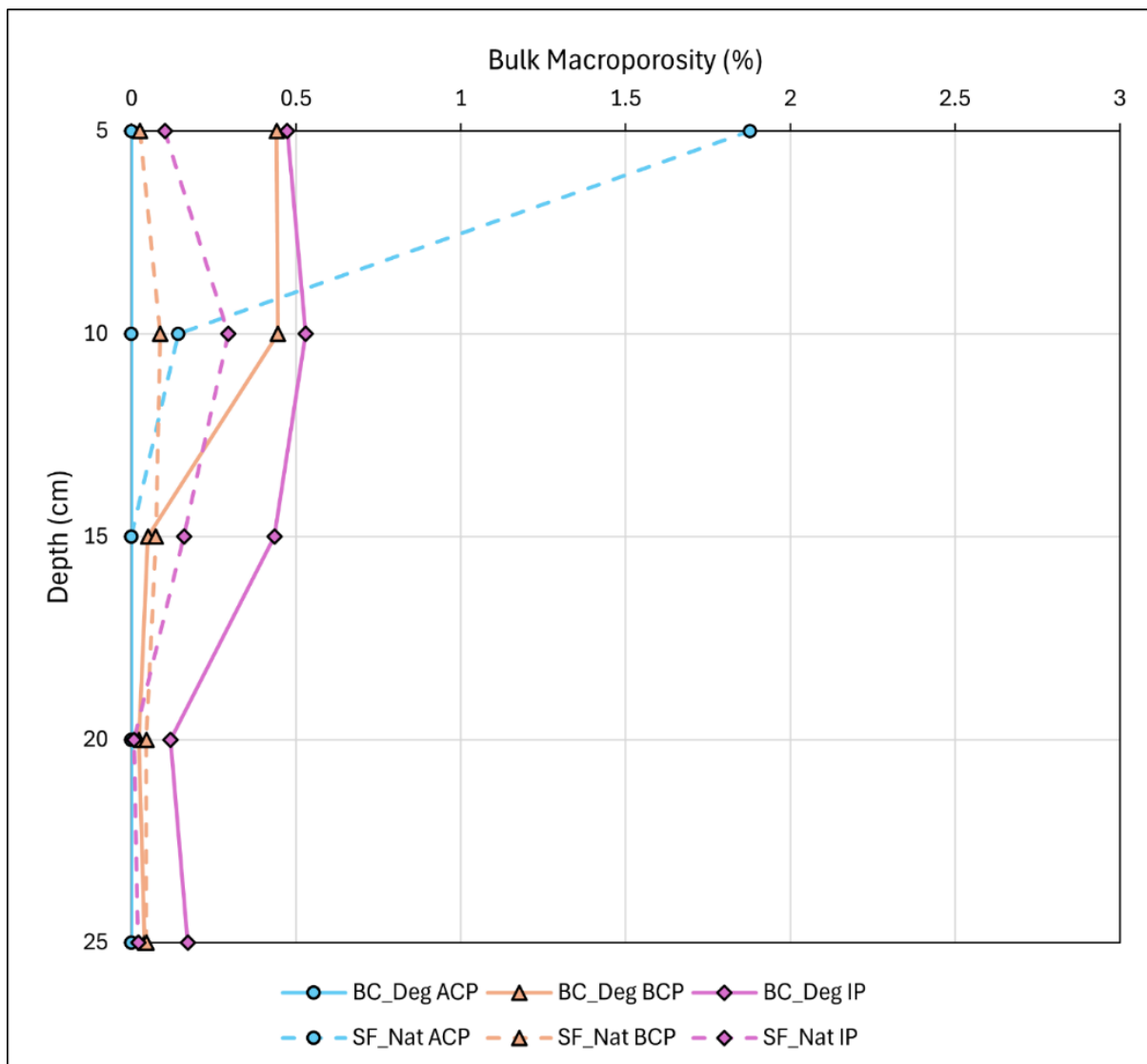
Figure 7.12: Bulk macroporosity depth profiles of atmosphere-connected (ACP), boundary-connected (BCP), and isolated porosity (IP) across control cores.

Figure 7.12 presents depth profiles of functionally relevant macroporosity for the control cores (BC_Deg – degraded; SF_Nat – near-natural), providing a baseline for comparison with restored sites and supporting earlier interpretations (Section 7.1.3c).

ii) Borrowdale:
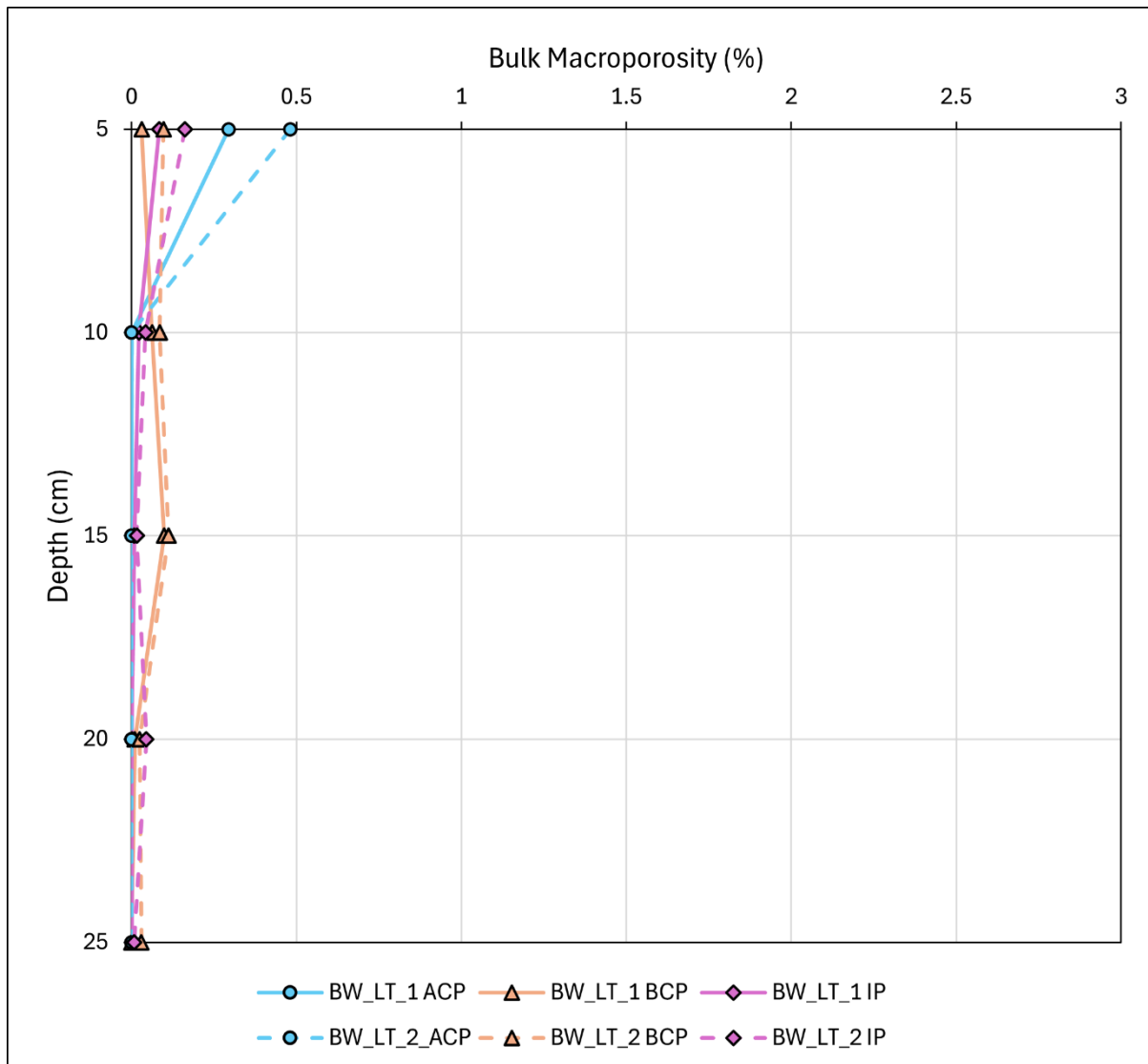
Figure 7.13: Bulk macroporosity depth profiles of atmosphere-connected (ACP), boundary-connected (BCP), and isolated porosity (IP) across Borrowdale cores (~10 years post-restoration, local turving).

Porosity types in Borrowdale cores are confined to the acrotelm (~10cm), with minimal macroporosity at depth (Figure 7.17a). This supports transitions toward microporosity over time, limiting vertical water and gaseous transfer (Section 7.2.3b). Compared to BC_Deg, reduced boundary-connected and isolated porosity indicates turving may suppress vertical and lateral drainage pathways after a decade, promoting water retention and saturation.

iii) Bampton Common:
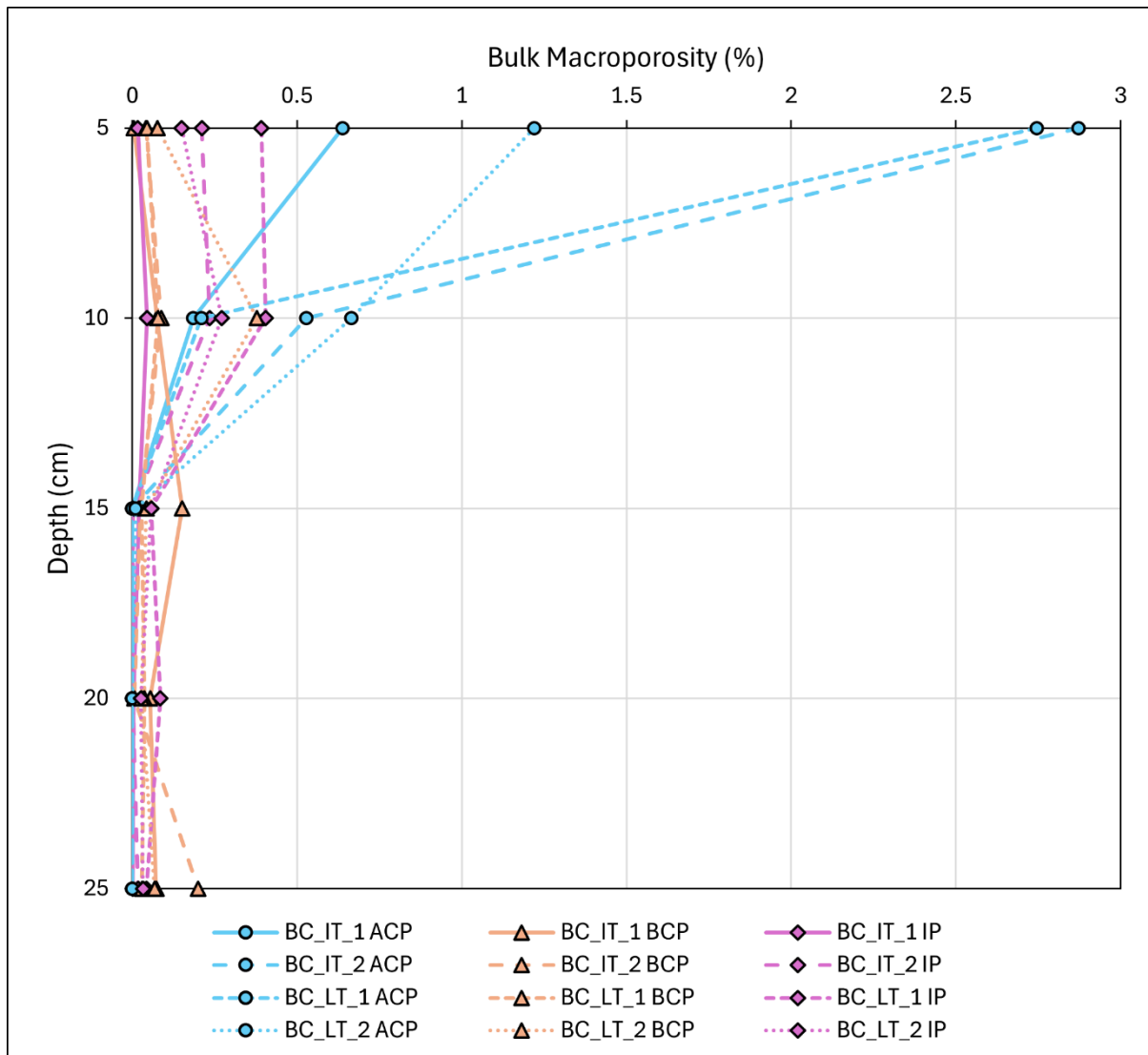
Figure 7.14: Bulk macroporosity depth profiles of atmosphere-connected (ACP), boundary-connected (BCP), and isolated porosity (IP) across Bampton Common cores (~5 years post-restoration, imported and local turving).

Atmosphere-connected porosity in Bampton Common cores is concentrated in the acrotelm, supporting water infiltration and limiting CH_4 release, though high values may increase CO_2 exchange. Porosity declines at depth, with minimal boundary-connected and isolated porosity beyond 10cm, suggesting acrotelm formation after ~5 years but limited mesotelm development, potentially due to poor bonding between turves and underlying peat (Figure 7.17b). This is further explored in Section 7.3.

iv) Shap Fells:
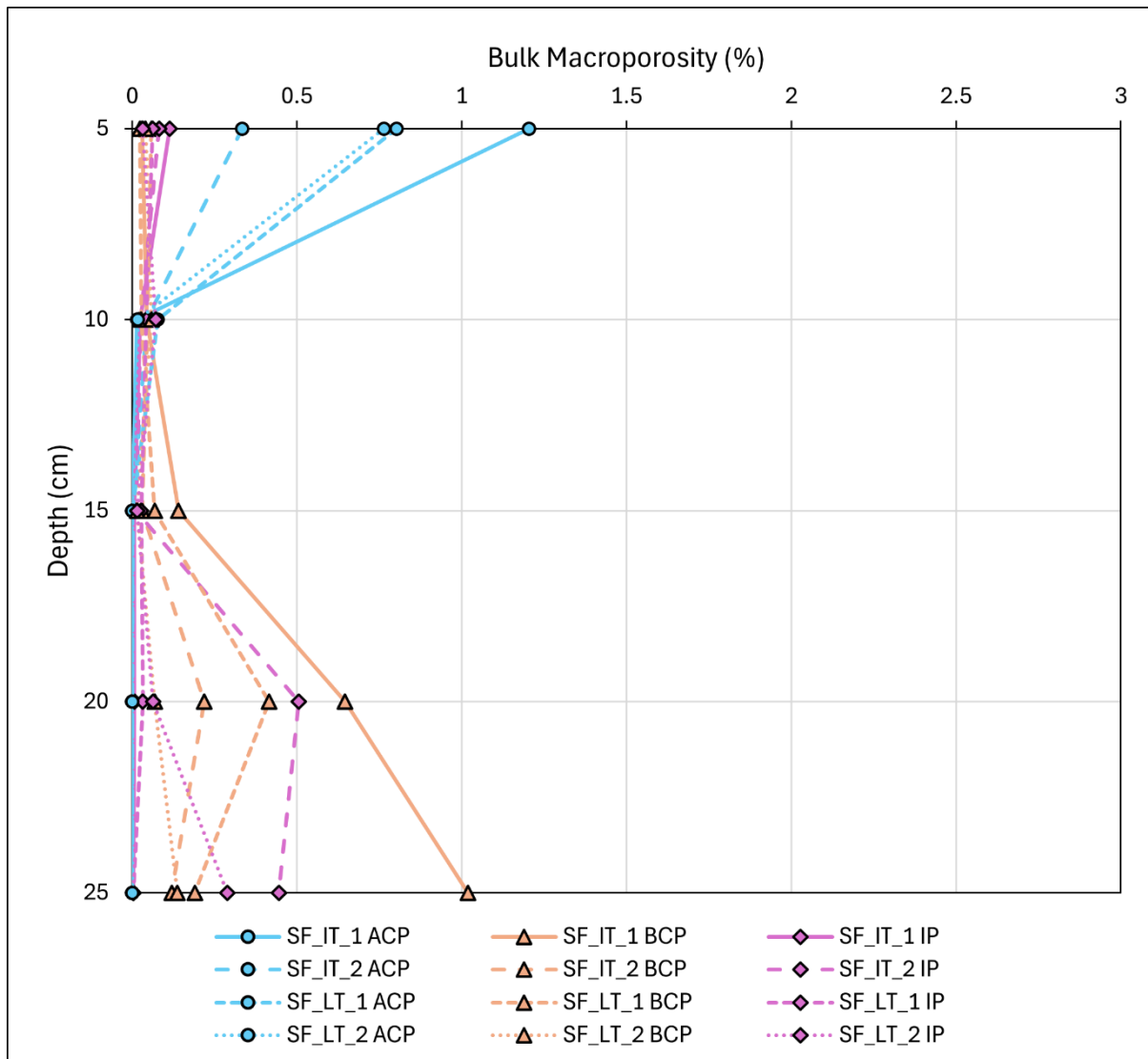
Figure 7.15: Bulk macroporosity depth profiles of atmosphere-connected (ACP), boundary-connected (BCP), and isolated porosity (IP) across Shap Fells cores (~2 years post-restoration, imported and local turving).

Shap Fells cores exhibit limited acrotelm development, with lower atmosphere-connected porosity than SF_Nat and higher boundary-connected porosity similar to BC_Deg. This indicates restricted surface to sub-surface exchange and continued drainage due to incomplete stratification after ~2 years. Reduced porosity between ~10-15cm may indicate the base of placed turves, compacted during restoration, suggesting ongoing integration of technique (Figure 7.17c), as seen in Chapter 6.

v) Stake Moss:
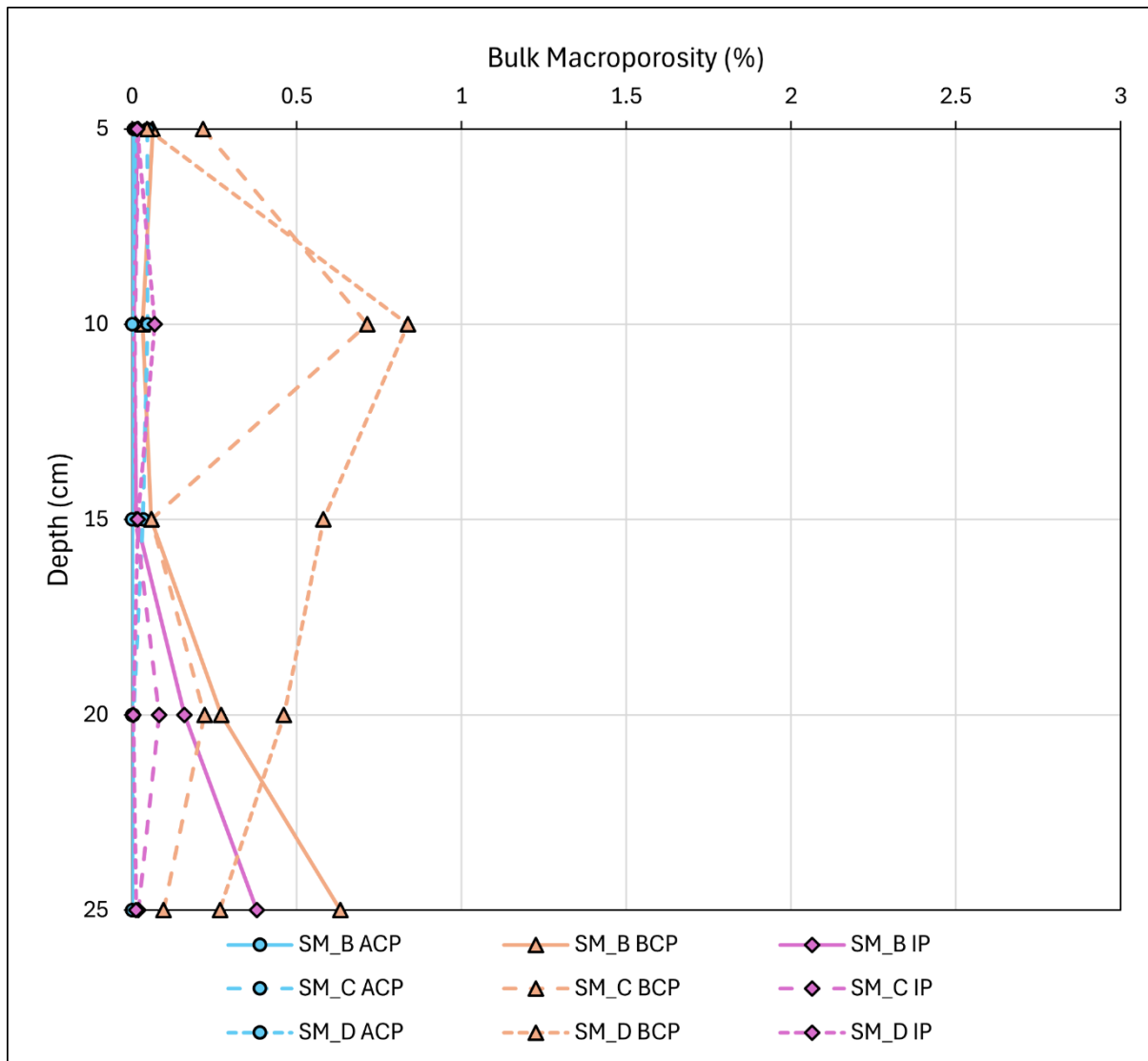
Figure 7.16: Bulk macroporosity depth profiles of atmosphere-connected (ACP), boundary-connected (BCP), and isolated porosity (IP) across Stake Moss cores (~2 years post-restoration, heather brash, coir logs, dams).

Stake Moss cores show lower atmosphere-connected porosity and higher boundary-connected porosity than Shap Fells, indicating more limited acrotelm development and persistent drainage after ~2 years using non-turving interventions. SM_C exhibits atmosphere-connected porosity extending into the catotelm, potentially enabling direct CH_4 release (Figure 7.17d). While functional layering remains weak, reduced isolated porosity compared to BC_Deg suggests some recovery of vertical connectivity.

Restoration promotes early acrotelm development by increasing atmosphere-connected porosity, facilitating effective surface water infiltration and limiting CH_4 release, particularly in turved sites. However, pore networks remain fragmented, with limited mesotelm development and ongoing drainage below the acrotelm in younger or non-turved sites, indicating incomplete functional recovery.
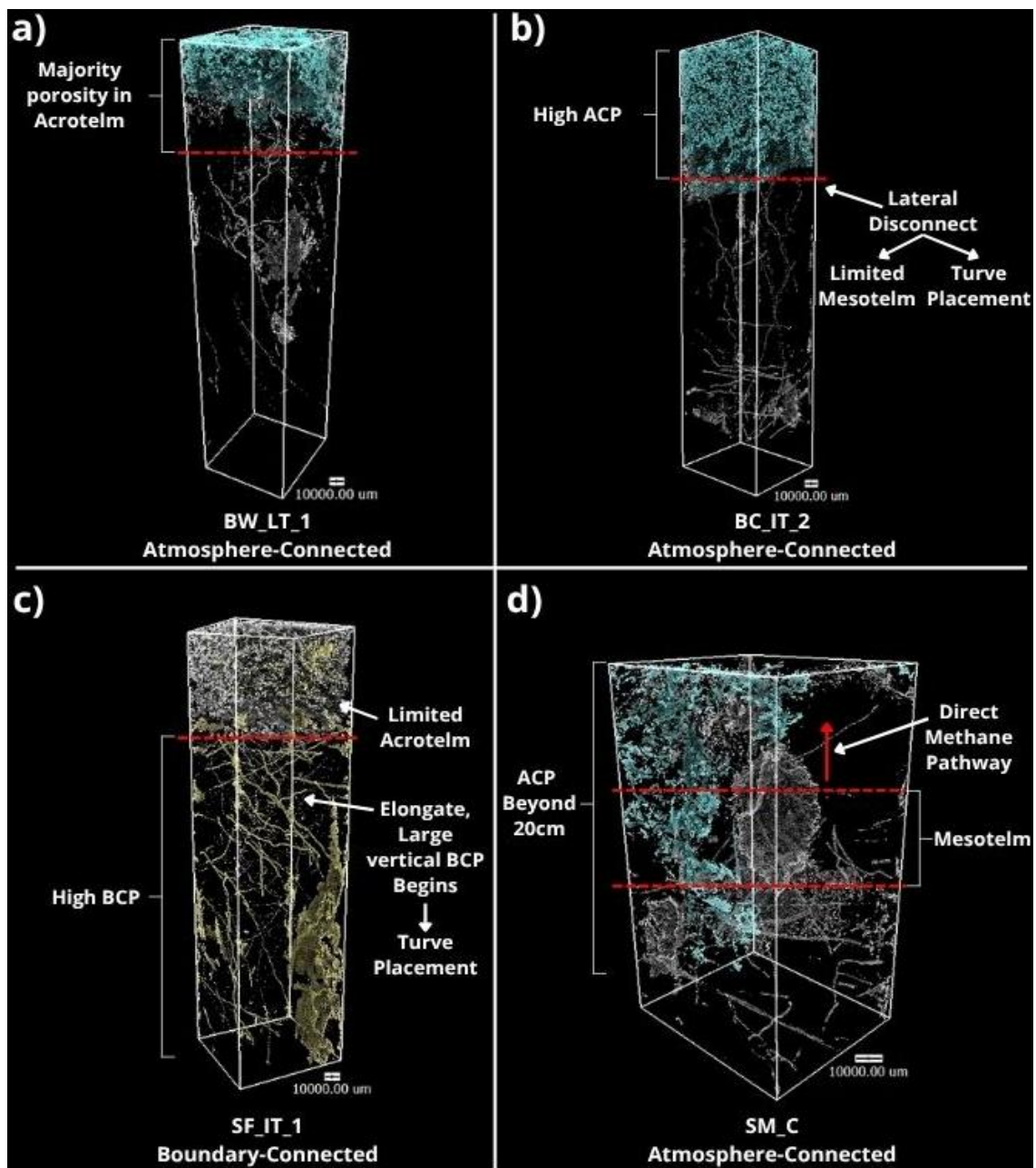
Figure 7.17: 3D visualisations of macroporosity types in select restored samples: a) BW_LT_1 – atmosphere-connected porosity (blue); b) BC_IT_2 – atmosphere-connected porosity (blue); c) SF_IT_1 – boundary-connected porosity (orange); d) SM_C – atmosphere-connected porosity (blue).

7.2.4 Summary of Structural Characteristics in Restored Samples

Restored cores show improved surface structure relative to degraded conditions, supporting early-stage surface to sub-surface interactions. However, structural recovery at depth remains limited, and no restored core replicates the stratified acrotelm–mesotelm–catotelm profile observed in near-natural conditions (SF_Nat), even after a decade, suggesting relationships with surface indicators (Chapter 5) and bulk and chemical properties (Chapter 6).

Restoration age influenced structural recovery:

- **Borrowdale (~10 years):** Low total macroporosity and reduced grayscale density suggest a transition toward microporosity, potentially driven by *Sphagnum* succession. However, persistent compaction indicates incomplete structural recovery.

- **Bampton Common (~5 years):** High surface porosity dominated by atmosphere-connected pores indicates acrotelm formation and potential for infiltration, but also increased CO_2 exchange.

- **Shap Fells and Stake Moss (~2 years):** Increased macroporosity at depth and lower surface porosity suggest relict drainage features and incomplete acrotelms.

Restoration technique affected pore type development:

- **Turved** cores displayed higher atmosphere-connected porosity, increasing surface water infiltration and early acrotelm development, associated with surface vegetation and moisture retention (discussed in Chapter 9).

- **Non-turved** cores retained higher boundary-connected porosity, consistent with degraded structure (BC_Deg) and ongoing drainage and carbon loss.

- **Isolated porosity** was lower than in BC_Deg across cores, suggesting some recovery of vertical connectivity and reduced gas accumulation.

- **Local** versus **imported turves** showed no consistent differences, though variability may indicate turve depth (quality) or compaction.

Microporosity patterns varied with restoration method:

- **Turved** sites at **Shap Fells** showed indicators of capillary water retention in the acrotelm and some mesotelm development.

- **Non-turved** sites at **Stake Moss** lacked stratification, retaining microporosity patterns similar to degraded conditions (BC_Deg).

> Findings indicate restoration initiates acrotelm development by increasing atmosphere-connected porosity, especially in turved sites, facilitating infiltration. However, boundary-connected porosity below the acrotelm often mirrors degraded conditions, suggesting ongoing drainage and limited mesotelm formation.

Although isolated porosity is often reduced relative to the degraded baseline, it does not support water, solute, or gas transport and is excluded from further analysis, except for shape-based assessment of gas bubble accumulation (Section 7.4.1a). Analyses focus on active atmosphere- and boundary-connected porosity, which govern exchange functions (Quinton *et al.*, 2009; Rezanezhad *et al.*, 2016). While bulk trends show transitional recovery of active pore space, functional capacity ultimately depends on pore size, which balances exchange and retention.

7.3 Functional Implications of Pore Size: Exchange and Retention

Pore size controls the rate and mechanism of water, solute, and gas movement (Rezanezhad *et al.*, 2009, 2010). Larger pores support advective transfer, while smaller pores restrict flow to diffusion and promote retention (Rezanezhad *et al.*, 2016; McCarter *et al.*, 2020). The size distribution of active atmosphere-connected and boundary-connected porosity is evaluated to determine whether restoration promotes exchange or retention relative to control baselines. Pores >1000mm^3 are classified as dominant due to their high capacity for transporting water, solutes, and gases. The depth of these pores is assessed to infer whether restoration increases vertical connectivity with the atmosphere or suppresses drainage pathways, supporting long-term carbon accumulation. This analysis also begins to evaluate the effectiveness of specific techniques. By examining vertical pore continuity, the structural integration of restoration interventions with underlaying peat can be assessed; particularly the placement and bonding of turves, as previously highlighted in Chapter 6. Due to the limited availability of direct supporting literature, subsequent inferences are grounded in the theoretical frameworks and findings cited earlier in this chapter.

7.3.1 Pore Size Distribution of Active Porosity

Pore size distribution of active porosity provides insight into functional behaviour by indicating whether pore networks support rapid exchange or promote retention:

- Large **atmosphere-connected pores** are more likely to support surface water infiltration and direct gas exchange with the atmosphere, while smaller pores may restrict infiltration or promote surface water retention.

- Large **boundary-connected pores** may indicate persistent or relict drainage features facilitating lateral or vertical export, particularly at depth, while smaller pores favour water and solute redistribution and regulation.

Atmosphere-connected and boundary-connected pore size distributions are compared across restored, degraded, and near-natural cores to evaluate whether restoration supports exchange or retention relative to baseline conditions. Pores are classified as small ($<1mm^3$), moderate ($1–1000mm^3$), or large ($>1000mm^3$), based on functional thresholds. Graphical statistics (mean, standard deviation, and skewness of φ) were calculated to characterise distributions (Chapter 3; Section 3.5.8).

a) Atmosphere-Connected Porosity
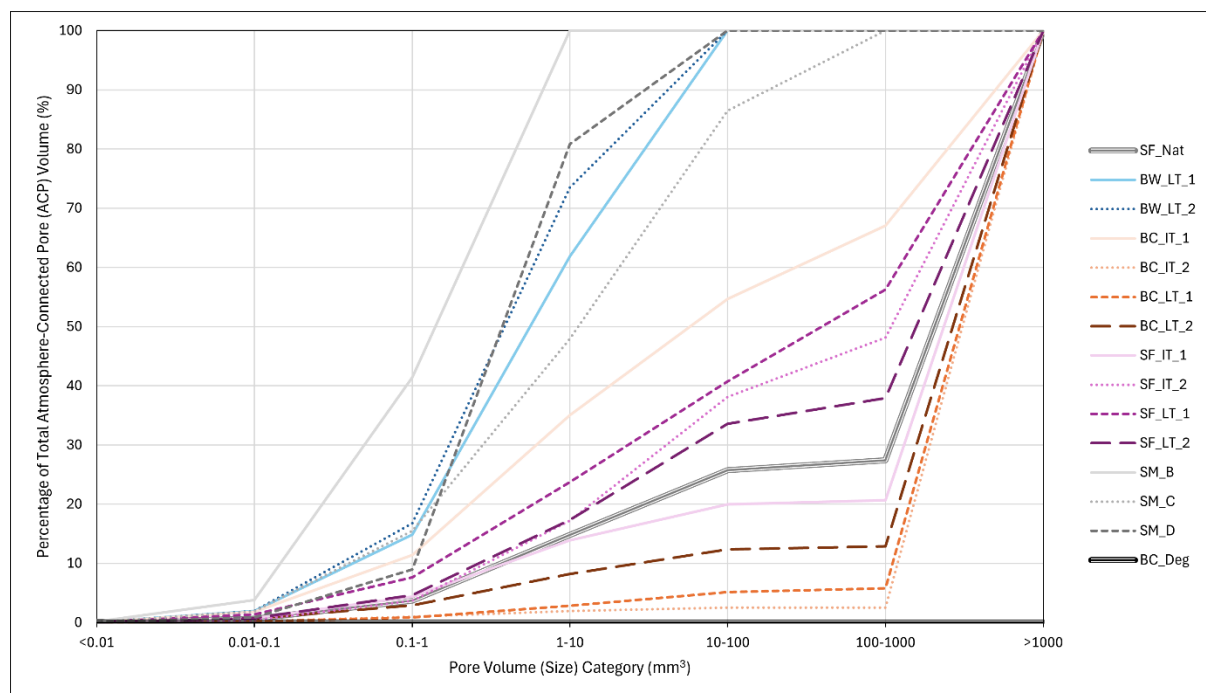
Figure 7.18: Pore size distribution of atmosphere-connected porosity (ACP) across cores, expressed as a cumulative percentage of the total macropore volume. Categories range from $<0.01mm^3$ (small) to $>1000mm^3$ (large).

i) Structural Description:

SF_Nat shows an even volume distribution across moderate to large pore sizes (10–1000mm^3), while **BC_Deg** contains no atmosphere-connected volume. **Bampton Common** and **Shap Fells** resemble SF_Nat, though Shap Fells has a greater proportion (~56%) within the 10–1000mm^3 range, whereas >90% of Bampton Common volume occurs in pores >1000mm^3. **Borrowdale** and **Stake Moss** cores exhibit >80% of volume in pores <1000mm^3, with no contribution from larger pores.

Table 7.6: Graphical statistics including mean, standard deviation, and skewness of phi (φ) for atmosphere-connected porosity pore size distribution (Figure 7.18).

Core ID	Mean φ	Standard Deviation (SD) φ	Skewness φ
BC_Deg	*0.00*	*0.00*	*0.00*
BW_LT_1	3.34	5.98	0.95
BW_LT_2	2.43	5.31	0.92
BC_IT_1	30.91	35.26	1.01
BC_IT_2	1031.12	1.57	1.00
BC_LT_1	1009.90	1.59	1.00
BC_LT_2	955.43	1.66	1.00
SF_IT_1	256.00	11.16	1.71
SF_IT_2	151.17	17.27	1.62
SF_LT_1	79.34	26.17	1.39
SF_LT_2	163.14	18.25	1.69
SM_B	0.64	5.03	1.13
SM_C	5.50	9.13	1.06
SM_D	2.25	3.41	0.93
SF_Nat	*205.07*	*14.62*	*1.71*

ii) Functional Interpretation:

SF_Nat shows moderate mean pore size (~205mm^3), heterogeneity (~15mm^3), and high skewness (1.71), indicating dominance by a few large pores, supporting surface water infiltration and regulated gas exchange. **BC_Deg** exhibiting no atmosphere-connected porosity supports surface hydrophobicity (identified in previous sections and Chapters 5 and 6). **Shap Fells** shows similar profiles to SF_Nat (mean φ = ~79–256mm^3; SD = ~11–26mm^3; skewness = 1.39–1.71), suggesting acrotelm recovery through large atmosphere-connected pores at the surface (Section 7.2.3c). **Bampton Common** exhibits large mean pore volumes (≥955mm^3), low heterogeneity (~1.6mm^3), and consistent skewness (~1.00), indicating a single dominant pore network enabling efficient water infiltration and gas exchange. **Borrowdale** and **Stake Moss** cores have low mean pore volumes (e.g., ~2.43–2.25mm^3) and skewness (~0.92–0.95), indicating smaller, more uniform pores with limited surface connectivity and higher retention capacity. Findings suggest relationships between surface moisture content, vegetation, and atmosphere-connected porosity (discussed in Chapter 9).

Restoration age and technique influence atmosphere-connected pore size distribution. Younger to moderate-aged (~2–5 years) turved cores support effective surface water infiltration and CO_2 exchange via large pores, while older (~10 years) turved and non-turved cores favour smaller pores, promoting retention/diffusion.

---

b) Boundary-Connected Porosity
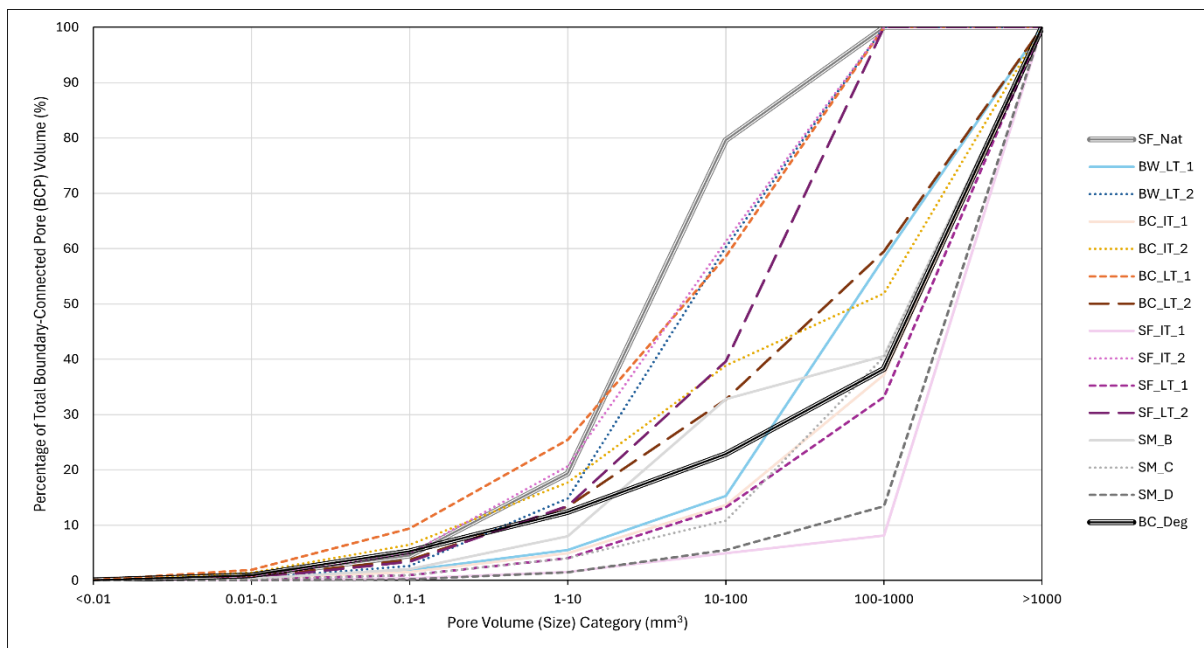
Figure 7.19: Pore size distribution of boundary-connected porosity (BCP) across cores, expressed as a cumulative percentage of the total macropore volume. Categories range from <0.01mm^3 (small) to >1000mm^3 (large).

i) Structural Description:

SF_Nat exhibits ~60% of boundary-connected volume between 1–100mm^3, with no contribution from large pores >1000mm^3. **BC_Deg** demonstrates a gradual increase across smaller pores sizes but is dominated by large pores, with >60% of volume >1000mm^3. **Turved** samples show variable profiles, with some (e.g., **SF_IT_2, SF_LT_2**) resembling SF_Nat with 33-61% of volume in the 10-100mm^3 range, while others (e.g., **BC_LT_2, BC_IT_2**) are similar to BC_Deg, with >50% of volume in large pores. **Stake Moss** cores consistently align with the degraded profile, exhibiting >90% of volume in large and <10% in smaller pores.

Table 7.7: Graphical statistics including mean, standard deviation, and skewness of phi (ϕ) for boundary-connected porosity pore size distribution (Figure 7.19).

Core ID	Mean ϕ	Standard Deviation (SD) ϕ	Skewness ϕ
BC_Deg	*230.77*	*10.82*	*1.63*
BW_LT_1	290.44	4.62	1.14
BW_LT_2	34.61	6.11	0.97
BC_IT_1	414.42	4.56	1.45
BC_IT_2	125.35	18.36	1.50
BC_LT_1	21.29	12.63	1.15
BC_LT_2	129.99	12.64	1.29
SF_IT_1	990.35	1.61	1.00
SF_IT_2	25.77	8.74	1.06
SF_LT_1	438.79	4.41	1.47
SF_LT_2	55.11	6.60	1.24
SM_B	222.46	11.05	1.62
SM_C	428.12	4.15	1.40
SM_D	948.79	1.66	1.00
SF_Nat	*17.37*	*5.27*	*1.01*

ii) Functional Interpretation:

SF_Nat shows low mean pore volume (~17mm^3), moderate heterogeneity (~5mm^3), and consistent skewness (1.01), indicating a uniform network of small to moderate sized pores promoting water and solute regulation and retention. **BC_Deg** has a considerably higher mean (~231mm^3), heterogeneity (~11mm^3), and skewness (1.63), suggesting sub-surface exchange through multiple large pores. There is no consistent trend by age or type across **turved** samples, with e.g., **BW_LT_1, BC_IT_1**, and **SF_IT_1** exceeding degraded mean volumes (>230mm^3) with low heterogeneity and skewness, implying large, singular exchange pathways, whereas others are similar to SF_Nat (e.g., **BW_LT_2, BC_LT_1, SF_IT_2**) indicating increased retention. Mean pore sizes in **Stake Moss** cores are close

to or exceed BC_Deg values, indicating persistent exchange pathways for water and solutes, indicative of drainage and erosion channels (dissolved and particulate organic carbon loss) (Chapter 2; Section 2.1.2; Figure 2.4; Holden, 2005b). Smaller boundary-connected pores in some turved cores suggest effective compaction, where deeper, larger pores have been compressed during turve placement (Figure 7.20). Others show a distinct shift in pore structure at ~10-15cm and persistent large voids, indicating weak contact between turves and underlying peat, as suggested in Section 7.2.3d (Figure 7.20). Findings demonstrate the influence of turve quality and placement on pore structure, with poor bonding reducing vertical connectivity, preserving drainage features, and increasing the risk of slippage. Additional pressure during placement or surface roughening may be required to improve structural integration and suppress drainage pathways.

> Turving can reduce boundary-connected pore size and promote retention, forming structures similar to near-natural conditions. However, large pores persist in some turved and non-turved cores, indicating incomplete drainage suppression and variability in technique effectiveness.
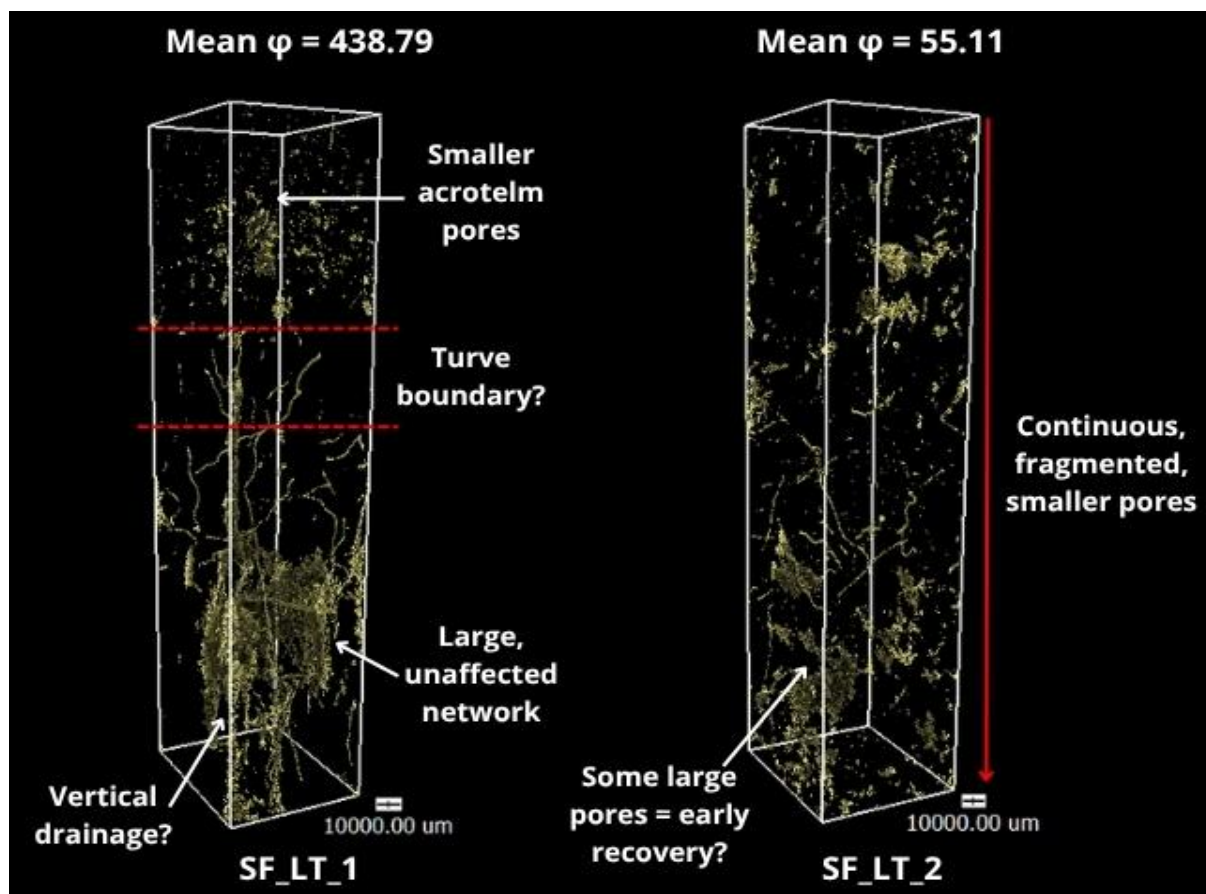
Figure 7.20: Boundary-connected porosity within Shap Fells locally turved cores (SF_LT_1 and SF_LT_2) showing contrasting mean pore volumes and the inference of turve placement effects on integrated structure.

7.3.2 Functionally Active Dominant Pores

Pore size distributions demonstrate large pores >1000mm^3 often contribute ~60-90% of active porosity volume, indicating a small number of large pores control most surface water infiltration, gas exchange, drainage, and solute transport. Their volume, abundance, and depth distribution therefore control key sub-surface functions. Table 7.8 quantifies the number of small, moderate, and large pores within atmosphere-connected and boundary-connected porosity.

Table 7.8: Total pore number across volumetric size categories: small (<0.01-1mm³); moderate (1-1000mm³); and large (>1000mm³) within active atmosphere-connected (ACP) and boundary-connected (BCP) porosity.

Core ID	Atmosphere-Connected Porosity			Boundary-Connected Porosity		
	Small (<0.01-1mm³)	Moderate (1-1000mm³)	Large (>1000mm³)	Small (<0.01-1mm³)	Moderate (1-1000mm³)	Large (>1000mm³)
BC_Deg	*0*	*0*	*0*	*5529*	*379*	*4*
BW_LT_1	2300	397	0	438	46	1
BW_LT_2	101	24	0	367	115	0
BC_IT_1	9752	1057	2	704	82	2
BC_IT_2	6455	255	1	3025	222	1
BC_LT_1	4001	357	1	2582	209	0
BC_LT_2	7386	503	1	2548	302	1
SF_IT_1	9184	948	1	1178	116	2
SF_IT_2	1346	317	1	2343	461	0
SF_LT_1	7275	734	1	841	110	2
SF_LT_2	4425	649	1	903	177	0
SM_B	32	3	0	1166	191	1
SM_C	831	125	0	722	111	1
SM_D	27	10	0	175	73	1
SF_Nat	*8292*	*1122*	*1*	*1259*	*231*	*0*

a) Structural Description

Atmosphere-connected porosity is frequently dominated by a single large pore (>1000mm³) in samples with high total volume (Section 7.2.3c). Moderate pores (1–1000mm³) are most numerous in SF_Nat (1122) and turved cores, while Stake Moss samples contain few. Small pores (<1mm³) exceed 7000 in SF_Nat and most turved cores, particularly Bampton Common.

Boundary-connected porosity follows a similar pattern. Large pores occur in high-volume cores (Section 7.2.3c), with BC_Deg containing the most (4). SF_Nat contains

none, and turved cores vary. Moderate pores are consistently present across cores. Small pores are abundant in BC_Deg (5529) but reduced in Stake Moss samples, which exhibit low total pore counts.

b) Functional Interpretation

Single, large **atmosphere-connected pores** support previous inferences that surface water infiltration and gas exchange are dominated by one primary network, contributing up to 90% of macroporosity volume (Section 7.3.1a). This is evident in Bampton Common cores, indicating increased capacity for surface water uptake and direct CO_2 exchange. Absence of large pores in Borrowdale and Stake Moss cores suggests reduced water infiltration. Higher counts of small and moderate pores in SF_Nat and turved cores relative to BC_Deg imply greater water retention and regulated solute exchange through more natural compaction, promoting saturation and long-term carbon storage.

Multiple, large **boundary-connected pores** in BC_Deg indicates persistent sub-surface drainage. SF_Nat contains none, consistent with increased water retention and regulated transfer. Turved cores vary, with some containing multiple large pores (e.g., BC_IT_1, SF_IT_1), supporting water and solute exchange, while others show none (e.g., BW_LT_2, BC_LT_1, SF_IT_2), suggesting retention through reduced boundary connectivity. This variation may indicate differences in turve placement effectiveness (Figure 7.20). High moderate and small pore abundance in BC_Deg may represent gas bubbles (Section 7.4.1a) connected to boundaries, while restored cores show values more comparable to SF_Nat, supporting a shift toward regulated water retention and carbon storage function.

Active porosity is often dominated by a small number of large pores ($>1000mm^3$), which account for most sub-surface functional capacity. Turved cores often develop large atmosphere-connected pores, enhancing water infiltration and gas exchange, while younger or non-turved sites typically retain large boundary-connected pores, indicating continued drainage and incomplete structural recovery.

7.3.3 Dominant Pore Distribution

Large pores ($>1000mm^3$) often account for the majority of active porosity volume, indicating they govern most functions, including exchange and retention. Analyses therefore focus on their volume and depth to infer functional roles. Depth position differentiates hydrological processes and gas exchange pathways:

- Large **atmosphere-connected pores** in the mesotelm or catotelm may act as direct CH_4 pathways to the atmosphere (Moore *et al.*, 2002), while those in the acrotelm more likely support CO_2 exchange.

- Shallow **boundary-connected pores** may indicate rooting or lateral flow, whereas deeper pores suggest drainage channels that lower water tables and increase dissolved and particulate organic carbon losses (Chapter 2; Section 2.1.2; Figure 2.4; Holden, 2005b).

Figure 7.21 presents the relative volume and depth of large ($>1000mm^3$) atmosphere- and boundary-connected pores.
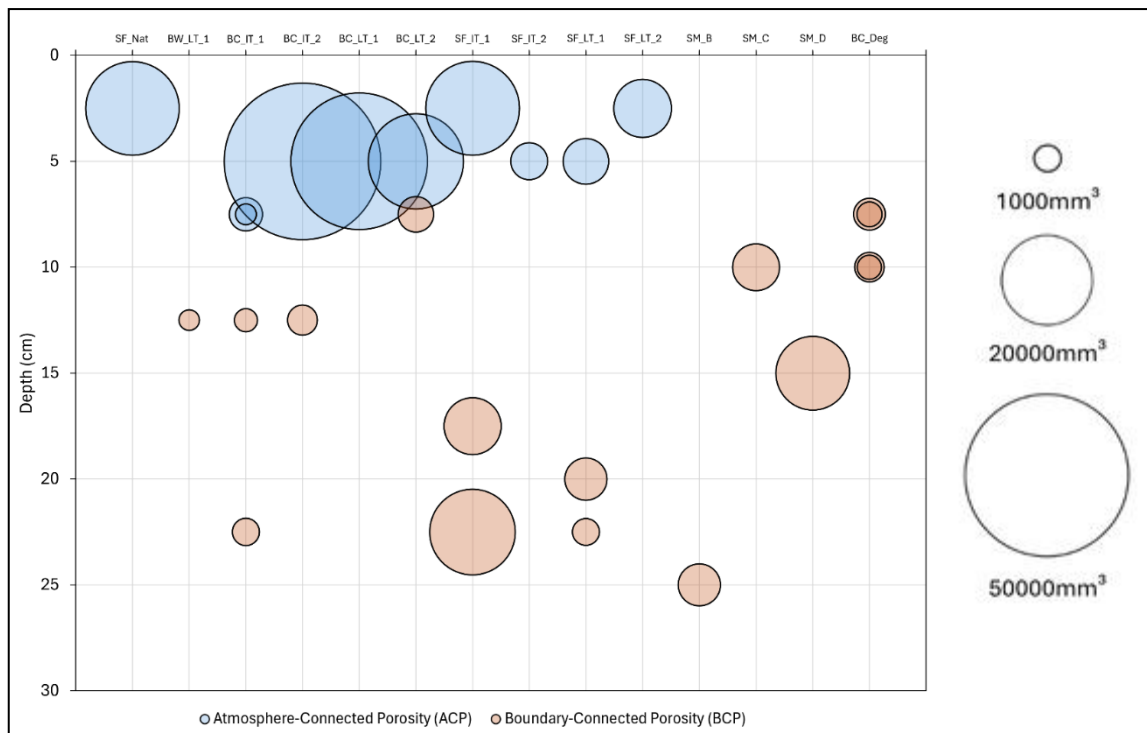
Figure 7.21: Depth (y-axis) and volume (relative bubble size – refer to key) of dominant pores (>1000mm³) across atmosphere-connected (ACP) and boundary-connected porosity (BCP). Note BW_LT_2 is not included as it attains no dominant pores.

a) Structural Description

Atmosphere-connected pores occur in the upper acrotelm (2.5–7.5cm), with the largest volumes in Bampton Common, where single pores account for up to 90% of total macroporosity (Figure 7.22a). Shap Fells and SF_Nat exhibit smaller volumes (Figure 7.22a). No large atmosphere-connected pores are present in Stake Moss or BC_Deg.

Boundary-connected pores occur below 10cm and extend to 25cm. In BC_Deg, four dominant pores exist at ~10cm with similar volumes (Figure 7.22b). Smaller, shallower boundary-connected pores are evident in older turved cores (Borrowdale, Bampton Common) (Figure 7.22b), while larger, deeper pores are present in younger turved (Shap Fells) and non-turved (Stake Moss) samples (Figure 7.22b).

b) Functional Interpretation

Large, shallow **atmosphere-connected pores** in Bampton Common suggest effective surface water infiltration and gas exchange, supporting contributions to high water table maintenance and CO_2 release. Smaller volumes in SF_Nat and Shap Fells indicate effective water infiltration but more regulated retention and gaseous exchange. Absence in Stake Moss and BC_Deg confirms limited surface connectivity and reduced water infiltration potential, promoting more oxic conditions and carbon loss.

More abundant, near-surface **boundary-connected pores** in BC_Deg indicate lateral drainage pathways lowering water tables and promoting hydrophobic surface conditions (Figure 7.22b). Shallow pores in older turved cores likely indicate acrotelm porosity from vegetation-root interactions (e.g., *Eriophorum vaginatum*, *Ericaceous* species (*Calluna vulgaris*, *Erica spp.*, *Vaccinium spp.*) and *Trichophorum cespitosum* species) with sample boundaries (Chapter 5; Section 5.2). Larger, deeper pores in younger turved (Shap Fells) and non-turved (Stake Moss) cores suggest incomplete suppression of drainage features or artefacts linked to turve placement after ~2 years. Absence at comparable depths in BC_Deg supports this interpretation. Findings support earlier recommendations to apply increased pressure during turve placement to enable bonding and reduce drainage (Section 7.3.1b).

> Dominant surface atmosphere-connected pores in turved cores increase infiltration and CO_2 exchange. Boundary-connected pore distributions indicate restoration age and technique, indicating the extent to which drainage channels are suppressed.
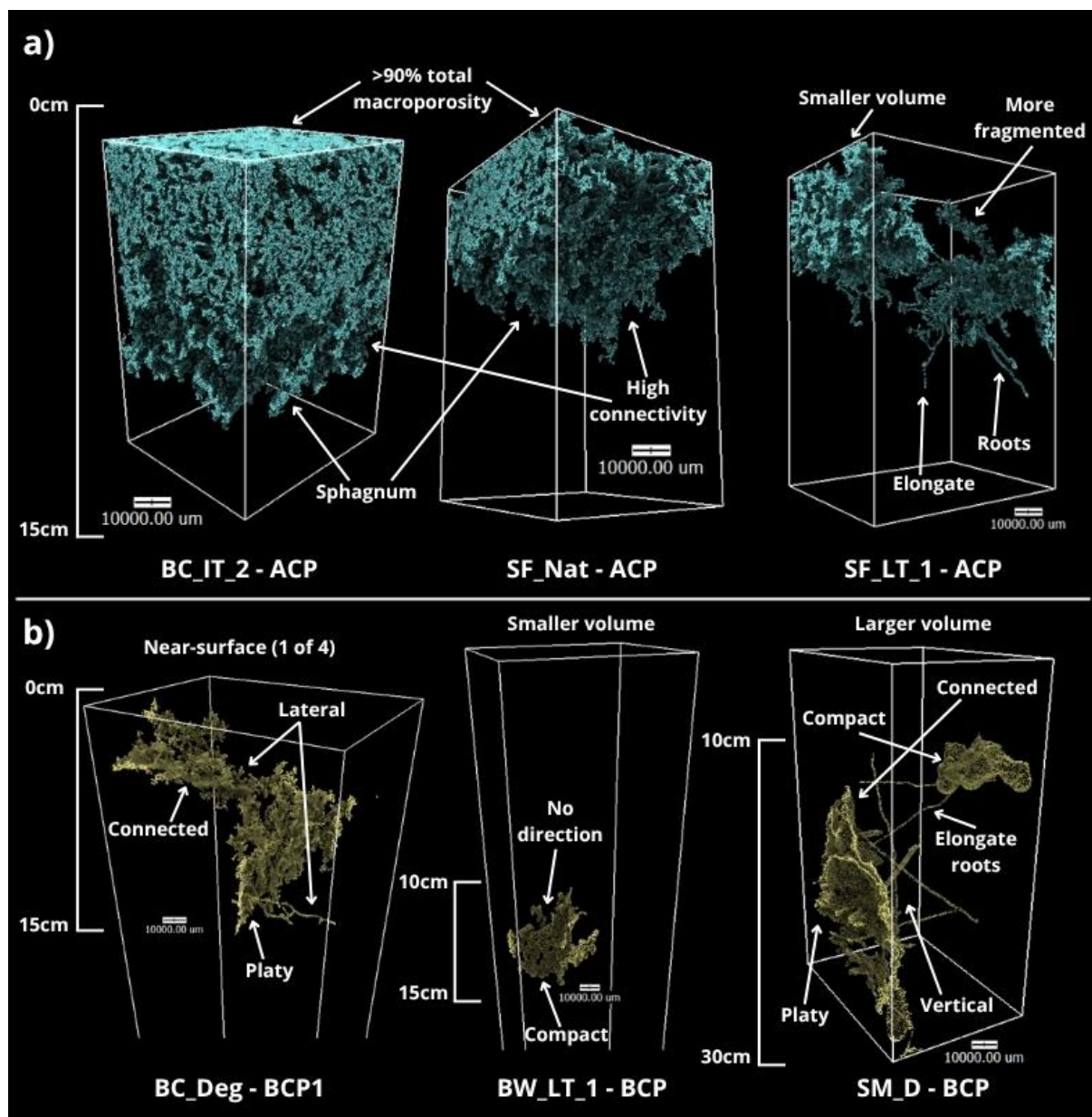
Figure 7.22: 3D visualisations of dominant (>1000mm^3) pores in select cores: a) atmosphere-connected (ACP); b) boundary-connected (BCP).

7.3.4 Summary of Pore Size Influence on Functional Behaviour

Active porosity is frequently dominated by one or two large pores (>1000mm^3), indicating single networks govern most functions. Pore size and distribution are shaped by restoration age and technique:

Atmosphere-connected porosity:

- Large pores in **turved cores** support effective surface water infiltration (Holden *et al.*, 2001; Holden, 2005b) and CO_2 exchange, often contributing >90% of macroporosity volume. This supports high saturation potential (Morris *et al.*, 2019), but may increase GHG flux and promote less water retention, indicating a trade-off between water retention and carbon loss.

- **Near-natural** and **Shap Fells** cores contain similarly sized and distributed pores, suggesting regulated exchange and functional recovery after ~2 years. **Bampton Common** and **Borrowdale** show more irregular distributions, indicating time-dependent structural shifts or variability in turve placement (quality) and site conditions.

- Absence of large pores in **Stake Moss** and the **degraded control** suggests poor infiltration and more oxic sub-surface conditions, promoting increased gas exchange through diffusion (Hoag and Price, 1997; McCarter *et al.*, 2020).

Boundary-connected porosity:

- Large boundary-connected pores dominate the **degraded control** and persist in some restored cores, indicating ongoing drainage and incomplete structural recovery (Chapter 2; Section 2.1.1).

- The **near-natural control** contains only small to moderate pores, supporting water retention and reduced solute export (e.g., dissolved and particulate organic carbon).

- Shallow pores in **older turved cores** likely result from vegetation–boundary interactions, indicating early acrotelm development and limited drainage.

- Smaller pores in some **turved** sites suggest bonding between turves and underlying peat, while larger pores in others indicate slippage or poor contact, emphasising the role of turving quality (e.g., compression and surface preparation) in suppressing drainage and promoting structural recovery.

> Functional recovery is supported in restored cores where dominant active pores indicate near-natural structures, particularly in turved samples. However, recovery remains dependent on restoration age, technique, and implementation quality.

While pore size indicates potential functional capacity, the ability of dominant pores to support water movement, solute transfer, and gas exchange depends on their structural characteristics, which control exchange efficiency (Rezanezhad *et al.*, 2010; Spencer *et al.*, 2017; Dale *et al.*, 2019; McCarter *et al.*, 2020) and long-term carbon accumulation (Rezanezhad *et al.*, 2016; Chirol *et al.*, 2021).

7.4 Structural Efficiency of Functionally Dominant Pores

Structural efficiency determines how effectively pores facilitate or restrict flow, influencing hydrological function and carbon dynamics. It is regulated by shape, complexity, connectivity (Quinton *et al.*, 2009; Rezanezhad *et al.*, 2016; Spencer *et al.*, 2017), and spatial organisation (Beckwith *et al.*, 2003), which together control the direction and rate of exchange (Figure 7.1; Chirol *et al.*, 2021).

This analysis builds on Chapter 6, where relatively insensitive bulk indicators (e.g., bulk density and moisture content) suggested limited recovery of water retention at depth. By directly assessing structural characteristics of large, functionally dominant pores, a more detailed interpretation of how restoration influences water retention, gas exchange, and

decomposition is provided. Findings further contribute to evaluating the effectiveness of specific interventions, particularly the extent to which placed turves integrate with underlying peat to support continuous pore networks, as evidenced by macropore size and vertical connectivity trends identified in the previous section.

7.4.1 Pore Shape

Pore shape influences whether networks promote retention or facilitate the movement of water, solutes, and gases, while also indicating decomposition and compaction processes. Elongate and platy pores typically support vertical or lateral transfer due to reduced hydraulic resistance, while compact (spherical) forms are more associated with retention and gas bubble formation (Strack *et al.*, 2006; McCarter *et al.*, 2020). The shape of dominant pores within atmosphere-connected (ACP) and boundary-connected porosity (BCP) therefore informs functional interpretations.

Pore shape was classified using Feret diameters along the x, y, and z axes (Chapter 3; Section 3.5.8, Table 3.9) and plotted using ternary diagrams based on the Sneed and Folk (1958) particle classification system, following Benn and Ballantyne (1993). Pores were categorised as elongate, platy, or compact (Figure 7.23). Isolated pores (IP) were also reintroduced to assess whether previously interpreted gas bubbles (Sections 7.1; 7.2) exhibit compact geometries, supporting their inferred origin as decomposition-driven gas accumulations. At depth (catotelm), these are associated with CH_4 produced via anoxic decomposition, while at the surface (acrotelm), they represent CO_2 generated through oxic decomposition and are more readily exchanged with the atmosphere via diffusion (Clymo, 1984; Baird *et al.*, 2004; Clymo and Bryant, 2008; Kettridge and Binley, 2011).
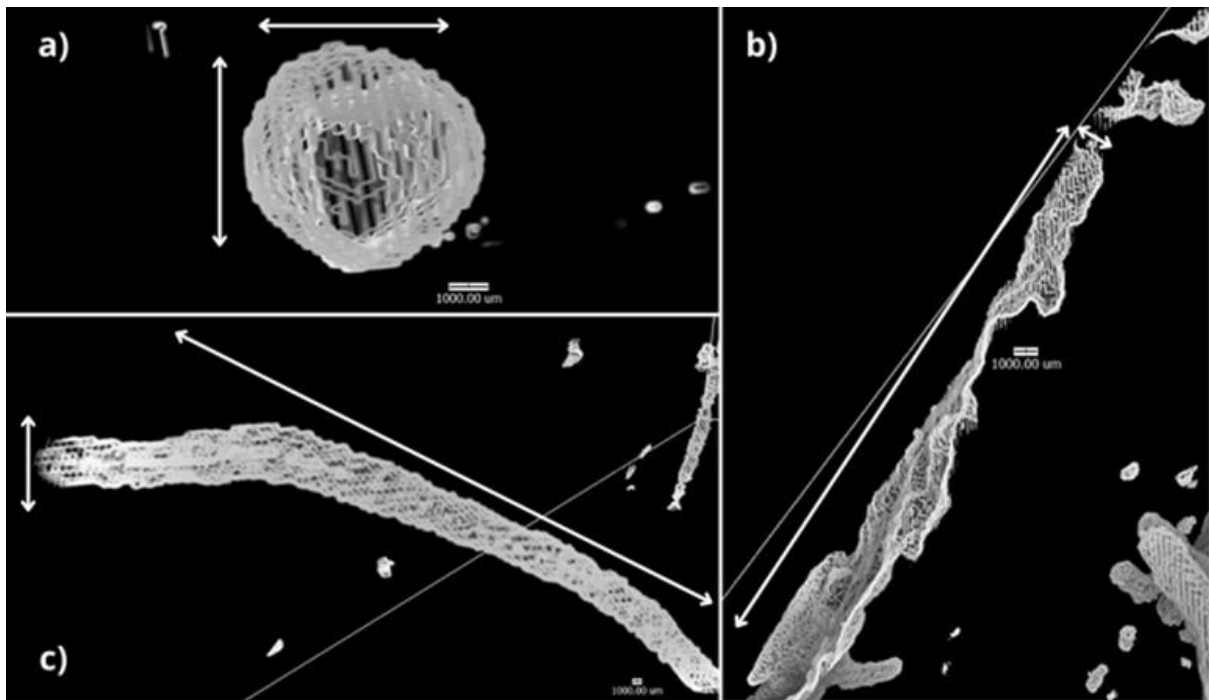
Figure 7.23: Example 3D visualisations of classified pore shapes based on Sneed and Folk (1958): a) compact – rounded or equant; b) platy – long, flat or widened; c) elongate – long, slender, and tube-like (length exceeding width).

a) Gas Bubble Interpretation

The first 250 small (<1mm^3) to moderate (1–1000mm^3) isolated pores were assessed to determine whether isolated porosity indicates compact, spherical forms characteristic of gas bubble accumulation. Figure 7.24 illustrates pore shape distributions across control and restored samples.
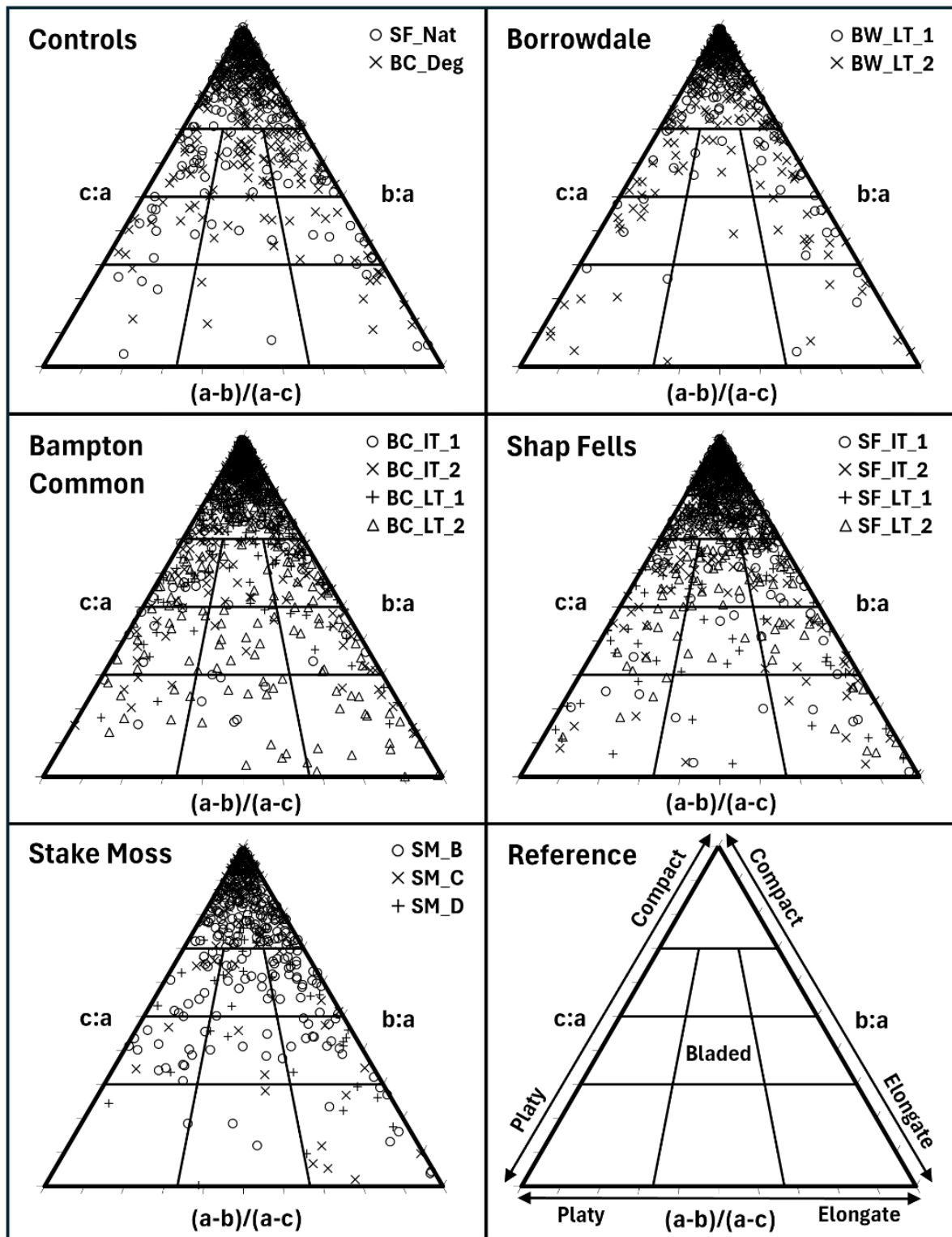
Figure 7.24: Ternary diagrams showing Sneed and Folk (1958) shape classifications for the first 250 small (<1mm^3) to moderate (1–1000mm^3) isolated pores in control and restored samples. Panels are grouped by site, with the reference diagram illustrating shape categories (platy, elongate, compact) to aid interpretation.

i) Structural Description:

Over 80% of isolated pores cluster near the apex of the ternary diagrams, indicating compact shapes. The remainder are evenly distributed across platy, bladed, and elongate classes, contributing minimally. No consistent differences are observed between control and restored samples.

ii) Functional Interpretation:

Dominance of compact shapes supports interpretations of **isolated porosity** representing gas bubbles. Some of the remaining 20% classified as platy or elongate may contribute to water retention, but spherical forms are characteristic of buoyant gas bubbles (Strack *et al.*, 2006; McCarter *et al.*, 2020). This aligns with CO_2 and CH_4 production through decomposition under oxic and anoxic conditions, respectively (Baird *et al.*, 2004; Strack *et al.*, 2005).

High isolated porosity proportions in **BC_Deg** are consistent with rapid oxic decomposition and associated CO_2 release. Low proportions in **SF_Nat** suggest slower CH_4 production under anoxic conditions or the presence of water-retentive voids. **Restored cores** show moderate proportions, supporting interpretations that rewetting and/or restoration operations (e.g., turve pressing or machinery tracking) reduce isolated porosity and slow decomposition. These interpretations are supported by bulk density, moisture content, and redox potential data (Chapter 6), further explored in Chapter 9.

> Isolated macropores exhibit compact geometries, supporting interpretations as rising gas bubbles (CO_2 and CH_4 depending on volume distribution; Sections 7.1.3; 7.2.3).

b) Dominant Active Pore Shapes

Figure 7.25 illustrates the shape classifications of dominant atmosphere-connected and boundary-connected pores (identified in Section 7.3.2).
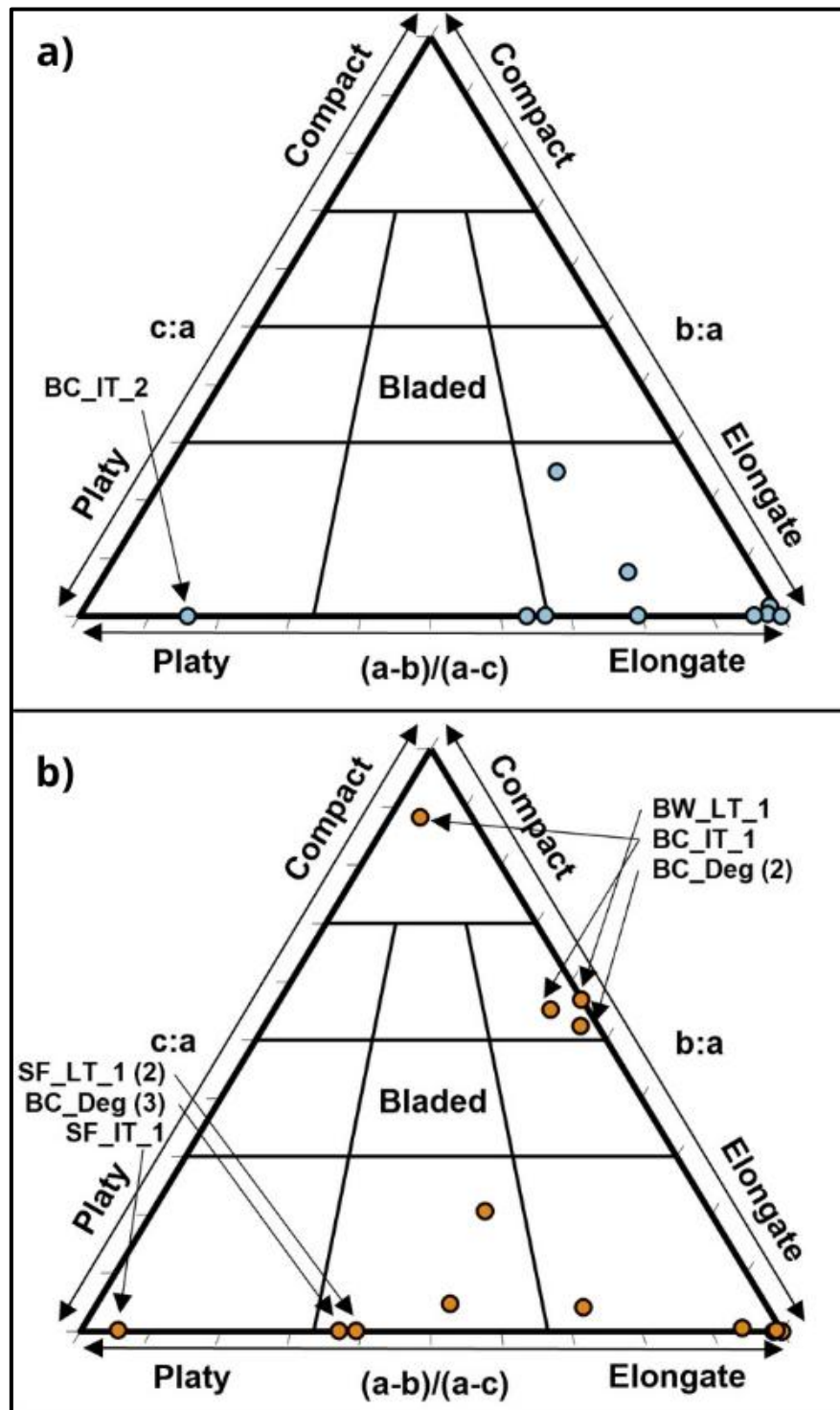
Figure 7.25: Ternary diagrams showing Sneed and Folk (1958) shape classifications of dominant pores across control and restored cores: a) atmosphere-connected (ACP); b) boundary-connected (BCP).

i) Structural Description:

Atmosphere-connected pores are predominantly elongate, with the exception of a platy form in BC_IT_2. **Boundary-connected pores** show more varied geometries, though most are elongate or platy. Compact forms are observed in BW_LT_1, BC_IT_1, and BC_Deg.

ii) Functional Interpretation:

Elongate **atmosphere-connected pores** support efficient vertical water infiltration and direct gas exchange with the atmosphere, especially in high-porosity turved samples (Sections 7.1.3; 7.2.3) (Figure 7.21a). The platy form in BC_IT_2 also enables exchange but likely promotes greater water retention due to increased surface area and flow resistance. Depending on orientation, this could increase CH_4 production by supporting methanotrophic communities (Chapter 2; Section 2.2.3; Ebrahimi and Or, 2017; Tian *et al.*, 2023).

Elongate **boundary-connected pores** promote lateral and vertical transfer beyond sample boundaries, indicating persistent drainage and potential carbon export. Platy forms (e.g., SF_LT_1, SF_IT_1) may indicate turve interfaces after ~2 years (Section 7.3.1b), or collapsed structures enabling diffuse flow (e.g., BC_Deg). Compact shapes likely impede flow, enhancing retention. The most elongate forms in BC_Deg and Stake Moss suggest continued drainage in degraded and non-turved sites.

> Dominant atmosphere-connected pores generally exhibit geometries supporting rapid exchange, while boundary-connected pore shapes vary, indicating restoration technique and structural recovery.

7.4.2 Pore Complexity

Pore shape provides a first-order understanding of network efficiency, distinguishing geometries facilitating rapid transfer from those promoting retention. However, shape does not capture internal structure. Pore complexity, defined as the number of branches per pore (Chapter 3; Section 3.5.8; Table 3.9), indicates tortuosity (in combination with Euler number, presented in the following section) and resistance to flow (Rezanezhad *et al.*, 2010; Kettridge and Binley, 2011; Spencer *et al.*, 2017; Gharedaghloo *et al.*, 2018). Highly branched pores reduce exchange efficiency and promote water or solute retention, whereas simpler structures enable more direct advective transfer (Spencer *et al.*, 2017).

This builds on previous size and shape analyses, which identified functional indicators such as large, atmosphere-connected pores supporting rapid infiltration and gas exchange. Complexity provides additional detail, quantifying internal structure and potential flow paths, enabling interpretation of relative retention. It also highlights discontinuities which may indicate limited structural integration, with implications for assessing restoration technique effectiveness.

Branch number is assessed alongside pore volume for dominant atmosphere-connected (ACP) and boundary-connected pores (BCP) (identified in Section 7.3.2) to evaluate whether larger pores exhibit greater or lower complexity, and how this varies across degraded, restored, and near-natural cores.

a) Atmosphere-Connected Pores

Higher branch numbers indicate increased tortuosity (further examined through Euler number in the following section), supporting regulated infiltration, advective gas exchange, and moisture retention. Large pores with low branching likely facilitate rapid exchange between the surface and atmosphere, particularly when elongate in shape (Section 7.4.1b).
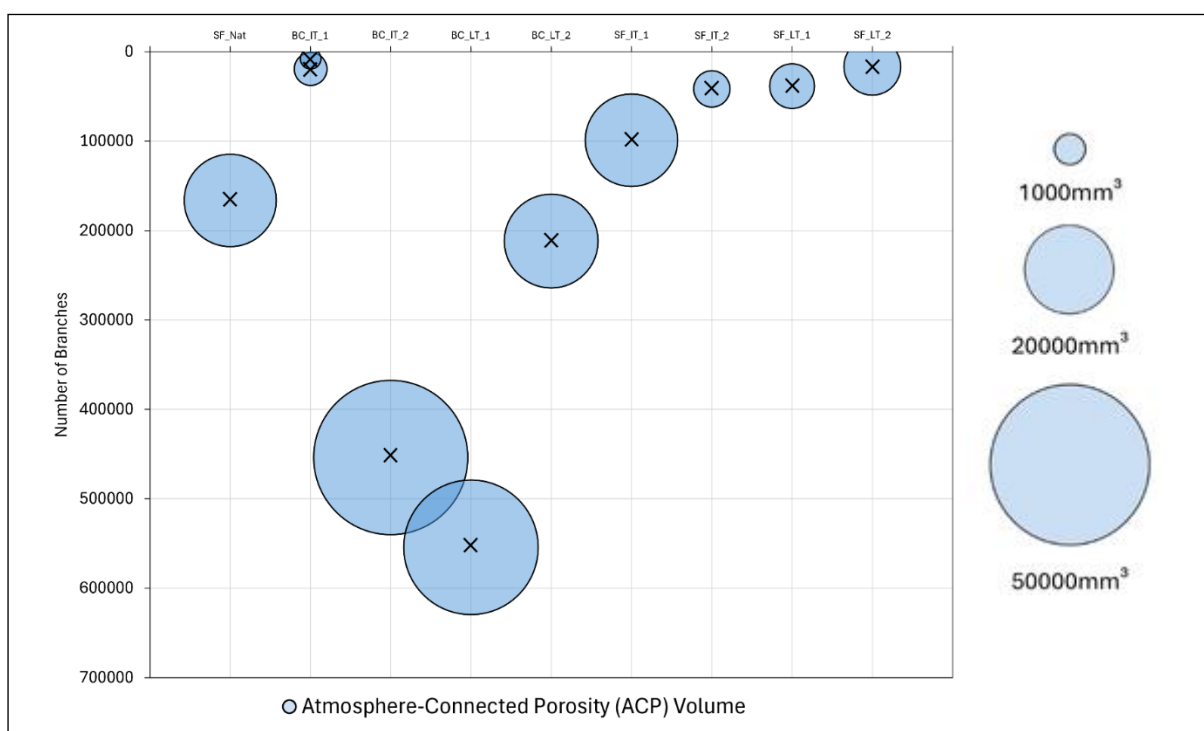
Figure 7.26: Number of branches (y-axis) and volume (relative bubble size – refer to key) of dominant pores >1000mm^3 across atmosphere-connected porosity (ACP). Note only the samples exhibiting dominant pores are included.

i) Structural Description:

Branch number generally increases with volume, indicating a positive relationship between size and complexity. Some variability is evident, with similarly sized pores displaying different branch counts (e.g., BC_LT_2 and SF_IT_1).

ii) Functional Interpretation:

Large, highly branched pores in **BC_IT_2** and **BC_LT_1** suggest increased retention and slower infiltration, contrasting with previous shape and bulk porosity inferences, indicating more water retention potential and development of a functional acrotelm (Figure 2.27a). However, their large volumes may still support increased CO_2 exchange (advective transport), which moves more readily than water (Gharedaghloo *et al.*, 2018; McCarter *et al.*, 2020). Simpler networks in **younger turved cores** (e.g., SF_IT_1) indicate reduced water retention and lower surface saturation potential (Figure 7.27b). **SF_Nat** shows intermediate complexity, consistent with balanced infiltration and retention, and more limited advective gas exchange.

> Large atmosphere-connected pores tend to exhibit greater complexity, with simpler networks more common in younger restored cores.
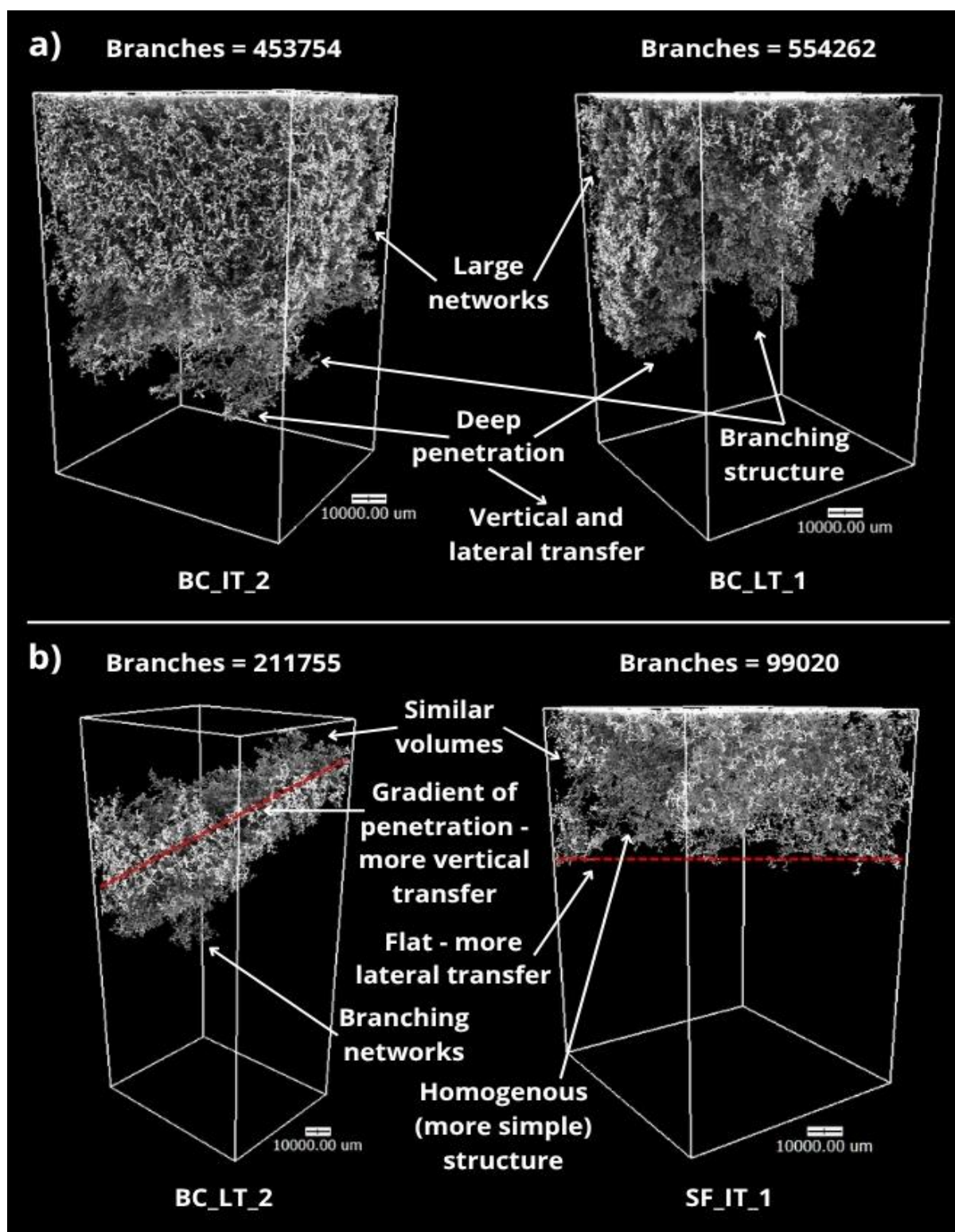
Figure 7.27: 3D visualisations of skeletonised pore branches for select dominant atmosphere-connected pores: a) large, branching pores within BC_IT_2 and BC_LT_2; b) comparable volume pores with different complexity within BC_LT_2 and SF_IT_1.

b) Boundary-Connected Porosity

Large, simple pores favour rapid lateral or vertical transfer, indicative of drainage and solute carbon losses, while complex networks suggest restricted flow and greater retention.
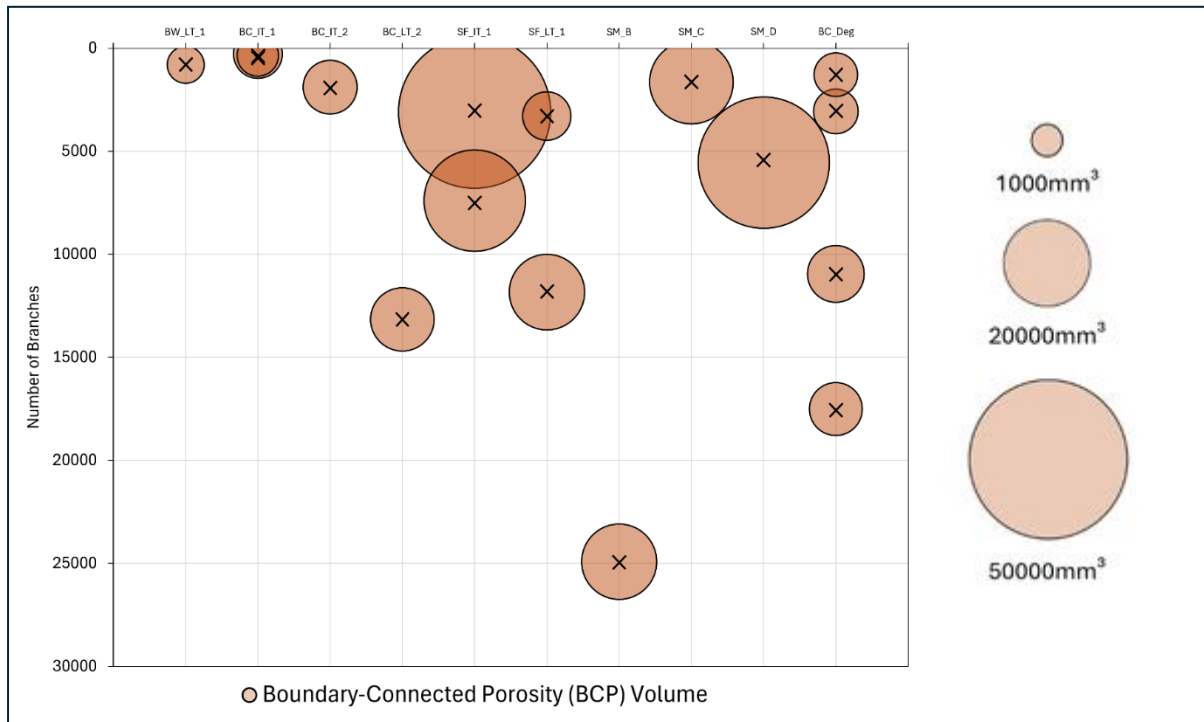
Figure 7.28: Number of branches (y-axis) and volume (relative bubble size – refer to key) of dominant pores >1000mm^3 across boundary-connected porosity (BCP). Note only the samples exhibiting dominant pores are included.

i) Structural Description:

Branch number varies independently of pore volume, with no consistent relationship between size and complexity. **Older turved cores** (BW_LT_1, BC_IT_1, BC_IT_2) contain smaller, less-branched networks, while **younger turved** (SF_IT_1, SF_LT_1) and **non-turved samples** (SM_C, SM_D) contain larger pores with similarly low complexity. **BC_Deg** shows multiple smaller pores with variable branching.

ii) Functional Interpretation:

Large, simple pores in **younger turved** and **non-turved cores** suggest efficient drainage and limited water retention, particularly at depths >15cm (Section 7.3.3) and where elongate geometries are present (Section 7.4.1b), supporting continued export of dissolved and particulate carbon (Figure 7.29a). This indicates incomplete suppression of drainage pathways after ~2 years or under indirect revegetation (e.g., coir logs, stone/timber dams). **Older turved cores** contain smaller, less complex pores consistent with bonding of placed turves and acrotelm development after ~5–10 years, which reduces drainage efficiency and slows decomposition (Figure 7.29b). Variable complexity in **BC_Deg** suggests fragmented or relict drainage structures linked to ongoing carbon loss.

> Complexity is independent of volume in dominant boundary-connected porosity and tends to decrease over time, indicating restoration effectiveness.
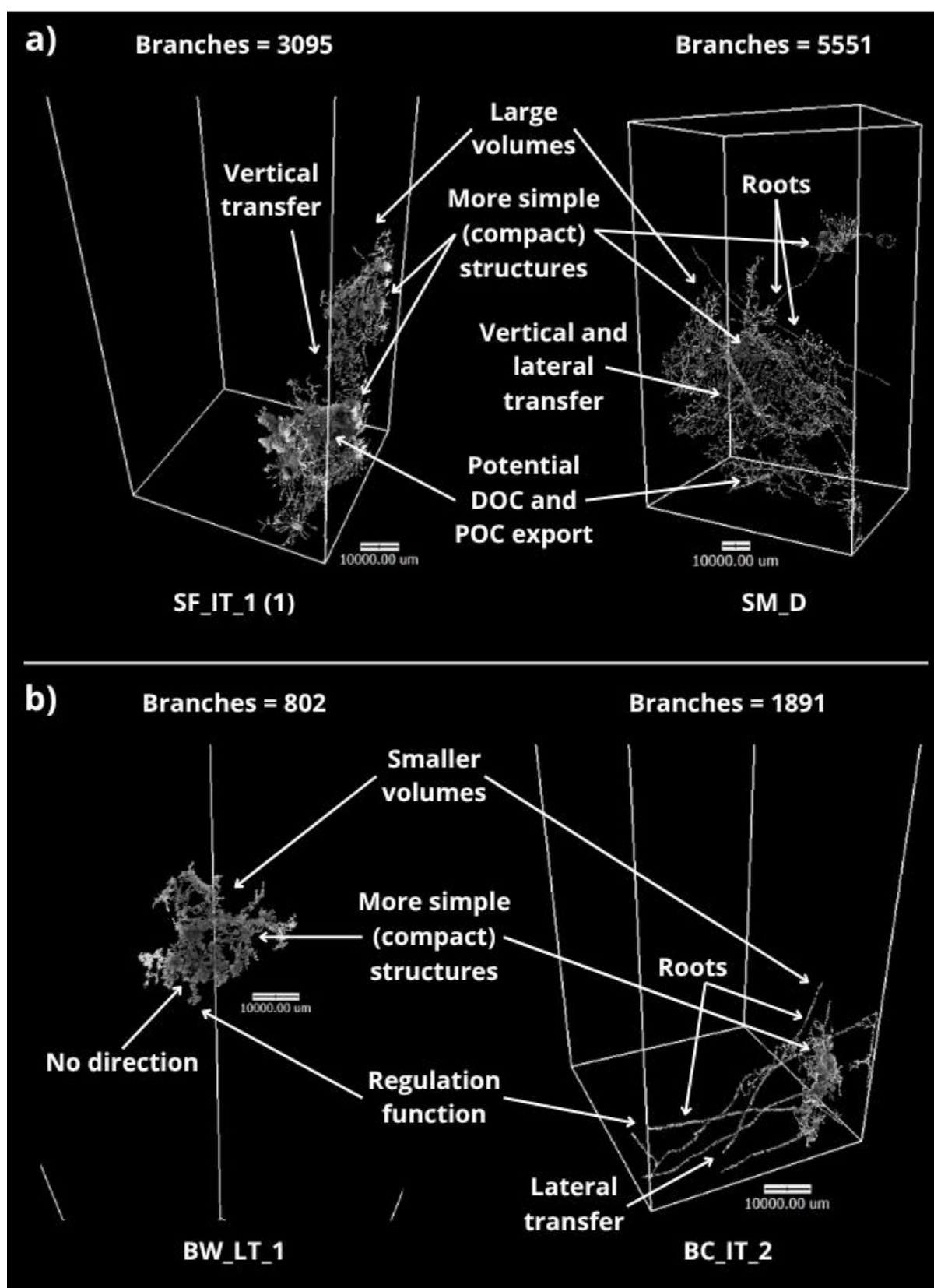
Figure 7.29: 3D visualisations of skeletonised pore branches for select dominant boundary-connected pores: a) large, more simple pores within SF_IT_1 and SM_D; b) small, simple pores within BW_LT_1 and BC_IT_2.

7.4.3 Pore Connectivity

While complexity captures the internal branching structure of pores, connectivity describes how well these branches form integrated networks, providing a more direct indicator of structural efficiency (Spencer *et al.*, 2017; Gong *et al.*, 2022). Complexity and connectivity inform tortuosity; complexity quantifies branching, while connectivity assesses whether branches form continuous loops or dead ends (Rezanezhad *et al.*, 2010; Kettridge and Binley, 2011; Gharedaghloo *et al.*, 2018). These characteristics influence retention versus exchange capacity and support interpretation of functional potential.

Connectivity is quantified using the Euler characteristic (Chapter 3; Section 3.5.8; Table 3.9). More negative values indicate highly connected, looped networks promoting water and solute retention; less negative values indicate simpler, more direct pathways facilitating rapid flow and gas exchange. Euler number is evaluated alongside pore volume for dominant atmosphere-connected (ACP) and boundary-connected pores (BCP) to determine whether large pores form tortuous, retentive systems or isolated, efficient paths. This builds on previous assessments of shape and complexity to further characterise structural efficiency across degraded, restored, and near-natural cores. Connectivity also enables assessment of restoration effectiveness by identifying whether interventions promote the development of redundant, retentive pathways supporting hydrological regulation.

a) Atmosphere-Connected Pores

More negative Euler numbers indicate highly connected, tortuous networks supporting regulated surface water infiltration and advective gas exchange though multiple, complex flow paths, consistent with high branch numbers (Section 7.4.2). Values nearer zero suggest simpler structures facilitating faster, more direct exchange between the atmosphere and sub-surface.
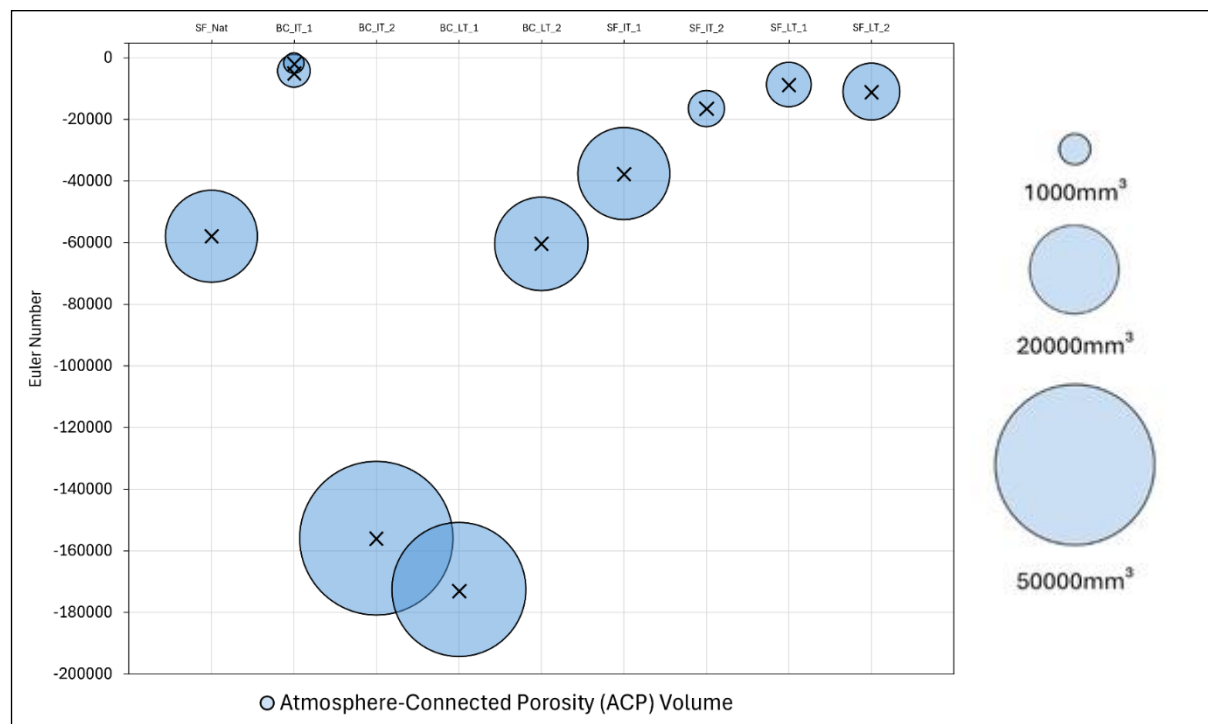
Figure 7.30: Euler number (y-axis) and volume (relative bubble size – refer to key) of dominant pores >1000mm³ across atmosphere-connected porosity (ACP). Note only the samples exhibiting dominant pores are included.

i) Structural Description:

Euler number generally decreases with pore volume, indicating larger pores are more connected. This resembles patterns observed in complexity (Section 7.4.2a), supporting the relationship between branch number and connectivity (tortuosity). Pores display negative Euler values, confirming connected networks.

ii) Functional Interpretation:

Larger pores form well-connected, complex pathways supporting surface water uptake as well as sub-surface water retention. This dual function is most evident in **turved samples** (e.g., BC_IT_2, BC_LT_1), where low Euler values correspond with high complexity and volume, suggesting developing acrotelm structure. Connectivity is greatest in **older turved** cores (e.g., **Bampton Common**), indicating improved structural integration and hydrological regulation. **SF_Nat** exhibits moderate connectivity, consistent with regulated but less efficient pathways than some restored samples. Consistently negative Euler values confirm atmosphere to sub-surface connectivity, indicative of functional recovery relative to **BC_Deg**.

Atmosphere-connected pores typically form well-connected, complex networks supporting exchange and retention, with efficiency increasing over time.

---

b) Boundary-Connected Pores

More negative Euler values indicate greater connectivity and increased potential for water and solute retention, challenges inferences of rapid drainage and solute export made in previous sections. Values closer to zero suggest limited connectivity and more direct lateral or vertical flow, promoting drainage and carbon loss.
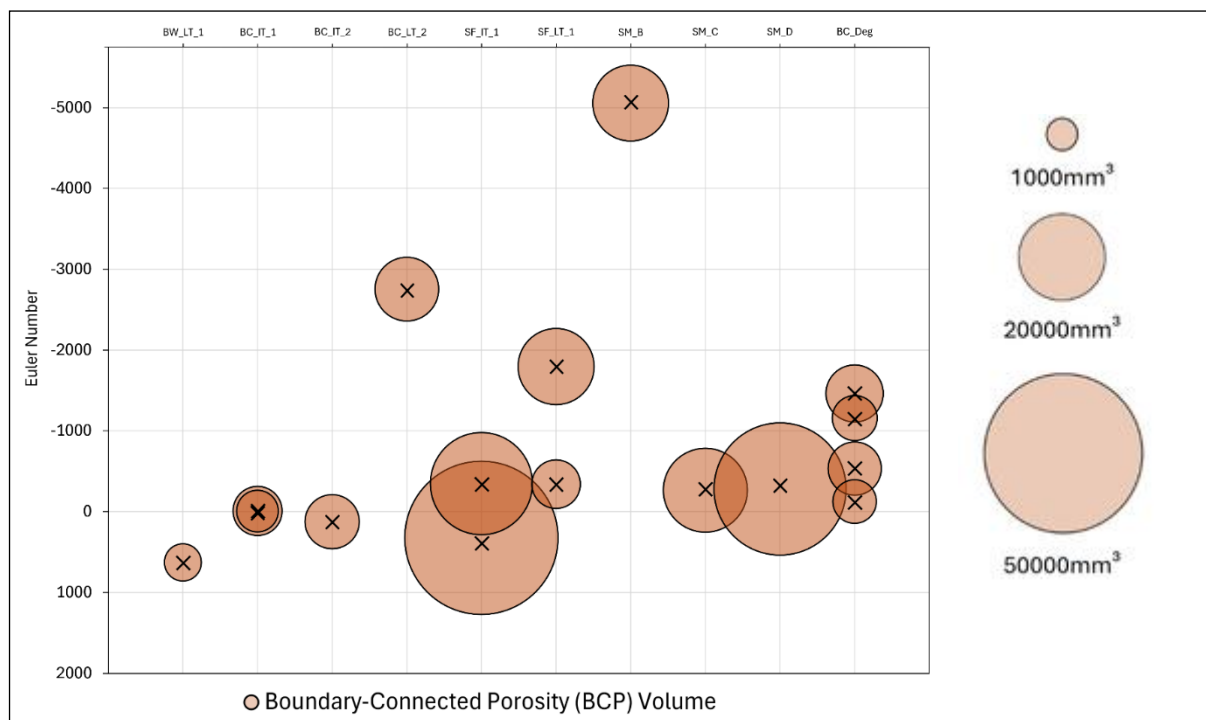
Figure 7.31: Euler number (y-axis) and volume (relative bubble size – refer to key) of dominant pores >1000mm³ across boundary-connected porosity (BCP). Note only the samples exhibiting dominant pores are included.

i) Structural Description:

Euler number shows no clear relationship with pore volume and varies independently. This resembles complexity patterns (Section 7.4.2b) and supports the relationship between branch number and connectivity (tortuosity). Values are typically closer to zero, indicating simpler, less interconnected structures.

ii) Functional Interpretation:

Less negative Euler numbers suggest more efficient lateral or vertical drainage with limited retention, particularly in **younger** and **non-turved samples**, where simpler structures indicate persistent drainage pathways. More negative values in **older turved cores** (e.g., BW_LT_1) may indicate improved pore integration and turve bonding ~10 years post-restoration, consistent with reduced drainage inferred from pore distribution

(Section 7.3.3) and shape (Section 7.4.1b). Absence of highly negative values supports their role as export pathways rather than retentive features.

> Boundary-connected pores exhibit simpler connectivity, promoting drainage and carbon loss, though older restored cores show indicators of increasing connectivity and water/solute retention potential.

7.4.4 Pore Anisotropy

While pore shape, complexity, and connectivity describe internal structure and infer network efficiency, anisotropy assesses the directional alignment of pores within the network (Beckwith *et al.*, 2003; Ketcham, 2005b; Spencer *et al.*, 2017; Gharedaghloo *et al.*, 2018). Isotropic pores lack preferred orientation and are typically associated with diffuse, multidirectional flow and increased retention (Gharedaghloo *et al.*, 2018). Anisotropic pores exhibit directional alignment, enhancing flow efficiency along dominant gradients, typically vertical pathways driven by gravity (Beckwith *et al.*, 2003; Cunliffe *et al.*, 2013).

Cores were extracted from gully sites (Chapter 3; Section 3.3; Figure 3.4), where pore networks may algin toward gully channels, promoting drainage and the export of dissolved and particulate organic carbon (Armstrong *et al.*, 2010; Rowson *et al.*, 2010; Wilson *et al.*, 2011; Evans *et al.*, 2018):

- High anisotropy in **atmosphere-connected pores** suggests vertically or slope-directed infiltration, potentially influenced by rooting species (Chapter 5; Section 5.2). This indicates rapid exchange and preferential flow toward drainage

systems, suggestive of reduced surface water retention and increased surface runoff potential (Holden *et al.*, 2006a; Wallage and Holden, 2011). Isotropy indicates more diffuse, multidirectional networks promoting water retention and reduced dissolved and particulate organic carbon export.

- High anisotropy in **boundary-connected pores** indicates persistent lateral or vertical drainage aligned with gully channels, supporting reduced water and solute retention and greater potential for carbon loss. Isotropy suggests suppressed drainage pathways and increased retention capacity.

Anisotropy is assessed across dominant active pores in degraded, restored, and near-natural cores to evaluate whether restoration influences pore orientation. This enables assessment of whether restoration disrupts structural alignment associated with degradation features, such as gully-directed drainage, and promotes functionality associated with saturated, anoxic conditions supporting carbon storage.

A threshold of 0.33 is applied: values >0.33 indicate directional alignment (anisotropy); values <0.33 indicate no preferred orientation (isotropy) (Beckwith *et al.*, 2003). Cores were extracted from south-facing slopes and oriented northward during image processing (Chapter 3; Section 3.5.4), allowing 3D visualisations to support interpretation of pore alignment relative to landscape position. Anisotropy values for total porosity were skewed by the high frequency of small, isotropic pores and are therefore excluded from analysis.

a) Dominant Active Pores

Table 7.9 presents anisotropy values and inferred directions for dominant atmosphere-connected (ACP) and boundary-connected (BCP) pores across cores.

Table 7.9: Anisotropy and inferred directional alignment of dominant atmosphere-connected (ACP) and boundary-connected (BCP) pores across cores. Anisotropy values >0.33 and oriented south/south-west/south-east are highlighted in bold. N/A indicates no dominant orientation (<0.33); / denotes data not available.

Core ID	ACP		BCP	
	Anisotropy	Inferred Direction	Anisotropy	Inferred Direction
BC_Deg	/	/	0.216	N/A
	/	/	0.138	N/A
	/	/	**0.899**	**SW**
	/	/	**0.782**	NE
BW_LT_1	/	/	**0.724**	NE
BW_LT_2	/	/	/	/
BC_IT_1	0.251	N/A	0	N/A
	0.298	N/A	**0.929**	**SE**
BC_IT_2	0.206	N/A	**0.804**	**SW**
BC_LT_1	0.217	N/A	/	/
BC_LT_2	0.162	N/A	**0.335**	W
SF_IT_1	0.209	N/A	**0.891**	**SW**
	/	/	**0.833**	W
SF_IT_2	**0.820**	**SW**	/	/
SF_LT_1	0.305	N/A	**0.549**	**SE**
	/	/	**0.558**	E
SF_LT_2	**0.809**	E	/	/
SM_B	/	/	0.263	
SM_C	/	/	**0.845**	NW
SM_D	/	/	**0.471**	N
SF_Nat	0.299	N/A	/	/

i) Structural Description:

Atmosphere-connected pores were generally isotropic (anisotropy < 0.33), indicating no dominant orientation. Exceptions were observed in younger turved cores (e.g., SF_IT_2, SF_LT_2), which exhibited high anisotropy (>0.80). SF_IT_2 was oriented south-west. **Boundary-connected pores** were typically anisotropic across cores, with values >0.70. Approximately 50% of these were aligned southward and occurred in turved samples.

ii) Functional Interpretation:

Generally low anisotropy in dominant **atmosphere-connected pores** suggests diffuse, multidirectional flow pathways supporting surface water retention. The lowest values

were observed in the older Bampton Common turved cores, suggesting turving may disrupt surface-aligned drainage structures and promote improved surface water retention after ~5 years. High anisotropy in younger turved cores, particularly SF_IT_2 aligned toward the gully, indicates persistent drainage and potential for water and solute loss after ~2 years. However, Figure 7.32a shows the dominant pore network in SF_IT_2 is associated with rooting species, indicating turve quality and early ecological recovery (Chapter 5; Section 5.2).

High anisotropy in **boundary-connected pores** across restored sites indicates persistent sub-surface drainage features aligned with lateral or vertical flow paths (Figure 7.32b). This suggests deeper pore networks remain structurally connected to gully systems or low-resistance pathways, potentially facilitating soil pipe formation and promoting water and solute loss (Holden and Burt, 2003; Holden, 2005a; Cunliffe *et al.*, 2013). Restoration appears to exert limited influence on deep pore orientation, with minimal variation across techniques or relative to degraded baselines, supporting earlier evidence of incomplete sub-surface recovery. The persistence of drainage features indicates incomplete bonding between placed turves and underlying peat, where a high-porosity gap enables continued flow and exchange. This highlights the potential benefit of increased turve compaction during placement or use of tracked machinery to disrupt deeper connections and promote sub-surface integration.

> High anisotropy in boundary-connected pores suggests persistent lateral drainage pathways unaffected by restoration, while isotropic atmosphere-connected pores support vertical infiltration and surface water retention over time.
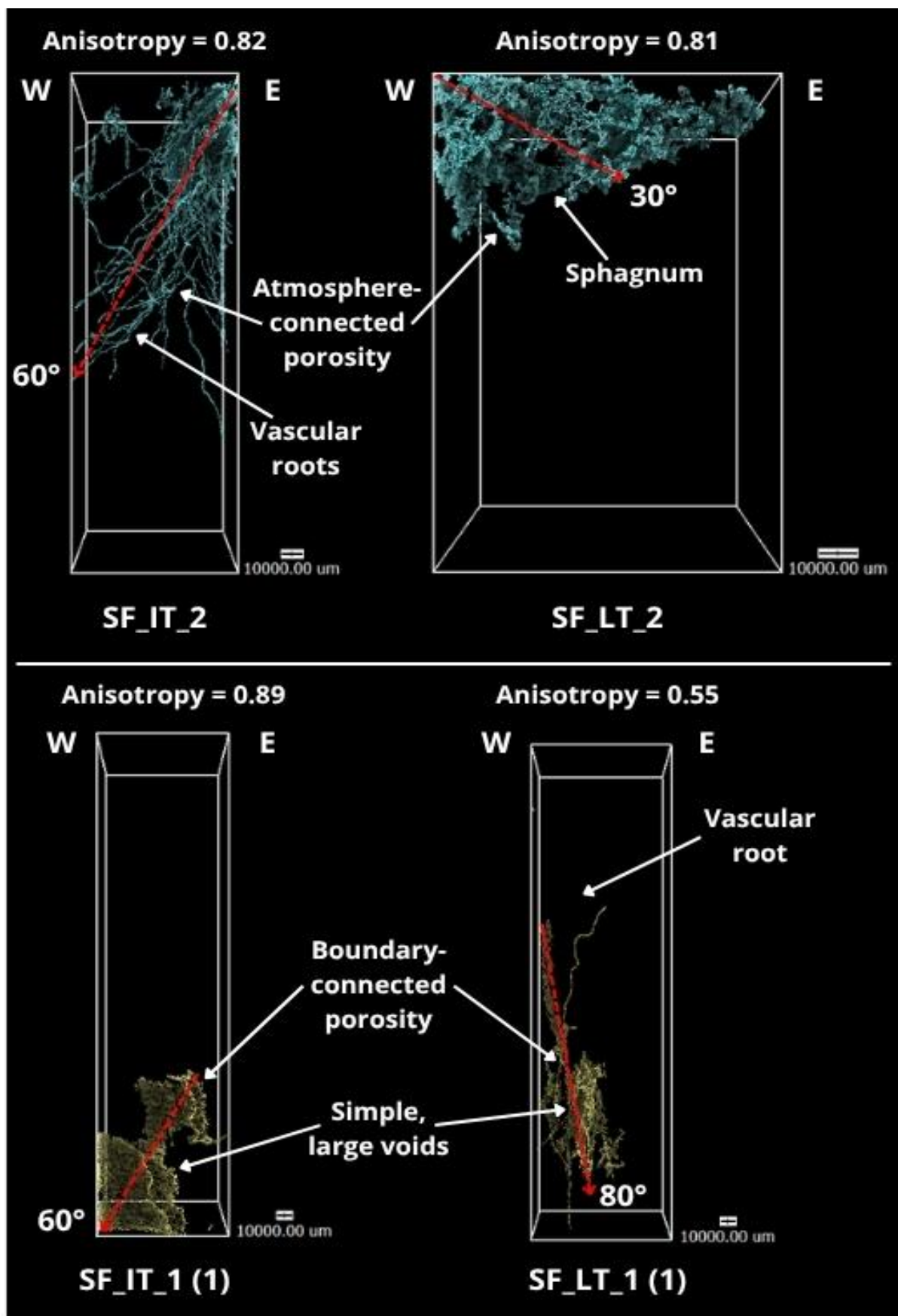
Figure 7.32: 3D visualisations of select dominant active pores illustrating anisotropy and inferred direction: a) SF_IT_2 and SF_LT_2 atmosphere-connected pores; b) SF_IT_1 (1) and SF_LT_1 (1) boundary-connected pores.

337

7.4.5 Summary of Structural Efficiency and Functional Implications

While pore size indicates functional capacity, the network efficiency of dominant active pores demonstrates functional behaviour beyond volume, providing additional context for interpreting exchange and retention:

Pore shape:

- Isolated pores were predominantly compact, consistent with gas bubbles from decomposition, confirming previous interpretations of decomposition processes (Sections 7.1; 7.2).

- Dominant atmosphere-connected pores were typically elongate, supporting vertical water infiltration and gaseous exchange.

- Elongate shapes in younger and non-turved cores suggest increased drainage potential, while platy or compact forms in older turved samples indicate retention over time, or structural collapse in the case of BC_Deg.

Pore complexity:

- Atmosphere-connected pore complexity generally increased with volume, particularly in older turved cores, indicating the development of more tortuous, retentive structures, challenging earlier volume-based interpretations of rapid exchange.

- Boundary-connected pore complexity was volume-independent and declined with restoration age, suggesting reduced drainage capacity and emerging stratification.

Pore connectivity:

- Atmosphere-connected pores exhibited consistently negative Euler numbers, which became more negative with volume, indicating well-connected, complex infiltrative networks supporting retention (alongside branch number).

- Boundary-connected pores exhibited less negative values, indicating simpler lateral flow networks. Reductions in older turved cores suggest partial structural integration, but legacy restoration impacts remained.

Pore anisotropy:

- Atmosphere-connected pores were generally isotropic in older turved sites, supporting regulated vertical infiltration and surface water retention over time.

- Boundary-connected pores remained anisotropic and frequently gully-oriented, consistent with drainage and carbon loss. Restoration did not disrupt these systems, even after ~5 years.

Findings demonstrate dominant pores change in structure and function with restoration age and technique. Turving promotes the development of more complex, connected, and isotropic atmosphere-connected networks, increasing vertical water infiltration and retention, characteristic of a functioning acrotelm. Boundary-connected pores often retain anisotropic, drainage-aligned traits, indicating incomplete suppression of legacy flow pathways and suggesting ongoing disturbance within the catotelm.

7.5 Chapter Synthesis and Discussion

By visualising and quantifying pore networks in degraded, near-natural, and restored blanket peatlands, μCT enabled key interpretations of functional behaviour, including water infiltration, retention, solute transfer, and gas exchange, beyond the resolution of surface (Chapter 5) or bulk chemical assessments (Chapter 6). Distinct structural features observed across cores helped explain these behaviours and evaluate restoration success. Figures 7.33 to 7.36 present summary illustrations for the near-natural target, degraded baseline, and two restored samples representing opposite ends of the structural recovery spectrum. These visualisations demonstrate how pore structures relate to functional capacity, exchange and retention potential, and network efficiency, and highlight the structural features most critical to sub-surface function (Figure 7.1).
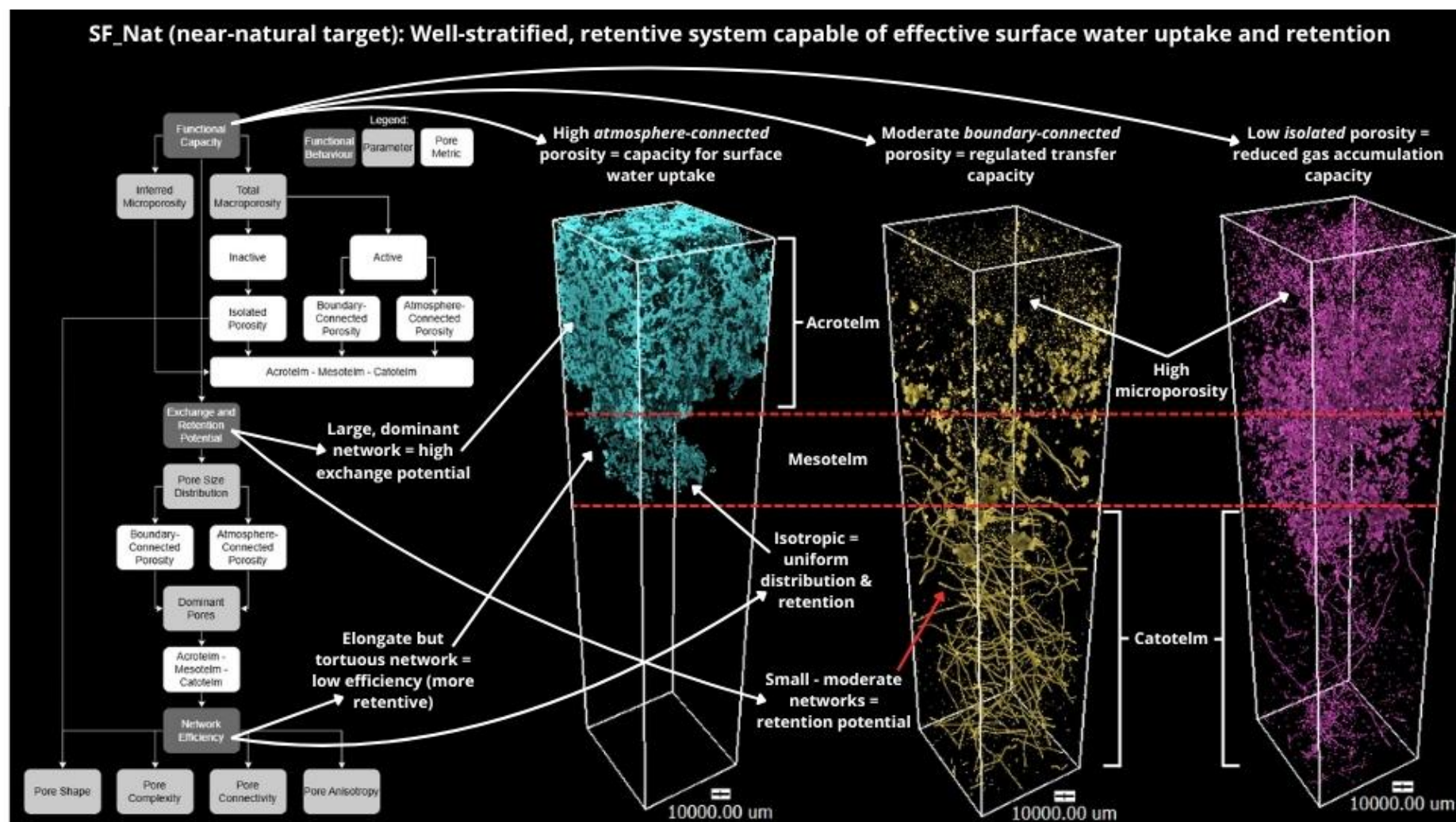
Figure 7.33: Summary of pore network structure and functional behaviour in the near-natural target (SF_Nat), showing stratified structure and features indicative of hydrological retention and carbon accumulation.

The near-natural target (SF_Nat) displays a well-stratified profile with clearly defined acrotelm, mesotelm, and catotelm layers (Figure 7.33). **Atmosphere-connected porosity** dominates near the surface, forming a vertically isotropic, tortuous pore network facilitating surface water infiltration (Holden *et al.*, 2001; Holden, 2005b), retention (Morris *et al.*, 2019), and regulated gas exchange (Kettridge and Binley, 2008), indicative of an intact, functional acrotelm transitioning into the mesotelm (Section 7.1). These features support saturated conditions favourable for peat-forming vegetation (e.g., *Sphagnum*) and contribute to long-term carbon accumulation through retarded decomposition (Chapter 2; Section 2.1.2). At depth, **boundary-connected porosity** is minimal and restricted to small-moderate networks (Section 7.3.1), indicating limited potential for rapid sub-surface transfer (e.g., drainage or solute loss through erosion). This suggests a more hydrologically retentive profile, with reduced exchange and greater capacity for water and carbon storage. **Isolated porosity** is also low, with compact geometries (Section 7.4.1), implying minimal gas bubble formation and vertical connectivity. Notably, the number of isolated pores are concentrated within the upper 15-20cm, possibly representing hyaline cells within intact *Sphagnum*, further supporting high surface productivity and net carbon accumulation (Chapter 2; Section 2.1.2). The combination of ineffective boundary-connected and isolated porosity in the sub-surface suggest an intact catotelm capable of carbon storage.

These features confirm SF_Nat as the structural target for functional recovery. It demonstrates how a stratified, vertically connected pore system underpins key hydrological and gaseous processes, such as water infiltration, retention, and diffusion resistance, required to maintain saturation and promote carbon accumulation in near-natural peatlands (Chapter 2; Sections 2.1, 2.2).
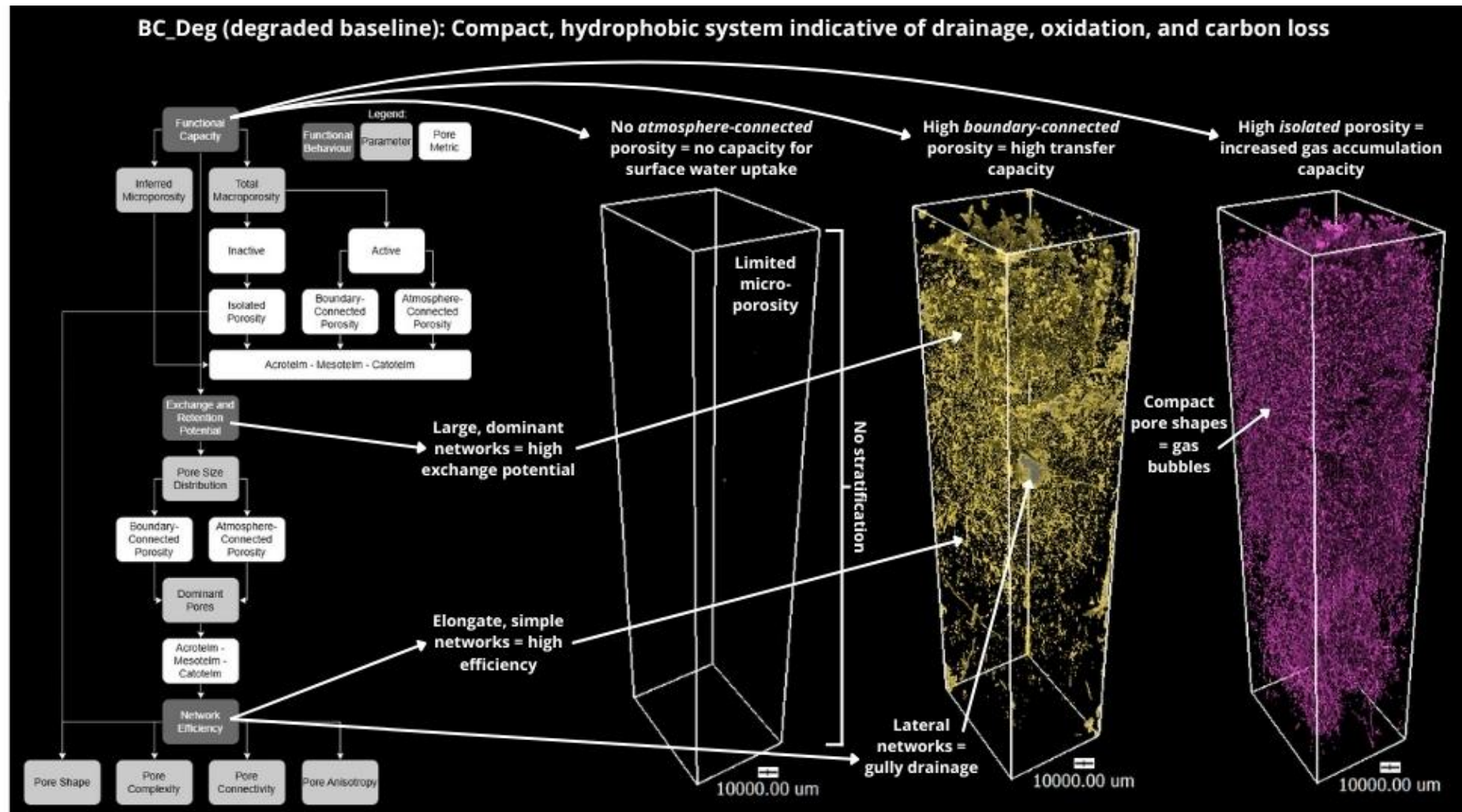
Figure 7.34: Summary of pore network structure and functional behaviour in the degraded baseline (BC_Deg), showing compact structure, lateral boundary-connected networks, and features indicative of drainage, fragmentation, and carbon loss.

The degraded baseline (BC_Deg) exhibits a compact, unstratified structure, lacking an acrotelm – mesotelm – catotelm (Figure 7.33). **Atmosphere-connected porosity** is absent, indicating limited capacity for surface water uptake (Section 7.1). This confirms absence of a functional acrotelm and mesotelm and suggests a hydrophobic surface layer contributing to poor saturation, restricted support for peat-forming species, and increased susceptibility to gas diffusion and desiccation (Chapter 2; Sections 2.2; 2.3.1).

The profile is dominated by **boundary-connected porosity**, forming laterally or gully-aligned elongate pores extending throughout (Sections 7.1; 7.3.1). These large, simple features promote sub-surface drainage, increase solute transfer potential (e.g., dissolved and particulate organic carbon), and reduce water retention. Pore size distribution supports this, showing four large, dominant pores facilitating exchange rather than storage (Section 7.4.2).

Isolated porosity is also increased and distributed throughout, with compact, rounded geometries consistent with gas bubble formation in unsaturated conditions (e.g., CO_2; Section 7.4.1). Increased isolated porosity suggests structural fragmentation and limited vertical continuity. Additionally, low inferred microporosity, particularly near the surface, further reduces the profile's capacity to retain water.

These structural characteristics support a system incapable of effective retention and highly susceptible to aerobic decomposition under unsaturated conditions. Dominance of simple, lateral boundary-connected pores, increased isolated porosity, and lack of vertical structure support high potential for drainage, rapid decomposition, and long-term carbon loss (Chapter 2; Sections 2.1.2; 2.4).
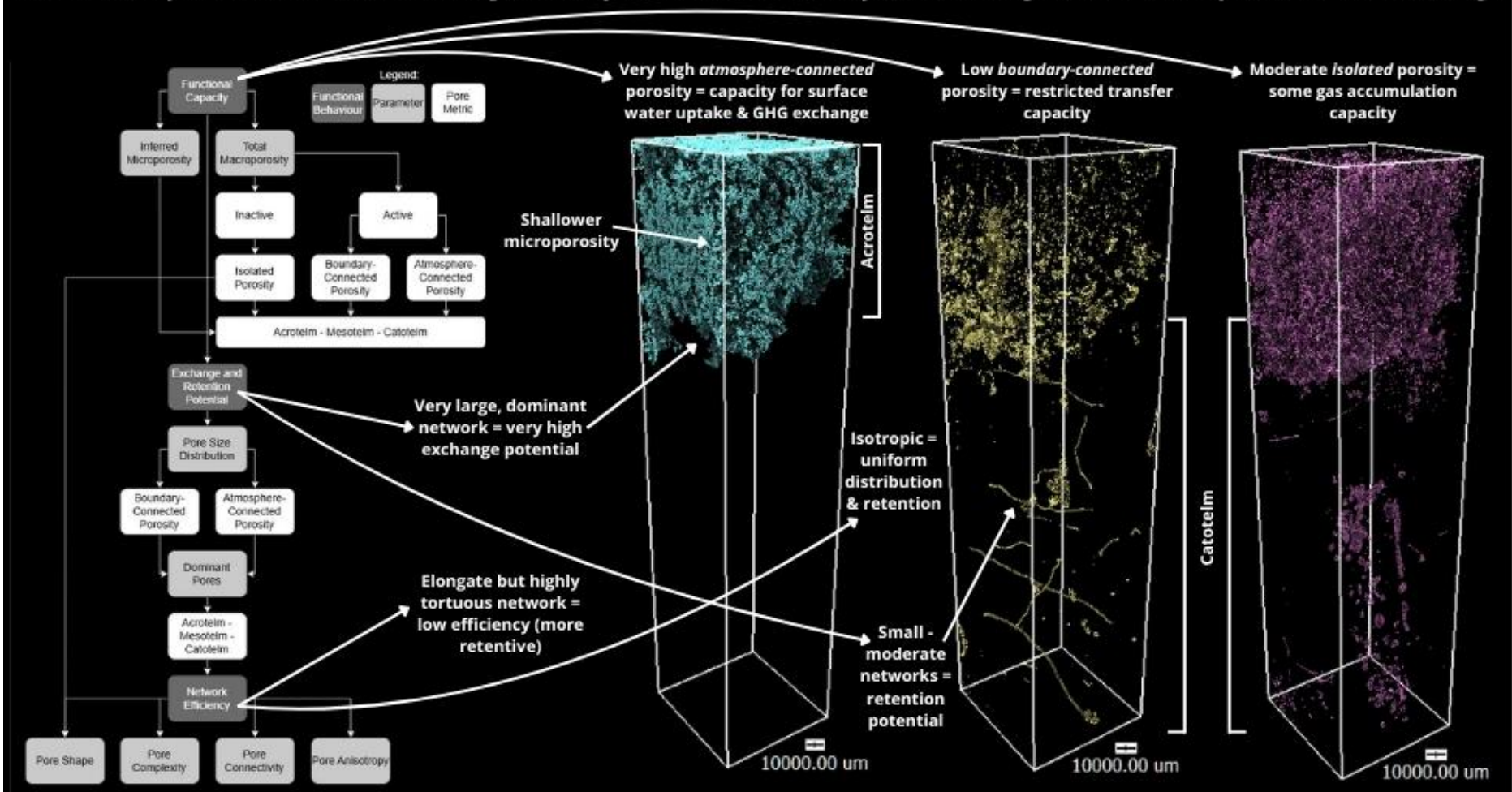
Figure 7.35: Summary of pore network structure and functional behaviour in the restored core BC_LT_1 (Bampton Common – Local Turving (1)), showing a developed acrotelm and reduced drainage features, but limited mesotelm development and structural recovery at depth.

Bampton Common – Local Turving (BC_LT_1) exhibits a partially stratified structure, with a developed acrotelm but no distinct mesotelm (Figure 7.34). **Atmosphere-connected porosity** dominates near the surface, forming a large, continuous, and tortuous network (Section 7.4.3). This indicates effective surface water uptake and a re-established functional acrotelm. However, its significant volume (nearly double SF_Nat) may support advective gas transport, increasing the potential for direct GHG exchange with the atmosphere (Chapter 2; Sections 2.1.2; 2.2.2). **Boundary-connected porosity** is reduced, comprising small–moderate pores comparable to SF_Nat (Section 7.3.1), indicating lower drainage potential and increased retention relative to BC_Deg. **Isolated porosity** is moderate, lower than in BC_Deg but still greater than SF_Nat, suggesting reduced aerobic decomposition but continued GHG production. Combined with extensive surface-connected networks, this supports potential for ongoing emissions. Inferred microporosity is shallow at depth, reflecting incomplete recovery of the lower profile. Absence of a defined mesotelm, characterised by intermediate microporosity and boundary-connected volume, suggests limited buffering between acrotelm and catotelm, potentially restricting long-term hydrological and carbon accumulation. This may reflect persistent over-compaction of turves even after ~5 years and highlights practical implications for improved placement (Section 7.2.3).

BC_LT_1 represents a functionally improved but structurally transitional system, showing divergence from the degraded baseline and partial alignment with the near-natural target. Dominant atmosphere-connected, and reduced boundary-connected and isolated pores indicate progressing recovery, though limitations at depth may restrict full functional restoration.
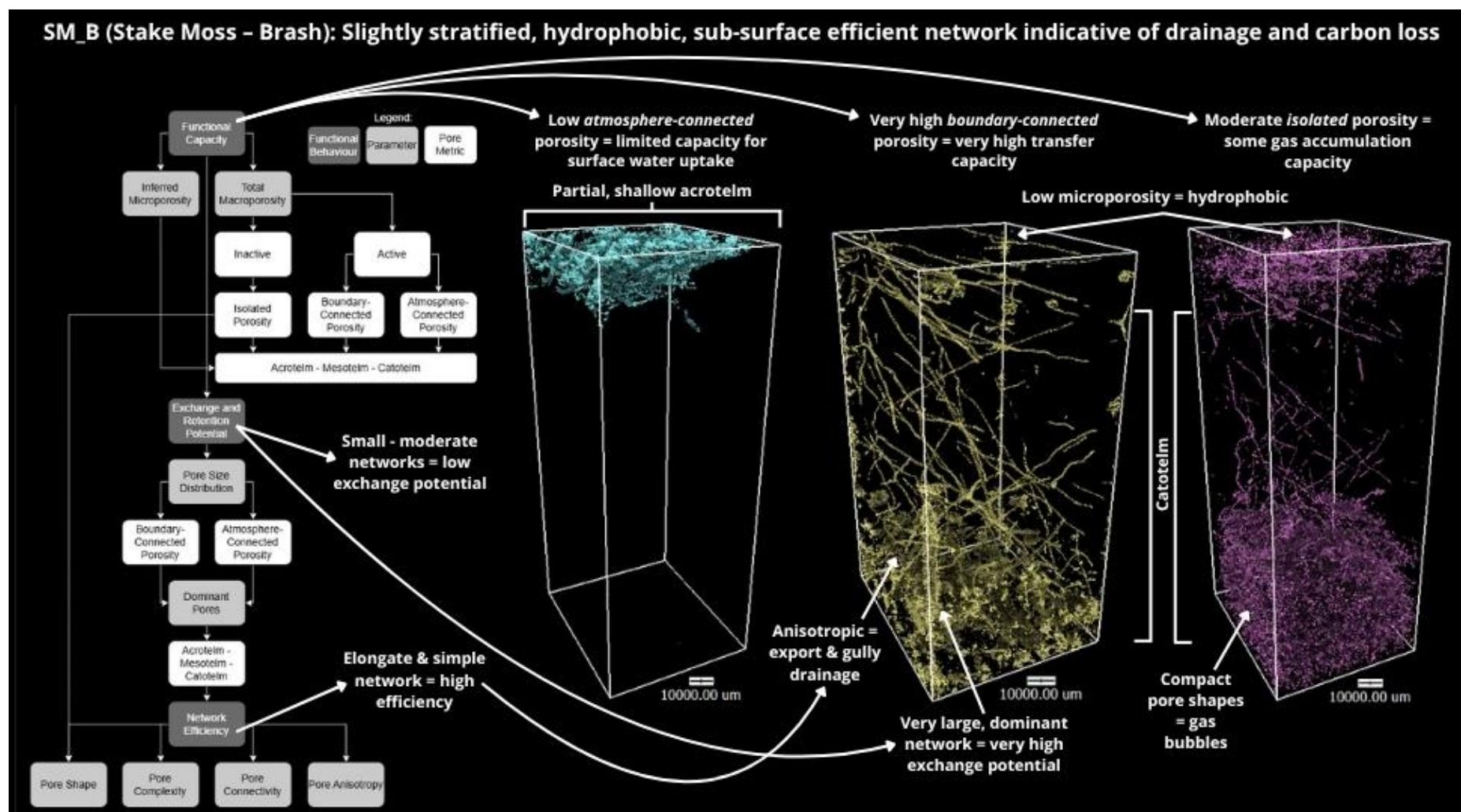
Figure 7.36: Summary of pore network structure and functional behaviour in the restored core SM_B (Stake Moss – Heather Brash Spreading), showing limited structural recovery, with dominant boundary-connected porosity and minimal microporosity indicative of continued drainage and carbon loss.

Stake Moss – Brash (SM_B) exhibits a poorly stratified profile, with a shallow, underdeveloped acrotelm and no mesotelm development (Figure 7.35). **Atmosphere-connected porosity** is low, limited to small, discontinuous pores near the surface (Section 7.2.3). This suggests restricted surface water infiltration and a weakly functional acrotelm, indicative of a relict hydrophobic layer contributing to drying and reduced support for peat-forming vegetation (Chapter 2; Sections 2.2; 2.3.1). **Boundary-connected porosity** dominates, forming a large, elongate, anisotropic network aligned with gully channels. While these structures differ slightly from BC_Deg, showing more vertical branching associated with vascular heather, they still promote efficient drainage, solute export, and advective gas exchange via roots (Moore *et al.*, 2002). Pore size and efficiency confirm these features facilitate rapid transfer, indicating limited hydrological recovery. **Isolated porosity** is moderate, with compact shapes distributed throughout (Section 7.4.1). Its reduction compared to BC_Deg suggests some influence of restoration on limiting aerobic decomposition, but its persistence indicates ongoing GHG production, similar to BC_LT_1. Distribution across surface and depth suggests CO_2 and CH_4 may be produced. Microporosity is minimal, further contributing to hydrophobicity and low retention.

These features describe a functionally limited system, structurally closer to the degraded baseline than the near-natural target or turved restorations. Persistence of large boundary-connected pores, minimal microporosity, and weak acrotelm formation indicate continued drainage, low saturation, and high carbon loss potential. Despite intervention, the lack of pore network recovery highlights the limited structural effectiveness of heather brash, particularly at depth, and reinforces the importance of restoration technique in supporting sub-surface functional recovery.

Figures 7.33–7.36 demonstrate the application of µCT in visualising, quantifying, and inferring how pore structure influences functional behaviour, and begin to hypothesise how restoration (across time and technique) affects sub-surface recovery. However, supporting these structural inferences with metrics of functional processes is required to evaluate restoration effectiveness. This involves correlating features such as atmosphere-connected porosity with bulk chemical indicators of saturation, including moisture content and redox potential (Eh) (Chapter 6), to confirm establishment of a functional acrotelm (Clymo, 1984; Clymo and Bryant, 2008). These relationships are explored at the start of Chapter 9 and provide a basis for evaluating restoration success.

µCT enabled a more detailed evaluation of restoration impacts by clearly distinguishing degraded and near-natural conditions and revealing structural differences across restoration techniques and ages; beyond those captured by surface (Chapter 5) or bulk chemical indicators (Chapter 6). These insights begin to explain *how* and *why* restored sites respond differently, highlighting the mechanisms underpinning functional recovery. Findings support a deeper understanding of restoration effectiveness and inform subsequent evaluation of specific intervention carbon costs and outcomes.

7.5.1 Lag in Deeper Sub-Surface Structural Recovery

µCT revealed structural recovery in the catotelm often lags behind near-surface changes in the acrotelm, which may be more closely associated with surface features (Chapter 5). For example, turving typically promoted acrotelm development through increased atmosphere-connected porosity, inferred to support *Sphagnum* succession (Figures

7.33–7.36). This may contribute to higher JNCC (2009) surface condition scores (explored in Chapter 9). However, deeper structural features, such as persistent boundary-connected or isolated porosity, remained only partially recovered, even after a decade. *This lag may help explain continued CH$_4$ emissions following restoration and the variable functional response observed across sites (Chapter 2; Section 2.4.2; Strack and Zuback, 2013; Cooper et al., 2014; Vanselow-Algan et al., 2015; Alderson et al., 2019).*

7.5.2 Role of the Mesotelm

µCT enabled clearer distinction of the acrotelm – mesotelm – catotelm profile than bulk and chemical indicators (Chapter 6), providing support for the diplotelmic model (Chapter 2; Section 2.1.1; Ingram, 1978; Clymo, 1984; Clymo and Bryant, 2008). An intact mesotelm, characterised my intermediate microporosity and moderate boundary-connected porosity, was observed only in the near-natural target. In restored sites, this transitional layer was typically absent or poorly developed, even after a decade, contributing to continued divergence from near-natural conditions. *Its absence helps explain delayed functional recovery (as discussed above) and carbon accumulation, reinforcing the mesotelm's role as a structural and hydrological buffer within the profile (Chapter 2; Section 2.1.1).* Moreover, its development appeared contingent on restoration technique, where over- or under-compression of turves may restrict formation, highlighting its potential as a structural metric for evaluating technique effectiveness.

7.5.3 Linking Pore Structure to Carbon Accumulation Potential

Visualising pore size, complexity, and connectivity helped identify structural conditions likely to influence carbon accumulation (Chapter 2; Section 2.1.2). Stratified, retentive

pore networks in near-natural peat (Figure 7.33) suggest conditions favourable for long-term carbon storage by supporting saturation, limiting oxygen availability, and reducing gas diffusion (Clymo, 1984; Belyea and Malmer, 2004; Clymo and Bryant, 2008). In contrast, degraded and non-turved restored cores (Figures 7.34; 7.36) exhibited drainage-prone structures, including dominant boundary-connected porosity and deep, oxidising profiles, potentially associated with greater CO_2 loss and CH_4 diffusion (Waddington and Price, 2000; Strack *et al.*, 2005; Evans *et al.*, 2016). *These structural patterns may help explain observed variation in GHG emissions and carbon accumulation potential (Chapter 2; Section 2.4.2) and provide a basis for interpreting bulk chemical trends in Chapter 9. They also inform the evaluation of restoration carbon costs and trade-offs in Chapter 8.*

7.5.4 Technique Effectiveness and Practical Considerations

µCT enabled structural differences between restoration techniques to be inferred, particularly pore connectivity and vertical continuity. Turved sites appeared more effective than heather brash spread in supporting the development of a functional acrotelm (Figure 7.35). However, variation between replicate cores, such as a 'porosity gap' or sharp changes in porosity between turves and underlying peat in SF_IT_1 and SF_LT_2, suggests implementation quality may influence outcomes. Similar features observed at Bampton Common indicate such discontinuities can persist for ~5 years, potentially limiting vertical connectivity and delaying mesotelm formation (Section 7.5.2).

Findings suggest practical refinements, such as applying moderate pressure during turve placement or using tracked machinery, may improve bonding, suppress drainage, and promote stratified development. While µCT indicates some interventions, particularly turving, may enhance sub-surface function (e.g., large, tortuous, isotropic atmosphere-connected pores), the carbon costs of implementation remain uncertain. For example, although machinery tracking may support hydrological recovery, associated emissions are not currently captured in standard accounting. As such, the relationship between structural improvement and the overall carbon balance of restoration projects remains unknown and is explored further in Chapter 8.

Table 7.10: Summary of research questions addressed in Chapter 7.

Research Question	Contribution/Implications
Research Question 1: Can surface indicators be used as a proxy to infer changes in sub-surface structure and function post-restoration?	Some alignment was observed between surface features (e.g., *Sphagnum*) and atmosphere-connected porosity near the surface (Chapter 9). However, deeper structural recovery (e.g., mesotelm or catotelm development) often lagged behind, indicating surface indicators may not reliably capture sub-surface function (Chapter 9).
Research Question 2: To what extent does the restoration of degraded blanket peatlands support the recovery of sub-surface structure and function?	µCT revealed partial sub-surface recovery following restoration, with turved sites showing greater development of atmosphere-connected porosity and stratification. However, key features such as mesotelm structure, microporosity, and vertical connectivity often remained underdeveloped, even after a decade. Findings highlight the importance of technique and time in driving sub-surface functional recovery.
Research Question 3: How do the carbon costs of interventions impact the carbon benefit potential of restoration?	Identified structural differences between techniques which may influence functional carbon outcomes (e.g., water retention, GHG emissions). While turving promoted favourable pore structures, potential carbon costs are not yet accounted for. Findings provide a basis for evaluating carbon trade-offs in Chapter 8.

Chapter 8: Evaluating the Carbon Costs of UK Blanket Peatland Restoration

The data presented here are currently under review for publication: Brennand, J.R., Barker, J.A., Manns, H. & Carr, S.J., 2025. Evaluating the carbon costs of UK blanket peatland restoration. Carbon Management. Taylor & Francis, and have been incorporated into the IUCN UK Peatland Code Carbon Savings Calculator (IUCN, 2025a).

Previous chapters have focussed on the condition and function of peatlands, evaluating ecological (Chapter 5), bulk chemical (Chapter 6), and structural (Chapter 7) responses to restoration across the surface and sub-surface. However, a complete assessment of restoration effectiveness requires evaluation of the interventions, specifically the carbon costs associated with their implementation (Chapter 1; Section 1.1). As outlined in Chapter 2; Section 2.5, a wide range of restoration techniques are applied across UK blanket peatlands, with multiple techniques prescribed to achieve the same objective (Thom *et al.*, 2019; NatureScot, 2021), yet their relative carbon and functional efficiency remains unknown, limiting understanding of their effectiveness and development.

Restoration is driven by climate policy objectives, particularly the aim of reducing carbon emissions from degraded peatlands (Chapter 2; Section 2.4.1). While chapter 7 provided a more detailed evaluation of how effectively different techniques restore sub-surface structure and function, offering greater sensitivity than existing surface (Chapter 5) and bulk chemical (Chapter 6) indicators, the carbon costs of implementing interventions have yet to be assessed. Addressing this gap introduces a new dimension to restoration

evaluation by enabling assessment of net carbon benefit, which integrates functional recovery (carbon savings) and emissions associated with intervention delivery (Chapter 2; Section 2.7).

Current carbon accounting frameworks, such as the IUCN UK Peatland Code, apply fixed deductions to projected carbon savings to account for uncertainty, leakage emissions, and the carbon costs associated with restoration delivery (Chapter 2; Section 2.7; IUCN, 2024b). A 10% deduction for carbon costs was previously applied; however, this figure had no empirical basis, potentially leading to over or under-estimation of project carbon savings. Acknowledging this gap, a Life Cycle Assessment (LCA) approach was adopted to calculate the CO_2eq emissions associated with the most common blanket peatland restoration interventions (Table 8.1). The assessment aimed to provide an evidence-based foundation for evaluating net carbon benefit and to support the credibility of carbon credit schemes and blended finance models for UK peatland restoration (Dunn and Freeman, 2011; Reed *et al.*, 2013, 2022; Bonn *et al.*, 2014; Moxey *et al.*, 2021; Chapter 2; Sections 2.4.1; 2.7).

Table 8.1: Common blanket peatland restoration interventions as described in Thom *et al.* (2019) and NatureScot (2022), classified by their fundamental roles in the restoration process.

Restoration Objective	Technique	Intervention	Description	Evidence of Application
Rewet	Gully/grip (drain) blocking	Heather bale dams	Used to block small grips. Installable by hand, helicopter, or machinery.	Armstrong *et al.* (2009)
		Peat dams	Made of humified peat, constructed with machinery for blocking small to medium-sized drains.	Armstrong *et al.* (2009); Green *et al.* (2017)
		Plastic piling/dams	Employed for blocking drains of varying sizes. Installable manually. Large composite dams (plastic piling plus humified peat) require machinery.	Armstrong *et al.* (2009)
		Stone dams	Used to obstruct large gullies and capture eroding sediment. Often delivered and installed by helicopter.	Armstrong *et al.* (2009); Howson *et al.* (2023)
		Timber dams	Installed into the peat on both sides of small to medium-sized drains to impede water and sediment flow. Installed manually or with machinery.	Howson *et al.* (2023)
	Surface/shallow bunding	Coir logs	Form shallow barriers across small gullies and areas with flowing water. Delivered by helicopter and installed by hand.	Parry *et al.* (2014)
		Peat bunds	Used to elevate water levels across extensive areas or block small gullies. Installed with machinery, typically excavators.	Parry *et al.* (2014); Green *et al.* (2017)
Revegetate	Direct establishment	Plug planting	Hand-installed plugs of peat-forming species like *Sphagnum* moss, at a rate of ~1 plug per 2m^2, across bare peat areas.	Caporn *et al.* (2017)
		Reprofiling + local turving (within excavator reach)	Using an excavator to reshape steep slopes to ~33°, redistributing ~1m^2 turves of peat from the gully area.	Holden *et al.* (2017)
		Reprofiling + imported turving (borrowed)	Using an excavator to reshape steep slopes to ~33°, redistributing ~1m^2 turves of peat from borrowed areas.	Parry *et al.* (2014); Holden *et al.* (2017)
	Indirect establishment	Geotextile (Geojute) application	Manually installed coir mesh to promote vegetation growth, delivered by helicopter, frequently accompanied by the spreading of heather brash.	Watts (2020)
		Heather brash spreading	Spread over bare peat areas to foster species establishment. Applied manually, with machinery, or aerially.	Parry *et al.* (2014); Watts (2020)
		Lime & fertiliser spreading	Distributed to raise pH and supply nutrients for vegetation growth in bare peat pans. Preferably applied by aerial delivery or machinery.	Shuttleworth *et al.* (2019)

8.1 Life Cycle Assessment Approach

The Life Cycle Assessment (LCA) evaluates three phases of peatland restoration, aligning with key LCA principles and scopes (Horne *et al.*, 2009; Hauschild, 2017; Chiu *et al.*, 2022): 1) raw exotic materials; 2) transportation of materials and project machinery; and 3) installation (Figure 8.1).
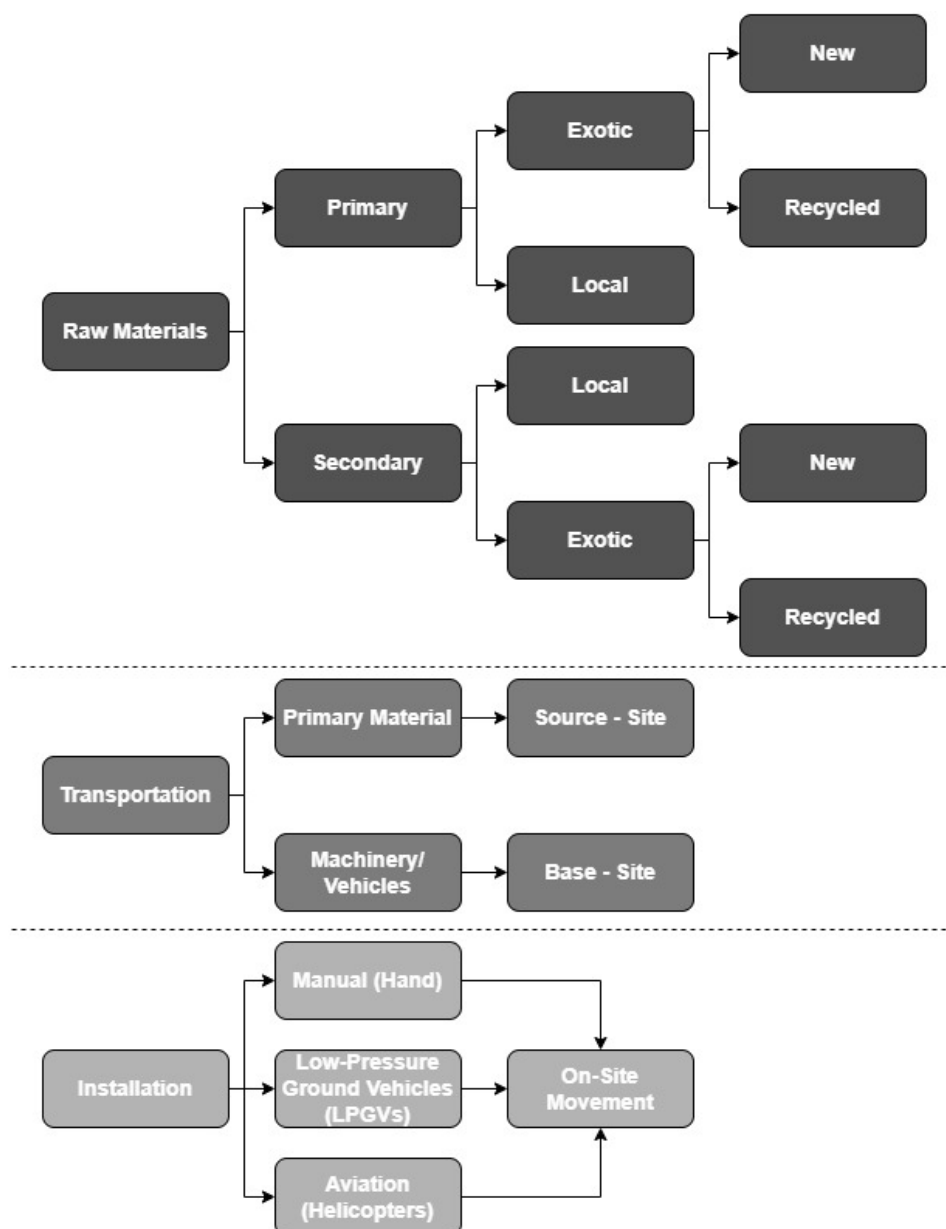
Figure 8.1: Elements considered in calculating the carbon costs for each assessed blanket peatland restoration approach. Scopes 1 and 2 emissions are included as well as some scope 3 emissions, including the direct emissions from products and vehicles (transport and distribution) (Chapter 3; Section 3.6; Figure 3.34).

Raw materials comprise primary and secondary exotic materials. Raw material costs include intermediate transport of primary materials, specifically movements around harvesting sites or depots. New and recycled variants of primary and secondary materials are considered, including the re-purposing of plastic (Alsabri and Al-Ghamdi, 2020). Transportation involves conveying primary materials to the site, alongside machinery and workers. Installation comprises the implementation of interventions, utilising manual (by hand), machinery-assisted (e.g., low-pressure ground vehicles), or helicopter-assisted approaches. Tables 8.2 and 8.3 summarise the LCA for rewetting and revegetation interventions assessed. This approach excludes 'end-of-life' (disposal) and supplier Scope 3 emissions but includes direct emissions from products and vehicles (Figure 8.1). This supports a consistent methodology across interventions, enabling robust comparisons of relative carbon costs across restoration approaches, though absolute carbon costs may be underestimated.

Table 8.2: Main LCA elements for each rewetting intervention, based on direct field observations and guidance in Thom *et al.* (2019) and NatureScot (2022). Primary data collection informs the delivery, transport, and install vehicle elements, while secondary data informs the 'average' intervention and material elements.

Average Intervention	Raw Materials	Transportation (Return)	Installation (Return/Round-Trip)	LCA References
Heather Bale Dam (1.5m long x 0.8m deep)	***Primary:*** - Harvested heather (exotic – translocation)	***Primary Material*** - Source (translocation site) – site (average 50% laden >17t rigid) ***Machinery (One-Time):*** - Origin – site (average 0% laden helicopter) - Depot – site (average 100% laden articulated (LPGV)) - Depot – site (average 100% laden 4x4 + trailer (argocat/softrack)) ***Workers (Daily):*** - Depot – site (average 50% laden 4x4)	***Manual (Hand):*** - Average 50% argocat/softrack onsite ***LPGV:*** - Average 9-14t excavator onsite and between interventions - Average 50% argocat/softrack onsite ***Helicopter:*** - Average 50% laden helicopter onsite - Average 50% argocat/softrack onsite	***Machinery/Vehicles:*** DESNZ (2023); European Rental Association (2023); Grogan & Matthews (2007); Rindlisbacher & Chabbey (2015)
Peat Dam (1.5m long x 1.2m deep)	***N/A***	***Machinery (One-Time):*** - Depot – site (average 100% laden articulated (LPGV)) - Depot – site (average 100% laden 4x4 + trailer (argocat/softrack)) ***Workers (Daily):*** - Depot – site (average 50% laden 4x4)	***Manual (Hand):*** - Average 50% argocat/softrack onsite ***LPGV:*** - Average 9-14t excavator onsite and between interventions - Average 50% argocat/softrack onsite	***Machinery/Vehicles:*** DESNZ (2023); European Rental Association (2023)
Plastic Piling/Dam (1.5m long x 1.2m deep)	***Primary:*** - PVC sheets (exotic – new or recycled): Includes 6 types with different thickness: Trench pile, EcoZ, Multilock, UltraU, Europile, UltraZ	***Primary Material:*** - Source (UK leading supplier) – site (average 50% laden 3.5t HGV) ***Machinery (One-Time):*** - Depot – site (average 100% laden articulated (LPGV)) - Depot – site (average 100% laden 4x4 + trailer (argocat/softrack)) ***Workers (Daily):*** - Depot – site (average 50% laden 4x4)	***Manual (Hand):*** - Average 50% argocat/softrack onsite ***LPGV:*** - Average 9-14t excavator onsite and between interventions - Average 50% argocat/softrack onsite	***Primary Materials:*** Alsabri *et al.* (2022); DESNZ (2023) ***Machinery/Vehicles:*** DESNZ (2023); European Rental Association (2023)
Stone Dam (775kg unit)	***Primary:*** - Gritstone (exotic)	***Primary Material:*** - Source (local quarry) – site (average 50% laden >17t rigid)	***Helicopter:*** - Average 50% laden helicopter onsite	***Primary Materials:*** Alsabri *et al.* (2022); Chrishna *et al.* (2011)

	Secondary: - Large dumpy bag (exotic - new or recycled)	**Machinery (One-Time):** - Origin – site (average 0% laden helicopter) - Depot – site (average 100% laden 4x4 + trailer (argocat/softrack)) **Workers (Daily):** - Depot – site (average 50% laden 4x4)	- Average 50% argocat/softrack onsite	**Machinery/Vehicles:** DESNZ (2023); European Rental Association (2023); Grogan & Matthews (2007); Rindlisbacher & Chabbey (2015)
Timber Dam (4 planks, 3m long x 0.75m deep)	**Primary:** - FSC timber (exotic – new or recycled)	**Primary Material:** - Source (UK leading supplier) – site (average 50% laden 3.5t HGV)	**Manual (Hand):** - Average 50% argocat/softrack onsite	**Primary Materials:** DESNZ (2023)
		Machinery (One-Time): - Depot – site (average 100% laden articulated (LPGV)) - Depot – site (average 100% laden 4x4 + trailer (argocat/softrack)) **Workers (Daily):** - Depot – site (average 50% laden 4x4)	**LPGV:** - Average 9-14t excavator onsite and between interventions - Average 50% argocat/softrack onsite	**Machinery/Vehicles:** DESNZ (2023); European Rental Association (2023)
Coir Log (2m long x 0.3m deep)	**Primary:** - Coir (exotic)	**Primary Material:** - Source (UK leading supplier) – site (average 50% laden 3.5t HGV)	**Manual (Hand):** - Average 50% argocat/softrack onsite	**Primary Materials:** DESNZ (2023); Grasselly *et al.* (2009)
	Secondary: - Chestnut stakes (exotic - new or recycled)	**Machinery (One-Time):** - Origin – site (average 0% laden helicopter) - Depot – site (average 100% laden 4x4 + trailer (argocat/softrack)) **Workers (Daily):** - Depot – site (average 50% laden 4x4)	**Helicopter:** - Average 50% laden helicopter onsite - Average 50% argocat/softrack onsite	**Machinery/Vehicles:** DESNZ (2023); European Rental Association (2023); Grogan & Matthews (2007); Rindlisbacher & Chabbey (2015)
Peat Bund (2m long x 0.3m deep)	**N/A**	**Machinery (One-Time):** - Depot – site (average 100% laden articulated (LPGV)) - Depot – site (average 100% laden 4x4 + trailer (argocat/softrack))	**Manual (Hand):** - Average 50% argocat/softrack onsite	**Machinery/Vehicles:** DESNZ (2023); European Rental Association (2023)
		Workers (Daily): - Depot – site (average 50% laden 4x4)	**LPGV:** - Average 9-14t excavator onsite and between interventions - Average 50% argocat/softrack onsite	

Table 8.3: Main LCA elements for each revegetation intervention (per hectare), based on direct field observations and guidance in Thom *et al*. (2019) and NatureScot (2022).Primary data collection informs the delivery, transport, and install vehicle elements, while secondary data informs the 'average' intervention and material elements.

Average Intervention	Raw Materials	Transportation (Return)	Installation (Return/Round-Trip)	LCA References
Plug Plants (mean of average edible flower and tomato) **Multiplier (ha): 5000**	***Primary:*** Edible flower/tomato cultivation (exotic - traditionally cultivated ('new') or sustainably cultivated ('recycled')) ***Secondary:*** Plastic packaging (exotic - new or recycled)	***Primary Material:*** - Source (UK leading supplier) – site (average 50% laden 3.5t HGV) ***Machinery (One-Time):*** - Depot – site (average 100% laden 4x4 + trailer (argocat/softrack)) ***Workers (Daily):*** - Depot – site (average 50% laden 4x4)	***Manual (Hand):*** - Average 50% argocat/softrack onsite	***Primary Materials:*** Almeida *et al*. (2014); Alsabri *et al*. (2022); Falla *et al*. (2022) ***Machinery/Vehicles:*** DESNZ (2023); European Rental Association (2023)
Reprofiling + Local Turves (33°, 1m²) **Multiplier (ha): 10000**	***N/A***	***Machinery (One-Time):*** - Depot – site (average 100% laden articulated (LPGV)) - Depot – site (average 100% laden 4x4 + trailer (argocat/softrack)) ***Workers (Daily):*** - Depot – site (average 50% laden 4x4)	***LPGV:*** - Average 9-14t excavator onsite and between interventions - Average 50% argocat/softrack onsite	***Machinery/Vehicles:*** DESNZ (2023); European Rental Association (2023)
Reprofiling + Imported Turves (33°, 1m²) **Multiplier (ha): 10000**	***N/A***	***Machinery (One-Time):*** - Depot – site (average 100% laden articulated (LPGV)) - Depot – site (average 100% laden 4x4 + trailer (argocat/softrack)) ***Workers (Daily):*** - Depot – site (average 50% laden 4x4)	***LPGV:*** - Average 9-14t excavator onsite, between interventions, and borrow pits - Average 50% argocat/softrack onsite	***Machinery/Vehicles:*** DESNZ (2023); European Rental Association (2023)
Geojute (72m² rolls) **Multiplier (ha): 139**	***Primary:*** - Coir (exotic) ***Secondary:*** - Chestnut stakes (exotic -	***Primary Material:*** - Source (UK leading supplier) – site (average 50% laden 3.5t HGV) ***Machinery (One-Time):*** - Origin – site (average 0% laden helicopter)	***Manual (Hand):*** - Average 50% argocat/softrack onsite ***Helicopter:***	***Primary Materials:*** DESNZ (2023); Grasselly *et al*. (2009) ***Machinery/Vehicles:*** DESNZ (2023); European Rental Association (2023);

	new or recycled) - Plastic pegs (exotic - new or recycled) - Steel pegs (exotic - new or recycled)	- Depot – site (average 100% laden 4x4 + trailer (argocat/softrack)) **Workers (Daily):** - Depot – site (average 50% laden 4x4)	- Average 50% laden helicopter onsite - Average 50% argocat/softrack onsite	Grogan & Matthews (2007); Rindlisbacher & Chabbey (2015)
Heather Brash (100kg bags) **Multiplier (ha): 2000**	**Primary:** - Harvested heather (exotic – translocation)	**Primary Material:** - Source (translocation site) – site (average 50% laden >17t rigid) **Machinery (One-Time):** - Origin – site (average 0% laden helicopter) - Depot – site (average 100% laden articulated (LPGV)) - Depot – site (average 100% laden 4x4 + trailer (argocat/softrack))	**Manual (Hand):** - Average 50% argocat/softrack onsite **LPGV:** - Average 9-14t excavator onsite - Average 50% argocat/softrack onsite	**Machinery/Vehicles:** DESNZ (2023); European Rental Association (2023); Grogan & Matthews (2007); Rindlisbacher & Chabbey (2015)
	Secondary: - Large dumpy bag (exotic - new or recycled)	**Workers (Daily):** - Depot – site (average 50% laden 4x4)	**Helicopter:** - Average 50% laden helicopter onsite - Average 50% argocat/softrack onsite	
Lime & Fertiliser (1t lime, 250kg fertiliser) **Multiplier (ha): 1**	**Primary:** - Ground lime (exotic - coal ('new') or gas fuelled extraction ('recycled')) - Average N:P:K fertiliser (exotic)	**Primary Material:** - Source (UK leading supplier) – site (average 50% laden >17t rigid & ferry (lime)) - Source (UK leading supplier) – site (average 50% laden 3.5t HGV (fertiliser))	**LPGV:** - Average 9-14t excavator onsite - Average 50% argocat/softrack onsite	**Primary Materials:** Alsabri *et al.* (2022); Flannery *et al.* (2022); Ouikhalfan *et al.* (2022)
		Machinery (One-Time): - Origin – site (average 0% laden helicopter) - Depot – site (average 100% laden articulated (LPGV)) - Depot – site (average 100% laden 4x4 + trailer (argocat/softrack))	**Helicopter:** - Average 50% laden helicopter onsite - Average 50% argocat/softrack onsite	**Machinery/Vehicles:** DESNZ (2023); European Rental Association (2023); Grogan & Matthews (2007); Rindlisbacher & Chabbey (2015)
	Secondary: - Large dumpy bag (exotic - new or recycled)	**Workers (Daily):** - Depot – site (average 50% laden 4x4)		

Restoration initiatives essentially rewet or revegetate sites (Table 8.1), with most projects using a mix of both. For rewetting, the approach adopted calculates carbon cost per intervention, appreciating different intensities of point measures per hectare may be required within individual projects (Table 8.2). For revegetation, the areal nature of interventions applied (Thom *et al.*, 2019; NatureScot, 2021) results in the estimation of carbon costs per hectare (Table 8.3). This approach offers flexibility based on the characteristics of each intervention type and enables grounded estimation of the total carbon costs of restoration at site level.

The choice of primary and secondary materials (new, recycled) along with installation method and resulting transportation, result in significant variation in carbon costs of restoration (Figure 8.2).
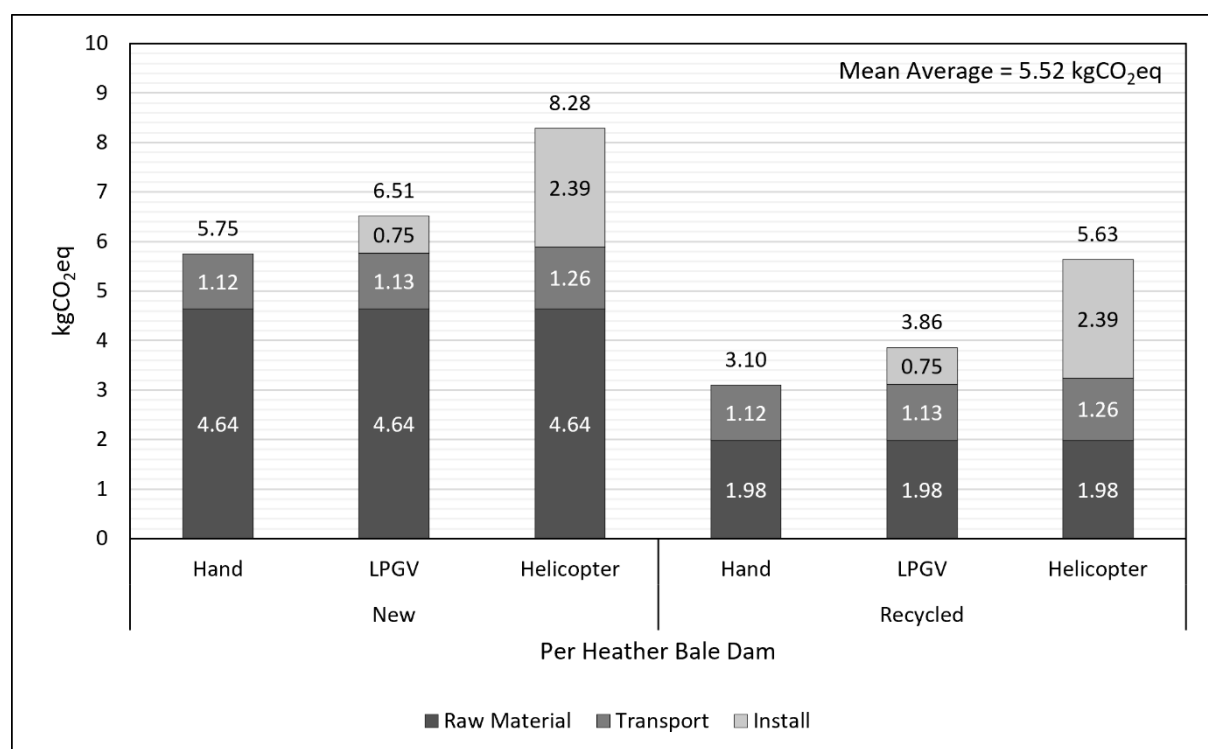
Figure 8.2: Example LCA breakdown for a heather bale dam as a rewetting intervention. The average carbon costs shown in this investigation represent the mean of all possible combinations (top right of the image).

8.1.1 Raw Materials

Raw materials comprise primary and secondary elements, where *secondary* materials are those facilitating transportation or installation of a **primary** element. For example, coir is the primary material in coir logs, while chestnut stakes act as **secondary** materials used to secure the logs (Table 8.2). **Local** materials refer to those acquired onsite, while **exotic** materials are non-local or imported through global supply chains, requiring transportation to the site, with **new** and **recycled** options. Carbon cost values ($kgCO_2eq$) for raw materials are derived from relevant LCA databases and literature (sources noted in Table 8.2 and Table 8.3). Where specific LCA data was unavailable, scope 1 and 2 emissions were calculated for traditional translocation harvesting methods (Table 8.2 and Table 8.3). For peat-forming plug plants like *Sphagnum*, an average value derived from the closest available comparators was applied (Table 8.3).

8.1.2 Transportation

Transportation mode and distances are always site-specific. Transportation can be partitioned into multiple stages:

1) Transportation of **primary materials** from source to the depot of a restoration contractor, or direct delivery to the site of restoration (Tables 8.2 and 8.3).

2) Transportation of **machinery** and **materials** from depot to site.

3) Commuting **personnel** from the organisation/depot to site.

The carbon costs of restoration interventions in this LCA represent indicative averages derived from 15 major peatland restoration projects (Table 8.4) conducted by three organisations (Moors for the Future, North Pennines National Landscape, Yorkshire Peat

Partnership). These averages represent return distance (km) and mode of transport for a 'typical' UK blanket peatland restoration effort. While these provide generalised transportation costs for individual interventions, case studies utilises actual distances and modes. Options for ground and water-based vehicles, specialist machinery, and helicopters (Tables 8.2 and 8.3) are given CO_2eq calculations based on UK Government data (DESNZ, 2023) for passenger and delivery vehicles, and the European Rental Association (2023) for specialist machinery such as excavators. Helicopter CO_2eq costs were also informed by Grogan & Matthews (2007) and Rindlisbacher & Chabbey (2015), as well as DESNZ (2023) for fuel consumption. Note that calculated CO_2eq costs do not include embedded emissions from vehicle or machinery manufacturing.

Table 8.4: Summary of the 15 peatland restoration projects used to derive average transport distances and details. Table includes the commissioning organisations, site locations, project years, and reference codes for detailed documentation listed in Appendix K.

Commissioning Organisation	Organisation Base	Site Name and Location (Grid Ref.)	Year of Project	Reference Code
Moors for the Future	Moorland Centre, Fieldhead, Hope Valley, S33 7ZA	Black Hill - SK 08772 91107	2003 - 2015	MFF-BlackHill
		Bleaklow - SK 09465 96069	2011 - 2015	MFF-Bleaklow
		Rishworth - SE 01301 17342	2010 - 2015	MFF-Rishworth
		Turley Holes - SD 98290 20720	2010 - 2015	MFF-TurleyHoles
North Pennines National Landscape	Martin Street, Stanhope, Bishop Auckland, DL13 2UY	Birkdale -NY 83839 27611	2018 - 2020	NP-Birkdale
		Dufton - NY 70000 28000	2018 - 2020	NP-Dufton
		Hartley Common - NY 82690 06707	2017 - 2019	NP-HartleyCommon
		Tynehead Fell - NY 76473 34716	2018 - 2020	NP-TyneheadFell
		Valance Lodge - NY 87251 34442	2020 - 2023	NP-VanceLodge
Yorkshire Peat Partnership	Unit 23, Skipton Auction Mart, Gargrave Road, Skipton, BD23 1UD	Fleet Moss - SD 86726 83509	2017 - 2023	YPP-FleetMoss
		Hareden Fell - SD 62040 49380	2018 - 2021	YPP-HaredenFell
		Holme House Fell - SD 57823 48167	2018 - 2021	YPP-HolmeHouseFell
		New House - SD 97317 80016	2018 - 2021	YPP-NewHouse
		Stake Moss - SD 93562 82482	2018 - 2021	YPP-StakeMoss
		Websters Meadow - SD 61232 50121	2018 - 2021	YPP-WebstersMeadow

Transport is categorised into one-time and recurring carbon costs (Tables 8.2 and 8.3). One-time costs cover machinery delivery, while recurring costs include daily worker transport. Transportation costs are calculated for interventions based on a 14-working-day period. This timeframe indicates typical operational constraints, service intervals, and equipment requirements, such as helicopter operating hours, which range from 75 to 180 (S. Ring, 2023, Heli-Lift Services, Oxford, UK, personal communication). This represents a continuous restoration block before machinery servicing is required, providing a logical basis for estimating average transport costs (servicing costs are not included). Optimal restoration efficiency is assumed within this framework to deliver consistent yet conservative estimates. However, in case study applications, actual project durations (in days) are used to offer greater accuracy in transportation cost calculations.

Considering return distances, a 50% load is applied for delivery vehicles transporting primary materials, as one leg of return journeys would be assumed unladen. Machinery transport assumes a 100% load, as LPGVs or access vehicles (e.g., argocat/softracks) will always be loaded onto transporters, except for helicopters. Workers are assumed to travel in an average 4x4 vehicle, with a 50% load to account for the maximum number of workers (4-5 individuals travelling). For primary material deliveries, the maximum vehicle load is accounted for, based on the number of interventions and their combined weight relative to the vehicle's capacity (Table 8.5). Exotic raw material sources are derived from restoration projects (Table 8.4). This approach provides a realistic and conservative estimate of transportation costs for each intervention. Note again actual distances are applied in case study applications.

Table 8.5: Maximum number of interventions (exotic) deliverable per trip based on the assumed delivery vehicle's load capacity. Note that one hectare of Geojute and heather brash spread requires two deliveries.

Intervention	Primary Material Weight (kg)	Assumed Delivery Vehicle and Maximum Load	Total Number of Interventions
Heather Bale Dam	40.00	>17t Rigid HGV = 17t	425
Plastic Piling/Dam	20.76	Average HGV = 3.5t	168
Stone Dam	750.00	>17t Rigid HGV = 17t	22
Timber Dam	96.00	Average HGV = 3.5t	36
Coir Log	9.00	Average HGV = 3.5t	388
Plug Plants	0.15	Average HGV = 3.5t	23333
Geojute	42.00 or 5838.00 per ha	Average HGV = 3.5t	83 or 139 per ha (requires 2 deliveries)
Heather Brash	100.00 or 20000.00 per ha	>17t Rigid HGV = 17t	170 or 200 per ha (requires 2 deliveries)
Lime & Fertiliser	1250.00 per ha (1000.00, lime; 250.00, fertiliser)	>17t Rigid HGV = 17t (lime) + Average HGV = 3.5t (fertiliser)	17 lime and 14 fertiliser

A systematic framework by which the transport carbon costs in this investigation (Equations 1-6) summarises the approach presented, offering a consistent approach to estimating emissions associated with material delivery, worker commuting, and machinery transport:

$$C_T = \frac{(C_{PM} \ X \ N_{PM}) + (C_W \ X \ D) + \ C_M}{N_1}$$

Equation 8.1

where:

- C_T: Total carbon cost per intervention ($kgCO_2eq$).

- C_{PM}: Carbon cost for transporting primary materials per trip ($kgCO_2eq$).

- N_{PM}: Number of trips required for primary materials, assuming maximum restoration efficiency over the project duration.

- C_W: Daily working commuting carbon cost ($kgCO_2eq$).

- D: Duration of the project (days; default = 14).

- C_M: One-time carbon cost for delivering machinery ($kgCO_2eq$).

- N_1: Number of interventions achievable within project duration.

$$C_{PM} = D_{PM} \; X \; E_V$$

Equation 8.2

where:

- D_{PM}: Distance travelled for material delivery (km).

- E_V: Emission factor for the vehicle used ($kgCO_2eq/km$).

$$N_{PM} = \frac{W_{PM}}{L_V}$$

Equation 8.3

where:

- W_{PM}: Total weight of primary materials (kg).

- L_V: Load capacity of the delivery vehicle (kg).

$$C_W = (D_W \ X \ E_{4x4}) + (D_V \ X \ E_s)$$

where:

- **D_W:** Daily commuting distance (km).

- **D_V:** Daily commuting distance onsite (km).

- **E_{4x4}:** Emissions factor for 4x4 vehicles (kgCO$_2$eq/km).

- **E_s:** Emissions factor for argocat/softrack

$$C_M = D_M \ X \ E_M$$

where:

- **D_M:** Distance for machinery delivery (km).

- **E_M:** Emissions factor for machinery transport vehicle (kgCO$_2$eq/km).

$$N_1 = \frac{D_{proj} \ X \ 8}{T_1}$$

where:

- **D_{proj}:** Project duration (days; default = 14).

- **8:** Conversion of days into working hours.

- **T_1:** Time required for one intervention to be installed (hours) (see below).

8.1.3 Installation

The CO_2eq installation cost is based on machinery time for point or area interventions, gathered from field trials and observations. For rewetting techniques, this includes moving between points (Tables 8.2 and 8.3) based on Thom *et al*. (2019) and NatureScot (2022). Movement costs between interventions are higher than for stationary use due to increased fuel consumption (DESNZ, 2023), varying with the machine used. Onsite worker movement is included in installation costs, using an average 50% laden argocat/softrack (loaded with workers and materials for one of the legs), assuming maximum restoration activity over the project duration (14-day or actual), forming the CO_2eq cost for manual installation. This aligns with a conservative estimate of total CO_2eq costs.

8.2 Carbon Costs of Restoration Interventions

Figure 8.3 shows carbon costs associated with individual rewetting interventions.
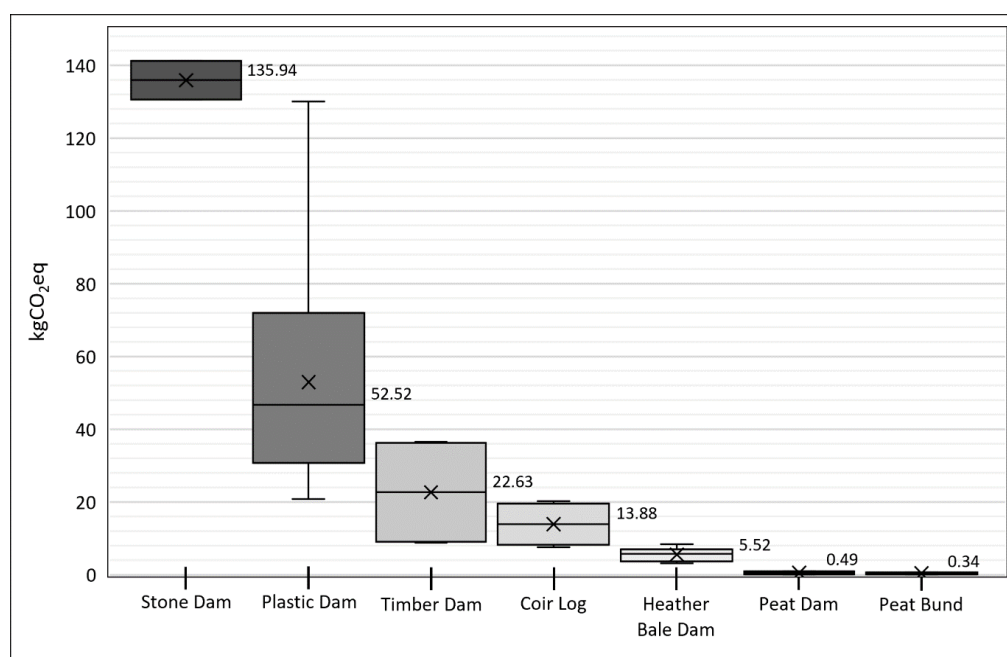
Figure 8.3: Carbon costs of various 'average' rewetting interventions evaluated. Crosses show the mean cost. Boxes represent the inclusive median, and whiskers indicate the range of minimum and maximum costs from all available options.

Carbon cost of rewetting interventions shows dramatic variation. For gully and grip blocking, stone dams have the highest carbon costs, some ~277 times greater than peat dams. For surface or shallow bunds, peat bunds have the lowest costs, while coir logs are ~40 times higher on average. Plastic dams show the greatest variance in carbon costs due to multiple sheet options and the use of recycled PVC or new materials (Table 8.2) (Alsabri and Al-Ghamdi, 2020).

Table 8.6 partitions each rewetting intervention into the three elements noted earlier. Interventions using exotic raw materials, (including translocated heather) demonstrate material costs that average ~71% of the total carbon costs. Installation usually constitutes the second-highest component of carbon cost across all interventions (~35% of total carbon cost), rising substantially if helicopters are deployed (Table 8.2). Across all rewetting interventions except those using local raw materials, transport is typically the smallest element of carbon costs at ~11%. Installation costs vary by intervention, dependent upon being hand, machine, or helicopter installed. Exceptions to this broad pattern include frequently hand-installed interventions like plastic and timber dams, and coir, where travel is greater due to dependence on global supply chains.

Table 8.6: Percentage breakdown of carbon costs for each 'average' rewetting intervention, detailing the distribution of costs across the three restoration phases.

Intervention	Raw Material (%)	Transport (%)	Install (%)
Stone dam	53.64	2.46	43.90
Plastic dam/Piling	94.99	4.02	0.99
Timber dam	74.19	21.34	4.48
Coir log	75.38	9.86	14.76
Heather bale dam	56.77	18.01	25.22
Peat dam	0.00	23.37	76.63
Peat bund	0.00	23.16	76.84

Figure 8.4 compares rewetting interventions by carbon cost per hectare.
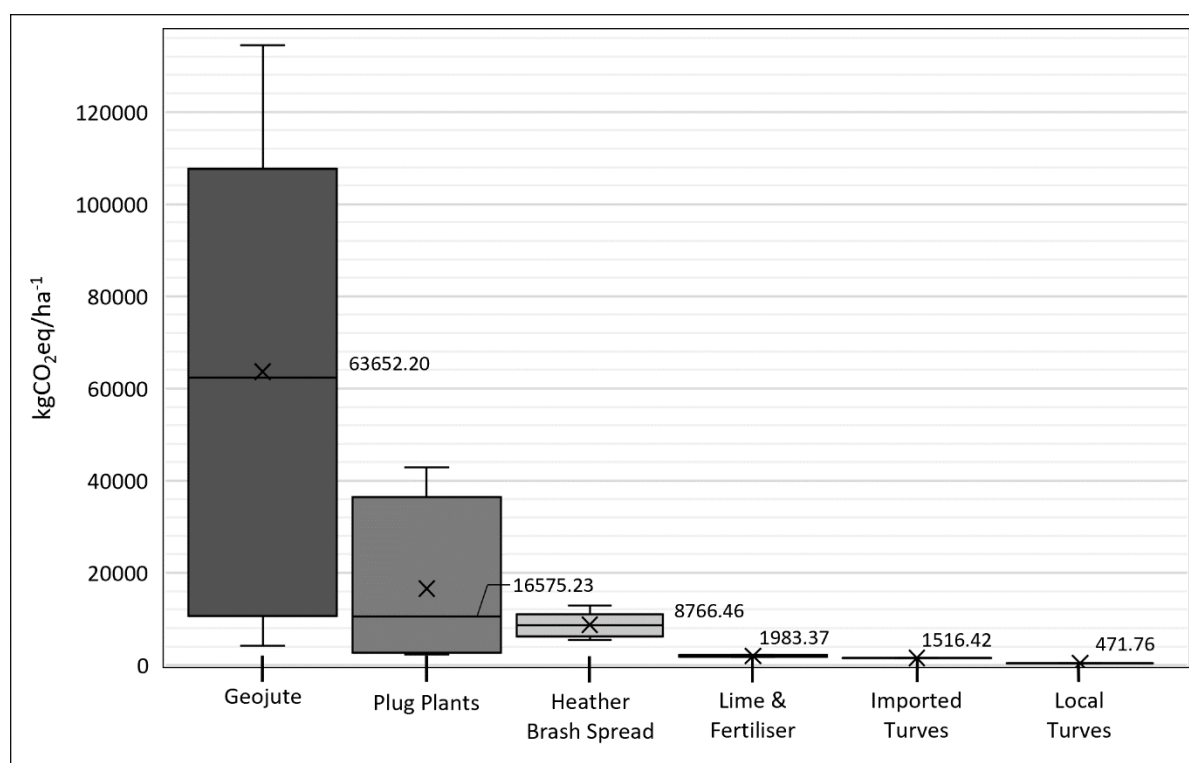
Figure 8.4: Carbon costs per hectare of numerous 'average' revegetating interventions assessed. Crosses show the mean cost. Boxes represent the inclusive median, and whiskers indicate the range of minimum and maximum costs from all available options.

Revegetation interventions per hectare also demonstrate significant variation in carbon costs. Geojute application, on average, exhibits the highest and most variable carbon cost, considerably higher than all other revegetation approaches. For direct revegetation techniques, plug plants had the greatest carbon cost, followed by imported and local turves, both of which significantly lower than plug plants. For indirect techniques use of lime and fertiliser displays the lowest carbon cost per hectare, while heather brash spreading and Geojute are ~4x or ~32x greater in carbon cost, respectively.

Geojute application also showed the greatest variance in revegetation carbon cost due to the multiple pegging options available (secondary raw materials), as shown in Table 8.3. It is also important to note that revegetation interventions, such as Geojute, are rarely

prescribed in isolation, and lime & fertiliser application is often prescribed for two follow-up applications in subsequent years, potentially doubling its carbon cost.

Partitioning the carbon cost of revegetation approaches (Table 8.7) show trends similar to rewetting interventions, whereby use of exotic raw materials dominates (~81%) the total carbon cost (except for translocated heather brash). Where locally-supplied materials (e.g., turves) are used, the majority of carbon cost is associated with installation.

Table 8.7: Percentage breakdown of carbon costs per hectare for each average revegetation intervention, listing the distribution of costs across the three restoration phases.

Intervention	Raw Material (%)	Transport (%)	Install (%)
Geojute	96.40	1.82	2.23
Plug plants	97.23	1.59	1.18
Heather brash spread	33.31	31.11	35.58
Lime & fertiliser application	96.30	1.27	2.43
Imported turves	0.00	10.33	89.67
Local turves	0.00	13.31	86.89

8.3 Application of Carbon Costs

As noted earlier, some components of the carbon costs presented in Figures 8.3 and 8.4, and Tables 8.6 and 8.7 are synthetic, based on indicative transport distances to site, and average durations of projects (Table 8.4). As such, the values presented above are indicative and enable relative comparison between techniques. To illustrate how the LCA approach can be applied in a real-world setting, carbon costs are applied to a case study example, contrasting the carbon costs at the end of the spectrum of options, and the proposed approach for the actual restoration.

Phase 2 of the Holcombe Moor restoration project in South Lancashire and Greater Manchester, England focuses on a ~35-hectare degraded blanket peatland plot. The proposed restoration plan (Table 8.8) estimates a total sequestration of 2,438,000 $kgCO_2eq$ over 30 years. The 15% reduction sets aside 366,000 $kgCO_2eq$, with 244,000 $kgCO_2eq$ (10%) accounting the carbon costs. After these adjustments, claimable emissions reductions amount to 2,072,000 $kgCO_2eq$, issued as Pending Issuance Units (PIUs) under the UK Peatland Code (IUCN, 2023). Table 8.8 also outlines two alternative restoration approaches for Holcombe Moor, based on the LCA data from this investigation (Figures 8.3 and 8.4): 1) a high-carbon-intensive approach; and 2) a low-carbon-intensive approach, both guided by Thom *et al.* (2019) NatureScot (2022).

Table 8.8: Proposed and alternative high and low-carbon approaches for Phase 2 of the Holcombe Moor blanket peatland restoration project (Taylor, N. 2024, Lancashire Peat Partnership, personal communication). Alternate approaches follow guidance from Thom *et al.* (2019) and NatureScot (2022).

Approach/Scenario	Objective	Technique	Intervention	Quantity
Proposed restoration plan	Rewet	Gully/grip (drain) blocking	Peat dams	53
			Stone dams	12
		Surface/shallow bunding	Peat bunds	2625
	Revegetate	Direct establishment	Imported turves	~0.5ha
			Local turves	~0.5ha
			Plug plants	~35ha (rate of 3500 ha^{-1})
		Indirect establishment	Heather brash	~1ha
			Lime & fertiliser	~1ha
High-carbon intensive restoration model	*Rewet*	*Gully/grip (drain) blocking*	*Stone dams*	*65*
		Surface/shallow bunding	*Coir logs*	*2625*
	Revegetate	*Direct establishment*	*Imported turves*	*~1ha*
			Plug plants	*~35ha (rate of 3500 ha^{-1})*
		Indirect establishment	*Geojute*	*~2ha*
Low-carbon intensive restoration model	*Rewet*	*Gully/grip (drain) blocking*	*Peat dams*	*65*
		Surface/shallow bunding	*Peat bunds*	*2625*
	Revegetate	*Direct establishment*	*Imported turves*	*~35ha*
			Local turves	*~1ha*
		Indirect establishment	*Lime & fertiliser*	*~2ha*

Figure 8.5 shows the time taken for the assumed post-restoration carbon sequestration and resulting PIUs (including the 'carbon cost buffer', based on IUCN 2024a) to compensate for carbon emissions arising from the three restoration scenarios in Table 8.8.
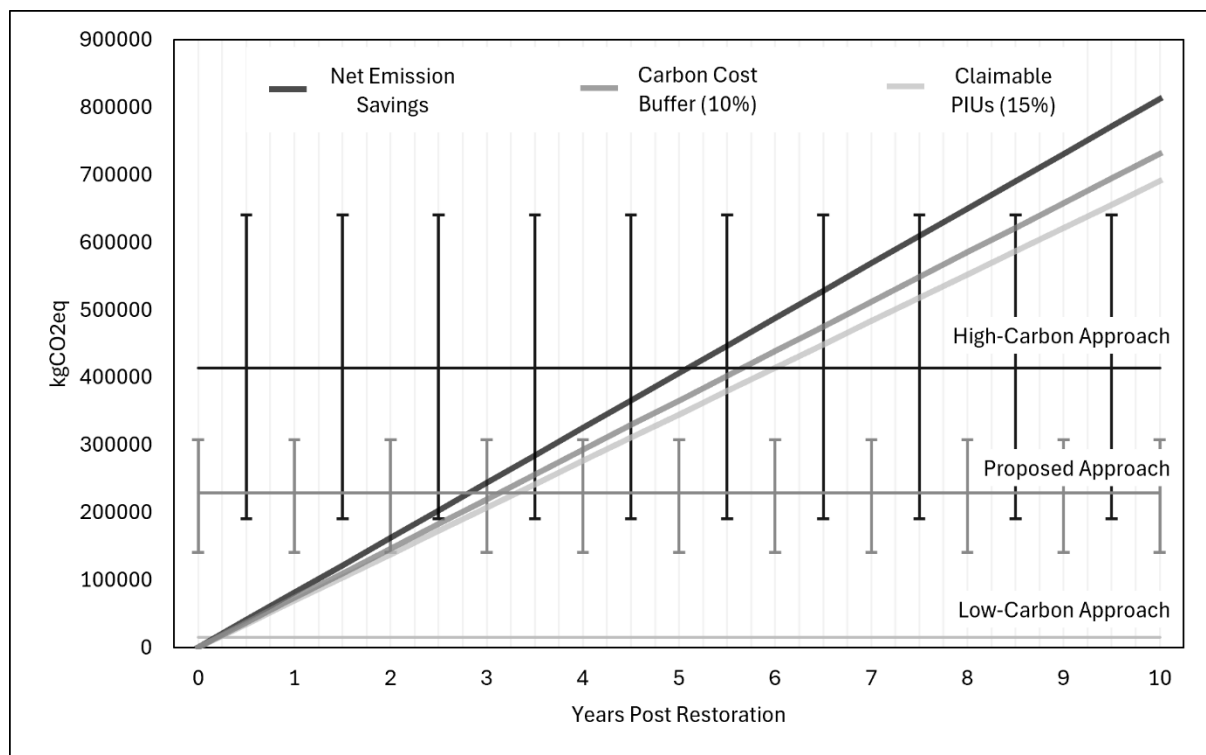
Figure 8.5: Average (horizontal), minimum (lower tier vertical), and maximum (higher tier vertical) carbon costs for the proposed (dark grey), high- (black), and low-carbon (light grey) approaches to the Holcombe Moor blanket peatland restoration, compared to the UK Peatland Code's estimated carbon savings and reductions (including the 'carbon cost buffer' and PIUs) from the first 10 years post-delivery.

There are clear differences between the three scenarios, ranging from less than a year up to ~8 years post-restoration before the carbon costs have been 'repaid' by assumed sequestration, and longer for the PIUs to enter a positive balance.

Figure 8.6 evaluates the adequacy of the 10% carbon cost and net 15% reduction used by the UK Peatland Code for PIU quantification across the restoration scenarios in Table 8.8.
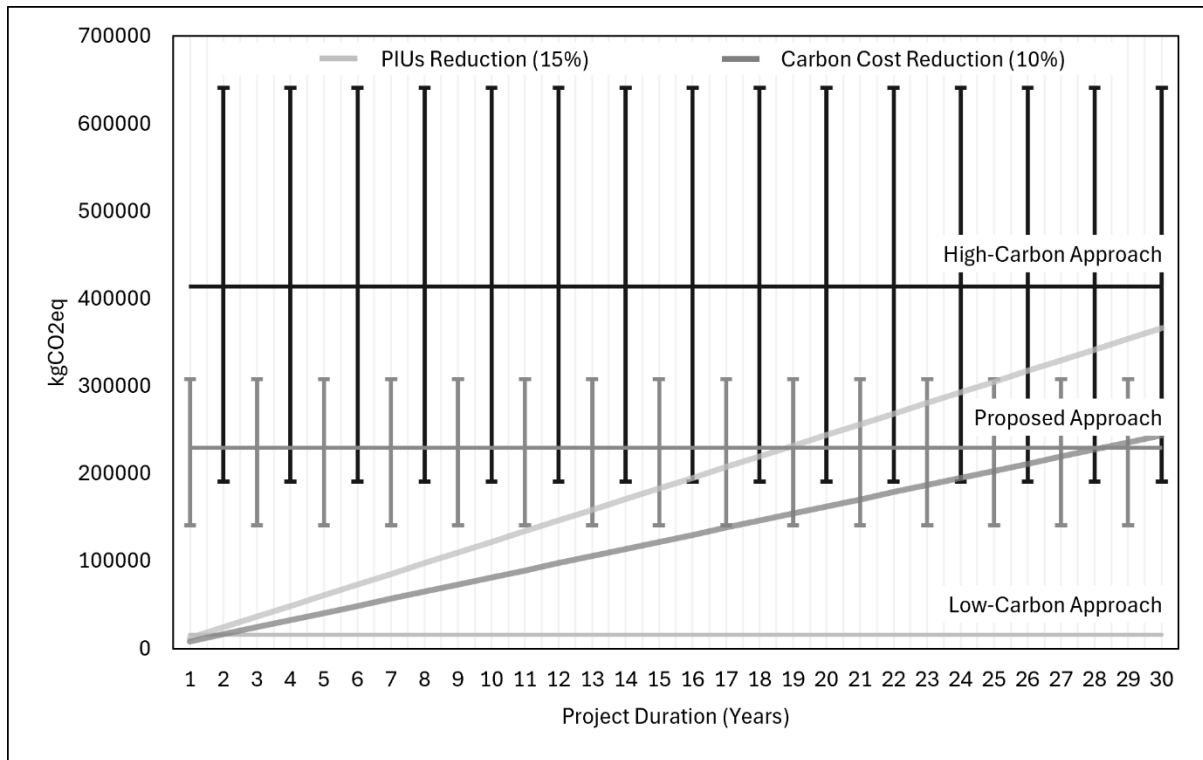
Figure 8.6: Average (horizontal), minimum (lower tier vertical), and maximum (higher tier vertical) carbon costs for the proposed (dark grey), high- (black), and low-carbon (light grey) approaches to the Holcombe Moor blanket peatland restoration, compared to the UK Peatland Code's emissions reductions, including the 10% carbon cost and net 15% reduction for estimated PIUs across the entire project duration.

For the proposed 'average' approach, the 10% reduction sufficiently covers the 30-year project duration, accounting for ~28 years, while the 15% reduction is adequate for ~19 years. The high-carbon approach is inadequate throughout the project under both 'average' and 'maximum' scenarios, requiring up to an additional ~23 years (53 years total) for reduction percentages to align with carbon costs. In contrast, the low-carbon approach achieves adequacy within ~1 year.

8.4 Chapter Synthesis and Discussion

While previous chapters evaluate the ecological (Chapter 5), bulk chemical (Chapter 6), and structural (Chapter 7) responses to restoration, these functional outcomes alone cannot determine restoration success if the emissions required to deliver them are unaccounted for. As restoration is increasingly financed through voluntary carbon markets (Chapter 2; Sections 2.4.1; 2.7), evaluating whether projects deliver net carbon benefit requires integration of both functional impacts and carbon costs.

8.4.1 Variation in Carbon Costs

The LCA demonstrated substantial variation in carbon costs across rewetting and revegetation techniques, influenced by intervention type, material origin, and delivery method. For rewetting, peat dams and bunds constructed from local peat incurred the lowest emissions. In contrast, interventions such as stone dams and coir logs showed significantly higher carbon costs due to use of exotic materials and reliance on helicopter delivery. For revegetation, plug planting and Geojute application were the most carbon intensive, whereas turving (local or imported) was more carbon efficient. *As explored in Chapter 9, these differences have direct implications when functional impacts are compared across techniques delivering similar goals (e.g., turving and heather brash spreading). Consequently, where multiple options exist for the same intervention, carbon costs become critical in determining net carbon benefit.*

8.4.2 Design and Delivery Considerations

The LCA also showed how carbon costs are distributed within interventions. Those dependent on materials through global supply chains or aerial delivery consistently generated the highest emissions, with raw materials often accounting for >90% of total carbon cost. Despite frequently recommended for inaccessible sites (Thom *et al.*, 2019; NatureScot, 2022), helicopter use was shown to be avoidable in many project contexts, with average restoration sites located only ~8km from the nearest access. Manul and low-pressure ground vehicle installation consistently resulted in lower carbon costs. *Alongside suggestions of optimal functional outcomes such as turve pressing and machinery tracking (Chapter 7; Section 7.4), findings demonstrate significant impact of technique selection on net carbon balance (further explored in Chapter 9).* Moreover, substitutions such as replacing steel with wooden pegs can further reduce emissions. Transport from depot to site was generally a minor contributor, highlighting carbon savings are most achievable through intervention design and material selection. *This is exemplified in the Holcombe Moor case study, where a higher-carbon intervention extended carbon offsetting times by over five decades compared to a lower-carbon alternative delivering the same objective.*

8.4.3 Implications for Policy and Carbon Markets

Findings challenge the adequacy of fixed carbon cost assumptions previously used in restoration carbon accounting. The standard 10% deduction applied by the IUCN UK Peatland Code (IUCN, 2024a) did not indicate the substantial variation in emissions across intervention types. Adoption of intervention-specific carbon accounting, as now incorporated into the Peatland Code Carbon Savings Calculator (IUCN, 2025a), enables

more accurate estimation of net carbon benefit and increases the credibility of issued credits.

Results further support the integration of carbon cost considerations into restoration planning, project design, and financing. While current decisions are typically based on ecological suitability and financial cost, carbon cost-efficiency should also be considered, particularly as blended finance models expand and private investment increases (Chapter 2; Section 2.4.1). In long-duration projects (typically 100 years), fixed carbon buffers may either over or underestimate actual emissions depending on intervention choice. However, this LCA does not recommend reducing buffer values, as future LCAs may reveal higher emissions for certain techniques (conservate approach applied). Instead, *findings emphasise the requirement to calculate actual project-specific emissions, in line with the direction now taken by the IUCN UK Peatland Code (IUCN, 2024a). This LCA provides the first empirical basis for refining carbon buffers and supports more robust, evidence-based adjustments to policy and market frameworks.*

Incorporating the carbon costs of delivery into assessments of restoration effectiveness contributes directly to the thesis aim of redefining what constitutes successful peatland restoration. *Findings demonstrate structurally and functionally effective interventions may not necessarily be carbon-efficient, and that credible, financeable restoration depends on balancing both outcomes*. Results provide the final component for Chapter 9, which evaluates the relative cost-efficiency of restoration strategies by integrating ecological, chemical, structural, and carbon cost data to inform a revised, evidence-based definition of restoration success.

Table 8.9: Summary of research questions addressed in Chapter 8.

Research Question	Contribution/Implications
Research Question 1: Can surface indicators be used as a proxy to infer changes in sub-surface structure and function post-restoration?	Not directly assessed, but surface indicators do not capture emissions associated with restoration implementation. While functional improvements may be observable at the surface (Chapter 5), these outcomes should be weighed against delivery emissions to assess net carbon benefit.
Research Question 2: To what extent does the restoration of degraded blanket peatlands support the recovery of sub-surface structure and function?	Not directly assessed, but interventions promoting favourable sub-surface outcomes (e.g., turving) vary in their carbon costs. These differences are important when evaluating whether functional benefits justify emissions incurred.
Research Question 3: How do the carbon costs of interventions impact the carbon benefit potential of restoration?	Substantial variation in carbon cost was observed across intervention types, delivery methods, and material choices. High-emission interventions (e.g., coir, stone dams, helicopter delivery) may reduce or delay carbon benefits. Findings provide the basis for evaluating restoration cost-efficiency in Chapter 9 and support the adoption of intervention-specific carbon accounting in policy and market frameworks.

Chapter 9: Evaluating Blanket Peatland Restoration

Evaluating the effectiveness of blanket peatland restoration requires a more integrated assessment of functional and carbon outcomes than is currently captured by surface-based monitoring (Chapter 2; Section 2.6), embedded within restoration policy (Chapter 2; Section 2.4.1), or used in carbon savings reporting (Chapter 2; Section 2.7). As demonstrated in Chapter 5, the JNCC (2009) *Common Standards Monitoring Guidance (CSM) for Upland Habitats: Blanket Bogs*, which informs condition assessment in the UK (Shepherd *et al.*, 2013; Alderson *et al.*, 2019; Birnie *et al.*, 2023; Crowle *et al.*, 2025), showed limited sensitivity to restoration impacts, despite evidence of ecological improvement. Although vegetation composition showed some response, surface-based assessments did not consistently align with restoration change (Chapter 5; Section 5.5).

Chapter 6 built on this limitation of restoration assessment, showing bulk and chemical indicators of sub-surface function, such as moisture content (saturation), pH (acidity), and Eh (anoxia) (Chapter 3; Section 3.3.4), only partially corresponded with surface condition, while others showed little or no relationship (Chapter 6; Section 6.2). This was further supported in Chapter 7, where µCT analysis revealed key pore network features regulating water retention, solute export, and gas exchange (Chapter 2; Section 2.2.3) often responded in the surface acrotelm, particularly through increased atmosphere-connected porosity, but remained largely unchanged at depth. In the catotelm, boundary-connected networks capable of rapid transfer and carbon export frequently persisted, even where surface condition had improved (Chapter 7; Section 7.5). Differences between surface indicators and sub-surface structure are explored in Section 9.2. Nevertheless, these contrasts between surface and sub-surface response,

where carbon storage is primarily governed (Chapter 2; Section 2.2), demonstrate a fundamental limitation in current monitoring and reporting, where carbon outcomes are indirectly inferred from surface indicators (Chapter 2; Section 2.6.2).

Collectively, findings support the evaluation of peatland restoration through a combined understanding of functional effectiveness and carbon efficiency. While Chapters 5 to 7 showed restoration can support ecological improvement and partial sub-surface recovery, Chapter 8 demonstrated the importance of accounting for the carbon costs associated with intervention delivery. With restoration increasingly funded through blended finance such as the Nature for Climate Peatland Grant Scheme (NCPGS) and Environmental Land Management (ELM) (Chapter 2; Section 2.4.1; Bonn *et al.*, 2014; Moxey *et al.*, 2021; Reed *et al.*, 2022; Chen *et al.*, 2023), robust evidence is required to validate carbon credit claims through schemes such as the IUCN UK Peatland Code (IUCN, 2024a) and attract private investment (Chapter 2; Section 2.7). Multiple techniques are often used to achieve the same restoration objective (Chapter 2; Section 2.5.3; Thom *et al.*, 2019; NatureScot, 2021), yet their structural and function outcomes (Chapters 5 – 7) and carbon costs (Chapter 8) vary significantly. Without evaluating both functional impact and carbon efficiency, restoration success may be overestimated or misrepresented, as explored in Section 9.3. This has direct implications for the IUCN UK Peatland Code, where carbon credits are awarded based on assumed surface recovery and emissions reductions (IUCN, 2024b), as well as for wider policy frameworks focusing solely on carbon benefits.

Building on the functional interpretations established through pore network analysis in Chapter 7; Section 7.5, structural indicators are considered alongside bulk and chemical properties to develop a more integrated understanding of sub-surface functional recovery. Exploring these relationships supports evaluation of restoration technique effectiveness and the carbon costs associated with delivering functional benefits.

9.1 Pore Structure and Bulk Chemical Indicators: Evaluating Sub-Surface Recovery

Understanding how structure supports key sub-surface functions is critical to evaluating restoration success (Chapter 2; Section 2.2) and informing concepts such as the diplotelmic model (Ingram, 1978; Clymo, 1984; Clymo and Bryant, 2008), which require spatial characterisation (Chapter 2; Section 2.1.1; Holden and Burt, 2003; Belyea and Baird, 2006; Morris *et al.*, 2011; Baird *et al.*, 2016). Porosity represents the primary structural control on hydrology, gaseous exchange, and carbon accumulation (Chapter 2; Section 2.1.3; Kettridge and Binley, 2008; 2011; Quinton *et al.*, 2009; Rezanezhad *et al.*, 2009; 2010; 2016; McCarter *et al.*, 2020). While total porosity determines the overall capacity for water, solute, and gas transport, it is the distribution of pore sizes controlling retention and exchange potential, and the shape, tortuosity, and orientation of pores influencing network efficiency in restored systems. For example, small, tortuous pores may support saturation and anoxia, whereas large, simple, networks can promote drainage and solute loss. As shown in Chapter 7; Section 7.5; Figures 3.33–3.36, functionally dominant pores vary in size, shape, and tortuosity across atmosphere-connected, boundary-connected, and isolated types, reflecting distinct roles in hydrological and biochemical function.

Pore network characteristics are compared with bulk and chemical indicators to evaluate whether functional behaviours inferred from porosity are supported by sub-surface evidence of functional processes. With a limited sample population, interpretation focusses on consistent trends and relationships across degraded, restored, and near-natural samples. These datasets provide a multi-scale understanding of key processes, including water retention, anoxia, and retarded decomposition, essential for *Sphagnum* succession, microtopographic variation, and long-term carbon accumulation (Chapter 2; Section 2.2). This forms the basis for assessing sub-surface functional recovery and evaluating restoration effectiveness across different timescales and interventions.

9.1.1 Relationships Between Pore Network Structure and Functional Indicators

Building on the µCT findings, key pore features associated with functional behaviour (Chapter 7; Section 7.5) are used to evaluate sub-surface recovery across target (near-natural), baseline (degraded), and restored conditions. These include effective atmosphere-connected porosity supporting surface water uptake and saturation, indicative of a functioning acrotelm, and reductions in boundary-connected and isolated porosity, reflecting a more retentive catotelm capable of maintaining anoxic conditions for retarded decomposition and reduced GHG emissions (Chapter 7; Section 7.5; Figures 7.33 – 7.36). Pore structure is compared with bulk and chemical indicators to assess alignment between structural characteristics and sub-surface function.

a) Target Conditions

The near-natural control (SF_Nat) provides a structural and functional target against which the effectiveness of restoration is assessed. As summarised in Chapter 7; Section 7.5; Figure 7.33, SF_Nat exhibited a well-stratified profile consistent with an intact acrotelm – mesotelm – catotelm transition. Pore network characteristics indicated effective surface water infiltration, retention, and reduced potential for drainage or aerobic decomposition, suggesting favourable conditions for long-term carbon storage. These features are explored in relation to corresponding bulk and chemical properties. Figure 9.1 offers a visual summary of SF_Nat, illustrating the alignment between key structural features and indicators of sub-surface function.
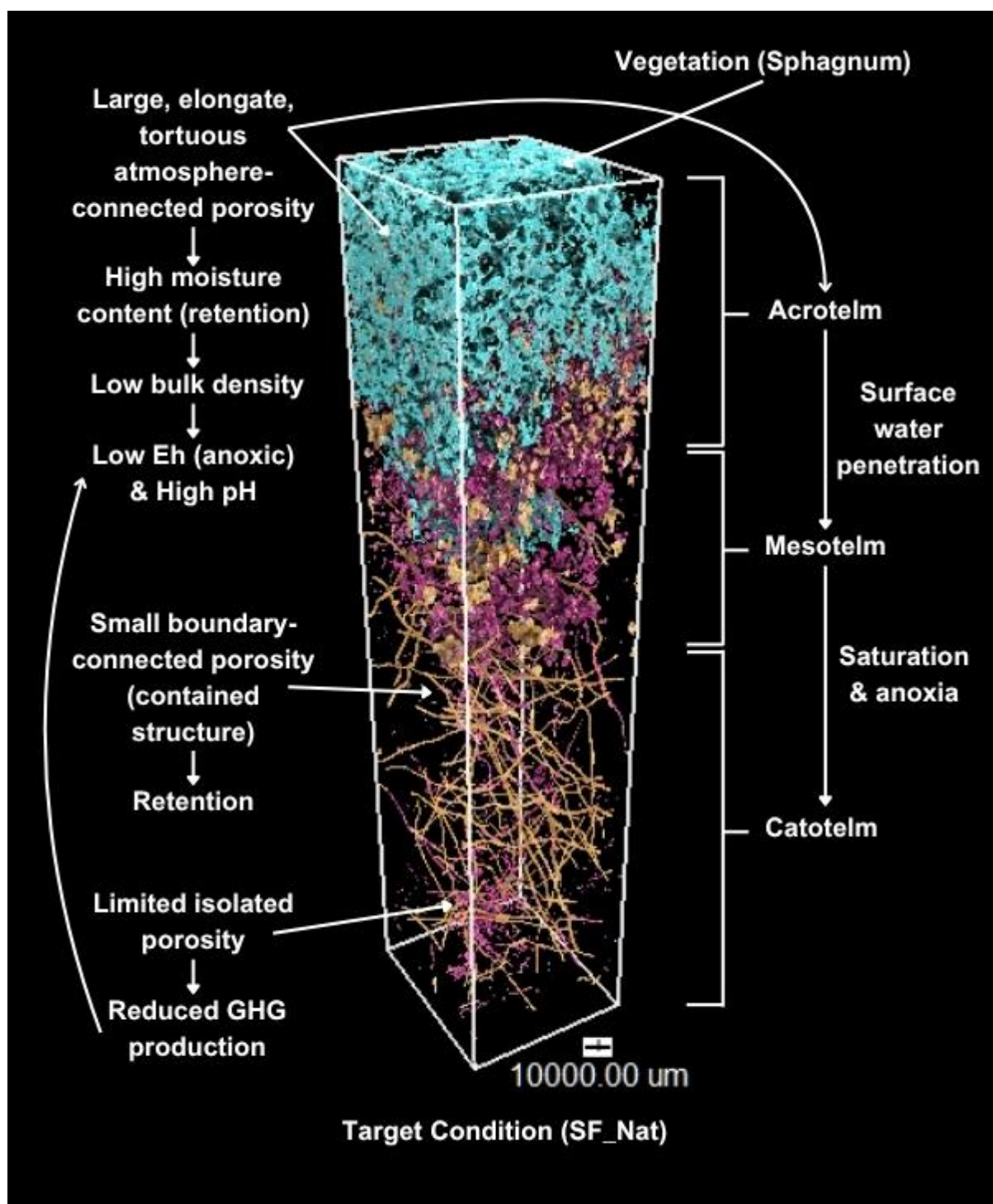
Figure 9.1: Annotated 3D visualisation of SF_Nat (near-natural target) showing atmosphere-connected porosity (blue); boundary-connected porosity (orange); isolated porosity (pink). Annotations indicate associated bulk and chemical properties and summarise combined structural and functional inferences.

i) Structural Attributes:

μCT analysis (Chapter 7) demonstrated a vertically connected structure with high surface macroporosity and inferred microporosity extending to ~15cm, before decreasing with depth, indicative of an acrotelm – mesotelm – catotelm transition (Chapter 7; Section 7.5; Figure 7.33). Atmosphere-connected porosity (ACP) dominated, forming a large, branching, surface-connected network supporting effective water uptake, retention, and regulation of advective gas transfer. This dominant network exhibited high tortuosity, suggesting increased water retention and GHG exchange regulation. Boundary-connected porosity (BCP) was restricted to smaller pores, visually consistent with non-orientated, narrow pathways contributing to regulated water and solute redistribution in deeper layers. Isolated porosity (IP) was low, supporting vertical continuity. The structure suggests a stratified, saturated, anoxic sub-surface with low surface bulk density, high moisture, and reduced temperature gradients, conductive to retarded decomposition and net carbon accumulation (Chapter 2; Sections 2.1; 2.2).

ii) Functional Indicators:

Bulk and chemical properties (Chapter 6) broadly support interpretations of near-natural structure and function. While total bulk density was similar to BC_Deg, it was considerably lower near the surface, aligning with high atmosphere-connected porosity and reduced compaction. Moisture content was significantly higher, particularly in the acrotelm, supporting effective water retention through a large, tortuous atmosphere-connected network. Eh was low and pH high, favourable for *Sphagnum* growth (explored in Section 9.2) and reduced GHG emissions. Temperature gradients were less steep than BC_Deg, indicating reduced microbial activity and lower CO_2 and CH_4 production under

saturated conditions. While Von-Post (humification) and greyscale density profiles (inferred microporosity) confirmed vertical stratification (intact acrotelm), Von-Post alone did not consistently indicate functional condition, similar to organic carbon content, supporting their limited sensitivity (Chapter 6; Section 6.1.3). Alternatively, this may also indicate minor disturbance, supporting the classification of SF_Nat as near-natural rather than pristine (Chapter 2; Section 2.3).

iii) Significance:

SF_Nat exhibits a stratified profile consistent with a functioning acrotelm – mesotelm – catotelm structure, supporting water retention, sustained anoxia, and reduced decomposition, favourable for long-term carbon accumulation. Pore network structure and bulk and chemical properties were largely aligned with functional interpretations, particularly in surface layers. These characteristics provide a representative structural and functional target for blanket peatland restoration.

b) Baseline conditions

The degraded core (BC_Deg) provides a structural and functional baseline against which recovery is assessed. As summarised in Chapter 7; Section 7.5; Figure 7.34, BC_Deg exhibited a compact, fragmented structure with limited macroporosity and inferred microporosity throughout. Pore networks were dominated by isolated and boundary-connected porosity, indicative of hydrophobic, oxygenated conditions, consistent with rapid decomposition and carbon loss. These features are evaluated in relation to corresponding bulk and chemical properties. Figure 9.2 presents a visual summary of findings.
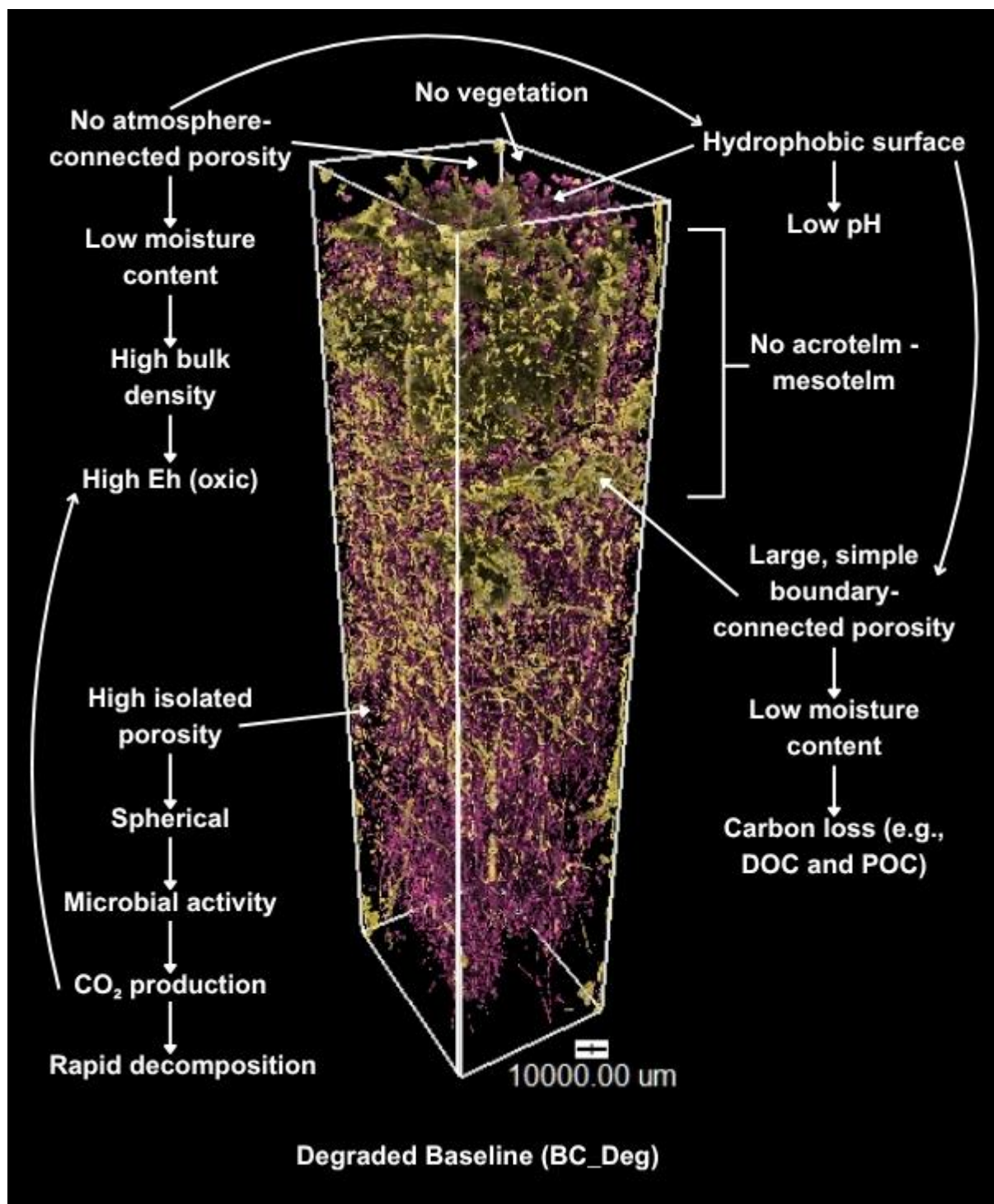
Figure 9.2: Annotated 3D visualisation of BC_Deg (degraded baseline) showing boundary-connected porosity (orange) and isolated porosity (pink). Annotations indicate associated bulk and chemical properties and summarise combined structural and functional inferences.

i) Structural Attributes:

µCT analysis (Chapter 7) demonstrated a compact structure with low macroporosity and inferred microporosity throughout. Isolated porosity (IP) dominated, forming compact, spherical shapes suggestive of gas accumulation associated with rapid oxic decomposition. No atmosphere-connected porosity (ACP) was detected, indicating a hydrophobic surface incapable of supporting surface water uptake or maintaining high water tables. Boundary-connected porosity (BCP) formed multiple dominant platy networks across depth, with 3D visualisations supporting lateral drainage pathways capable of exporting water and solutes out of the system. These networks exhibited low tortuosity, with at least one orientated toward the gully channel. Findings indicate a dry, oxic sub-surface, consistent with increased bulk density, higher temperature gradients, and greater humification, indicative of increased microbial activity, accelerated decomposition, and net carbon loss through CO_2 emissions and dissolved and particulate organic carbon export (Chapter 2; Sections 2.1; 2.2).

ii) Functional Indicators:

Bulk and chemical properties (Chapter 6) support structural interpretations of functional degradation. High bulk density and low moisture content, particularly in the upper 10cm, align with the absence of atmosphere-connected porosity and reduced water retention due to active boundary-connected networks. Increased Eh and low pH near the surface are consistent with a structure facilitating drainage and promoting hydrophobicity, limiting vegetation recovery (as demonstrated in Section 9.2) and supporting CO_2 production under rapid oxic decomposition. Von-Post humification values reaching H7 within the first 30cm further support ongoing decomposition. Only

organic carbon content showed no clear correspondence with pore structure, aligning with previous observations of its limited sensitivity (Chapter 6; Section 6.1.1).

iii) Significance:

Degraded peat lacks an acrotelm and mesotelm, exhibiting a structurally and functionally degraded catotelm. This supports sustained carbon loss and GHG emissions, with limited capacity for biodiversity support or water regulation. Characteristics support BC_Deg as a representative baseline for degraded blanket peatland condition. Bulk and chemical properties aligned with pore network findings, suggesting their potential as accessible proxies for sub-surface condition in degraded systems. In particular, Eh could act as an indirect proxy for oxic decomposition and CO_2 production under aerated conditions.

c) Restored conditions

Restored cores exhibited transitional structures between degraded and near-natural conditions. As summarised in Chapter 7; Section 7.5; Figures 7.35 and 7.36, μCT analysis demonstrated partial recovery, with evidence of acrotelm development and improved vertical connectivity. However, no mesotelm was observed, and deeper profiles retained features indicative of structural degradation. Figure 9.3 summarises findings from an intermediate restored core, illustrating typical structural features and their alignment with functional indicators.
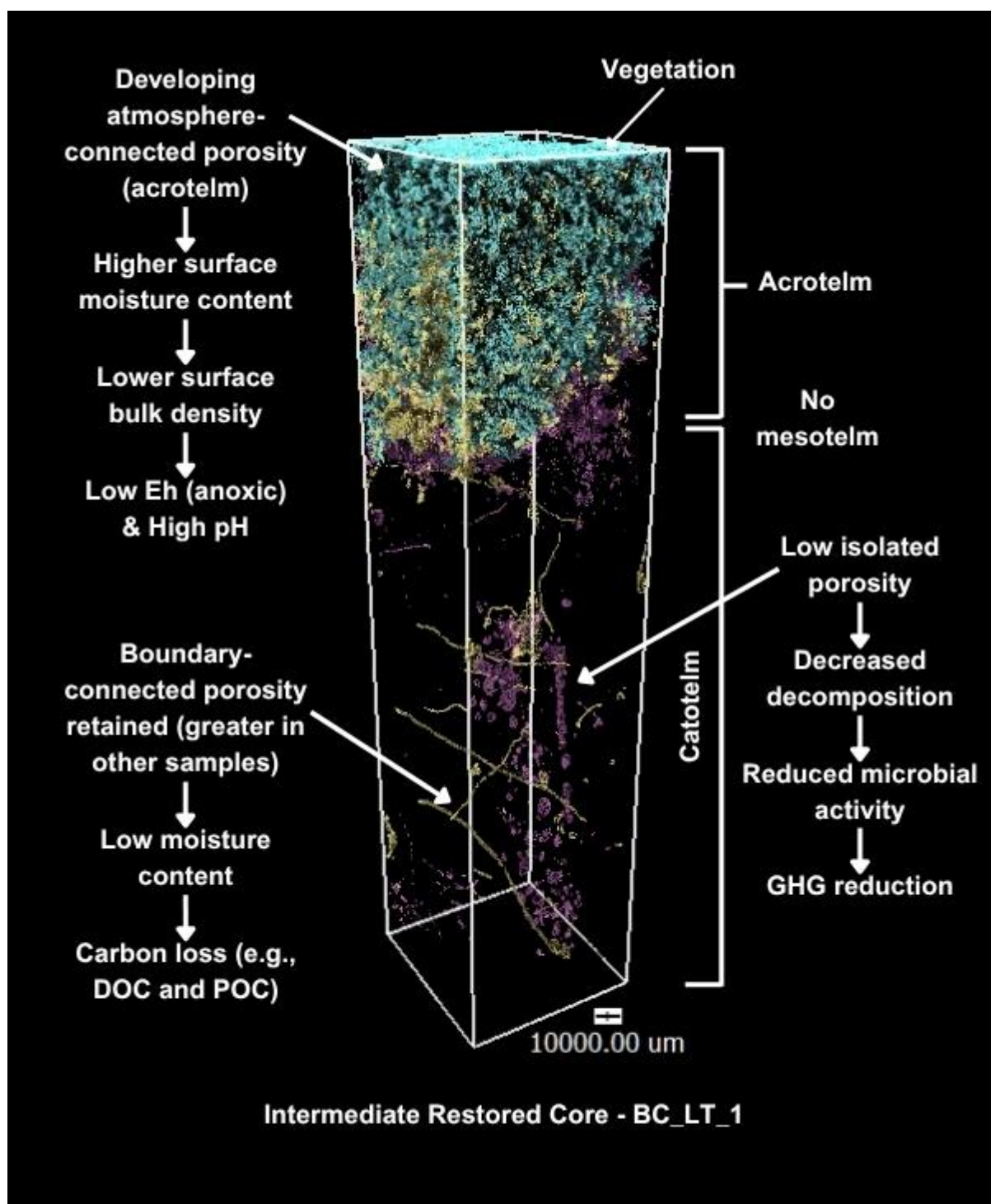
Figure 9.3: Annotated 3D visualisation of BC_LT_1 (intermediate restored core) showing atmosphere-connected porosity (blue); boundary-connected porosity (orange); isolated porosity (pink). Annotations indicate associated bulk and chemical properties and summarise combined structural and functional inferences.

i) Structural Attributes:

μCT analysis (Chapter 7) indicated increased surface macroporosity and inferred microporosity in the upper 5–10cm relative to the degraded baseline (BC_Deg), associated with the development of atmosphere-connected porosity (ACP). However, atmosphere-connected networks were either undeveloped, characterised by smaller, simpler structures with limited capacity for surface water uptake, or overly large (but still tortuous), facilitating greater advective gas exchange than observed in the near-natural target (SF_Nat). Occasionally, atmosphere-connected porosity extended into the deeper catotelm, suggesting persistence of preferential flow paths for CH_4 release (Moore *et al.*, 2002).

Boundary-connected porosity (BCP) remained present in most restored cores with greater volumes than SF_Nat, sometimes forming low-tortuosity networks in deeper layers similar to BC_Deg. While less abundant, their persistence indicates continued sub-surface drainage and incomplete disruption of degraded structure. Isolated porosity (IP) was reduced relative to BC_Deg, suggesting some improvement in vertical connectivity, but remained higher than SF_Nat, consistent with incomplete stratification and ongoing decomposition. Findings indicate partial structural recovery, primarily in surface layers, while deeper profiles remain largely degraded and structurally unresponsive to restoration.

ii) Functional Indicators:

Bulk and chemical properties (Chapter 6) showed mixed correspondence with pore structures but broadly supported inferences of partial recovery. Most restored cores exhibited higher bulk density than controls (reduced isolated porosity), potentially

indicating compaction associated with disturbance or continued decomposition. However, lower surface values in profiles aligned with increased atmosphere-connected porosity, suggesting acrotelm formation. Moisture content was generally more similar to BC_Deg, particularly at depth, supporting oxic conditions and ongoing decomposition. Yet surface moisture was often higher, again indicating functional recovery at the surface.

Eh was lower in restored cores than BC_Deg, despite relatively high bulk density and lower moisture content. This suggests atmosphere-connected porosity plays a role in maintaining sub-surface anoxia and retarding decomposition (functional acrotelm). pH was consistently higher in restored cores compared to BC_Deg, while temperature gradients were shallower, favourable for *Sphagnum* succession and reduced microbial activity, consistent with early-stage acrotelm development.

iii) Significance:

Findings support the use of the diplotelmic model in interpreting restored peat structure, particularly the role of the acrotelm. Moreover, Eh and pH could act as potential proxies for understanding sub-surface structure and function. Below ~15cm, bulk and chemical profiles shifted, supporting the structural interpretation of an absent mesotelm. SF_Nat demonstrates this transitional layer characterised by declining atmosphere-connected porosity to no contribution, negligible isolated, and minimal boundary-connected porosity, supporting water retention and a change from oxic to anoxic decomposition. Its absence in restored samples suggests a disconnect between surface and sub-surface structure and function. Furthermore, bulk and chemical properties beyond did not clearly capture the influence of boundary-connected porosity, despite its role in water regulation and solute export. This demonstrates the requirement for complementary hydrological

and dissolved and particulate organic carbon monitoring to assess sub-surface flow processes not captured by standard bulk or chemical indicators. As with the control cores, Von-Post humification and organic carbon content were largely insensitive to structural variation, confirming their limited value as indicators of sub-surface recovery.

Restored cores showed partial structural recovery, with developing acrotelms but no mesotelm and minimal change in the catotelm. Restoration reduces degradation impacts, improving surface anoxia and moisture, which may support retarded decomposition and lower GHG emissions (Chapter 2; Section 2.1.2). However, near-natural conditions are not achieved after a decade. The diplotelmic model, expanded to include the mesotelm (Clymo and Bryant, 2008), offers a useful framework for assessing recovery. Bulk and chemical indicators capture surface structure, but deeper processes require additional monitoring.

9.1.2 Influence of Restoration Age and Technique on Sub-Surface Structure and Function

Chapters 6 and 7 demonstrated both restoration age and technique influence the extent of sub-surface structural and functional recovery. Older turved sites (~10 years, Borrowdale) generally supported more stable biochemical conditions, such as lower Eh, higher pH, and more retentive pore networks than younger interventions (~5 years, Bampton Common; ~2 years, Shap Fells), with gradients of recovery observed across sites. Comparisons between techniques applied ~2 years ago further showed turving at Shap Fells promoted greater structural development, particularly atmosphere-connected porosity in the acrotelm, than heather brash spreading at Stake Moss. While less directly comparable, coir log and stone/timber dam interventions also retained

deeper degradation features and limited porosity impact relative to turved sites. However, restoration outcomes did not consistently align with near-natural conditions based on time or technique alone, with inter-site variability evident and no clear differences observed between local and imported turves.

Structural (Chapter 7) and functional (Chapter 6) properties are analysed further to assess the influence of restoration age and technique, building on the baseline and target conditions established in Section 9.1.1 (Figures 9.1–9.3). Age-related trends are examined across turved sites restored ~2 (Shap Fells), ~5 (Bampton Common), and ~10 years ago (Borrowdale). Differences in revegetation technique are evaluated by comparing turving at Shap Fells with heather brash spreading at Stake Moss over similar timescales (~2 years). Additional insights are drawn from coir log and stone/timber dam interventions, although interpretation is limited due to their distinct roles in rewetting.

a) Time Post-Restoration

Figure 9.4 compares turved cores restored ~5 years apart from Borrowdale (~10 years) and Bampton Common (~5 years) to evaluate how restoration age typically influences porosity development and sub-surface functional recovery. Visualisation prioritises the ~5-year gradient between Bampton Common and Borrowdale, as the ~3-year difference between Shap Fells (~2 years) and Bampton Common was less pronounced.
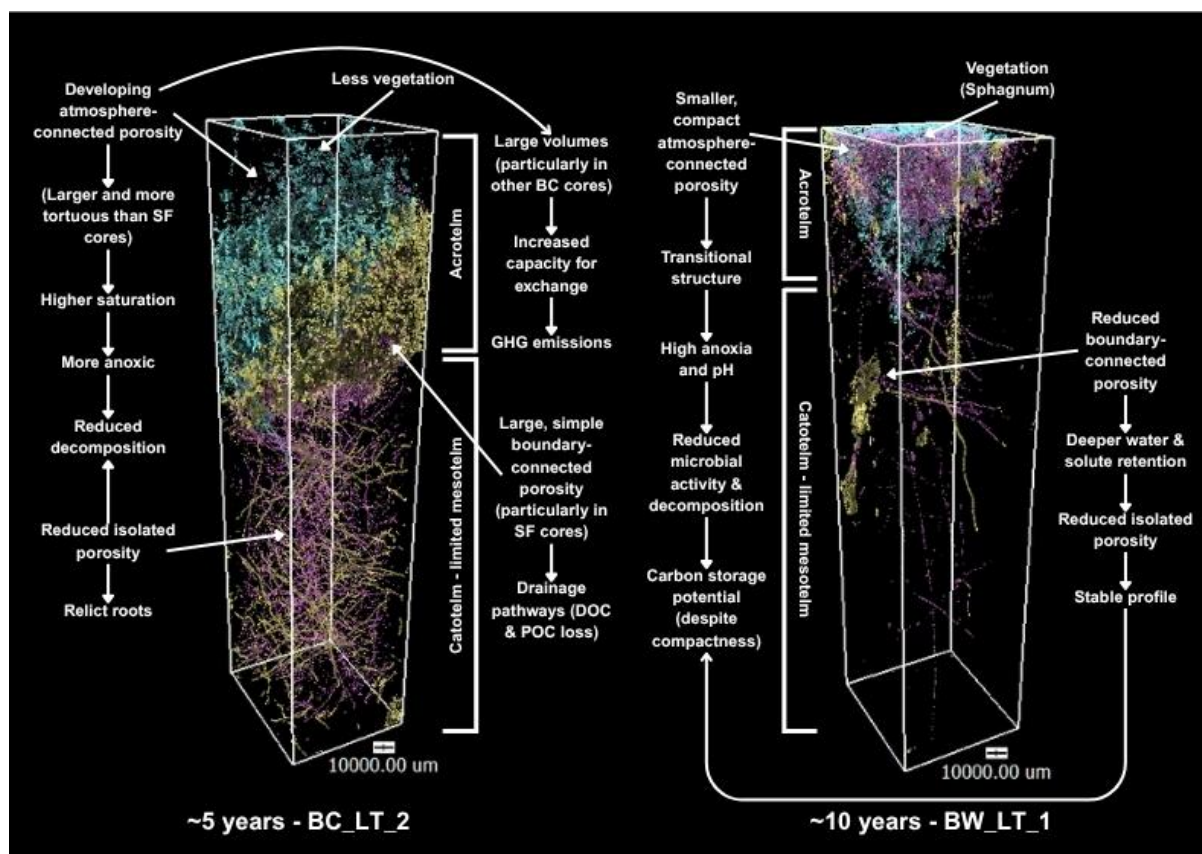
Figure 9.4: Annotated 3D visualisation of the structural and functional impacts of time since restoration between two example cores (~5 years, BC_LT_2; ~10 years, BW_LT_1). Atmosphere-connected porosity (blue); boundary-connected porosity (orange); isolated porosity (pink). Annotations indicate associated bulk and chemical properties and summarise combined structural and functional inferences.

After **~2 years**, cores from **Shap Fells** exhibited initial acrotelm development. µCT demonstrated emerging atmosphere-connected porosity (ACP) in the upper 5cm, while bulk and chemical properties showed reduced bulk density and increased moisture content. Atmosphere-connected networks were relatively tortuous and vertically oriented but often discontinuous, supporting restricted infiltration and retention. This is consistent with increased Eh compared to older restored cores. Boundary-connected porosity (BCP) remained dominant, with low tortuosity suggesting efficient sub-surface drainage and solute export. Isolated porosity (IP) was reduced compared to the degraded baseline, yet bulk density remained high and moisture content lower at depth, supporting more oxic decomposition. Findings indicate early-stage structural and functional

recovery, with improvement relative to degraded conditions, but less alignment with the near-natural target (refer to visualisations in Chapter 7; Section 7.2).

By **~5 years** post-restoration, atmosphere-connected porosity in **Bampton Common** cores became more extensive and tortuous, supporting improved surface infiltration and retention. Moisture content increased in upper layers, and Eh declined, indicating emergence of a more anoxic profile. However, atmosphere-connected volumes exceeded those of the near-natural core, suggesting potential for increased advective GHG exchange. Boundary-connected porosity persisted at depth, and isolated porosity remained present but reduced, consistent with intermediate bulk density. Findings indicate increased surface functionality (acrotelm) but incomplete structure at depth (mesotelm – catotelm) (Figure 9.4).

After **~10 years**, **Borrowdale** cores showed reduced atmosphere-connected volume and continuity relative to younger sites. However, surface microporosity inferences, lower Eh, and increased pH suggested water retention may be supported by vegetation (e.g., *Sphagnum*) and surface structure (explored further in Section 9.2). Boundary-connected porosity was minimal, and isolated porosity was negligible, indicating a more compact but hydrologically stable profile. Moisture content and Eh supported anoxic conditions, while shallower temperature gradients indicated suppressed microbial activity. Notably, Shap Fells and Bampton Common cores showed more inter-site variability, supporting a consistent sub-surface in older sites. Findings suggest time reduces structurally over-efficient features (e.g., large atmosphere-connected porosity) while supporting improved sub-surface function, despite a more compact structure.

Time is a critical driver of structural and functional recovery in restored peatlands, challenging 5-year assumptions embedded in project monitoring (Chapter 2; Section 2.4.2) and carbon accounting frameworks (Chapter 2; Section 2.7). Despite indicators of improvement, restored sites did not align with near-natural conditions even after a decade. Notably, the transition from Bampton Common (~5 years) to Borrowdale (~10 years) cores suggests restored sites may evolve toward a more compact but functionally stable structure over time. This raises considerations for defining restoration success, particularly where the objective is to return natural function (Chapter 2; Section 2.4.2).

b) Restoration Technique

Figure 9.5 compares turved and heather brash restored cores from Shap Fells and Stake Moss (~2 years post-restoration) to assess the influence of revegetation technique on sub-surface structure and function.

Turved cores from **Shap Fells** exhibited early indicators of sub-surface structural and functional recovery, primarily through increased atmosphere-connected porosity (ACP) in the acrotelm, supporting higher surface moisture, increased pH, and reduced Eh compared to degraded conditions (BC_Deg). However, structure remained compact with high bulk density and deep boundary-connected porosity (BCP), indicating restricted vertical continuity and limited restoration impact at depth.
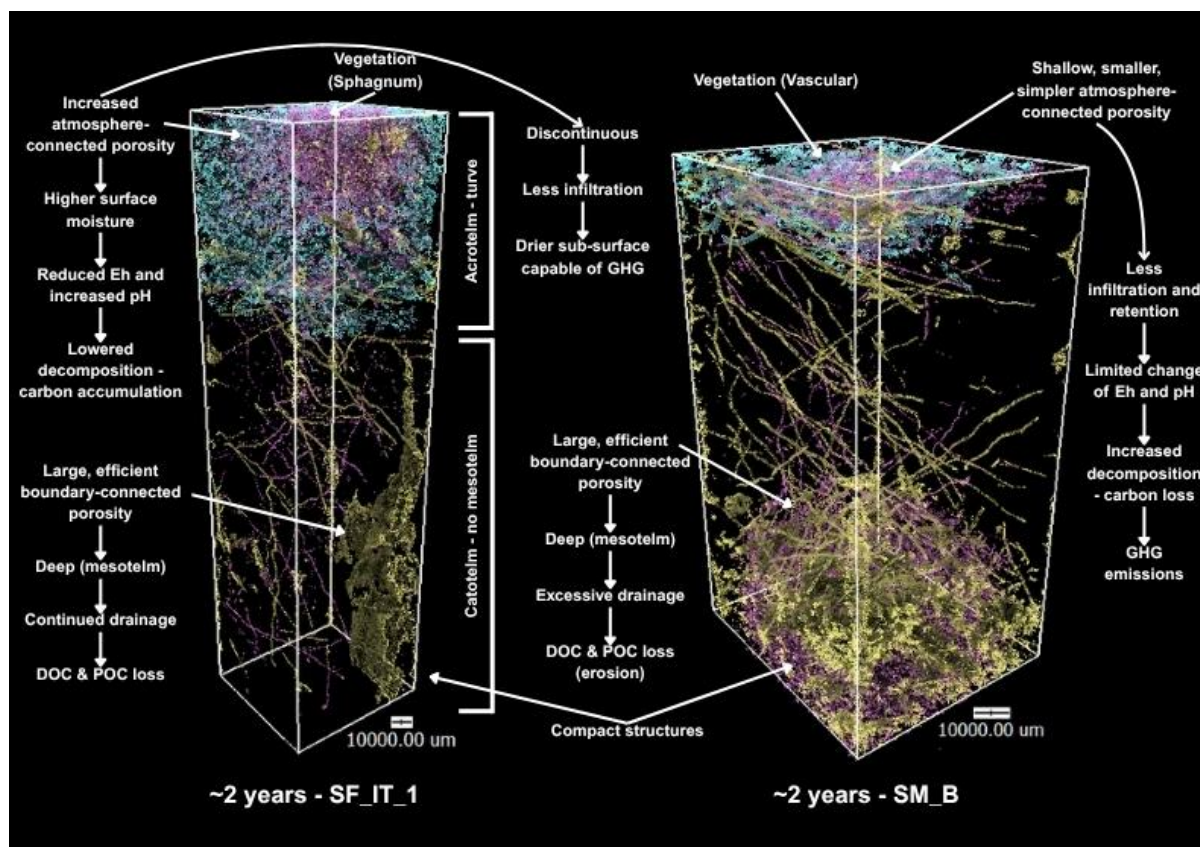
Figure 9.5: Annotated 3D visualisation of the structural and functional impacts of restoration technique between two comparable example cores (~2 years, SF_IT_1 (turving); ~2 years, SM_B (heather brash)). Atmosphere-connected porosity (blue); boundary-connected porosity (orange); isolated porosity (pink). Annotations indicate associated bulk and chemical properties and summarise combined structural and functional inferences.

Not all variation in turved sites was attributable to time (Section 9.1.2a). Structural inconsistencies at Shap Fells and Bampton Common suggest placement technique influences outcomes. Porosity 'gaps' between the acrotelm and catotelm (~15 cm) indicated poor contact, promoting lateral boundary-connected flow and limiting mesotelm development. In contrast, abrupt transitions suggested over-compression, with both reducing vertical continuity. Findings support surface roughening and moderate compression to improve turve integration (Chapter 7; Section 7.3.1). No consistent differences between local and imported turves were observed, highlighting placement as equally important as turve origin.

Stake Moss cores, representing alternative techniques including **heather brash spreading (SM_B), coir logs (SM_C), and stone/timber dams (SM_D),** retained more characteristics associated with the degraded baseline (BC_Deg). Atmosphere-connected porosity was minimal, particularly in SM_B, limiting surface water uptake and retention, as demonstrated in reduced moisture content and higher Eh. At SM_C, atmosphere-connected porosity extended beyond 20cm, indicating a direct path for CH_4 loss through advective transport (Moore *et al.*, 2002). Boundary-connected porosity was also greater in volume and efficiency, with 3D visualisations showing large cracks, branching roots, and degraded catotelm features, especially in SM_B. Although isolated porosity was lower than in BC_Deg, indicating some structural improvement, cores remained distinct from near-natural targets.

Turving is a more effective technique for reinstating sub-surface structure and function. By installing an intact acrotelm, turving promotes atmosphere-connected porosity development, improved surface moisture retention, and more anoxic conditions favourable for GHG reduction.

9.1.3 Sub-Surface Structural and Functional Recovery: Synthesis and Implications

Evaluating divergence from degraded baselines and alignment with near-natural targets is essential for assessing restoration effectiveness. Integrating key pore structural characteristics (Chapter 7; Section 7.5) with bulk and chemical indicators (Chapter 6) reveals pore networks regulating water retention, decomposition, and gas exchange; critical to long-term carbon accumulation and function. This integration directly answers

Research Question 2 and provides a baseline for evaluating surface to sub-surface relationships (Research Question 1) and carbon efficiency (Research Question 3).

Near-natural peat exhibited a clear diplotelmic profile comprising acrotelm, mesotelm, and catotelm layers (Ingram, 1978; Clymo, 1984; Clymo and Bryant, 2008). The mesotelm, previously under-characterised (Chapter 2; Section 2.1.1; Holden and Burt, 2003; Belyea and Baird, 2006; Morris *et al.*, 2011; Baird *et al.*, 2016), emerged as a critical transitional zone, buffering oxic – anoxic boundaries and enabling transitional shifts in pore type and function. This supports its inclusion in conceptual models and addresses requirements for improved mesotelm characterisation (Belyea and Baird, 2006; Morris and Waddington, 2011). Vertical continuity across atmosphere-connected, boundary-connected, and isolated pores was associated with increased water retention, reduced decomposition, and stratified function. *Alignment with bulk chemical indicators, such as low surface bulk density, high moisture, and low Eh, supports the suitability of SF_Nat as a scientifically grounded target for functional restoration.*

Degraded peat consistently lacked a functional acrotelm or mesotelm and was dominated by boundary-connected and isolated porosity. These features facilitated vertical and lateral drainage, oxic decomposition, and continued carbon loss. Relationships between pore structure and bulk chemical properties, such as low moisture content, high Eh, and compacted profiles, supports the use of the degraded site as a reliable baseline. *Findings suggest bulk and chemical indicators can act as cost-effective proxies for sub-surface condition in degraded systems.*

Restored peat exhibited partial sub-surface recovery. While atmosphere-connected porosity developed in the acrotelm, mesotelm formation was absent, and the underlying

catotelm often retained degraded characteristics. Improved surface anoxia indicated positive structural change, yet persistent boundary-connected pores continued to promote drainage and decomposition. Although some surface-level bulk chemical indicators showed improvement, most were less responsive to structural recovery in deeper layers. *This demonstrates a disconnect between bulk chemical indicators and pore network function, revealing limitations in current monitoring protocols (Chapter 2; Section 2.6.2).*

Restoration age influenced the extent of recovery. After ~2 years (Shap Fells), initial acrotelm formation was evident, but vertical continuity was limited and drainage pathways persisted, indicating early-stage recovery with minimal functional benefit. By ~5 years (Bampton Common), more extensive atmosphere-connected porosity and improved near-surface conditions were observed, though over-efficient gas pathways and continued boundary-connected drainage suggested incomplete recovery. At ~10 years (Borrowdale), atmosphere-connected porosity declined, yet deeper profiles showed indicators of consolidation rather than renewed degradation, with improved Eh regulation, reduced decomposition, and more stable biochemical conditions. *Findings indicate restored sites evolve structurally over time, transitioning toward more compact but functionally stable profiles. However, alignment with near-natural targets may require longer timescales than the 5-year assumptions currently embedded in policy and carbon credit validation schemes (Chapter 2; Sections 2.4; 2.7).*

Restoration technique also impacted sub-surface recovery. Turving promoted atmosphere-connected porosity and surface rewetting, but variation in implementation, such as turve placement, led to inconsistent outcomes. Poor bonding between turves

and underlying layers, including porosity gaps or compression-induced compaction, disrupted vertical continuity and limited mesotelm development. *This supports recommendations for surface roughening and moderate compression to support integration.* In contrast, alternative techniques such as heather brash spreading, coir logs, and stone/timber dams yielded pore structures resembling degraded conditions, with limited atmosphere-connected porosity and efficient boundary-connected drainage. Although isolated porosity was sometimes reduced, sub-surface conditions remained largely unsuitable for retention or carbon accumulation. *Findings highlight the importance of both technique selection and implementation quality in achieving effective restoration.*

Collectively, findings offer a more comprehensive understanding of how restoration influences sub-surface structure and function in blanket peatlands. Although restored cores diverged from degraded baselines, they did not align with near-natural targets, even after a decade. These are similar findings to Spencer *et al*. (2017) in restored saltmarshes and questions what the goals of restoration should be and what can be claimed in terms of the outcomes of restoration. *Restoration success cannot be assumed based on intervention alone; it depends on implementation quality and time for structural response.*

> Findings highlight the value of integrating µCT-based assessments into evaluations of functional recovery. However, the extent to which sub-surface processes are reflected in surface conditions remains unclear, demonstrating a critical gap in current monitoring frameworks and limiting the reliability of policy tools reliant on surface indicators (Research Question 1).

9.2 Evaluating the Effectiveness of Surface Indicators in Capturing Sub-Surface Function

Surface indicators underpin peatland restoration assessment across the UK, informing national monitoring frameworks (JNCC, 2009; Shepherd *et al.*, 2013; IUCN, 2018; Birnie *et al.*, 2023; Crowle *et al.*, 2025) and carbon credit schemes such as the IUCN UK Peatland Code (Birnie and Smyth, 2013; Smyth *et al.*, 2015; IUCN, 2024b). The JNCC (2009) *Common Standards Monitoring Guidance (CSM) for Upland Habitats: Blanket Bogs* provides a standardised, surface-based approach using vegetation composition, cover, and disturbance, as rapid, scalable proxies for condition (Billett *et al.*, 2010; Shepherd *et al.*, 2013; Alderson *et al.*, 2019; Crowle *et al.*, 2025). These indicators also inform carbon savings estimates (Couwenberg *et al.*, 2011; Birnie and Smyth, 2013; Lopatin *et al.*, 2019) and the generation of tradable carbon units in voluntary carbon markets (Smyth *et al.*, 2015; IUCN, 2024b).

Chapters 5 and 6 highlighted key limitations of the JNCC (2009) surface indicators in detecting recovery in restored sites, largely due to threshold-based criteria. Even when treated as continuous variables, surface scores showed weak correlations with sub-surface bulk and chemical properties, limiting their ability to reflect processes governing long-term carbon accumulation. Findings question the suitability of surface-based monitoring for restoration assessment and carbon accounting. Building on this and the integrated understanding of sub-surface function presented in Section 9.1, the effectiveness of JNCC (2009) condition scores is now evaluated to determine whether surface indicators reliably capture functional recovery in restored blanket peatlands (Research Question 1).

9.2.1 Capturing Sub-Surface Function Using JNCC (2009) Surface Indicators

Evaluating surface condition alongside sub-surface structural and functional descriptors explores the degree to which JNCC (2009) *Common Standards Monitoring Guidance (CSM) for Upland Habitats: Blanket Bogs* indicates hydrological, biochemical, and carbon dynamic function across degraded, restored, and near-natural sites. Table 9.1 presents a comparison between the JNCC (2009) condition scores (Chapter 5; Section 5.5.1) and qualitative assessments of sub-surface structure and associated bulk and chemical properties indicative of functionality (Section 9.1).

Threshold-based application of JNCC (2009) distinguished degraded and near-natural sites, but lacked sensitivity to detect recovery in restored cores (discussed in Chapter 5). Therefore, the condition scores derived from continuous JNCC (2009) survey data and are used to better represent variation across restored sites (Chapter 5; Section 5.5.1; Table 5.4).

Table 9.1: Comparison of JNCC (2009) surface condition scores with qualitative assessments of sub-surface structure and function across control and restored cores. ACP = atmosphere-connected porosity; BCP = boundary-connected porosity; IP = isolated porosity; BD = bulk density; MC = moisture content; Eh = redox potential.

Core ID	JNCC (2009) Condition Score	Sub-Surface Structure	Sub-Surface Function
BC_Deg	*0.21*	*No acrotelm or mesotelm. Dominated by BCP and IP. High compaction and fragmentation.*	*High BD, low MC, high Eh. Indicates oxic decomposition and increased carbon loss.*
BW_LT	0.76	Transitional structure: weak acrotelm–mesotelm development. Limited ACP, some stratification; compact deeper layers with reduced BCP.	High BD, moderate MC, increased pH and lower Eh. Evidence of sub-surface anoxia and retarded decomposition.
BC_IT	0.68	Acrotelm to catotelm transition present. Over-efficient ACP; BCP persists at depth; reduced IP.	High BD, increased surface MC, moderate Eh reduction. Indicates partial hydrological function.
BC_LT	0.75	Similar to BC_IT, mesotelm remains absent.	Surface MC and BD improved. Sub-surface remains partially oxic.
SF_IT	0.66	ACP developing with fragmented stratification. BCP remains dominant at depth.	Higher MC, slight BD reduction. pH and Eh not yet comparable to near-natural.
SF_LT	0.76	Comparable to SF_IT; mesotelm absent but improved surface structure.	MC and BD approach near-natural values. Moderate functional recovery.
SM_B	0.47	Limited ACP; rooted compact structure with dominant BCP. Early-stage recovery.	High BD, low MC, and Eh. Functionally degraded.
SM_C	0.62	Similar to SM_B with slightly deeper ACP penetration. Stratification absent.	Moderately improved MC, but still high BD and low Eh. Functionally limited.
SM_D	0.61	Comparable to SM_B and SM_C. Dominant BCP persists. Stratification absent.	Subtle chemical improvement; oxic conditions remain.
SF_Nat	*0.88*	*Well-developed, stratified acrotelm, mesotelm, and catotelm. High ACP connectivity.*	*Low BD, high MC, low Eh. Fully anoxic profile supports low decomposition and carbon retention.*

a) Relationships Between Surface and Sub-Surface

Table 9.1 and Figure 9.6 demonstrate JNCC (2009) surface condition scores reliably distinguish near-natural (SF_Nat) and degraded (BC_Deg) conditions, aligning with findings in Chapters 5 and 6.
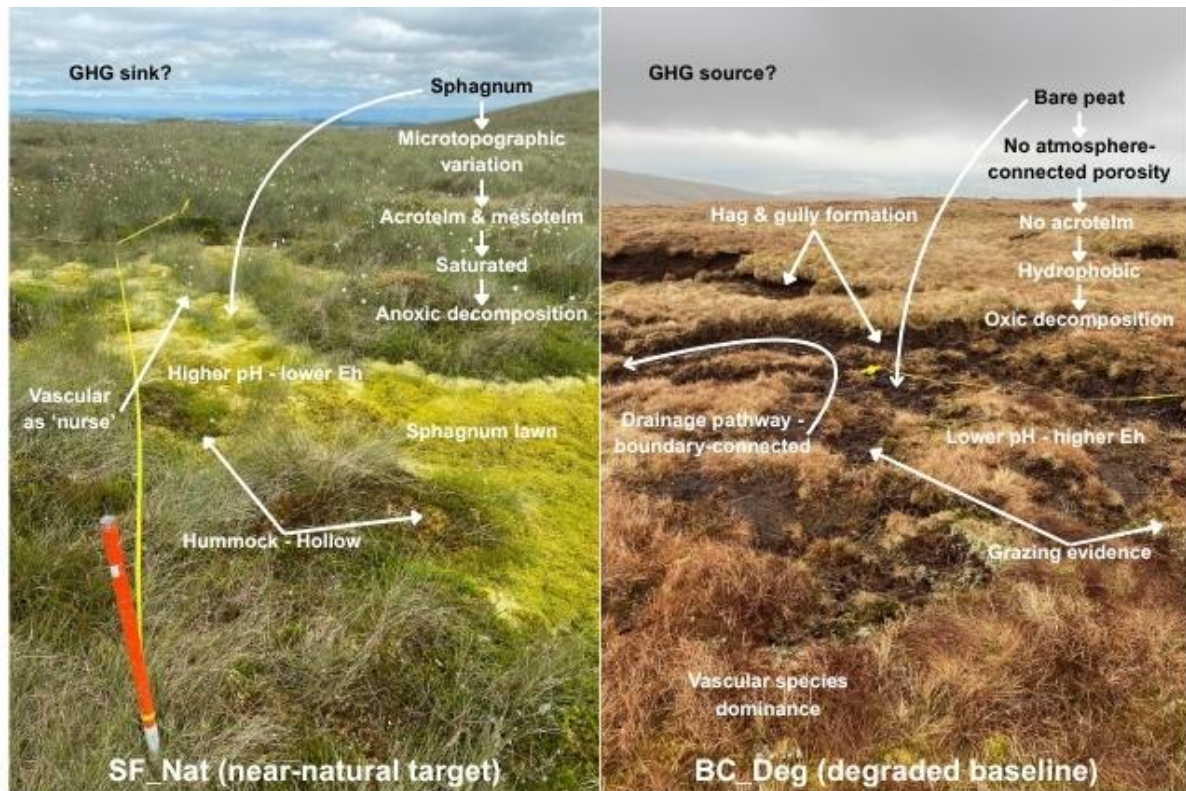
Figure 9.6: Annotated images of the near-natural (SF_Nat - left) and degraded control (BC_Deg – right) plots showing contrasting surface and sub-surface conditions.

SF_Nat shows the highest condition score (0.88) and most structurally and functionally intact sub-surface, including stratified acrotelm – mesotelm – catotelm layers, high and tortuous atmosphere-connected porosity, low surface bulk density, and saturated, anoxic conditions conductive to carbon accumulation. Notably, SF_Nat was the only core to exhibit an intact mesotelm, supporting the role of this layer in peat formation (Section 9.1.3). **BC_Deg** records the lowest surface score (0.22), consistent with compact, fragmented sub-surface structure dominated by boundary-connected and

isolated porosity, high surface bulk density, and oxic conditions (hydrophobic layer). These patterns correlate with surface indicators. SF_Nat exhibits the highest *Sphagnum* cover (~33%), low browsing (demonstrating effective exclusion zones; Chapter 5), and minimal degradation, while BC_Deg shows low indicator species richness, dominance of vascular species, and extensive bare peat and disturbance, including *Sphagnum* damage (Figure 9.6).

However, the relationship between surface condition and sub-surface recovery becomes less consistent across restored sites. **Borrowdale – Local Turving (BW_LT)** records a high surface condition score (0.76) and increased *Sphagnum* cover, yet the sub-surface remains transitional across both cores, lacking mesotelm development and diverging from SF_Nat after a decade. This correlates with PCA results (Chapter 5; Section 5.2.4), where BW_LT clusters nearer SF_Nat in vegetation composition but remains structurally distinct. **Shap Fells – Local Turving (SF_LT)** records a similar surface score after ~2 years (0.76), despite reduced sub-surface development, including persistent boundary-connected pores at depth and oxic conditions supporting rapid decomposition. These patterns are also evident across **Bampton Common – Imported (BC_IT)** and **Local Turved (BC_LT)** sites, suggesting surface indicators can overestimate recovery and fail to capture sub-surface structural change over time. This may represent surface assessments evaluating the condition of the placed turves rather than the functional recovery of the peatland.

Findings support that sub-surface recovery lags behind surface change, and that restoration age is not a reliable predictor of condition.

Surface condition scores captured variation between revegetation techniques, but not between rewetting methods or turve materials. Clear differences were observed between turving at Shap Fells (SF_IT, SF_LT) and heather brash spreading at Stake Moss (SM_B) (Figure 9.7).

Figure 9.7: Annotated images of the SF_LT (left) and SM_B (right) sites showing contrasting surface and sub-surface conditions.

Turving at Shap Fells exhibited higher condition scores (0.66-0.76), partial acrotelm development, and increased anoxia and pH, conditions associated with ~25% *Sphagnum* cover. **Heather brash spreading** at Stake Moss recorded the lowest surface condition score among restored sites (0.47), alongside minimal atmosphere-connected porosity and effective boundary-connected networks at depth, associated with vascular species dominance and evidence of drainage. Findings support turving as a more

effective technique in restoring an intact acrotelm and promoting sub-surface recovery, as well as surface biodiversity (Figure 9.7).

However, finer-scale surface variation between **local** and **imported turves**, such as increased species richness, cover, and reduced disturbance in local turves (Chapter 5), did not correspond to measurable differences in sub-surface structure and function. Furthermore, **coir log** (SM_C) and **dam** (SM_D) treatments exhibited moderate surface scores (0.61-0.62), yet shared compact, unstratified sub-surface structure, dominated by boundary-connected porosity and oxic conditions consistent with drainage.

> Findings demonstrate limited capacity of surface condition scores to detect technique variation in sub-surface recovery.

b) Identifying Potential Proxies

Figure 9.8 presents a conceptual summary of how JNCC (2009) surface indicators may relate to underlying sub-surface structural and functional characteristics across sites. Relationships are informed by a combination of qualitative (Chapter 7; Section 7.5 and Section 9.1.1) and quantitative (Chapter 6; Section 6.2) analysis, but are not statistically significant due to limited populations. Moreover, improvements often occurred independently. For example, while *Sphagnum* cover may relate to increased atmosphere-connected porosity and surface saturation, supporting an intact acrotelm, boundary-connected porosity often persisted, sustaining continued sub-surface degradation in the catotelm (Section 9.2.1.c). Nevertheless, the framework contributes to integrating sub-surface understanding into existing surface-based monitoring and carbon accounting approaches, offering insights relevant to Research Question 1.
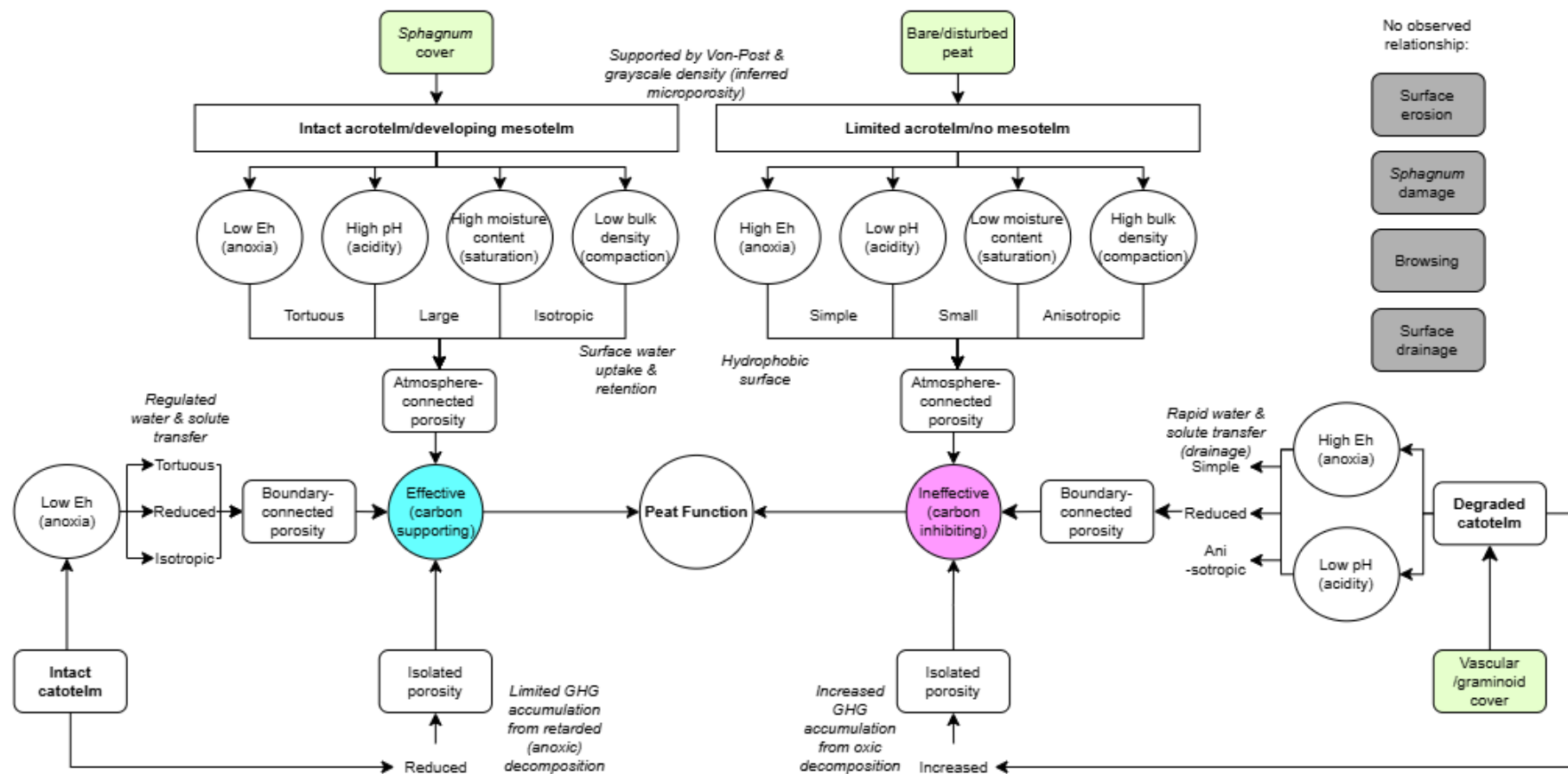
Figure 9.8: Summary diagram illustrating how JNCC (2009) surface indicators may correspond to sub-surface structural and functional characteristics observed across restored blanket peatland sites.

Sites dominated by **vascular and graminoid species** (e.g., Stake Moss, Shap Fells) exhibited greater boundary-connected porosity, limited acrotelm development, and more oxic, acidic sub-surface conditions, supporting drainage, decomposition, and likely increased GHG emissions. In contrast, turved sites showed greater ***Sphagnum* cover**, with increased atmosphere-connected porosity, higher surface moisture, and increased pH, despite receiving similar JNCC (2009) condition scores. This discrepancy reflects the equal weighting of indicator species in JNCC (2009), which overlooks compositional differences influencing sub-surface hydrological and biochemical function (Chapter 5; Section 5.5.2).

Some correspondence was observed between **bare peat extent** and poor acrotelm development. *Sphagnum* cover promoted atmosphere-connected porosity and vertical continuity, while persistent bare peat or damaged ground limited recovery by maintaining hydrophobic surface layers that restricted water infiltration and sustained oxic, acidic profiles. Although some interventions disrupted these layers to support surface to sub-surface exchange, passive revegetation methods such as heather brash spreading failed to initiate acrotelm formation, suggesting a more direct approach may be required (e.g., optimal turve pressing; Section 9.1.2).

Other indicators. such as surface erosion, drainage, *Sphagnum* damage, and browsing, showed limited or inconsistent correspondence with sub-surface characteristics in early-stage restorations. However, their influence may be greater at other sites. For instance, differences between grazing exclusion zones at Shap Fells and Bampton Common (Chapter 5; Section 5.3) suggest browsing may have a more pronounced impact at heavily grazed sites.

Findings demonstrate the limited ability of JNCC (2009) to distinguish structurally functional from non-functional ecological indicators in restored sites, especially where favourable surface appearances obscure sub-surface degradation (Section 9.2.1c). Nevertheless, potential proxy relationships involving *Sphagnum* presence, vascular/graminoid dominance, and bare peat cover could improve existing monitoring frameworks using current indicators.

c) Recommendations for Surface-Based Assessment

Based on the evaluation of JNCC (2009) *Common Standards Monitoring Guidance (CSM) for Upland Habitats: Blanket Bogs* in capturing sub-surface structure and function, and its critical assessment in Chapters 5 and 6, the following recommendations are proposed to support future use of the framework in peatland restoration monitoring protocols, including those adopted by Natural England (Shepherd *et al.*, 2013; Crowle *et al.*, 2025) and NatureScot (Birnie *et al.*, 2023), as well as those used for carbon savings estimates (IUCN, 2024b).

Reliance on binary and threshold-based criteria should be reconsidered. Findings from combined analysis of surface and sub-surface indicators support earlier recommendations in Chapter 5 to remove binary and threshold-based criteria. These restrict the ability of surface indicators to measure restoration success and mask sub-surface processes related to carbon accumulation. By collecting and reporting actual values (or simplified categorical data), a richer dataset can be produced, increasing understanding of wider ecosystem service benefits such as biodiversity gain, which is

increasingly important in future blended finance models (Chapter 2; Section 2.4; Reed *et al.*, 2013; Bonn *et al.*, 2014, 2016a; IUCN, 2025b).

The presence and proportion of *Sphagnum* should receive specific attention rather than being combined with other bryophyte, vascular, and graminoid species into a single indicator group. *Sphagnum* should be emphasised, particularly as a proxy for atmosphere-connected porosity, hydrological function, reduced acidity (from degraded baselines), and net carbon accumulation. The exclusion of *Sphagnum fallax* from favourable condition classification is especially challenging in restored contexts, where its early establishment may indicate sub-surface functional recovery (Chapter 5; Section 5.6). Furthermore, the associated microtopographic complexity introduced by *Sphagnum* may be integrated into current frameworks as an additional proxy for surface roughness (reduced surface run off and water uptake), acrotelm development, and long-term carbon benefit (Belyea and Clymo, 2001; Belyea and Malmer, 2004) Chapter 5; Section 5.5.2).

Greater emphasis should be placed on the extent of bare peat, which often correlates with hydrophobic surface layers and oxic sub-surface conditions associated with carbon loss. These indicators may serve as a proxy for reduced water infiltration, restricted vertical continuity, acidity, and CO_2 emissions, demonstrating the requirement for direct disturbance in restoration to reinstate acrotelm development (e.g., optimum turve placement). Consequently, bare peat should be weighted more heavily in monitoring frameworks, particularly in carbon accounting protocols, rather than grouped with other degradation indicators (e.g., disturbed ground; JNCC, 2009).

Restoration technique should be documented and interpreted alongside surface condition scores. Removal of binary thresholds enables more meaningful assessments of functional recovery, yet without contextual information on the intervention applied, condition scores risk misinterpretation. As demonstrated in Chapters 6 and 7, different techniques influence sub-surface processes in different ways (e.g., turving versus heather brash spreading in supporting acrotelm formation), making it essential to consider implementation alongside condition outcomes. Despite this, restoration technique is rarely recorded in current reporting (Chapter 2; Section 2.5).

These refinements remain grounded in existing monitoring and carbon accounting protocols enabling swift adoption (Research Question 1). They also provide a framework for more accurate, scalable evaluations of recovery, particularly when integrated with remote sensing, to assess condition beyond the surface (Chapter 2; Section 2.6.2; Luscombe *et al.*, 2015; Lees *et al.*, 2019, 2021; Alshammari *et al.*, 2020; Minasny *et al.*, 2024).

9.2.2 Capturing Sub-Surface Function Using Surface Indicators: Synthesis and Implications

Surface indicators, including those used in the JNCC (2009) *Common Standards Monitoring Guidance (CSM) for Upland Habitats: Blanket Bogs*, do not consistently capture sub-surface structural and functional recovery in restored sites. While they effectively distinguish degraded and near-natural conditions, their limited sensitivity restricts their ability to evaluate gradual recovery. This has implications for current monitoring and reporting frameworks, particularly those using indirect surface proxies for carbon accounting, such as the IUCN UK Peatland Code (IUCN, 2024b). In their current

form, these tools risk overestimating restoration success by failing to detect lagging or incomplete sub-surface recovery.

Some surface indicators captured sub-surface structure and function more effectively than others. *Sphagnum* presence aligned with characteristics such as increased atmosphere-connected porosity, improved pH, and reduced Eh, indicative of an intact acrotelm. In contrast, bare peat and vascular/graminoid dominated sites were associated with compacted, oxic profiles lacking vertical continuity and water retention in the catotelm. *Findings support the use of Sphagnum cover, vascular/graminoid dominance, and bare peat extent as surface proxies for hydrological and biochemical function.* However, current frameworks do not adequately distinguish between functionally distinct surface states, limiting their interpretive value, and these indicators do not necessarily tell the whole story.

Although surface condition scores improved with restoration, gains often occurred independently of sub-surface structural recovery, particularly at depth (Section 9.1.1). Increases in *Sphagnum* cover, reduced vascular/graminoid dominance, and minimal bare peat contributed to higher scores and were associated with functional layer development, including acrotelm formation and improved water retention. However, mesotelm formation remained absent across restored cores, and boundary-connected networks persisted, enabling drainage even where *Sphagnum* had established. *This disconnect suggests vegetation change may precede sub-surface recovery, particularly in turved sites, obscuring the true extent of restoration success.*

Restoration technique was a key determinant of sub-surface structure and function. Turved sites showed improved atmosphere-connected porosity and biochemical

416

conditions compared to sites restored with heather brash (and coir logs or stone/timber dams). However, these differences were not always captured by surface scores, particularly in early-stage restorations where vegetation cover obscured underlying structural degradation. *This highlights the importance of recording and contextualising surface assessments by intervention type,* as recommended in Chapter 2 (Section 2.5).

Refinements grounded in current practice could address these limitations. These include removing binary thresholds, recording actual values or simplified categories, increasing the weighting of *Sphagnum* (including species such as *Sphagnum fallax*), treating bare peat as a standalone degradation indicator, and recording restoration technique alongside surface data. Incorporating pH and Eh as proxies for sub-surface structure and function could improve interpretation and alignment with sub-surface indicators without introducing new methodologies (Chapter 6; Section 6.2). These refinements would also support integration with remote sensing approaches, enabling more accurate and scalable evaluations of condition and carbon outcomes (Luscombe *et al.*, 2015; Lees *et al.*, 2019, 2021; Alshammari *et al.*, 2020; Minasny *et al.*, 2024).

Findings confirm the limited ability of surface indicators to capture sub-surface structural and functional recovery (Research Question 1), particularly in the context of restoration monitoring and carbon credit validation. Without integration of sub-surface data and restoration context, there is a risk of overestimating recovery outcomes. Monitoring frameworks should place greater emphasis on intervention effectiveness and carbon efficiency to support robust, evidence-based assessment (Research Question 3).

9.3 Evaluating Technique Effectiveness: Function and Net Carbon Benefit

Peatland restoration aims to rewet and revegetate degraded sites (Holden *et al.*, 2004; Parry *et al.*, 2014; Thom *et al.*, 2016), reducing carbon emissions and recovering ecosystem services (Chapter 2; Sections 2.4.2; 2.5; Bain *et al.*, 2011; Bonn *et al.*, 2014, 2016a; Evans *et al.*, 2017). Widely adopted guidance, including *Conserving Bogs: The Management Handbook* (Thom *et al.*, 2019) and *Peatland ACTION – Technical Compendium* (NatureScot, 2021), recommend a range of interventions designed to meet these objectives, differing in material composition and method of installation (Chapter 2; Section 2.5). However, as demonstrated in Sections 9.1 and 9.2, functional recovery varies by technique, with some approaches supporting more functional outcomes than others (detailed in Chapters 5, 6, and 7). This suggests specific interventions may be more effective in delivering long-term carbon benefits and wider ecosystem service gains (Chapter 5; Section 2.5).

Moreover, Chapter 8 identified significant variation in the carbon costs of restoration interventions, with emissions differing by orders of magnitude depending on raw materials, transportation, and installation. As carbon remains the primary metric in restoration success (Chapter 2; Sections 2.6; 2.7), these differences have implications for reporting and carbon accounting under the IUCN UK Peatland Code (IUCN, 2024a). Some techniques may deliver increased functional recovery (including reduced GHG emissions) and lower carbon costs, offering greater carbon efficiency. Others may incur high carbon costs relative to their functional benefits, undermining their contribution to climate mitigation and limiting their viability as financeable nature-based solutions

(Drever *et al.*, 2021). This is critical considering the variable response of sites to restoration, with some remaining net GHG sources for decades post-intervention (Chapter 2; Section 2.4.2; Cooper *et al.*, 2014; Vanselow-Algan *et al.*, 2015). Findings support the requirement to evaluate technique effectiveness on carbon balance but also broader ecosystem service delivery, with implications for finance and reporting frameworks (Whitfield *et al.*, 2011; Grand-Clement *et al.*, 2013; Reed *et al.*, 2013, 2022; Bonn *et al.*, 2014, 2016a; Stoneman *et al.*, 2016; Wichmann *et al.*, 2016; IUCN, 2025b).

9.3.1 Restoration Technique and Functional Recovery

Restoration technique influenced the degree of functional recovery, as demonstrated through comparisons between local and imported turves at Bampton Common and Shap Fells, and between turving and heather brash spreading as revegetation interventions across Shap Fells and Stake Moss, respectively, where sites represented ~2 years post-restoration. While less comparable due to differing objectives, contrasts were also observed across coir log and stone/timber dam installation approaches, as well as local turving at Borrowdale, representing a longer-term restoration example. Findings build on Sections 9.1 and 9.2, demonstrating how material source and installation method influenced surface and sub-surface structure and function, with implications for long-term carbon accumulation.

a) Turving approaches

Across Bampton Common and Shap Fells, minimal variation in sub-surface structure was observed between **locally sourced** and **imported turves**. Both exhibited mixed stratification, with no evidence of mesotelm development, indicators of gaps between placed turves or over-compaction (poor bonding), and persistent boundary-connected

porosity, indicative of incomplete hydrological recovery. Findings suggest installation method, rather than turve origin, was the primary determinant of structural restoration. Effective installation should therefore focus on disrupting the degraded, hydrophobic surface layer prior to placement and supporting compression of the turve into the underlying peat to promote vertical continuity (Chapter 7; Section 7.4). This would reduce the risk of slippage and increase intervention resilience.

However, **locally sourced turves** more consistently supported improved sub-surface bulk chemical properties and biodiversity gain. They were associated with reduced temperature gradients, indicative of lower microbial activity and GHG emissions, and exhibited more consistent profiles across bulk and chemical indicators. Findings suggest better integration with the underlying peat, possibly due to reduced spatial variability in site conditions. Local turves also consistently exhibited higher species richness and greater *Sphagnum* cover, indicating higher-quality turves with more intact acrotelms, potentially preserved by limited disturbance during transport. As discussed in Section 9.2, *Sphagnum* serves as a proxy for atmosphere-connected porosity and surface water uptake capacity, suggesting local turving may support more retentive sub-surfaces over time. This is supported by the functional recovery observed in local turves at Borrowdale.

Despite structural inconsistencies, findings support local turving as a more effective technique, particularly in biodiversity gain, due to closer alignment with site-specific conditions and more intact structures through limited transport. Nevertheless, turved sites remained structurally and functionally distinct from near-natural conditions, even after a decade. This demonstrates the importance of aligning turve selection and

placement with site-specific objectives and highlights the requirement to integrate structural, biochemical, and vegetation indicators when evaluating success.

b) Alternative methods

Comparisons between **turved** sites at Shap Fells and **heather brash spreading** at Stake Moss demonstrated distinct differences in sub-surface structure and function, despite similar time since restoration (~2 years). Cores from **Shap Fells**, irrespective of turve origin, demonstrated early signs of acrotelm recovery, evidenced by increased atmosphere-connected porosity and inferred microporosity near the surface. This was supported by increased surface wetness, reduced compaction, lowered Eh, and the presence of *Sphagnum*. While surface disturbances (e.g., damaged ground and bare peat) and sub-surface degradation (e.g., large, lateral boundary-connected pores at depth) remained, findings indicate the initiation of functional recovery. The heather-brash site at **Stake Moss** exhibited limited vertical stratification, with no clear acrotelm development and a higher proportion of efficient boundary-connected porosity at depth, promoting lateral drainage and solute export. This related to poor water retention capacity, indicated at the surface by the absence of *Sphagnum*, the highest erosion potential (lowest peat regrowth), and in sub-surface bulk chemical properties, which exhibited high Eh, low pH, and indicators of rapid decomposition. These contrasts are demonstrated in Figure 9.7.

Although both interventions aimed to revegetate reprofiled gullies, findings suggest turving produced more favourable conditions for surface to sub-surface integration and functional recovery within ~2 years. This is likely due to the contrasting material used. Heather brash promotes vascular dominance and relies on successional development

over time, whereas turving introduces an intact acrotelm and physically disrupts underlying degraded structures through tracking and compression, facilitating rapid surface to sub-surface integration.

While not directly comparable due to differing objectives, **coir log** and **damming** interventions at Stake Moss were associated with less functional outcomes than turved sites. Sub-surface structures exhibited poor stratification and limited acrotelm development, with boundary-connected porosity dominating at depth, supporting more oxic, acidic, and compact conditions conducive to carbon loss. Surface vegetation indicated these limitations. *Sphagnum* was largely absent or restricted to species other than *Sphagnum cuspidatum*, which was consistently present across turved sites. Persistent disturbance, particularly bare peat and damaged *Sphagnum* further restricted recovery. In contrast, **turving** introduced an intact acrotelm and supported development of tortuous pore networks capable of water retention, promoting anoxia and creating conditions more favourable for carbon accumulation. Findings suggest turving may be most effective when coupled with rewetting approaches such as coir log installation or damming, helping to retain water introduced by rewetting interventions. Integrating structural re-vegetation (e.g., turving) with hydrological techniques therefore represents a more effective strategy than using heather or grass-spread approaches, accelerating surface and sub-surface recovery. However, as demonstrated in Chapter 2; Section 2.5 (Thom *et al.*, 2019; NatureScot, 2021), multiple combinations of restoration techniques are available, associated with significantly different carbon costs influencing net carbon-benefits (Chapter 8).

9.3.2 Carbon Costs as an Indicator of Success

Chapter 8 demonstrated the carbon costs of blanket peatland restoration interventions vary substantially, ranging from ~0.34 $kgCO_2eq$ (peat bunds) to ~135.94 $kgCO_2eq$ (stone dams) for individual rewetting techniques, and ~471.76 $kgCO_2eq/ha$ (local turves) to ~63,652.20 $kgCO_2eq/ha$ (Geojute) for revegetation at the hectare scale. Interventions involving exotic materials sourced through global supply chains (e.g., coir) or helicopter delivery incurred the highest emissions, while those using local materials (e.g., peat) and manual or low-pressure ground machinery were significantly lower. At the project scale, these differences become impactful, with carbon-intensive interventions potentially offsetting or delaying net carbon benefits (Chapter 8; Section 8.3). Although greater carbon costs may be justifiable if they deliver greater functional benefits (Drever *et al.*, 2021), this trade-off remains unassessed. As carbon represents the dominant metric used to assess restoration success (Chapter 2; Section 2.6) and secure private finance (Chapter 2; Section 2.7), integrating carbon costs into accounting frameworks such as the IUCN UK Peatland Code (IUCN, 2024a) is critical for increasing robustness and attracting investment.

a) Carbon Costs Versus Functional Benefit

Table 9.2 presents carbon cost data from Chapter 8 to quantify the carbon costs associated with interventions at **Shap Fells** and **Stake Moss**. This enables a comparative assessment of functional recovery and carbon efficiency across sites adopting local, low-carbon techniques versus those using exotic, carbon-intensive approaches (Chapter 4; Section 4.2).

Table 9.2 Breakdown of total carbon costs associated with comparable (~2 years post-restoration; revegetation of gully sides) restorations at Shap Fells and Stake Moss using average raw material, transport, and installation data from Chapter 8. *Note the stone and timber dam figure accounts for the actual number of stone versus timber applications (Chapter 4; Section 4.3.1), representing a combined total.

Site	Intervention	Number/Hectares	Total Carbon Emissions (kgCO$_2$eq)	Total Restoration Emissions (kgCO$_2$eq)
Stake Moss	Heather Brash (SM_B)	6.34 ha	72,780	**106,070**
	Coir Logs (SM_C)	1,217	15,860	
	Stone/Timber Dams (SM_D)*	423	17,430	
Shap Fells	Imported Turving (SF_IT)	9.01 ha	2,680	**3,050**
	Local Turving (SF_LT)	0.91 ha	370	

Heather brash spreading at Stake Moss incurred substantially higher carbon costs (~72,780 kgCO$_2$e/ha) than **turving** at Shap Fells (~3,050 kgCO$_2$e/ha in total), even when heather brash was applied to an additional 2.67ha. Despite this higher cost, SM_B showed limited structural and functional recovery, with surface and sub-surface characteristics resembling the degraded control. Turving at Shap Fells supported early-stage acrotelm formation (e.g., effective atmosphere-connected porosity), increased saturation, and *Sphagnum* re-establishment. Findings indicate greater carbon costs does not necessarily yield greater functional benefit.

This relationship is visualised in Figure 9.9, which presents a carbon cost–function plot for each intervention type. Functional scores were derived by normalising observed indicators from Figure 9.8 onto a 0–10 scale and weighting them against JNCC (2009) condition scores to reflect carbon efficiency (functional benefit relative to carbon cost) at each site (including Borrowdale and Bampton Common). While structural indicators

are based on qualitative interpretation and data includes anomalies such as the mineral layer identified in BC_IT_1, the infographic illustrates the lack of correlation between intervention carbon cost and functional benefit, with some high-emission techniques delivering limited recovery, and lower-emission approaches supporting more effective restoration.
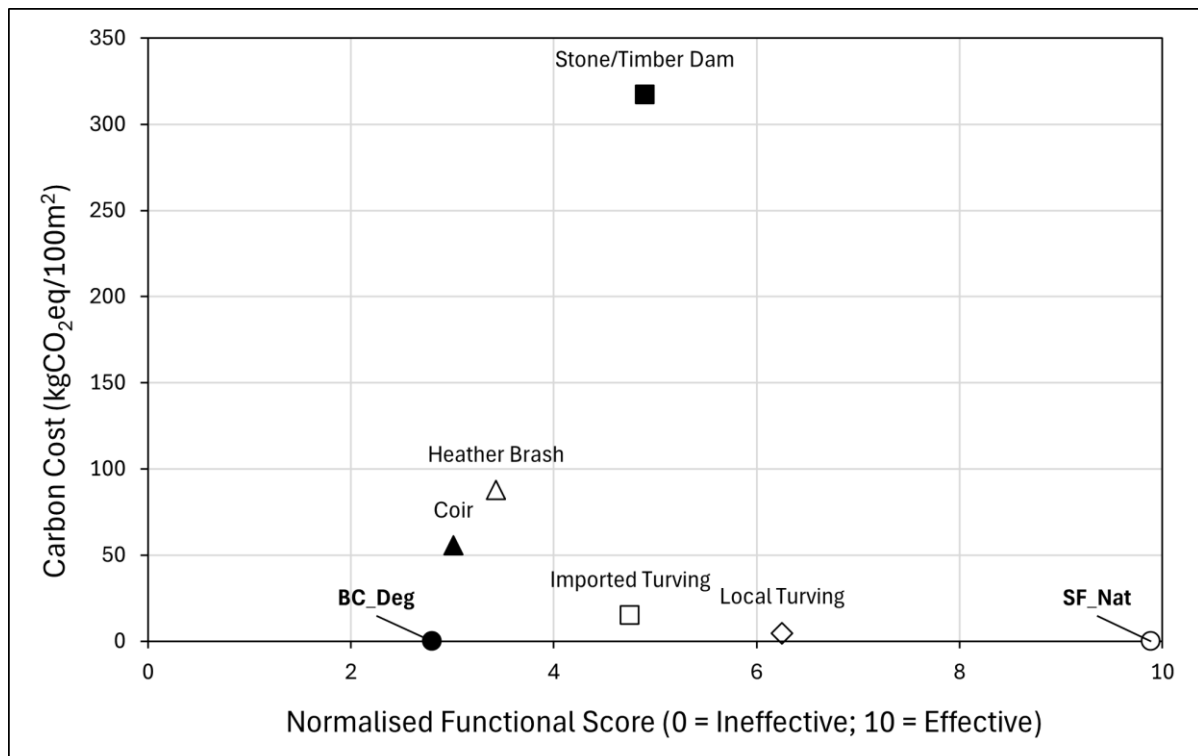
Figure 9.9: Comparison of mean normalised functional indicator scores and total carbon costs (kgCO$_2$e) for selected restoration interventions. Functional metrics include porosity types, bulk density, moisture content, pH, Eh, and *Sphagnum*, vascular/graminoid, and bare peat cover (see Figure 9.8). Carbon costs are derived from Chapter 8.

While not directly comparable, **coir logs** and **stone/timber dams** also incurred considerably higher emissions with less evidence of functional recovery (Figure 9.9). When evaluated alongside functional outcomes, it may be justifiable to supplement such interventions with low-carbon local turves. This could increase surface hydrology and biodiversity at minimal additional carbon cost, improving functional potential and reducing future GHG emissions. Findings demonstrate how integrating carbon cost data

with functional recovery can improve restoration planning, supporting more efficient and net sequestration-aligned delivery.

b) Trade-offs Between Carbon Costs and Functional Outcome

Beyond the sites evaluated in this investigation, additional interventions assessed in Chapter 8 further contextualise restoration efficiency. Techniques such as **Geojute application** (~63,652.20 kgCO$_2$eq/ha), **plug planting** (~16,575.23 kgCO$_2$eq/ha), and **plastic piling** (~52.52 kgCO$_2$eq) exhibited significantly higher carbon costs than local interventions such as **peat dams** (~0.49 kgCO$_2$eq) and **bunds** (~0.34 kgCO$_2$eq). Interventions using exotic materials or helicopter delivery demonstrated emissions orders of magnitude greater than those based on locally sourced materials, manually or low ground-pressure vehicle installed. While such techniques are often necessary to stabilise severely degraded peat (Parry *et al.*, 2014; Thom *et al.*, 2016) or access remote areas (Thom *et al.*, 2019; NatureScot, 2021), findings suggest they do not deliver functional outcomes comparable to near-natural targets, even after a decade. As evidenced by the Holcombe Moor case study (Chapter 8), carbon-intensive interventions may cumulatively offset benefits, delaying net transitions from source to sink.

Findings support the requirement to prioritise techniques promoting long-term carbon storage functions while minimising carbon costs, particularly considering the extended timescales and variable carbon outcomes associated with peatland restoration (Chapter 2; Section 2.4.2; Cooper *et al.*, 2014; Vanselow-Algan *et al.*, 2015; Alderson *et al.*, 2019). They further support the inclusion of broader ecosystem benefits as part of restoration success, better justifying interventions and attracting private investment.

9.3.3 Implications for the IUCN UK Peatland Code

The IUCN UK Peatland Code is the primary mechanism for quantifying, verifying, and financing carbon savings from peatland restoration through voluntary carbon markets in the UK (Reed *et al.*, 2013; Hooker and Wentworth, 2024; IUCN, 2024a). Until recently, it did not explicitly account for the carbon costs of restoration, instead applying a uniform 10% deduction from projected carbon savings as a 'carbon cost buffer'; lacking empirical evidence (IUCN, 2024a). This research directly addressed that gap. The carbon cost data presented in Chapter 8 have now been incorporated into the updated IUCN UK Peatland Code Carbon Savings Calculator (Brennand *et al.*, 2025; IUCN, 2025a). This integration allows restoration projects to quantify the emissions associated with selected interventions, enabling site-specific estimation of net carbon savings and more accurate PIU calculations. While the updated tool has not yet been widely adopted, it allows decision-makers to evaluate the carbon intensity of interventions during the design phase. This promotes greater transparency and provides an environmental incentive to select more sustainable approaches, supporting carbon accounting integrity and increased credit returns.

However, while intervention emissions are now better accounted for, **the current Peatland Code Field Protocol (IUCN, 2024b) fails to capture sub-surface structural functions indicative of long-term carbon storage**. For example, *Sphagnum* cover is a key proxy for acrotelm development, supporting atmospheric connections, water retention, and reduced decomposition (Section 9.2), yet this is not currently used to inform emissions factors or carbon savings estimates (Birnie and Smyth, 2013; Smyth *et al.*, 2015). As with other versions of condition assessment (JNCC, 2009; Shepherd *et al.*,

2013; Birnie *et al.*, 2023; Crowle *et al.*, 2025), greater integration of functional indicators could refine emissions factors further (Chapter 2; Section 2.7), increasing or decreasing estimated savings based on more accurate condition. *Incorporating such metrics would align carbon valuation with function, improving the credibility and accuracy of peatland carbon accounting.*

This development increases the robustness of carbon savings estimates, previously limited by proxy assumptions (Chapter 2; Section 2.6) **and simplified models** (Chapter 2; Section 2.1.1). *Improved credibility could increase investor confidence, supporting the role of the Peatland Code within blended finance models and supporting uptake of peatland restoration as a nature-based solution in national climate policy; addressing a critical financial barrier in restoration delivery* (Chapter 2; Section 2.4.2; Moxey *et al.*, 2021). Long-term, this could also increase the value of carbon credits, currently priced at ~£15-25 per verified Peatland Carbon Unit (PCU) though not yet traded, by demonstrating measurable reductions in intervention emissions and improved accountability.

However, **carbon costs should not be the only determining factor of intervention choice.** While findings indicate lower-carbon intensive approaches (e.g., local turving) can deliver greater functional outcomes, conclusions are based on a limited number of sites and sub-samples. Practical factors, such as the quality and availability of turves, can also influence intervention success. *Carbon costs should therefore be one component of a wider decision tree, assisting projects to tailor intervention selection to site conditions and net functional benefit, rather than relying on standardised guidance (Thom et al., 2019; NatureScot, 2021) overlooking spatial variability.*

Equally, **restoration techniques provide benefits beyond carbon** (Reed *et al.*, 2013; Bonn *et al.*, 2014; Thom *et al.*, 2016; Wichmann *et al.*, 2016; Alderson *et al.*, 2019). For example, while local and imported turves showed similar sub-surface structural outcomes, local turving supported greater biodiversity through increased species richness and *Sphagnum* cover. Yet, *as these ecosystem services are not factored into financial valuation, there is little incentive for decision-makers to prioritise higher-biodiversity approaches, which could lead to greater long-term functional outcomes*. Similar arguments apply to peat versus stone dams, where local approaches provide greater ecological benefit with significantly lower emissions. These considerations have broader implications for restoration policy and practice.

9.3.4 Technique Carbon Efficiency: Synthesis and Implications

Restoration interventions vary significantly in their capacity to deliver functional recovery and net carbon benefit (carbon efficiency). These differences reflect both the type of intervention and the way it is implemented. Evidence from Chapters 5, 6, 7, and 8 highlight technique selection (Chapter 2; Section 2.5) influences ecological, biochemical, and hydrological outcomes and should be evaluated in relation to the carbon costs incurred (Research Question 3). This has direct implications for carbon accounting frameworks such as the IUCN UK Peatland Code, which currently overlook technique-specific variation in functional benefits.

Turving emerged as the most effective revegetation method for restoring hydrological function, supporting atmosphere-connected porosity, increased *Sphagnum* cover, and reduced acidity and Eh; conditions promoting carbon accumulation. In contrast, techniques such as heather brash spreading showed poor integration between surface

and sub-surface layers, with structural characteristics indicative of continued degradation. *Findings demonstrate the importance of intervention type in restoring sub-surface structure and function.*

Material source and installation approach influenced outcomes. Locally sourced turves outperformed imported alternatives in terms of surface biodiversity and biochemical recovery, likely due to reduced disturbance and better preservation of acrotelm integrity. However, structural parameters such as porosity and stratification were similar between turving types, suggesting *installation quality is as important as material origin in supporting sub-surface recovery*.

Higher carbon costs did not equate to greater functional benefit. Heather brash, coir logs, and dam installations incurred significantly higher emissions than local turving but failed to demonstrate comparable structural or functional improvement. This demonstrates the requirement to evaluate interventions based on their cost-efficiency in delivering ecosystem services. *Findings support prioritisation of low-carbon, high-function methods in restoration planning*.

Insights inform the IUCN UK Peatland Code, where *incorporating carbon cost data into the Carbon Savings Calculator (IUCN, 2024a) can improve the credibility and transparency of projected savings (PIUs)*. Moreover, the IUCN UK Peatland Code Field Protocol (IUCN, 2024b) currently overlooks key indicators of sub-surface recovery, such as *Sphagnum* cover, which serves as a proxy for acrotelm development and hydrological function. *Integrating such indicators would refine emissions factors and better align carbon accounting with actual restoration success*.

While carbon cost is now included in restoration finance, it should inform rather than dictate intervention choice. Practical considerations such as site accessibility, intervention feasibility, and co-benefits like biodiversity gain should also be included in decision-making. *Findings support the development of a decision tree balancing functional outcomes, carbon costs, and logistical constraints.* There is also an opportunity to incorporate the economics of restoration feasibility (Chapter 10; Section 10.3).

Findings confirm peatland restoration assessments should move beyond surface indicators and assumed recovery timelines. Integrating carbon costs with functional recovery supports a revised understanding of restoration success that is functionally effective, financeable as a nature-based solution, and aligned with long-term carbon sequestration goals (Research Question 3).

9.4 Evaluating Blanket Peatland Restoration: Answering the Research Questions

Blanket peatland restoration effectiveness was evaluated using an integrated approach combining surface ecological assessments, sub-surface bulk and chemical analyses, 3D X-ray micro-computed tomography (μCT), and Life Cycle Assessment (LCA) across degraded, restored, and near-natural sites. This research offers a multidimensional evaluation of functional restoration outcomes and their delivery costs. Findings are presented in relation to the three research questions, each addressing a distinct element of restoration effectiveness:

Research Question 1: Can surface indicators be used as a proxy to infer changes in sub-surface structure and function post-restoration?

Surface indicators under JNCC (2009) reliably distinguished degraded and near-natural conditions, where sub-surface structure and function were significantly different. However, they overestimated recovery in restored sites, showing more favourable condition despite weak correspondence with sub-surface functions such as compaction (bulk density), saturation (moisture content), acidity (pH), and anoxia (Eh). µCT analysis confirmed key sub-surface processes, particularly in deeper layers, such as drainage through boundary-connected porosity and gas accumulation in isolated pores, were not captured by surface assessment.

Sphagnum cover and associated microtopographic complexity showed some alignment with atmosphere-connected porosity and inferred hydrological function through an intact acrotelm (Belyea and Clymo, 2001; Belyea and Malmer, 2004). In contrast, bare peat corresponded with absent atmosphere-connected porosity and deep boundary-connected networks capable of exporting water and solutes, representing a hydrophobic surface layer. Vascular/graminoid dominance was similarly associated with degraded sub-surface structure. These indicators also showed the strongest relationships with surface pH and Eh, suggesting potential as improved proxies and warranting greater weighting within assessment frameworks. However, surface indicators did not consistently capture differences in restoration technique, age, or structural development

at depth. Indicators often worked in isolation, with drainage features persisting below the surface despite *Sphagnum* development.

> Surface metrics provide useful insights into ecological condition but do not reliably capture sub-surface structural or functional recovery, especially in restored sites. Select indicators such as *Sphagnum* cover and bare peat extent show potential as proxies but require refinement to better align with sub-surface processes.

Research Question 2: To what extent does the restoration of degraded blanket peatlands support the recovery of sub-surface structure and function?

Restoration supported measurable improvements in sub-surface function, primarily through the development of atmosphere-connected porosity at the surface, indicative of a functioning acrotelm. This represents early improvements in surface water uptake, retention, and reduced decomposition. However, complete vertical stratification (acrotelm – mesotelm – catotelm) and continuity were only observed in the near-natural sample. Restored cores lacked a mesotelm, and catotelm layers retained degraded characteristics.

Functional recovery improved over time. Older sites such as Borrowdale (~10 years) exhibited greater sub-surface anoxia and hydrological regulation than younger sites like Shap Fells (~2 years). Restoration technique also influenced outcomes. Turving was most effective in promoting vertical pore development, atmosphere-connected porosity, and surface saturation. In contrast, alternative revegetation approaches such as heather

brash spreading showed limited structural development and retained degraded features at depth, including extensive boundary-connected networks capable of facilitating drainage and erosion. Inter-site variability demonstrated the importance of installation quality and material origin. Locally sourced turves showed better structural integration and biodiversity outcomes than imported.

> Restoration supports progressive recovery of sub-surface structure and function, with time and technique as drivers. However, restored sites remain structurally and functionally distinct from near-natural targets, even after a decade, demonstrating requirement for long-term monitoring and improved intervention design.

Research Question 3: How do the carbon costs of interventions impact the carbon benefit potential of restoration?

Restoration incurs significantly variable carbon costs depending on technique, raw material choice, and installation method. Life Cycle Assessment (LCA) showed interventions using local materials and manual or low-pressure ground vehicle installation (e.g., peat dams, bunds, local turves) produced the lowest emissions. In contrast, those relying on global supply chains (exotic materials) or helicopter delivery (e.g., stone dams and coir logs) incurred carbon costs orders of magnitude greater.

Carbon-intensive interventions did not provide improved functional outcomes. Sites restored using low-carbon techniques, particularly locally sourced turves, often showed better sub-surface structural recovery and biodiversity. Integrating functional recovery with carbon costs defined carbon efficiency as the delivery of long-term functional

benefits at minimal carbon cost; establishing a critical metric of restoration effectiveness.

This approach has already informed updates to the IUCN UK Peatland Code Carbon Savings Calculator, improving the transparency and accuracy of carbon credit reporting (Brennand *et al.,* 2025; IUCN, 2025b). While carbon remains central to restoration finance, its effectiveness as a success metric is weak, demonstrating the value of broader ecosystem services, such as biodiversity, as complementary funding mechanisms.

> Restoration success should be evaluated in terms of carbon efficiency, defined as the delivery of long-term functional benefits at minimal carbon cost. Including carbon costs in project planning, procurement, and reporting enables more credible, sustainable, and financeable restoration strategies.

Chapter 10: Conclusion - Implications for Practice, Policy, and Future Research

The research presented in this thesis provides practical and policy relevant insight to improve how blanket peatland restoration is delivered, evaluated, and financed. Restoration effectiveness was assessed based on sub-surface structural recovery, functional benefits, and carbon costs, which have been largely absent from previous evaluations. This was achieved through an integrated methodology combining established field assessment with innovative approaches, including 3D X-ray micro-computed tomography (µCT), Life Cycle Assessment (LCA), and depth dependent bulk chemical analysis, supported by a bespoke sampling framework tailored to large, heterogeneous landscapes. Assessments were grounded in accessible, standardised monitoring approaches to support real-world uptake. Consequently, there are clear opportunities to refine practitioner guidance, improve monitoring and carbon accounting methodologies, and expand the evidence base for research-led, sustainable, and financeable blanket peatland restoration in the UK as an effective nature-based solution.

10.1 Implications for Practice

Practitioners are increasingly expected to deliver effective and financeable restoration outcomes (Bonn *et al.*, 2014; 2016a; Stoneman *et al.*, 2016; IUCN, 2024d). Findings from this investigation demonstrate opportunities to improve how blanket peatland restoration is designed, implemented, and evaluated.

Functional outcomes should guide technique selection. Rather than assuming similarity across interventions, practitioners and decision-makers should prioritise approaches demonstrating measurable improvements in hydrological function, biodiversity, and sub-surface structure, such as increased *Sphagnum* cover, water retention, and acrotelm development, over those selected for cost or convenience. This investigation identified turving as a more effective revegetation technique than heather brash-spreading. Therefore, it should be prioritised where feasible. *However, current tendering processes often favour speed and cost over functional outcomes. Introducing scoring criteria reflecting carbon efficiency, biodiversity gain, and functional improvement would support more sustainable, evidence-based restoration.*

Restoration effectiveness is also influenced by its method of implementation. This research demonstrated practical factors, such as surface preparation (roughening to disrupt hydrophobic layers), compression to improve turve bonding (reducing boundary-connected porosity or preventing over-compaction), and the careful handling of revegetation materials (transporting imported turves from ecologically similar donor sites), directly influence structural integration and functional recovery. Existing guidance (e.g., Thom *et al.*, 2019; NatureScot, 2021) should be refined to incorporate these considerations. Decision trees could further support practitioners by enabling tailored intervention selection based on site-specific factors including degradation type, access restrictions, carbon costs, and functional goals. *Such tools would help move practice beyond general prescriptions toward more functionally and carbon effective restoration.*

Refinements to support functionally effective techniques depend on informed practice. Training, demonstrations, and post-project evaluations would help build the capacity required to deliver functional restoration. *Inter-site variability observed in this investigation supports a shift from prioritising intervention quantity to focusing on intervention quality, where success is evaluated by functional outcomes rather than spatial coverage or surface appearance*; an approach that should be reflected in future policy and funding mechanisms.

10.2 Implications for Policy

As governments increasingly aim to operationalise climate mitigation and biodiversity targets through peatland restoration as a nature-based solution (Reed *et al.*, 2022; Strack *et al.*, 2022; Wentworth, 2022), findings of this thesis have direct relevance for peatland policy in the UK and internationally. These policy implications go beyond improving existing tools such as the IUCN UK Peatland Code, supporting a broader shift in how restoration is understood, financed, and regulated. The focus should be on measurable function rather than assumed outcomes, recognising the range of ecological, hydrological, and climate services restored peatlands provide (Grand-Clement *et al.*, 2013; Thom *et al.*, 2016).

UK and international policies prioritise carbon as the principal metric for success. This investigation demonstrates restoration effectiveness is better captured through a combination of structural, hydrological, and ecological indicators, some of which are already assessed within existing frameworks (e.g., biodiversity gain within JNCC, 2009). However, relying on these as indirect proxies for carbon results in less accurate assessments of restoration outcomes, particularly as sub-surface recovery remains

variable and incompletely understood. *Policy should therefore integrate additional indicators of biodiversity, water regulation, and sub-surface functionality to better align with ecosystem service delivery targets and the broader role of peatlands as nature-based solutions.*

There is a clear opportunity to improve private financing mechanisms. Schemes such as the IUCN UK Peatland Code (IUCN, 2024a) currently do not include biodiversity and hydrological benefits in their eligibility and valuation criteria. This research showed techniques such as local turving offer dual benefits by supporting both carbon efficiency (lower carbon costs and greater functional gain) and increased species richness, particularly through *Sphagnum* establishment. *Embedding such indicators within valuation models would strengthen the investment rationale and promote more environmentally beneficial interventions.*

Integration of carbon cost data into the IUCN UK Peatland Code sets a precedent. Inclusion of Life Cycle Assessment (LCA) data from this investigation in the IUCN UK Peatland Code Carbon Savings Calculator (Brennand *et al*., 2025; IUCN, 2025b; 2025c) demonstrates how carbon accounting can be made more accurate and transparent within voluntary carbon markets. *Countries developing similar frameworks, such as Canada, Chile, Argentina, and parts of Scandinavia, should incorporate carbon efficiency and functional indicators from the start to avoid the oversimplifications seen in earlier UK models.*

Policy mechanisms should incentivise low-carbon, high-function restoration. This investigation identified technique carbon efficiency as a critical determinant of restoration effectiveness. Carbon cost-weighted grant schemes, updated funding

criteria, and procurement standards rewarding low-emission delivery and the use of locally sourced materials could support more sustainable restoration outcomes. Where feasible, sourcing local materials, such as timber/heather instead of coir imported through global supply chains, may also deliver economic co-benefits by supporting local industries. As carbon crediting evolves from voluntary to compliance, robust accounting and the integration of broader ecosystem service benefits will be essential. *Findings from this research provide a framework to support this transition, improving the credibility, integrity, and policy alignment of carbon financing mechanisms.*

GHG accounting frameworks should be updated to better capture sub-surface function. This investigation demonstrated a disconnect between surface indicators and sub-surface functional response. Current emissions factors used in restoration assessment rely on indirect proxies not grounded in actual sub-surface condition. Consequently, carbon savings estimates misrepresent functional recovery. *Policy and financing mechanisms such as the IUCN UK Peatland Code (IUCN, 2024a) should therefore support further research to develop improved emissions factors based on functional indicators such as Sphagnum and bare peat cover, as well as bulk chemical metrics including pH and Eh.*

Assumptions of carbon benefit should be re-evaluated. Findings from sites restored a decade ago showed sub-surface structure and function continued to lag behind surface condition. This challenges the five-year assumptions of functional recovery and carbon benefit currently embedded in restoration monitoring and crediting frameworks (IUCN, 2024a). *Carbon accounting models should reflect longer timescales of sub-surface recovery to improve the credibility of peatland restoration claims.* This becomes

particularly important when considering the carbon efficiency of techniques, where intervention choice can offset net carbon benefit by up to a decade. This is now partially addressed through updated emissions reductions in the IUCN UK Peatland Code (Brennand *et al.*, 2025; IUCN, 2024a).

10.3 Opportunities for Future Research

The findings from this thesis support a revised framework for evaluating blanket peatland restoration effectiveness, based on sub-surface structure, function, and carbon cost. Further research is suggested to develop more effective operational tools, financial models, and scalable monitoring approaches grounded in this revised understanding.

Integrating biodiversity into valuation models is a critical next step. Expanding financing schemes such as the IUCN UK Peatland Code Carbon Savings Calculator to incorporate biodiversity benefits (IUCN, 2025b), alongside project carbon costs (IUCN, 2025c), would support a more comprehensive valuation of restoration benefits. *This would strengthen the financial case for techniques delivering high functional gains which remain undervalued using carbon-only metrics.*

Evaluation of emerging restoration techniques is required. As new interventions are developed, their functional effectiveness and carbon efficiency should be evaluated through updated emissions factors and integration into emissions calculators (IUCN, 2024a). *Continued refinement based on empirical evidence will support continued relevance and scientific credibility.*

Incorporating financial costs will improve decision-making. Combining financial costs with carbon costs and functional benefit data would enable more informed decisions by landowners, policymakers, and investors. *A holistic cost–benefit approach would help identify interventions that deliver maximum environmental and economic value.*

Validation of structural indicators through direct GHG flux measurement is required. While key pore network features identified using µCT were used to infer carbon dynamics, these relationships require validation through in situ GHG flux measurements. *Empirical validation would increase the reliability of structural indicators in carbon modelling and further support their integration into policy frameworks.*

Applying the structure – function – carbon cost framework across peatland types would improve global understanding. Although this research focused on UK blanket bogs, the approach is transferable to raised bogs, fens, and tropical or boreal peatlands. The development of a bespoke sampling framework, designed to extract limited samples for µCT from large, heterogeneous landscapes, enables this transferability. *Comparative studies using this framework across diverse peatland systems would refine global understanding of sub-surface recovery processes and ecosystem service delivery.*

Remote sensing offers new opportunities for proxy development at scale. Functional indicators such as *Sphagnum* cover, inferred acrotelm development, and vertical stratification could be assessed using UAVs, LiDAR, or hyperspectral imaging, enabling landscape-scale monitoring and improved surface-based interpretation of sub-surface processes. A key contribution to knowledge would be linking seasonal changes in porosity, particularly the expansion and contraction of atmosphere-connected pore

networks, with 'bog breathing' dynamics, increasing understanding of peatland resilience and functional capacity (Howie *et al.*, 2018; Lees *et al.*, 2019; 2021; Andersen *et al.*, 2024).

Advances in image analysis could operationalise μCT at scale. This research demonstrated the value of μCT in evaluating the structural and functional impacts of peatland restoration. μCT enabled the quantification and classification of pore networks, distinguishing distinct roles of atmosphere-connected, boundary-connected, and isolated porosity in regulating surface water uptake, retention, solute transport, and gas exchange; critical to long-term carbon accumulation (Chapter 2; Section 2.1.2). It revealed macropore function is often controlled by a single dominant network extending through the profile, advancing previous understanding from micropore-scale studies in discontinuous samples (Chapter 2; Section 2.1.1; Kettridge and Binley; 2008; 2011; Quinton *et al.*, 2009; Rezanezhad *et al.*, 2009, 2010, 2016). The method also confirmed a disconnect between surface condition and sub-surface function, particularly when compared with key bulk and chemical indicators such as bulk density, moisture content, pH, and Eh. Importantly, μCT supported the conceptualisation of the mesotelm as a distinct transitional zone between active and inactive zones (Chapter 2; Section 2.1.1; (Clymo and Bryant, 2008; Belyea and Baird, 2006; Morris *et al.*, 2011; Baird *et al.*, 2016).

Collectively, these insights address long-standing knowledge gaps in structure and function relationships, particularly in restored systems, and establish a methodological foundation for evaluating restoration effectiveness. As cost-effective scanning technologies and AI-driven segmentation tools continue to develop, μCT is likely to become increasingly accessible. Wider adoption would enable the integration of

structure – function – carbon cost relationships into practical, scalable monitoring frameworks aligned with policy and financing mechanisms.

10.4 Concluding Remarks

The findings from this thesis provide a better understanding of restoration effectiveness by moving beyond threshold-based surface indicators to measurable sub-surface structural and functional recovery. By combining innovative 3D X-ray micro-computed tomography (µCT) with established bulk and chemical indicators, this research assesses what effective restoration looks like beneath the surface.

µCT was applied for the first time to evaluate restoration impact using continuous, intact cores, facilitated by a bespoke sampling approach. This allowed detailed characterisation of pore structure and function across depth, advancing understanding beyond previous studies based on discontinuous or destructively sampled peat. The method identified dominant macropore networks, distinguished functionally active and inactive pores, and clarified the role of transitional layers such as the mesotelm, providing new insight into structural and functional relationships. Critically, it revealed disconnects between surface indicators and sub-surface function, demonstrating the limitations of surface-based assessments in capturing functionality.

Analysis was grounded in current monitoring protocols, enabling critical evaluation of JNCC (2009) indicators and identifying surface features more closely aligned with sub-surface function. When applied beyond binary classification, and combined with remote sensing and ground-truthing, indicators such as *Sphagnum* cover, bare peat extent, surface pH, and Eh offer scalable, accessible tools for monitoring restoration success.

This study presents an original application of Life Cycle Assessment (LCA) to quantify the carbon costs of peatland restoration interventions. By associating these costs with structural and functional impacts, it introduces a carbon efficiency indicator, balancing emissions against functional benefit. Collectively, findings reveal significant variation in technique emissions and demonstrate more carbon-intensive approaches do not necessarily support greater functional recovery.

A bespoke, tailored sampling framework was developed to extract representative peat cores across large, heterogeneous landscapes. This approach enabled the selection of sites and cores capturing variation in age, technique, and condition, supporting µCT analysis in representing restoration impacts. By accounting for spatial heterogeneity and variability, the framework supports the validity of structural and functional interpretations. It offers a transferable model for future research and monitoring.

Collectively, findings have direct relevance for restoration practice and policy. They support refinement of monitoring protocols, prioritisation of low-carbon, high-function interventions, and updates to carbon accounting frameworks such as the IUCN UK Peatland Code. The research also advocates for recognising benefits beyond carbon, including improved hydrological regulation, biodiversity gains, and long-term ecosystem resilience. Through associating sub-surface recovery to intervention type and emissions cost, this research enables more credible, cost-effective, and functionally aligned restoration strategies, supporting the role of peatlands as a nature-based solution to the climate and biodiversity crises.

Restoration that fails to restore peatland function, or costs more carbon than it saves within a reasonable timescale, risks becoming part of the problem, not the solution. In contrast, restoring function delivers benefits beyond carbon, which policy and finance mechanisms are increasingly seeking to secure.

Appendices

A) µCT scanning parameters used for the Nikon XTH 225 and Nikon Custom 450 systems:

Table 1: Nikon XTH 225.

Scanner: Nikon XTH 225			
Stage Position		**Optimise Image**	
X	Locked	Binning	x1
Y	28	Digital Correction	x1
Magnification	657	Beam Energy	190
Rotation	360°	Beam Current	100
Tilt	Locked	Resulting Power	19
Imaging	0		
Stage Position Results		**Optimise Image Results**	
Geometric Magnification	1.557	Exposure	3.00fps
		Exposure Time	0.33s
Effective Pixel Size	81.55µm	Gain	30dB
Projection Setup		**Acquisition**	
Num. Projections	2001	~0.75 hours	
Frames	2		

Table 2: Nikon Custom 450 – Batch scan of three parts (1590 slices each): top, middle, bottom.

Scanner: Nikon Custom 450 – 1 of 3			
Stage Position		**Optimise Image**	
X	Locked	Binning	x1
Y	113	Digital Correction	x1
Magnification	368	Beam Energy	190
Rotation	360°	Beam Current	100
Tilt	Locked	Resulting Power	19
Imaging	0		
Stage Position Results		**Optimise Image Results**	
Geometric Magnification	3.913	Exposure	5.65fps
		Exposure Time	0.0177s
Effective Pixel Size	51.11µm	Gain	30dB
Projection Setup		**Acquisition**	
Num. Projections	3201	~0.75 hours (each) – Total: ~2.25 hours	
Frames	2		

B) µCT reconstruction parameters used for the Nikon XTH 225 and Nikon Custom 450 systems:

Table 3: Nikon XTH 225.

Software: CTPro3D (Filtered Back-Projection Algorithm)			
Centre of Rotation		**Initial Processing**	
Automatic?	Yes	Beam Hardening	Preset 2
Accuracy	High Quality	Scatter Reduction	0
Slice Detection	Dual	Noise Reduction	Preset 1
Outputs:			
Interpolation?		Yes (Linear)	
Attenuation Scaling		0.20 (low) – 99.80 (high)	
Format		TIFF Stack Single	
Processing Time		~2 hours	

Table 4: Nikon Custom 450 – Batch scan of three parts (1590 slices each): top, middle, bottom.

Software: CTPro3D (Filtered Back-Projection Algorithm) – 1 of 3			
Centre of Rotation		**Initial Processing**	
Automatic?	Manual	Beam Hardening	Preset 3
Accuracy	High Quality	Scatter Reduction	0
Slice Detection	Dual	Noise Reduction	Preset 1
Outputs:			
Interpolation?		Yes (Linear)	
Attenuation Scaling		0.20 (low) – 99.80 (high)	
Format		TIFF Stack Single	
Processing Time		~2 hours (each) – Total: ~6 hours	

C) Signal processing steps for each core across High Flux Bay, Nikon XTH 225, and Nikon Custom 450 systems:

Table 5: Signal processing steps in ImageJ for each core and the size of file output.

Core ID	Scanner	Rescale Volume (62.6732066%)	Remove Slices (Top & Bottom)	Rotate (Image - Transform - Rotate (North))	3D Crop (Plugins - Stacks - Crop 3D)	Contrast Stretch (Image - Adjust Brightness/ Contrast)
BC_Deg	Nikon Xtek 225kV High Flux Bay	1_Rescaled_BC_Deg - TIFF Files: 7.75MB each; 30.6GB	Top: 3576 - 4047 (473) Bottom: 0 - 307 (308) - TIFF Files: 7.75MB each; 27.3GB	Angle: 53.20	x from 998 - 2335; y from 1092 - 2415; z from 1 - 3268; value: 50 - TIFF Files: 1.24MB each; 4.38GB	Greyscale range: 7585 - 44898
BW_LT_1	Nikon Xtek 225kV High Flux Bay	1_Rescaled_BW_LT_1 - TIFF Files: 7.14MB each; 28.2GB	Top: 3886 - 4047 (162) Bottom: 0 - 163 (164) - TIFF Files: 7.14MB each; 25.9GB	Angle: 104	x from 477 - 1345; y from 570 - 1347; z from 1 - 3722; value: 50 - TIFF Files: 1.28MB each; 4.68GB	Greyscale range: 7623 - 44907
BW_LT_2	Nikon XTH 225	/	Top: 2251 - 2295 (45) Bottom: 0 - 96 (97) - TIFF Files: 4.06MB each; 8.22GB	Angle: -120	x from 654 - 1587; y from 660 - 1401; z from 1 - 2154; value: 50 - TIFF Files: 1.32MB each; 2.78GB	Greyscale range: 4216 - 51324
BC_IT_1	Nikon Xtek 225kV High Flux Bay	1_Rescaled_BC_IT_1 - TIFF Files: 4.67MB each; 18.4GB	Top: 3965 - 4047 (83) Bottom: 0 - 144 (145) - TIFF Files: 4.67MB each; 16.6GB	Angle: -36.6	x from 364 - 1245; y from 350 - 1193; z from 1 - 3820; value: 50 - TIFF Files: 1.41MB each; 5.29GB	Greyscale range: 7638 - 44937
BC_IT_2	Nikon Xtek 225kV High Flux Bay	1_Rescaled_BC_IT_2 - TIFF Files: 5.24MB each; 20.7GB	Top: 3995 - 4047 (53) Bottom: 0 - 149 (150) - TIFF Files: 5.24MB each; 18.4GB	Angle: -167	x from 332 - 1225; y from 492 - 1279; z from 1 - 3845; value: 50 - TIFF Files: 1.34MB each; 5.04GB	Greyscale range: 7656 - 44944
BC_LT_1	Nikon Xtek 225kV High Flux Bay	1_Rescaled_BC_LT_1 - TIFF Files: 5.13MB each; 20.3GB	Top: 3849 - 4047 (199) Bottom: 0 - 156 (157) - TIFF Files: 5.13MB each; 18.5GB	Angle: 42.7	x from 390 - 1268; y from 410 - 1232; z from 1 - 3692; value: 50 - TIFF Files: 1.37MB each; 4.97GB	Greyscale range: 7621 - 44918
BC_LT_2	Nikon Xtek 225kV High Flux Bay	1_Rescaled_BC_LT_2 - TIFF Files: 5.06MB each; 20.3GB	Top: 3953 - 4047 (95) Bottom: 0 - 149 (150) - TIFF Files: 5.06MB each; 17.2GB	Angle: -4.8	x from 588 - 2035; y from 699 - 1923; z from 1 - 3803; value: 50 - TIFF Files: 1.31MB each; 4.47GB	Greyscale range: 7655 - 44953
SF_IT_1	Nikon Xtek 225kV High Flux Bay	1_Rescaled_SF_IT_1 - TIFF Files: 5.95MB each; 23.5GB	Top: 3986 - 4047 (62) Bottom: 0 - 144 (145) - TIFF Files: 5.95MB each; 21.7GB	Angle: 23.7	x from 414 - 1270; y from 456 - 1360; z from 1 - 3841; value: 50 - TIFF Files: 1.47MB each; 5.54GB	Greyscale range: 7606 - 44929
SF_IT_2	Nikon Custom 450	1_Rescaled_SF_IT_2 - TIFF Files: 2.99MB each; 13.9GB	/	/	x from 227 - 1056; y from 252 - 1043; z from 1 - 4773; value: 50 - TIFF Files: 1.25MB each; 5.84GB	Greyscale range: 3515 - 35902
SF_LT_1	Nikon Xtek 225kV High Flux Bay	1_Rescaled_SF_LT_1 - TIFF Files: 5.03MB each; 19.8GB	Top: 3806 - 4047 (242) Bottom: 0 - 148 (149) - TIFF Files: 5.03MB each; 17.9GB	Angle: 157.1	x from 344 - 1266; y from 454 - 1180; z from 1 - 3657; value: 50 - TIFF Files: 1.27MB each; 4.57GB	Greyscale range: 7633 - 44898
SF_LT_2	Nikon Xtek 225kV High Flux Bay	1_Rescaled_SF_LT_2 - TIFF Files: 5.24MB each; 20.7GB	Top: 3966 - 4047 (82) Bottom: 0 - 146 (147) - TIFF Files: 5.24MB each; 18.9GB	Angle: 190.5	x from 338 - 1247; y from 494 - 1249; z from 1 - 3819; value: 50 - TIFF Files: 1.31MB each; 4.89GB	Greyscale range: 7651 - 44951
SM_B	Nikon XTH 225	/	Top: 2196 - 2295 (100) Bottom: 0 - 99 (100) - TIFF Files: 4.09MB each; 9.19GB	Angle: -75.1	x from 1132 - 2067; y from 1232 - 2031; z from 1 - 2096; value: 50 - TIFF Files: 1.42MB each; 2.92GB	Greyscale range: 4223 - 51367
SM_C	Nikon XTH 225	/	Top: 2200 - 2295 (96) Bottom: 0 - 97 (98) - TIFF Files: 4.16MB each; 8.52GB	Angle: -17.4	x from 1132 - 2067; y from 1248 - 2033; z from 1 - 2102; value: 50 - TIFF Files: 1.40MB each; 2.88GB	Greyscale range: 4249 - 51349
SM_D	Nikon XTH 225	/	Top: 2270 - 2295 (27) Bottom: 0 - 93 (94)- TIFF Files: 4.32MB each; 8.85GB	Angle: 21.2	x from 1100 - 2103; y from 1216 - 1951; z from 1 - 2175; value: 50 - TIFF Files: 1.40MB each; 2.99GB	Greyscale range: 4237 - 51399
SF_Nat	Nikon Xtek 225kV High Flux Bay	1_Rescaled_SF_Nat - TIFF Files: 5.42MB each; 21.4GB	Top: 3865 - 4047 (182) Bottom: 0 - 149 (150) - TIFF Files: 5.42MB each; 19.2GB	Angle: 0.70	x from 661 - 2023; y from 707 - 1955; z from 1 - 3715; value: 50 - TIFF Files: 1.23MB each; 4.38GB	Greyscale range: 7602 - 44906

D) Segmentation of total pore space (TPS) for each core across High Flux Bay, Nikon XTH 225, and Nikon Custom 450 systems:

Table 6: Segmentation steps in ImageJ of total pore space (TPS) for each core and the size of file output.

Core ID	Scanner	Thresholding - Total Pore Space (TPS)	Quantifying - TPS	Thresholding Adjustments - TPS
BC_Deg	Nikon Xtek 225kV High Flux Bay	Threshold greyscale range: 0 - 26471 5_TPS_BC_Deg - TIFF Files: 652KB each; 2.30GB	Area/Volume Fraction BC_Deg_TPS_AreaVolume_Fraction - Excel File: 9KB	Despeckle x1
BW_LT_1	Nikon Xtek 225kV High Flux Bay	Threshold greyscale range: 0 - 26471 5_TPS_BW_LT_1 - TIFF Files: 660KB each; 2.34GB	Area/Volume Fraction BW_LT_1_TPS_AreaVolume_Fraction - Excel File: 9KB	Despeckle x1
BW_LT_2	Nikon XTH 225	Threshold greyscale range: 0 - 39835 (0.57%)	Area/Volume Fraction BW_LT_2_TPS_AreaVolume_Fraction - Excel File: 9KB	Despeckle x1
BC_IT_1	Nikon Xtek 225kV High Flux Bay	Threshold greyscale range: 0 - 26471 5_TPS_BC_IT_1 - TIFF Files: 727KB each; 2.64GB	Area/Volume Fraction BC_IT_1_TPS_AreaVolume_Fraction - Excel File: 9KB	Despeckle x1
BC_IT_2	Nikon Xtek 225kV High Flux Bay	Threshold greyscale range: 0 - 26471 5_TPS_BC_IT_2 - TIFF Files: 688KB each; 2.52GB	Area/Volume Fraction BC_IT_2_TPS_AreaVolume_Fraction - Excel File: 9KB	Despeckle x1
BC_LT_1	Nikon Xtek 225kV High Flux Bay	Threshold greyscale range: 0 - 26471 5_TPS_BC_LT_1 - TIFF Files: 706KB each; 2.48GB	Area/Volume Fraction BC_LT_1_TPS_AreaVolume_Fraction - Excel File: 9KB	Despeckle x1
BC_LT_2	Nikon Xtek 225kV High Flux Bay	Threshold greyscale range: 0 - 26471 5_TPS_BC_LT_2 - TIFF Files: 672KB each; 2.44GB	Area/Volume Fraction BC_LT_2_TPS_AreaVolume_Fraction - Excel File: 9KB	Despeckle x1
SF_IT_1	Nikon Xtek 225kV High Flux Bay	Threshold greyscale range: 0 - 26471 5_TPS_SF_IT_1 - TIFF Files: 757KB each; 2.77GB	Area/Volume Fraction SF_IT_1_TPS_AreaVolume_Fraction - Excel File: 9KB	Despeckle x1
SF_IT_2	Nikon Custom 450	Threshold greyscale range: 0 - 34181 5_TPS_SF_IT_2 - TIFF Files: 642KB each; 2.92GB	Area/Volume Fraction SF_IT_2_TPS_AreaVolume_Fraction - Excel File: 9KB	Despeckle x1
SF_LT_1	Nikon Xtek 225kV High Flux Bay	Threshold greyscale range: 0 - 26471 5_TPS_SF_LT_1 - TIFF Files: 655KB each; 2.28GB	Area/Volume Fraction SF_LT_1_TPS_AreaVolume_Fraction - Excel File: 9KB	Despeckle x1
SF_LT_2	Nikon Xtek 225kV High Flux Bay	Threshold greyscale range: 0 - 26471 5_TPS_SF_LT_2 - TIFF Files: 672KB each; 2.44GB	Area/Volume Fraction SF_LT_2_TPS_AreaVolume_Fraction - Excel File: 9KB	Despeckle x1
SM_B	Nikon XTH 225	Threshold greyscale range: 0 - 39835 5_TPS_SM_B - TIFF Files: 731KB each; 1.46GB	Area/Volume Fraction SM_B_TPS_AreaVolume_Fraction - Excel File: 9KB	Despeckle x1
SM_C	Nikon XTH 225	Threshold greyscale range: 0 - 39835 5_TPS_SM_C - TIFF Files: 718KB each; 1.44GB	Area/Volume Fraction SM_C_TPS_AreaVolume_Fraction - Excel File: 9KB	Despeckle x1
SM_D	Nikon XTH 225	Threshold greyscale range: 0 - 39835 5_TPS_SM_D - TIFF Files: 721KB each; 1.49GB	Area/Volume Fraction SM_D_TPS_AreaVolume_Fraction - Excel File: 9KB	Despeckle x1
SF_Nat	Nikon Xtek 225kV High Flux Bay	Threshold greyscale range: 0 - 26471 5_TPS_SF_Nat - TIFF Files: 651KB each; 2.30GB	Area/Volume Fraction SF_Nat_TPS_AreaVolume_Fraction - Excel File: 9KB	Despeckle x1

E) Isolation of isolated porosity (IP), atmosphere-connected (ACP), and boundary-connected (BCP):

Table 7: Isolation and quantification of isolated porosity (IP) in ImageJ for each core including the size of file output.

Core ID	Scanner	Particle Analyser Parameters - IP	Particle Analyser IP ID/Output	Convert IP to Binary (Threshold: 1)	Quantifying - IP
BC_Deg	Nikon Xtek 225kV High Flux Bay	Exclude on Edges; Feret diameter; Thickness; Surface area; Enclosed volume; Euler characteristic - Min volume: 4882860 micron3; Surface resampling: 2; Show particle stack	7_IP_PS_BC_Deg + BC_Deg_IP_Particle_Analysis - TIFF Files: 2.54MB each; 9.22GB + Excel File - 29.9MB	8_Binary_IP_BC_Deg - TIFF Files: 652KB each; 2.30GB	Area/Volume Fraction BC_Deg_IP_AreaVolume_Fraction - Excel File: 9KB
BW_LT_1	Nikon Xtek 225kV High Flux Bay	Exclude on Edges; Feret diameter; Thickness; Surface area; Enclosed volume; Euler characteristic - Min volume: 4882860 micron3; Surface resampling: 2; Show particle stack	7_IP_PS_BW_LT_1 + BW_LT_1_IP_Particle_Analysis - TIFF Files: 2.58MB each; 9.38GB + Excel File - 2.79MB	8_Binary_IP_BW_LT_1 - TIFF Files: 660KB each; 2.34GB	Area/Volume Fraction BW_LT_1_IP_AreaVolume_Fraction - Excel File: 9KB
BW_LT_2	Nikon XTH 225	Exclude on Edges; Feret diameter; Thickness; Surface area; Enclosed volume; Euler characteristic - Min volume: 4882860 micron3; Surface resampling: 2; Show particle stack	7_IP_PS_BW_LT_2 + BW_LT_2_IP_Particle_Analysis - TIFF Files: 2.64MB each; 5.56GB + Excel File - 3024KB	8_Binary_IP_BW_LT_2 - TIFF Files: 677KB each; 1.39GB	Area/Volume Fraction BW_LT_2_IP_AreaVolume_Fraction - Excel File: 9KB
BC_IT_1	Nikon Xtek 225kV High Flux Bay	Exclude on Edges; Feret diameter; Thickness; Surface area; Enclosed volume; Euler characteristic - Min volume: 4882860 micron3; Surface resampling: 2; Show particle stack	7_IP_PS_BC_IT_1 + BC_IT_1_IP_Particle_Analysis - TIFF Files: 2.84MB each; 10.5GB + Excel File - 1580KB	8_Binary_IP_BC_IT_1 - TIFF Files: 727KB each; 2.64GB	Area/Volume Fraction BC_IT_1_IP_AreaVolume_Fraction - Excel File: 9KB
BC_IT_2	Nikon Xtek 225kV High Flux Bay	Exclude on Edges; Feret diameter; Thickness; Surface area; Enclosed volume; Euler characteristic - Min volume: 4882860 micron3; Surface resampling: 2; Show particle stack	7_IP_PS_BC_IT_2 + BC_IT_2_IP_Particle_Analysis - TIFF Files: 2.68MB each; 10.0GB + Excel File - 14135KB	8_Binary_IP_BC_IT_2 - TIFF Files: 688KB each; 2.52GB	Area/Volume Fraction BC_IT_2_IP_AreaVolume_Fraction - Excel File: 9KB
BC_LT_1	Nikon Xtek 225kV High Flux Bay	Exclude on Edges; Feret diameter; Thickness; Surface area; Enclosed volume; Euler characteristic - Min volume: 4882860 micron3; Surface resampling: 2; Show particle stack	7_IP_PS_BC_LT_1 + BC_LT_1_IP_Particle_Analysis - TIFF Files: 2.76MB each; 9.95GB + Excel File - 11.8MB	8_Binary_IP_BC_LT_1 - TIFF Files: 706KB each; 2.48GB	Area/Volume Fraction BC_LT_1_IP_AreaVolume_Fraction - Excel File: 9KB
BC_LT_2	Nikon Xtek 225kV High Flux Bay	Exclude on Edges; Feret diameter; Thickness; Surface area; Enclosed volume; Euler characteristic - Min volume: 4882860 micron3; Surface resampling: 2; Show particle stack	7_IP_PS_BC_LT_2 + BC_LT_2_IP_Particle_Analysis - TIFF Files: 2.62MB each; 9.76GB + Excel File - 9981KB	8_Binary_IP_BC_LT_2 - TIFF Files: 672KB each; 2.44GB	Area/Volume Fraction BC_LT_2_IP_AreaVolume_Fraction - Excel File: 9KB
SF_IT_1	Nikon Xtek 225kV High Flux Bay	Exclude on Edges; Feret diameter; Thickness; Surface area; Enclosed volume; Euler characteristic - Min volume: 4882860 micron3; Surface resampling: 2; Show particle stack	7_IP_PS_SF_IT_1 + SF_IT_1_IP_Particle_Analysis - TIFF Files: 2.95MB each; 11.1GB + Excel File - 2.61MB	8_Binary_IP_SF_IT_1 - TIFF Files: 757KB each; 2.77GB	Area/Volume Fraction SF_IT_1_IP_AreaVolume_Fraction - Excel File: 9KB
SF_IT_2	Nikon Custom 450	Exclude on Edges; Feret diameter; Thickness; Surface area; Enclosed volume; Euler characteristic - Min volume: 4882860 micron3; Surface resampling: 2; Show particle stack	7_IP_PS_SF_IT_2 + SF_IT_2_IP_Particle_Analysis - TIFF Files: 2.50MB each; 11.6GB + Excel File - 9160KB	8_Binary_IP_SF_IT_2 - TIFF Files: 642KB each; 2.92GB	Area/Volume Fraction SF_IT_2_IP_AreaVolume_Fraction - Excel File: 9KB
SF_LT_1	Nikon Xtek 225kV High Flux Bay	Exclude on Edges; Feret diameter; Thickness; Surface area; Enclosed volume; Euler characteristic - Min volume: 4882860 micron3; Surface resampling: 2; Show particle stack	7_IP_PS_SF_LT_1 + SF_LT_1_IP_Particle_Analysis - TIFF Files: 2.56MB each; 9.14GB + Excel File - 2.61MB	8_Binary_IP_SF_LT_1 - TIFF Files: 655KB each; 2.28GB	Area/Volume Fraction SF_LT_1_IP_AreaVolume_Fraction - Excel File: 9KB
SF_LT_2	Nikon Xtek 225kV High Flux Bay	Exclude on Edges; Feret diameter; Thickness; Surface area; Enclosed volume; Euler characteristic - Min volume: 4882860 micron3; Surface resampling: 2; Show particle stack	7_IP_PS_SF_LT_2 + SF_LT_2_IP_Particle_Analysis - TIFF Files: 2.62MB each; 9.79GB + Excel File - 3.297KB	8_Binary_IP_SF_LT_2 - TIFF Files: 672KB each; 2.44GB	Area/Volume Fraction SF_LT_2_IP_AreaVolume_Fraction - Excel File: 9KB
SM_B	Nikon XTH 225	Exclude on Edges; Feret diameter; Thickness; Surface area; Enclosed volume; Euler characteristic - Min volume: 4882860 micron3; Surface resampling: 2; Show particle stack	7_IP_PS_SM_B + SM_B_IP_Particle_Analysis - TIFF Files: 2.85MB each; 5.84GB + Excel File - 12899KB	8_Binary_IP_SM_B - TIFF Files: 731KB each; 1.46GB	Area/Volume Fraction SM_B_IP_AreaVolume_Fraction - Excel File: 9KB
SM_C	Nikon XTH 225	Exclude on Edges; Feret diameter; Thickness; Surface area; Enclosed volume; Euler characteristic - Min volume: 4882860 micron3; Surface resampling: 2; Show particle stack	7_IP_PS_SM_C + SM_C_IP_Particle_Analysis - TIFF Files: 2.80MB each; 5.76GB + Excel File - 2694KB	8_Binary_IP_SM_C - TIFF Files: 718KB each; 1.44GB	Area/Volume Fraction SM_C_IP_AreaVolume_Fraction - Excel File: 9KB
SM_D	Nikon XTH 225	Exclude on Edges; Feret diameter; Thickness; Surface area; Enclosed volume; Euler characteristic - Min volume: 4882860 micron3; Surface resampling: 2; Show particle stack	7_IP_PS_SM_D + SM_D_IP_Particle_Analysis - TIFF Files: 2.82MB each; 5.99GB + Excel File - 729KB	8_Binary_IP_SM_D - TIFF Files: 721KB each; 1.49GB	Area/Volume Fraction SM_D_IP_AreaVolume_Fraction - Excel File: 9KB
SF_Nat	Nikon Xtek 225kV High Flux Bay	Exclude on Edges; Feret diameter; Thickness; Surface area; Enclosed volume; Euler characteristic - Min volume: 4882860 micron3; Surface resampling: 2; Show particle stack	7_IP_PS_SF_Nat + SF_Nat_IP_Particle_Analysis - TIFF Files: 2.54MB each; 9.23GB + Excel File - 4.44MB	8_Binary_IP_SF_Nat - TIFF Files: 651KB each; 2.30GB	Area/Volume Fraction SF_Nat_IP_AreaVolume_Fraction - Excel File: 9KB

Table 8: Isolation and quantification of atmosphere-connected porosity (ACP) in ImageJ for each core including the size of file output.

Core ID	Scanner	Particle Analyser Parameters - TPS	Thresholding - Atmosphere-Connected Porosity & Surface Air (ACP+Air)	Erode/Dilate - ACP+Air	Shape Smoothing - ACP+Air	3D Surface Air - ACP+Air	Image Calculator - ACP	Quantifying ACP	Particle Analyser Parameters - ACP
BC_Deg	Nikon Xtek 225kV High Flux Bay	Min volume: 4882860 micron3; Surface resampling: 2; Show particle stack	Threshold greyscale range: 18353 - 18355 11_ACP+Air_BC_Deg - TIFF Files: 652KB each; 2.30GB	Erode x 6/Dilate x6 12_Surface_Air_BC_Deg - TIFF Files: 652KB each; 2.30GB	Relative proportion FDs (%): 7 13_Smooth_BC_Deg	Gaussian Blur 3D (Sigma: 3) + Tresholding (2) 14_3D_SA_BC_Deg	11_ACP+Air_BC_Deg subtract 14_3D_SA_BC_Deg 15_ACP_BC_Deg	Area/Volume Fraction BC_Deg_ACP_AreaVolume_Fraction - Excel File: 9KB	Feret diameter; Thickness; Surface area; Enclosed volume; Euler characteristic - Min volume: 4882860 micron3; Surface resampling: 6; Show particle stack
BW_LT_1	Nikon Xtek 225kV High Flux Bay	Min volume: 4882860 micron3; Surface resampling: 2; Show particle stack	Threshold greyscale range: 4854 - 4856 11_ACP+Air_BW_LT_1 - TIFF Files: 660KB each; 2.34GB	Erode x 6/Dilate x6 12_Surface_Air_BW_LT_1 - TIFF Files: 660KB each; 2.34GB	Relative proportion FDs (%): 7 13_Smooth_BW_LT_1	Gaussian Blur 3D (Sigma: 3) + Tresholding (2) 14_3D_SA_BW_LT_1	11_ACP+Air_BW_LT_1 subtract 14_3D_SA_BW_LT_1 15_ACP_BW_LT_1	Area/Volume Fraction BW_LT_1_ACP_AreaVolume_Fraction - Excel File: 9KB	Feret diameter; Thickness; Surface area; Enclosed volume; Euler characteristic - Min volume: 4882860 micron3; Surface resampling: 6; Show particle stack
BW_LT_2	Nikon XTH 225	Min volume: 4882860 micron3; Surface resampling: 2; Show particle stack	Threshold greyscale range: 13152 - 13154 11_ACP+Air_BW_LT_2 - TIFF Files: 677KB each; 1.39GB	Erode x 6/Dilate x6 12_Surface_Air_BW_LT_2 - TIFF Files: 677KB each; 1.39GB	Relative proportion FDs (%): 7 13_Smooth_BW_LT_2	Gaussian Blur 3D (Sigma: 3) + Tresholding (2) 14_3D_SA_BW_LT_2	11_ACP+Air_BW_LT_2 subtract 14_3D_SA_BW_LT_2 15_ACP_BW_LT_2	Area/Volume Fraction BW_LT_2_ACP_AreaVolume_Fraction - Excel File: 9KB	Feret diameter; Thickness; Surface area; Enclosed volume; Euler characteristic - Min volume: 4882860 micron3; Surface resampling: 6; Show particle stack
BC_IT_1	Nikon Xtek 225kV High Flux Bay	Min volume: 4882860 micron3; Surface resampling: 2; Show particle stack	Threshold greyscale range: 4110 - 4112 11_ACP+Air_BC_IT_1 - TIFF Files: 727KB each; 2.64GB	Erode x 6/Dilate x6 12_Surface_Air_BC_IT_1 - TIFF Files: 727KB each; 2.64GB	Relative proportion FDs (%): 7 13_Smooth_SA_BC_IT_1	Gaussian Blur 3D (Sigma: 3) + Tresholding (2) 14_3D_SA_BC_IT_1	11_ACP+Air_BC_IT_1 subtract 14_3D_SA_BC_IT_1 15_ACP_BC_IT_1	Area/Volume Fraction BC_IT_1_ACP_AreaVolume_Fraction - Excel File: 9KB	Feret diameter; Thickness; Surface area; Enclosed volume; Euler characteristic - Min volume: 4882860 micron3; Surface resampling: 6; Show particle stack
BC_IT_2	Nikon Xtek 225kV High Flux Bay	Min volume: 4882860 micron3; Surface resampling: 2; Show particle stack	Threshold greyscale range: 29895 - 29897 11_ACP+Air_BC_IT_2 - TIFF Files: 688KB each; 2.52GB	Erode x 6/Dilate x6 12_Surface_Air_BC_IT_2 - TIFF Files: 688KB each; 2.52GB	Relative proportion FDs (%): 7 13_Smooth_SA_BC_IT_2	Gaussian Blur 3D (Sigma: 3) + Tresholding (2) 14_3D_SA_BC_IT_2	11_ACP+Air_BC_IT_2 subtract 14_3D_SA_BC_IT_2 15_ACP_BC_IT_2	Area/Volume Fraction BC_IT_2_ACP_AreaVolume_Fraction - Excel File: 9KB	Feret diameter; Thickness; Surface area; Enclosed volume; Euler characteristic - Min volume: 4882860 micron3; Surface resampling: 6; Show particle stack
BC_LT_1	Nikon Xtek 225kV High Flux Bay	Min volume: 4882860 micron3; Surface resampling: 2; Show particle stack	Threshold greyscale range: 29156 - 29158 11_ACP+Air_BC_LT_1 - TIFF Files: 706KB each; 2.48GB	Erode x 6/Dilate x6 12_Surface_Air_BC_LT_1 - TIFF Files: 706KB each; 2.48GB	Relative proportion FDs (%): 7 13_Smooth_SA_BC_LT_1	Gaussian Blur 3D (Sigma: 3) + Tresholding (2) 14_3D_SA_BC_LT_1	11_ACP+Air_BC_LT_1 subtract 14_3D_SA_BC_LT_1 15_ACP_BC_LT_1	Area/Volume Fraction BC_LT_1_ACP_AreaVolume_Fraction - Excel File: 9KB	Feret diameter; Thickness; Surface area; Enclosed volume; Euler characteristic - Min volume: 4882860 micron3; Surface resampling: 6; Show particle stack
BC_LT_2	Nikon Xtek 225kV High Flux Bay	Min volume: 4882860 micron3; Surface resampling: 2; Show particle stack	Threshold greyscale range: 27637 - 27639 11_ACP+Air_BC_LT_2 - TIFF Files: 672KB each; 2.44GB	Erode x 6/Dilate x6 12_Surface_Air_BC_LT_2 - TIFF Files: 672KB each; 2.44GB	Relative proportion FDs (%): 7 13_Smooth_SA_BC_LT_2	Gaussian Blur 3D (Sigma: 3) + Tresholding (2) 14_3D_SA_BC_LT_2	11_ACP+Air_BC_LT_2 subtract 14_3D_SA_BC_LT_2 15_ACP_BC_LT_2	Area/Volume Fraction BC_LT_2_ACP_AreaVolume_Fraction - Excel File: 9KB	Feret diameter; Thickness; Surface area; Enclosed volume; Euler characteristic - Min volume: 4882860 micron3; Surface resampling: 6; Show particle stack

SF_IT_1	Nikon Xtek 225kV High Flux Bay	Min volume: 4882860 micron3; Surface resampling: 2; Show particle stack	Threshold greyscale range: 30261 - 30263 11_ACP+Air_SF_IT_1 - TIFF Files: 757KB each; 2.77GB	Erode x 6/Dilate x6 12_Surface_Air_SF_IT_1 - TIFF Files: 757KB each; 2.77GB	Relative proportion FDs (%): 7 13_Smooth_SA_SF_IT_1	Gaussian Blur 3D (Sigma: 3) + Tresholding (2) 14_3D_SA_SF_IT_1	11_ACP+Air_SF_IT_1 subtract 14_3D_SA_SF_IT_1 15_ACP_SF_IT_1	Area/Volume Fraction SF_IT_1_ACP_AreaVolume_Fraction - Excel File: 9KB	Feret diameter; Thickness; Surface area; Enclosed volume; Euler characteristic - Min volume: 4882860 micron3; Surface resampling: 6; Show particle stack
SF_IT_2	Nikon Custom 450	Min volume: 4882860 micron3; Surface resampling: 2; Show particle stack	Threshold greyscale range: 18530 - 18532 11_ACP+Air_SF_IT_2 - TIFF Files: 642KB each; 2.92GB	Erode x 6/Dilate x6 12_Surface_Air_SF_IT_2 - TIFF Files: 642KB each; 2.92GB	Relative proportion FDs (%): 7 13_Smooth_SA_SF_IT_2	Gaussian Blur 3D (Sigma: 3) + Tresholding (2) 14_3D_SA_SF_IT_2	11_ACP+Air_SF_IT_2 subtract 14_3D_SA_SF_IT_2 15_ACP_SF_IT_2	Area/Volume Fraction SF_IT_2_ACP_AreaVolume_Fraction - Excel File: 9KB	Feret diameter; Thickness; Surface area; Enclosed volume; Euler characteristic - Min volume: 4882860 micron3; Surface resampling: 6; Show particle stack
SF_LT_1	Nikon Xtek 225kV High Flux Bay	Min volume: 4882860 micron3; Surface resampling: 2; Show particle stack	Threshold greyscale range: 1316 - 1318 11_ACP+Air_SF_LT_1 - TIFF Files: 655KB each; 2.28GB	Erode x 6/Dilate x6 12_Surface_Air_SF_LT_1 - TIFF Files: 655KB each; 2.28GB	Relative proportion FDs (%): 7 13_Smooth_SA_SF_LT_1	Gaussian Blur 3D (Sigma: 3) + Tresholding (2) 14_3D_SA_SF_LT_1	11_ACP+Air_SF_LT_1 subtract 14_3D_SA_SF_LT_1 15_ACP_SF_LT_1	Area/Volume Fraction SF_LT_1_ACP_AreaVolume_Fraction - Excel File: 9KB	Feret diameter; Thickness; Surface area; Enclosed volume; Euler characteristic - Min volume: 4882860 micron3; Surface resampling: 6; Show particle stack
SF_LT_2	Nikon Xtek 225kV High Flux Bay	Min volume: 4882860 micron3; Surface resampling: 2; Show particle stack	Threshold greyscale range: 9477 - 9479 11_ACP+Air_SF_LT_2 - TIFF Files: 672KB each; 2.44GB	Erode x 6/Dilate x6 12_Surface_Air_SF_LT_2 - TIFF Files: 672KB each; 2.44GB	Relative proportion FDs (%): 7 13_Smooth_SA_SF_LT_2	Gaussian Blur 3D (Sigma: 3) + Tresholding (2) 14_3D_SA_SF_LT_2	11_ACP+Air_SF_LT_2 subtract 14_3D_SA_SF_LT_2 15_ACP_SF_LT_2	Area/Volume Fraction SF_LT_2_ACP_AreaVolume_Fraction - Excel File: 9KB	Feret diameter; Thickness; Surface area; Enclosed volume; Euler characteristic - Min volume: 4882860 micron3; Surface resampling: 6; Show particle stack
SM_B	Nikon XTH 225	Min volume: 4882860 micron3; Surface resampling: 2; Show particle stack	Threshold greyscale range: 7766 - 7768 11_ACP+Air_SM_B - TIFF Files: 731KB each; 1.46GB	Erode x 6/Dilate x6 12_Surface_Air_SM_B - TIFF Files: 731KB each; 1.46GB	Relative proportion FDs (%): 7 13_Smooth_SA_SM_B	Gaussian Blur 3D (Sigma: 3) + Tresholding (2) 14_3D_SA_SM_B	11_ACP+Air_SM_B subtract 14_3D_SA_SM_B 15_ACP_SM_B	Area/Volume Fraction SM_B_ACP_AreaVolume_Fraction - Excel File: 9KB	Feret diameter; Thickness; Surface area; Enclosed volume; Euler characteristic - Min volume: 4882860 micron3; Surface resampling: 6; Show particle stack
SM_C	Nikon XTH 225	Min volume: 4882860 micron3; Surface resampling: 2; Show particle stack	Threshold greyscale range: 9505 - 9507 11_ACP+Air_SM_C - TIFF Files: 718KB each; 1.44GB	Erode x 6/Dilate x6 12_Surface_Air_SM_C - TIFF Files: 718KB each; 1.44GB	Relative proportion FDs (%): 7 13_Smooth_SA_SM_C	Gaussian Blur 3D (Sigma: 3) + Tresholding (2) 14_3D_SA_SM_C	11_ACP+Air_SM_C subtract 14_3D_SA_SM_C 15_ACP_SM_C	Area/Volume Fraction SM_C_ACP_AreaVolume_Fraction - Excel File: 9KB	Feret diameter; Thickness; Surface area; Enclosed volume; Euler characteristic - Min volume: 4882860 micron3; Surface resampling: 6; Show particle stack
SM_D	Nikon XTH 225	Min volume: 4882860 micron3; Surface resampling: 2; Show particle stack	Threshold greyscale range: 4319 - 4321 11_ACP+Air_SM_D - TIFF Files: 721KB each; 1.49GB	Erode x 6/Dilate x6 12_Surface_Air_SM_D - TIFF Files: 721KB each; 1.49GB	Relative proportion FDs (%): 7 13_Smooth_SA_SM_D	Gaussian Blur 3D (Sigma: 3) + Tresholding (2) 14_3D_SA_SM_D	11_ACP+Air_SM_D subtract 14_3D_SA_SM_D 15_ACP_SM_D	Area/Volume Fraction SM_D_ACP_AreaVolume_Fraction - Excel File: 9KB	Feret diameter; Thickness; Surface area; Enclosed volume; Euler characteristic - Min volume: 4882860 micron3; Surface resampling: 6; Show particle stack
SF_Nat	Nikon Xtek 225kV High Flux Bay	Min volume: 4882860 micron3; Surface resampling: 2; Show particle stack	Threshold greyscale range: 19594 - 19596 11_ACP+Air_SF_Nat - TIFF Files: 651KB each; 2.30GB	Erode x 6/Dilate x6 12_Surface_Air_SF_Nat - TIFF Files: 651KB each; 2.30GB	Relative proportion FDs (%): 7 13_Smooth_BW_SF_LT_1	Gaussian Blur 3D (Sigma: 3) + Tresholding (2) 14_3D_SA_SF_Nat	11_ACP+Air_SF_Nat subtract 14_3D_SA_SF_Nat 15_ACP_SF_Nat	Area/Volume Fraction SF_Nat_ACP_AreaVolume_Fraction - Excel File: 9KB	Feret diameter; Thickness; Surface area; Enclosed volume; Euler characteristic - Min volume: 4882860 micron3; Surface resampling: 6; Show particle stack

Table 9: Isolation and quantification of boundary-connected porosity (BCP) in ImageJ for each core including the size of file output.

Core ID	Scanner	Image Calculator - Boundary-Connected Porosity & IP (BCP+IP)	Particle Analyser Parameters - BCP+IP	Image Calculator - BCP	Quantifying - BCP
BC_Deg	Nikon Xtek 225kV High Flux Bay	6_Dspk_TPS_BC_Deg subtract 11_EPS_BC_Deg 17_BCP+IP_BC_Deg - TIFF Files: 652KB each; 2.30GB	Feret diameter; Thickness; Surface area; Enclosed volume; Euler characteristic - Min volume: 4882860 micron3; Surface resampling: 2; Show particle stack	17_BCP+IP_BC_Deg subtract 8_Binary_IP_BC_Deg	Area/Volume Fraction BC_Deg_BCP_AreaVolume_Fraction - Excel File: 9KB
BW_LT_1	Nikon Xtek 225kV High Flux Bay	6_Dspk_TPS_BW_LT_1 subtract 11_EPS_BW_LT_1 17_BCP+IP_BW_LT_1 - TIFF Files: 660KB each; 2.34GB	Feret diameter; Thickness; Surface area; Enclosed volume; Euler characteristic - Min volume: 4882860 micron3; Surface resampling: 2; Show particle stack	17_BCP+IP_BW_LT_1 subtract 8_Binary_IP_BW_LT_1	Area/Volume Fraction BW_LT_1_BCP_AreaVolume_Fraction - Excel File: 9KB
BW_LT_2	Nikon XTH 225	6_Dspk_TPS_BW_LT_2 subtract 11_EPS_BW_LT_2 17_BCP+IP_BW_LT_2 - TIFF Files: 677KB each; 1.39GB	Feret diameter; Thickness; Surface area; Enclosed volume; Euler characteristic - Min volume: 4882860 micron3; Surface resampling: 2; Show particle stack	17_BCP+IP_BW_LT_2 subtract 8_Binary_IP_BW_LT_2	Area/Volume Fraction BW_LT_2_BCP_AreaVolume_Fraction - Excel File: 9KB
BC_IT_1	Nikon Xtek 225kV High Flux Bay	6_Dspk_TPS_BC_IT_1 subtract 11_EPS_BC_IT_1 17_BCP+IP_BC_IT_1 - TIFF Files: 727KB each; 2.64GB	Feret diameter; Thickness; Surface area; Enclosed volume; Euler characteristic - Min volume: 4882860 micron3; Surface resampling: 2; Show particle stack	17_BCP+IP_BC_IT_1 subtract 8_Binary_IP_BC_IT_1	Area/Volume Fraction BC_IT_1_BCP_AreaVolume_Fraction - Excel File: 9KB
BC_IT_2	Nikon Xtek 225kV High Flux Bay	6_Dspk_TPS_BC_IT_2 subtract 11_EPS_BC_IT_2 17_BCP+IP_BC_IT_2 - TIFF Files: 688KB each; 2.52GB	Feret diameter; Thickness; Surface area; Enclosed volume; Euler characteristic - Min volume: 4882860 micron3; Surface resampling: 2; Show particle stack	17_BCP+IP_BC_IT_2 subtract 8_Binary_IP_BC_IT_2	Area/Volume Fraction BC_IT_2_BCP_AreaVolume_Fraction - Excel File: 9KB
BC_LT_1	Nikon Xtek 225kV High Flux Bay	6_Dspk_TPS_BC_LT_1 subtract 11_EPS_BC_LT_1 17_BCP+IP_BC_LT_1 - TIFF Files: 706KB each; 2.48GB	Feret diameter; Thickness; Surface area; Enclosed volume; Euler characteristic - Min volume: 4882860 micron3; Surface resampling: 2; Show particle stack	17_BCP+IP_BC_LT_1 subtract 8_Binary_IP_BC_LT_1	Area/Volume Fraction BC_LT_1_BCP_AreaVolume_Fraction - Excel File: 9KB
BC_LT_2	Nikon Xtek 225kV High Flux Bay	6_Dspk_TPS_BC_LT_2 subtract 11_EPS_BC_LT_2 17_BCP+IP_BC_LT_2 - TIFF Files: 672KB each; 2.44GB	Feret diameter; Thickness; Surface area; Enclosed volume; Euler characteristic - Min volume: 4882860 micron3; Surface resampling: 2; Show particle stack	17_BCP+IP_BC_LT_2 subtract 8_Binary_IP_BC_LT_2	Area/Volume Fraction BC_LT_2_BCP_AreaVolume_Fraction - Excel File: 9KB
SF_IT_1	Nikon Xtek 225kV High Flux Bay	6_Dspk_TPS_SF_IT_1 subtract 11_EPS_SF_IT_1 17_BCP+IP_SF_IT_1 - TIFF Files: 757KB each; 2.77GB	Feret diameter; Thickness; Surface area; Enclosed volume; Euler characteristic - Min volume: 4882860 micron3; Surface resampling: 2; Show particle stack	17_BCP+IP_SF_IT_1 subtract 8_Binary_IP_SF_IT_1	Area/Volume Fraction SF_IT_1_BCP_AreaVolume_Fraction - Excel File: 9KB
SF_IT_2	Nikon Custom 450	6_Dspk_TPS_SF_IT_2 subtract 11_EPS_SF_IT_2 17_BCP+IP_SF_IT_2 - TIFF Files: 642KB each; 2.92GB	Feret diameter; Thickness; Surface area; Enclosed volume; Euler characteristic - Min volume: 4882860 micron3; Surface resampling: 2; Show particle stack	17_BCP+IP_SF_IT_2 subtract 8_Binary_IP_SF_IT_2	Area/Volume Fraction SF_IT_2_BCP_AreaVolume_Fraction - Excel File: 9KB
SF_LT_1	Nikon Xtek 225kV High Flux Bay	6_Dspk_TPS_SF_LT_1 subtract 11_EPS_SF_LT_1 17_BCP+IP_SF_LT_1 - TIFF Files: 655KB each; 2.28GB	Feret diameter; Thickness; Surface area; Enclosed volume; Euler characteristic - Min volume: 4882860 micron3; Surface resampling: 2; Show particle stack	17_BCP+IP_SF_LT_1 subtract 8_Binary_IP_SF_LT_1	Area/Volume Fraction SF_LT_1_BCP_AreaVolume_Fraction - Excel File: 9KB
SF_LT_2	Nikon Xtek 225kV High Flux Bay	6_Dspk_TPS_SF_LT_2 subtract 11_EPS_SF_LT_2 17_BCP+IP_SF_LT_2 - TIFF Files: 672KB each; 2.44GB	Feret diameter; Thickness; Surface area; Enclosed volume; Euler characteristic - Min volume: 4882860 micron3; Surface resampling: 2; Show particle stack	17_BCP+IP_SF_LT_2 subtract 8_Binary_IP_SF_LT_2	Area/Volume Fraction SF_LT_2_BCP_AreaVolume_Fraction - Excel File: 9KB
SM_B	Nikon XTH 225	6_Dspk_TPS_SM_B subtract 11_EPS_SM_B 17_BCP+IP_SM_B - TIFF Files: 731KB each; 1.46GB	Feret diameter; Thickness; Surface area; Enclosed volume; Euler characteristic - Min volume: 4882860 micron3; Surface resampling: 2; Show particle stack	17_BCP+IP_SM_B subtract 8_Binary_IP_SM_B	Area/Volume Fraction SM_B_BCP_AreaVolume_Fraction - Excel File: 9KB
SM_C	Nikon XTH 225	6_Dspk_TPS_SM_C subtract 11_EPS_SM_C 17_BCP+IP_SM_C - TIFF Files: 718KB each; 1.44GB	Feret diameter; Thickness; Surface area; Enclosed volume; Euler characteristic - Min volume: 4882860 micron3; Surface resampling: 2; Show particle stack	17_BCP+IP_SM_C subtract 8_Binary_IP_SM_C	Area/Volume Fraction SM_C_BCP_AreaVolume_Fraction - Excel File: 9KB
SM_D	Nikon XTH 225	6_Dspk_TPS_SM_D subtract 11_EPS_SM_D 17_BCP+IP_SM_D - TIFF Files: 721KB each; 1.49GB	Feret diameter; Thickness; Surface area; Enclosed volume; Euler characteristic - Min volume: 4882860 micron3; Surface resampling: 2; Show particle stack	17_BCP+IP_SM_D subtract 8_Binary_IP_SM_D	Area/Volume Fraction SM_D_BCP_AreaVolume_Fraction - Excel File: 9KB
SF_Nat	Nikon Xtek 225kV High Flux Bay	6_Dspk_TPS_SF_Nat subtract 11_EPS_SF_Nat 17_BCP+IP_SF_Nat - TIFF Files: 651KB each; 2.30GB	Feret diameter; Thickness; Surface area; Enclosed volume; Euler characteristic - Min volume: 4882860 micron3; Surface resampling: 2; Show particle stack	17_BCP+IP_SF_Nat subtract 8_Binary_IP_SF_Nat	Area/Volume Fraction SF_Nat_BCP_AreaVolume_Fraction - Excel File: 9KB

F) Selected top three most intensive 50x50m grid units for Borrowdale, Bampton Common, and Shap Fells:
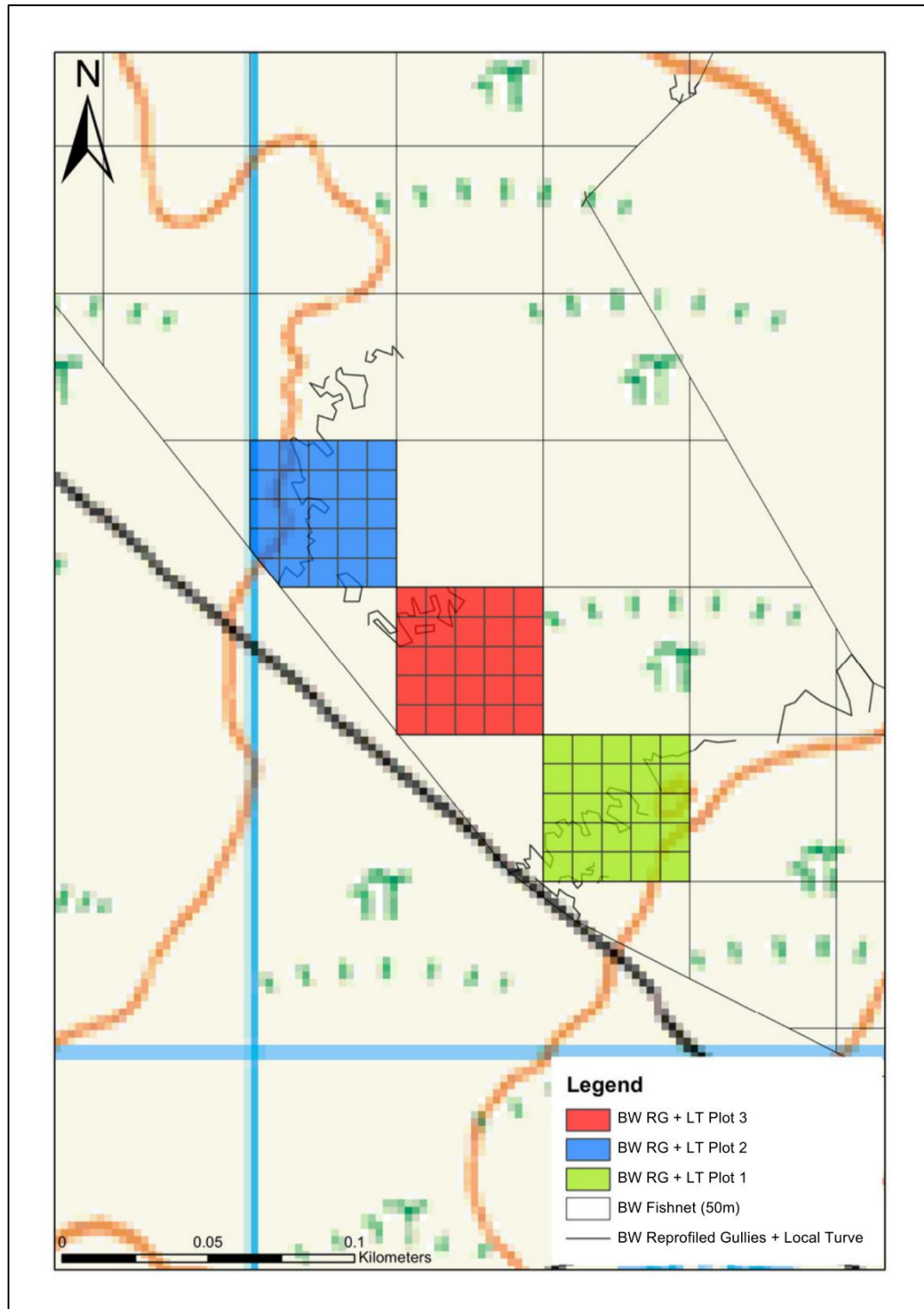
Figure 1: Selected top three most intensive 50x50m grid units at Borrowdale (BW) based on total lengths of reprofiled and locally turved (RG + LT) gullies. Internal grids relate to ground-truthing assessments.
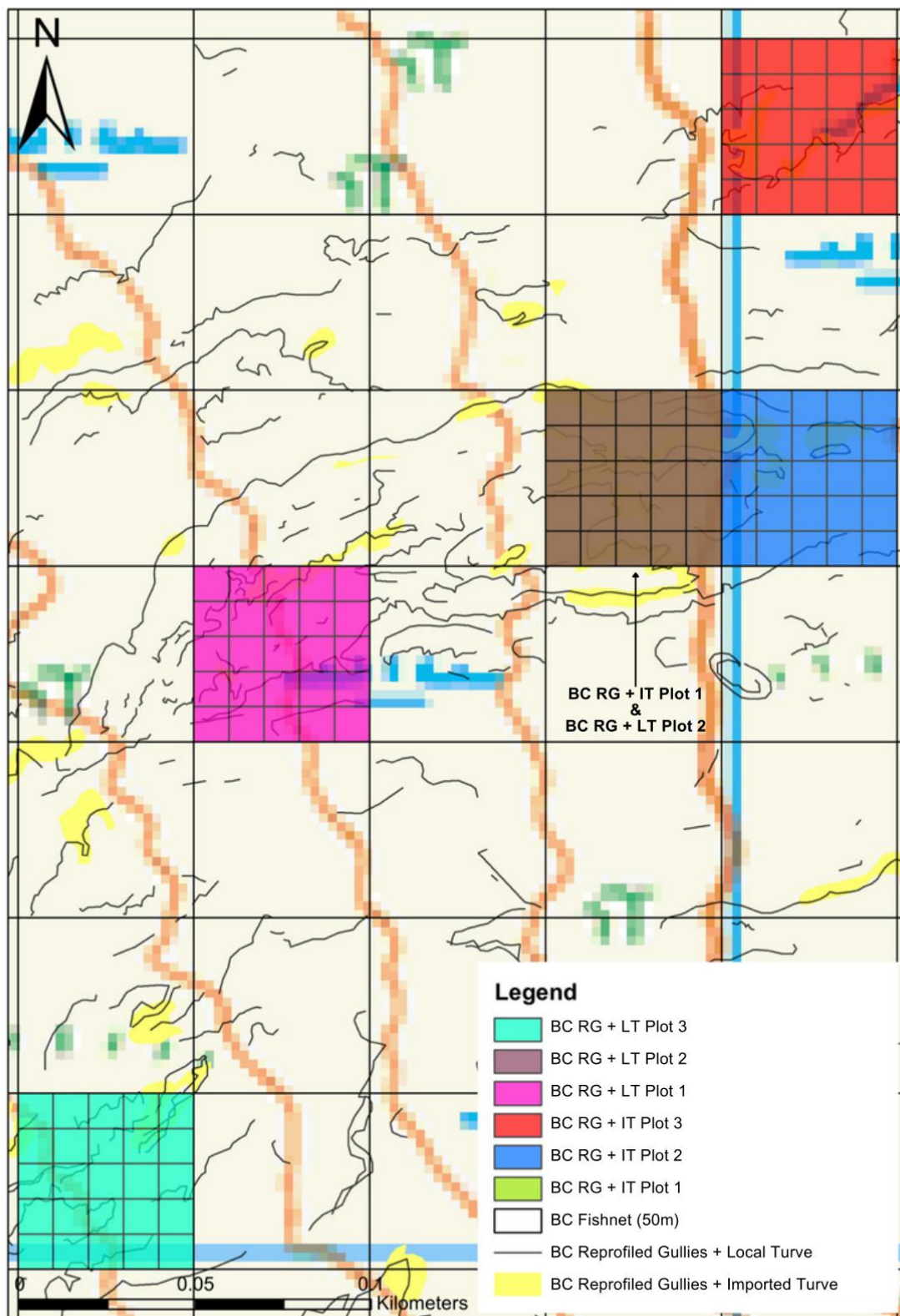
Figure 2: Selected top three most intensive 50x50m grid units at Bampton Common (BC) for total lengths of reprofiled and locally turved (RG + LT) and reprofiled and imported turved (RG + IT) gullies. Internal grids relate to ground-truthing assessments.
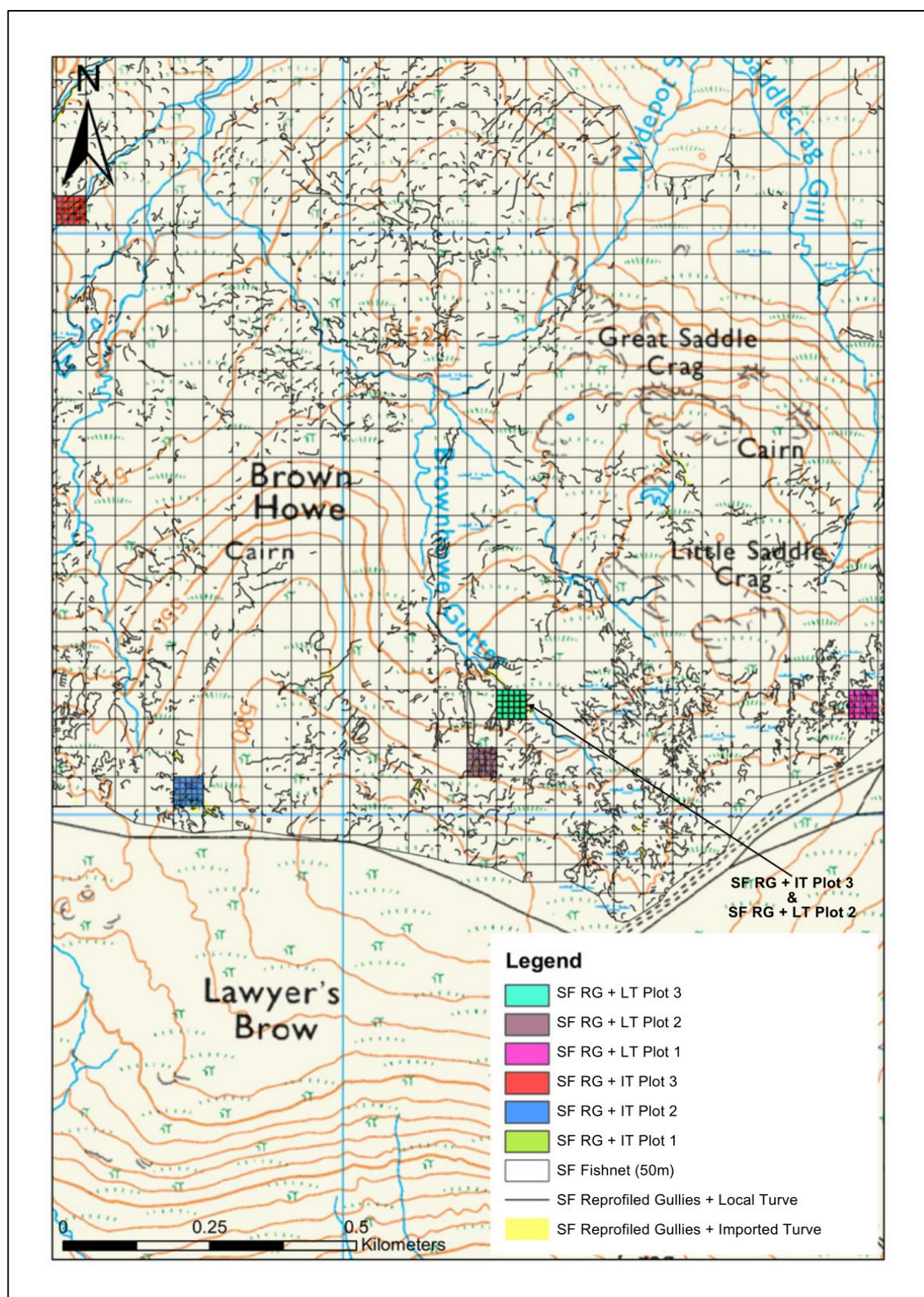
Figure 3: Selected top three most intensive 50x50m grid units at Shap Fells (SF) for total lengths of reprofiled and locally turved (RG + LT) and reprofiled and imported turved (RG + IT) gullies. Internal grids relate to ground-truthing assessments.

G) JNCC (2009) indicator species of favourable condition and sensitive areas:

Figure 4: JNCC (2009) indicator species of favourable condition.

Table 10: Summary of JNCC (2009) 'sensitive areas' prone to disturbance.

Code	Sensitive Area
(a)	Slopes >18°
(b)	Areas dominated by *Sphagnum*, mosses, liverworts, or lichens
(c)	Hummocky terrain with well-developed *Sphagnum* lawns or cotton-grass tussocks creating micro-topographic variation
(d)	Pools, wet hollows, haggs, erosion gullies, and areas within 5–10m of watercourses

H) Final survey area selection for Borrowdale, Shap Fells, and Stake Moss:
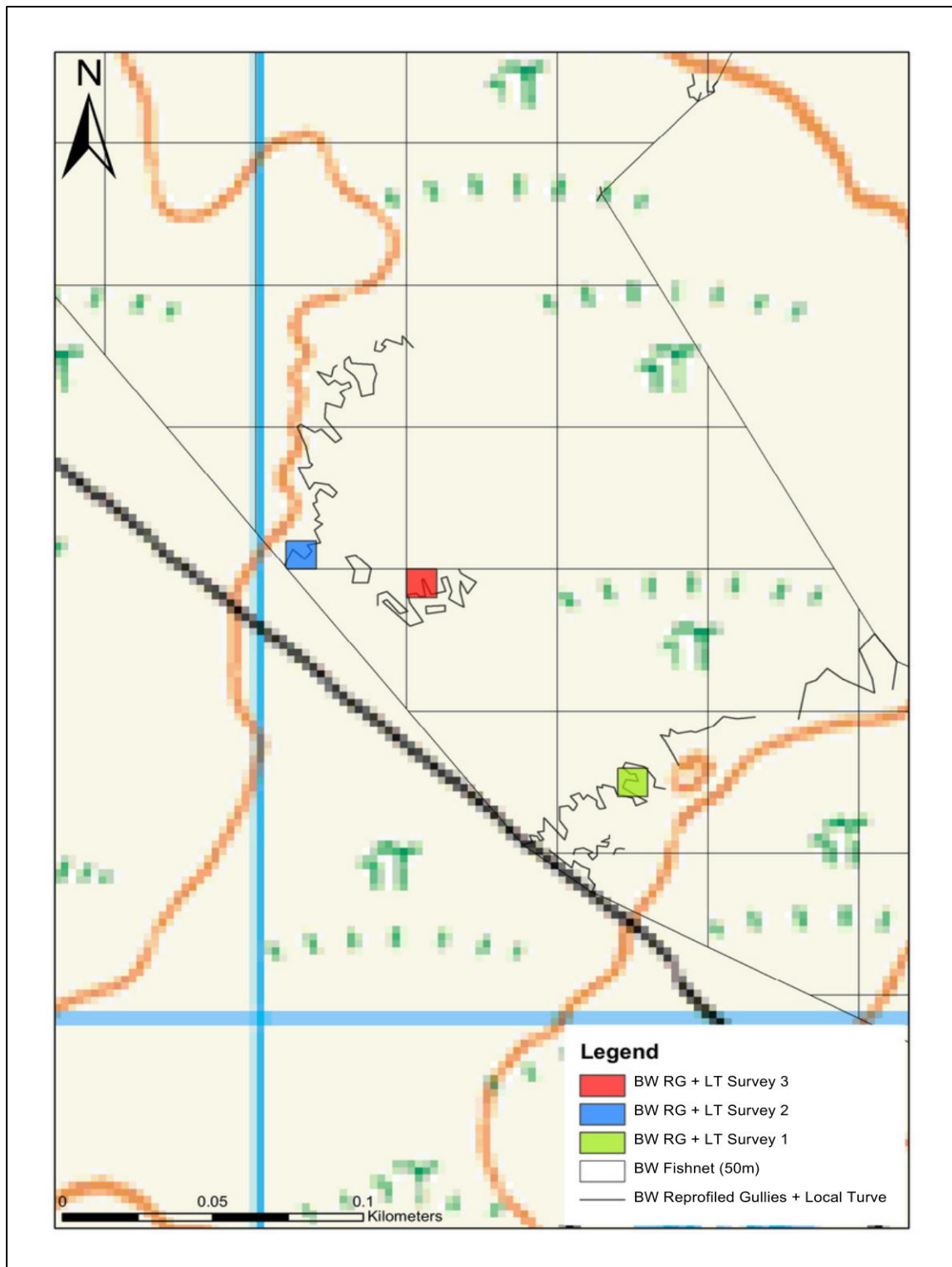
Figure 5: Selected 10x10m survey sub-plots at Borrowdale (BW) based on total lengths of reprofiled and locally turved (RG + LT) gullies.
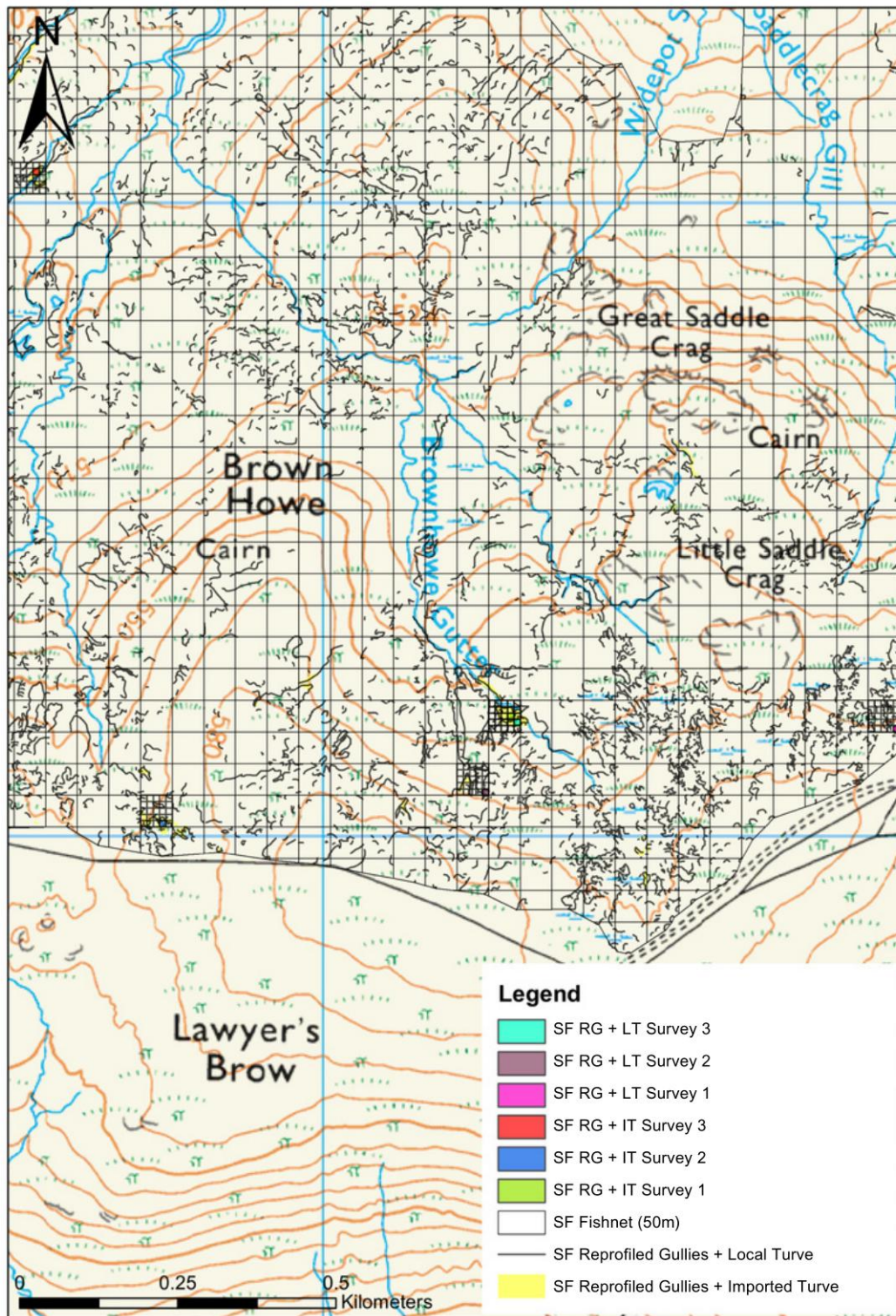
Figure 6: Selected 10x10m survey sub-plots at Shap Fells (SF) for total lengths of reprofiled and locally turved (RG + LT) and reprofiled and imported turved (RG + IT) gullies.
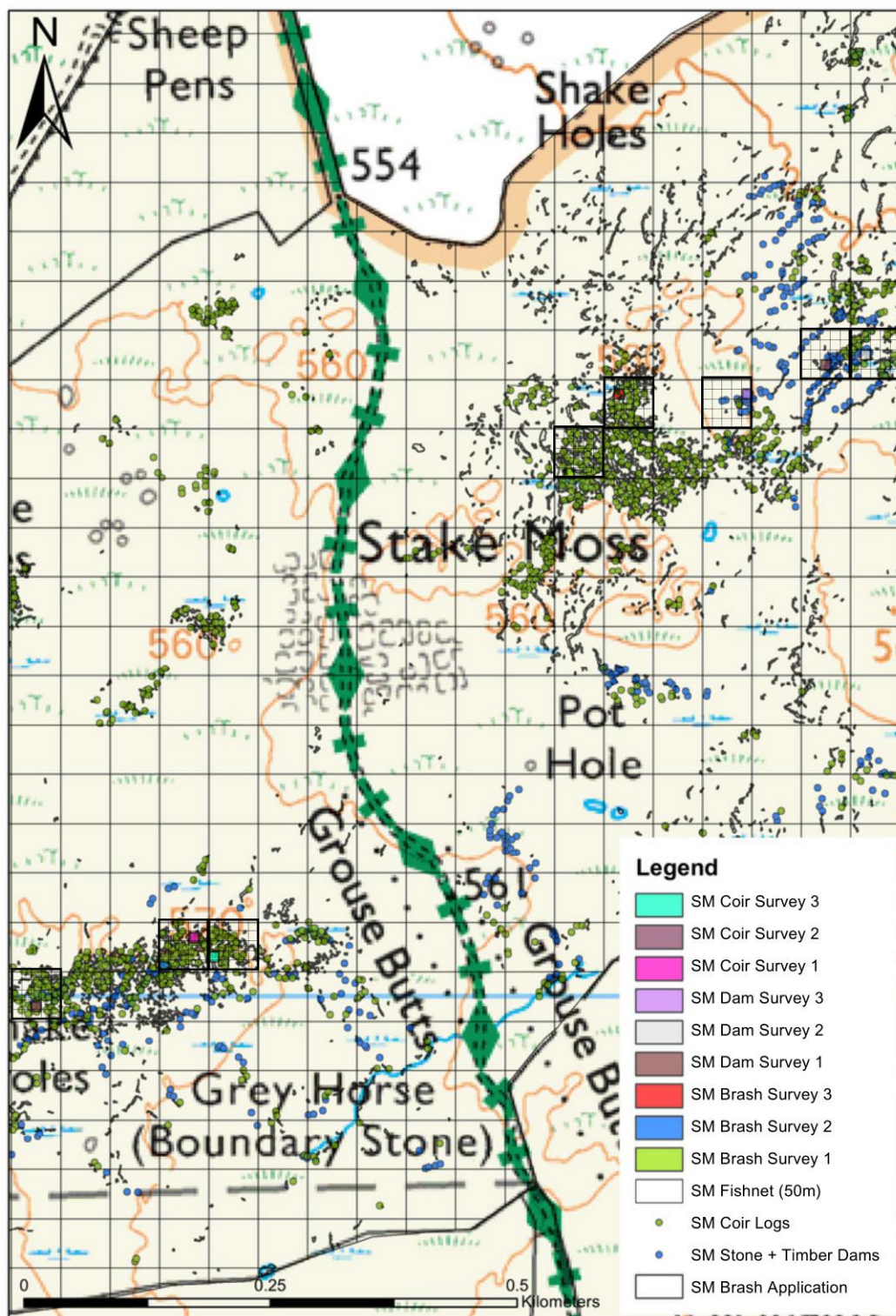
Figure 7: Selected 10x10m survey sub-plots at Stake Moss (SM) for total area of heather brash spread (Brash), quantity of stone/timber dams (Dam), and quantity of coir logs (Coir) within gullies.

I) JNCC (2009) survey sheet used to collect surface condition data:

Table 11: JNCC (2009) data collection sheet example.

Site:																									
Dominant Feature & Peat Regrowth (%)			**Non-*Sphagnum* Indicator Species (%)**																					**Microtopography (n)**	
Plot	Loc.	PRG	AP	AS	BN	CB	CV	CS	DS	ES	EN	EA	EV	MT	MG	NO	N-C L	PM	RL	RC	RA	TC	VS	Hu	Ho
1																									
2																									
3																									
4																									
5																									
6																									
7																									
8																									
9																									
10																									
11																									
12																									
13																									
14																									
15																									
16																									
17																									
18																									
19																									
20																									
21																									
22																									
23																									
24																									
25																									

***Sphagnum* Species (%)**												**Degradation (%)**								**Sensitive Areas**	
Plot	S.Au	S.Ca	S.Cu	S.De	S.Fa	S.Fi	S.Fu	S.Ma	S.Pa	S.Pap	S.Su	S.Te	BP	AD	ER	BR	BU	DG	SD	Inv.	Typ.	Pool?	Rest?	Notes
1																								
2																								
3																								
4																								
5																								
6																								
7																								
8																								
9																								
10																								
11																								
12																								
13																								
14																								
15																								
16																								
17																								
18																								
19																								
20																								
21																								
22																								
23																								
24																								
25																								

J) Plot-scale (4m^2) JNCC (2009) data:
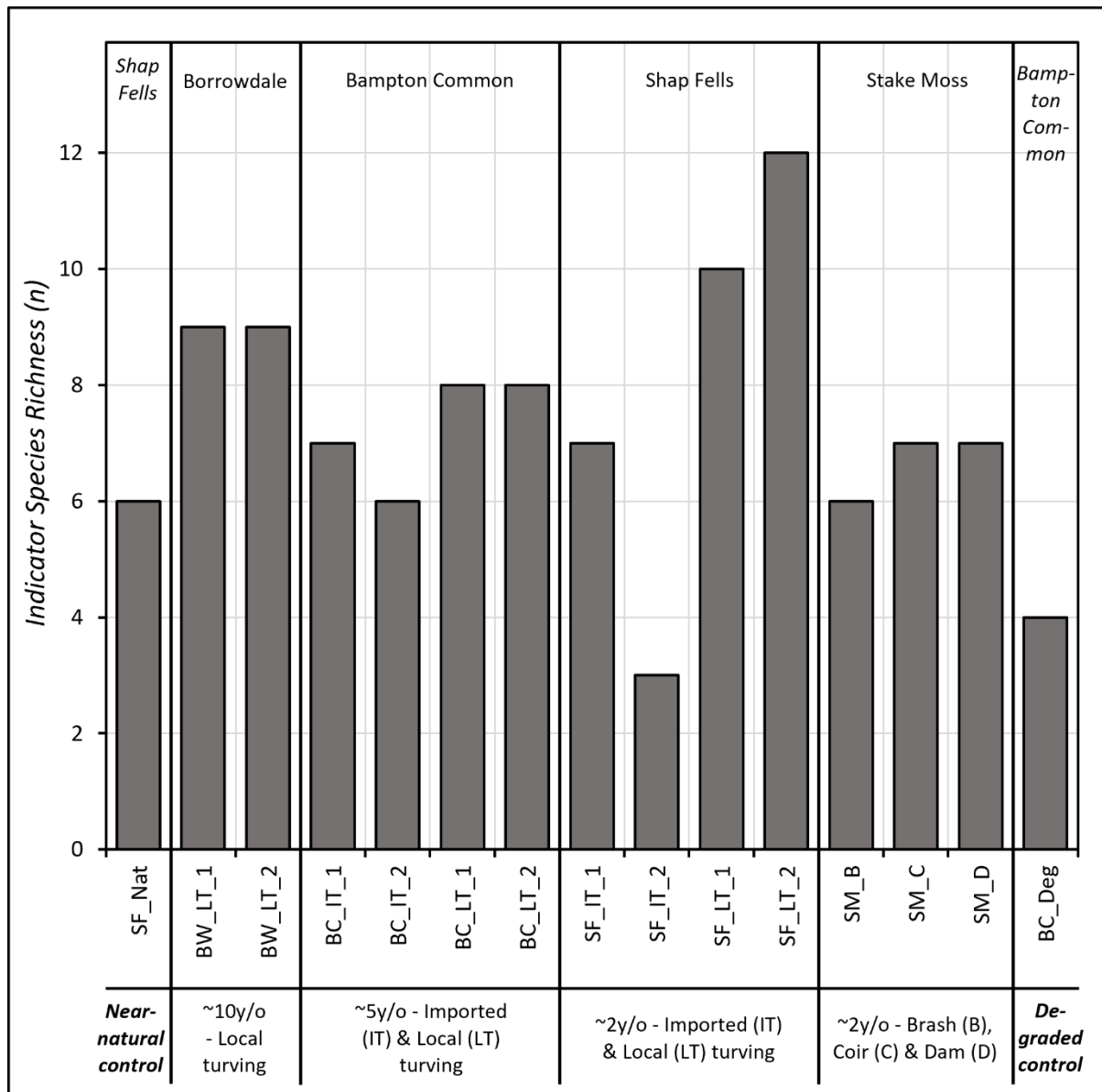
Figure 5: Indicator species richness (JNCC, 2009) across selected restoration and control plots (4m^2). Each plot represents the most favourable condition within its site, showcasing effective restoration. For turved sites (BW_LT, BC_IT, BC_LT, SF_IT, SF_LT), duplicate samples were assessed, as indicated by numerical site codes. Black vertical lines separate sites based on restoration age and technique (described in bottom text). The blanket bog complex for each site is labelled at the top.
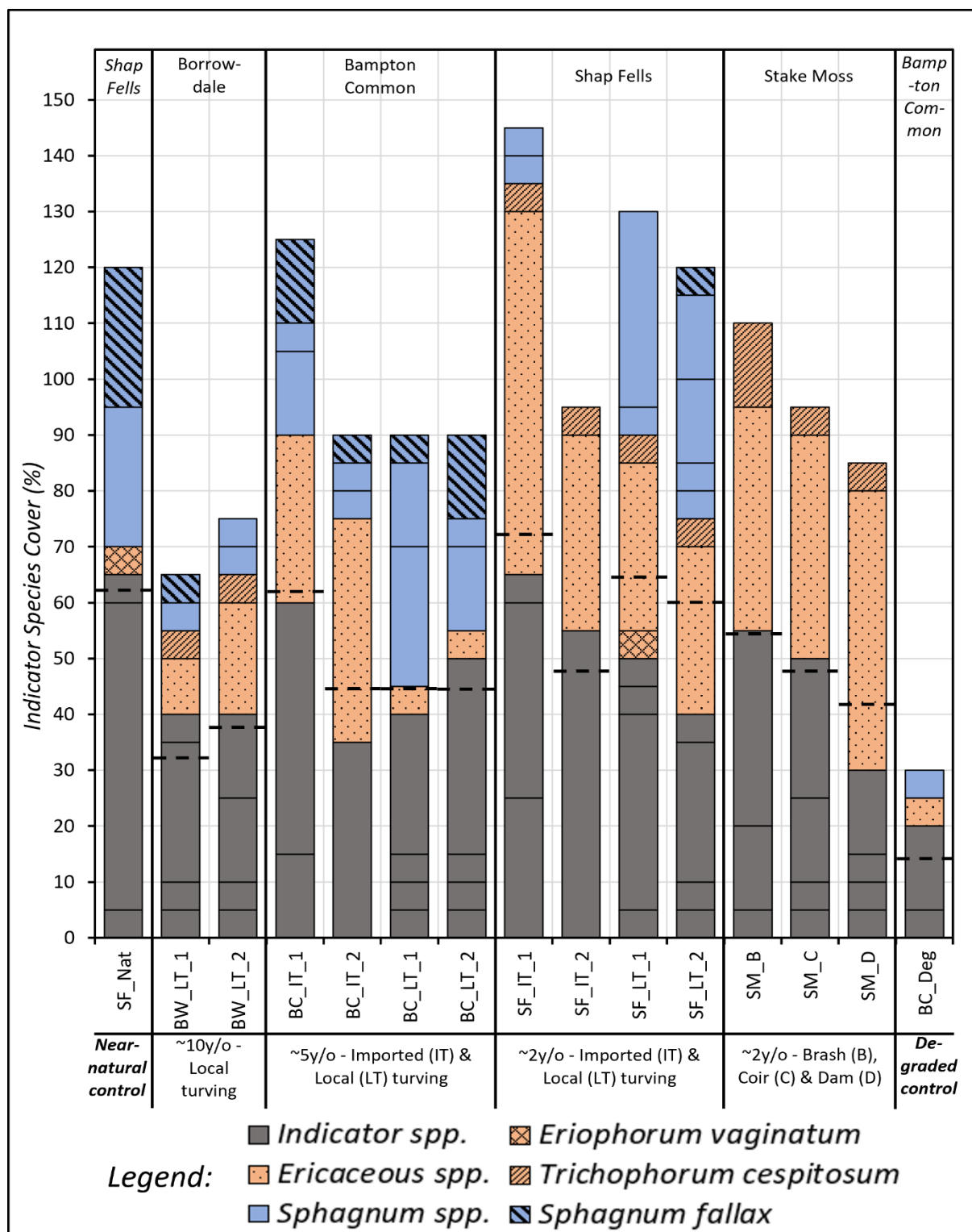
Figure 6: Total indicator species cover (JNCC, 2009) across selected restored and control plots (4m²). Stacked bars represent the contribution of indicator species. *Eriophorum vaginatum*, *Ericaceous* species, and *Trichophorum cespitosum* are highlighted in orange. *Sphagnum* species are shown in blue, with *Sphagnum fallax* distinguished by bold diagonal lines. Other indicator species are outlined in grey. Dashed horizontal lines mark the 50% cover threshold. Values may exceed 100% due to categorical data assessment (Chapter 4; Section 4.3.7). Black vertical lines separate sites by restoration age and technique, with blanket bog complexes labelled at the top.
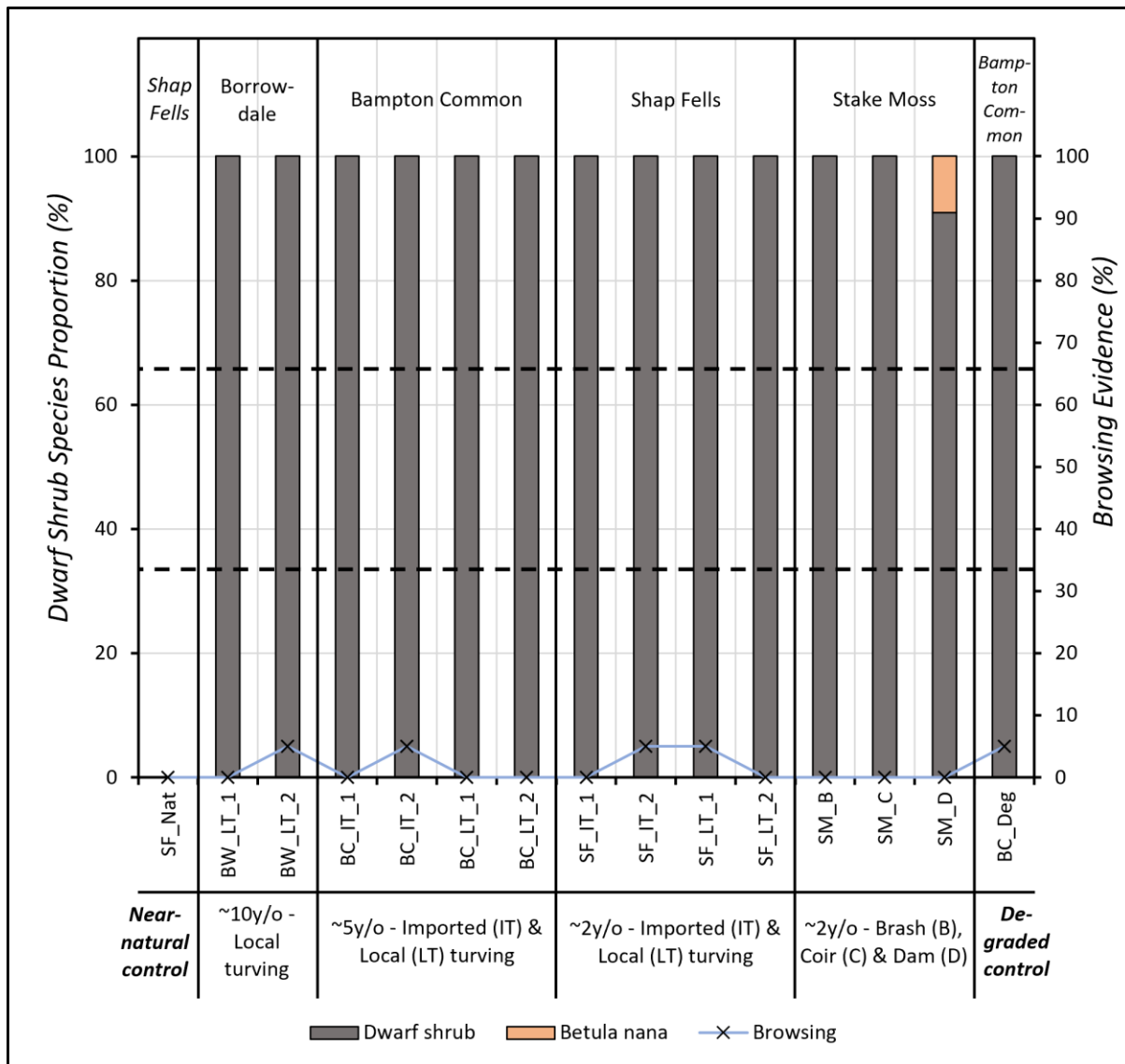
Figure 7: Dwarf shrub species proportions and browsing evidence across restored, near-natural, and degraded plots (4m^2). *Betula nana* is highlighted in orange to assess whether browsing exceeds the 66% threshold (indicated by a horizontal dashed line), while all other dwarf shrub species are shown in grey, with the 33% threshold also marked by a horizontal dashed line. The blue line represents browsing evidence. Black vertical lines separate sites by restoration age and technique, with blanket bog complexes labelled at the top.
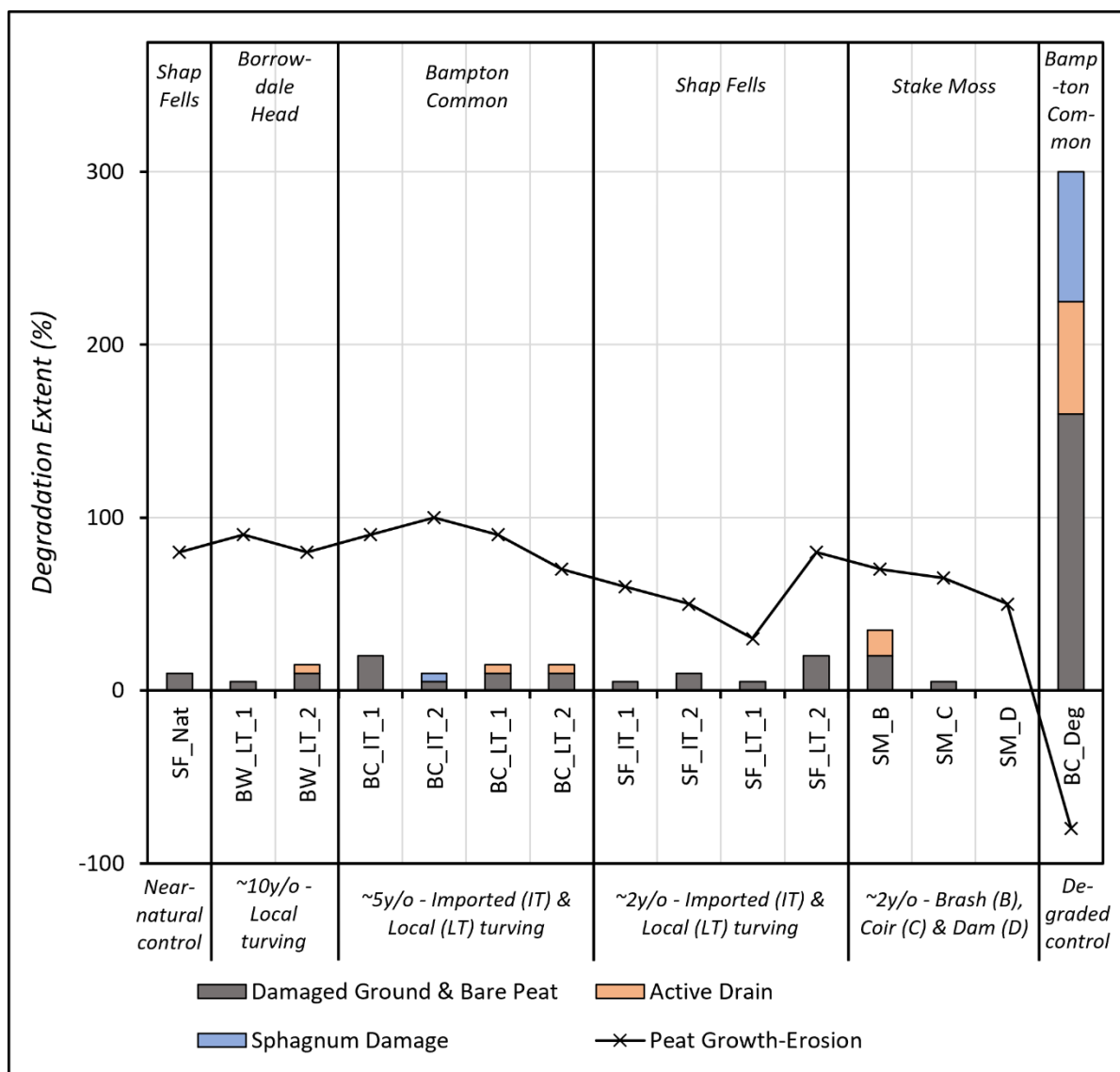
Figure 8: Total degradation extent and relative contributions of damaged ground and bare peat (grey), active drains (orange), and *Sphagnum* damage (blue) across selected restored, near-natural, and degraded plots (4m^2). Peat growth minus erosion is represented by the black line. Black vertical lines separate sites by restoration age and technique, with blanket bog complexes labelled at the top.

Table 12: Revised condition scores for selected 4m^2 plots used in sub-surface chemical and μCT analysis. These represent the most favourable conditions within each site, identified through JNCC (2009) assessment and normalised scoring.

Criterion	BC_Deg	BW_LT_1	BW_LT_2	BC_IT_1	BC_IT_2	BC_LT_1	BC_LT_2	SF_IT_1	SF_IT_2	SF_LT_1	SF_LT_2	SM_B	SM_C	SM_D	SF_Nat
C1	0.33	0.75	0.75	0.58	0.50	0.67	0.67	0.58	0.25	0.83	1.00	0.50	0.58	0.58	0.50
C2	0.21	0.45	0.52	0.86	0.62	0.62	0.62	1.00	0.66	0.90	0.83	0.76	0.66	0.59	0.83
C3	0.10	0.20	0.20	0.70	0.30	0.90	0.70	0.20	0.00	0.80	0.90	0.00	0.00	0.00	1.00
C4	1.00	0.87	0.87	0.93	0.93	1.00	1.00	0.93	0.93	0.80	0.87	0.73	0.87	0.87	0.93
C5	0.00	1.00	0.00	1.00	0.00	1.00	1.00	1.00	0.00	0.00	1.00	1.00	1.00	1.00	0.00
C6	0.00	0.94	0.89	0.94	1.00	0.94	0.83	0.78	0.72	0.61	0.89	0.83	0.81	0.72	0.89
C7	0.00	1.00	0.94	0.94	1.00	0.94	0.94	0.94	0.94	0.94	0.82	0.94	1.00	1.00	0.94
C8	0.00	0.93	0.93	0.80	0.93	0.93	0.93	1.00	0.93	1.00	0.93	0.80	0.93	1.00	0.93
C9	0.00	1.00	0.92	1.00	1.00	0.92	0.92	1.00	1.00	1.00	1.00	0.77	1.00	1.00	1.00
C10	0.00	1.00	1.00	1.00	0.93	1.00	1.00	1.00	0.00	1.00	1.00	0.00	0.00	0.00	1.00
Score	0.16	0.81	0.70	0.88	0.72	0.89	0.86	0.84	0.54	0.79	0.92	0.63	0.68	0.68	0.80

K) LCA supporting information

Table 13: Supporting references with their respective code to the 15 peatland restoration projects used to derive average transport distances and details for this study, as listed in Table 8.4.

Reference Code	Project Links
MFF-BlackHill	https://www.iucn-uk-peatlandprogramme.org/projects/black-hill-moorlife-project?destination=/projects-map%3Fsearch%3DMoors%2520for%2520the%2520Future
MFF-Bleaklow	https://www.iucn-uk-peatlandprogramme.org/projects/bleaklow-moorlife-project-0?destination=/projects-map%3Fsearch%3DMoors%2520for%2520the%2520Future
MFF-Rishworth	https://www.iucn-uk-peatlandprogramme.org/projects/rishworth-common-moorlife-project?destination=/projects-map%3Fsearch%3DMoors%2520for%2520the%2520Future
MFF-TurleyHoles	https://www.iucn-uk-peatlandprogramme.org/projects/turley-holes-moorlife-project?destination=/projects-map%3Fsearch%3DMoors%2520for%2520the%2520Future
NP-Birkdale	https://northpennines.org.uk/wp-content/uploads/2024/02/D2-Birkdale-2021-FINAL.pdf
NP-Dufton	https://northpennines.org.uk/wp-content/uploads/2024/02/D5.4-Dufton-2022.pdf
NP-HartleyCommon	https://northpennines.org.uk/wp-content/uploads/2024/02/Hartley-Common-Site-Management-Plan.pdf
NP-TyneheadFell	https://northpennines.org.uk/wp-content/uploads/2024/02/D5.4-Tynehead-Fell.pdf
NP-VanceLodge	https://northpennines.org.uk/wp-content/uploads/2024/02/Valance-Lodge-and-Langdon-Fell-Site-Managment-Plans.pdf
YPP-FleetMoss	https://www.yppartnership.org.uk/sites/default/files/2019-11/191121%202009_2019%20full%20report%20TT_0.pdf https://www.iucn-uk-peatlandprogramme.org/projects/fleet-moss-moor?destination=/projects-map%3Fsearch%3DYorkshire%2520Peat%2520Partnership
YPP-HaredenFell	https://www.yppartnership.org.uk/sites/default/files/2019-11/191121%202009_2019%20full%20report%20TT_0.pdf https://www.iucn-uk-peatlandprogramme.org/projects/hareden-fell?destination=/projects-map%3Fsearch%3DYorkshire%2520Peat%2520Partnership
YPP-HolmeHouseFell	https://www.yppartnership.org.uk/sites/default/files/2019-11/191121%202009_2019%20full%20report%20TT_0.pdf https://www.iucn-uk-peatlandprogramme.org/projects/holme-house-fell?destination=/projects-map%3Fsearch%3DYorkshire%2520Peat%2520Partnership
YPP-NewHouse	https://www.yppartnership.org.uk/sites/default/files/2019-11/191121%202009_2019%20full%20report%20TT_0.pdf https://www.iucn-uk-peatlandprogramme.org/projects/new-house?destination=/projects-map%3Fsearch%3DYorkshire%2520Peat%2520Partnership
YPP-StakeMoss	https://www.yppartnership.org.uk/sites/default/files/2019-11/191121%202009_2019%20full%20report%20TT_0.pdf https://www.iucn-uk-peatlandprogramme.org/projects/stake-moss?destination=/projects-map%3Fsearch%3DYorkshire%2520Peat%2520Partnership
YPP-WebstersMeadow	https://www.yppartnership.org.uk/sites/default/files/2019-11/191121%202009_2019%20full%20report%20TT_0.pdf https://www.iucn-uk-peatlandprogramme.org/projects/websters-meadow-langden-head?destination=/projects-map%3Fsearch%3DYorkshire%2520Peat%2520Partnership

References

Al Shammary, A. A. G., Kouzani, A. Z., Kaynak, A., Khoo, S. Y., Norton, M. and Gates, W. (2018). Soil bulk density estimation methods: a review. *Pedosphere*, 28(4), pp. 581–596. https://doi.org/10.1016/S1002-0160(18)60034-7

Alderson, D. M., Evans, M. G., Shuttleworth, E. L., Pilkington, M., Spencer, T., Walker, J. and Allott, T. E. H. (2019). Trajectories of ecosystem change in restored blanket peatlands. *Science of the Total Environment*, 665, pp. 785–796. https://doi.org/10.1016/j.scitotenv.2019.02.095

Alexander, P. D., Bragg, N. C., Meade, R., Padelopoulos, G. and Watts, O. (2008). Peat in horticulture and conservation: the UK response to a changing world. *Mires and Peat*, 3, Article 08. https://doi.org/10.19189/001c.128260

Allott, T. E. H., Evans, M. G., Lindsay, J. B., Agnew, C. T., Freer, J. E., Jones, A. and Parnell, M. (2009). *Water tables in Peak District blanket peatlands*. Moors for the Future Report No. 17. Edale: Moors for the Future Partnership, 51 pp. Available at: https://research.manchester.ac.uk/en/publications/water-tables-in-peak-district-blanket-peatlands

Almeida, J., Achten, W. M. J., Verbist, B., Heuts, R. F., Schrevens, E. and Muys, B. (2014). Carbon and water footprints and energy use of greenhouse tomato production in Northern Italy. *Journal of Industrial Ecology*, 18(6), pp. 898–908. https://doi.org/10.1111/jiec.12169

Alsabri, A. **and Al Ghamdi**, S. G. (2020). Carbon footprint and embodied energy of PVC, PE, and PP piping: perspective on environmental performance. *Energy Reports*, 6 (8), pp. 364–370. https://doi.org/10.1016/j.egyr.2020.11.173

Alshammari, L., Boyd, D. S., Sowter, A., Marshall, C., Andersen, R., Gilbert, P., Marsh, S. and Large, D. J. (2020). Use of surface motion characteristics determined by InSAR to assess peatland condition. *Journal of Geophysical Research: Biogeosciences*, 125(1), e2018JG004953. https://doi.org/10.1029/2018JG004953

Alshehri, A., Dunn, C., Freeman, C., Hugron, S., Jones, T. and Rochefort, L. (2020). A potential approach for enhancing carbon sequestration during peatland restoration using low cost, phenolic rich biomass supplements. *Frontiers in Environmental Science*, 8, Article 48, pp. 1–12. https://doi.org/10.3389/fenvs.2020.00048

Andersen, R., Farrell, C., Graf, M. D., Muller, F., Calvar, E., Frankard, P., Caporn, S. J. M. and Anderson, P. (2017). An overview of the progress and challenges of peatland restoration in Western Europe. *Restoration Ecology*, 25(2), pp. 271–282. https://doi.org/10.1111/rec.12415

Andersen, R., Felgate, S., Fernandez-Garcia, P., Gaffney, P., Gilbert, P., Hancock, M., Large, D., Leith, F., Marshall, C., Mayor, D., McIlveny, J., Monteith, D., Pickard, A., Sanders, R., Sterk, H. P. and Williamson, B. (2021). Impact of land management on fire resilience and carbon fate in blanket bogs: the FireBlanket project. *EGU General*

Assembly 2021, online, 19–30 April 2021. EGU21-9505. https://doi.org/10.5194/egusphere-egu21-9505

Andersen, R., Fernandez Garcia, P., Martin Walker, A., Klein, D., Marshall, C., Large, D. J., Hughes, R. and Hancock, M. H. (2024). Blanket bog vegetation response to wildfire and drainage suggests resilience to low severity, infrequent burning. *Fire Ecology*, 20(1), Article 26, pp. 1–16. https://doi.org/10.1186/s42408-024-00256-0

Anderson, B. J., Arroyo, B. E., Collingham, Y. C., Etheridge, B., Fernandez De Simon, J., Gillings, S., Gregory, R. D., Leckie, F. M., Sim, I. M. W., Thomas, C. D., Travis, J. and Redpath, S. M. (2009). Using distribution models to test alternative hypotheses about a species' environmental limits and recovery prospects. *Biological Conservation*, 142(3), pp. 488–499. https://doi.org/10.1016/j.biocon.2008.10.036

Anderson, R. **and Peace**, A. (2017). Ten-year results of a comparison of methods for restoring afforested blanket bog. *Mires and Peat*, 19(6), pp. 1–23. https://doi.org/10.19189/MaP.2015.OMB.214

Apori, S. O., McMillan, D., Giltrap, M. and Tian, F. (2022). Mapping the restoration of degraded peatland as a research area: a scientometric review. *Frontiers in Environmental Science*, 10, Article 942788, pp. 1–22. https://doi.org/10.3389/fenvs.2022.942788

Arganda-Carreras, I., Kaynig, V., Rueden, C., Eliceiri, K. W., Schindelin, J., Cardona, A. and Seung, H. S. (2017). Trainable Weka Segmentation: a machine learning tool for microscopy pixel classification. *Bioinformatics*, 33(15), pp. 2424–2426. https://doi.org/10.1093/bioinformatics/btx180

Armstrong, A., Holden, J., Kay, P., Foulger, M., Gledhill, S., McDonald, A. T. and Walker, A. (2009). Drain blocking techniques on blanket peat: a framework for best practice. *Journal of Environmental Management*, 90(11), pp. 3512–3519. https://doi.org/10.1016/j.jenvman.2009.06.003

Armstrong, A., Holden, J., Kay, P., Francis, B., Foulger, M., Gledhill, S., McDonald, A. T. and Walker, A. (2010). The impact of peatland drain-blocking on dissolved organic carbon loss and discolouration of water; results from a national survey. *Journal of Hydrology*, 381(1–2), pp. 112–120. https://doi.org/10.1016/j.jhydrol.2009.11.031

Armstrong, A., Holden, J., Luxton, K. and Quinton, J. N. (2012). Multi-scale relationship between peatland vegetation type and dissolved organic carbon concentration. *Ecological Engineering*, 47, pp. 182–188. https://doi.org/10.1016/j.ecoleng.2012.06.027

Artz, R. R. E., Chapman, S. J., Robertson, A. H. J., Potts, J. M., Laggoun Défarge, F., Gogo, S., Comont, L., Disnar, J.-R. and Francez, A.-J. (2008). FTIR spectroscopy can predict organic matter quality in regenerating cutover peatlands. *Soil Biology and Biochemistry*, 40(2), pp. 515–527. https://doi.org/10.1016/j.soilbio.2007.09.019

Artz, R., Saunders, M., Yeluripati, J., Chapman, S., Moxley, J., Malcolm, H. and Couwenberg, J. (2014). *Implications for longer-term policy and implementation into the AFOLU Inventory of the IPCC 2013 Supplement to the 2006 Guidelines: Wetlands*. ClimateXChange/Scottish Government Report. Edinburgh: ClimateXChange, 53 pp. Available at: https://www.climatexchange.org.uk/wp-

content/uploads/2023/09/part_2_cxc_briefing_on_ipcc_2013_wetlands_supplement.pdf

Artz, R., Evans, C., Crosher, I., Hancock, M., Scott-Campbell, M., Pilkington, M., Jones, P., Chandler, D., McBride, A., Ross, K. and Weyl, R. (2019). *The State of UK Peatlands: An Update*. IUCN UK Peatland Programme Report. Edinburgh: IUCN UK Peatland Programme, 50 pp. Available at: https://www.iucn-uk-peatlandprogramme.org/sites/default/files/2024-05/State%20of%20UK%20Peatlands%20an%20update%20Sept%202019.pdf

ASTM International. (2000). *ASTM D2974-00: Standard Test Methods for Moisture, Ash, and Organic Matter of Peat and Other Organic Soils*. Annual Book of ASTM Standards, Vol. 04.08. West Conshohocken, PA: ASTM International.

ASTM International. (2007). *ASTM D2974-07: Standard Test Methods for Moisture, Ash, and Organic Matter of Peat and Other Organic Soils*. Annual Book of ASTM Standards, Vol. 04.08. West Conshohocken, PA: ASTM International, 4 pp.

Bacon, K. L., Baird, A. J., Blundell, A., Bourgault, M.-A., Chapman, P. J., Dargie, G., Dooling, G. P., Gee, C., Holden, J., Kelly, T., McKendrick-Smith, K. A., Morris, P. J., Noble, A., Palmer, S. M., Quillet, A., Swindles, G. T., Watson, E. J. and Young, D. M. (2017). Questioning ten common assumptions about peatlands. *Mires and Peat*, 19(12), pp. 1–23. https://doi.org/10.19189/MaP.2016.OMB.253

Bain, C. G., Bonn, A., Stoneman, R., Chapman, S., Coupar, A., Evans, M., Gearey, B., Howat, M., Joosten, H., Keenleyside, C., Labadz, J., Lindsay, R., Littlewood, N., Lunt, P., Miller, C. J., Moxey, A., Orr, H., Reed, M., Smith, P. and Worrall, F. (2011). *IUCN UK Commission of Inquiry on Peatlands*. IUCN UK Peatland Programme Report. Edinburgh: IUCN UK Peatland Programme, 112 pp. Available at: https://www.researchgate.net/publication/224807079_IUCN_UK_Commission_of_inquiry_on_peatlands/stats#fullTextFileContent

Baird, A. J. (1997). Field estimation of macropore functioning and surface hydraulic conductivity in a fen peat. *Hydrological Processes*, 11(3), pp. 287–295. https://doi.org/10.1002/(SICI)1099-1085(19970315)11:3<287::AID-HYP443>3.0.CO;2-L

Baird, A. J. **and Waldron**, S. (2004). Ebullition of methane-containing gas bubbles from near-surface Sphagnum peat. *Geophysical Research Letters*, 31(21), L21505. https://doi.org/10.1029/2004GL021157

Baird, A. J., Holden, J. and Chapman, P. J. (2009). *A literature review of evidence on emissions of methane in peatlands*. Defra Project SP0574. Leeds: University of Leeds, 54 pp. Available at: https://randd.defra.gov.uk/ProjectDetails?ProjectId=15992

Baird, A. J., Milner, A. M., Blundell, A., Swindles, G. T. and Morris, P. J. (2016). Microform scale variations in peatland permeability and their ecohydrological implications. *Journal of Ecology*, 104(2), pp. 531–544. https://doi.org/10.1111/1365-2745.12530

Baird, A. J. **and Low**, R. G. (2022). The water table: its conceptual basis, its measurement and its usefulness as a hydrological variable. *Hydrological Processes*, 36(6), e14622. https://doi.org/10.1002/hyp.14622

Baker, S. J., Perry, M. C., Betts, R. A., Schoenecker, J. and Pellegrini, A. F. A. (2025). Spikes in UK wildfire emissions driven by peatland fires in dry years. *Environmental Research Letters*, 20(3), 034028. https://doi.org/10.1088/1748-9326/adafc6

Baldocchi, D. D. (2003). Assessing the eddy covariance technique for evaluating carbon dioxide exchange rates of ecosystems: past, present and future. *Global Change Biology*, 9(4), pp. 479–492. https://doi.org/10.1046/j.1365-2486.2003.00629.x

Ballard, C. E., McIntyre, N., Wheater, H. S., Holden, J. and Wallage, Z. E. (2011). Hydrological modelling of drained blanket peatland. *Journal of Hydrology*, 407(1–4), pp. 81–93. https://doi.org/10.1016/j.jhydrol.2011.07.005

Beck, H. E., Zimmermann, N. E., McVicar, T. R., Vergopolan, N., Berg, A. and Wood, E. F. (2018). Present and future Köppen-Geiger climate classification maps at 1 km resolution. *Scientific Data*, 5(1), Article 180214, pp. 1–12. https://doi.org/10.1038/sdata.2018.214

Beckwith, C. W., Baird, A. J. and Heathwaite, A. L. (2003). Anisotropy and depth-related heterogeneity of hydraulic conductivity in a bog peat II: modelling the effects on groundwater flow. *Hydrological Processes*, 17(1), pp. 89–101. https://doi.org/10.1002/hyp.1116

BEIS (2021). *2019 UK Greenhouse Gas Emissions: Final Figures*. National Statistics, February 2021. London: Department for Business, Energy and Industrial Strategy, 42 pp. Available at: https://assets.publishing.service.gov.uk/media/60198cd5d3bf7f70bc2e1ee7/2019_Final_greenhouse_gas_emissions_statistical_release.pdf

Bell, M. C., Ritson, J. P., Verhoef, A., Brazier, R. E., Templeton, M. R., Graham, N. J. D., Freeman, C. and Clark, J. M. (2018). Sensitivity of peatland litter decomposition to changes in temperature and rainfall. *Geoderma*, 331, pp. 29–37. https://doi.org/10.1016/j.geoderma.2018.06.002

Belyea, L. R. **and Clymo**, R. S. (2001). Feedback control of the rate of peat formation. *Proceedings of the Royal Society B: Biological Sciences*, 268(1473), pp. 1315–1321. https://doi.org/10.1098/rspb.2001.1665

Belyea, L. R. **and Malmer**, N. (2004). Carbon sequestration in peatland: patterns and mechanisms of response to climate change. *Global Change Biology*, 10(7), pp. 1043–1052. https://doi.org/10.1111/j.1529-8817.2003.00783.x

Belyea, L. R. **and Baird**, A. J. (2006). Beyond "The limits to peat bog growth": cross-scale feedback in peatland development. *Ecological Monographs*, 76(3), pp. 299–322. https://doi.org/10.1890/0012-9615(2006)076[0299:BTLTPB]2.0.CO;2

Bendle, J. M., Palmer, A. P. and Carr, S. J. (2015). A comparison of micro-CT and thin section analysis of Lateglacial glaciolacustrine varves from Glen Roy, Scotland. *Quaternary Science Reviews*, 114, pp. 61–77. https://doi.org/10.1016/j.quascirev.2015.02.008

Bengtsson, F., Granath, G. and Rydin, H. (2016). Photosynthesis, growth, and decay traits in *Sphagnum* – a multispecies comparison. *Ecology and Evolution*, 6(10), pp. 3325–3341. https://doi.org/10.1002/ece3.2119

Benn, D. I. **and Ballantyne**, C. K. (1993). The description and representation of particle shape. *Earth Surface Processes and Landforms*, 18(7), pp. 665–672. https://doi.org/10.1002/esp.3290180709

Beven, K. **and Germann**, P. (2013). Macropores and water flow in soils revisited. *Water Resources Research*, 49(6), pp. 3071–3092. https://doi.org/10.1002/wrcr.20156

Biasi, C., Lind, S. E., Pekkarinen, N. M., Huttunen, J. T., Shurpali, N. J., Hyvönen, N. P., Repo, M. E. and Martikainen, P. J. (2008). Direct experimental evidence for the contribution of lime to CO_2 release from managed peat soil. *Soil Biology & Biochemistry*, 40(10), pp. 2660–2669. https://doi.org/10.1016/j.soilbio.2008.07.011

Billett, M. F., Deacon, C. M., Palmer, S. M., Dawson, J. J. C. and Hope, D. (2006). Connecting organic carbon in stream water and soils in a peatland catchment. *Journal of Geophysical Research*, 111 (G2), G02010. https://doi.org/10.1029/2005JG000065

Billett, M. F., Charman, D. J., Clark, J. M., Evans, C. D., Evans, M. G., Ostle, N. J., Worrall, F., Burden, A., Dinsmore, K. J., Jones, T., McNamara, N. P., Parry, L., Rowson, J. G. and Rose, R. (2010). Carbon balance of UK peatlands: current state of knowledge and future research challenges. *Climate Research*, 43(15-29), pp. 1–17. https://doi.org/10.3354/cr00903

Birnie, R. **and Smyth**, M.-A. (2013). *Case Study on Developing the Market for Carbon Storage and Sequestration by Peatlands*. Report for Natural England/Defra, NE0136. London: Department for Environment, Food and Rural Affairs, 123 pp. Available at: http://randd.defra.gov.uk/Default.aspx?Menu=Menu&Module=More&Location=None&ProjectID=18522&FromSearch=Y&Publisher=1&SearchText=NE0136&SortString=ProjectCode&SortOrder=Asc&Paging=10#Description

Birnie, R., Taylor, E. and Smyth, M.-A. (2023). *Peatland Condition Assessment*. Edinburgh: PeatlandACTION, 8 pp. Available at: https://www.nature.scot/sites/default/files/2023-02/Guidance-Peatland-Action-Peatland-Condition-Assessment-Guide-A1916874.pdf

Bjørn, A., Owsianiak, M., Molin, C. and Laurent, A. (2018). Main characteristics of LCA. In: Hauschild, M., Rosenbaum, R. and Olsen, S. (eds), *Life Cycle Assessment*. Cham: Springer, pp. 9–16. https://doi.org/10.1007/978-3-319-56475-3_2

Boelter, D. H. (1968). *Important physical properties of peat materials*. In: Proceedings of the Third International Peat Congress, 18–23 August 1968, Québec, Canada. Ottawa: Department of Energy, Mines and Resources and National Research Council of Canada, pp. 150–154. Available at: https://research.fs.usda.gov/treesearch/12921

Bonn, A., Reed, M. S., Evans, C. D., Joosten, H., Bain, C., Farmer, J., Emmer, I., Couwenberg, J., Moxey, A., Artz, R., Tanneberger, F., von Unger, M., Smyth, M.-A. and Birnie, D. (2014). Investing in nature: Developing ecosystem service markets for peatland restoration. *Ecosystem Services*, 9, pp. 54–65. https://doi.org/10.1016/j.ecoser.2014.06.011

Bonn, A., Allott, T., Evans, M., Joosten, H. and Stoneman, R. (2016a). Peatland restoration and ecosystem services: nature-based solutions for societal goals. In: A. Bonn, T. Allott, M. Evans, H. Joosten and R. Stoneman (eds) *Peatland Restoration and Ecosystem Services: Science, Policy and Practice*. Ecological Reviews. Cambridge: Cambridge University Press, pp. 402–417.
https://doi.org/10.1017/CBO9781139177788.021

Bonn, A., Allott, T., Evans, M., Joosten, H. and Stoneman, R. (eds) (2016b). *Peatland Restoration and Ecosystem Services: Science, Policy and Practice*. Cambridge: Cambridge University Press, 493 pp. https://doi.org/10.1017/CBO9781139177788

Breuwer, A., Heijmans, M. M. P. D., Gleichman, M. and Robroek, B. J. M. (2009). Response of *Sphagnum* species mixtures to increased temperature and nitrogen availability. *Plant Ecology*, 204(1), pp. 97–111. https://doi.org/10.1007/s11258-009-9571-x

Brennand, J. R., Barker, J. A., Manns, H. and Carr, S. J. (2025). Evaluating the carbon costs of UK blanket peatland restoration. *Carbon Management*, 16(1), e2574026. https://doi.org/10.1080/17583004.2025.2574026

BSI (1990a). *BS 1377-3:1990. Methods of Test for Soils for Civil Engineering Purposes – Part 3: Chemical and Electro-chemical Tests*. London: British Standards Institution.

BSI (1990b). *BS 1377-2:1990. Methods of Test for Soils for Civil Engineering Purposes – Part 2: Classification Tests*. London: British Standards Institution.

Bushberg, J. T., Seibert, J. A., Leidholdt, E. M. Jr. and Boone, J. M. (2012). *The Essential Physics of Medical Imaging*. 3rd edn. Philadelphia: Lippincott Williams & Wilkins.

Callebaut, F., Gabriels, D., Minjauw, W. and De Boodt, M. (1982). Redox potential, oxygen diffusion rate, and soil gas composition in relation to water table level in two soils. *Soil Science*, 134(3), pp. 149–156. https://doi.org/10.1097/00010694-198209000-00001

Carless, D., Kulessa, B., Booth, A. D., Drocourt, Y., Sinnadurai, P., Street-Perrott, F. A. and Jansson, P. (2021). An integrated geophysical and GIS-based approach improves estimation of peatland carbon stocks. *Geoderma*, 402, 115176. https://doi.org/10.1016/j.geoderma.2021.115176

Carr, S. J., Diggens, L. M. and Spencer, K. L. (2020). There is no such thing as undisturbed soil and sediment sampling: sampler-induced deformation of salt marsh sediments revealed by 3D X-ray computed tomography. *Journal of Soils and Sediments*, 20, pp. 2960–2976. https://doi.org/10.1007/s11368-020-02655-7

CCC (2020). *Land Use: Policies for a Net Zero UK*. London: Committee on Climate Change, 123 pp. Available at: https://www.theccc.org.uk/wp-content/uploads/2020/01/Land-use-Policies-for-a-Net-Zero-UK.pdf

Chambers, F. M., Beilman, D. W. and Yu, Z. (2011). Methods for determining peat humification and for quantifying peat bulk density, organic matter and carbon content for palaeostudies of climate and peatland carbon dynamics. *Mires and Peat*, 7(7), pp. 1–10. https://doi.org/10.19189/001c.128415

Chapin, F. S. III, Woodwell, G. M., Randerson, J. T., Rastetter, E. B., Lovett, G. M., Baldocchi, D. D., Clark, D. A., Harmon, M. E., Schimel, D. S., Valentini, R., Wirth, C., Aber, J. D., Cole, J. J., Goulden, M. L., Harden, J. W., Heimann, M., Howarth, R. W., Matson, P. A., McGuire, A. D., Melillo, J. M., Mooney, H. A., Neff, J. C., Houghton, R. A., Pace, M. L., Ryan, M. G., Running, S. W., Sala, O. E., Schlesinger, W. H. and Schulze, E. D. (2006). Reconciling carbon cycle concepts, terminology, and methods. *Ecosystems*, 9, pp. 1041–1050. https://doi.org/10.1007/s10021-005-0105-7

Chapman, S. J. (2009). Carbon stocks in Scottish peatlands — a comparison of land use. *Soil Use and Management*, 25(2), pp. 105–112. https://doi.org/10.1111/j.1475-2743.2009.00219.x

Chapman, S., Artz, R. and Donnelly, D. (2012). *Carbon Savings from Peat Restoration*. ClimateXChange Report. Edinburgh: ClimateXChange, 17 pp. Available at: https://www.climatexchange.org.uk/wp-content/uploads/2023/09/carbon_savings_from_peat_restoration.pdf

Chapman, S. J., Farmer, J., Main, A. and Smith, J. (2017). Refining pedotransfer functions for estimating peat bulk density. *Mires and Peat*, 19(23), pp. 1–11. https://doi.org/10.19189/MaP.2017.OMB.281

Charman, D. (2002). *Peatlands and Environmental Change*. Chichester: John Wiley & Sons. ISBN: 978-0-470-96990-0

Charman, D. J., Beilman, D. W., Blaauw, M., Booth, R. K., Brewer, S., Chambers, F. M., Christen, J. A., Gallego-Sala, A., Harrison, S. P., Hughes, P. D. M., Jackson, S. T., Korhola, A., Mauquoy, D., Mitchell, F. J. G., Prentice, I. C., van der Linden, M., De Vleeschouwer, F., Yu, Z. C., Alm, J., Bauer, I. E., Corish, Y. M. C., Garneau, M., Hohl, V., Huang, Y., Karofeld, E., Le Roux, G., Loisel, J., Moschen, R., Nichols, J. E., Nieminen, T. M., MacDonald, G. M., Phadtare, N. R., Rausch, N., Sillasoo, Ü., Swindles, G. T., Tuittila, E.-S., Ukonmaanaho, L., Väliranta, M., van Bellen, S., van Geel, B., Vitt, D. H. and Zhao, Y. (2013). Climate-related changes in peatland carbon accumulation during the last millennium. *Biogeosciences*, 10(2), pp. 929–944. https://doi.org/10.5194/bg-10-929-2013

Chen, C., Loft, L., Sattler, C. and Matzdorf, B. (2023). Developing regional voluntary carbon markets for peatlands: innovation processes and influencing factors. *Climate Policy*, 23(2), pp. 238–253. https://doi.org/10.1080/14693062.2022.2160300

Chimner, R. A., Ott, C. A., Perry, C. H. and Kolka, R. K. (2014). Developing and evaluating rapid field methods to estimate peat carbon. *Wetlands*, 34, pp. 1241–1246. https://doi.org/10.1007/s13157-014-0574-6

Chirol, C., Carr, S. J., Spencer, K. L. and Moeller, I. (2021). Pore, live root and necromass quantification in complex heterogeneous wetland soils using X-ray computed tomography. *Geoderma*, 387, 114898, pp. 1–11. https://doi.org/10.1016/j.geoderma.2020.114898

Chiu, Y., Yang, Y. and Morse, C. (2022). Quantifying carbon footprint for ecological river restoration. *Environment, Development and Sustainability*, 24, pp. 952–970. https://doi.org/10.1007/s10668-021-01477-y

Clarke, J. L., Welch, D. and Gordon, I. J. (1995). The influence of vegetation pattern on the grazing of heather moorland by red deer and sheep. II. The impact on heather. *Journal of Applied Ecology*, 32(1), pp. 166–176. https://doi.org/10.2307/2404426

Clymo, R. S. **and Hayward**, P. M. (1982). The ecology of *Sphagnum*. In A. J. E. Smith (ed.) *Bryophyte Ecology*. Dordrecht: Springer, pp. 229–289. https://doi.org/10.1007/978-94-009-5891-3_8

Clymo, R. S. (1984). The limits to peat bog growth. *Philosophical Transactions of the Royal Society of London B: Biological Sciences*, 303(1117), pp. 605–654. https://doi.org/10.1098/rstb.1984.0002

Clymo, R. S., Turunen, J. and Tolonen, K. (1998). Carbon accumulation in peatland. *Oikos*, 81, pp. 368–388. https://doi.org/10.2307/3547057

Clymo, R. S. **and Bryant**, C. L. (2008). Diffusion and mass flow of dissolved carbon dioxide, methane and dissolved organic carbon in a 7 m deep raised peat bog. *Geochimica et Cosmochimica Acta*, 72(8), pp. 2048–2066. https://doi.org/10.1016/j.gca.2008.01.032

Cnudde, V. **and Boone**, M. N. (2013). High-resolution X-ray computed tomography in geosciences: a review of the current technology and applications. *Earth-Science Reviews*, 123, pp. 1–17. https://doi.org/10.1016/j.earscirev.2013.04.003

Collier, S. M., Green, S. M., Inman, A., Hopkins, D. W., Kendall, H., Jahn, M. M. and Dungait, J. A. J. (2020). Effect of farm management on topsoil organic carbon and aggregate stability in water: a case study from Southwest England, UK. *Soil Use and Management*, 37(1), pp. 49–62. https://doi.org/10.1111/sum.12658

Comas, X., Kettridge, N., Binley, A., Slater, L., Parsekian, A., Baird, A. J., Strack, M. and Waddington, J. M. (2014). The effect of peat structure on the spatial distribution of biogenic gases within bogs. *Hydrological Processes*, 28(22), pp. 5483–5494. https://doi.org/10.1002/hyp.10056

Cook, S., Peacock, M., Evans, C. D., Page, S. E., Whelan, M., Gauci, V. and Khoon, K. L. (2016). Cold storage as a method for the long-term preservation of tropical dissolved organic carbon. *Mires and Peat*, 18(25), pp. 1–8. https://doi.org/10.19189/MaP.2016.OMB.249

Cooper, M. D. A., Evans, C. D., Zielinski, P., Levy, P. E., Gray, A., Peacock, M., Norris, D., Fenner, N. and Freeman, C. (2014). Infilled ditches are hotspots of landscape methane flux following peatland re-wetting. *Ecosystems*, 17, pp. 1227–1241. https://doi.org/10.1007/s10021-014-9791-3

Couwenberg, J., Thiele, A., Tanneberger, F., Augustin, J., Bärisch, S., Dubovik, D., Liashchynskaya, N., Michaelis, D., Minke, M., Skuratovich, A. and Joosten, H. (2011). Assessing greenhouse gas emissions from peatlands using vegetation as a proxy. *Hydrobiologia*, 674, pp. 67–89. https://doi.org/10.1007/s10750-011-0729-x

Crishna, N., Banfill, P. F. G. and Goodsir, S. (2011). Embodied energy and CO_2 in UK dimension stone. *Resources, Conservation and Recycling*, 55(12), pp. 1265–1273. https://doi.org/10.1016/j.resconrec.2011.06.014

Crowle, A., Diack, I., Glaves, D., Key, D. and Lindsay, R. (2025). *Definition of Favourable Conservation Status for Blanket Bog*. RP2967. London: Natural England, 43 pp. Available at: https://publications.naturalengland.org.uk/file/5731662867202048

Cunliffe, A. M., Baird, A. J. and Holden, J. (2013). Hydrological hotspots in blanket peatlands: spatial variation in peat permeability around a natural soil pipe. *Water Resources Research*, 49(9), pp. 5342–5354. https://doi.org/10.1002/wrcr.20435

Curran, M. A. (2013). Life cycle assessment: a review of the methodology and its application to sustainability. *Current Opinion in Chemical Engineering*, 2(3), pp. 273–277. https://doi.org/10.1016/j.coche.2013.02.002

DAERA (2022). *Northern Ireland Peatland Strategy 2022–2040*. Department of Agriculture, Environment and Rural Affairs, Northern Ireland, 36 pp. Available at: https://www.daera-ni.gov.uk/sites/default/files/consultations/daera/NI%20Peatland%20Strategy%20-%20Copy%20for%20EQIA%20Consultation.%20%208-8-2022.%20PDF_0.PDF

Dale, J., Cundy, A. B., Spencer, K. L., Carr, S. J., Croudace, I. W., Burgess, H. M. and Nash, D. J. (2019). Sediment structure and physicochemical changes following tidal inundation at a large open coast managed realignment site. *Science of the Total Environment*, 660 (10), pp. 1419–1432. https://doi.org/10.1016/j.scitotenv.2018.12.323

Dalva, M. **and Moore**, T. (1993). The influence of temperature and water table position on carbon dioxide and methane emissions from laboratory columns of peatland soils. *Journal of Soil Science*, 44(4), pp. 651–664. https://doi.org/10.1111/j.1365-2389.1993.tb02330.x

Davey, E., Wigand, C., Johnson, R., Sundberg, K., Morris, J. and Roman, C. T. (2011). Use of computed tomography imaging for quantifying coarse roots, rhizomes, peat, and particle densities in marsh soils. *Ecological Applications*, 21(6), pp. 2156–2171. https://doi.org/10.1890/10-2037.1

Davies, G. M., Gray, A., Rein, G. and Legg, C. J. (2013). Peat consumption and carbon loss due to smouldering wildfire in a temperate peatland. *Forest Ecology and Management*, 308, pp. 169–177. https://doi.org/10.1016/j.foreco.2013.07.051

Davies, G. M., Kettridge, N., Stoof, C. R., Gray, A., Ascoli, D., Fernandes, P. M., Marrs, R., Allen, K. A., Doerr, S. H., Clay, G. D., McMorrow, J. and Vandvik, V. (2016). The role of fire in UK peatland and moorland management: the need for informed, unbiased debate. *Philosophical Transactions of the Royal Society B: Biological Sciences*, 371(1696), Article 20150342, pp. 1–17. https://doi.org/10.1098/rstb.2015.0342

DEFRA (2021a). *England Peat Action Plan*. London: Department for Environment, Food & Rural Affairs, 40 pp. Available at: https://assets.publishing.service.gov.uk/media/6116353fe90e07054eb85d8b/england-peat-action-plan.pdf

DEFRA (2021b). *Environmental Land Management Scheme*. London: Department for Environment, Food & Rural Affairs, 56 pp. Available at: https://www.nao.org.uk/wp-content/uploads/2021/09/The-Environmental-Land-Management-scheme.pdf

DEFRA and Rural Payments Agency (2024). *Environmental Land Management: Recent Changes to the Sustainable Farming Incentive and Countryside Stewardship Schemes*. London: Department for Environment, Food and Rural Affairs, 16 pp. Available at: https://lordslibrary.parliament.uk/environmental-land-management-recent-changes-to-the-sustainable-farming-incentive-and-countryside-stewardship-schemes/

DESNZ (2023). *Greenhouse Gas Reporting: Conversion Factors 2023 (Full Set for Advanced Users)*. London: Department for Energy Security and Net Zero. Updated 28 June 2023. Available at: https://assets.publishing.service.gov.uk/media/649c5358bb13dc0012b2e2b7/ghg-conversion-factors-2023-full-file-update.xlsx

Dipper (2022). *Peatlands Restoration: Delivering effective plans and strategies on the ground. UK Strategy Progress: Scotland*. Presented at the IUCN UK Peatland Programme Conference, Aberystwyth, October 2022. Scottish Government.

Done, A. **and Muir**, R. (2008). The landscape history of grouse shooting in the Yorkshire Dales. *Rural History*, 12(2), pp. 195–210. https://doi.org/10.1017/S0956793300002442

Doube, M., Klosowski, M. M., Arganda-Carreras, I., Cordelières, F. P., Dougherty, R. P., Jackson, J. S., Schmid, B., Hutchinson, J. R. and Shefelbine, S. J. (2010). BoneJ: free and extensible bone image analysis in ImageJ. *Bone*, 47(6), pp. 1076–1079. https://doi.org/10.1016/j.bone.2010.08.023

Douglas, D. J. T., Buchanan, G. M., Thompson, P., Amar, A., Fielding, D. A., Redpath, S. M. and Wilson, J. D. (2015). Vegetation burning for game management in the UK uplands is increasing and overlaps spatially with soil carbon and protected areas. *Biological Conservation*, 191, pp. 243–250. https://doi.org/10.1016/j.biocon.2015.06.014

Drever, C. R., Cook-Patton, S. C., Akhter, F., Badiou, P. H., Chmura, G. L., Davidson, S. J., Desjardins, R. L., Dyk, A., Fargione, J. E., Fellows, M., Filewod, B., Hessing-Lewis, M., Jayasundara, S., Keeton, W. S., Kroeger, T., Lark, T. J., Le, E., Leavitt, S. M., LeClerc, M. E. and Kurz, W. A. (2021). Natural climate solutions for Canada. *Science Advances*, 7(23), eabd6034. https://doi.org/10.1126/sciadv.abd6034

Đuka, A., Vusić, D., Horvat, D., Šušnjar, M., Pandur, Z. and Papa, I. (2017). LCA studies in forestry—stagnation or progress? *Croatian Journal of Forest Engineering*, 38(2), pp. 311–326. https://crojfe.com/site/assets/files/4089/duka.pdf

Dunn, C. **and Freeman**, C. (2011). Peatlands: our greatest source of carbon credits? *Carbon Management*, 2(3), pp. 289–301. https://doi.org/10.4155/cmt.11.23

Dunn, C., Jones, T. G., Roberts, S. and Freeman, C. (2016). Plant species effects on the carbon storage capabilities of a blanket bog complex. *Wetlands*, 36, pp. 47–58. https://doi.org/10.1007/s13157-015-0714-7

Ebrahimi, A. **and Or**, D. (2017). Mechanistic modeling of microbial interactions at pore to profile scale resolve methane emission dynamics from permafrost soil. *Journal of Geophysical Research: Biogeosciences*, 122(5), pp. 1216–1238. https://doi.org/10.1002/2016JG003674

European Rental Association (2023). *Equipment CO₂ Calculator*. Available at: https://equipmentcalculator.org/en

European Union (1992). *Council Directive 92/43/EEC on the Conservation of Natural Habitats and of Wild Fauna and Flora*. European Union, 44 pp. Available at: http://data.europa.eu/eli/dir/1992/43/oj

Evans, R. (1997). Soil erosion in the UK initiated by grazing animals: a need for a national survey. *Applied Geography*, 17(3), pp. 127–141. https://doi.org/10.1016/S0143-6228(97)00002-7

Evans, M. **and Warburton**, J. (2005). Sediment budget for an eroding peat-moorland catchment in northern England. *Earth Surface Processes and Landforms*, 30(5), pp. 557–577. https://doi.org/10.1002/esp.1153

Evans, M., Warburton, J. and Yang, J. (2006). Eroding blanket peat catchments: global and local implications of upland organic sediment budgets. *Geomorphology*, 79(1–2), pp. 45–57. https://doi.org/10.1016/j.geomorph.2005.09.015

Evans, C. D., Renou-Wilson, F. and Strack, M. (2016). The role of waterborne carbon in the greenhouse gas balance of drained and re-wetted peatlands. *Aquatic Sciences*, 78, pp. 573–590. https://doi.org/10.1007/s00027-015-0447-y

Evans, C., Artz, R., Moxley, J., Smyth, M.-A., Taylor, E., Archer, N., Burden, A., Williamson, J., Donnelly, D., Thomson, A., Buys, G., Malcolm, H., Wilson, D., Renou-Wilson, F. and Potts, J. (2017). *Implementation of an Emissions Inventory for UK Peatlands*. Wallingford: Centre for Ecology and Hydrology, 93 pp. Available at: https://uk-air.defra.gov.uk/reports/cat07/1904111135_UK_peatland_GHG_emissions.pdf

Evans, C. D., Peacock, M., Green, S. M., Holden, J., Chapman, P. J., Lebron, I., Callaghan, N., Grayson, R. and Baird, A. J. (2018). The impact of ditch blocking on fluvial carbon export from a UK blanket bog. *Hydrological Processes*, 32(13), pp. 2141–2154. https://doi.org/10.1002/hyp.13158

Evans, C. D., Peacock, M., Baird, A. J., Artz, R. R. E., Burden, A., Callaghan, N., Chapman, P. J., Cooper, H. M., Coyle, M., Craig, E., Cumming, A., Dixon, S., Gauci, V., Grayson, R. P., Helfter, C., Heppell, C. M., Holden, J., Jones, D. L., Kaduk, J., Levy, P., Matthews, R., McNamara, N. P., Misselbrook, T., Oakley, S., Page, S. E., Rayment, M., Ridley, M., Stanley, K. M., Williamson, J. L., Worrall, F., and Morrison, R. (2021). Overriding water table control on managed peatland greenhouse gas emissions. *Nature*, 593, pp. 548–552. https://doi.org/10.1038/s41586-021-03523-1

Falla, N. M., Contu, S., Demasi, S., Caser, M. and Scariot, V. (2020). Environmental impact of edible flower production: a case study. *Agronomy*, 10(4), 579. https://doi.org/10.3390/agronomy10040579

Farmer, J., Matthews, R., Smith, P., Langan, C., Hergoualc'h, K., Verchot, L. and Smith, J. U. (2014). Comparison of methods for quantifying soil carbon in tropical peats. *Geoderma*, 214–215, pp. 177–183. https://doi.org/10.1016/j.geoderma.2013.09.013

Fenner, N. **and Freeman**, C. (2011). Drought-induced carbon loss in peatlands. *Nature Geoscience*, 4, pp. 895–900. https://doi.org/10.1038/ngeo1323

Ferguson, P. **and Lee**, J. A. (1983). Past and present sulphur pollution in the southern Pennines. *Atmospheric Environment*, 17(6), pp. 1131–1137. https://doi.org/10.1016/0004-6981(83)90336-0

Freeman, C., Ostle, N. and Kang, H. (2001). An enzymic "latch" on a global carbon store. *Nature*, 409, pp. 149. https://doi.org/10.1038/35051650

Frolking, S., Roulet, N. T., Moore, T. R., Richard, P. J. H., Lavoie, M. and Muller, S. D. (2001). Modeling northern peatland decomposition and peat accumulation. *Ecosystems*, 4, pp. 479–498. https://doi.org/10.1007/s10021-001-0105-1

Frolking, S., Roulet, N. T., Moore, T. R., Lafleur, P. M., Bubier, J. L. and Crill, P. M. (2002). Modeling seasonal to annual carbon balance of Mer Bleue Bog, Ontario, Canada. *Global Biogeochemical Cycles*, 16(3), pp. 1–21. https://doi.org/10.1029/2001GB001457

Gagnon, Z. E. **and Glime**, J. M. (1992). The pH-lowering ability of *Sphagnum magellanicum* Brid. *Journal of Bryology*, 17(1), pp. 47–57. https://doi.org/10.1179/jbr.1992.17.1.47

Gallego-Sala, A. V., Charman, D. J., Harrison, S. P., Li, G. and Prentice, I. C. (2016). Climate-driven expansion of blanket bogs in Britain during the Holocene. *Climate of the Past*, 12(1), pp. 129–136. https://doi.org/10.5194/cp-12-129-2016

Garnett, M. H., Ineson, P. and Stevenson, A. C. (2000). Effects of burning and grazing on carbon sequestration in a Pennine blanket bog, UK. *Holocene*, 10(6), pp. 729–736. https://doi.org/10.1191/09596830094971

Gharedaghloo, B., Price, J. S., Rezanezhad, F. and Quinton, W. L. (2018). Evaluating the hydraulic and transport properties of peat soil using pore network modeling and X-ray micro-computed tomography. *Journal of Hydrology*, 561, pp. 494–508. https://doi.org/10.1016/j.jhydrol.2018.04.007

Gibbs, H. K. **and Salmon**, J. M. (2015). Mapping the world's degraded lands. *Applied Geography*, 57, pp. 12–21. https://doi.org/10.1016/j.apgeog.2014.11.024

Givelet, N., Le Roux, G., Cheburkin, A., Chen, B., Frank, J., Goodsite, M. E., Kempter, H., Krachler, M., Noernberg, T., Rausch, N., Rheinberger, S., Roos Barraclough, F., Sapkota, A., Scholz, C. and Shotyk, W. (2004). Suggested protocol for collecting, handling and preparing peat cores and peat samples for physical, chemical, mineralogical and isotopic analyses. *Journal of Environmental Monitoring*, 6(5), pp. 481–492. https://doi.org/10.1039/B401601G

Gong, L., Nie, L., Xu, Y., Ji, X. and Liu, B. (2022). Characterization of micro-scale pore structure and permeability simulation of peat soil based on 2D/3D X-ray computed tomography images. *Eurasian Soil Science*, 55, pp. 790–801. https://doi.org/10.1134/S1064229322060060

Gorham, E. (1991). Northern peatlands: role in the carbon cycle and probable responses to climatic warming. *Ecological Applications*, 1(2), pp. 182–195. https://doi.org/10.2307/1941811

Gorham, E., Lehman, C., Dyke, A., Clymo, D. and Janssens, J. (2012). Long-term carbon sequestration in North American peatlands. *Quaternary Science Reviews*, 58, pp. 77–82. https://doi.org/10.1016/j.quascirev.2012.09.018

Government (2021). *Net Zero Strategy: Build Back Greener*. London: HM Government, 368 pp. Available at: https://assets.publishing.service.gov.uk/media/6194dfa4d3bf7f0555071b1b/net-zero-strategy-beis.pdf

Grand-Clement, E., Anderson, K., Smith, D., Luscombe, D., Gatis, N., Ross, M. and Brazier, R. E. (2013). Evaluating ecosystem goods and services after restoration of marginal upland peatlands in South West England. *Journal of Applied Ecology*, 50(2), pp. 324–334. https://doi.org/10.1111/1365-2664.12039

Gray, A., Davies, G. M., Domènech, R., Taylor, E. and Levy, P. E. (2021). Peatland wildfire severity and post-fire gaseous carbon fluxes. *Ecosystems*, 24, pp. 713–725. https://doi.org/10.1007/s10021-020-00545-0

Grasselly, D., Hamm, F., Quaranta, G. and Vitrou, J. (2009). Carbon footprint of coconut fibre (coir) substrates. *Interprofessional Technical Centre for Fruit and Vegetables (CTIFL)*, Infos-CTIFL 249, pp. 55–59. https://www.cabidigitallibrary.org/doi/full/10.5555/20093081674

Green, S. M., Baird, A. J., Holden, J., Reed, D., Birch, K. and Jones, P. (2017). An experimental study on the response of blanket bog vegetation and water tables to ditch blocking. *Wetlands Ecology and Management*, 25, pp. 703–716. https://doi.org/10.1007/s11273-017-9545-z

Green, S. M., Baird, A. J., Evans, C. D., Peacock, M., Holden, J., Chapman, P. J. and Smart, R. P. (2018). Methane and carbon dioxide fluxes from open and blocked ditches in a blanket bog. *Plant and Soil*, 424, pp. 619–638. https://doi.org/10.1007/s11104-017-3543-z

Gregg, R., Elias, J., Alonso, I., Crosher, I., Muto, P. and Morecroft, M. (2021). *Carbon storage and sequestration by habitat: a review of the evidence (2nd edn)*. London: Natural England, 243 pp. Available at: https://publications.naturalengland.org.uk/file/6257983284838400

Gribbe, S., Blume-Werry, G. and Couwenberg, J. (2020). Digital, three-dimensional visualization of root systems in peat. *Soil Systems*, 4(1), Article 13. https://doi.org/10.3390/soilsystems4010013

Grieve, I. **and Gilvear**, D. (2008). Effects of wind farm construction on concentrations and fluxes of dissolved organic carbon and suspended sediment from peat catchments at Braes of Doune, central Scotland. *Mires and Peat*, 4, Article 03, pp. 1–11. https://doi.org/10.19189/001c.128271

Grogan, P. **and Matthews**, S. (2007). *CO_2 Emissions Calculator for Small Aircrafts*. Kingston, Canada: Queen's University. Available at: https://www.queensu.ca/terrestrial-ecosystem-ecology/sites/teelwww/files/uploaded_files/Resources%20and%20Data/CO2%20emis

sions%20calculator%20for%20travel%20in%20small%20fixed-wing%20and%20helicopter%20aircraft.xlsx

Grootjans, A. P., Hensgens, G., Hogenboom, R., Aarts, B., Manschot, J. and Roelofs, J. G. M. (2016). Ecohydrological analysis of a groundwater-influenced blanket bog: Occurrence of *Schoenus nigricans* in Roundstone Bog, Connemara, Ireland. *Mires and Peat*, 18, Article 10, pp. 1–13. https://doi.org/10.19189/MaP.2015.OMB.177

Günther, A., Barthelmes, A., Huth, V., Joosten, H., Jurasinski, G., Koebsch, F. and Couwenberg, J. (2020). Prompt rewetting of drained peatlands reduces climate warming despite methane emissions. *Nature Communications*, 11, Article 1644. https://doi.org/10.1038/s41467-020-15499-z

Haapalehto, T. O., Vasander, H., Jauhiainen, S., Tahvanainen, T. and Kotiaho, J. S. (2011). The effects of peatland restoration on water table depth, elemental concentrations, and vegetation: 10 years of changes. *Restoration Ecology*, 19(5), pp. 587–598. https://doi.org/10.1111/j.1526-100X.2010.00704.x

Hamard, S., Robroek, B. J. M., Allard, P.-M., Signarbieux, C., Zhou, S., Saesong, T., de Baaker, F., Buttler, A., Chiapusio, G., Wolfender, J.-L., Bragazza, L. and Jassey, V. E. J. (2019). Effects of *Sphagnum* leachate on competitive *Sphagnum* microbiome depend on species and time. *Frontiers in Microbiology*, 10, Article 2042, pp. 1–17. https://doi.org/10.3389/fmicb.2019.02042

Hanna, R. D. **and Ketcham**, R. A. (2017). X-ray computed tomography of planetary materials: A primer and review of recent studies. *Chemie der Erde – Geochemistry*, 77(4), pp. 547–572. https://doi.org/10.1016/j.chemer.2017.01.006

Haraguchi, A. (1991). Effects of water table oscillation on redox property of peat in a floating mat. *Journal of Ecology*, 79(4), pp. 1113–1121. https://doi.org/10.2307/2261102

Harenda, K. M., Lamentowicz, M., Samson, M. and Chojnicki, B. H. (2018). The role of peatlands and their carbon storage function in the context of climate change. In: Zieliński, T. and Sagan, I. (eds.) *Interdisciplinary Approaches for Sustainable Development Goals*. GeoPlanet: Earth and Planetary Sciences, pp. 169–184. https://doi.org/10.1007/978-3-319-71788-3_12

Hauschild, M. Z., Rosenbaum, R. K. and Olsen, S. I. (2017). *Life Cycle Assessment: Theory and Practice*. 1st edn. Cham: Springer. 1216 pp. https://doi.org/10.1007/978-3-319-56475-3

Heinemeyer, A., Asena, Q., Burn, W. L. and Jones, A. L. (2018). Peatland carbon stocks and burn history: Blanket bog peat core evidence highlights charcoal impacts on peat physical properties and long-term carbon storage. *Geo: Geography and Environment*, 5(2), e00063, pp. 1–15. https://doi.org/10.1002/geo2.63

Helliwell, J. R., Sturrock, C. J., Grayling, K. M., Tracy, S. R., Flavel, R. J., Young, I. M., Whalley, W. R. and Mooney, S. J. (2013). Applications of X-ray computed tomography for examining biophysical interactions and structural development in soil systems: A review. *European Journal of Soil Science*, 64(3), pp. 279–297. https://doi.org/10.1111/ejss.12028

Hilasvuori, E., Akujärvi, A., Fritze, H., Karhu, K., Laiho, R., Mäkiranta, P., Oinonen, M., Palonen, V., Vanhala, P. and Liski, J. (2013). Temperature sensitivity of decomposition in a peat profile. *Soil Biology and Biochemistry*, 67, pp. 47–54. https://doi.org/10.1016/j.soilbio.2013.08.009

Hoag, R. S. **and Price**, J. S. (1997). The effects of matrix diffusion on solute transport and retardation in undisturbed peat in laboratory columns. *Journal of Contaminant Hydrology*, 28(3), pp. 193–205. https://doi.org/10.1016/S0169-7722(96)00085-X

Hogg, E. H. (1993). Decay potential of hummock and hollow *Sphagnum* peats at different depths in a Swedish raised bog. *Oikos*, 66(2), pp. 269–278. https://doi.org/10.2307/3544814

Hoey, T. P. (2004). Particle-size analysis. In Evans, D. J. A. and Benn, D. I. (eds) *A Practical Guide to the Study of Glacial Sediments*. London: Arnold, 34(2), Chapter 3, 232 pp. https://doi.org/10.1111/j.1502-3885.2005.tb01018.x

Holden, J. **and Burt**, T. P. (2003). Hydrological studies on blanket peat: the significance of the acrotelm–catotelm model. *Journal of Ecology*, 91(1), pp. 86–102. https://doi.org/10.1046/j.1365-2745.2003.00748.x

Holden, J., Chapman, P. J. and Labadz, J. C. (2004). Artificial drainage of peatlands: hydrological and hydrochemical process and wetland restoration. *Progress in Physical Geography*, 28(1), pp. 95–123. https://doi.org/10.1191/0309133304pp403ra

Holden, J. (2005a). Controls of soil pipe frequency in upland blanket peat. *Journal of Geophysical Research: Earth Surface*, 110(F1), F01002, pp. 1–15. https://doi.org/10.1029/2004JF000143

Holden, J. (2005b). Peatland hydrology and carbon release: why small-scale process matters. *Philosophical Transactions of the Royal Society A*, 363(1837), pp. 2891–2913. https://doi.org/10.1098/rsta.2005.1671

Holden, J., Evans, M. G., Burt, T. P. and Horton, M. (2006). Impact of land drainage on peatland hydrology. *Journal of Environmental Quality*, 35(5), pp. 1764–1778. https://doi.org/10.2134/jeq2005.0477

Holden, J., Chapman, P. J., Lane, S. N. and Brookes, C. (2006). Impacts of artificial drainage of peatlands on runoff production and water quality. In: *Developments in Earth Surface Processes*, Vol. 9. International Association of Hydrological Sciences, Chapter 22, pp. 501–528. https://doi.org/10.1016/S0928-2025(06)09022-5

Holden, J., Shotbolt, L., Bonn, A., Burt, T. P., Chapman, P. J., Dougill, A. J., Fraser, E. D. G., Hubacek, K., Irvine, B., Kirkby, M. J., Reed, M. S., Prell, C., Stagl, S., Stringer, L. C., Turner, A. and Worrall, F. (2007). Environmental change in moorland landscapes. *Earth-Science Reviews*, 82(1–2), pp. 75–100. https://doi.org/10.1016/j.earscirev.2007.01.003

Holden, J., Kirkby, M. J., Lane, S. N., Milledge, D. G., Brookes, C. J., Holden, V. and McDonald, A. T. (2008). Overland flow velocity and roughness properties in peatlands. *Water Resources Research*, 44(6), W06415. https://doi.org/10.1029/2007WR006052

Holden, J., Wallage, Z. E., Lane, S. N. and McDonald, A. T. (2011). Water table dynamics in undisturbed, drained and restored blanket peat. *Journal of Hydrology*, 402(1–2), pp. 103–114. https://doi.org/10.1016/j.jhydrol.2011.03.010

Holden, J., Green, S. M., Baird, A. J., Grayson, R. P., Dooling, G. P., Chapman, P. J., Evans, C. D., Peacock, M. and Swindles, G. (2017). The impact of ditch blocking on the hydrological functioning of blanket peatlands. *Hydrological Processes*, 31(3), pp. 525–539. https://doi.org/10.1002/hyp.11031

Hooker, H. **and Wentworth**, J. (2024). *Carbon Offsetting*. POSTnote 713. London: UK Parliamentary Office of Science and Technology, 22 pp. Available at: https://researchbriefings.files.parliament.uk/documents/POST-PN-0713/POST-PN-0713.pdf

Horne, R. E., Grant, T. and Verghese, K. L. (2009). Prospects for life cycle assessment development and practice in the quest for sustainable consumption. In: *Life Cycle Assessment: Principles, Practice and Prospects*. Collingwood, VIC: CSIRO Publishing, pp. 161–172. https://doi.org/10.1071/9780643097964

House, J., Gallego-Sala, A., Clark, J. and Orr, H. (2011). *Vulnerability of Upland Peatland Services to Climate Change*. Report SC070036. Environment Agency. https://doi.org/10.13140/RG.2.2.11558.93761

Howie, S. A. **and Hebda**, R. J. (2018). Bog surface oscillation (mire breathing): a useful measure in raised bog restoration. *Hydrological Processes*, 32(11), pp. 1518–1530. https://doi.org/10.1002/hyp.11622

Howson, T., Evans, M., Allott, T., Shuttleworth, E., Johnston, A., Rees, J., Milledge, D., Edokpa, D., Lockyer, C., Kay, M., Spencer, T., Brown, D., Goudarzi, S. and Pilkington, M. (2023). Peatland gully restoration with stone and timber dams (Kinder Plateau, UK). *Ecological Engineering*, 195, 107066. https://doi.org/10.1016/j.ecoleng.2023.107066

Hu, Y., Limaye, A. and Lu, J. (2020). Three-dimensional segmentation of computed tomography data using Drishti Paint: new tools and developments. *Royal Society Open Science*, 7, 201033. https://doi.org/10.1098/rsos.201033

Huang, C. C. (2002). Holocene landscape development and human impact in the Connemara Uplands, Western Ireland. *Journal of Biogeography*, 29(2), pp. 153–165. https://doi.org/10.1046/j.1365-2699.2002.00661.x

Huang, Y., Ciais, P., Luo, Y., Zhu, D., Wang, Y., Qiu, C., Goll, D. S., Guenet, B., Makowski, D., De Graaf, I., Leifeld, J., Kwon, M. J., Hu, J. and Qu, L. (2021). Tradeoff of CO_2 and CH_4 emissions from global peatlands under water table drawdown. *Nature Climate Change*, 11(7), pp. 618–622. https://doi.org/10.1038/s41558-021-01059-w

Hutchinson, G. L. **and Mosier**, A. R. (1981). Improved soil cover method for field measurement of nitrous oxide fluxes. *Soil Science Society of America Journal*, 45(2), pp. 311–316. https://doi.org/10.2136/sssaj1981.03615995004500020017x

Ingram, H. A. P. (1978). Soil layers in mires: function and terminology. *Journal of Soil Science*, 29(2), pp. 224–227. https://doi.org/10.1111/j.1365-2389.1978.tb02053.x

IPCC (2013). *2013 Supplement to the 2006 IPCC Guidelines for National Greenhouse Gas Inventories: Wetlands*. Hiraishi, T., Krug, T., Tanabe, K., Srivastava, N., Baasansuren, J., Fukuda, M. and Troxler, T. G. (eds). Geneva: Intergovernmental Panel on Climate Change, 354 pp. Available at: https://www.ipcc.ch/site/assets/uploads/2018/03/Wetlands_Supplement_Entire_Report.pdf

IPCC (2014). *Summary for Policymakers*. In: *Climate Change 2014: Mitigation of Climate Change. Contribution of Working Group III to the Fifth Assessment Report of the Intergovernmental Panel on Climate Change*. Edenhofer, O., Pichs-Madruga, R., Sokona, Y. et al. (eds). Cambridge: Cambridge University Press, 32 pp. Available at: https://www.ipcc.ch/site/assets/uploads/2018/02/ipcc_wg3_ar5_summary-for-policymakers.pdf

IPCC (2021). *Summary for Policymakers*. In: *Climate Change 2021: The Physical Science Basis. Contribution of Working Group I to the Sixth Assessment Report of the Intergovernmental Panel on Climate Change*. Masson-Delmotte, V., Zhai, P., Pirani, A. et al. (eds). Cambridge: Cambridge University Press, 2409 pp. Available at: https://www.ipcc.ch/report/ar6/wg1/downloads/report/IPCC_AR6_WGI_FullReport.pdf

IPCC (2022a). *Technical Summary*. In: *Climate Change 2022: Impacts, Adaptation and Vulnerability. Contribution of Working Group II to the Sixth Assessment Report of the Intergovernmental Panel on Climate Change*. Pörtner, H.-O., Roberts, D. C., Tignor, M. et al. (eds). Cambridge: Cambridge University Press, 3068 pp. Available at: https://www.ipcc.ch/report/ar6/wg2/downloads/report/IPCC_AR6_WGII_FullReport.pdf

IPCC (2022b). *Climate Change 2022: Mitigation of Climate Change. Contribution of Working Group III to the Sixth Assessment Report of the Intergovernmental Panel on Climate Change*. Shukla, P. R., Skea, J., Slade, R. et al. (eds). Cambridge: Cambridge University Press, 2042 pp. Available at: https://www.ipcc.ch/report/ar6/wg3/downloads/report/IPCC_AR6_WGIII_FullReport.pdf

IPCC (2023a). *Climate Change 2023: Synthesis Report. Contribution of Working Groups I, II and III to the Sixth Assessment Report of the Intergovernmental Panel on Climate Change*. Lee, H. and Romero, J. (eds). Geneva: Intergovernmental Panel on Climate Change, 186 pp. Available at: https://www.ipcc.ch/report/ar6/syr/downloads/report/IPCC_AR6_SYR_FullVolume.pdf

IPCC (2023b). *The Earth's Energy Budget, Climate Feedbacks and Climate Sensitivity*. In: *Climate Change 2021 – The Physical Science Basis*. Contribution of Working Group I to the Sixth Assessment Report of the Intergovernmental Panel on Climate Change. Cambridge: Cambridge University Press, pp. 923–1056. https://doi.org/10.1017/9781009157896.009

Ise, T., Dunn, A. L., Wofsy, S. C. and Moorcroft, P. R. (2008). High sensitivity of peat decomposition to climate change through water table feedback. *Nature Geoscience*, 1, pp. 763–766. https://doi.org/10.1038/ngeo331

Ise, T., Dunn, A. L., Wofsy, S. C. and Moorcroft, P. R. (2010). Simulating peatland methane dynamics coupled to a mechanistic model of biogeochemistry, hydrology and

energy: implications to climate change. In: Simard, S. W. (ed.) *Climate Change and Variability*. London: InTech, pp. 331–354. https://doi.org/10.5772/9815

ISO (2006). *ISO 14044:2006 – Environmental Management – Life Cycle Assessment – Requirements and Guidelines*. 1st edn. Geneva: International Organization for Standardization, 46 pp. Available at: https://www.iso.org/standard/38498.html

IUCN (2018). *UK Peatland Strategy 2018–2040*. Edinburgh: International Union for the Conservation of Nature, 48 pp. Available at: https://live-twt-d8-iucn.pantheonsite.io/sites/default/files/2024-03/UK%20Peatland%20Strategy%202018_2040.pdf

IUCN (2024a). *Peatland Code: Version 2.1*. Edinburgh: International Union for the Conservation of Nature, 18 pp. Available at: https://www.iucn-uk-peatlandprogramme.org/sites/default/files/2025-09/Peatland%20Code%20V2.1%20-%20Web%20Final-Sept%202025.pdf

IUCN (2024b). *Peatland Code Field Protocol: Version 2.1*. Edinburgh: International Union for the Conservation of Nature, 18 pp. Available at: https://www.iucn-uk-peatlandprogramme.org/sites/default/files/2025-09/Peatland%20Code%20V2.1%20-%20Web%20Final-Sept%202025.pdf

IUCN (2024c). *Peatlands and Methane*. Edinburgh: International Union for the Conservation of Nature, 7 pp. Available at: https://live-twt-d8-iucn.pantheonsite.io/sites/default/files/2025-06/202407_Briefing%20Doc%20-%20Peatlands%20and%20Methane_04%20ONLINE%20%281%29.pdf

IUCN (2024d). *UK Peatland Strategy: Progress Report 2024*. Edinburgh: International Union for the Conservation of Nature, 60 pp. Available at: https://www.iucn-uk-peatlandprogramme.org/sites/default/files/2025-09/202408_IUCN%20UK%20Peatland%20Programme%20UK%20Strategy_07.pdf

IUCN (2025a). *Adoption of University of Cumbria PhD student's carbon calculator brings national and international significance*. Edinburgh: International Union for the Conservation of Nature. Available at: https://www.iucn-uk-peatlandprogramme.org/news/adoption-university-cumbria-phd-students-carbon-calculator-brings-national-and-international

IUCN (2025b). *Biodiversity Methodology Guidance Document*. Edinburgh: International Union for the Conservation of Nature, 15 pp. Available at: https://www.iucn-uk-peatlandprogramme.org/sites/default/files/2025-05/Peatland%20Code%20and%20Woodland%20Carbon%20Code%20FIRNS%20Biodiversity%20Methodology%20Public%20Consultation%20Extended%20Summary%20Report.pdf

IUCN (2025c). *UK Carbon Price Index*. Edinburgh: International Union for the Conservation of Nature. Available at: https://www.iucn-uk-peatlandprogramme.org/uk-carbon-price-index

JNCC (2009). *Common Standards Monitoring Guidance for Upland Habitats*. Peterborough: Joint Nature Conservation Committee, 107 pp. Available at:

https://data.jncc.gov.uk/data/78aaef0b-00ef-461d-ba71-cf81a8c28fe3/CSM-UplandHabitats-2009.pdf

JNCC (2011). *UK Biodiversity Action Plan: Priority Habitat Descriptions*. JNCC Research Report (December). Peterborough: Joint Nature Conservation Committee, 103 pp. Available at: https://data.jncc.gov.uk/data/2728792c-c8c6-4b8c-9ccd-a908cb0f1432/UKBAP-PriorityHabitatDescriptions-Rev-2011.pdf

Joosten, H. (2009). *The Global Peatland CO_2 Picture: Peatland Status and Drainage-Related Emissions in All the Countries of the World*. Wageningen: Wetlands International, 36 pp. Available at: https://www.wetlands.org/download/5010/?tmstv=1763894145

Joosten, H., Couwenberg, J. and von Unger, M. (2016). International carbon policies as a new driver for peatland restoration. In: A. Bonn, T. Allott, M. Evans, H. Joosten and R. Stoneman (eds.) *Peatland Restoration and Ecosystem Services: Science, Policy and Practice*. Cambridge: Cambridge University Press, pp. 291–313. https://doi.org/10.1017/CBO9781139177788.016

Joosten, H., Sirin, A., Couwenberg, J., Laine, J. and Smith, P. (2016). The role of peatlands in climate regulation. In: A. Bonn, T. Allott, M. Evans, H. Joosten and R. Stoneman (eds.) *Peatland Restoration and Ecosystem Services: Science, Policy and Practice*. Cambridge: Cambridge University Press, pp. 63–76. https://doi.org/10.1017/CBO9781139177788.005

Joosten, H. (2021). *Global Guidelines for Peatland Rewetting and Restoration*. Ramsar Technical Report No. 11. Gland, Switzerland: Ramsar Convention Secretariat, 77 pp. Available at: https://www.ramsar.org/sites/default/files/documents/library/rtr11_peatland_rewetting_restoration_e.pdf

Joshi, P., Schroth, M. H. and Sander, M. (2021). Redox properties of peat particulate organic matter: quantification of electron accepting capacities and assessment of electron transfer reversibility. *Journal of Geophysical Research: Biogeosciences*, 126(8), e2021JG006329, pp. 1–18. https://doi.org/10.1029/2021JG006329

Kahlert, H., Steinhardt, T., Behnert, J. and Scholz, F. (2004). A new calibration-free pH probe for in situ measurements of soil pH. *Electroanalysis*, 16(20), pp. 2058–2064. https://doi.org/10.1002/elan.200403059

Kalhori, A., Wille, C., Gottschalk, P., Li, Z., Hashemi, J., Kemper, K. and Sachs, T. (2024). Temporally dynamic carbon dioxide and methane emission factors for rewetted peatlands. *Communications Earth & Environment*, 5, Article 62. https://doi.org/10.1038/s43247-024-01226-9

Kasischke, E. S. (2000). Boreal ecosystems in the global carbon cycle. In E. S. Kasischke and B. J. Stocks (eds.) *Fire, Climate Change, and Carbon Cycling in the Boreal Forest*. Ecological Studies, vol. 138. Berlin & New York: Springer, pp. 19–30. https://doi.org/10.1007/978-0-387-21629-4_2

Kechavarzi, C., Dawson, Q., Bartlett, M. and Leeds-Harrison, P. B. (2010). The role of soil moisture, temperature and nutrient amendment on CO_2 efflux from agricultural

peat soil microcosms. *Geoderma*, 154(3–4), pp. 203–210. https://doi.org/10.1016/j.geoderma.2009.02.018

Keller, T., Lamandé, M., Peth, S., Berli, M., Delenne, J.-Y., Baumgarten, W., Rabbel, W., Radjai, F., Rajchenbach, J., Selvadurai, A. P. S. and Or, D. (2013). An interdisciplinary approach towards improved understanding of soil deformation during compaction. *Soil and Tillage Research*, 128, pp. 61–80. https://doi.org/10.1016/j.still.2012.10.004

Kermorvant, C., D'Amico, F., Bru, N., Caill-Milly, N. and Robertson, B. (2019). Spatially balanced sampling designs for environmental surveys. *Environmental Monitoring and Assessment*, 191(8), Article 524. https://doi.org/10.1007/s10661-019-7666-y

Ketcham, R. A. (2005a). Computational methods for quantitative analysis of three-dimensional features in geological specimens. *Geosphere*, 1(1), pp. 32–41. https://doi.org/10.1130/GES00001.1

Ketcham, R. A. (2005b). Three-dimensional grain fabric measurements using high-resolution X-ray computed tomography. *Journal of Structural Geology*, 27(7), pp. 1217–1228. https://doi.org/10.1016/j.jsg.2005.02.006

Kettridge, N. **and Binley**, A. (2008). X-ray computed tomography of peat soils: measuring gas content and peat structure. *Hydrological Processes*, 22(25), pp. 4827–4837. https://doi.org/10.1002/hyp.7097

Kettridge, N. **and Binley**, A. (2011). Characterization of peat structure using X-ray computed tomography and its control on the ebullition of biogenic gas bubbles. *Journal of Geophysical Research: Biogeosciences*, 116 (G1), G01024, pp. 1–13. https://doi.org/10.1029/2010JG001478

Kettridge, N., Turetsky, M. R., Sherwood, J. H., Thompson, D. K., Miller, C. A., Benscoter, B. W., Flannigan, M. D., Wotton, B. M. and Waddington, J. M. (2015). Moderate drop in water table increases peatland vulnerability to post-fire regime shift. *Scientific Reports*, 5, Article 8063, pp. 1–4. https://doi.org/10.1038/srep08063

Klingenfuß, C., Roßkopf, N., Walter, J., Heller, C. and Zeitz, J. (2014). Soil organic matter to soil organic carbon ratios of peatland soil substrates. *Geoderma*, 235–236, pp. 410–417. https://doi.org/10.1016/j.geoderma.2014.07.010

Koehler, A. K., Sottocornola, M. and Kiely, G. (2011). How strong is the current carbon sequestration of an Atlantic blanket bog? *Global Change Biology*, 17(1), pp. 309–319. https://doi.org/10.1111/j.1365-2486.2010.02180.x

Lafleur, P. M., Moore, T. R., Roulet, N. T. and Frolking, S. (2005). Ecosystem respiration in a cool temperate bog depends on peat temperature but not water table. *Ecosystems*, 8, pp. 619–629. https://doi.org/10.1007/s10021-003-0131-2

Lees, K. J., Quaife, T., Artz, R. R. E., Khomik, M., Sottocornola, M., Kiely, G., Hambley, G., Hill, T., Saunders, M., Cowie, N. R., Ritson, J. and Clark, J. M. (2019). A model of gross primary productivity based on satellite data suggests formerly afforested peatlands undergoing restoration regain full photosynthesis capacity after five to ten years. *Journal of Environmental Management*, 246, pp. 594–604. https://doi.org/10.1016/j.jenvman.2019.03.040

Lees, K. J., Artz, R. R. E., Chandler, D. M., Aspinall, T., Boulton, C. A., Buxton, J., Cowie, N. R. and Lenton, T. M. (2021). Using remote sensing to assess peatland resilience by estimating soil surface moisture and drought recovery. *Science of the Total Environment*, 761, 143312, pp. 785–796. https://doi.org/10.1016/j.scitotenv.2020.143312

Leifeld, J., Müller, M. and Fuhrer, J. (2011). Peatland subsidence and carbon loss from drained temperate fens. *Soil Use and Management*, 27(2), pp. 170–176. https://doi.org/10.1111/j.1475-2743.2011.00327.x

Leifeld, J. **and Menichetti**, L. (2018). The underappreciated potential of peatlands in global climate change mitigation strategies. *Nature Communications*, 9(1), Article 1071, pp. 1–7. https://doi.org/10.1038/s41467-018-03406-6

Levy, P. E. **and Gray**, A. (2015). Greenhouse gas balance of a semi-natural peatbog in northern Scotland. *Environmental Research Letters*, 10, 094019. https://doi.org/10.1088/1748-9326/10/9/094019

Li, Y., Henrion, M., Moore, A., Lambot, S., Opfergelt, S., Vanacker, V., Jonard, F. and Van Oost, K. (2024). Factors controlling peat soil thickness and carbon storage in temperate peatlands based on UAV high-resolution remote sensing. *Geoderma*, 449, 117009. https://doi.org/10.1016/j.geoderma.2024.117009

Limaye, A. (2012). Drishti: a volume exploration and presentation tool. In: *Developments in X-Ray Tomography VIII*. Proceedings of SPIE, 85060X. https://doi.org/10.1117/12.935640

Lindsay, R.A., Charman, D.J., Everingham, F., O'Reilly, R.M., Palmer, M.A., Rowell, T.A. and Stroud, D.A. (1988). *Part I: Peatland Ecology*. In: *The Flow Country – The Peatlands of Caithness and Sutherland*. Peterborough: Joint Nature Conservation Committee, 174 pp. Available at: https://uel-repository.worktribe.com/OutputFile/480290

Lindsay, R. (2010a). *Climate-Related Changes in Peatland Carbon Accumulation*. Edinburgh: IUCN UK Peatland Programme. Available at: https://www.iucn-uk-peatlandprogramme.org/sites/default/files/2019-07/Peatbogs_and_carbon.pdf

Lindsay, R. (2010b). *Peatbogs and Carbon: A Critical Synthesis*. Edinburgh: IUCN UK Peatland Programme, 315 pp. Available at: https://www.iucn-uk-peatlandprogramme.org/sites/default/files/2024-03/Peatbogs_and_carbon.pdf

Lindsay, R., Birnie, R. and Clough, J. (2014a). *Grazing and Trampling*. IUCN UK Peatland Programme Briefing Note No. 7. https://doi.org/10.13140/2.1.2920.6729

Lindsay, R., Birnie, R. and Clough, J. (2014b). *Impacts of Artificial Drainage on Peatlands*. IUCN UK Peatland Programme Briefing Note No. 3. Edinburgh: IUCN UK Peatland Programme, 8 pp. Available at: https://www.iucn-uk-peatlandprogramme.org/sites/default/files/2024-03/Briefing%203%20Impacts%20of%20Artificial%20Drainage%20on%20Peatlands.pdf

Loisel, J. **and Yu**, Z. (2013). Surface vegetation patterning controls carbon accumulation in peatlands. *Geophysical Research Letters*, 40(200), pp. 5508–5513. https://doi.org/10.1002/grl.50744

Luscombe, D. J., Anderson, K., Gatis, N., Grand-Clement, E. and Brazier, R. E. (2015). Using airborne thermal imaging data to measure near-surface hydrology in upland ecosystems. *Hydrological Processes*, 29(6), pp. 1656–1668. https://doi.org/10.1002/hyp.10285

Lopatin, J., Kattenborn, T., Galleguillos, M., Perez-Quezada, J. F. and Schmidtlein, S. (2019). Using aboveground vegetation attributes as proxies for mapping peatland belowground carbon stocks. *Remote Sensing of Environment*, 231, 111217. https://doi.org/10.1016/j.rse.2019.111217

Liu, H., Price, J., Rezanezhad, F. and Lennartz, B. (2020). Centennial-scale shifts in hydrophysical properties of peat induced by drainage. *Water Resources Research*, 56(10), e2020WR027538. https://doi.org/10.1029/2020WR027538

Liu, W., Grootjans, A. P., Everts, H., Fritz, C. and de Vries, N. (2020). Estimation of greenhouse gas emission reductions based on vegetation changes after rewetting in Drentsche Aa brook valley. *Mires and Peat*, 26, Article 02. https://doi.org/10.19189/MaP.2019.OMB.StA.1767

Ma, L., Zhu, G., Chen, B., Zhang, K., Niu, S., Wang, J., Ciais, P. and Zuo, H. (2022). A globally robust relationship between water table decline, subsidence rate, and carbon release from peatlands. *Communications Earth & Environment*, 3, Article 254. https://doi.org/10.1038/s43247-022-00590-8

Mackenzie, C. (2024). *UK Nature Finance in 20 Posts*. 9 October. Available at: https://www.linkedin.com/pulse/uk-nature-finance-30-posts-craig-mackenzie-dsdpe/

Mäkilä, M. (2011). Carbon accumulation in pristine and drained mires. In: K. Nenonen and P. Nurmi (eds) *Geoscience for Society: 125th Anniversary Volume*. Geological Survey of Finland, Special Paper 49. Espoo, pp. 171–177. https://www.osti.gov/etdeweb/biblio/1037422

Malik, A. A., Puissant, J., Buckeridge, K. M., Goodall, T., Jehmlich, N., Chowdhury, S., Gweon, H. S., Peyton, J. M., Mason, K. E., van Agtmaal, M., Blaud, A., Clark, I. M., Whitaker, J., Pywell, R. F., Ostle, N., Gleixner, G. and Griffiths, R. I. (2018). Land-use-driven change in soil pH affects microbial carbon cycling processes. *Nature Communications*, 9, 3591. https://doi.org/10.1038/s41467-018-05980-1

Marshall, C., Sterk, H. P., Gilbert, P. J., Andersen, R., Bradley, A. V., Sowter, A., Marsh, S. and Large, D. J. (2022). Multiscale variability and the comparison of ground and satellite radar-based measures of peatland surface motion for peatland monitoring. *Remote Sensing*, 14(2), 336. https://doi.org/10.3390/rs14020336

Mastrantonis, S., Langlois, T., Radford, B., Spencer, C., de Lestang, S. and Hickey, S. (2024). Revealing the impact of spatial bias in survey design for habitat mapping: A tale of two sampling designs. *Remote Sensing Applications: Society and Environment*, 36, 101327. https://doi.org/10.1016/j.rsase.2024.101327

McCarter, C. P. R. **and Price**, J. S. (2013). The hydrology of the Bois-des-Bel bog peatland restoration: 10 years post-restoration. *Ecological Engineering*, 55, pp. 73–81. https://doi.org/10.1016/j.ecoleng.2013.02.003

McCarter, C. P. R., Rezanezhad, F., Quinton, W. L., Gharedaghloo, B., Lennartz, B., Price, J., Connon, R. and Van Cappellen, P. (2020). Pore-scale controls on hydrological and geochemical processes in peat: Implications on interacting processes. *Earth-Science Reviews*, 207, 103227. https://doi.org/10.1016/j.earscirev.2020.103227

Mello, G., Ferreira Dias, M. and Robaina, M. (2020). Wind farms life cycle assessment review: CO_2 emissions and climate change. *Energy Reports*, 6(S8), pp. 214–219. https://doi.org/10.1016/j.egyr.2020.11.104

Milne, R. **and Brown**, T. A. (1997). Carbon in the vegetation and soils of Great Britain. *Journal of Environmental Management*, 49(4), pp. 413–433. https://doi.org/10.1006/jema.1995.0118

Minasny, B., Berglund, Ö., Connolly, J., Hedley, C., de Vries, F., Gimona, A., Kempen, B., Kidd, D., Lilja, H., Malone, B., McBratney, A., Roudier, P., O'Rourke, S., Rudiyanto, Padarian, J., Poggio, L., ten Caten, A., Thompson, D., Tuve, C. and Widyatmanti, W. (2019). Digital mapping of peatlands – A critical review. *Earth-Science Reviews*, 196, 102870. https://doi.org/10.1016/j.earscirev.2019.05.014

Minasny, B., Adetsu, D. V., Aitkenhead, M., Artz, R. R. E., Baggaley, N., Barthelmes, A., Beucher, A., Caron, J., Conchedda, G., Connolly, J., Deragon, R., Evans, C., Fadnes, K., Fiantis, D., Gagkas, Z., Gilet, L., Gimona, A., Glatzel, S., Greve, M. H., Habib, W., Hergoualc'h, K., Hermansen, C., Kidd B. D., Koganti, T., Kopansky, D., Large, J, D., Larmola, T., Lilly, A., Liu, H., Marcus, M., Middleton, M., Morrison, K., Jes, P, R., Quaife, T., Rochefort, L., Rudiyanto, Toca, L., Tubiello N, F., Lystbæk, W, P., Weldon, S., Widyatmanti, W., Williamson, J., Zak, D. (2024). Mapping and monitoring peatland conditions from global to field scale. *Biogeochemistry*, 167, pp. 383–425. https://doi.org/10.1007/s10533-023-01084-1

Moore, P. D. (1975). Origin of blanket mires. *Nature*, 256(5519), pp. 267–269. https://doi.org/10.1038/256267a0

Moore, P. D. (1993). The origin of blanket mire, revisited. In F. M. Chambers (ed.) *Climate Change and Human Impact on the Landscape*. Dordrecht: Springer, pp. 217–224. https://doi.org/10.1007/978-94-010-9176-3_18

Moore, P. D. (2002). The future of cool temperate bogs. *Environmental Conservation*, 29(1), pp. 3–20. https://doi.org/10.1017/S0376892902000024

Moore, T. R., Bubier, J. L., Frolking, S. E., Lafleur, P. M. and Roulet, N. T. (2002). Plant biomass and production and CO_2 exchange in an ombrotrophic bog. *Journal of Ecology*, 90(1), pp. 25–36. https://doi.org/10.1046/j.0022-0477.2001.00633.x

Moore, P. A., Morris, P. J. and Waddington, J. M. (2015). Multi-decadal water-table manipulation alters peatland hydraulic structure and moisture retention. *Hydrological Processes*, 29(13), pp. 2970–2982. https://doi.org/10.1002/hyp.10416

Morris, P. J. **and Waddington**, J. M. (2011). Groundwater residence time distributions in peatlands: Implications for peat decomposition and accumulation. *Water Resources Research*, 47(2). https://doi.org/10.1029/2010WR009492

Morris, P. J., Waddington, J. M., Benscoter, B. W. and Turetsky, M. R. (2011). Conceptual frameworks in peatland ecohydrology: Looking beyond the two-layered (acrotelm–catotelm) model. *Ecohydrology*, 4(1), pp. 1–11. https://doi.org/10.1002/eco.191

Morris, P. J., Baird, A. J. and Belyea, L. R. (2015). Bridging the gap between models and measurements of peat hydraulic conductivity. *Water Resources Research*, 51(7), pp. 5353–5364. https://doi.org/10.1002/2015WR017264

Morris, P. J., Baird, A. J., Eades, P. A. and Surridge, B. W. J. (2019). Controls on near-surface hydraulic conductivity in a raised bog. *Water Resources Research*, 55(2), pp. 1531–1543. https://doi.org/10.1029/2018WR024566

Moxey, A., Smyth, M. A., Taylor, E. and Williams, A. P. (2021). Barriers and opportunities facing the UK Peatland Code: A case-study of blended green finance. *Land Use Policy*, 108, 105594. https://doi.org/10.1016/j.landusepol.2021.105594

Natural England (2001). *The Upland Management Handbook (SC26)*. London: Natural England. Available at: https://publications.naturalengland.org.uk/publication/82050

Natural England (2016). *Peaty Soils Location (England)*. Natural England Open Data Publication. London: Natural England. Available at: https://naturalengland-defra.opendata.arcgis.com/datasets/Defra::peaty-soils-location-england/about

Natural England (2022). *Priority Habitats Inventory*. London: Natural England. Available at: https://naturalengland-defra.opendata.arcgis.com/datasets/Defra::priority-habitats-inventory-england/about

Natural England (2025). *A New Peat Map for England*. UK Government Blog. London: Natural England. Available at: https://naturalengland.blog.gov.uk/2025/05/12/a-new-peat-map-for-england/

Natural England and DEFRA (2021). *Nature for Climate Peatland Grant Scheme*. London: Department for Environment, Food & Rural Affairs. Available at: https://www.gov.uk/guidance/nature-for-climate-peatland-grant-scheme

NatureScot (2021). *Peatland ACTION – Technical Compendium: Restoration 7 – Stabilisation and Revegetation*. Edinburgh: NatureScot. Available at: https://www.nature.scot/doc/peatland-action-technical-compendium-restoration-7-stabilisation-and-revegetation

Niedermeier, A. **and Robinson**, J. S. (2007). Hydrological controls on soil redox dynamics in a peat-based, restored wetland. *Geoderma*, 137(3–4), pp. 318–326. https://doi.org/10.1016/j.geoderma.2006.08.027

Noble, A., Palmer, S. M., Glaves, D. J., Crowle, A., Brown, L. E. and Holden, J. (2018). Prescribed burning, atmospheric pollution and grazing effects on peatland vegetation composition. *Journal of Applied Ecology*, 55(2), pp. 559–569. https://doi.org/10.1111/1365-2664.12994

North Pennines National Landscape (2024). *The Great North Bog: Financing Document*. Penrith: North Pennines National Landscape, 23 pp. Available at: https://northpennines.org.uk/wp-content/uploads/2024/02/Great-North-Bog-Financing-Document.pdf

Natural Resources Wales (2020). *National Peatland Action Programme 2020–2025*. Cardiff: Natural Resources Wales, 36 pp. Available at: https://cdn.cyfoethnaturiol.cymru/692545/national-peatlands-action-programme.pdf

Natural Resources Wales (2022). *Production of the Peatlands of Wales Map – Soil Policy Evidence Programme*. Cardiff: Natural Resources Wales, 40 pp. Available at: https://www.gov.wales/sites/default/files/publications/2022-03/production-peatlands-wales-map-spep2020-21-03.pdf

O'Kelly, B. C. (2004). Accurate determination of moisture content of organic soils using the oven-drying method. *Drying Technology*, 22(7), pp. 1767–1776. https://doi.org/10.1081/DRT-200025642

O'Kelly, B. C. **and Pichan**, S. P. (2014). Effect of decomposition on physical properties of fibrous peat. *Environmental Geotechnics*, 1(1), pp. 22–32. https://doi.org/10.1680/envgeo.13.00012

O'Kelly, B. C. **and Sivakumar**, V. (2014). Water content determinations for peat and other organic soils using the oven-drying method. *Drying Technology*, 32(6), pp. 631–643. https://doi.org/10.1080/07373937.2013.849728

Page, S. E. **and Baird**, A. J. (2016). Peatlands and global change: Response and resilience. *Annual Review of Environment and Resources*, 41, pp. 35–57. https://doi.org/10.1146/annurev-environ-110615-085520

Parry, L. E., Charman, D. J. and Noades, J. P. W. (2012). A method for modelling peat depth in blanket peatlands. *Soil Use and Management*, 28(4), pp. 614–624. https://doi.org/10.1111/j.1475-2743.2012.00447.x

Parry, L. E., Holden, J. and Chapman, P. J. (2014). Restoration of blanket peatlands. *Journal of Environmental Management*, 133, pp. 193–205. https://doi.org/10.1016/j.jenvman.2013.11.033

Peacock, M., Jones, T. G., Futter, M. N., Freeman, C., Gough, R., Baird, A. J., Green, S. M., Chapman, P. J., Holden, J. and Evans, C. D. (2018). Peatland ditch blocking has no effect on dissolved organic matter (DOM) quality. *Hydrological Processes*, 32(26), pp. 3891–3906. https://doi.org/10.1002/hyp.13297

Peacock, M., Gauci, V., Baird, A. J., Burden, A., Chapman, P. J., Cumming, A., Evans, J. G., Grayson, R. P., Holden, J., Kaduk, J., Morrison, R., Page, S., Pan, G., Ridley, L. M., Williamson, J., Worrall, F. and Evans, C. D. (2019). The full carbon balance of a rewetted cropland fen and a conservation-managed fen. *Agriculture, Ecosystems and Environment*, 269, pp. 1-12. https://doi.org/10.1016/j.agee.2018.09.020

Pearce-Higgins, J. W. **and Yalden**, D. W. (2004). Habitat selection, diet, arthropod availability and growth of a moorland wader: The ecology of European Golden Plover *Pluvialis apricaria* chicks. *Ibis*, 146 (2), pp. 335–346. https://doi.org/10.1111/j.1474-919X.2004.00278.x

Perdana, L. R., Ratnasari, N. G., Ramadhan, M. L., Palamba, P., Nasruddin and Nugroho, Y. S. (2018). Hydrophilic and hydrophobic characteristics of dry peat. *IOP*

Conference Series: Earth and Environmental Science, 105, 012063. https://doi.org/10.1088/1755-1315/105/1/012083

Petrescu, A. M. R., Lohila, A., Tuovinen, J. P., Baldocchi, D. D., Desai, A. R., Roulet, N. T., Vesala, T., Dolman, A. J., Oechel, W. C., Marcolla, B., Friborg, T., Rinne, J., Matthes, J. H., Merbold, L., Meijide, A., Kiely, G., Sottocornola, M., Sachs, T., Zona, D. and Cescatti, A. (2015). The uncertain climate footprint of wetlands under human pressure. *Proceedings of the National Academy of Sciences of the United States of America*, 112(15), pp. 4594–4599. https://doi.org/10.1073/pnas.1416267112

Petrokofsky, G., Kanamaru, H., Achard, F., Goetz, S. J., Joosten, H., Holmgren, P., Lehtonen, A., Menton, M. C., Pullin, A. S. and Wattenbach, M. (2012). Comparison of methods for measuring and assessing carbon stocks and carbon stock changes in terrestrial carbon pools: A systematic review protocol. *Environmental Evidence*, 1(6). https://doi.org/10.1186/2047-2382-1-6

Pilkington, M., Walker, J. and Maskill, R. (2016). *Vegetation trajectories on bare peat stabilisation sites*. Moors for the Future Partnership Report. Derbyshire: Moors for the Future Partnership, 55 pp. Available at: https://www.moorsforthefuture.org.uk/__data/assets/pdf_file/0030/87186/2016-Trajectories-for-impacts-of-revegetation-Annex-1-Vegetation.pdf

Plumptre, A. J., Baisero, D., Benítez-López, A., Faurby, S., Gallego-Zamorano, J., Kühl, H. S., Luna-Aranguré, C., Vázquez-Domínguez, E., Voigt, M., Wich, S., and Wint, G. R. W. (2022). Response: Where might we find ecologically intact communities? *Frontiers in Forests and Global Change*, 5, Article 880353. https://doi.org/10.3389/ffgc.2022.880353

Prat-Guitart, N., Rein, G., Hadden, R. M., Belcher, C. M. and Yearsley, J. M. (2016). Effects of spatial heterogeneity in moisture content on the horizontal spread of peat fires. *Science of the Total Environment*, 572, pp. 1422–1430. https://doi.org/10.1016/j.scitotenv.2016.02.145

Prescott, C. E. (2010). Litter decomposition: What controls it and how can we alter it to sequester more carbon in forest soils? *Biogeochemistry*, 101, pp. 133–149. https://doi.org/10.1007/s10533-010-9439-0

Preston, M. D., Smemo, K. A., McLaughlin, J. W. and Basiliko, N. (2012). Peatland microbial communities and decomposition processes in the James Bay Lowlands, Canada. *Frontiers in Microbiology*, 3, Article 70. https://doi.org/10.3389/fmicb.2012.00070

Price, J. (1997). Soil moisture, water tension, and water table relationships in a managed cutover bog. *Journal of Hydrology*, 202(1–2), pp. 21–32. https://doi.org/10.1016/S0022-1694(97)00037-1

Price, J. S., Heathwaite, A. L. and Baird, A. J. (2003). Hydrological processes in abandoned and restored peatlands: An overview of management approaches. *Wetlands Ecology and Management*, 11, pp. 65–83. https://doi.org/10.1023/A:1022046409485

Proctor, M. C. F. **and Maltby**, E. (1998). Relations between acid atmospheric deposition and the surface pH of some ombrotrophic bogs in Britain. *Journal of Ecology*, 86(2), pp. 329–340. https://doi.org/10.1046/j.1365-2745.1998.00254.x

Quinton, W. L., Gray, D. M. and Marsh, P. (2000). Subsurface drainage from hummock-covered hillslopes in the Arctic tundra. *Journal of Hydrology*, 237(1–2), pp. 113–125. https://doi.org/10.1016/S0022-1694(00)00304-8

Quinton, W. L., Hayashi, M. and Carey, S. K. (2008). Peat hydraulic conductivity in cold regions and its relation to pore size and geometry. *Hydrological Processes*, 22(15), pp. 2829–2837. https://doi.org/10.1002/hyp.7027

Quinton, W. L., Elliot, T., Price, J. S., Rezanezhad, F. and Heck, R. (2009). Measuring physical and hydraulic properties of peat from X-ray tomography. *Geoderma*, 153(1–2), pp. 269–277. https://doi.org/10.1016/j.geoderma.2009.08.010

Ramchunder, S. J., Brown, L. E. and Holden, J. (2009). Environmental effects of drainage, drain-blocking and prescribed vegetation burning in UK upland peatlands. *Progress in Physical Geography*, 33(1), pp. 49–79. https://doi.org/10.1177/0309133309105245

Ramsar Convention (1971). *Final Act of the International Conference on the Conservation of Wetlands and Waterfowl*. Ramsar: Nature and Natural Resources, 17 pp. Available at: https://www.ramsar.org/sites/default/files/documents/library/final_act_ramsar_conference1971.pdf

Ramsar Convention (2003). *The Ramsar Strategic Plan 2003–2008*. Gland, Switzerland: Ramsar Convention Secretariat, 53 pp. Available at: https://www.ramsar.org/sites/default/files/documents/pdf/key_strat_plan_2003_e.pdf

Rebitzer, G., Ekvall, T., Frischknecht, R., Hunkeler, D., Norris, G., Rydberg, T., Schmidt, W. P., Suh, S., Weidema, B. P. and Pennington, D. W. (2004). Life cycle assessment Part 1: Framework, goal and scope definition, inventory analysis, and applications. *Environment International*, 30(5), pp. 701–720. https://doi.org/10.1016/j.envint.2003.11.005

Rebmann, C., Aubinet, M., Schmid, H., Arriga, N., Aurela, M., Burba, G., Clement, R., De Ligne, A., Fratini, G., Gielen, B., Grace, J., Graf, A., Gross, P., Haapanala, S., Herbst, M., Hörtnagl, L., Ibrom, A., Joly, L., Kljun, N. and Franz, D. (2018). ICOS eddy covariance flux-station site setup: A review. *International Agrophysics*, 32, pp. 471–494. https://doi.org/10.1515/intag-2017-0044

Reed, M. S., Bonn, A., Evans, C. D., Joosten, H., Bain, C., Farmer, J., Emmer, I., Couwenberg, J., Moxey, A., Artz, R. R. E., Tanneberger, F., von Unger, M., Smyth, M., Birnie, R., Inman, I., Smith, S., Quick, T., Cowap, C. and Prior, S. (2013). *Towards the development of a UK Peatland Code: Payments for Ecosystem Services*. Leeds: Sustainability Research Institute, 117 pp. Available at: https://uel-repository.worktribe.com/OutputFile/479748

Reed, M. S., Curtis, T., Gosal, A., Kendall, H., Andersen, S. P., Ziv, G., Attlee, A., Fitton, R. G., Hay, M., Gibson, A. C., Hume, A. C., Hill, D., Mansfield, J. L., Martino, S., Olesen, A.

S., Prior, S., Rodgers, C., Rudman, H. and Tanneberger, F. (2022). Integrating ecosystem markets to co-ordinate landscape-scale public benefits from nature. *PLoS ONE*, 17(1), e0258334, pp. 1–27. https://doi.org/10.1371/journal.pone.0258334

Rezanezhad, F., Quinton, W. L., Price, J. S., Elrick, D., Elliot, T. R. and Heck, R. J. (2009). Examining the effect of pore size distribution and shape on flow through unsaturated peat using computed tomography. *Hydrology and Earth System Sciences*, 13(10), pp. 1993–2002. https://doi.org/10.5194/hess-13-1993-2009

Rezanezhad, F., Quinton, W. L., Price, J. S., Elliot, T. R., Elrick, D. and Shook, K. R. (2010). Influence of pore size and geometry on peat unsaturated hydraulic conductivity computed from 3D computed tomography image analysis. *Hydrological Processes*, 24(21), pp. 2983–2994. https://doi.org/10.1002/hyp.7709

Rezanezhad, F., Price, J. S., Quinton, W. L., Lennartz, B., Milojevic, T. and Van Cappellen, P. (2016). Structure of peat soils and implications for water storage, flow and solute transport: A review update for geochemists. *Chemical Geology*, 429, pp. 75–84. https://doi.org/10.1016/j.chemgeo.2016.03.010

Rindlisbacher, T. **and Chabbey**, L. (2015). *Guidance on the Determination of Helicopter Emissions*. 2nd edn. Bern: Federal Office of Civil Aviation (FOCA), 32 pp. Available at: https://www.bazl.admin.ch/dam/bazl/de/dokumente/Fachleute/Regulationen_und_Grundlagen/guidance_on_the_determinationofhelicopteremissions.pdf.download.pdf/guidance_on_the_determinationofhelicopteremissions.pdf

Robertson, G. S., Newborn, D., Richardson, M. and Baines, D. (2017). Does rotational heather burning increase red grouse abundance and breeding success on moors in northern England? *Wildlife Biology*, 2017(SP1), pp. 1–10. https://doi.org/10.2981/wlb.00227

Robinson, M. **and Armstrong**, A. C. (1988). The extent of agricultural field drainage in England and Wales, 1971–80. *Transactions of the Institute of British Geographers*, 13(1), pp. 19–28. https://doi.org/10.2307/622772

Rochefort, L., Quinty, F., Campeau, S., Johnson, K. and Malterer, T. J. (2003). North American approach to the restoration of *Sphagnum*-dominated peatlands. *Wetlands Ecology and Management*, 11, pp. 3–20. https://doi.org/10.1023/A:1022011027946

Rosenberry, D. O., Glaser, P. H., Siegel, D. I. and Weeks, E. P. (2003). Use of hydraulic head to estimate volumetric gas content and ebullition flux in northern peatlands. *Water Resources Research*, 39(3), 1066–1075. https://doi.org/10.1029/2002WR001377

Roulet, N. T., Ash, R., Quinton, W. and Moore, T. (1993). Methane flux from drained northern peatlands: Effect of a persistent water table lowering on flux. *Global Biogeochemical Cycles*, 7(4), pp. 749–769. https://doi.org/10.1029/93GB01931

Rowell, D. L. (1994). *Soil Science: Methods and Applications*. 1st edn. London: Routledge, 268 pp. https://doi.org/10.4324/9781315844855

Rowell, T. A. (1988). *The Peatland Management Handbook*. Peterborough: Nature Conservancy Council.

Rowson, J. G., Gibson, H. S., Worrall, F., Ostle, N., Burt, T. P. and Adamson, J. K. (2010). The complete carbon budget of a drained peat catchment. *Soil Use and Management*, 26(3), pp. 261–273. https://doi.org/10.1111/j.1475-2743.2010.00274.x

Rydin, H. **and Jeglum**, J.K. (2013). *The Biology of Peatlands*, 2nd edn. Biology of Habitats Series. Oxford: Oxford University Press, 382 pp. https://www.researchgate.net/publication/264545254_The_biology_of_peatlands_second_edition

Scanlon, D. **and Moore**, T. (2000). Carbon dioxide production from peatland soil profiles: The influence of temperature, oxic/anoxic conditions and substrate. *Soil Science*, 165(2), pp. 153–160. https://doi.org/10.1097/00010694-200002000-00006

Schellekens, J., Bindler, R., Martínez-Cortizas, A., McClymont, E. L., Abbott, G. D., Biester, H., Pontevedra-Pombal, X. and Buurman, P. (2015). Preferential degradation of polyphenols from *Sphagnum*: 4-Isopropenylphenol as a proxy for past hydrological conditions in *Sphagnum*-dominated peat. *Geochimica et Cosmochimica Acta*, 150, pp. 74–89. https://doi.org/10.1016/j.gca.2014.12.003

Schindelin, J., Arganda-Carreras, I., Frise, E., Kaynig, V., Longair, M., Pietzsch, T., Preibisch, S., Rueden, C., Saalfeld, S., Schmid, B., Tinevez, J.-Y., White, D. J., Hartenstein, V., Eliceiri, K., Tomancak, P. and Cardona, A. (2012). Fiji: An open-source platform for biological-image analysis. *Nature Methods*, 9, pp. 676–682. https://doi.org/10.1038/nmeth.2019

Scholz, K., Ejarque, E., Hammerle, A., Kainz, M., Schelker, J. and Wohlfahrt, G. (2021). Atmospheric CO_2 exchange of a small mountain lake: Limitations of eddy covariance and boundary layer modelling methods in complex terrain. *Journal of Geophysical Research: Biogeosciences*, 126(7), e2021JG006286. https://doi.org/10.1029/2021JG006286

Schulte, E. E. **and Hopkins**, B. G. (2015). Estimation of soil organic matter by weight loss-on-ignition. In *Soil Organic Matter: Analysis and Interpretation*, 46, pp. 59–61. https://doi.org/10.2136/sssaspecpub46.c3

Seybold, C. A., Mersie, W., Huang, J. and McNamee, C. (2002). Soil redox, pH, temperature and water-table patterns of a freshwater tidal wetland. *Wetlands*, 22, pp. 149–158. https://doi.org/10.1672/0277-5212(2002)022[0149:SRPTAW]2.0.CO;2

Shepherd, M., Labadz, J., Caporn, S., Crowle, A., Goodison, R., Rebane, M. and Waters, R. (2013). *Natural England Review of Upland Evidence – Restoration of Degraded Blanket Bog*. Sheffield: Natural England, 94 pp. Available at: https://publications.naturalengland.org.uk/file/10510011

Shuttleworth, E. L., Evans, M. G., Hutchinson, S. M. and Rothwell, J. J. (2015). Peatland restoration: Controls on sediment production and reductions in carbon and pollutant export. *Earth Surface Processes and Landforms*, 40(4), pp. 459–472. https://doi.org/10.1002/esp.3645

Shuttleworth, E. L., Evans, M. G., Pilkington, M., Spencer, T., Walker, J., Milledge, D. and Allott, T. E. H. (2019). Restoration of blanket peat moorland delays stormflow from

hillslopes and reduces peak discharge. *Journal of Hydrology X*, 2, Article 100006. https://doi.org/10.1016/j.hydroa.2018.100006

Silins, U. **and Rothwell**, R. L. (1998). Forest peatland drainage and subsidence affect soil water retention and transport properties in an Alberta peatland. *Soil Science Society of America Journal*, 62(4), pp. 1048–1055. https://doi.org/10.2136/sssaj1998.03615995006200040028x

Sloan, T. J., Payne, R. J., Anderson, A. R., Bain, C., Chapman, S., Cowie, N., Gilbert, P., Lindsay, R., Mauquoy, D., Newton, A. J. and Andersen, R. (2018). Peatland afforestation in the UK and consequences for carbon storage. *Mires and Peat*, 23, Article 01, pp. 1–17. https://doi.org/10.19189/MaP.2017.OMB.315

Smith, J., Nayak, D. R. and Smith, P. (2014). Wind farms on undegraded peatlands are unlikely to reduce future carbon emissions. *Energy Policy*, 66, pp. 585–591. https://doi.org/10.1016/j.enpol.2013.10.066

Smyth, M.-A., Taylor, E., Birnie, R., Artz, R., Evans, C., Gray, A., Moxey, A., Prior, S., Littlewood, N., Dickie, I. and Bonaventura, M. (2015). *Developing peatland carbon metrics and financial modelling to inform the pilot phase UK Peatland Code*. Report to Defra (Project NR0165). Crichton Carbon Centre, Dumfries. Available at: https://www.iucn-uk-peatlandprogramme.org/search?search=sites%20default%20files%202021%2012%20Defra%2013239%20Peatland%20Code%20metrics%20Final%20report%202015%20pdf

Sneed, E. D. **and Folk**, R. L. (1958). Pebbles in the Lower Colorado River, Texas: A study in particle morphogenesis. *The Journal of Geology*, 66(2), pp. 114–150. https://doi.org/10.1086/626490

SNH (2015). *Scotland's National Peatland Plan: Working for Our Future.* Edinburgh: Scottish Natural Heritage, 52 pp. Available at: https://www.nature.scot/sites/default/files/2023-06/Publication%202015%20-%20Scotland%27s%20National%20Peatland%20Plan%20-%20for%20print%20only.pdf

Sottocornola, M., Laine, A., Kiely, G., Byrne, K. A. and Tuittila, E. S. (2009). Vegetation and environmental variation in an Atlantic blanket bog in south-western Ireland. *Plant Ecology*, 203, pp. 69–81. https://doi.org/10.1007/s11258-008-9510-2

Spencer, K. L., Carr, S. J., Diggens, L. M., Tempest, J. A., Morris, M. A. and Harvey, G. L. (2017). The impact of pre-restoration land use and disturbance on sediment structure, hydrology and the sediment geochemical environment in restored saltmarshes. *Science of the Total Environment*, 587–588, pp. 47–58. https://doi.org/10.1016/j.scitotenv.2016.11.032

Stanek, W. **and Silc**, T. (1977). Comparisons of four methods for determination of degree of peat humification (decomposition) with emphasis on the Von Post method. *Canadian Journal of Soil Science*, 57(2), pp. 109–117. https://doi.org/10.4141/cjss77-015

Stimson, A. G., Allott, T. E. H., Boult, S., Evans, M. G., Pilkington, M. and Holland, N. (2017). Water quality impacts of bare peat revegetation with lime and fertiliser application. *Applied Geochemistry*, 85(A), pp. 97–105. https://doi.org/10.1016/j.apgeochem.2017.09.003

Stoneman, R., Bain, C., Locky, D., Mawdsley, N., McLaughlan, M., Kumaran-Prentice, S., Reed, M. and Swales, V. (2016). Policy drivers for peatland conservation. In: A. Bonn, T. Allott, M. Evans, H. Joosten and R. Stoneman (eds) *Peatland Restoration and Ecosystem Services: Science, Policy and Practice*. Ecological Reviews. Cambridge: Cambridge University Press,pp. 375–401. https://doi.org/10.1017/CBO9781139177788.020

Strack, M. **and Waddington**, J. M. (2005). Dynamics of biogenic gas bubbles in peat and their effects on peatland biogeochemistry. *Global Biogeochemical Cycles*, 19. 2004GB002330. https://doi.org/10.1029/2004GB002330

Strack, M. **and Waddington**, J. M. (2007). Response of peatland carbon dioxide and methane fluxes to a water table drawdown experiment. *Global Biogeochemical Cycles*, 21(1), GB1007. https://doi.org/10.1029/2006GB002715

Strack, M., Kellner, E. and Waddington, J. M. (2006). Effect of entrapped gas on peatland surface level fluctuations. *Hydrological Processes*, 20(17), pp. 3611–3622. https://doi.org/10.1002/hyp.6518

Strack, M. **and Price**, J. S. (2009). Moisture controls on carbon dioxide dynamics of peat–*Sphagnum* monoliths. *Ecohydrology*, 2(1), pp. 34–41. https://doi.org/10.1002/eco.36

Strack, M., Waddington, J.M., Turetsky, M., Roulet, N.T. and Byrne, K.A. (2008). *Northern peatlands, greenhouse gas exchange and climate change*. In: Peatlands and Climate Change. Jyväskylä: International Peat Society, pp. 44–69. https://pure.ul.ie/en/publications/northern-peatlands-greenhouse-gas-exchange-and-climate-change/

Strack, M. **and Zuback**, Y. C. A. (2013). Annual carbon balance of a peatland 10 years following restoration. *Biogeosciences*, 10(5), pp. 2885–2896. https://doi.org/10.5194/bg-10-2885-2013

Strack, M., Cagampan, J., Fard, G. H., Keith, A. M., Nugent, K., Rankin, T., Robinson, C., Strachan, I. B., Waddington, J. M. and Xu, B. (2016). Controls on plot-scale growing-season CO_2 and CH_4 fluxes in restored peatlands: Do they differ from unrestored and natural sites? *Mires and Peat*, 17, Article 5. https://doi.org/10.19189/MaP.2015.OMB.216

Strack, M., Davidson, S. J., Hirano, T. and Dunn, C. (2022). The potential of peatlands as nature-based climate solutions. *Current Climate Change Reports*, 8, pp. 71–82. https://doi.org/10.1007/s40641-022-00183-9

Susilawati, H. L., Setyanto, P., Ariani, M., Hervani, A. and Inubushi, K. (2016). Influence of water depth and soil amelioration on greenhouse gas emissions from peat soil columns. *Soil Science and Plant Nutrition*, 62(1), pp. 57–68. https://doi.org/10.1080/00380768.2015.1107459

Suwanit, W. **and Gheewala**, S. H. (2011). Life cycle assessment of mini-hydropower plants in Thailand. *International Journal of Life Cycle Assessment*, 16, pp. 849–858. https://doi.org/10.1007/s11367-011-0311-9

Swenson, M. M., Regan, S., Bremmers, D. T. H., Lawless, J., Saunders, M. and Gill, L. W. (2019). Carbon balance of a restored and cutover raised bog: Implications for restoration and comparison to global trends. *Biogeosciences*, 16(3), pp. 713–731. https://doi.org/10.5194/bg-16-713-2019

Tallis, J. H. (1995). Climate and erosion signals in British blanket peats: The significance of *Racomitrium lanuginosum* remains. *Journal of Ecology*, 83(6), pp. 1021–1030. https://doi.org/10.2307/2261183

Tallis, J. H. (1998). Growth and degradation of British and Irish blanket mires. *Environmental Reviews*, 6(2), pp. 81–122. https://doi.org/10.1139/er-6-2-81

Thom, T., Evans, M., Evans, C. and Allott, T. (2016). Blanket mire restoration and its impact on ecosystem services. In: A. Bonn, T. Allott, M. Evans, H. Joosten and R. Stoneman (eds) *Peatland Restoration and Ecosystem Services: Science, Policy and Practice*. Ecological Reviews. Cambridge: Cambridge University Press, pp. 153–169. https://doi.org/10.1017/CBO9781139177788.010

Thom, T., Hanlon, A., Lindsay, R., Richards, J., Stoneman, R. and Brooks, S. (2019). *Conserving Bogs: The Management Handbook*, 2nd edn. Peterborough: IUCN UK Peatland Programme, 207 pp. Available at: https://www.yppartnership.org.uk/sites/default/files/2019-09/Conserving%20Bogs%20The%20Management%20Handbook%202nd%20Edition.pdf

Thompson, D. B. A., MacDonald, A. J., Marsden, J. H. and Galbraith, C. A. (1995). Upland heather moorland in Great Britain: A review of international importance, vegetation change and some objectives for nature conservation. *Biological Conservation*, 71(2), pp. 163–178. https://doi.org/10.1016/0006-3207(94)00043-P

Tian, W., Wang, H., Xiang, X., Loni, P. C., Qiu, X., Wang, R., Huang, X. and Tuovinen, O. H. (2023). Water table level controls methanogenic and methanotrophic communities and methane emissions in a *Sphagnum*-dominated peatland. *Microbiology Spectrum*, 11(5), e01992-23. https://doi.org/10.1128/spectrum.01992-23

Tokarz, E. **and Urban**, D. (2015). Soil redox potential and its impact on microorganisms and plants of wetlands. *Journal of Ecological Engineering*, 16(3), pp. 20–30. https://doi.org/10.12911/22998993/2801

Tokida, T., Miyazaki, T. and Mizoguchi, M. (2005). Ebullition of methane from peat with falling atmospheric pressure. *Geophysical Research Letters*, 32(13), GL022949. https://doi.org/10.1029/2005GL022949

Tolonen, K. **and Turunen**, J. (1996). Accumulation rates of carbon in mires in Finland and implications for climate change. *Holocene*, 6(2), pp. 171–178. https://doi.org/10.1177/095968369600600204

Toniolo, S., Mazzi, A., Fedele, A., Aguiari, F. and Scipioni, A. (2017). Life cycle assessment to support the quantification of the environmental impacts of an event. *Environmental Impact Assessment Review*, 63, pp. 12–22. https://doi.org/10.1016/j.eiar.2016.07.007

Trippier, B., Robinson, P., Colson, D. and Hutchinson, J. (2020). *Developing a Framework for Using Earth Observation Imagery to Monitor Peatland Condition.* JNCC Report No. 667. Peterborough: Joint Nature Conservation Committee, 56 pp. Available at: https://data.jncc.gov.uk/data/958df51f-2e7c-4d2b-92f0-eac84c2a86af/JNCC-Report-667-FINAL-WEB.pdf

Turetsky, M., Wieder, K., Halsey, L. and Vitt, D. (2002). Current disturbance and the diminishing peatland carbon sink. *Geophysical Research Letters*, 29(11), pp. 21-1-21-4. https://doi.org/10.1029/2001GL014000

Turner, E. K., Worrall, F. and Burt, T. P. (2013). The effect of drain blocking on the dissolved organic carbon (DOC) budget of an upland peat catchment in the UK. *Journal of Hydrology*, 479, pp. 169–179. https://doi.org/10.1016/j.jhydrol.2012.11.059

Turunen, J., Roulet, N. T., Moore, T. R. and Richard, P. J. H. (2004). Nitrogen deposition and increased carbon accumulation in ombrotrophic peatlands in eastern Canada. *Global Biogeochemical Cycles*, 18(3), GB002154. https://doi.org/10.1029/2003GB002154

UNEP (2017). *Smoke on the Water: Countering Global Threats from Peatland Loss and Degradation*. Arendal, Norway: GRID–Arendal, 72 pp. Available at: https://globalpeatlands.org/sites/default/files/2022-08/smoke%20on%20the%20water%20countering%20global%20threats%20from%20peatland%20loss%20and%20degradation.pdf

UNFCCC (1998). Kyoto Protocol to the United Nations Framework Convention on Climate Change. *Journal of Environmental Law*, 10(1), pp. 215–224. https://doi.org/10.1093/jel/10.1.215

United Nations (2011). *Ad Hoc Working Group on Further Commitments for Annex I Parties under the Kyoto Protocol – Sixteenth Session, Part Four*. Durban: United Nations, 11 pp. Available at: https://unfccc.int/resource/docs/2011/awg16/eng/l03a02.pdf

United Nations (2015). *Adoption of the Paris Agreement*. Conference of the Parties, Twenty-First Session (COP21). Paris: United Nations, 32 pp. Available at: https://unfccc.int/resource/docs/2015/cop21/eng/l09r01.pdf

United Nations Climate Change (2020). *Global Warming Potentials (IPCC Fourth Assessment Report)*. Available at: https://unfccc.int/process/transparency-and-reporting/greenhouse-gas-data/greenhouse-gas-data-unfccc/global-warming-potentials

Urbanová, Z. **and Picek**, T. (2019). *How are peat bogs affected by drainage?* LIFE for MIRES. Available at: https://life.npsumava.cz/en/2021/06/17/how-are-peat-bogs-affected-by-drainage/

Urquhart, C. **and Gore**, A. J. P. (1973). The redox characteristics of four peat profiles. *Soil Biology and Biochemistry*, 5(5), pp. 659–666. https://doi.org/10.1016/0038-0717(73)90056-4

Van Breemen, N. (1995). How *Sphagnum* bogs down other plants. *Trends in Ecology & Evolution*, 10(7), pp. 270–275. https://doi.org/10.1016/0169-5347(95)90007-1

Van der Molen, P. C., Schalkoort, M. and Smit, R. (1994). Vegetation and ecology of hummock–hollow complexes on an Irish raised bog. *Biology and Environment: Proceedings of the Royal Irish Academy*, 94B(2), pp. 145–175. http://www.jstor.org/stable/20499927

Vanselow-Algan, M., Schmidt, S. R., Greven, M., Fiencke, C., Kutzbach, L. and Pfeiffer, E. M. (2015). High methane emissions dominated annual greenhouse gas balances 30 years after bog rewetting. *Biogeosciences*, 12(14), pp. 4361–4371. https://doi.org/10.5194/bg-12-4361-2015

Verhoeven, J. T. A. **and Liefveld**, W. M. (1997). The ecological significance of organochemical compounds in *Sphagnum*. *Plant Biology*, 46(2), pp. 117–130. https://doi.org/10.1111/plb.1997.46.2.117

Von Post, L. (1922). *Svensk torvtäkt: några ord om torv och torvanvändning i Sverige*. *Svenska Mosskulturföreningens Tidskrift*, 1, pp. 1–7.

Waddington, J. M. **and Price**, J. S. (2000). Effect of peatland drainage, harvesting, and restoration on atmospheric water and carbon exchange. *Physical Geography*, 21, pp. 433–451. https://doi.org/10.1080/02723646.2000.10642719

Waddington, J. M., Morris, P. J., Kettridge, N., Granath, G., Thompson, D. K. and Moore, P. A. (2015). Hydrological feedbacks in northern peatlands. *Ecohydrology*, 8(1), pp. 113–127. https://doi.org/10.1002/eco.1493

Wallage, Z. E., Holden, J. and McDonald, A. T. (2006). Drain blocking: An effective treatment for reducing dissolved organic carbon loss and water discolouration in a drained peatland. *Science of the Total Environment*, 367(2–3), pp. 811–821. https://doi.org/10.1016/j.scitotenv.2006.02.010

Wallage, Z. E. **and Holden**, J. (2011). Near-surface macropore flow and saturated hydraulic conductivity in drained and restored blanket peatlands. *Soil Use and Management*, 27(2), pp. 247–254. https://doi.org/10.1111/j.1475-2743.2011.00336.x

Wang, M., Wang, S., Cao, Y., Jiang, M., Wang, G. and Dong, Y. (2021). The effects of hummock–hollow microtopography on soil organic carbon stocks and soil labile organic carbon fractions in a sedge peatland in Changbai Mountain, China. *Catena*, 201, 105204. https://doi.org/10.1016/j.catena.2021.105204

Ward, S. E., Bardgett, R. D., McNamara, N. P., Adamson, J. K. and Ostle, N. J. (2007). Long-term consequences of grazing and burning on northern peatland carbon dynamics. *Ecosystems*, 10, pp. 1069–1083. https://doi.org/10.1007/s10021-007-9080-5

Watts, S. H. (2020). *Revegetation of upland eroded bare peat using heather brash and geotextiles in the presence and absence of grazing*. *Mires and Peat*, 26, Article 29. https://doi.org/10.19189/MAP.2019.AJB.STA.1902

Weber, T. K. D., Iden, S. C. and Durner, W. (2017). A pore-size classification for peat bogs derived from unsaturated hydraulic properties. *Hydrology and Earth System Sciences*, 21(12), pp. 6185–6200. https://doi.org/10.5194/hess-21-6185-2017

Wentworth, J. (2022). *Reducing peatland emissions*. POSTnote No. 668. London: Parliamentary Office of Science and Technology, 8 pp. Available at: https://post.parliament.uk/research-briefings/post-pn-0668/

Weston, D. J., Timm, C. M., Walker, A. P., Gu, L., Muchero, W., Schmutz, J., Shaw, A. J., Tuskan, G. A., Warren, J. M. and Wullschleger, S. D. (2015). Sphagnum physiology in the context of changing climate: Emergent influences of genomics, modelling and host-microbiome interactions on understanding ecosystem function. *Plant, Cell & Environment*, 38(9), pp. 1737–1751. https://doi.org/10.1111/pce.12458

Whitehead, S. C. **and Baines**, D. (2018). Moorland vegetation responses following prescribed burning on blanket peat. *International Journal of Wildland Fire*, 27(10), pp. 658–664. https://doi.org/10.1071/WF18019

Whitfield, S., Reed, M., Thomson, K., Christie, M., Stringer, L. C., Quinn, C. H., Anderson, R., Moxey, A. and Hubacek, K. (2011). Managing peatland ecosystem services: Current UK policy and future challenges in a changing world. *Scottish Geographical Journal*, 127(3), pp. 209–230. https://doi.org/10.1080/14702541.2011.616864

Wichmann, S., Brander, L., Schäfer, A., Schaafsma, M., van Beukering, P., Tinch, D. and Bonn, A. (2016). Valuing peatland ecosystem services. In: A. Bonn, T. Allott, M. Evans, H. Joosten and R. Stoneman (eds) *Peatland Restoration and Ecosystem Services: Science, Policy and Practice*. Ecological Reviews. Cambridge: Cambridge University Press, pp. 314–338. https://doi.org/10.1017/CBO9781139177788.017

Wickland, K. P., Striegl, R. G., Neff, J. C. and Sachs, T. (2006). Effects of permafrost melting on CO_2 and CH_4 exchange of a poorly drained black spruce lowland. *Journal of Geophysical Research: Biogeosciences*, 111(G2), G000099. https://doi.org/10.1029/2005JG000099

Wijeyesekera, D. C., John, L. M. S. A. and Adnan, Z. (2016). Embedded empiricisms in soft soil technology. *IOP Conference Series: Materials Science and Engineering*, 136, 012001. https://doi.org/10.1088/1757-899X/136/1/012001

Wilder Carbon (2024). *Wilder Carbon – Update on Projects and Buyers, Together with Plans for a Nature and Climate Credit*. 7 pp. Available at: https://ecosystemsknowledge.net/wp-content/uploads/2024/06/WilderCarbonFAQs.pdf

Wilson, D., Alm, J., Laine, J., Byrne, K. A., Farrell, E. P. and Tuittila, E. S. (2009). Rewetting of cutaway peatlands: Are we re-creating hot spots of methane emissions? *Restoration Ecology*, 17(6), pp. 796–806. https://doi.org/10.1111/j.1526-100X.2008.00416.x

Wilson, D., Blain, D., Couwenberg, J., Evans, C., Murdiyarso, D., Page, S., Renou-Wilson, F., Rieley, J., Strack, M. and Tuittila, E. S. (2016). Greenhouse gas emission

factors associated with rewetting of organic soils. *Mires and Peat*, 17, Article 4. https://doi.org/10.19189/MaP.2016.OMB.222

Wilson, L., Wilson, J., Holden, J., Johnstone, I., Armstrong, A. and Morris, M. (2010). Recovery of water tables in Welsh blanket bog after drain blocking: Discharge rates, time scales and the influence of local conditions. *Journal of Hydrology*, 391(3–4), pp. 237–248. https://doi.org/10.1016/j.jhydrol.2010.05.002

Wilson, L., Wilson, J., Holden, J., Johnstone, I., Armstrong, A. and Morris, M. (2011). Ditch blocking, water chemistry and organic carbon flux: Evidence that blanket bog restoration reduces erosion and fluvial carbon loss. *Science of the Total Environment*, 409(11), pp. 2010–2018. https://doi.org/10.1016/j.scitotenv.2011.02.036

Wiltshire, J., Hekman, J. and Fernández Milan, B. (2019). *Carbon loss and economic impacts of a peatland wildfire in north-east Sutherland, Scotland, May 2019*. Report for WWF-UK, Issue 3. Oxfordshire: WWF-UK, 23 pp. Available at: https://www.wwf.org.uk/sites/default/files/2019-11/Carbon%20loss%20and%20economic%20impacts%20of%20a%20peatland%20wildfire%20in%20north-east%20Sutherland.pdf

Wolf, C., Klein, D., Weber-Blaschke, G. and Richter, K. (2016). Systematic review and meta-analysis of life cycle assessments for wood energy services. *Journal of Industrial Ecology*, 20(4), pp. 743–763. https://doi.org/10.1111/jiec.12321

World Resources Institute & World Business Council for Sustainable Development (2011). *Corporate Value Chain (Scope 3) Accounting and Reporting Standard: Supplement to the GHG Protocol Corporate Accounting and Reporting Standard*. Washington, DC: WRI & WBCSD, 5 pp. Available at: https://ghgprotocol.org/sites/default/files/standards/Corporate-Value-Chain-Accounting-Reporing-Standard_041613_2.pdf

Worrall, F., Reed, M., Warburton, J. and Burt, T. (2003). Carbon budget for a British upland peat catchment. *Science of the Total Environment*, 312(1–3), pp. 133–146. https://doi.org/10.1016/S0048-9697(03)00226-2

Worrall, F., Evans, M. G., Bonn, A., Reed, M. S., Chapman, D. and Holden, J. (2009). Can carbon offsetting pay for upland ecological restoration? *Science of the Total Environment*, 408(1), pp. 26–36. https://doi.org/10.1016/j.scitotenv.2009.09.022

Worrall, F., Clay, G., Marrs, R. and Reed, M. (2010). *Impacts of burning management on peatlands*. IUCN Investing in Peatlands Conference, Durham, UK. Available at: https://research.manchester.ac.uk/en/publications/impacts-of-burning-management-on-peatlands/

Worrall, F., Rowson, J. G., Evans, M. G., Pawson, R., Daniels, S. and Bonn, A. (2011). Carbon fluxes from eroding peatlands: The carbon benefit of revegetation following wildfire. *Earth Surface Processes and Landforms*, 36(11), pp. 1487–1498. https://doi.org/10.1002/esp.2174

Worrall, F. **and Clay**, G. D. (2012). The impact of sheep grazing on the carbon balance of a peatland. *Science of the Total Environment*, 438, pp. 426–434. https://doi.org/10.1016/j.scitotenv.2012.08.084

Xu, J., Morris, P. J., Liu, J. and Holden, J. (2018). PEATMAP: Refining estimates of global peatland distribution based on a meta-analysis. *Catena*, 160, pp. 134–140. https://doi.org/10.1016/j.catena.2017.09.010

Young, D. M., Baird, A. J., Morris, P. J. and Holden, J. (2017). Simulating the long-term impacts of drainage and restoration on the ecohydrology of peatlands. *Water Resources Research*, 53(8), pp. 6510–6522. https://doi.org/10.1002/2016WR019898

Young, D. M., Baird, A. J., Charman, D. J., Evans, C. D., Gallego-Sala, A. V., Gill, P. J., Hughes, P. D. M., Morris, P. J. and Swindles, G. T. (2019). Misinterpreting carbon accumulation rates in records from near-surface peat. *Scientific Reports*, 9, Article 17939. https://doi.org/10.1038/s41598-019-53879-8

Young, D. M., Baird, A. J., Gallego-Sala, A. V. and Loisel, J. (2021). A cautionary tale about using the apparent carbon accumulation rate obtained from peat cores. *Scientific Reports*, 11, Article 9547. https://doi.org/10.1038/s41598-021-88766-8

Yu, Z. (2011a). Holocene carbon flux histories of the world's peatlands: Global carbon-cycle implications. *Holocene*, 21(5), pp. 761–774. https://doi.org/10.1177/0959683610386982

Yu, Z., Beilman, D. W., Frolking, S., MacDonald, G. M., Roulet, N. T., Camill, P. and Charman, D. J. (2011b). Peatlands and their role in the global carbon cycle. *Eos*, 92(12), pp. 97–98. https://doi.org/10.1029/2011EO120001

Yu, Z. (2011c). Global peatland dynamics since the Last Glacial Maximum. *Geophysical Research Letters*, 37(13), L043584. https://doi.org/10.1029/2010GL043584

Yu, Z. C. (2012). Northern peatland carbon stocks and dynamics: A review. *Biogeosciences*, 9(10), pp. 4071–4085. https://doi.org/10.5194/bg-9-4071-2012

Zeh, L., Igel, T. M., Schellekens, J., Limpens, J., Bragazza, L. and Kalbitz, K. (2020). Vascular plants affect properties and decomposition of moss-dominated peat, particularly at elevated temperatures. *Biogeosciences*, 17(19), pp. 4797–4813. https://doi.org/10.5194/bg-2019-503